PACE-2023

The Second International Congress on the Phenomenological Aspects of Civil Engineering

Atatürk University, Erzurum, TÜRKİYE

20-23 June 2023

Transactions of the PACE-2023

ISSN 2791-6405

Edited by Abdulkadir Cüneyt Aydın

Transactions of The Second International Congress on the Phenomenological Aspects of Civil Engineering

Edited by
Abdulkadir Cüneyt Aydın
Atatürk University

Publishing

20-23 June 2023
Erzurum-Turkey

ISSN 2791-6405

Published by ACA Publishing ®, a trademark of ACADEMY ®
Müftü Solakzade Mah. 78. Sk. 4/2, Yıldızkent 25070-Palandöken/Erzurum
E-mail: info@acapublishing.com https://www.acapublishing.com

ORGANIZERS

ACADEMY Sağlık Hiz. Müh. İnş. Taah.
Elekt. Yay. Tic. San. Ltd. Şti.

CONTRIBUTORS

Foreword

Civil engineering is as old as mankind, and, which will be forever. The civilization, which includes all applied sciences is the basics of civil engineering. Thus, the gap, between pure science and enhancing quality of life is the wisdom of civil engineering, which is a combination of art, craft, and mathematics. Thereby, the Congress name should imply the scientific era, which is inspected intensively as long as mankind. That means also, many things have done before. This concept, gathered us to decide a name, which can be memorized and remembered easily, harmonic, and emphasized the openness of the Congress. Withal, the abbreviation of the Congress has to be a meaningful word. For a pandemic world, to activate the scientific impression to our lives, International Congress on Phenomenological Aspects of Civil Engineering (PACE) get in life.

As the above-mentioned sense, PACE-2023 aimed to get in touch the academicians, researchers and practitioners in the civil engineering, geological engineering, geophysical engineering, architectural engineering, architecture, and landscape architecture related topics from all around the world to review recent trends, topics, problems, and innovations of knowledge and understanding in the relevant areas to share the knowledge that the present, and the future pose. It is hoped that the transactions of the PACE-2023 will provide a fruitful background for up grading the branch, through an appropriate exchange of information between all researchers, scientists and industrial scholars.

The impression for a congress is very important, especially, when it's executed for the second time, also. Thus, 15 keynotes from all over the world are selected for wider audience. About 48 manuscripts from 15 countries are submitted; however, we could only accept 23 of them. All authors are submitted their full manuscripts except, the 2 of the ones, who submitted their works, as abstracts. Withal, only the presented submissions are included within this transactions e-book. The reviews of the papers were undertaken by the Scientific Committee of the congress and only the accepted ones were announced for the congress. The editor is deeply grateful to all for their effort in enhancing the quality of the transactions. At the end, the PACE-2023 Congress is executed with 15 Keynotes, 31 presentations, and 157 participants from 14 countries. Hereby, the manuscripts were about 77% from out of Turkey, which implies the globality of the Congress. We think, the Congress got the pace...!

I would like to thank to all participants of the congress, especially the session chairs and Keynotes from all over the world; to get in touch at PACE-2023, At the second stage, all PACE-2023 Committee members, they have done their best to get in life this Congress. Without their grateful support, the PACE-2023 would not have been the great success it was.

We look forward to get in touch again in the next congress, PACE-2025.

Abdulkadir Cüneyt Aydın

Editor & Chairman of the PACE-2023

COMMITTEES

Chairman

Prof. Dr. Abdulkadir Cüneyt Aydın, Ataturk University, TURKEY

Secretary

Assoc. Prof. Dr. Mahyar MAALI, Erzurum Technical University, TURKEY

Organizing Committee

Prof. Dr. Abdulkadir KAN, Ataturk University, TURKEY

Prof. Dr. İbrahim TÜRKMEN, İnönü University, TURKEY

Prof. Dr. Mehmet Burhan KARAKOÇ, İnönü University, TURKEY

Assoc. Prof. Dr. Çağlar Özer, Ataturk University, TURKEY

Assoc. Prof. Dr. Gökhan KAPLAN, Ataturk University, TURKEY

Assoc. Prof. Dr. İlker TEKİN, Karabuk University, TURKEY

Assoc. Prof. Dr. Mahmut KILIÇ, Ataturk University, TURKEY

Assoc. Prof. Dr. Merve MAALI, Erzurum Technical University, TURKEY

Assoc. Prof. Dr. Sinan SEZEK, Ataturk University, TURKEY

Assist. Prof. Dr. Ali ÖZ, Ataturk University, TURKEY

Assist. Prof. Dr. Barış Bayrak, Kafkas University, TURKEY

Dr. Haluk Görkem Alcan, Kafkas University, TURKEY

Scientific Committee

Abbas HEYDARI, Sharif University of Technology, IRAN

Abdelhafid KHELIDJ, Nantes University, FRANCE

Abdullah DİLSİZ, Yıldırım Beyazıt University, TURKEY

Adem DOGANGUN, Uludag University, TURKEY

Ahmet Can ALTUNIŞIK, Karadeniz Technical University, TURKEY

Arvin FARID, Boise State University, USA

Ayfer DÖNMEZ ÇAVDAR Karadeniz Technical University, TURKEY

Ayman S. MOSALLAM, University of California, USA

Aynur KAZAZ, Akdeniz University, TURKEY

Ayse DALOGLU, Karadeniz Technical University, TURKEY

Badee ALSHAMERİ, National University of Sciences and Technology (NUST), PAKİSTAN

Baki ÖZTÜRK, Hacettepe University, TURKEY

Beyhan BAYHAN, Bursa Technical University, TURKEY

Çağla Meral AKGÜL, Middle East Technical University, TURKEY

Erfan NAJAF, Islamic Azad University, South Tehran Branch, Tehran, IRAN

Esra Mete GÜNEYİSİ, Gaziantep University, TURKEY

Fatih ÇELİK, Niğde Ömer Halisdemir University, TURKEY

Fauzan Mohd. JAKARNİ, University Putra Malaysia, MALAYSIA

Gökhan ÖZDEMİR, Eskişehir Technical University, TURKEY

Hossain SHOWKATI, Urmia University, IRAN

Ilker Bekir TOPCU, Osmangazi University, TURKEY

Halit YAZICI, Dokuz Eylul University, TURKEY

Hatem A. Abou-SENNA, University of Central Florida, USA

Helmi Zulhaidi Mohd SHAFRI, Universiti Putra, MALAYSIA

Izzet Ufuk CAGDAS, Akdeniz University, TURKEY

Jelena BLEIZIFFER, University of Zagreb, CROTIA

Jian JIANG, China University of Mining and Technology, CHINA

Kadir GÜLER, İstanbul Technical University, TURKEY

Kemal BEYEN, Kocaeli University, TURKEY

Le Hoang AN, Ton Duc Thang University, VIETNAM

Mahmut FIRAT, Inonu University, TURKEY

Marko SERAFIMOV, Methodius University, MACEDONIA

Mehmet İNAN, Oregon University, USA

Merve MAALI, Erzurum Technical University, TURKEY

Mohamed MOULI, ENSET, ALGERIA

Mohammad Arif KAMAL Aligarh Muslim University, INDIA

Mojtaba B. SİRJANİ, Norfolk State University, USA

Naimul HAQUE, East West University, BANGLADESH

Nasr-Eddine BOUHAMOU, University Center Nour Bachir of El-Bayadh, ALGERİA

Osman Hamdy OSMAN, Zagazig University, EGYPT

Saaid ZAKI, Institute of Nano Technology, EGYPT

Said KENAI, University of Blidal, ALGERIA

Sakir ERDOGDU, Karadeniz Technical University, TURKEY
Sinan SEZEK, Ataturk University, TURKEY

Slimane MERDACI, Liabes Djillali University, ALGERIA

Sogol FALLAH, University College of Dublin, IRELAND

Suada DZEBO, University of Sarajevo, SARAJEVO

Suleyman ADANUR, Karadeniz Technical University, TURKEY

Suman SAHA, National Institute of Technology Durgapur, INDIA

Şemsi YAZICI, Ege University, TURKEY

Tanay KARADEMİR, Istanbul Bilgi University, Turkey

Tayfun UYGUNOGLU, Afyon Kocatepe University, TURKEY

Xintao LIU, Hong Kong Polytechnic University, HONG KONG

Vahid JAHANGIRI, University of Mohaghegh Ardabili, IRAN

Yao YU, North Dakota State University, USA

Yusuf AYVAZ, Yildiz Technical University, TURKEY

Conference Staff

Res. Assist. Ph.D. Candidate Oğuzhan Çelebi

Ph.D. Candidate Ahmad Jamshid Sadid

Ph.D. Candidate Aysan Ardalani

Ph.D. Candidate Oğuzhan Akarsu

Contents

KEYNOTE SPEAKERS

PACE-2023

The Second International Congress on the Phenomenological Aspects of Civil Engineering

Keynote

20-23 June 2023

Synthesis of Environmentally Friendly Lightweight Artificial Aggregates

Mo Kim Hung

Associate Professor, University of Malaya, Kuala Lumpur, MALAYSIA

Corresponding Author E-mail: khmo@um.edu.my

Keywords

Woody solid waste ash,
Palm oil fuel ash,
Cold-bonded artificial aggregates,
Geopolymer.

Abstract

The presentation covers the latest development of environmentally friendly lightweight artificial aggregate developed at the University Malaya, Malaysia. The first part involves utilizing bio-based solid waste ash, namely woody solid waste ash and palm oil fuel ash to produce cold-bonded artificial aggregates. Cement-based and alkali-activated based cold-bonded artificial aggregates are produced, which can meet the lightweight aggregate requirement of bulk density and achieve adequate strength. The granulating parameters such as granulating speed, rotation angle and water content to produce the cold-bonded artificial aggregates are also optimized. Secondly, the potential of foamed fly ash-based geopolymer aggregate for heavy metal ion removal is explored. The geopolymer aggregate is produced with a simple moulding method and with increasing foaming agent, the geopolymer aggregate can achieve lightweight bulk density and acceptable strength. More importantly, the increasing porosity due to the foaming helps increase surface area of heavy metal ion adsorption, thus improving the removal efficiency under optimal pH and contact time.

PACE-2023

The Second International Congress on the Phenomenological Aspects of Civil Engineering

Keynote

20-23 June 2023

Structural Health Monitoring of Civil Engineering Structures

Ahmet Can Altunışık

Professor, Karadeniz Tecnical University, Department of Civil Engineering, Trabzon, TURKEY

Corresponding Author E-mail: ahmetcan8284@hotmail.com

Keywords

Earthquake,
Wind, flood, vehicle load and external loads,
Material defects,
Workmanship defect.

Abstract

Many special engineering structures such as buildings, bridges, towers, historical monuments, dams and tunnels are exposed to various environmental effects throughout their service life, gradually accumulating damage or are suddenly damaged due to natural disasters.
Structural Health Monitoring System that allows continuous or periodic monitoring of structures due to uncertainties such as natural factors, ground conditions, material deformations due to time. As a result of the environmental effects they are exposed to, these engineering structures, which can cause great financial and emotional damage when collapsed, need to be determined by using developing methods and their current conditions should be constantly observed.

PACE-2023

The Second International Congress on the Phenomenological Aspects of Civil Engineering

Keynote

20-23 June 2023

Seismic Performances of Engineering Structures During the February 6, 2023 Kahramanmaraş, Türkiye, Earthquakes (M7.7 and M7.6)

Alemdar Bayraktar

Professor, University of British Columbia, CANADA

Corresponding Author E-mail: alemdarbayraktar@gmail.com

Keywords

Earthquake,

Active faults,

Aftershocks,

Kahramanmaras,

Seismic performances.

Abstract

In order to ensure the durability of a structure both over time and against potentially catastropic earthquake, - proper structural design (Good geotech + Good structural = Good design), - correct construction, - correct inspection, - adequate maintenance of the structures along their life Professional engineering system should be implemented. New construction technologies and strengthening techniques for the damaged buildings can be developed. Shear walls are very important for improving the earthquake performance of buildings. The building design software (black box) should be used with care. After many earthquakes, the undamaged structures in the region was tired. It is important to check the structural safety of undamaged buildings and other engineering structures after the earthquakes with structural health monitoring methods. Before new structures are allowed to be used, one of the best solutions may be to check the health of the structure using a non-destructive experimental method..

1. Active Faults and Seismic Hazard of Türkiye

According to the Türkiye Earthquake Hazard Map published in 2018, a large part of Türkiye is located in areas with high seismic risk.

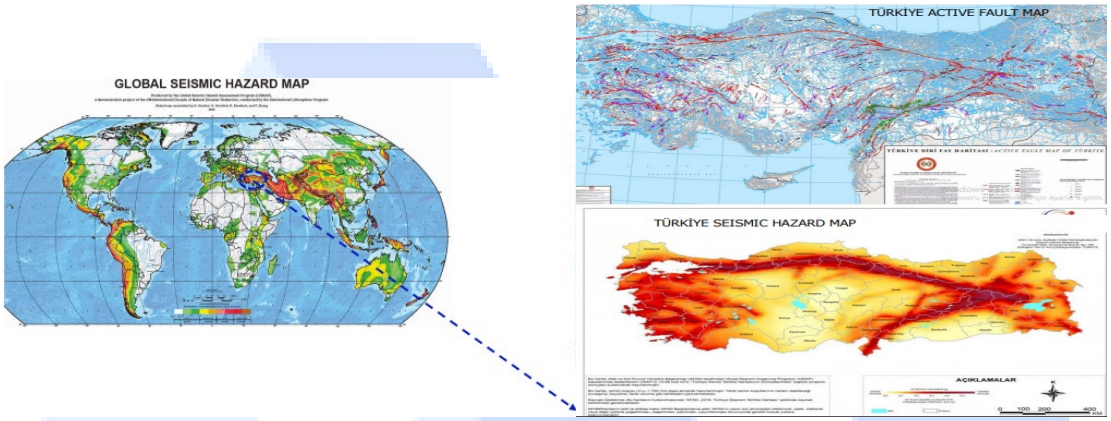

Global Seismic Hazard Map – Türkiye Active Fault Map – Türkiye Seismic Hazard Map

Türkiye is located between the Eurasian Plate in the north and the African-Arabian Plates in the south.

- The Arabian plate is moving towards the northeast with respect to the Anatolian plate at approximately 10-11 mm/yr.
- Two main major faults of Türkiye are North Anatolian Fault (NAF) and East Anatolian Fault (EAF).

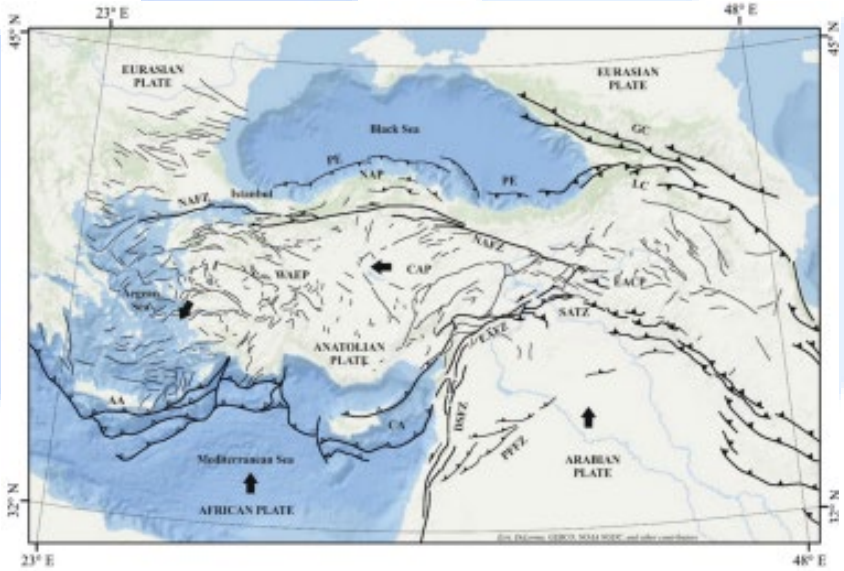

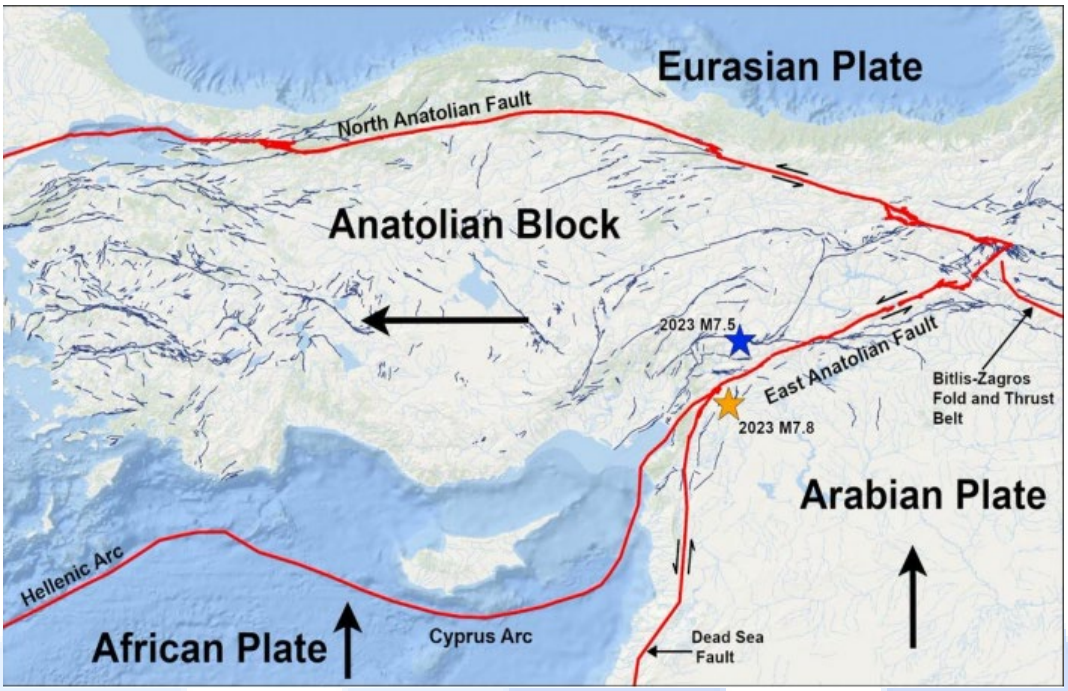

North Anatolian Fault (NAF) and East Anatolian Fault (EAF)

The fault mechanism of the East Anatolian Fault Zone (EAFZ), which is about 450km long, is NE-trending left-lateral strikeslip fault system that lies between Karlıova and Hatay.

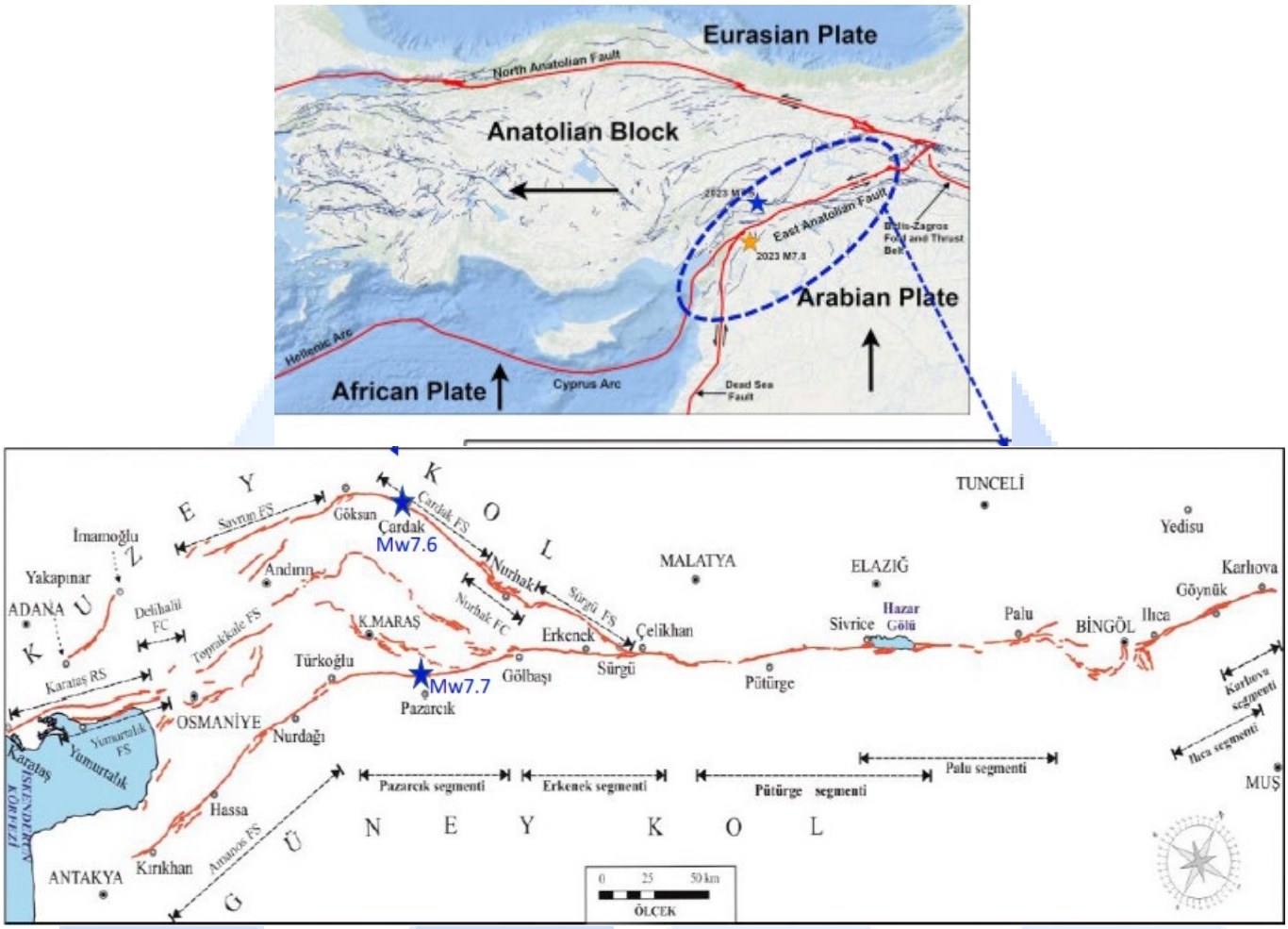

Duman and Emre (2013)

2. Historical Seismicity of Türkiye and the Earthquake Region

- In Türkiye, more than 20 earthquakes with a magnitude of 7 or higher have occurred since 1900. Between 1900 and 2023, 269 earthquakes resulted in loss of life and damage have occurred.

- The biggest historical earthquakes in terms of casualties and severe damage are 1939 Erzincan (Ms7.9) and 17 August 1999 Kocaeli (Mw7.6), 12 Nowember 1999 Düzce (Mw 7.5).

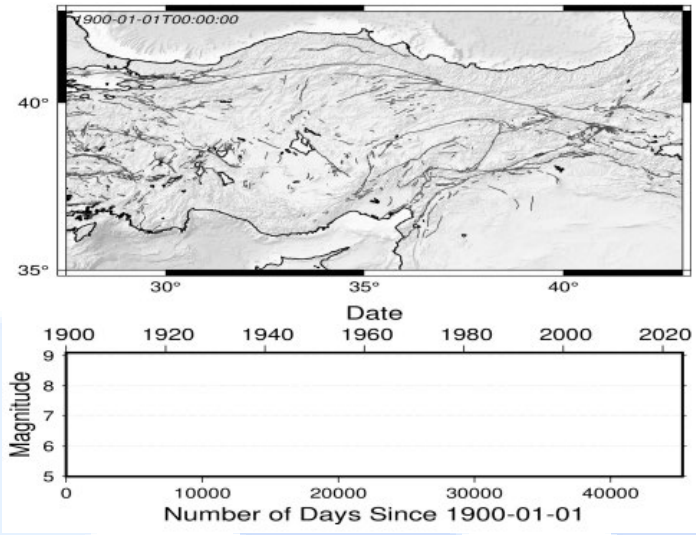
1900-01-01T00:00:00
40°
35°
30°
35°
40°
Date
1900
1920
1940
1960
1980
2000
2020
Magnitude
9
8
7
6
5
0
10000
20000
30000
40000
Number of Days Since 1900-01-01

Location	Date	Ms	Mw	Magnitude
Pütürge - Malatya	04.12.1905	6.8		IX
Şarköy - Tekirdağ	09.08.1912	7.4		X
Burdur	03.10.1914	7.0		IX
Tokat	24.01.1916	7.1		
Ayvalık - Balıkesir	18.11.1919	7.0		IX
Köprüköy - Erzurum	13.09.1924	6.8		IX
Offshore Kaş	18.03.1926	6.8		X
Offshore Datça	26.06.1926	7.7		IX
Kaman - Kırşehir	19.04.1938	6.6		
Dikili - İzmir	22.09.1939	6.6		
Çayırlı - Erzincan	26.12.1939	7.9		
Erbaa - Tokat	20.12.1942	7.0		
Adapazarı - Sakarya	20.06.1943	6.6		
Ilgaz - Çankırı	26.11.1943	7.2		
Gerede - Bolu	01.02.1944	7.3		
Offshore Edremit	06.10.1944	6.8		
Offshore Izmir	23.07.1949	6.6		
Tercan - Erzincan / Yedisu - Bingöl	17.08.1949	6.7		
Çerkeş - Çankırı	13.08.1951	6.9		
Yenice - Gönen - Çanakkale	18.03.1953	7.2		
Söke - Aydın	16.07.1955	6.8		
Mediterranean Sea	25.04.1957	7.1		
Abant - Bolu	26.05.1957	7.1		
Karacabey - Bursa	06.10.1964	7.0		
Varto - Muş	19.08.1966	6.9		
Adapazarı - Sakarya	22.07.1967	6.8		
Offshore Bartın	03.09.1968	6.5		
Alaşehir - Manisa	28.03.1969	6.5		
Çavdarhisar - Kütahya	28.03.1970	7.2		
Bingöl	22.05.1971	6.8		
Lice - Diyarbakır	06.09.1975	6.6		
Çaldıran - Van	24.11.1976		7.0	
Narman - Erzurum	30.10.1983		6.6	
Armenia	07.12.1988		6.7	
Erzincan	13.03.1992		6.6	
Gölcük - Kocaeli	17.08.1999		7.6	
Düzce - Bolu	12.11.1999		7.1	
Sultandağı - Afyon	03.02.2002		6.5	
Merkez - Van	23.10.2011		7.1	IX
Offshore Bodrum (Gökova Gulf)	21.07.2017		6.5	VII
Sivrice - Elazığ	24.01.2020		6.8	IX
Offshore Seferihisar, Izmir	30.10.2020		6.6	VIII
Pazarcık - Kahramanmaraş	06.02.2023		7.7	XI
Elbistan - Kahramanmaraş	06.02.2023		7.6	X
Defne - Hatay	20.02.2023		6.4	IX

Source: AFAD

Historical earthquakes of the EAFZ:

• Palu earthquake in 1789

• A series of earthquakes occurred including the earthquakes of 1822, 1866, 1872, 1874, 1875, 1893.

• Malatya earthquake in 1905. The EAFZ entered a relatively calm period in the 20th century after this earthquake until 1971.

• Bingöl earthquake of May 22, 1971 (M=6.8),

• Doğanşehir earthquakes of May 5, 1986 (M=5.8) and May 6, 1986 (M=5.6)

• Despite having a quieter period in the 20th century and not producing earthquakes greater than magnitude 7, the DAFS still experienced a total of 13 earthquakes (Ms>5.0) that caused damage, although none of them exceeded Ms=6.8.

• In the 2000s, the EAFZ entered a more active period, with destructive earthquakes occurring in Bingöl on May 1, 2003 (Mw 6.3), Karlıova Bingöl on March 14, 2005 (Mw 5.8), Doğanyol Malatya on February 21, 2007 (Mw 5.7), Kovancılar Elazığ on March 8, 2010 (Mw 6.1), Sivrice Elazığ on January 24, 2020 (Mw 6.8), and Karlıova Bingöl on June 14, 2020 (Mw 5.7).

• On February 6, 2023, the most recent earthquakes occurred on the EAFZ, with a magnitude of Mw 7.7 in Pazarcık (Kahramanmaraş) at 04:17 Turkey time and Mw 7.6 in Elbistan (Kahramanmaraş) at 13:24.

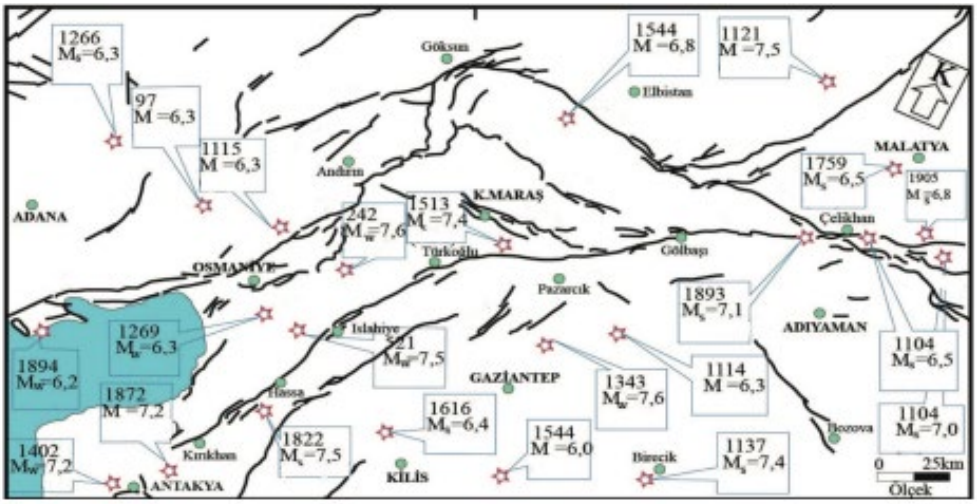

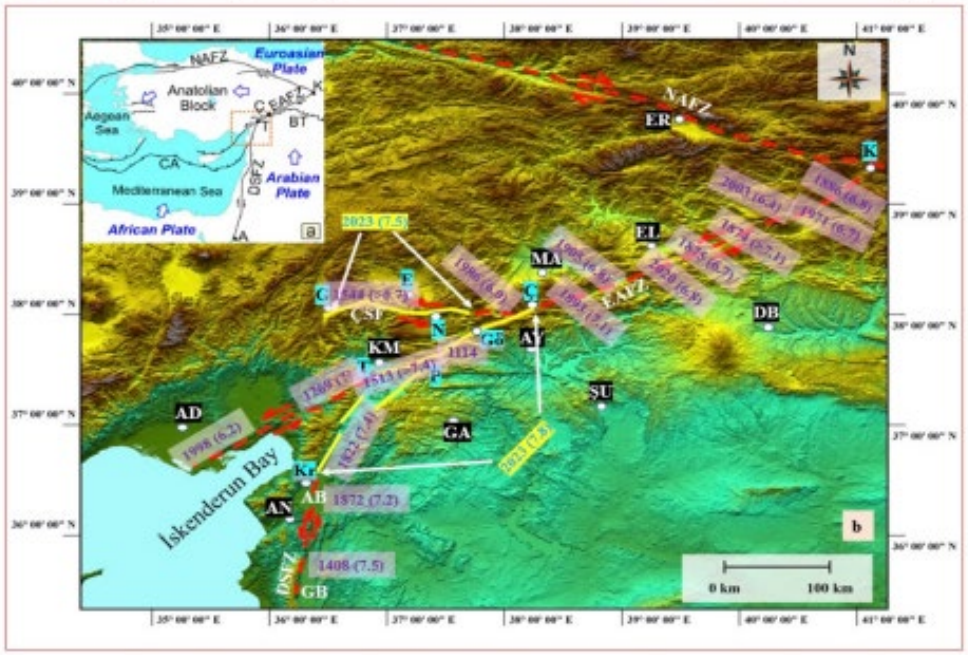

3. Main and Aftershocks of the 6 February 2023 Kahramanmaras Earthquakes (Mw 7.7 and Mw 7.6)

- The events took place on February 6, 2023 near the city of Kahramanmaraş while most people were asleep:
- The first main shock (Pazarcık) was Mw7.7 (04:17 a.m.)
- The earthquakes came as winter storms impacted the region, with freezing temperatures and snowfall.
- Aftershock (Nurdağı-Mw6.6) after ten minutes later (4:28 a.m.)

- Second mainshock came with Mw7.6 (Elbistan) after 9 hours later from the Mw7.7 (13:24 p.m.), 95 km to the northeast of the Mw7.7 event. • A big one came with Mw6.4 (Yayladağ) on February 20, 2023 (17:04 p.m.).

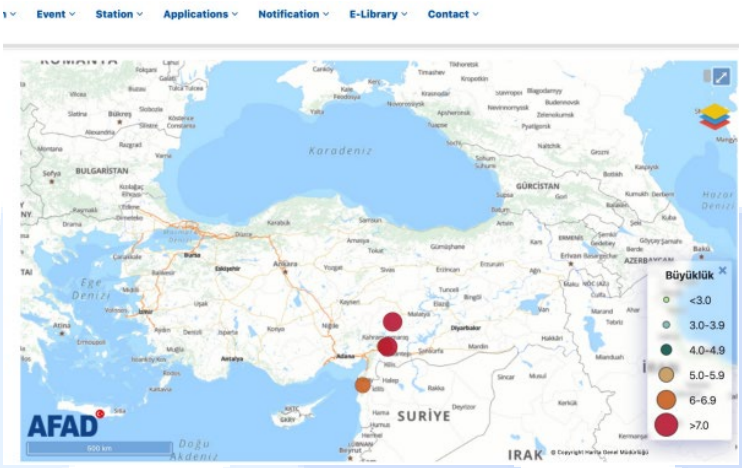

Search | Search | S-File | Statistics | TS Time Zone

Date(UTC)	Latitude	Longitude	Depth	Type	Magnitude	Location	EventID		
06-02-2023 01:17:32	37.288	37.043	8.6	MW	7.7	Pazarcık (Kahramanmaraş)	543428	Detail	S-File
06-02-2023 01:28:16	37.304	36.92	6.2	MW	6.6	Nurdağı (Gaziantep)	543431	Detail	S-File
06-02-2023 10:24:47	38.089	37.239	7	MW	7.6	Elbistan (Kahramanmaraş)	543593	Detail	S-File
20-02-2023 17:04:27	36.037	36.021	21.73	MW	6.4	Yayladağı (Hatay)	551067	Detail	S-File

AFAD (2023)

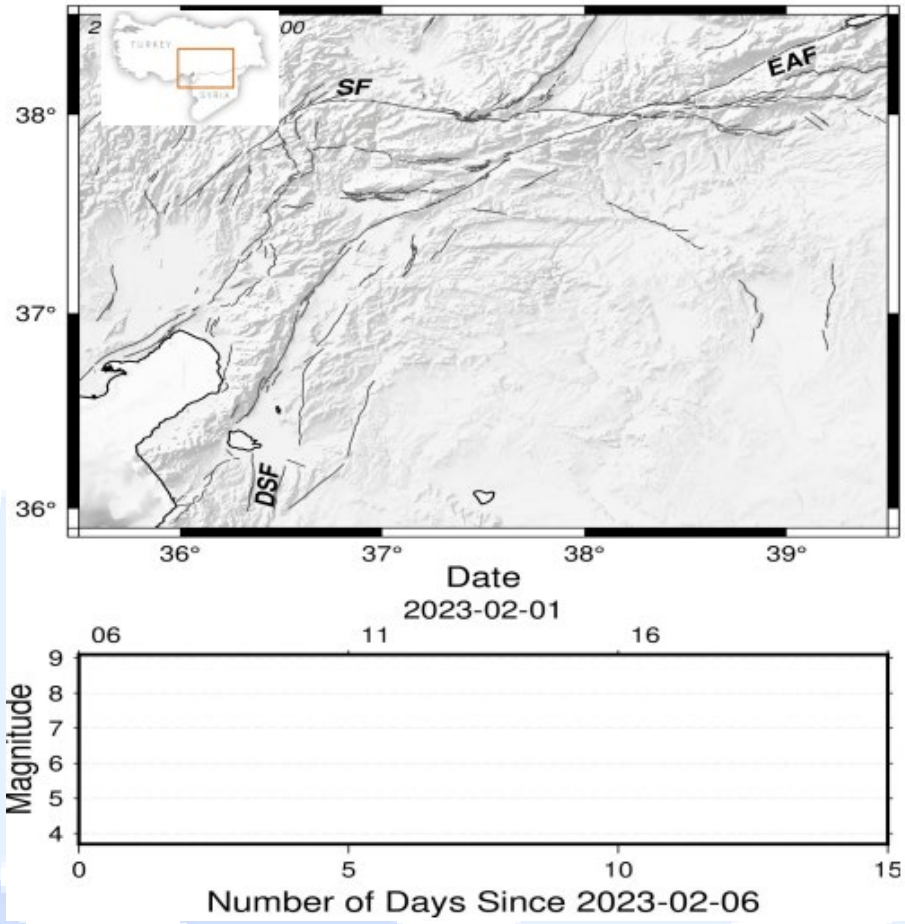
SF
EAF
DSF
38°
37°
36°
36°
37°
38°
39°
Date
2023-02-01
06
11
16
Magnitude
9
8
7
6
5
4
0
5
10
15
Number of Days Since 2023-02-06

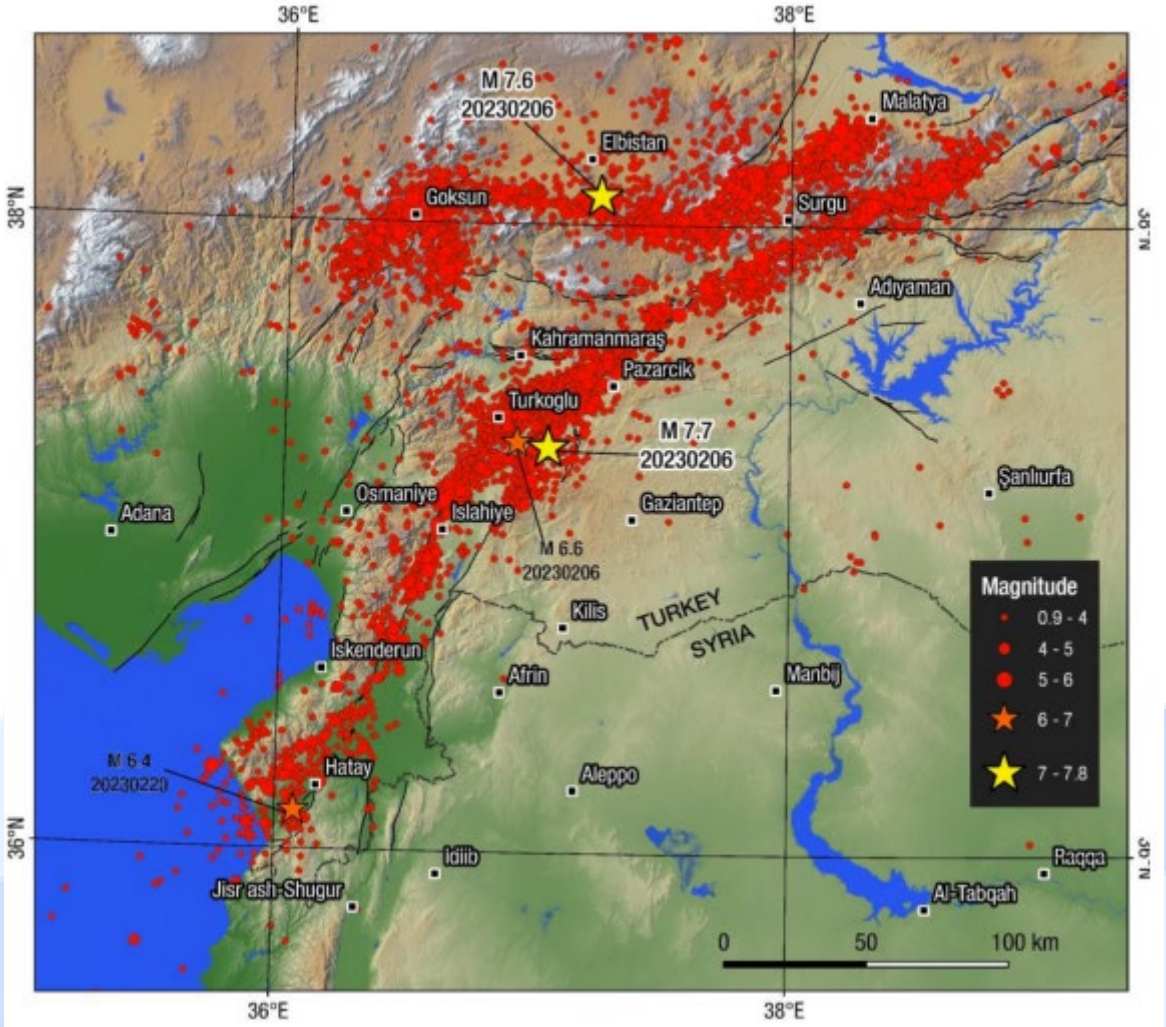

Figure ?. Main and aftershocks of the earthquakes Mw 7.7, Mw6.6, Mw7.5 and Mw 6.4

- The events affected the cities of Kahramanmaraş, Adıyaman, Hatay, Osmaniye, Gaziantep, Kilis, Şanlıurfa, Diyarbakır, Malatya, Adana, and Elazığ with residents of over 14 million, and north part of Syria. More than 55,000 deaths have been reported across southern Türkiye and northwestern Syria.
- Most damages occurred in Gaziantep-Nurdağ-Islahiye, Adıyaman-Center-Gölbaşı, Kahramanmaraş-Türkoğlu-Elbistan-Dulkadiroğlu, Hatay-Antakya due to the proximity of these cities to the faults.

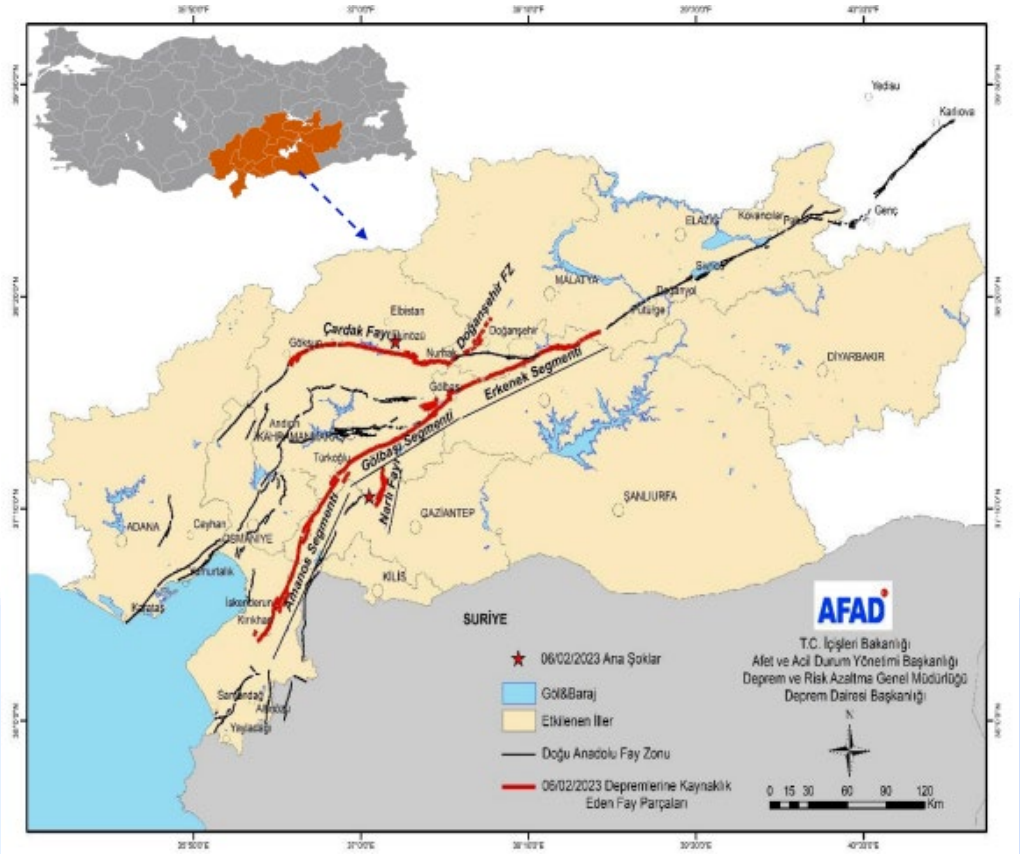

Yerleşim Merkezi	Deprem üslerine olan mesafe (km)		Yakın olduğu diri fay ve mesafesi
	Pazarcık Mw7.7	Elbistan Mw7.6	
Adana, Çukurova	157	209	Misis Fayı, 31 km Ecemiş Fayı Pozantı segmenti, 120 km
Adıyaman, İl Merkezi	125	100	Güneydoğu Anadolu Bindirme Zonu, 6.3 km Doğu Anadolu Fay Zonu Erkenek Segmenti, 26.0 km
Çelikhan	134	90	Doğu Anadolu Fay Zonu Erkenek Segmenti, 1.0 km (kayma zonu)
Gaziantep, İl Merkezi	48	126	Ölüdeniz Fay Zonu Narlı Segmenti,36.0 km
İslahiye	46	130	Doğu Anadolu Fay Zonu Amanos Segmenti, 0.9 km (kayma zonu)
Nurdağı	30	111	Doğu Anadolu Fay Zonu Amanos Segmenti, 2.3 km
Hatay İl Merkezi	122	209	Antakya Fay Zonu 0.0 km (kayma zonu) Ölüdeniz Fay Zonu Hacıpaşa Segmenti, 19.4 km * Ölüdeniz Fay Zonu Armanaz Segmenti, 31 km Ölüdeniz Fay Zonu Sermada Segmenti, 50 km**
İskenderun	110	191	İskenderun fayı Payas Segmenti, 7.9 km (kayma zonu) Doğu Anadolu Fay Zonu Amanos Segmenti, 18.0 km
Hassa	72	161	Doğu Anadolu Fay Zonu Amanos Segmenti, 0.0 km
Kırıkhan	108	197	Doğu Anadolu Fay Zonu Amanos Segmenti, 0.0 km (kayma zonu)
Samandağ	163	250	Antakya Fay Zonu, 3.8 km (kayma zonu) Antakya Fay Zonu Ana Segment, 10.0 km Ölüdeniz Fay Zonu Hacıpaşa segmenti 34.0 km
Kahramanmaraş Merkez	35	63	Doğu Anadolu Fay Zonu Pazarcık Segmenti, 14.9 km Kahramanmaraş Fay Zonu, 0.0 km (Kayma zonu)***
Nurhak	82	23	Sürgü Fayı, 0.0 km (Kayma Zonu) (Kayma zonu)****
Pazarcık	31	67	Doğu Anadolu Fay Zonu Pazarcık Segmentine 7.8 km Ölüdeniz Fay Zonu Narlı Segmentin,16.1 km,
Osmaniye	73	142	İskenderun Fay Zonu Osmaniye Segmenti, 0.0 km (kayma zonu) Tahtakale fayı, 5.9 km *****
Malatya, İl Merkezi	163	99	Doğanşehir Fayına 28.0 km Doğu Anadolu Fay Zonu Pütürge Segmentine 34.0 km
Doğanşehir	116	100	Sürgü fayına 7.6 km (kayma zonu) Doğanşehir fay zonuna 3.6 km

BGD (2023)

3.1. Surface Fault Ruptures

- The mainshock centered on Pazarcık ruptured the Erkenek (between Çelikhan and Gölbaşı, 65km), Gölbaşı (between Gölbaşı and Türkoğlu, 90km), and Amanos
- (between Türkoğlu and Kırıkhan, 110km) segments of the DAFS as well as the Narlı segment at the northern end of the Ölüdeniz Fault System along a fault line.
- The second earthquake centered on Elbistan was related to the Çardak Fault and the Doğanşehir Fault Zone based on field observations.
- The Geophysical modeling results also clearly reveal that the rupture times of the Mw 7.7 and Mw 7.6 earthquakes are approximately 100 s and 60 s,
- respectively.
- The largest horizontal displacement after both earthquakes was obtained at Ekinözü as 4.7 m (Mw 7.7).
-

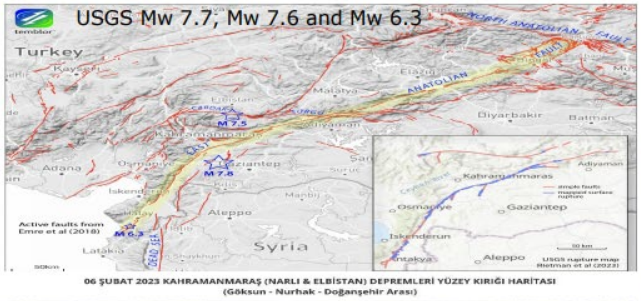

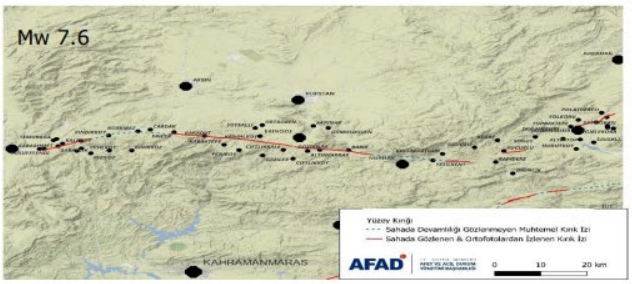

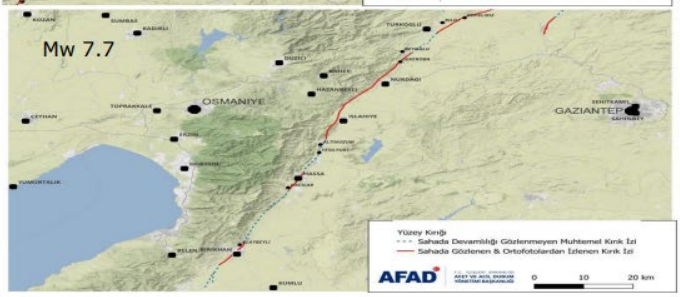

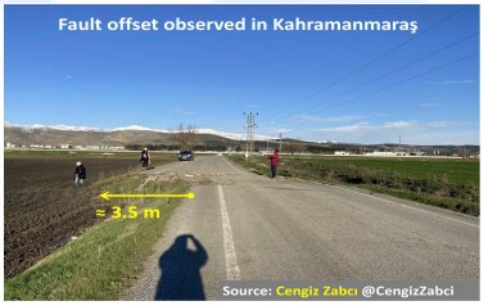
Fault offset observed in Kahramanmaraş
≈ 3.5 m
Source: Cengiz Zabcı @CengizZabci


TP (2023)

3.2. Strong Ground Motion Records of the 6 February 2023 Kahramanmaras Earthquakes (Mw 7.7 and Mw 7.6)

- Ore than 800 strong-motion stations, operated by AFAD (Disaster and Emergency Management Authority) recorded the February 6, 2023, Kahramanmaraş earthquakes.
- Records can be downloaded from https://tadas.afad.gov.tr

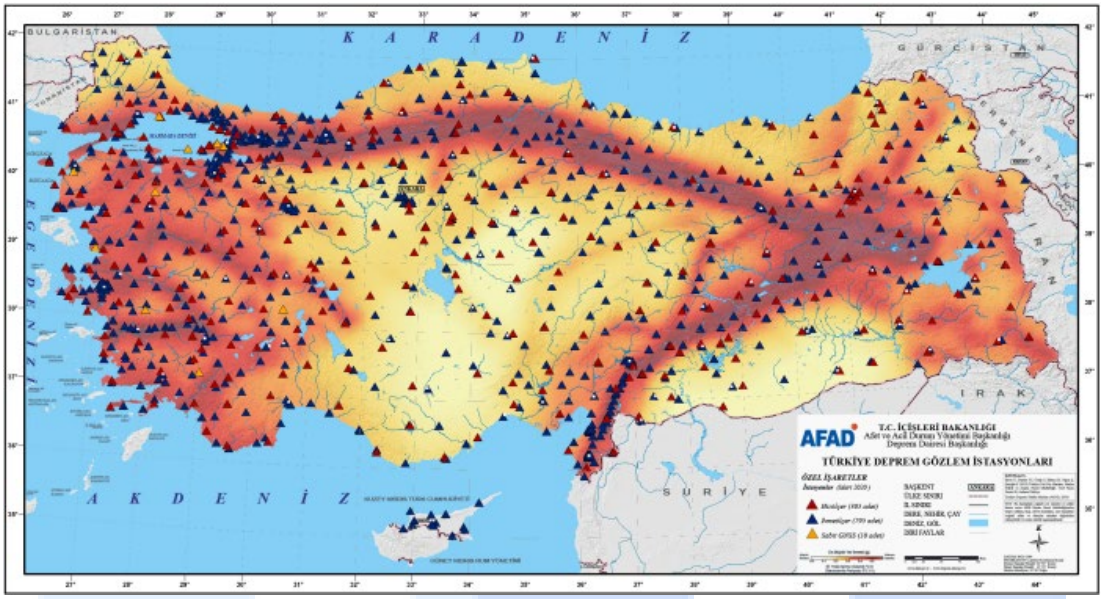

- Large strike-slip earthquakes are generally associated with near-fault effects, such as rupture directivity pulses (directivity refers to energy focused along the fault in the direction of rupture, which can result in a large pulse of motion), which can be identified from examining the velocity and displacement time histories from an earthquake.

- Such ground motions have the potential to cause severe damage, especially to long-period structures.

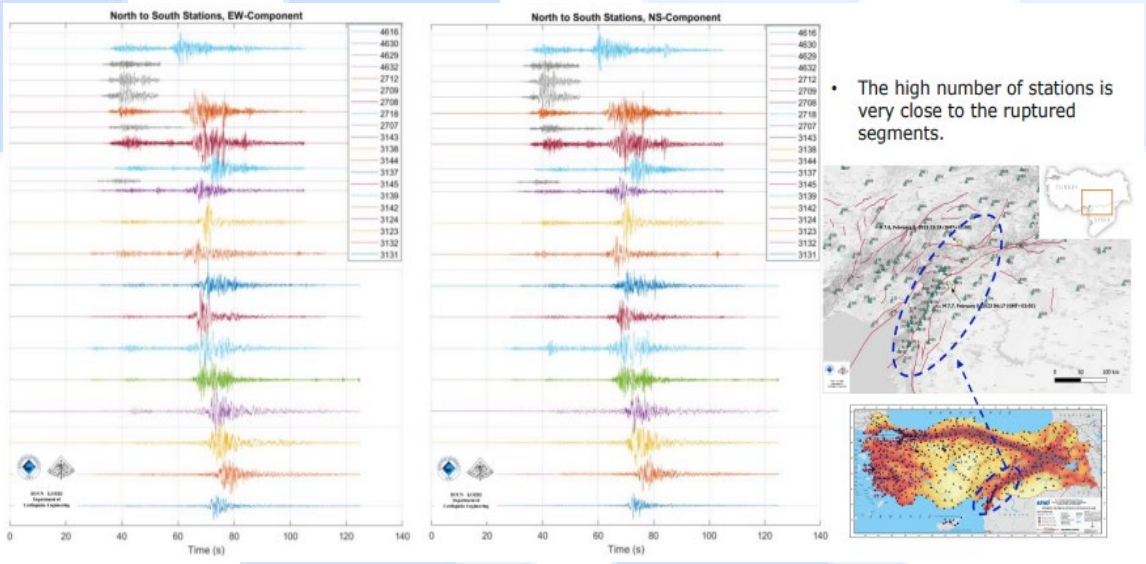

- The maximum recorded horizontal PGA 1347 cm/s2 (1.37g), observed 146 km from the epicenter along the north-south direction at station 3129 due to combined effects of forward directivity, basin effects, and site amplification
- The horizontal PGA at the station closest to the epicenter (No. 4616) is 0.58g.
- Between the two main shock earthquakes (Mw 7.7 and Mw7.6), serious aftershocks occurred at locations very close to the first one.

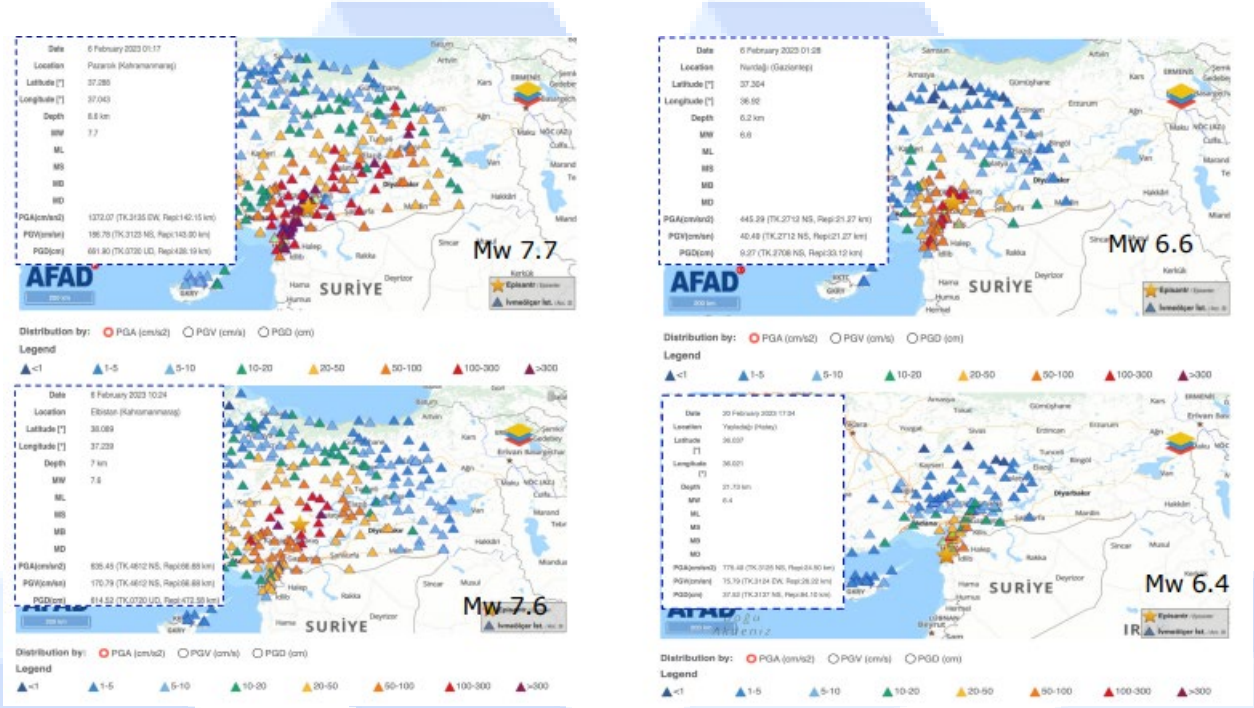

- It is seen that the peak horizontal and vertical ground acceleration values of the 2023 Kahramanmaraş earthquake are larger than the highest horizontal and vertical ground acceleration values of the 1999 Kocaeli earthquake, respectively.

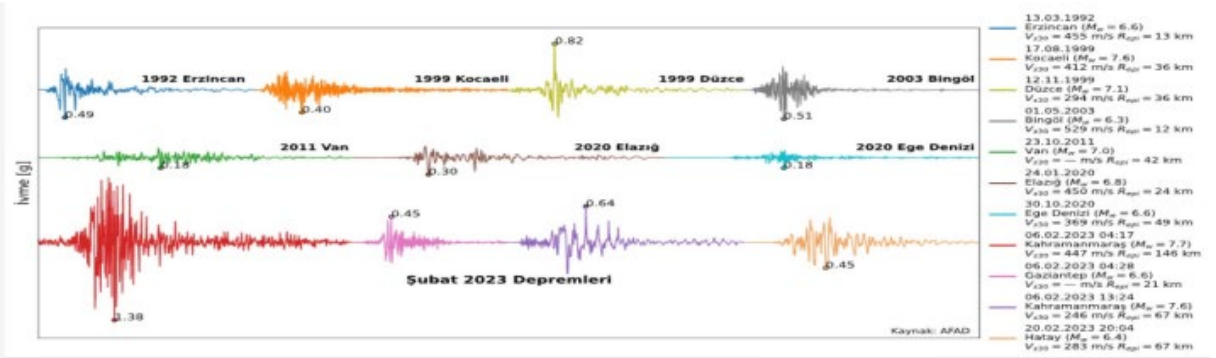
1992 Erzincan
1999 Kocaeli
1999 Düzce
2003 Bingöl
2011 Van
2020 Elazığ
2020 Ege Denizi
Şubat 2023 Depremleri
İvme [g]
Kaynak: AFAD

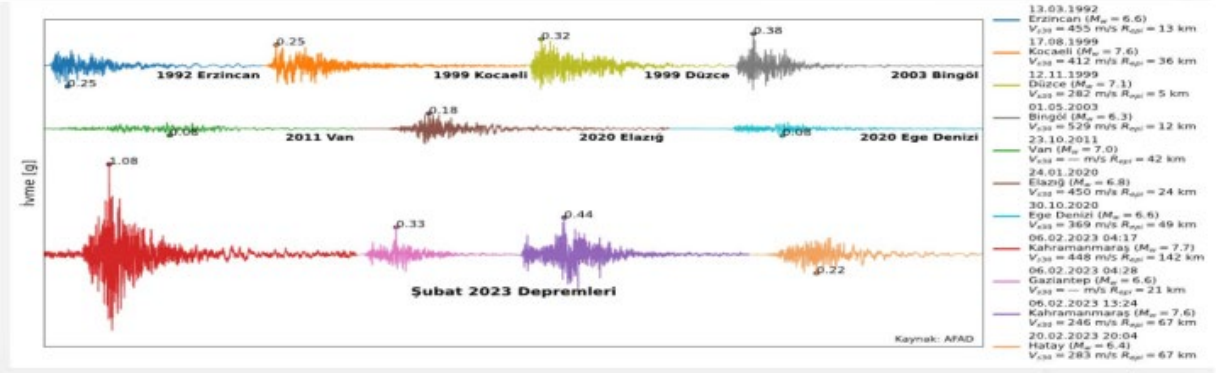
1992 Erzincan
1999 Kocaeli
1999 Düzce
2003 Bingöl
2011 Van
2020 Elazığ
2020 Ege Denizi
Şubat 2023 Depremleri
İvme [g]
Kaynak: AFAD

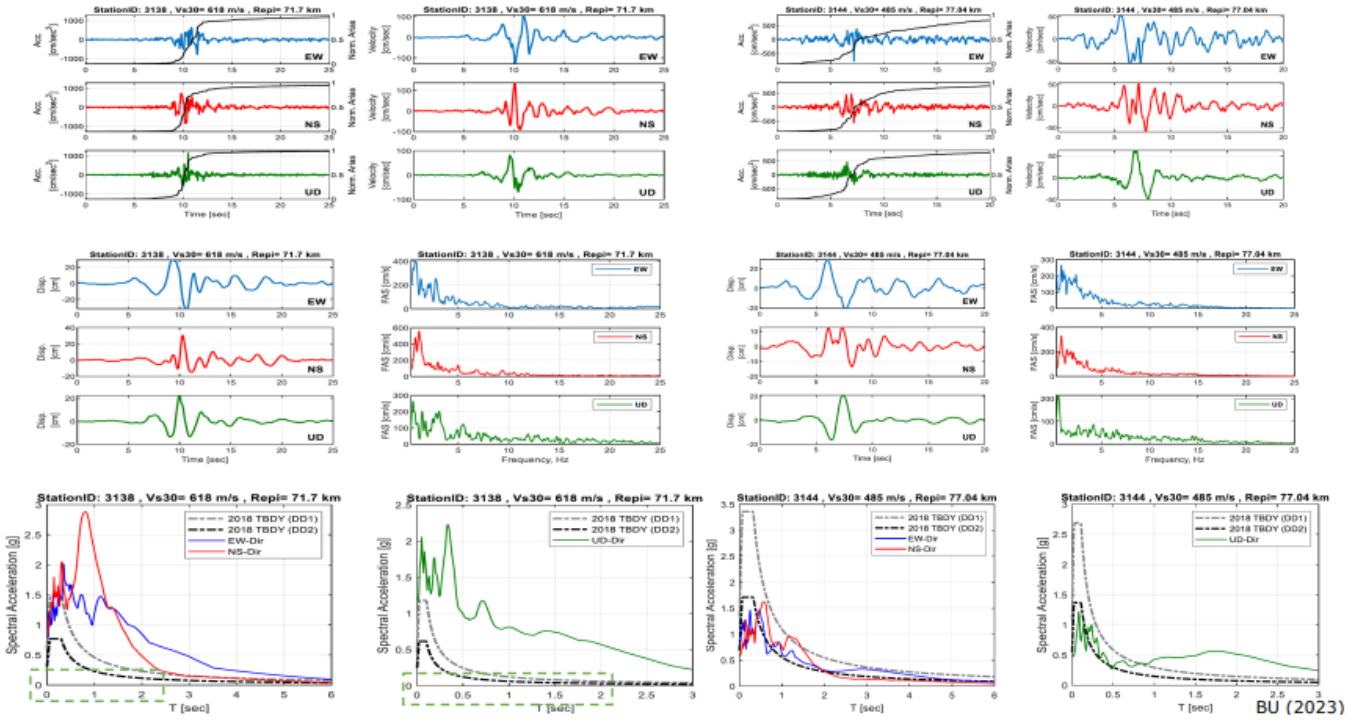
BU (2023)

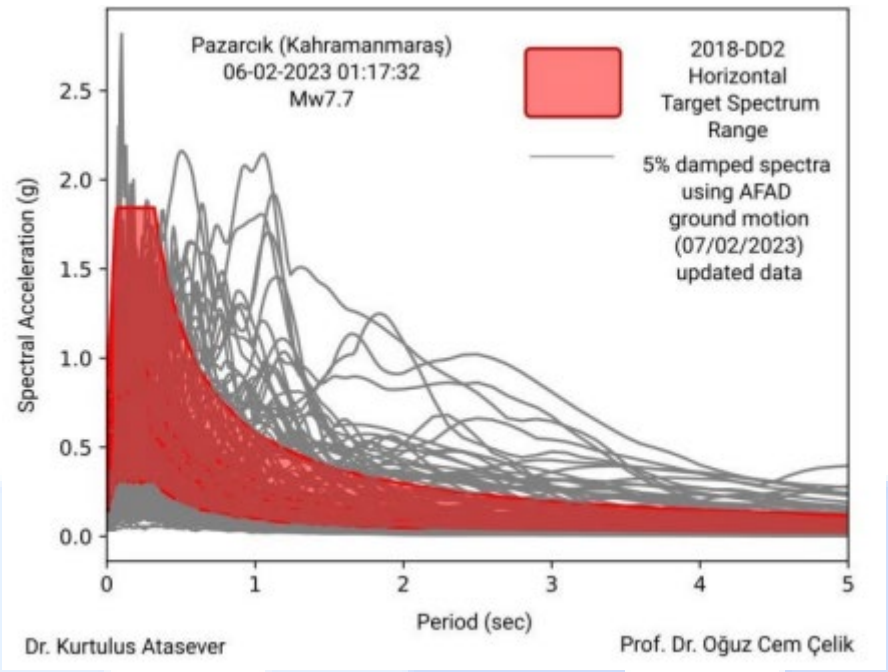

- Residential buildings are generally designed considering the 475-year return period (10% in 50 years) spectrum in TEC.
- Despite stations located on stiff soil conditions; the response spectra of the components show clear amplifications also in the longer periods with a particular peak around 1.2 seconds.
- The design response spectra for residential buildings (i.e. maximum design earthquake with a return period of 475 years) are exceeded for a wide period range, whereas the maximum credible earthquake level (return period of 2475 years) response spectra is generally exceeded for long periods especially in soft soils, in certain regions.
- This implies that in Gaziantep (İslahiye and Nurdağı districts), Hatay, Kahramanmaraş, and Adıyaman the buildings were subjected to seismic actions larger than Turkish Earthquake Code design levels.
- Earthquake demands were higher than the expected.

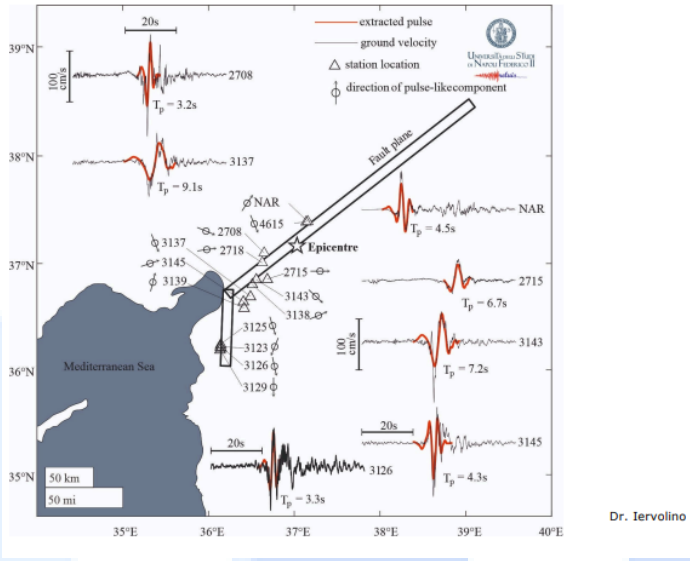

- Design PGA in fraction of g's corresponding to a 10% probability of exceedance in 50 years (475-year return period) in the affected region.
- The region near Kahramanmaras in Türkiye has a high seismicity with a PGA larger than 0.5g throughout the zone for a 475-year return period.

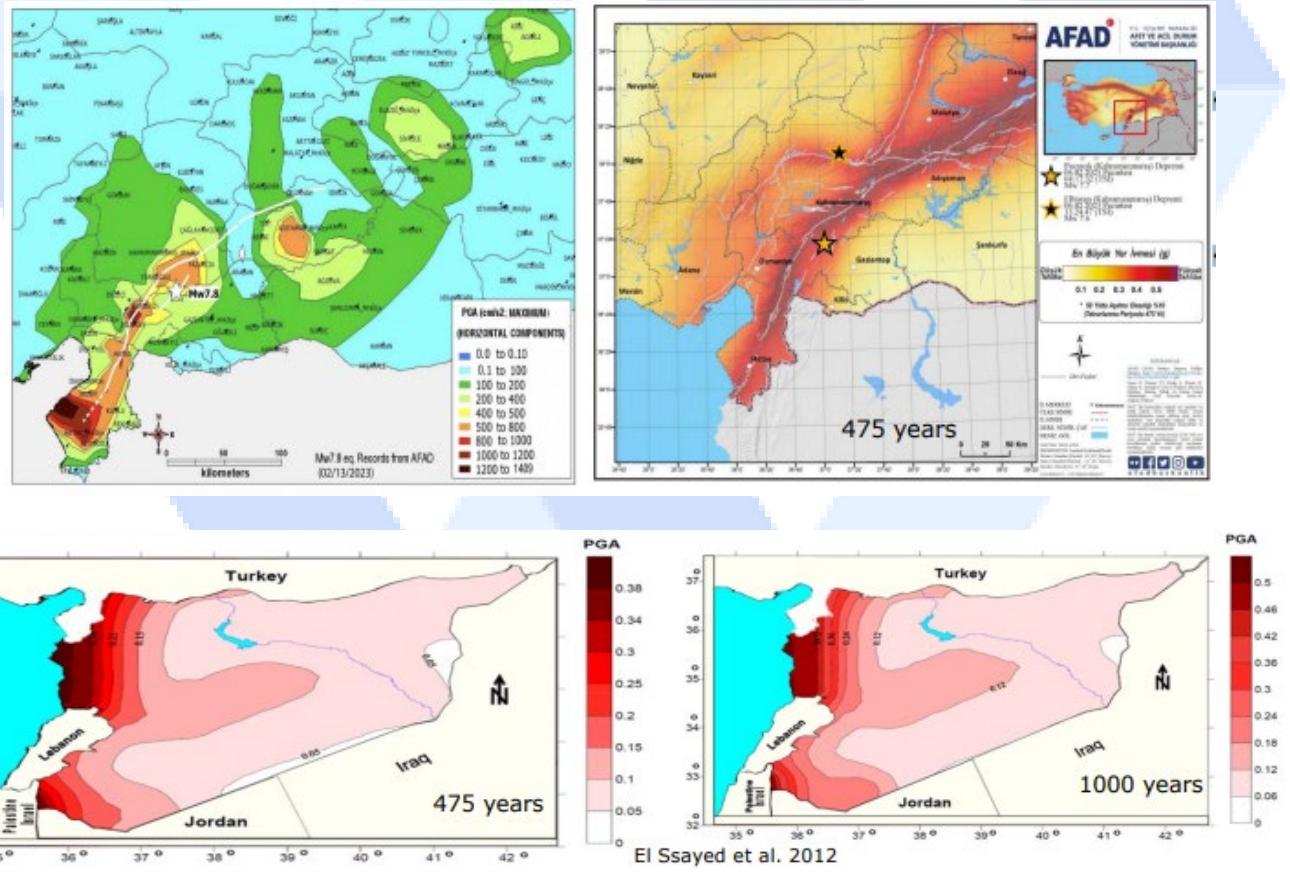

3.3. Liquefaction

- In the magnitude-7.7 earthquake, extensive liquefaction was observed at the shores of lakes in Gölbaşı (Adıyaman), in the İskenderun Port wharf area, Turkoğlu, and in Antakya near Asi River.

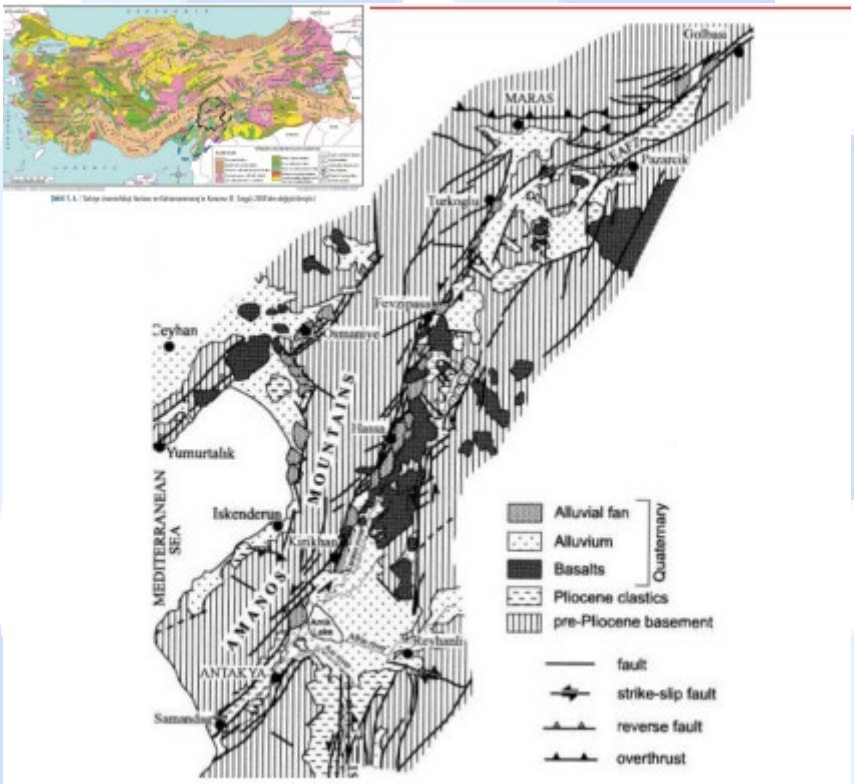

Regional geological map of the Karasu Rift. (simplified from 1:500000 by Rojay et al.2001)
DST: Dead Sea transform fault zone, EAFZ: East Anatolian fault zone.

Preliminary mapping of liquefaction phenomena triggered by the February 6 2023 M7.7 earthquake, Türkiye / Syria, based on remote sensing data

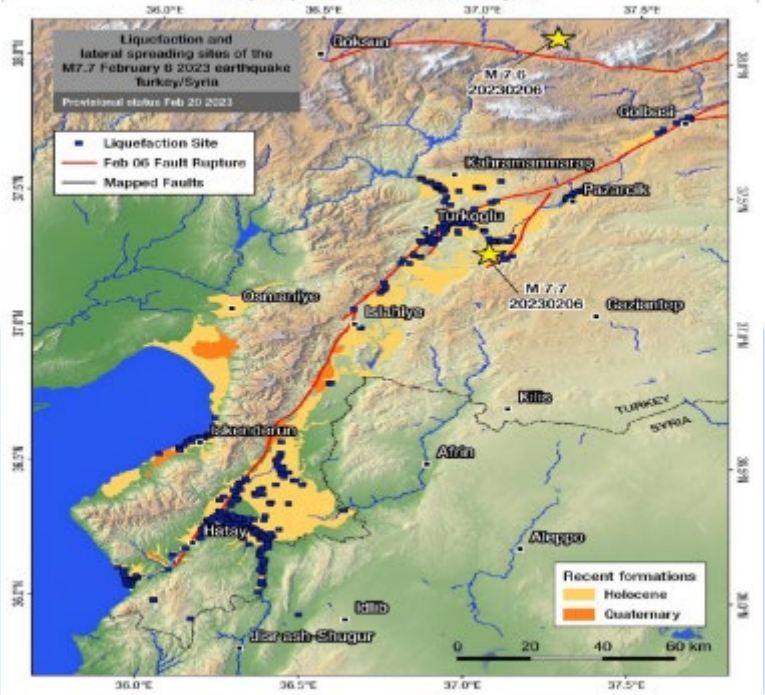

Overview map of liquefaction and lateral spreading sites identified and mapped using satellite imagery. Areas with major concentrations of liquefaction manifestations are Amik plain north of Hatay/Antakya, the extensive fluvial basins near to the M7.7 epicenter and the coastal plains of Hatay/Antakya and Iskenderun. Simplified geology from MTA (2002).

Newsletter of
Environmental, Disaster, and Crises Management Strategies
ISSN 2653-9454
Issue No. 29, February 2023 | 112

LIQUEFACTION PHENOMENA TRIGGERED BY THE 6 FEBRUARY 2023 EARTHQUAKES

Earthquake-triggered liquefaction phenomena and subsidence reported from the northeastern end of the Hatay city center. Source: https://twitter.com/geodesist_a/status/1624410147853414400

- Soil liquefaction occurs when a saturated or partially saturated soil lacking cohesion substantially loses strength and stiffness in response to earthquake ground motion.
- In other words, soil behaves like a liquid.
- Liquefaction that occurs beneath buildings and other structures can cause major damage leading to severely tilted buildings, ground subsidence and lateral flow of soil during strong earthquakes.

METU (2023)

https://www.haberturk.com/video/haber/izle/binalar-sivilasma-tehlikesi-ortadan-kaldirilmadan-projelendirilip-insa-edilmis/797131

- Soil conditions induced seismic demands caused heavily damage and collapse
- Insufficient foundations
- Overturning of buildings due to bearing-capacity failure on soft soil under strong seismic moment.
- In regions such as Hatay-Antakya and Adıyaman-Gölbaşı, buildings collapsed due to soil liquefaction, either by sinking into the ground or tilting to the side entirely or partially sinking into the liquefied ground obliquely depending on the characteristics of their foundation system.

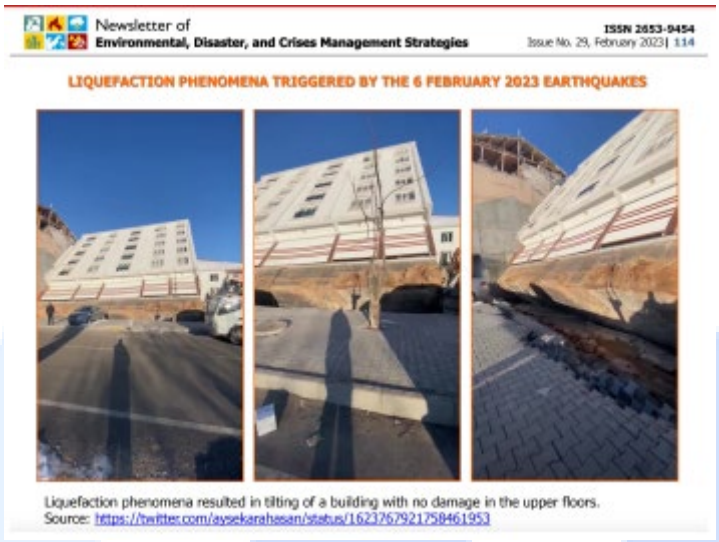

- RC Building with pile foundation - 1.5m settlement

- Liquefactioninduced bearing capacity failures

https://www.linkedin.com/search/results/content/?keywords=sıvılaşma&sid=VTR&update=urn%3Ali%3Afs_updateV2%3A(urn%3Ali%3Aactivity%3A7043298308118786048%2CBLENDED_SEARCH_FEED%2CEMPTY%2CDEFAULT%2Cfalse)

3.4. Performance of RC Structures

History of the Turkish Earthquake Codes:

- Zelzele Mıntıkalarında Yapılacak İnşaata Ait İtalyan Yapı Talimatnamesi (1940)
- Zelzele Mıntıkaları Muvakkat Yapı Talimatnamesi (1944)
- Türkiye Yersarsıntısı Bölgeleri Yapı Yönetmeliği (1949)
- Yersarsıntısı Bölgelerinde Yapılacak Yapılar Hakkında Yönetmelik (1953)
- Afet Bölgelerinde Yapılacak Yapılar Hakkında Yönetmelik (ABYYHY-1962)
- Afet Bölgelerinde Yapılacak Yapılar Hakkında Yönetmelik (ABYYHY-1968)
- Afet Bölgelerinde Yapılacak Yapılar Hakkında Yönetmelik (ABYYHY-1975)
- Afet Bölgelerinde Yapılacak Yapılar Hakkında Yönetmelik (ABYYHY-1998)
- Deprem Bölgelerinde Yapılacak Binalar Hakkında Yönetmelik (DBYBHY-2007)
- Turkish Earthquake Code (TEC-2018)
- Türkiye Earthquake Hazard Map (2018)
- New Code for Reinforced Concrete Design (2000)

Regulations:

- Natural Disaster Insurance Institution (DASK) (2000)
- Building Inspection Law (2001, 2011)

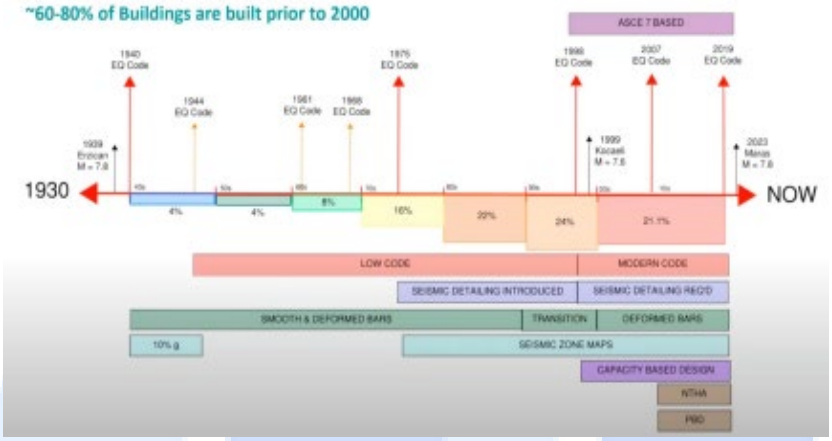

- The total population of the 11 provinces affected by the earthquake was recorded as 14,013 ,196 people for the year 2022. Additionally, there are 1,738,035 temporary residents under protection in the earthquake zone, who are migrants.

- The total number of buildings in the region is approximately 2. 6 million. Approximately 90 % of this building stock consists of residential buildings, 6% are commercial buildings, and 3% are public buildings. The number of houses (flat) in the 11 provinces affected by the earthquake was around 5. 6

- million as of the year 2022, and their share in the total housing stock in Turkey is 14 .05 %.

- The losses of the insurance sector and the income losses of small businesses along with macroeconomic effects, it is estimated that the total burden of the disaster caused by the earthquake on the Turkish economy is approximately 2 trillion TL (103.6 billion dollars). This magnitude is predicted to reach approximately 9 % of the 2023 gross domestic product.

Number of Total Buildings in Earthquake-Affected Provinces

Province	Resident	Workplace	Public	Other	Overall Total
Adana	404,502	29,920	8,916	7,779	451,117
Adıyaman	107,242	5,765	4,370	3,119	120,496
Diyarbakır	199,138	11,412	11,964	3,165	225,679
Elazığ	106,569	7,221	2,872	7,051	123,713
Gaziantep	269,212	22,829	5,480	8,162	305,683
Hatay	357,467	33,511	10,382	5,489	406,849
Kahramanmaraş	219,351	12,358	6,879	4,565	243,153
Kilis	33,399	1,526	1,651	736	37,312
Malatya	159,896	8,370	6,670	4,051	178,987
Osmaniye	128,163	9,428	3,105	2,384	143,080
Şanlıurfa	347,902	18,847	11,790	4,089	382,628
Total in 11 Provinces	2,332,841	161,187	74,079	50,590	2,618,697

Source: Spatial Population Registration System (SPRS)

- As of March 6, 2023, damage assessment studies have been conducted on 1 ,712 ,182 buildings in 11 provinces affected by the earthquake. Accordingly, 35 ,355 buildings have collapsed, 17 ,491 buildings need to be urgently demolished, and 179 ,786 buildings have been identified as having severe damage, 40 ,228 buildings have moderate damage, and 431 ,421 buildings have minor damage. Among the buildings that have collapsed or suffered major damage, there are also historical and cultural structures, schools, administrative buildings, hospitals, and hotels, in addition to residential buildings.

- Total number of residential buildings that fall under the categories of needing urgent demolition, collapsed, or heavily damaged is determined as 518 ,009. The number of moderately damaged residential buildings is estimated as 131 ,577, and the number of lightly damaged residential buildings is estimated as 1 ,279 ,727. Based on this data, a total of 2 ,273 ,551 people have directly faced housing problems after the earthquake. The ongoing effects of the earthquakes and the conditions in the earthquake region deepen the housing problem.

- Around half of the buildings in the affected regions of Türkiye were constructed before 2000, i. e., before modern principles of earthquake design were implemented in the Turkish Seismic Code.

- In Syria, more than 22 ,000 buildings were affected by the earthquakes, with 2 ,850 of them partially/completely collapsed or severely damaged.

- 86. 7 % of buildings in the earthquake zone are reinforced concrete, while 95. 4 % of apartments are reinforced concrete. 2. 4 % of the buildings are steel, 3. 5 % are load -bearing masonry, and 3. 6 % are prefabricated. The other category includes wood, mixed, or unidentified load -bearing systems, and the share of other load -bearing systems is quite low.

Number of Buildings Included in Damage Assessment (6 March 2023)

Status	Number of Buildings	Number of Detached Units
Undamaged	860,006	2,387,163
Lightly Damaged	431,421	1,615,817
Moderately Damaged	40,228	166,132
Severely Damaged	179,786	494,588
Collapsed	35,355	96,100
Requiring Urgent Demolition	17,491	60,728
Not Assessed	147,895	296,508
Total	1,712,182	5,117,036

Source: MoEUCC

Damage Control Report by Province (as of 06 March 2023)

	Total Number of Urgent + Severely Damaged + Collapsed Houses	Number of Moderately Damaged Houses	Number of Lightly Damaged Houses
Adana	2,952	11,768	71,072
Adıyaman	56,256	18,715	72,729
Diyarbakır	8,602	11,209	113,223
Elazığ	10,156	15,22	31,151
Gaziantep	29,155	20,251	236,497
Kahramanmaraş	99,326	17,887	161,137
Malatya	71,519	12,801	107,765
Hatay	215,255	25,957	189,317
Kilis	2,514	1,303	27,969
Osmaniye	16,111	4,122	69,466
Şanlıurfa	6,163	6,041	199,401
Total	518,009	131,577	1,279,727

Source: MoEUCC

Load-Bearing Systems of Buildings in Earthquake-Affected Region

(%)	Reinforced Concrete	Steel	Masonry	Prefabricated	Other
Building	86,7	2,4	3,5	3,6	3,9
Apartment	95,4	0,4	1,3	0,6	2,3

Source: Ministry of Interior, SPRS

Note: Data collected for buildings and apartments with a building permit.

SBB (2023)


İHA
PERBİR

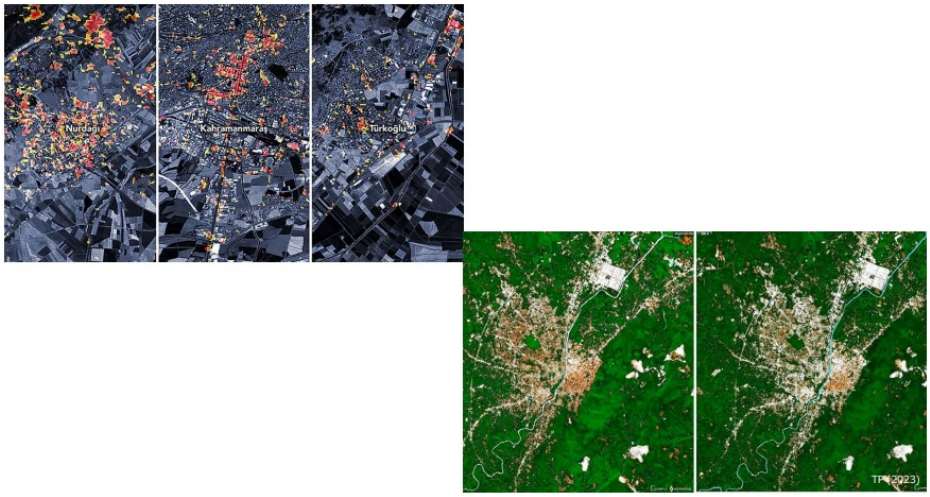
Nurdağı
Kahramanmaraş
Türkoğlu
TF (2023)

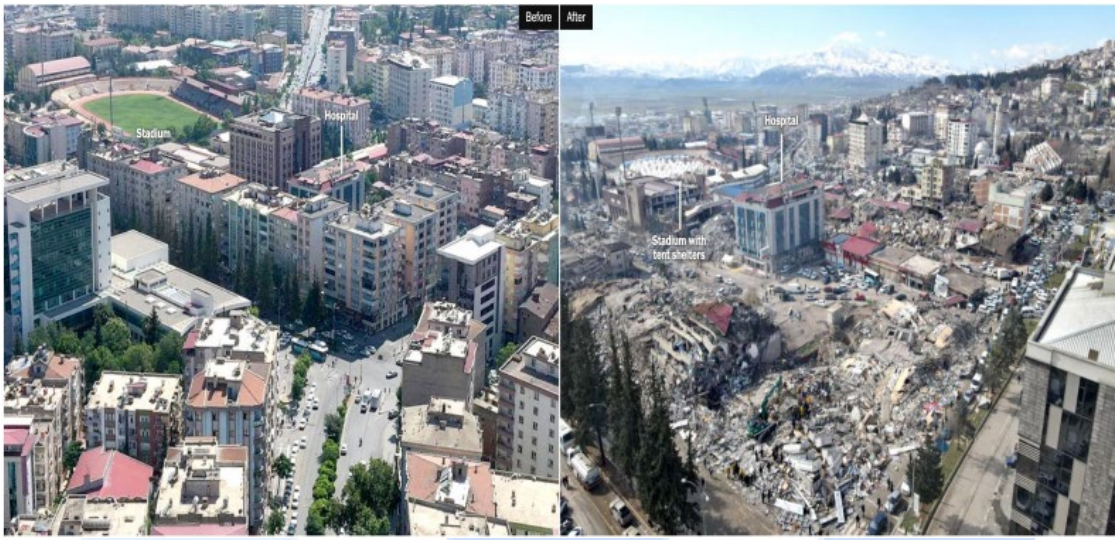
Before
After
Stadium
Hospital
Hospital
Stadium with tent shelters


TP (2023)


TP (2023)


The majority of the buildings in rubble have either completely or partially turned into a mechanism due to the collapse of their first floors, causing all floors above them to fall.
TP (2023)


The buildings were rubble.
TP (2023)

Similar types of damage were observed in many prior earthquakes throughout Turkey.

The rubble of 70% of the total 56,956 collapsed/urgently to be demolished buildings in the earthquake zone has been removed (April 13, 2023).

The rubble of 70% of the total 56,956 collapsed/urgently to be demolished buildings in the earthquake zone has been removed (April 13, 2023).

Some reasons for the extensive damages and collapses of a huge number of RC buildings:

- High seismic intensity ((large PGA, PGV, PGD and spectral values),
- Earthquake sequence (back-to-back effect),
- Near-fault effects, basin effect, soil amplification
- Shallow earthquakes (less than 10km),
- Long effective duration of the acceleration records,
- Proximity to the cities,
- Very long affected fault systems,
- Underestimation of seismic demands in design,
- Age of the buildings,
- Liquefaction,
- Low bearing capacity of the foundations,
- Low quality of the concrete and steel materials
- Insufficient geotechnical site investigations prior to building construction,
- Inadequacy of the cross-sectional dimensions,
- Reinforcement detailing errors on the columns, beams, shear walls and joints,

- Insufficient shear walls,
- Load bearing system elements were not constructed in accordance with the regulations,
- Insufficient engineering design due to the blind use of building design software,
- Different floor levels of the buildings,
- Slab without beams (using of flexible joist slabs (flat slab),
- The presence of soft story in the ground level (as a commercial story) or above was caused pancake-type collapse,
- First story high heights,
- Short column effects,
- Pounding (impact) effects,
- Cantilever effects,
- A significant part of the relevant damages occurred due to the fact that the connection between the load-bearing system elements and the concrete block bricks used as infill walls. They did not allow deformation during the earthquake.
- Buildings having periods around of 0.5-2s completely collapsed or heavily damaged,
- Lack of control in the design and construction phases

- The majority of collapses occurred within the outline of their floor plans.

- The extensive inelastic action at the critical joints in the RC buildings caused the formation of a hinge at the connection of columns with the beams, thereby creating mechanisms that led to pancake-type collapses, where the floors pile up on each other.

- When the buildings that collapsed or suffered severe damage in earthquakes in the last 30 years, including the earthquakes in Erzincan (1992), Dinar (1995), Ceyhan (1998), Gölcük and Düzce (1999), Afyon and Bingöl (2002), Elazığ (2010 and 2020), Van (2011), and İzmir (2020), are examined, it is seen that there are similar damages.

- Some buildings patly collapsed.

- The collapse of one building among neighboring parcels and buildings with similar sizes, while the other remains standing, could be due to some of the irregularities in one but not the other.

- It should also be considered that there may be differences in ground conditions (thickness of alluvium on the main rock), material and workmanship quality between parcels.


TP (2023)


• The lengths of the column rebars that form the upper floor are found to be shorter than required.


A soft-story is a floor that is structurally significantly more flexible and weaker than the others


The presence of a soft story increases deformation demands very significantly, and puts the entire burden of energy dissipation on the first story structural elements, as opposed to distributing the burden along the entire height of the building.

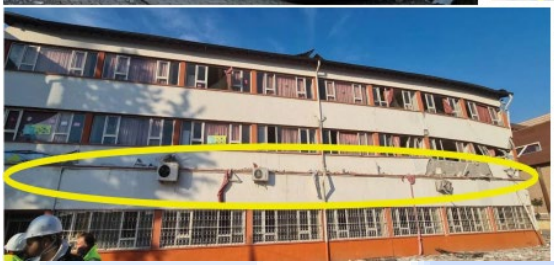


TP (2023)

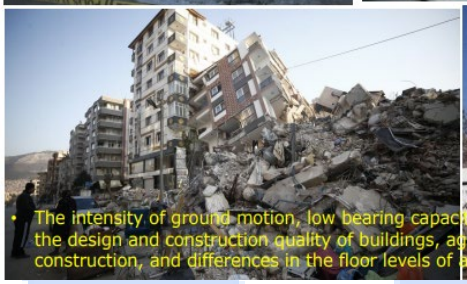


• The intensity of ground motion, low bearing capacities of the soils on which foundations are placed, deficiencies in the design and construction quality of buildings, age of buildings, non-compliance with regulations in their construction, and differences in the floor levels of adjacent buildings (impact effect).
TP (2023)

TP (2023)



- Insufficeint shear walls, even in >10 story buildings


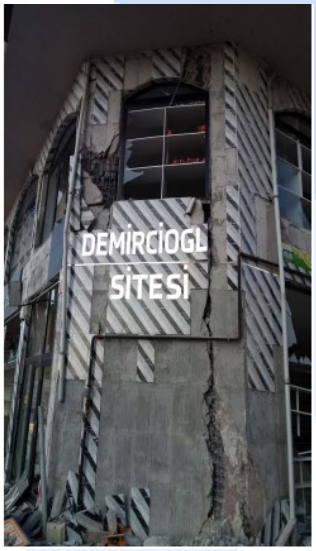


Lack of column confinement and poor detailing
Inadequate steel reinforcement (in size and number of longitudinal bars)
A good "workmanship" is much more valuable than the "theoretical modeling".
TP (2023)


Classical failure of columns and shear walls due to several reasons: poor quality of concrete, columnties not having 135 degree hooks and having large spacing, etc.
TP(2023)

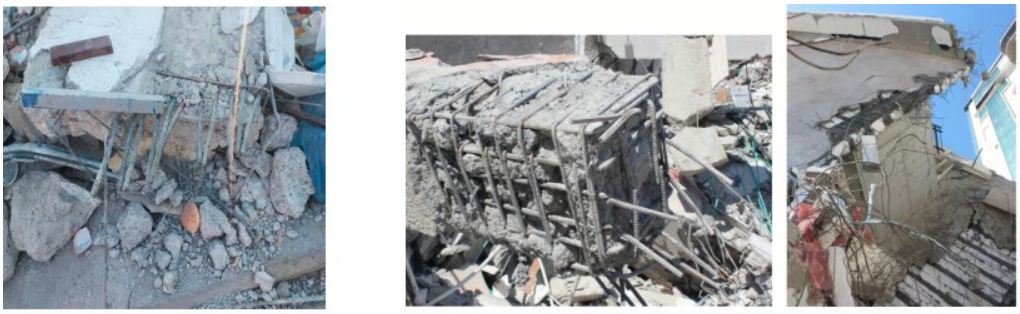

Typical deficiencies of the frame buildings constructed before 2000 were the use of plain reinforcing bars, insufficient steel reinforcement detailing and possibly low concrete strength resulting in heavy damage and collapse

TP (2023)

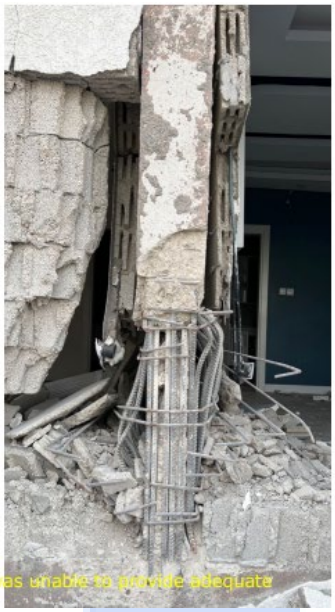

- Necessary reinforcement details were not applied in column-beam connections in collapsing buildings, and that the spacing of stirrups is sparse and stirrup hooks are at right angles.

- Many buildings have experienced beam-column joint failures.

L-shaped central column failure from the ground story of a framed building.

https://www.linkedin.com/in/oğuz-cem-çelik-oguz-c-celik-54082022/recent-activity/

Residual story drift

https://www.linkedin.com/feed/update/urn:li:activity:7048162998208610304/

- Low concrete quality and strength. There is a serious weakness in the materials used in both old and new reinforced concrete structures.
- Steel bars smooth instead of ridged.
- Some ridged rebars coming from abroad were fractured.
- Especially for buildings constructed before 2001 when ready-mixed concrete was not yet widely used.

- One of the most important non-structural damage in the region was observed in the infill walls.
- The infill walls were severely damaged and failed under combined in and out of plane effects.
- The damage was similar in all the infill walls made of hollow clay brick, autoclaved aerated concrete or bims blocks, indicating that none of the block materials showed good seismic performance.





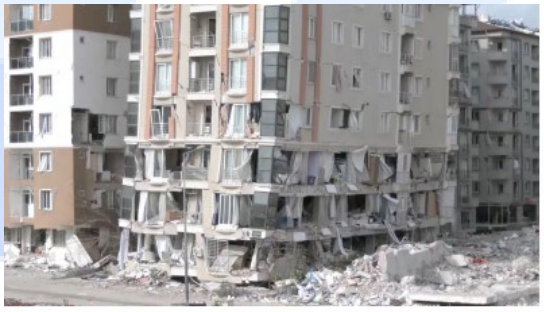



During the Mw 7.8 and Mw 7.5 earthquake sequence, damage to stairs and stairwells collapse were reported. The residents of these buildings were not able to evacuate the building due to the collapse of stairwells.
TP (2023)


Antakya


T24
HAFTALIK
T24
DEPREM BÖLGESİNDE

- Fallen panels from the ceiling and blocked corridor, indicating loss of functionality and giving evidence of the significant interior damage that can occur even if the exterior looks undamaged (EERI (2023)

Nurdağ Devlet Hastanesi

- Renaissance Residence was a residential building in Ekinci, Antakya, that fell over in February of 2023 during the first earthquake.
- The building is 12 floors high and has a total 249 homes, 2 shops. The building is divided into 4 blocks. The area that the building takes up on the ground is 10,500 square meters (113,000 sq ft).
- The building was built between 2011 and 2012.
- At least 800 people died.


Rönesans Residence - Hatay


Rönesans Residence - Hatay


Rönesans Residence - Hatay

Rönesans Residence – Hatay

Potential reasons for this failure: (1) Inadequate foundation or, (2) Initiation of the collapse of the structure from one side (sidesway collapse), resulting in the toppling of the structure. The sidesway collapse occurs due to lateral dynamic instability at large lateral displacements, when the lateral strength of the structure degrades significantly (EERI (2023).

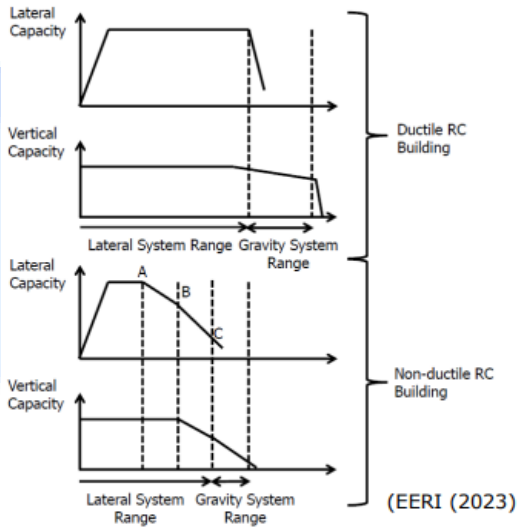

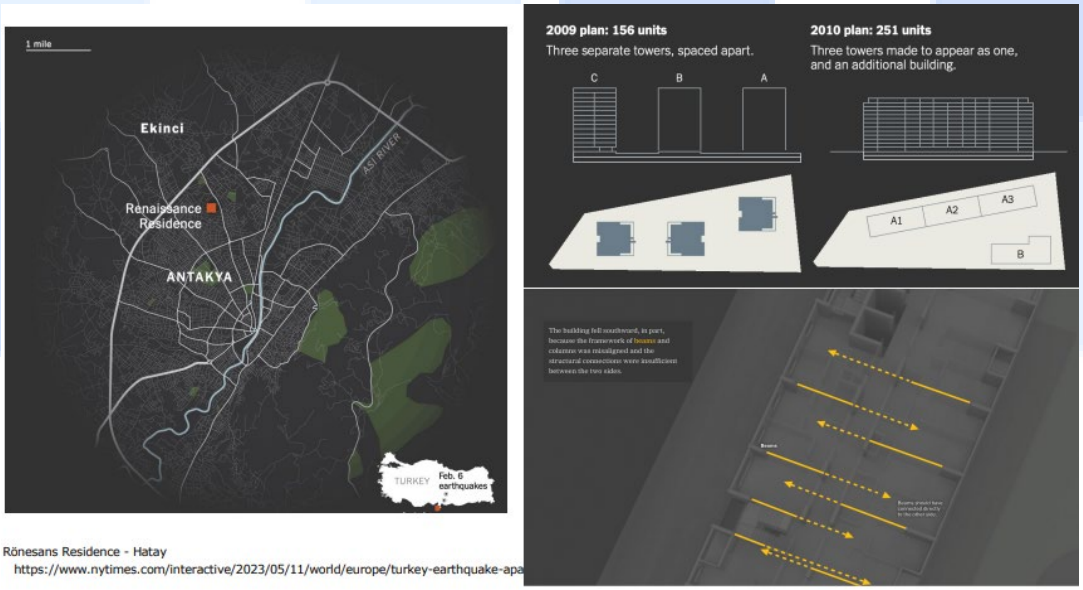

Rönesans Residence - Hatay
https://www.nytimes.com/interactive/2023/05/11/world/europe/turkey-earthquake-apa

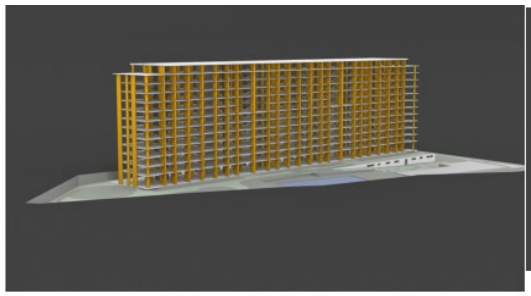

Rönesans Residence - Hatay
https://www.nytimes.com/interactive/2023/05/11/world/europe/turkey-earthquake-apartment-building-collapse.html

Rönesans Residence - Hatay
https://www.nytimes.com/interactive/2023/05/11/world/europe/turkey-earthquake-apartment-building-collapse.html

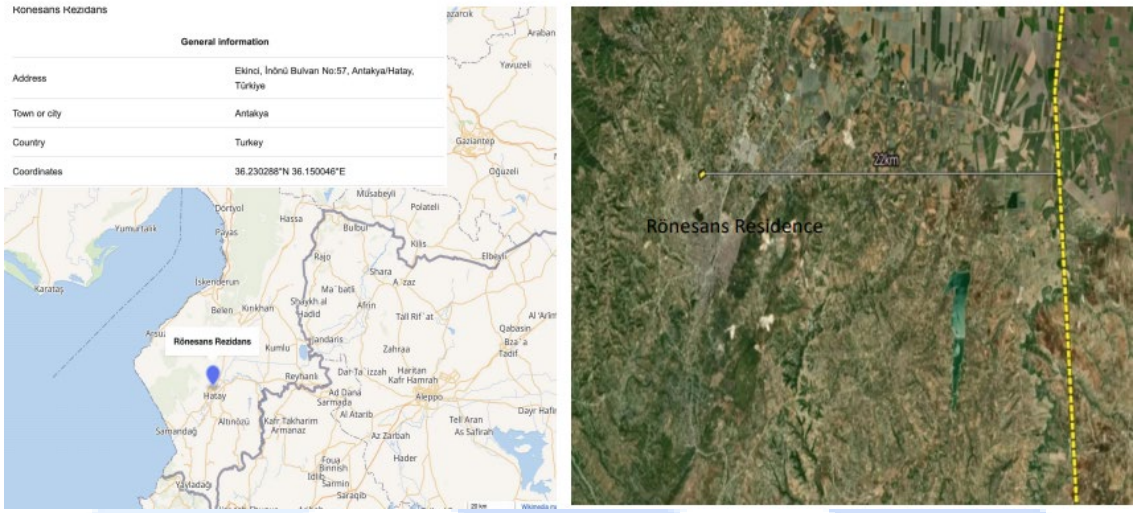
Rönesans Rezidans
General information
Address
Ekinci, İnönü Bulvarı No:57, Antakya/Hatay, Türkiye
Town or city
Antakya
Country
Turkey
Coordinates
36.230288°N 36.150046°E
Rönesans Residence
22km

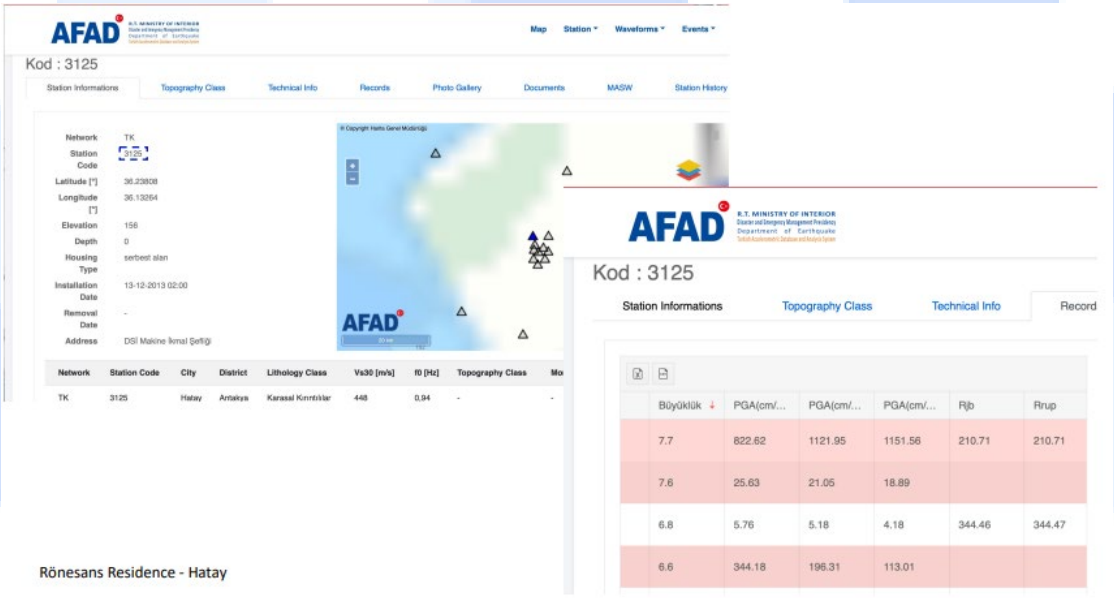
AFAD
Kod : 3125
Station Informations
Topography Class
Technical Info
Records
Photo Gallery
Documents
MASW
Station History
Network
Station Code
Latitude [°]
Longitude [°]
Elevation
Depth
Housing Type
Installation Date
Removal Date
Address
Rönesans Residence - Hatay
Kod : 3125
Station Informations
Topography Class
Technical Info
Record
Büyüklük
PGA(cm/...
Rjb
Rrup

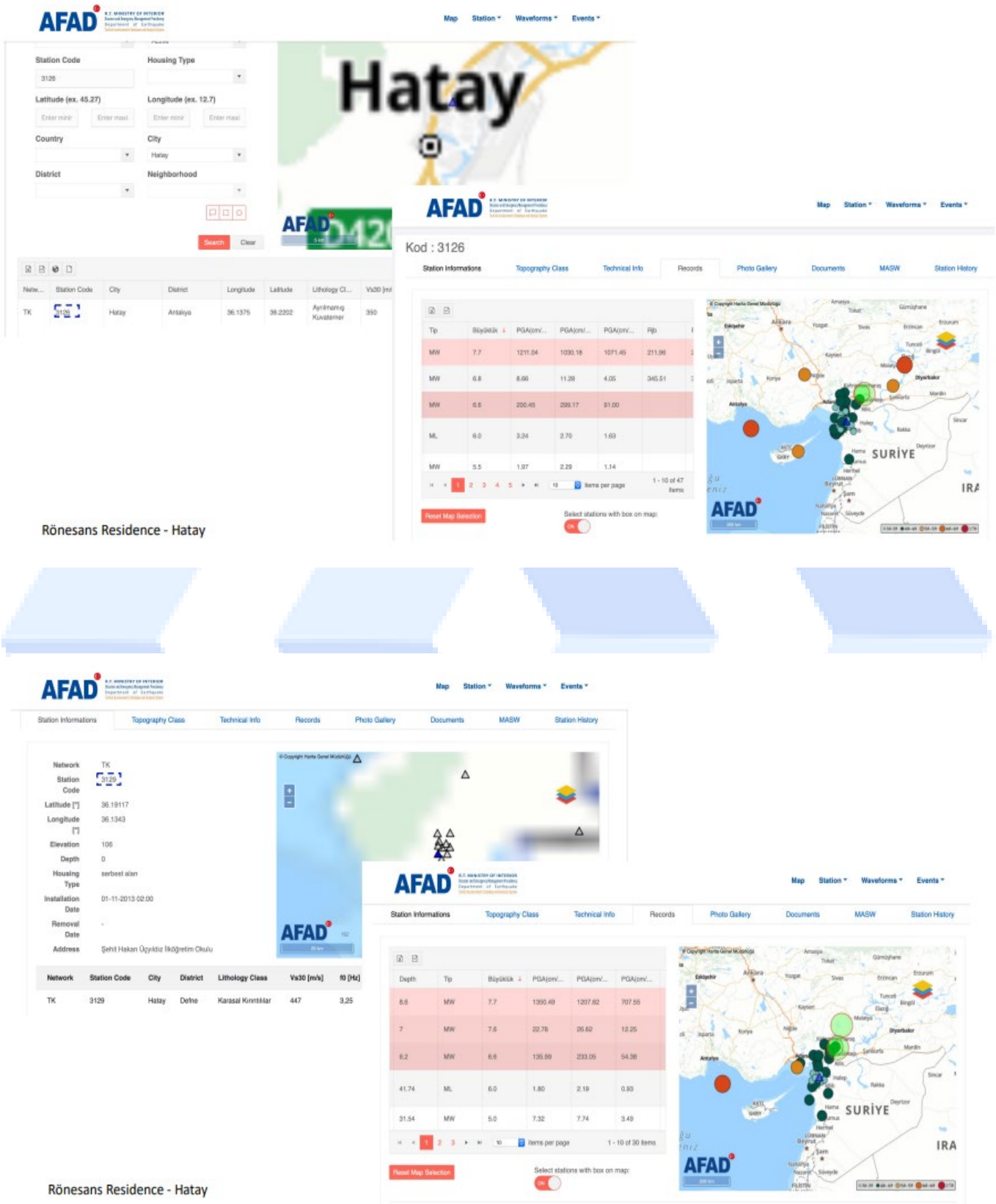
AFAD
Map
Station
Waveforms
Events
Station Code
Housing Type
Latitude (ex. 45.27)
Longitude (ex. 12.7)
Country
City
District
Neighborhood
Search
Clear
Hatay
Kod : 3126
Station Informations
Topography Class
Technical Info
Records
Photo Gallery
Documents
MASW
Station History
Reset Map Selection
Select stations with box on map:
SURİYE
Rönesans Residence - Hatay
Network
Station Code
Latitude [°]
Longitude [°]
Elevation
Depth
Housing Type
Installation Date
Removal Date
Address
Şehit Hakan Üçyıldız İlköğretim Okulu
Lithology Class
Vs30 [m/s]
f0 [Hz]
Karasal Kırıntılılar
447
3,25

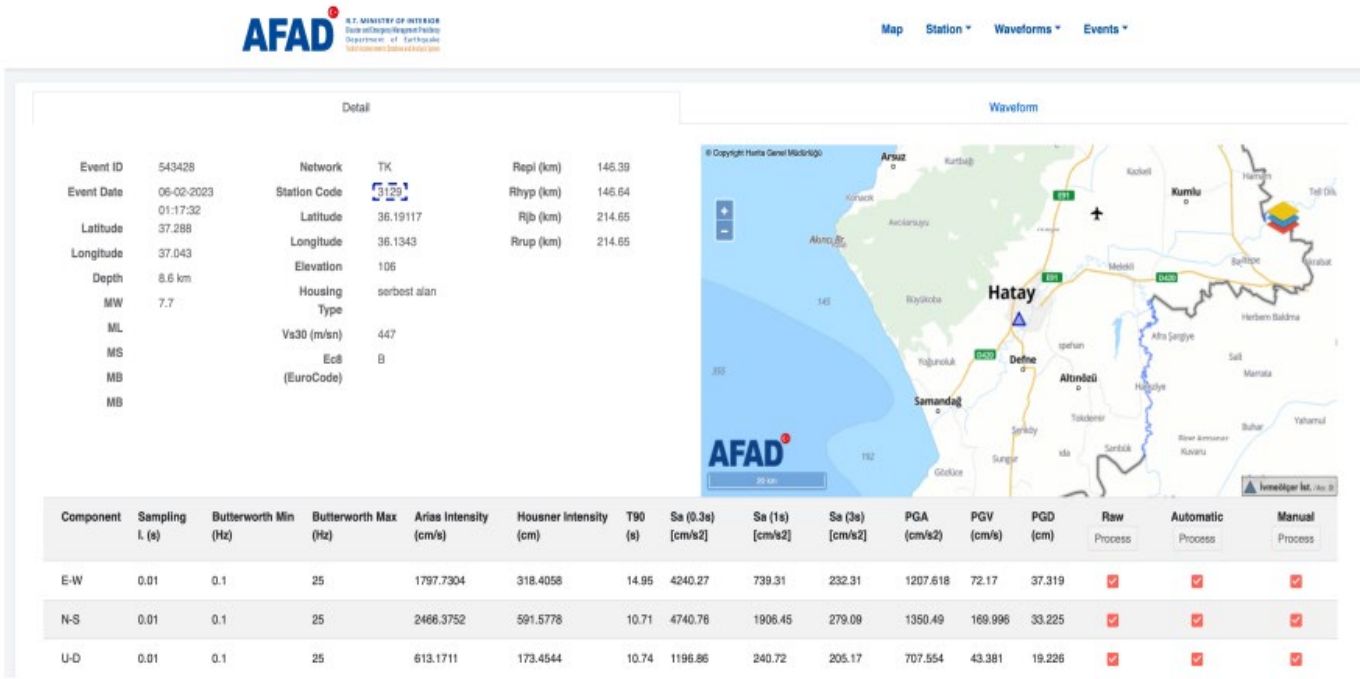

Component	Sampling I. (s)	Butterworth Min (Hz)	Butterworth Max (Hz)	Arias Intensity (cm/s)	Housner Intensity (cm)	T90 (s)	Sa (0.3s) [cm/s2]	Sa (1s) [cm/s2]	Sa (3s) [cm/s2]	PGA (cm/s2)	PGV (cm/s)	PGD (cm)	Raw Process	Automatic Process	Manual Process
E-W	0.01	0.1	25	1797.7304	318.4058	14.95	4240.27	739.31	232.31	1207.618	72.17	37.319	☑	☑	☑
N-S	0.01	0.1	25	2466.3752	591.5778	10.71	4740.76	1906.45	279.09	1350.49	169.996	33.225	☑	☑	☑
U-D	0.01	0.1	25	613.1711	173.4544	10.74	1196.86	240.72	205.17	707.554	43.381	19.226	☑	☑	☑

Rönesans Residence - Hatay

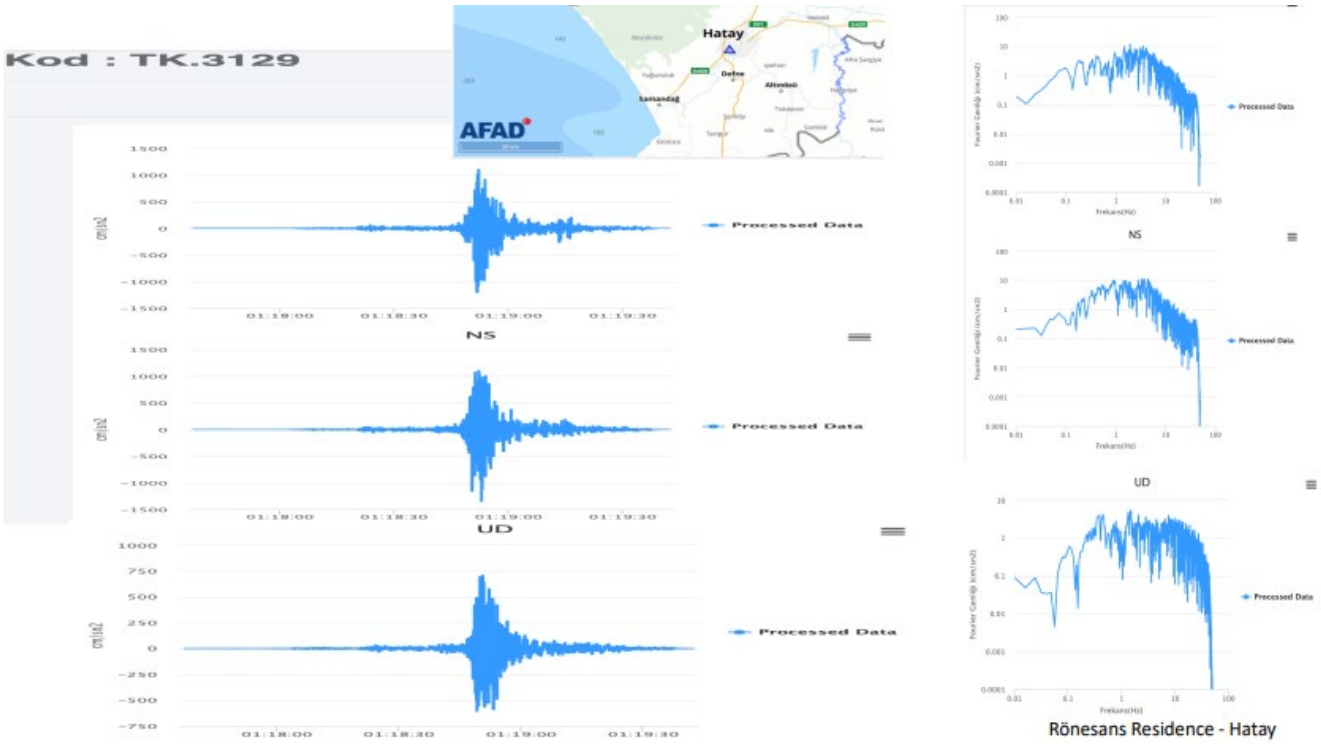

- Tunnel form buildings in the region performed in an outstanding manner with some damage in the coupling beams and infill walls due to the following key reasons: i) the use of more shear wall area more than usually 2.5% of the floor area, ii) siting at stiff soil or rock sites, iii) mid-rise construction ranging from (4 to 8 stories).

- This performance provided further confidence in the use of significant shear wall area for the buildings constructed in high seismic zones.

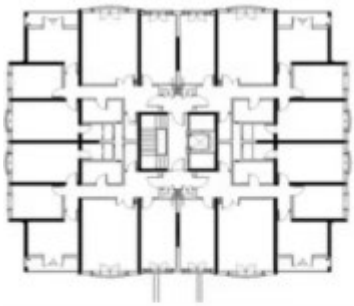

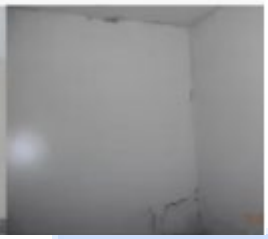


RC Tunnel Form

- The strengthened buildings with the addition of shear walls, fiber reinforced polymers collapsed while some damage was observed.


- All base-isolated hospitals were operational after the earthquake sequence.

- The intensity of the ground motion, the structural system, design, and construction quality were decisive in the building performance.

3.5. Performance of Precast Structures

- Many older prefabricated buildings have experienced significant damages or some partially or totally collapsed from many reasons: mainly from weak connection and detailing, insufficient diaphragm effect.

3.6. Performance of Steel Structures

- The 11 provinces in the earthquake zone have a rich cultural texture in terms of cultural structures, civil architecture examples, ruins, monuments, martyrs' memorials, and preserved streets.
- There are approximately 8,500 works in the cultural heritage category in the region.
- As of February 25, 2023, examinations have been conducted for 2,863 out of 8,444 artifacts in the cultural heritage category.
- It has been determined that 169 of these structures have collapsed, 535 have suffered heavy damage, 390 have suffered moderate damage, 721 have suffered minor damage, and 1,048 have not been damaged.

Cultural Assets in Earthquake-Affected Provinces

Provinces	Streets Under Protection	Monuments	Administrative Buildings	Cultural Structures	Martyrs Cemeteries	Military Structures	Industrial and Commercial Structures	Religious Structures	Cemeteries	Civil Architecture	Ruins	Total in Province
Adana	3	1	54	143	5	39	85	75	56	320	95	876
Adıyaman	-	2	2	46	-	6	7	54	14	8	25	164
Diyarbakır	-	-	70	261	3	11	4	153	90	606	22	1,220
Elazığ	-	1	36	89	1	5	-	72	22	80	9	315
Gaziantep	-	4	36	95	-	6	22	77	36	797	8	1,081
Hatay	2	3	50	144	3	16	53	114	85	576	62	1,108
Kahramanmaraş	-	9	5	58	1	25	41	46	32	327	17	561
Kilis	-	2	5	28	-	5	13	35	4	356	4	452
Malatya	-	4	23	119	2	5	14	99	35	454	10	765
Osmaniye	-	1	13	24	3	8	1	19	25	45	26	165
Şanlıurfa	14	1	26	155	2	7	13	120	74	1301	24	1,737
Total	19	28	320	1.162	20	133	253	864	473	4.870	302	8,444

3.7. Performance of Masonry Structures

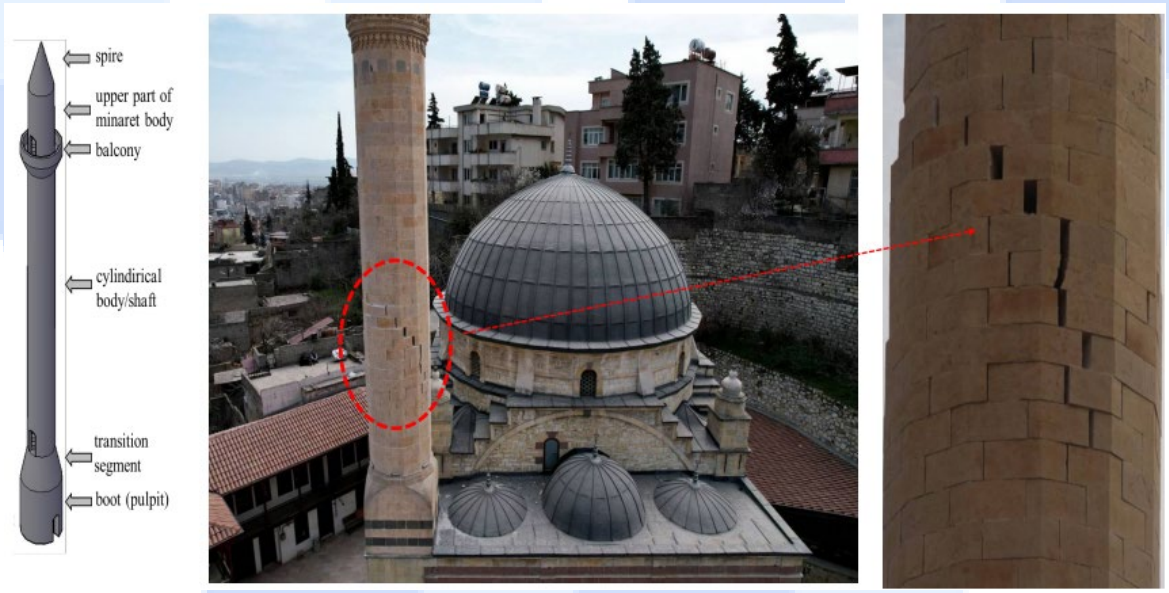

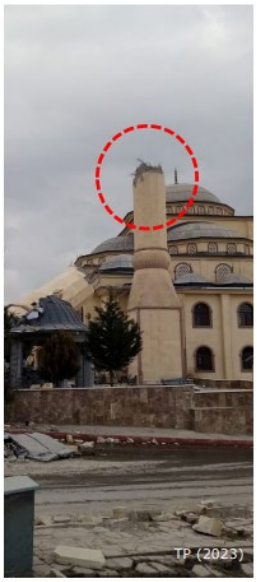

- Karakuş Tümülüs Handshake Pillar in Adıyaman, Türkiye, 2,000- year-old and height of 10m.

TP (2023)

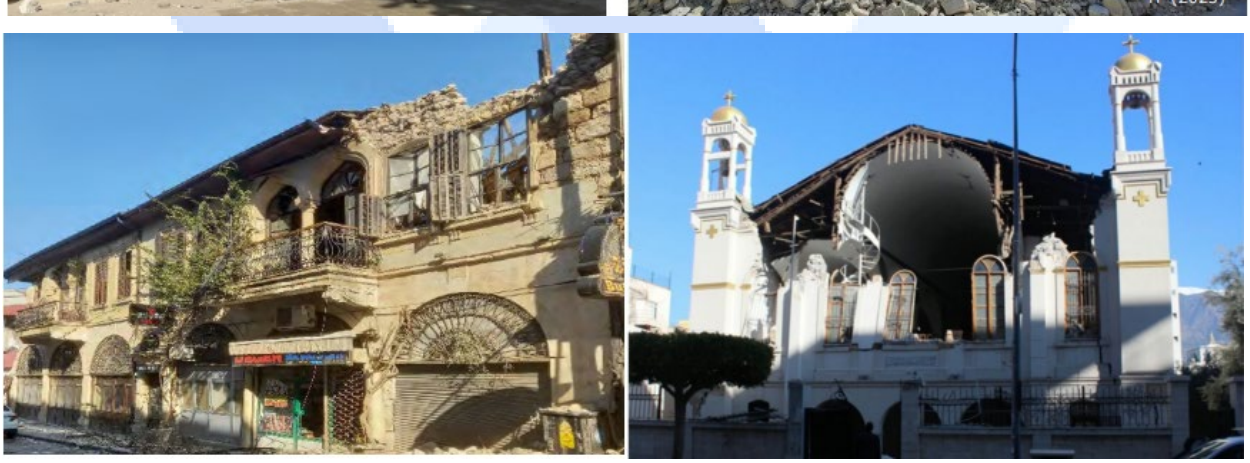






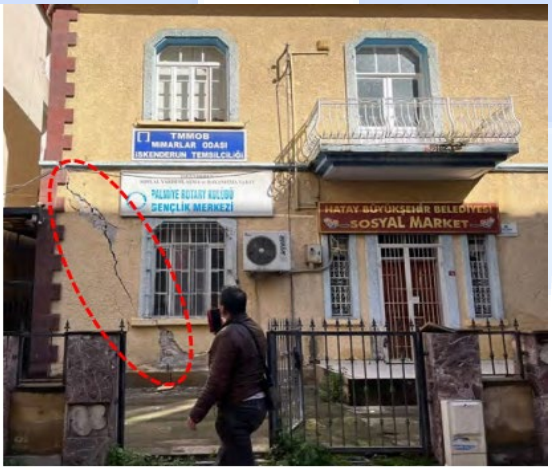
TMMOB
MİMARLAR ODASI
PALMİYE ROTARY KULÜBÜ
GENÇLİK MERKEZİ
HATAY BÜYÜKŞEHİR BELEDİYESİ
SOSYAL MARKET





TP (2023)

3.8. Performance of Electricity Transmission and Pipeline Systems

- Significant damages have occurred to the electricity distribution lines and transformer centers, and water and sanitation systems in the region, particularly in Hatay, Gaziantep, Kahramanmaraş, and Adıyaman.
- 11 poles connecting a 1,128 km long electricity transmission line have collapsed.
- There has been damage to the transformer center and equipment, which has a total power of 4,088 MVA.
- There have been approximately 20 explosions and malfunctions in the natural gas transmission lines at around 20 different points.

Water and Sanitation Damage Status

Item	Unit	Quantity	Cost* (TRY)	Data Source
Potable Water Supply Line	km	169	1,595,000,000	DSI
Water Treatment Plant	m^3/day	135,000	25,000,000	DSI
Water Reservoirs	m^3	10,000	50,000,000	DSI
Potable Water Supply Line	km	185	2,119,000,000	ILBANK
Water Treatment Plant	piece	2	1,765,000,000	ILBANK
Water Reservoirs	piece	23	112,900,000	ILBANK
Potable Water Network	km	488	1,405,000,000	ILBANK
Sewer Network	km	1,842	6,262,000,000	ILBANK
Wastewater Treatment Plant	piece	7	1,595,000,000	ILBANK
Pumping Station	piece	5	51,000,000	ILBANK
Potable Water Network	km	241	29,000,000	SPA
Catchment Construction	piece	5	800,000	SPA
Water Tank	piece	22	71,000,000	SPA
Total			15,080,700,000	

* Calculated based on repair/replacement needs for damaged parts and potential equipment needs. Approximate costs were estimated by using unit prices and past tender data. An average cost was not included, as each infrastructure involves different unit costs.

3.9. Performance of Dams

- There are 142 hydroelectric power plants (HPP) in the region.
- 19 percent of the total number of dams and 39 percent of the hydraulic installed capacity in Turkey are located in the disaster area.
- There are also 45 MW licensed solar power plant, 924 MW wind power plant, and biomass and waste heat power plants with a total installed capacity of 224 MW in the earthquake zone.
- In the region, there are large dams with large storage capacity such as Atatürk Dam, Karakaya, Keban, Kartalkaya Dam, and Büyükkaraçay Dam.
- Dam heights in the region change from 19m to 201m.
- Construction years of the dams change from 1970 to 2021.
- Proximity of dams to epicenter is from approximately 15km to 200km.
- Different level of damages took place in 14 dams.
- The estimated damage amount for the 14 dams is 2.7 billion Turkish liras (141.8 million dollars).

Status of Major Dams that Sustained Damage in Earthquake-Affected Region

Name of Storage Facility	Body Volume (m3)	Status of Damage	Estimated Cost of Damage (TRY)*
Hatay-Reyhanlı Dam	20,730,055	Moderately Damaged (may continue operations only after reinforcement)	750,000,000
Malatya-Sultansuyu Dam	3,205,000	Severely Damaged (must be reconstructed)	705,000,000
Osmaniye-Bahçe Ariklikaş Pond	615,000	Severely Damaged (must be reconstructed)	260,000,000
Kahramanmaraş-Kartalkaya Dam	1,452,000	Moderately Damaged (may continue operations only after reinforcement)	250,000,000
Malatya-Erkenek Pond	370,000	Moderately Damaged (may continue operations only after reinforcement)	250,000,000
Malatya-Sürgü Dam	1,220,000	Moderately Damaged (may continue operations only after reinforcement)	100,000,000
Hatay-Yarseli Dam	3,000,000	Lightly Damaged (may continue operations after minor repair)	100,000,000
Hatay-Büyükkaraçay Dam	2,500,000	Lightly Damaged (may continue operations after minor repair)	50,000,000
Hatay-Hassa Demrek Pond	358,325	Lightly Damaged (may continue operations after minor repair)	45,000,000
Osmaniye-Kalecik Dam	843,000	Lightly Damaged (may continue operations after minor repair)	40,000,000
Hatay-Samandağ Karamanlı Pond	359,000	Lightly Damaged (may continue operations after minor repair)	40,000,000
Malatya-Çat Dam	2,500,000	Lightly Damaged (may continue operations after minor repair)	35,000,000
Hatay-Kırıkhan Kurtlusoğuksu Pond	362,872	Lightly Damaged (may continue operations after minor repair)	30,000,000
Gaziantep-Nurdağı Hamidiye Pond	150,000	Lightly Damaged (may continue operations after minor repair)	20,000,000
TOTAL			2,675,000,000

* While damage assessment on facilities continues, the damage has been determined holistically and as an estimate as it is not possible to feed water to the channels due to seasonal conditions.

- Kartalkaya Dam with height of 57m is a rock fill dam constructed in 1972 in Pazarcik-Kahramanmaraş.
- Distance from the Mw7.7 epicenters is 38km.
- Serious cracks occurred along the dam crest.

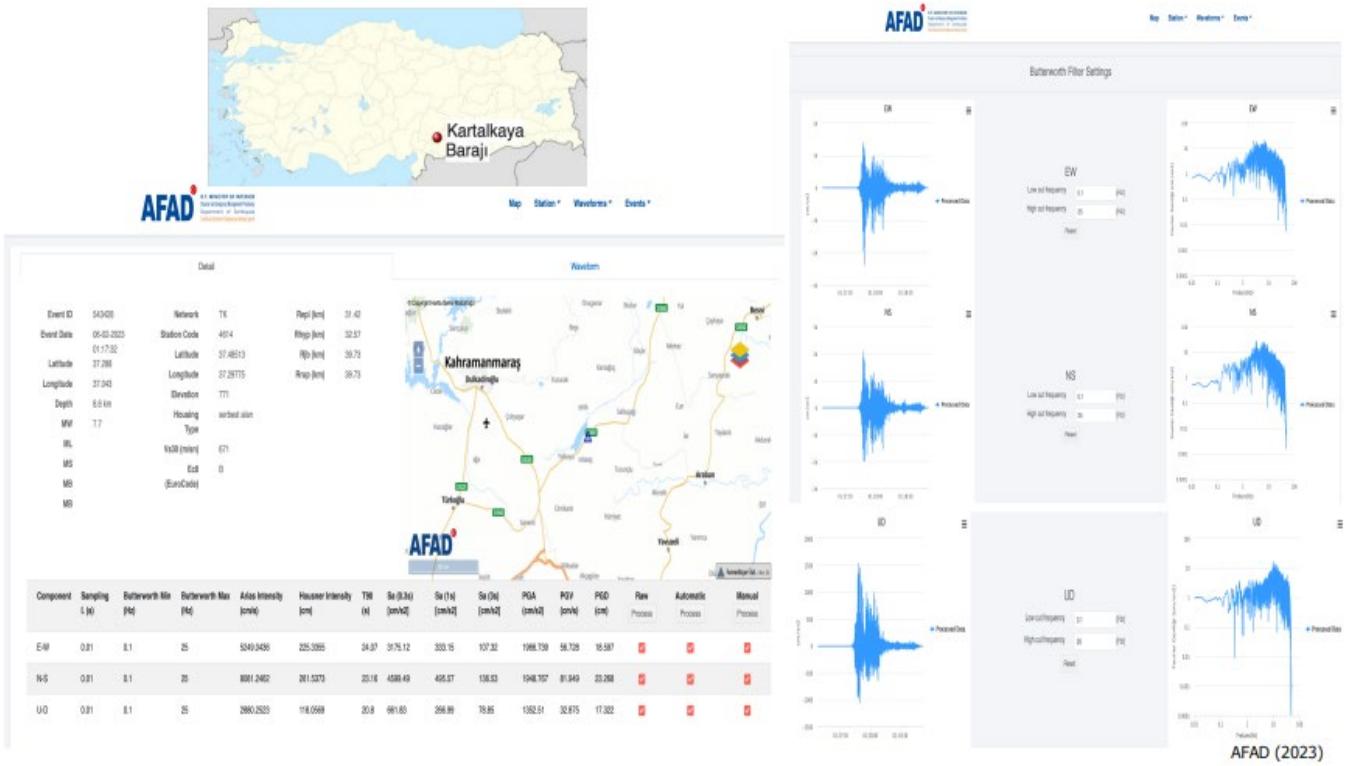
Kartalkaya
Baraji
AFAD
Map
Station *
Waveforms *
Events *
Detail
Waveform
Kahramanmaraş
Butterworth Filter Settings
EW
NS
UD
AFAD (2023)

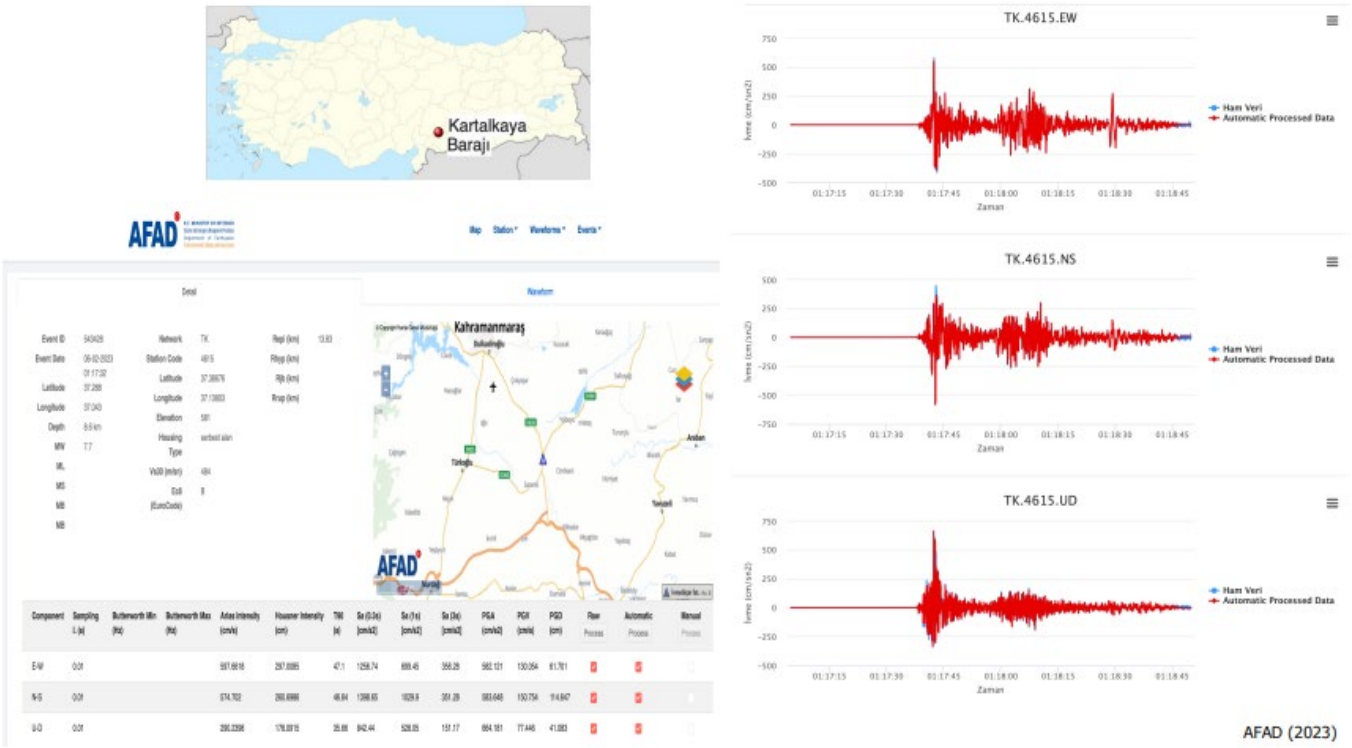

- Sultansuyu Dam is a embankment dam constructed in Malatya in 1992. The height 60 m (from talveg) and crest length 721m.
- Distance from M7.7 from 156km, from M7.6 70km.

- It is 8.8 km away from Malatya Fault Zone- Akçadağ segment. There is no other dam under the influence of near source (closer than 10 km to the active fault zone).
- Serious cracks occurred along the crest and upstream face of the dam
- The reservoir was discharged after the earthquake.

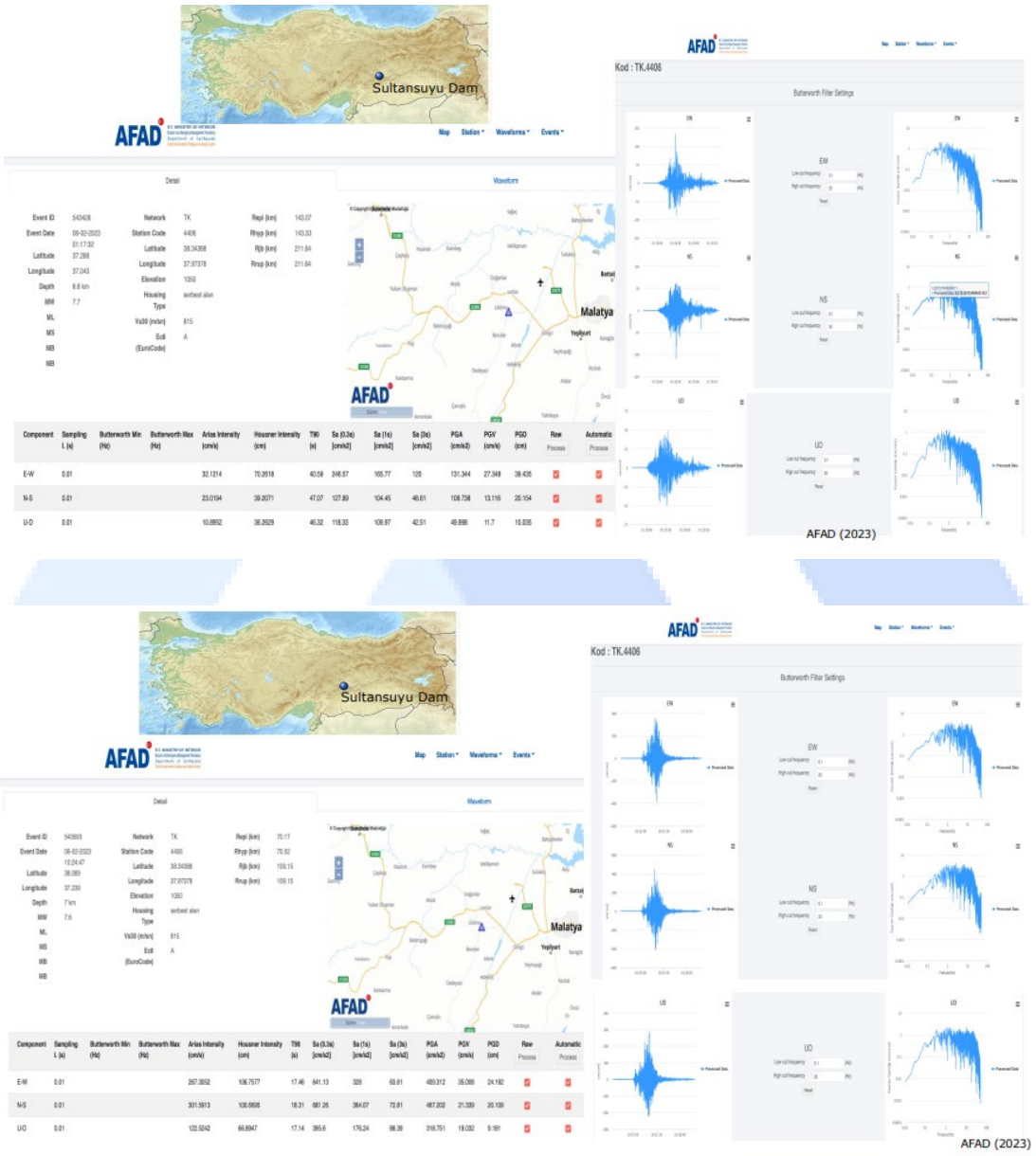

- Arıklıkaş pond with height of 33m is a rock fill dam constructed in 1998 in Bahçe-Osmaniye.
- Serious cracks occurred along the dam crest and upstream face.

- Malatya Sürgü Dam with height of 55m is an embankment dam constructed in 1969 in Malatya.

- Cracks occurred along the dam crest due to Mw 7.6.

- Maydanki (Afrin) Dam (in Syria) is an embankment dam, and it is 73 m high, with a crest length of 983 m.
- It is located near the south-west border of Turkey.
- Serious cracks occurred along the crest of the dam.
- It was reported that the reservoir has been emptied after the earthquake.

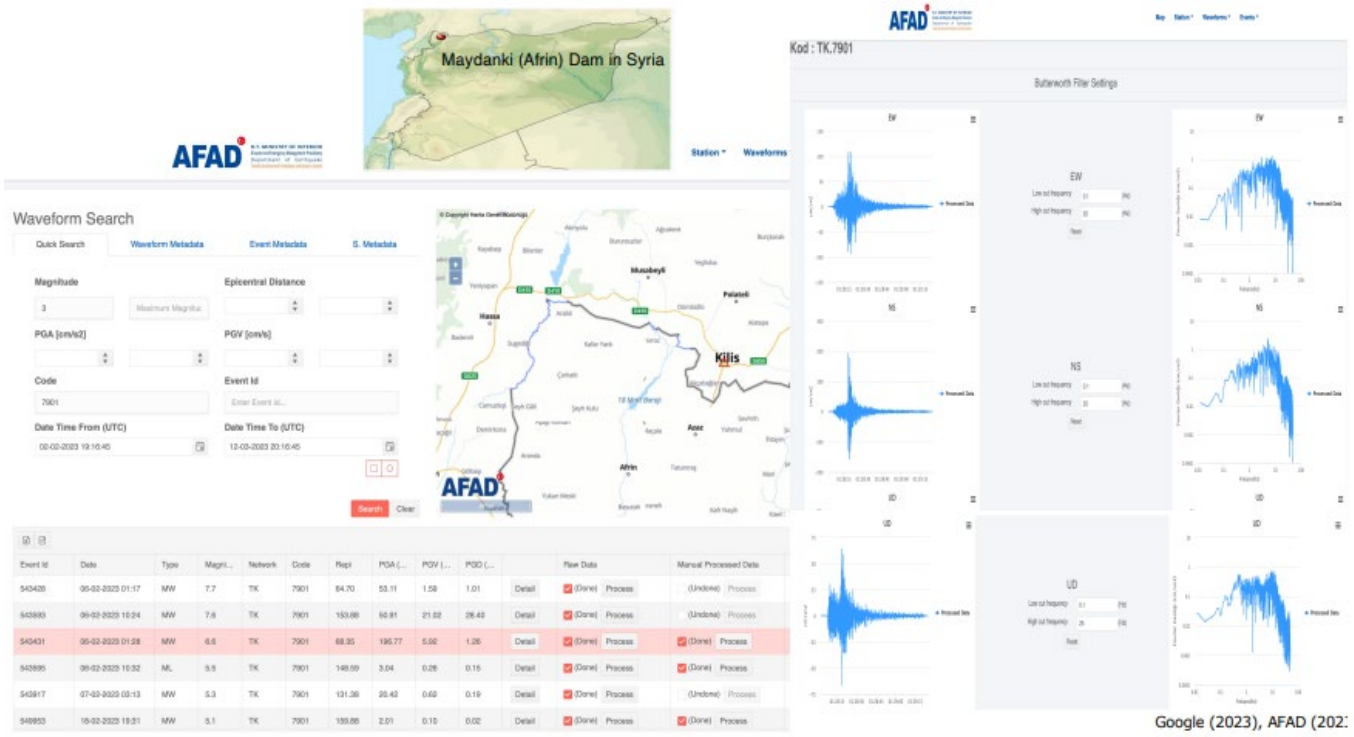
Maydanki (Afrin) Dam in Syria
AFAD
Waveform Search
Quick Search
Waveform Metadata
Event Metadata
S. Metadata
Magnitude
Epicentral Distance
PGA [cm/s2]
PGV [cm/s]
Code
Event Id
Date Time From (UTC)
Date Time To (UTC)
Search
Clear
Kilis
Musabeyli
Hassa
Afrin
Azaz
Kod : TK.7901
Butterworth Filter Settings
EW
NS
UD
Google (2023), AFAD (202

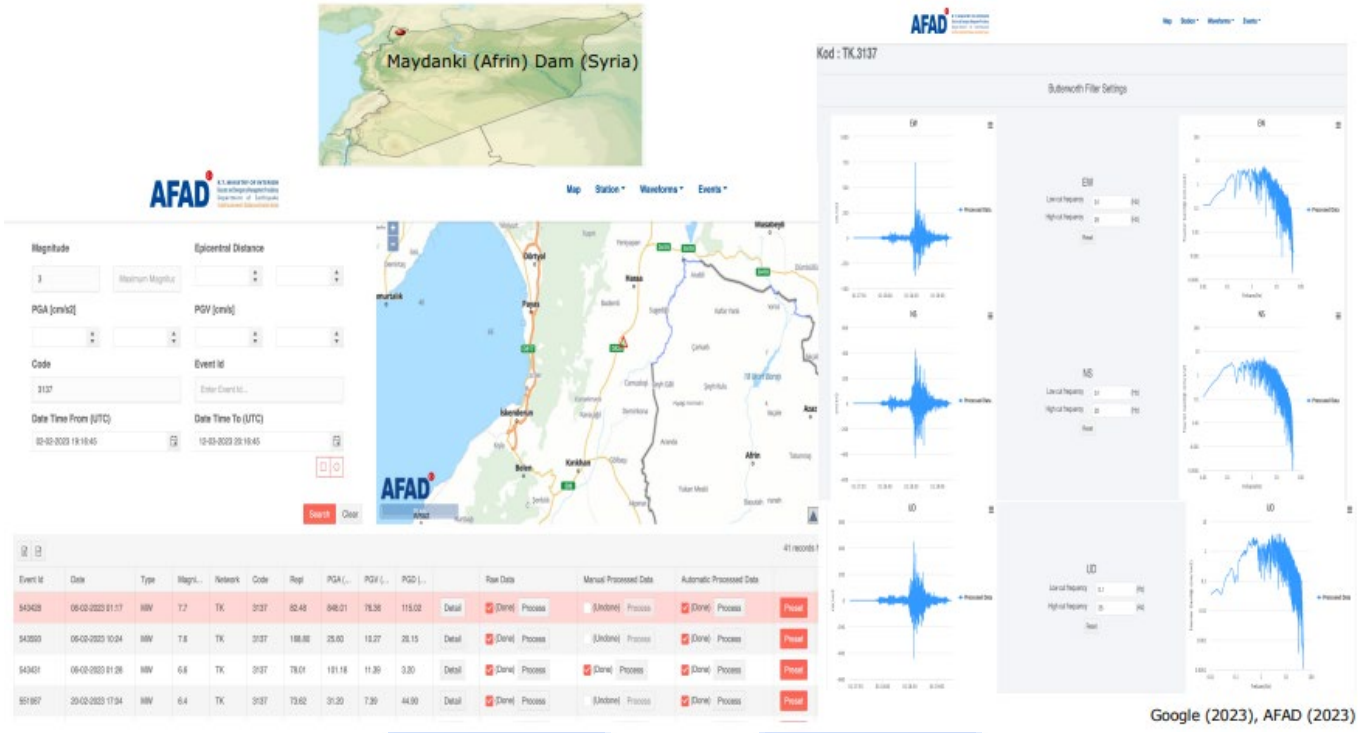
Maydanki (Afrin) Dam (Syria)
AFAD
Map
Station
Waveforms
Events
Magnitude
Epicentral Distance
PGA [cm/s2]
PGV [cm/s]
Code
Event Id
Date Time From (UTC)
Date Time To (UTC)
Search
Clear
Kod : TK.3137
Butterworth Filter Settings
EW
NS
UD
Google (2023), AFAD (2023)

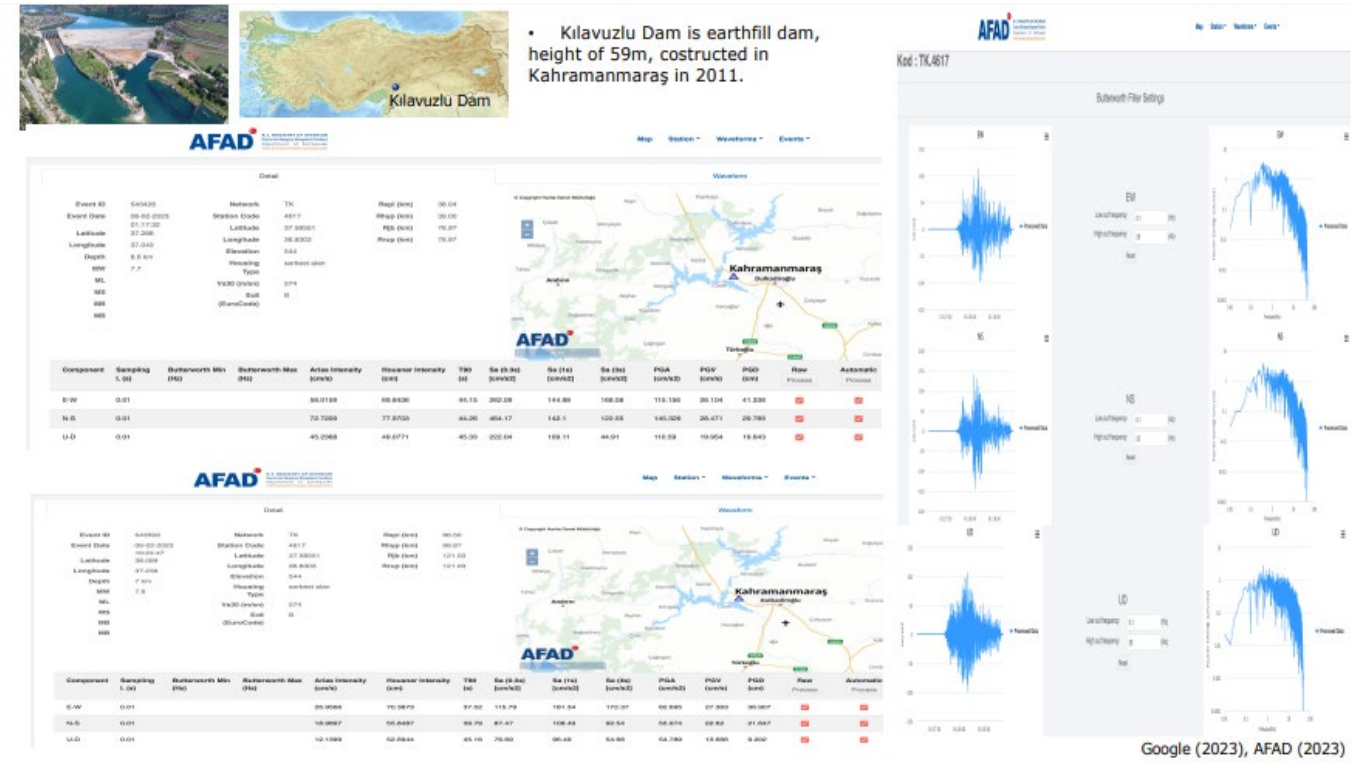

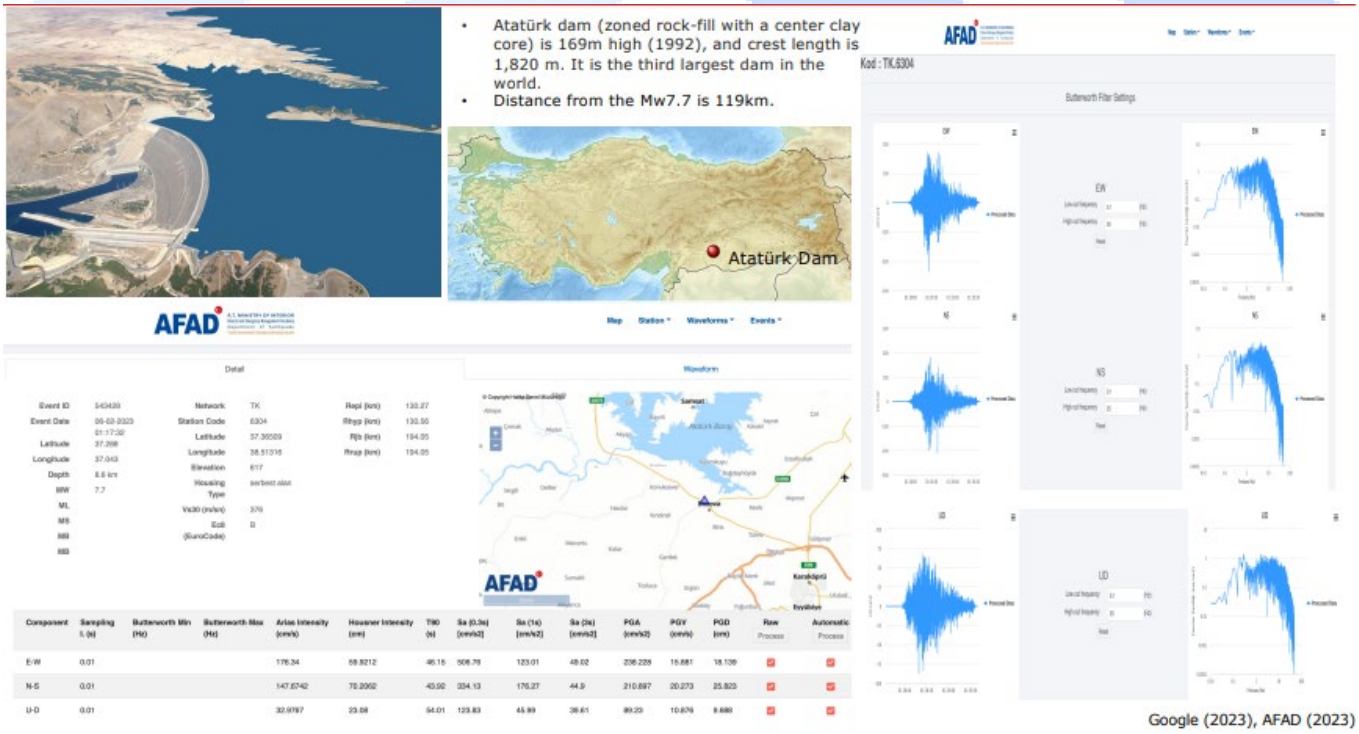

3.10. Performance of Bridges

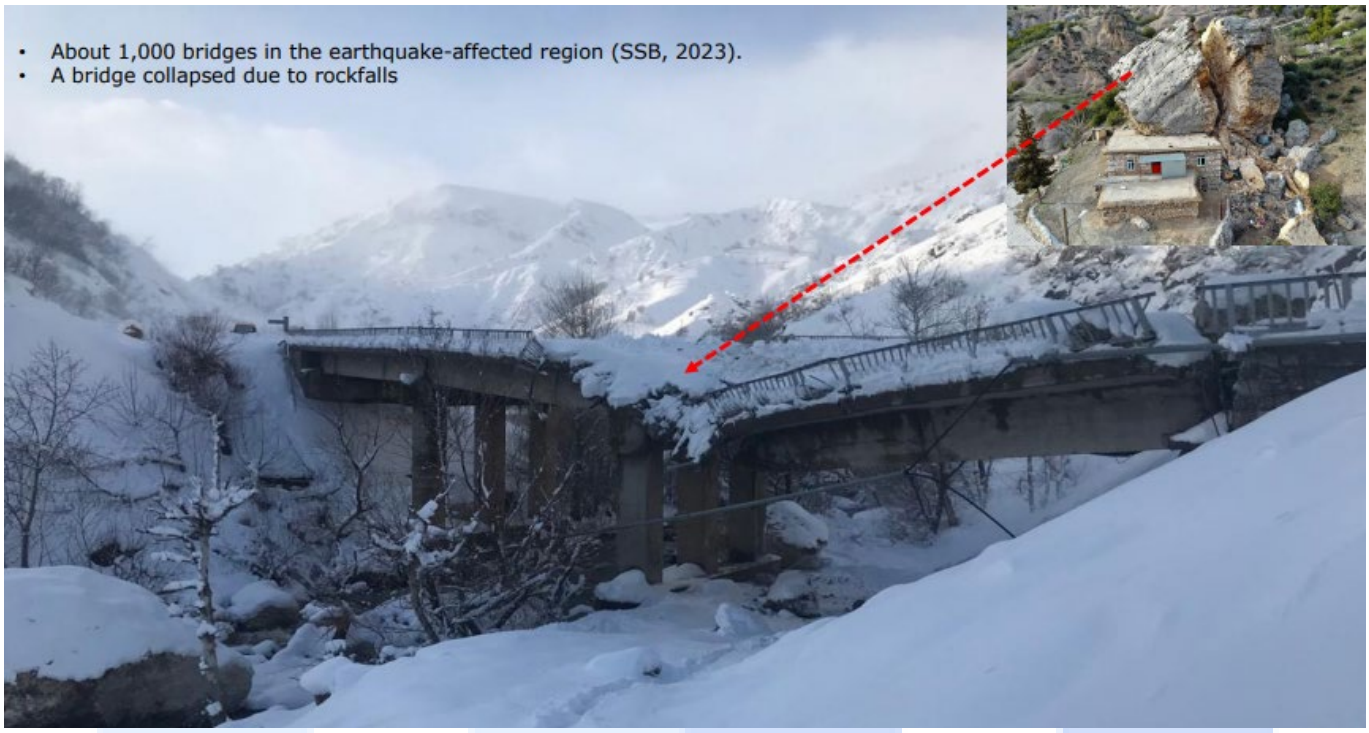
• About 1,000 bridges in the earthquake-affected region (SSB, 2023).
• A bridge collapsed due to rockfalls

Batıayaz Köprüsü

- Expansion joint movements

- Damper damage at expansion joint

- Bridge column (diamater 3m) damage (plastic hinge, spalling of cover concrete, buckled vertical rebar and yielded transverse rebars





- Lateral/vertical bending damage at mid-span of interior girder

- Damage to end of bridge precast girder



- Exterior and interior shear key failure




https://www.linkedin.com/posts/farzad-haghi-25806283_bridgeengineering-earthquakeengineering-bridgeconstruction-activity-7047163840358199296-3_XB/?utm_source=share&utm_medium=member_android

- Kömürhan cable-stayed bridge constructed in 2020.

- Total length of the bridge is 660m (main span 380m, deck width 23m) and it has been designed with a single invert Y pylon with height of 165.5m.

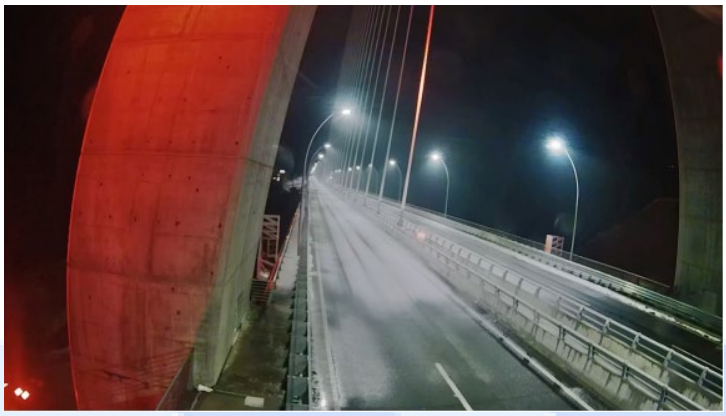

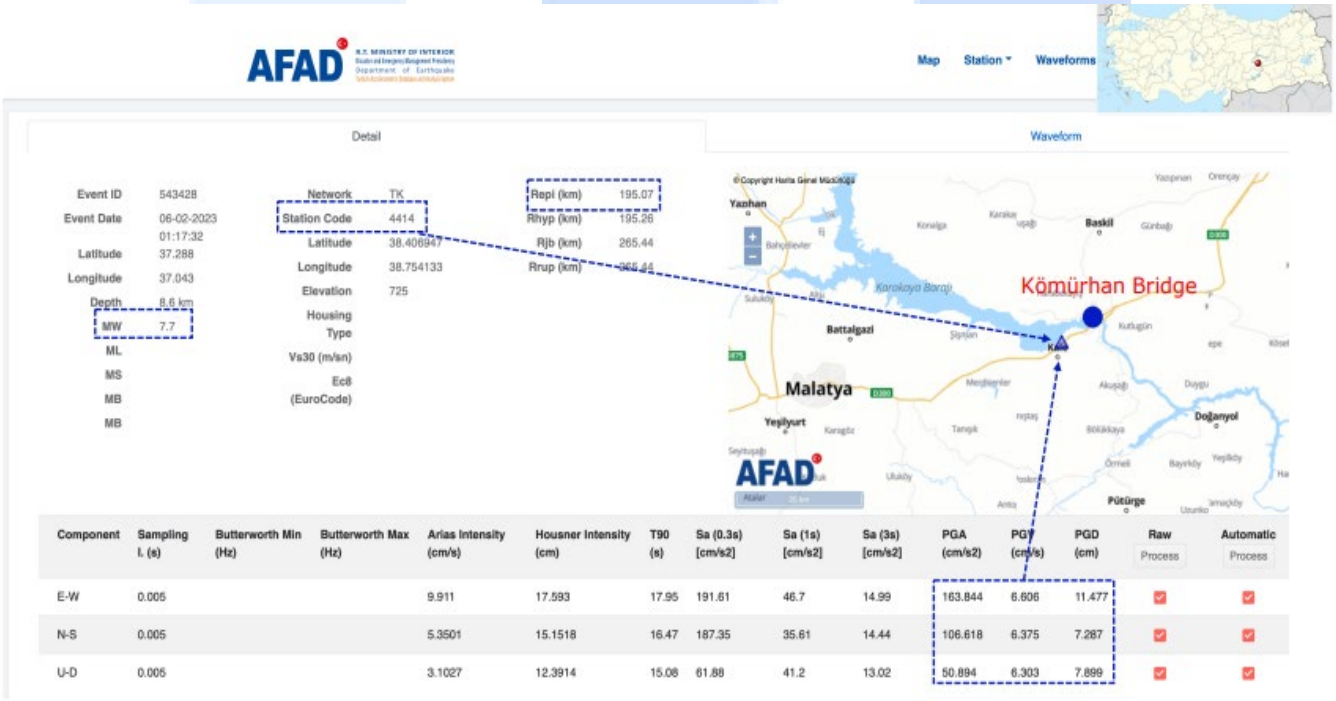

Component	Sampling I. (s)	Butterworth Min (Hz)	Butterworth Max (Hz)	Arias Intensity (cm/s)	Housner Intensity (cm)	T90 (s)	Sa (0.3s) [cm/s2]	Sa (1s) [cm/s2]	Sa (3s) [cm/s2]	PGA (cm/s2)	PGV (cm/s)	PGD (cm)	Raw Process	Automatic Process
E-W	0.005			9.911	17.593	17.95	191.61	46.7	14.99	163.844	6.606	11.477	☑	☑
N-S	0.005			5.3501	15.1518	16.47	187.35	35.61	14.44	106.618	6.375	7.287	☑	☑
U-D	0.005			3.1027	12.3914	15.08	61.88	41.2	13.02	50.894	6.303	7.899	☑	☑

AFAD (2023)

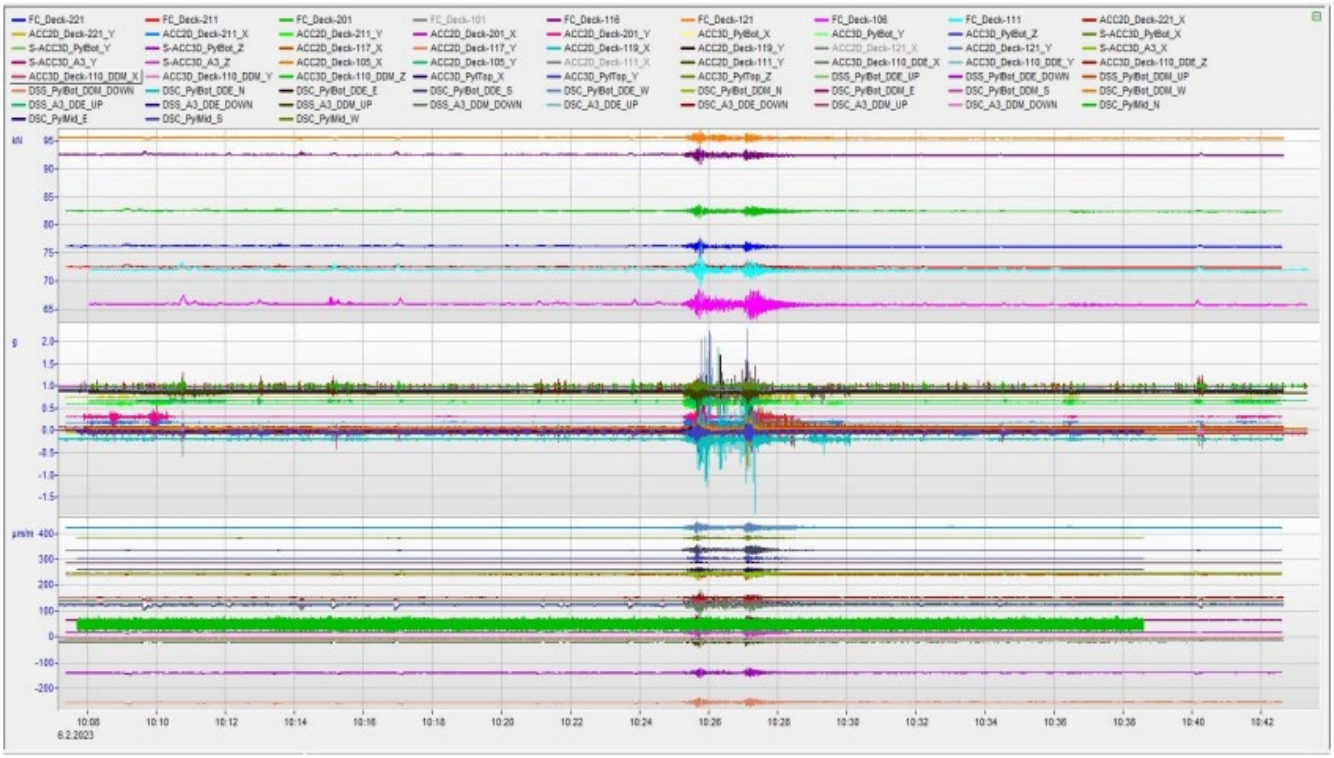
FC_Deck-221
FC_Deck-211
FC_Deck-201
FC_Deck-101
FC_Deck-116
FC_Deck-121
FC_Deck-106
FC_Deck-111
ACC2D_Deck-221_X
ACC2D_Deck-221_Y
ACC2D_Deck-211_X
ACC2D_Deck-211_Y
ACC2D_Deck-201_X
ACC2D_Deck-201_Y
ACC3D_PyBot_X
ACC3D_PyBot_Y
ACC3D_PyBot_Z
S-ACC3D_PyBot_X
S-ACC3D_PyBot_Y
S-ACC3D_PyBot_Z
ACC2D_Deck-117_X
ACC2D_Deck-117_Y
ACC2D_Deck-119_X
ACC2D_Deck-119_Y
ACC2D_Deck-121_X
ACC2D_Deck-121_Y
S-ACC3D_A3_X
S-ACC3D_A3_Y
S-ACC3D_A3_Z
ACC2D_Deck-105_X
ACC2D_Deck-105_Y
ACC2D_Deck-111_X
ACC2D_Deck-111_Y
ACC3D_Deck-110_DDE_X
ACC3D_Deck-110_DDE_Y
ACC3D_Deck-110_DDE_Z
ACC3D_Deck-110_DDM_X
ACC3D_Deck-110_DDM_Y
ACC3D_Deck-110_DDM_Z
ACC3D_PylTop_X
ACC3D_PylTop_Y
ACC3D_PylTop_Z
DSS_PyBot_DDE_UP
DSS_PyBot_DDE_DOWN
DSS_PyBot_DDM_UP
DSS_PyBot_DDM_DOWN
DSC_PyBot_DDE_N
DSC_PyBot_DDE_E
DSC_PyBot_DDE_S
DSC_PyBot_DDE_W
DSC_PyBot_DDM_N
DSC_PyBot_DDM_E
DSC_PyBot_DDM_S
DSC_PyBot_DDM_W
DSS_A3_DDE_UP
DSS_A3_DDE_DOWN
DSS_A3_DDM_UP
DSS_A3_DDM_DOWN
DSC_A3_DDE_UP
DSC_A3_DDE_DOWN
DSC_A3_DDM_UP
DSC_A3_DDM_DOWN
DSC_PyMid_N
DSC_PyMid_E
DSC_PyMid_S
DSC_PyMid_W
kN
g
μm/m
10:08
10:10
10:12
10:14
10:16
10:18
10:20
10:22
10:24
10:26
10:28
10:30
10:32
10:34
10:36
10:38
10:40
10:42
6.2.2023

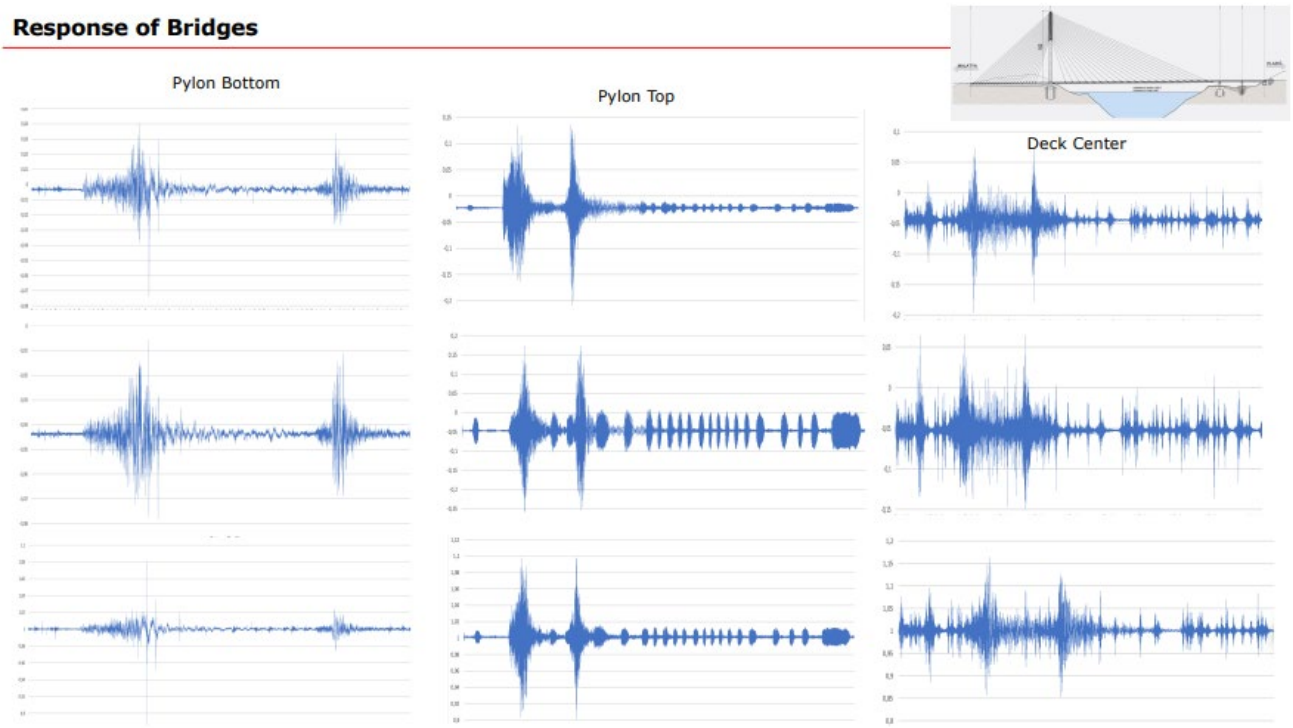

3.11. Performance of Tunnels

- Erkenek Tunnel is a twin-tube tunnel with a length of 1,816 m.

- RC tunnel structures in general performed well during and after the event.
- No serious damages were observed in the highway tunnels.
- Some concrete spalling, and minor portal damages were observed.

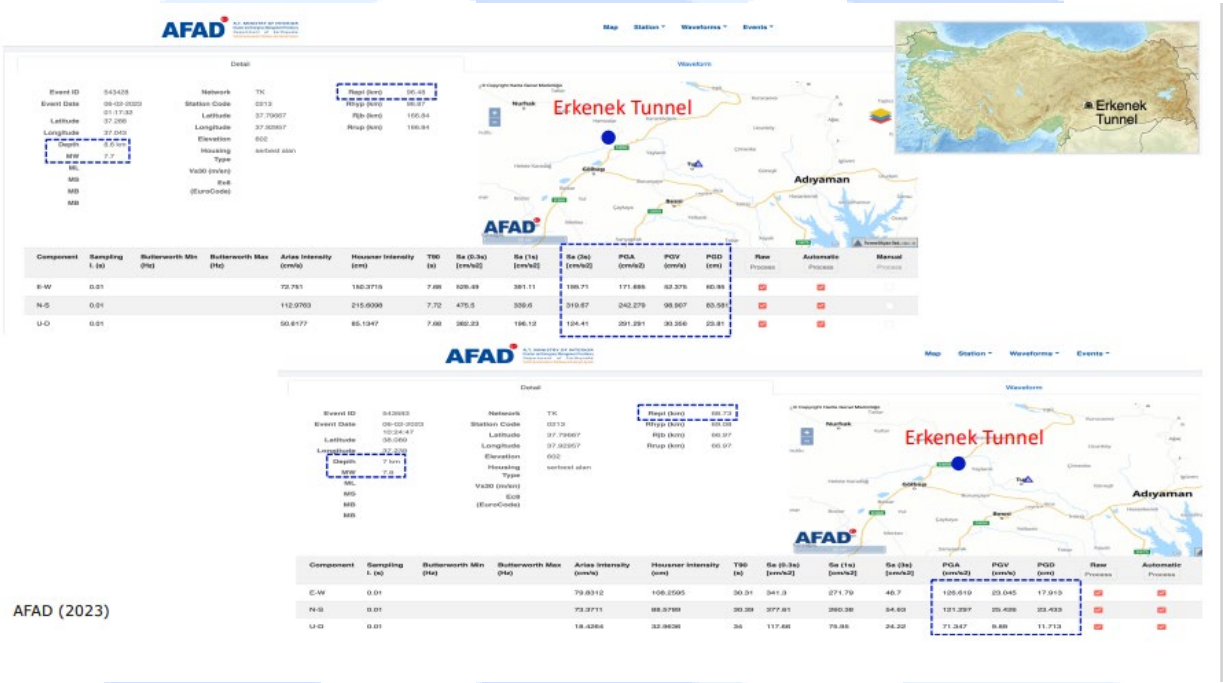

AFAD (2023)

3.12. Performance of Highways

- 15 percent of the existing highway network in Turkey, 12 percent of the state road network, and 14 percent of the provincial road network are located in the earthquake-affected provinces.

- Surface fault rupture-induced serious deformations, offset, buckling, uplift and subsidence on asphalt roads, highways, railway tracks as well as on unpaved roads and farmlands.

SBB (2023), TP (2023)




3.13. Performance of Railways

- The total length of the railway in the disaster zone is 1,275 km.
- The railway network's Mersin-Adana-Osmaniye-Narlı, ToprakkaleIskenderun, Fevzipaşa-Islahiye, Köprüağzı-Kahramanmaraş, NizipGaziantep-Narlı, Narlı-Malatya, Çetinkaya-Malatya, Malatya-Elazığ, and Malatya-Yolçatı-Diyarbakır sections have also been affected by the earthquakes.
- Generally, there have been collapses in tunnels, line deformations, landslides, rockfalls, and structural damage to bridges on the lines.

3.14. Performance of Airport Runway

- Hatay airport experienced some damage to its runway due to soil and foundation problems and was closed to air traffic in the first three days after the earthquakes.

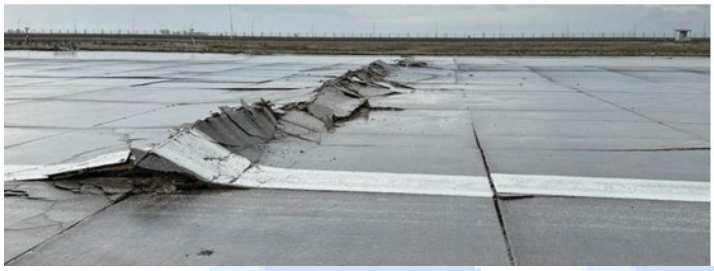

3.15. Performance of Ports

- There are 13 ports operated by the private sector in the Iskenderun Gulf (SSB (2023)).
- Serious damages and a big fire occurred in Iskenderun port.

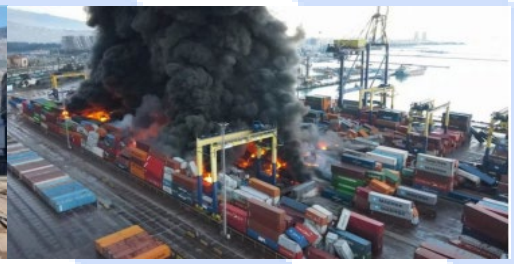

3.16. Performance of Retaining Walls

- Cracks, tilt, lateral displacement and damages on retaining walls were observed

4. Conclusions and Recommendations

Some conclusions and recommendations:

- In order to ensure the durability of a structure both over time and against potentially catastropic earthquake, - proper structural design (Good geotech + Good structural = Good design), - correct construction, - correct inspection, - adequate maintenance of the structures along their life
- Professional engineering system should be implemented.
- New construction technologies and strengthening techniques for the damaged buildings can be developed.
- Shear walls are very important for improving the earthquake performance of buildings.
- The building design software (black box) should be used with care.
- After many earthquakes, the undamaged structures in the region was tired. It is important to check the structural safety of undamaged buildings and other engineering structures after the earthquakes with structural health monitoring methods.
- Before new structures are allowed to be used, one of the best solutions may be to check the health of the structure using a non-destructive experimental method.

References

[1.] AFAD (2023a), 06 Şubat 2023 Pazarcik (Kahramanmaraş) Mw 7.7 ve Elbistan (Kahramanmaraş) Mw 7.6 Depremlerine İlişkin Ön Değerlendirme Raporu, Deprem Dairesi Başkanliği, Ankara, 9 Şubat 2023.

[2.] AFAD (2023b), 06 Şubat 2023 Kahramanmaraş (Pazarcık ve Elbistan) Depremleri Saha Çalişmalari Ön Değerlendirme Raporu, AFAD Deprem Dairesi Başkanliği, Ankara, 24 Şubat 2023.

[3.] Anadolu Ajansı, Türkiye.

[4.] BBC (2023), Turkey–Syria earthquakes 2023, Turkey earthquake: UK team to assess building damage by Rebecca Morelle and Alison Francis.

[5.] BGD (2023), Baraj Güvenliği Derneği, Ankara.

[6.] BU (2023), Kahramanmaraş - Gaziantep Türkiye M7.7 Earthquake, 6 February 2023 (04:17 GMT+03:00) Strong Ground Motion and Building Damage Estimations Preliminary Report (v6), 16.02.2023 (v6) by Ufuk Hancılar, Karin Şeşetyan, Eser Çaktı, Erdal Şafak, Nesrin Yenihayat, Fatma S. Malcıoğlu, Kökcan Dönmez, Tuğçe Tetik, Hakan Süleyman.

[7.] DEU (2023), 06 Şubat 2023, 04:17, Mw=7.7, H=9 Km Pazarcik (Kahramanmaraş) Depremi, 06 Şu Bat 2023, 13:24, Mw=7.6, H=7 Km Elbistan (Kahramanmaraş) Depremi, 20 Şubat 2023, 20:04, Mw=6.4, H=22 Km Defne (Hatay) Depremi Raporu, 03.03.2023.

[8.] Dowell, R.K. (2023), Mw 7.8 Turkiye (Turkey) Earthquake of 2023, Reconnaissance Report of Observed Structural Bridge Damage, Report No. SERP-23/03, San Diego State University, March 2023.

[9.] Duman, T. Y., Emre, Ö. (2013). The East Anatolian Fault: geometry, segmentation and jog characteristics. Geological Society, London, Special Publications, 372(1), 495-529, https://doi.org/10.1144/SP372.14.

[10.] EERI (2023), Joint PVRR: 2023 Türkiye Earthquake Sequence, PRJ-3824, Released: 3/29/2023.

[11.] El Ssayed, H. M., Zaineh, H. E., Dojcinovski, D., Mihailov, V. (2012) "Re-Evaluations of Seismic Hazard of Syria," International Journal of Geosciences, Sept. 3, 847-855.

[12.] Erdik, M., Tümsa, M. B. D., Pınar, A., Altunel, E., and Zülfikar, A. C., 2023, A preliminary report on the February 6, 2023 earthquakes in Türkiye, http://doi.org/10.32858/temblor.297.

[13.] Garini, E. and Gazetas,G. (2023), The 2 earthquakes of February 6th 2023 in Turkey & Syria, First Preliminary Report (8-2-23) Structural Damages, NTUA, Greece.

[14.] Garini, E. and Gazetas, G. (2023), The 2 earthquakes of February 6th 2023 in Turkey & Syria, Second Preliminary Report (8-2-23) Emergence of Fault Rupture, Accelerograms, NTUA, Greece.

[15.] Haghi, F. (2023), https://www.linkedin.com/posts/farzad-haghi-25806283_bridgeengineering-earthquakeengineering-bridgeconstruction-activity7047163840358199296-3_XB/?utm_source=share&utm_medium=member_android

[16.] IMO (2023), TMMOB İnşaat Mühendisleri Odasi 6 Şubat 2023 Kahramanmaraş Pazarcik ve Elbistan Depremleri Ön Değerlendirme Raporu, 14 Şubat 2023.

[17.] IMO (2023), TMMOB Mimarlar Odası 6 Şubat 2023 Depremleri Tespit ve Değerlendirme Raporu, 23 Şubat 2023. • International Press, February 2023.

[18.] Independent (2023), Cataclysmic earthquakes in Turkey and Syria sent a dire warning to America's West Coast. Will anyone listen?

[19.] ITU (2023), Pazarcık (Kahramanmaraş) ve Elbistan (Kahramanmaraş) (Mw 7,8 ve Mw 7,7) Depremleri Ön ve Nihai Raporları, Şubat ve Mart 2023.

[20.] JRC (2023), M7.8 and M7.5 Earthquakes in Türkiye and Syria, JRC Scientific Analysis: Update#2 8 Feb 2023 19:00 UTC.

[21.] KRDAE (2023), Kandilli Rasathanesi ve DAE Bölgesel Deprem-Tsunami Izleme ve Değerlendirme Merkezi, 06 Şubat 2023 Sofalaca Şehitkamil Gaziantep Depremi , İstanbul

[22.] Lekkas, E., Carydis, P., Vassilakis, E., Mavroulis, S., Argyropoulos, I., Sarantopoulou, A., Mavrouli, M., Konsolaki, A., Gogou, M., Katsetsiadou, K.-N., Kotsi, E., Spyrou, N.-I., Diakakis, M., Kranis, H., Skourtsos, E., Lozios, S., Soukis, K. (2023). The 6 February 6 2023 Turkey-Syria Earthquakes. Newsletter of Environmental, Disaster and Crises Management Strategies, 29, ISSN 2653-9454, DOI: 10.13140/RG.2.2.17643.82726.

[23.] Magnitude 7.8 SOUTHERN TURKEY, February 6, 2023at 01:17:35 UTC, Teachable Moments are a service of The Earth Scope Consortium and The University of Portland.

[24.] METU (2023), Preliminary Reconnaissance Report on February 6, 2023, Pazarcık Mw=7.7 and Elbistan Mw=7.6, Kahramanmaraş-Türkiye Earthquakes, February 20, 2023.

[25.] MTA (2023a), 06 Şubat 2023 Pazarcik (Kahramanmaraş) Depremi (Mw 7,7) Saha Gözlem Raporlari Serisi 1- Amanos Segmenti Rapor No: 14121, Maden Tetkik ve Arama Genel Müdürlüğü, Jeoloji Etütleri Dairesi 14 Şubat 2023, Ankara.

[26.] MTA (2023b), 06 ŞUBAT 2023 Pazarcik (Kahramanmaraş) (Mw 7,7) ve Elbistan (Kahramanmaraş) (Mw 7,6) Depremleri Bilgi Notu, Jeoloji Etütleri Dairesi Başkanliği 08 Şubat 2023, Ankara.

[27.] OCHA/UNDAC (2023), Türkiye: 2023 Earthquakes Situation Report No. 2 As of 19 February 2023.

[28.] Reuters (2023), 7.8 magnitude quake, 5.03.2023.

[29.] SBB (2023), 2023 Kahramanmaraş ve Hatay Depremleri Raporu, SBB Deprem Sonrası Değerlendirme Raporu, Mart 2023, Ankara, Türkiye, https://www.sbb.gov.tr/2023-kahramanmaras-ve-hatay-depremleri-raporu/.

[30.] Stein, R.S.., Toda, S., Özbakir, A. D., Sevilgen, V., Gonzalez-Huizar, H., Lotto, G., Sevilgen, S. 2023, Interactions, stress changes, mysteries, and partial forecasts of the 2023 Kahramanmaraş, Türkiye, earthquakes, Temblor, http://doi.org/10.32858/temblor.299 (Temblor, Interactions, stress changes, mysteries, and partial forecasts of the 2023 Kahramanmaraş, Türkiye, earthquakes, POSTED ON MARCH 2, 2023 BY TEMBLOR).

[31.] Taftsoglou, M., Valkaniotis, S., Karantanellis, E., Goula, E., Papathanassiou, G. (2023), Preliminary mapping of liquefaction phenomena triggered by the February 6 2023 M7.7 earthquakes, Türkiye / Syria, based on remote sensing data, February 23 2023.

[32.] The Atlantic (2023), A Month Since the Devastating Earthquake in Turkey, Alan Taylor, March 8, 2023.

[33.] TP (2023), Turkish Press, Türkiye.

[34.] TURKONFED (2023), 2023 Kahramanmaraş Depremi Afet Ön Değerledirme Raporu, 10 Şubat 2023.

[35.] USGS (2023), The M7.8 and M7.5 Kahramanmaraş Earthquake Sequence struck near Nurdağı, Turkey (Türkiye) on February 6, 2023.

[36.] YDMP (2023), Yapı Deprem Mühendisliği Platformu, İstanbul, 2023.

[37.] Zahradník, J., Turhan, F., Sokos, E. (2023), Multiple-point seismic source models of the catastrophic Turkish earthquakes of February 6, 2023, EMSC on February 20, 2023.

[38.] 06.02.2023 Kahramanmaraş Merkezli Depremlerin Saha İncelemelerine ait İHA Fotoğraflari.

PACE-2023

The Second International Congress on the Phenomenological Aspects of Civil Engineering

Keynote

20-23 June 2023

Ultra High Performance Fiber Concrete (Uhpfc) as A Repair Material

Bassam A. Tayeh

Professor, Islamic University of Gaza, PALESTINE

Corresponding Author E-mail: btayeh@iugaza.edu.ps

Keywords

NC and UHPFC,

Slant shear test,

Splitting tensile test,

Interfacial failure,

Sand-blasted method,

Micro structure.

Abstract

A large number of existing concrete structures worldwide are in urgent need for effective and durable repair. However, up to half of all concrete repairs are estimated to fail. The interfacial transition zone between new and old concrete is the weakest section in repaired concrete. The objectives of this research are investigate the bond strength characteristics between NC substrate and UHPFC as a repair material, examine the short and long term transport properties of the interfacial bond between NC substrate and UHPFC, quantify the influence of surface roughness of NC substrate on the interfacial bond characteristics of composite UHPFC/NC substrate, assess the influence of substrate surface moisture condition on the interfacial bond characteristics of composite UHPFC/NC substrate. As a result, the bond strength in the slant shear test and splitting tensile test was very strong, as the interfacial failure occurred after the damage of the NC substrate. The results of the pull-off test and flexural test showed that failure occurred in the substrates in all specimens at all test ages. The results of RCPT, gas permeability, water permeability and porosity tests confirmed that UHPFC has very low permeability. UHPFC improved the resistance of the NC substrate against the penetration of chloride and other aggressive fluids. The permeability behavior of OV bonded specimens was very close to that of monolithic UHPFC samples. The results showed that the substrate surface properties were required to ensure efficient bonding between concrete substrate surfaces and overlay materials. In this study, the sand-blasted method was demonstrated to be the most efficient technique. There is good correlation between the substrate roughness parameters and the splitting cylinder tensile test results and the slant shear test results. The SEM results proved that the use of UHPFC as a repair material can improve the microstructure of the interface zone.

1. Introduction

A large number of existing concrete structures worldwide are in urgent need for effective and durable repair. However, up to half of all concrete repairs are estimated to fail [1]. Concrete repairs are often per-ceived to lack both early age performance and long-term durability. Approximately 75% of the failures can be attributed to the lack of durability. This inadequate performance is often ascribed to the lack of an effective and perfect bond [2].

The interfacial transition zone between new and old concrete is the weakest section in repaired concrete [3-5]. Good bonding at the interfaces in the repaired concrete structures is important for safety, durability, and better resistance against penetration of harmful substances [6-7].

Ultra high performance fiber concrete (UHPFC) is one of the breakthroughs in concrete technology, providing significant improvement in strength, workability, ductility, and durability compared with normal concrete. The properties of UHPFC are enhanced through the reduction of the amount of water, elimination of all coarse aggregates, use of highly refined silica fume, and introduction of steel fibers [8-10].

2. Literature

The research on the application of UHPFC as a new construction material and a new repair material is still in progress. There is a serious gap of information available about the behavior of UHPFC as a repair material. Furthermore, further investigations on the short- and long-term bonding performance of UHPFC under different surface preparations conditions and varying the moisture content of the NC substrate are required. Hence, the present research attempts to study the short- and long-term bond characteristics between old concrete substrate with different surface preparations and different moisture conditions, in order to fill the knowledge gaps.

3. Research Objectives

- To investigate the bond strength characteristics between NC substrate and UHPFC as a repair material.
- To examine the short and long term transport properties of the interfacial bond between NC substrate and UHPFC.
- To quantify the influence of surface roughness of NC substrate on the interfacial bond characteristics of composite UHPFC/NC substrate.
- To assess the influence of substrate surface moisture condition on the interfacial bond characteristics of composite UHPFC/NC substrate.

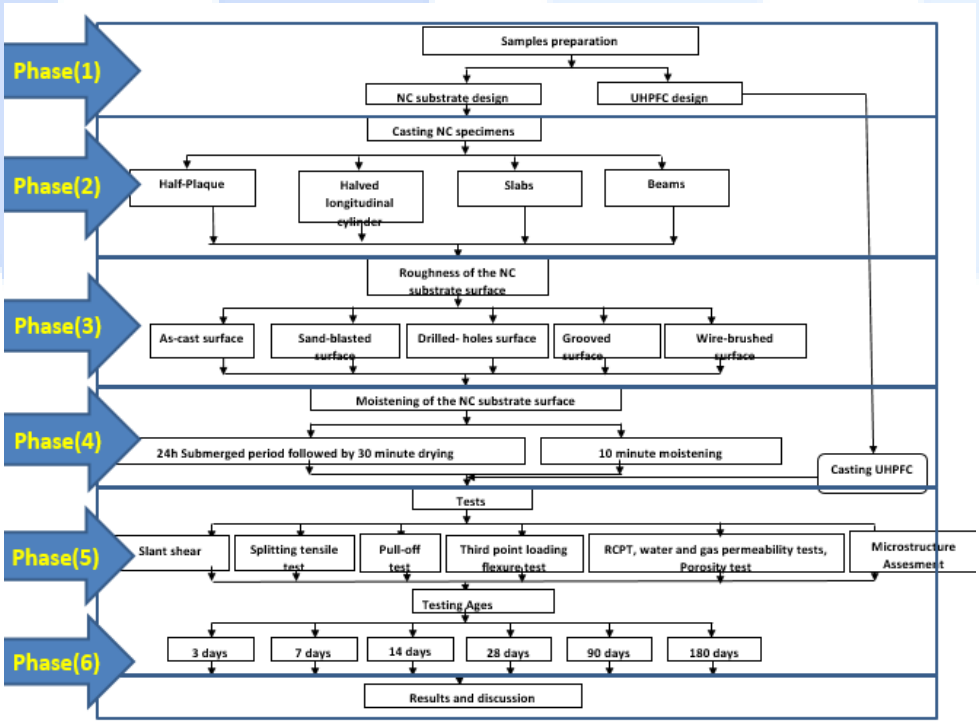

Figure 1. Research Objectives

Table 1. Mix proportions for NC substrate and UHPFC

Concrete Type (kg/m3)	NC substrate	UHPFC
OPC (Type 1, 42.5)	400	768
Coarse Aggregate (max. 12.5mm)	930	-
River Sand (F.M. =2.4)	873	-
Mining Sand (100-1180mm)	-	1140
Silica Fume (23.7 m2/g)	-	192
Steel Fiber (Lf = 10mm, df =0.2mm)	-	157
Superplasticizer (PCE-based)	4	40
Water	200	144
Total	2407	2441
W/B	0.5	0.15

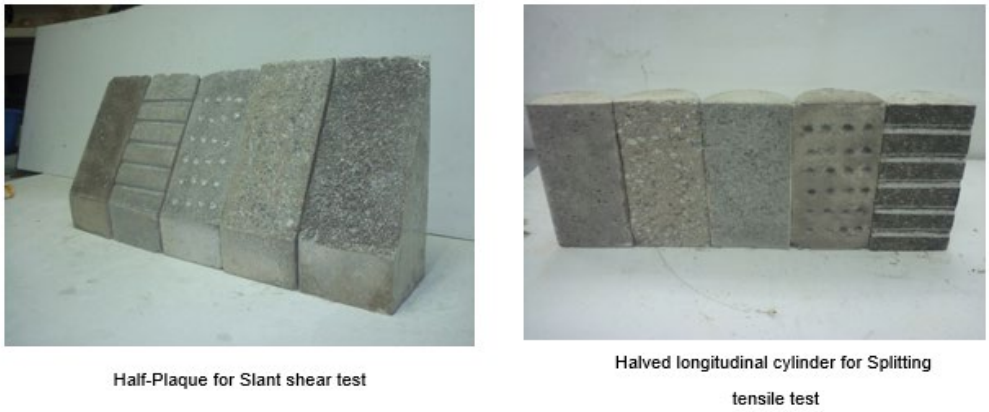

Figure 2. Slabs for Pull off test

Figure 3. Beams for Flexural test

Figure 4. Slant shear, Splitting tensile, Pull off and Flexural test

Figure 5. Rapid chloride permeability test

Figure 6. Gas and water permeability test

Figure 7. Porosity test

Figure 8. Scanning electron microscopy and energy dispersive X-ray spectroscopy (SEM/EDS)

4. Results and Discussion

4.1. Slant shear test results

4.1.1. Failure modes

Observation on the slant shear composite specimens after testing shows four different types of failure modes:

- ✓ Type A: pure interfacial failure (a complete de-bonding at the transition zone) where no cracking and fracturing can be observed
- ✓ Type B: interfacial failure combined with minor NC substrate cracking or damage.
- ✓ Type C: interfacial failure combined with substrate fracture.
- ✓ Type D: substratum failure with good interface (with good bonding at the interface)

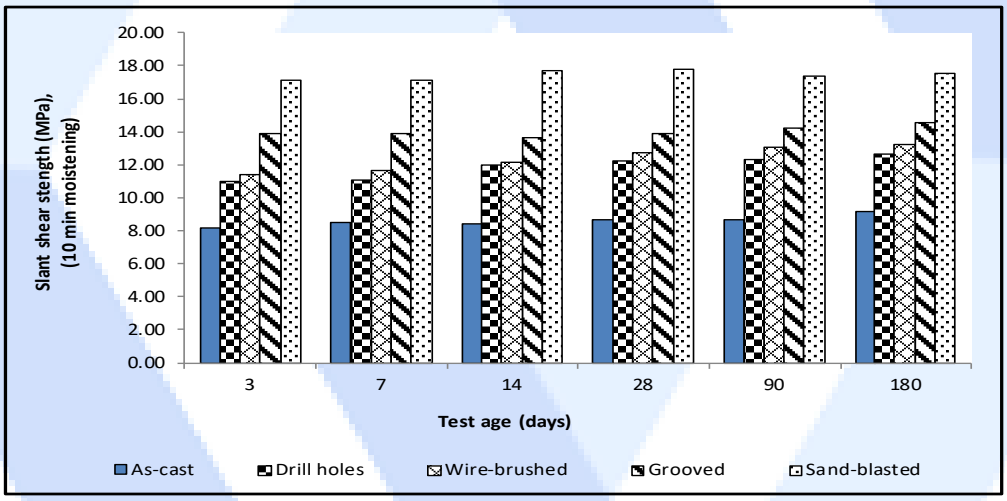

Figure 9. Average slant shear strength for the different types of substrate surface at different ages (10 min. moistening)

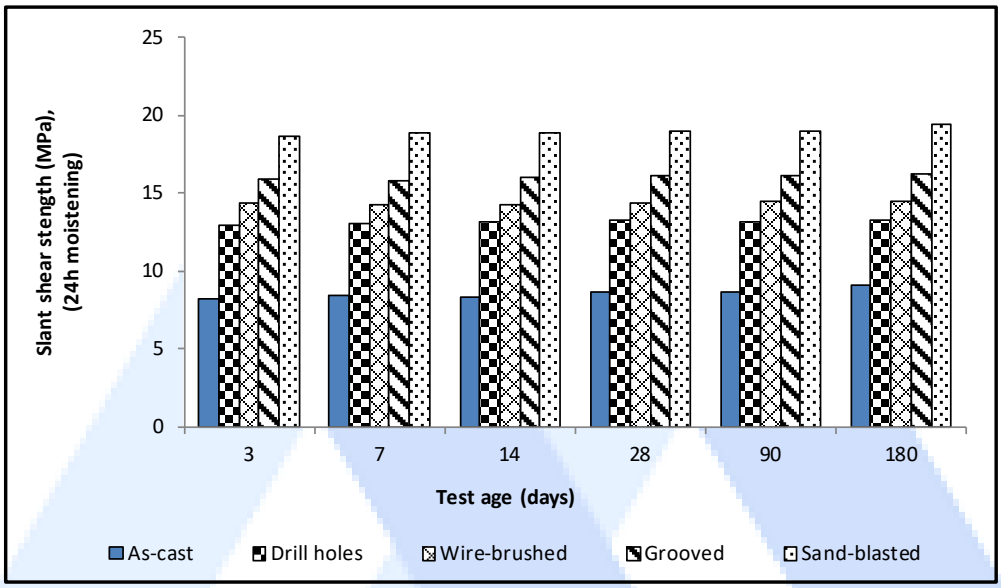

Figure 10. Average slant shear strength for the different type of substrate surface at different ages. (24 h moistening)

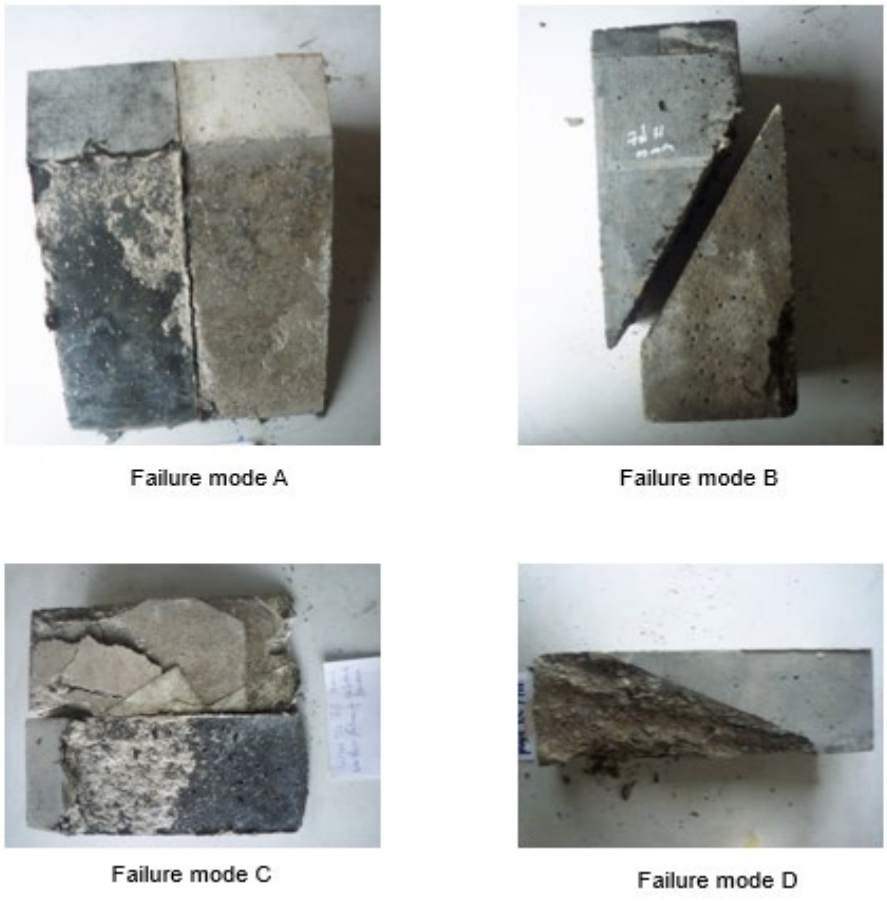

Figure 11. Failure modes for slant shear strength

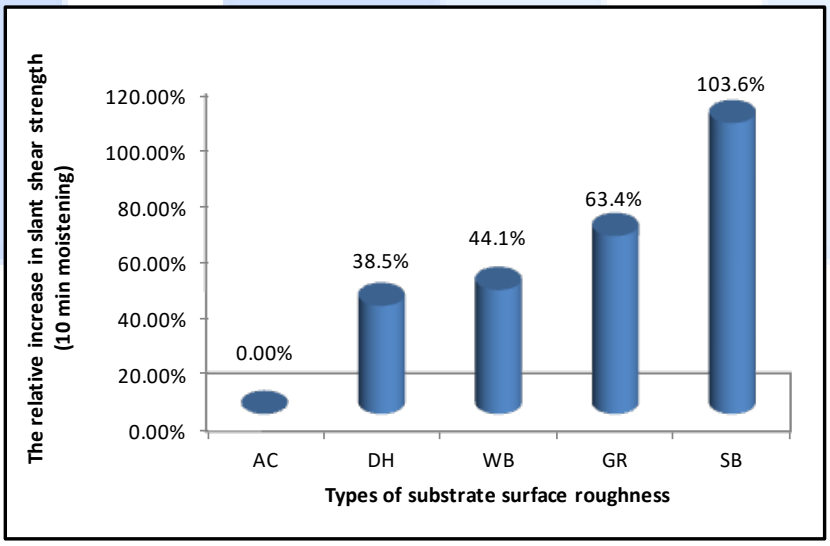

Figure 12. The average relative increase in slant shear strength for the different types of substrate surface roughness at all ages (10 min. moistening)

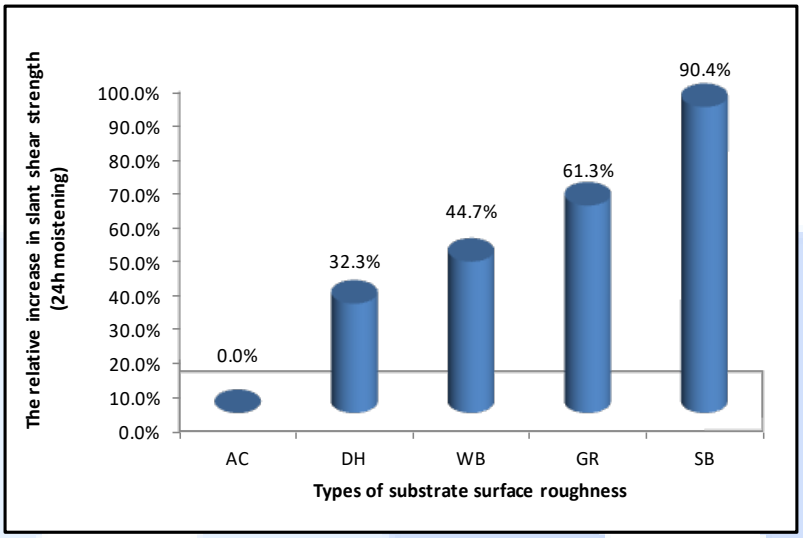

Figure 13. The average relative increase in slant shear strength for the different types of substrate surface roughness at all ages (24h. moistening)

4.2. Splitting tensile strength test results

4.2.1. Failure modes

The observed failure modes of the composites after the splitting tensile test. The modes of failure can be classified into three categories:

Type A = complete interfacial failure (de-bonding of the composite at the interface)

Type B = interfacial failure combined with partial substratum failure

Type C = substratum failure (with good bonding at the interface)

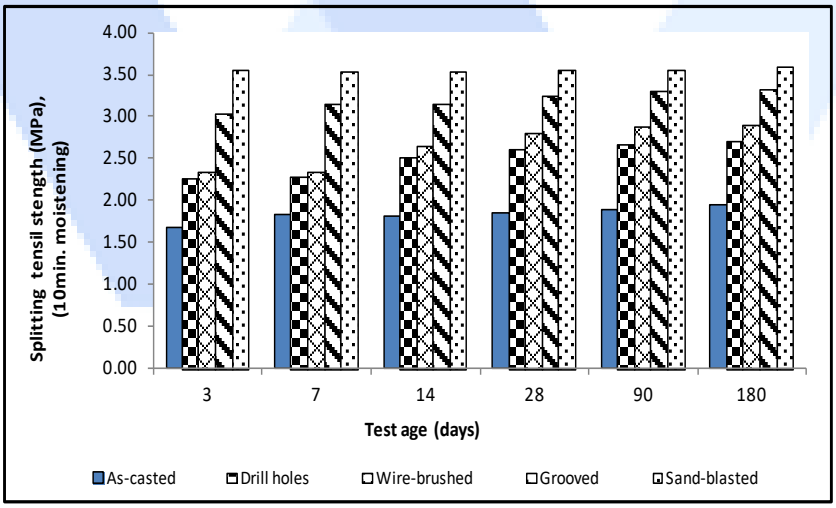

Figure 14. Average splitting tensile strength for different types of substrate surface at different ages (10 min. moistening)

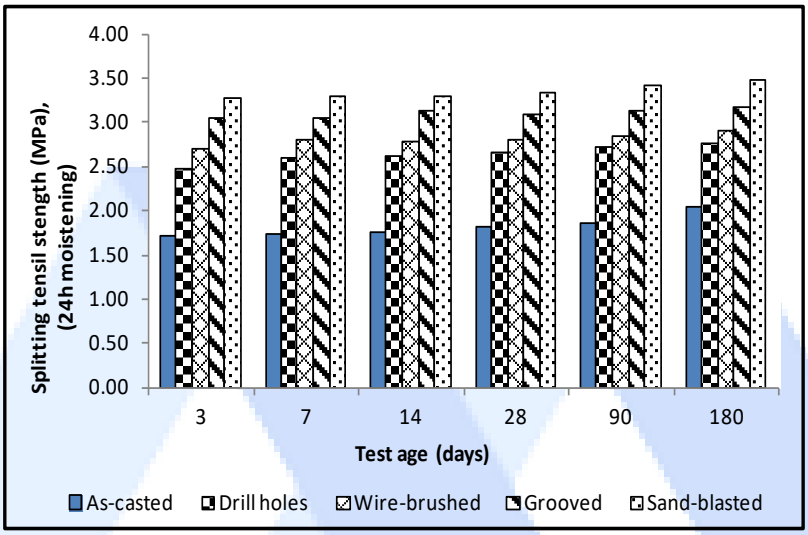

Figure 15. Average splitting tensile strength for different types of substrate surface at different ages (24 h moistening)

Figure 16. Failure modes splitting tensile strength

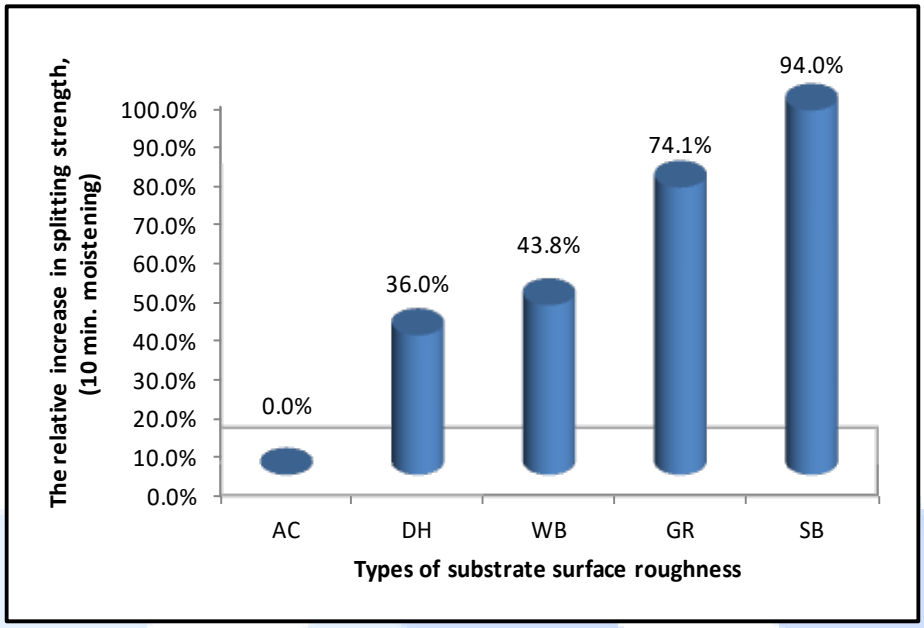

Figure 17. Average relative increase in splitting tensile strength for different types of substrate surface roughness at all ages (10 min moistening)

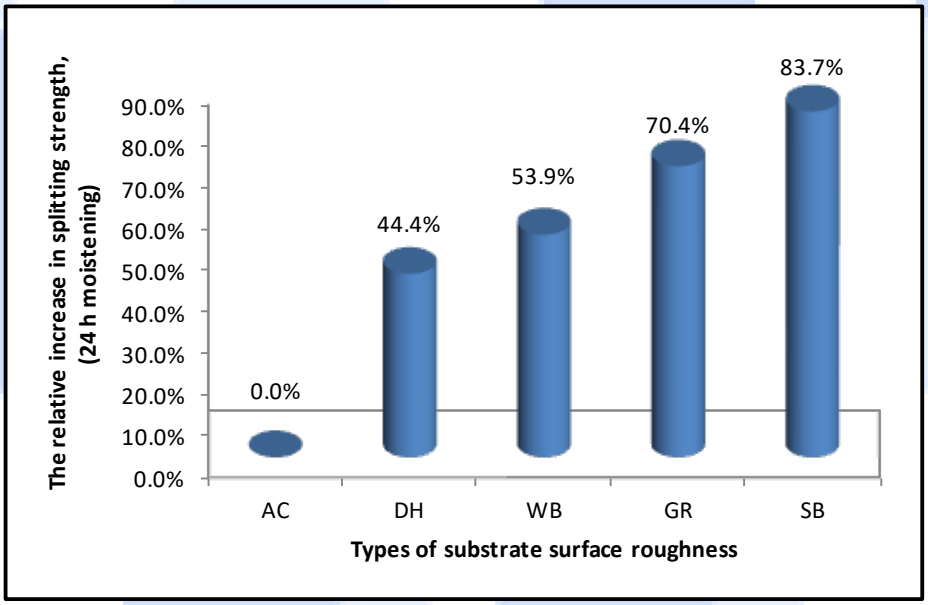

Figure 18. Average relative increase in splitting tensile strength for different types of substrate surface roughness at all ages (24h. moistening)

4.3. Pull-off test

The results of pull-off test showed that in all specimens and at all ages of the test, the failure occurred in the NC substrate, indicating a strong bond with the UHPFC.

Figure 19. (a) Pull off test set-up for the composite specimen, (b) Failure through the NC substrate

4.4. Flexural test

The results of flexural test clearly showed that all failures occurred via the NC substrate.

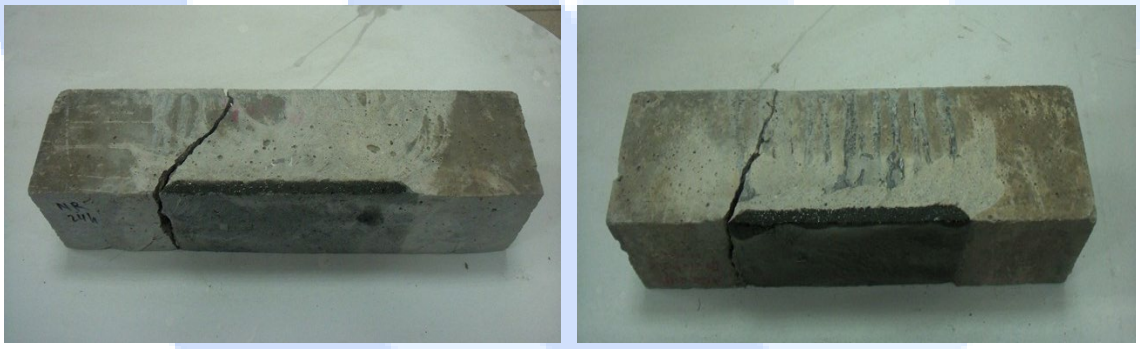

(a) (b)

(c)

Figure 20. Flexural failure of composite UHPFC/NC substrate, (a) as-cast surface, (b) wire-brushed surface and (c) sand-blasted surface

4.5. The permeability properties of the NC substrate, UHPFC and composite UHPFC/NC substrate Rapid chloride permeability test

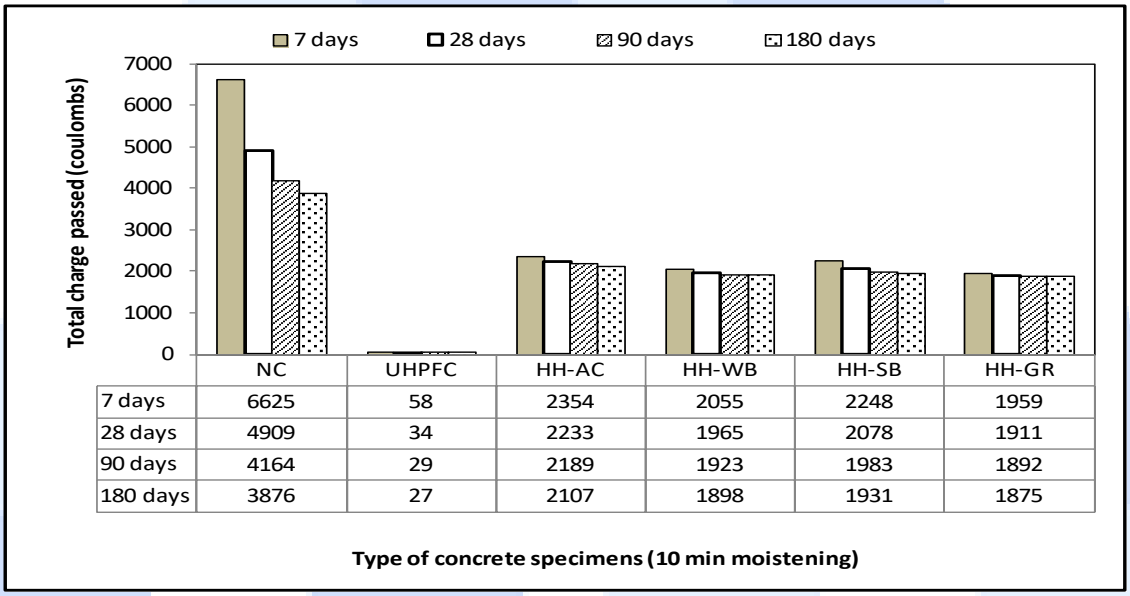

	NC	UHPFC	HH-AC	HH-WB	HH-SB	HH-GR
7 days	6625	58	2354	2055	2248	1959
28 days	4909	34	2233	1965	2078	1911
90 days	4164	29	2189	1923	1983	1892
180 days	3876	27	2107	1898	1931	1875

Figure 21. Comparison of the rapid chloride permeability test results between NC substrate, UHPFC and composite UHPFC/NC substrate (HH, 10 min moistening)

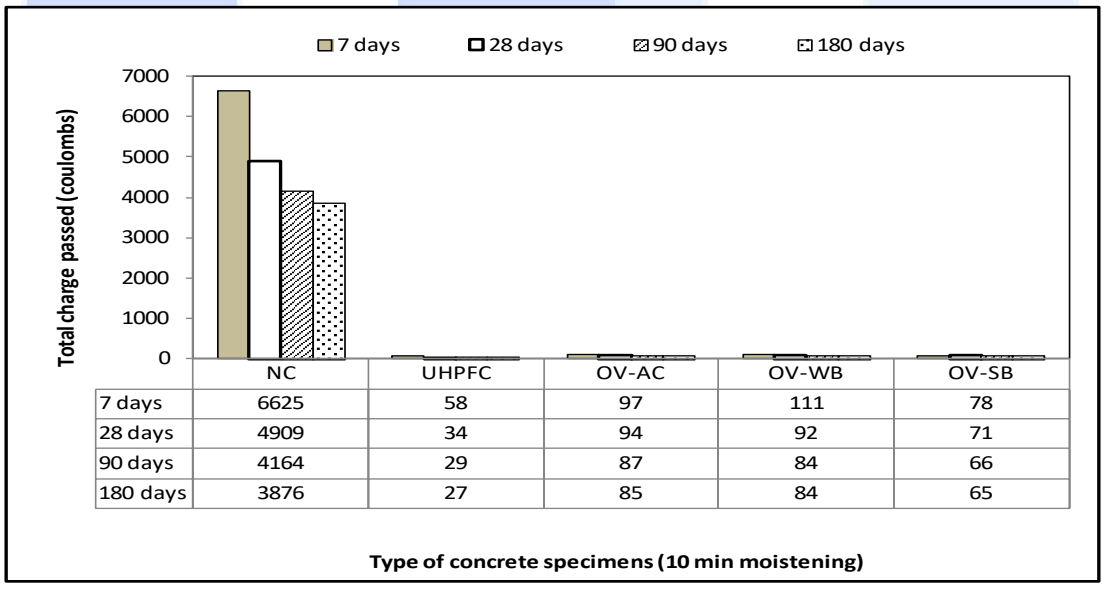

	NC	UHPFC	OV-AC	OV-WB	OV-SB
7 days	6625	58	97	111	78
28 days	4909	34	94	92	71
90 days	4164	29	87	84	66
180 days	3876	27	85	84	65

Figure 22. Comparison of the rapid chloride permeability test results between NC substrate, UHPFC and composite UHPFC/NC substrate (OV, 10 min moistening)

4.6. Gas permeability

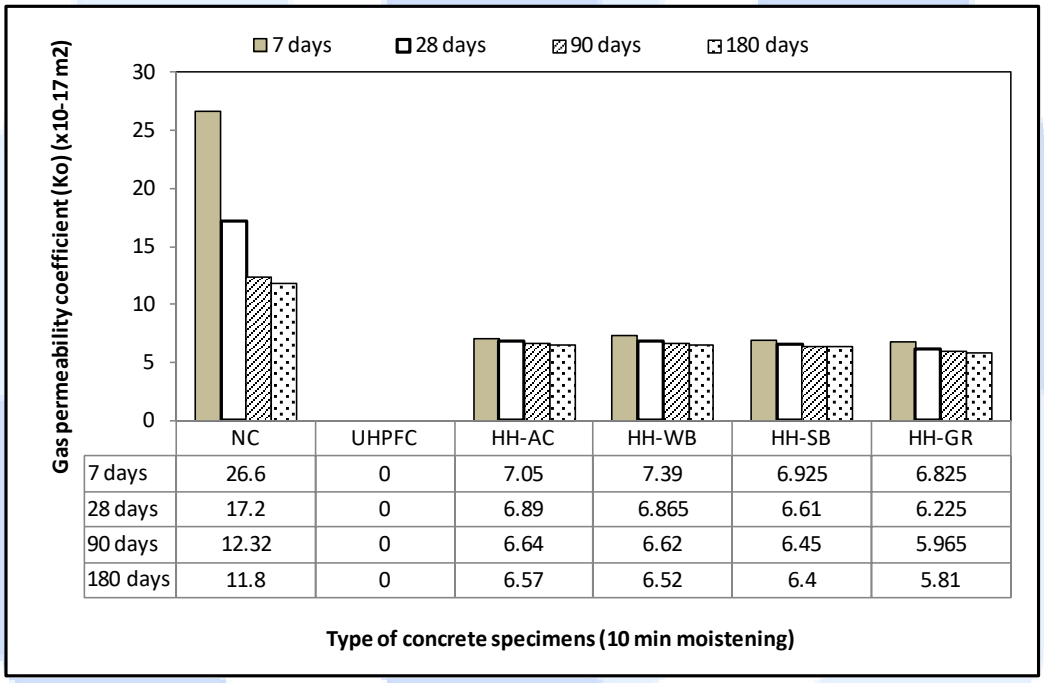

	NC	UHPFC	HH-AC	HH-WB	HH-SB	HH-GR
7 days	26.6	0	7.05	7.39	6.925	6.825
28 days	17.2	0	6.89	6.865	6.61	6.225
90 days	12.32	0	6.64	6.62	6.45	5.965
180 days	11.8	0	6.57	6.52	6.4	5.81

Figure 23. Comparison of the gas permeability test results between NC substrate, UHPFC and composite UHPFC/NC substrate (HH, 10 min moistening)

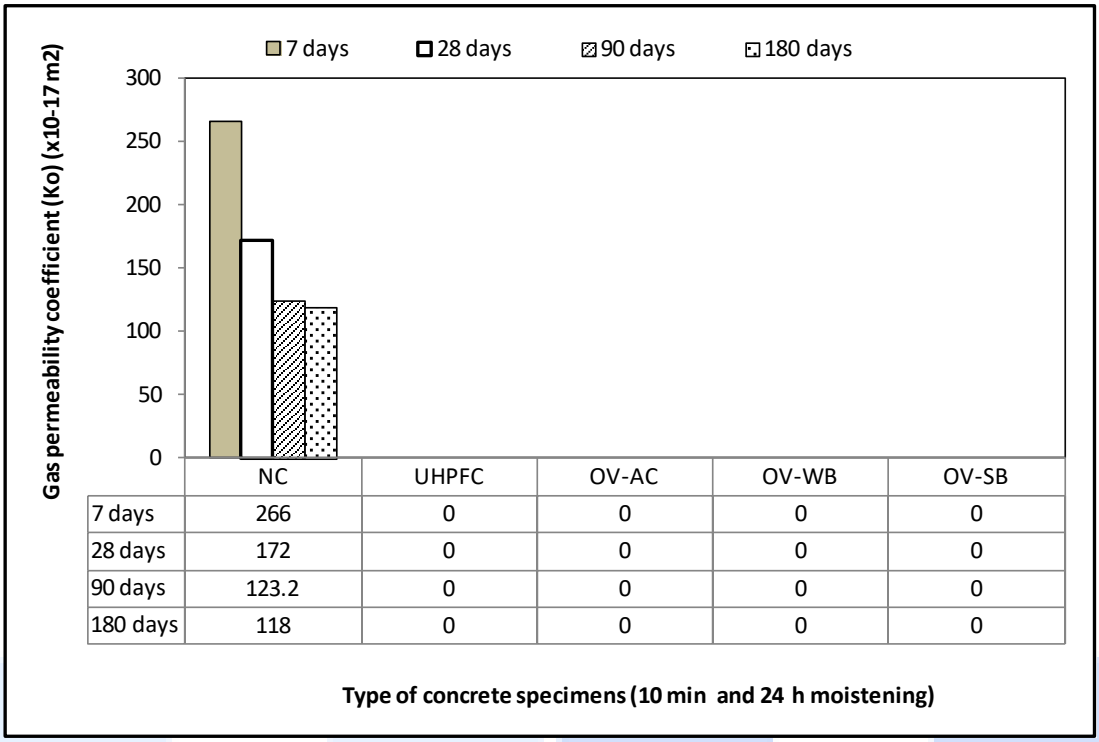

	NC	UHPFC	OV-AC	OV-WB	OV-SB
7 days	266	0	0	0	0
28 days	172	0	0	0	0
90 days	123.2	0	0	0	0
180 days	118	0	0	0	0

Figure 24. Comparison of the gas permeability test results between NC substrate, UHPFC and composite UHPFC/NC substrate (OV, 10 min and 24 h moistening)

4.7. Water permeability

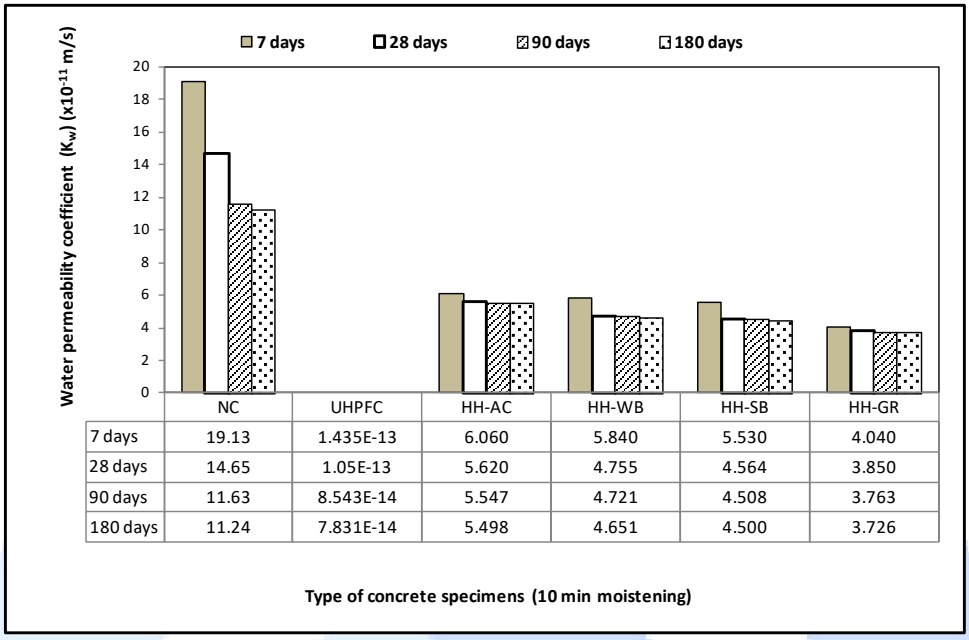

	NC	UHPFC	HH-AC	HH-WB	HH-SB	HH-GR
7 days	19.13	1.435E-13	6.060	5.840	5.530	4.040
28 days	14.65	1.05E-13	5.620	4.755	4.564	3.850
90 days	11.63	8.543E-14	5.547	4.721	4.508	3.763
180 days	11.24	7.831E-14	5.498	4.651	4.500	3.726

Figure 25. Comparison of the water permeability test results between NC substrate, UHPFC and composite UHPFC/NC substrate (HH, 10 min moistening)

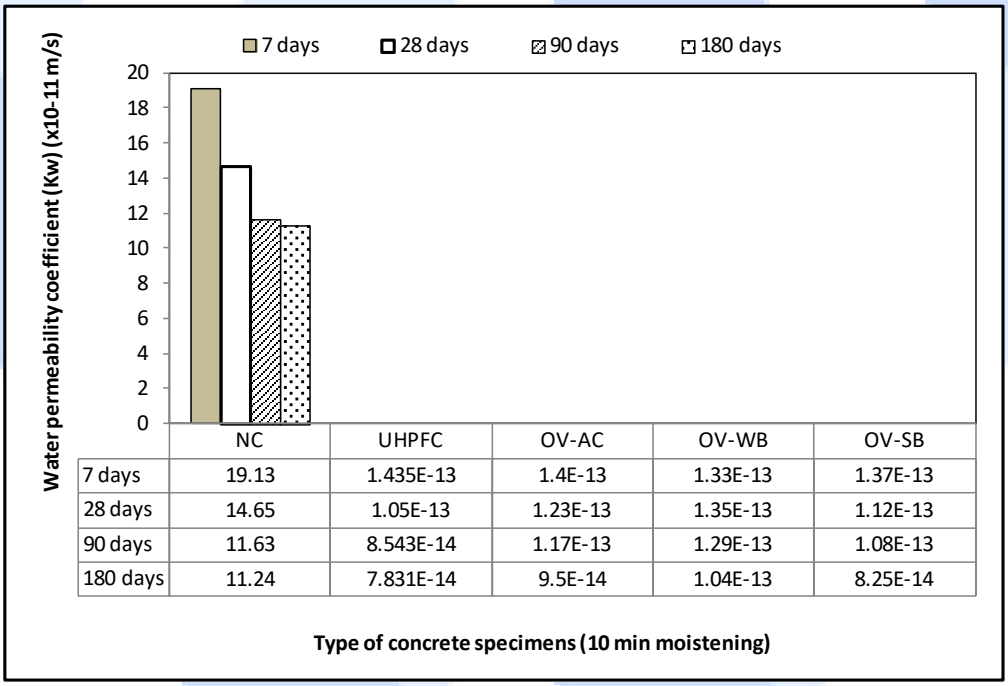

	NC	UHPFC	OV-AC	OV-WB	OV-SB
7 days	19.13	1.435E-13	1.4E-13	1.33E-13	1.37E-13
28 days	14.65	1.05E-13	1.23E-13	1.35E-13	1.12E-13
90 days	11.63	8.543E-14	1.17E-13	1.29E-13	1.08E-13
180 days	11.24	7.831E-14	9.5E-14	1.04E-13	8.25E-14

Figure 26. Comparison of the water permeability test results between NC substrate, UHPFC and composite UHPFC/NC substrate (OV, 10 min moistening)

4.8. Porosity Test

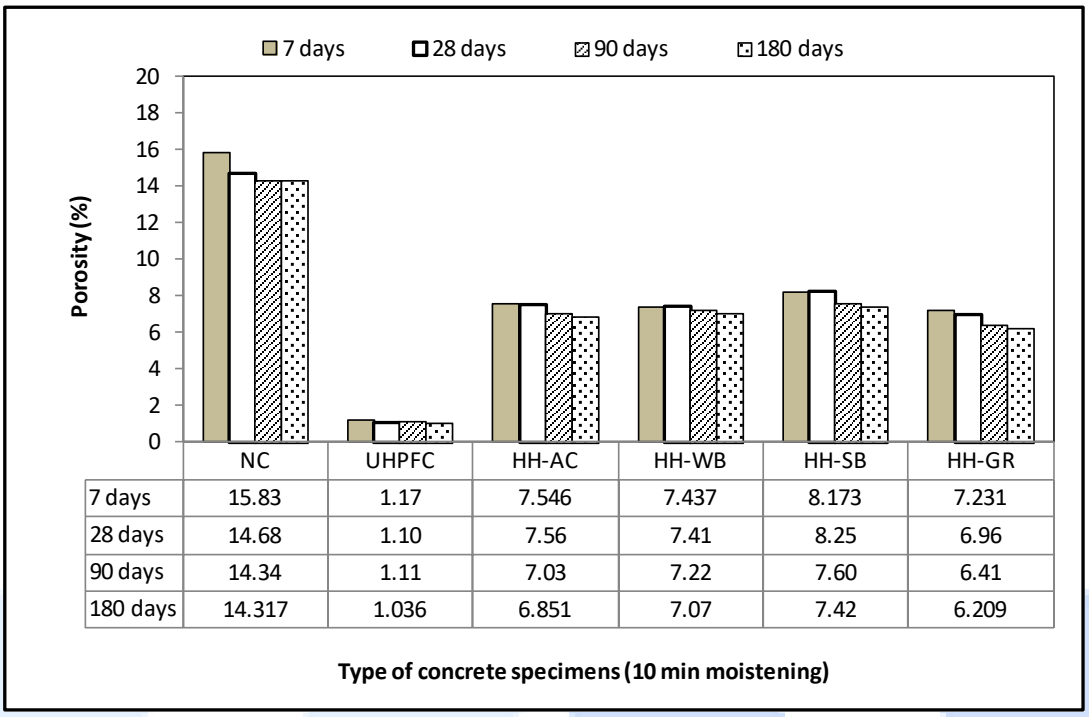

	NC	UHPFC	HH-AC	HH-WB	HH-SB	HH-GR
7 days	15.83	1.17	7.546	7.437	8.173	7.231
28 days	14.68	1.10	7.56	7.41	8.25	6.96
90 days	14.34	1.11	7.03	7.22	7.60	6.41
180 days	14.317	1.036	6.851	7.07	7.42	6.209

Figure 27. Comparison of the porosity test results between NC substrate, UHPFC and composite UHPFC/NC substrate (HH, 10 min moistening)

5. Conclusion

- The bond strength in the slant shear test and splitting tensile test was very strong, as the interfacial failure occurred after the damage of the NC substrate.
- The results of the pull-off test and flexural test showed that failure occurred in the substrates in all specimens at all test ages.
- The results of RCPT, gas permeability, water permeability and porosity tests confirmed that UHPFC has very low permeability.
- UHPFC improved the resistance of the NC substrate against the penetration of chloride and other aggressive fluids.
- The permeability behavior of OV bonded specimens was very close to that of monolithic UHPFC samples.
- The results showed that the substrate surface properties were required to ensure efficient bonding between concrete substrate surfaces and overlay materials.
- In this study, the sand-blasted method was demonstrated to be the most efficient technique.
- There is good correlation between the substrate roughness parameters and the splitting cylinder tensile test results and the slant shear test results.
- The SEM results proved that the use of UHPFC as a repair material can improve the microstructure of the interface zone

PACE-2023

The Second International Congress on the Phenomenological Aspects of Civil Engineering

Keynote

20-23 June 2023

Analysis of Silo Supporting Ring Beams Resting on Discrete Supports Using a Stiffness Criterion

Cem Topkaya[1,*], J. Michael Rotter[2], Özer Zeybek[3]

[1]*Professor, Department of Civil Engineering, Middle East Technical University, Ankara, Turkey*

[2]*Institute for Infrastructure and Environment, University of Edinburgh, EH9 3JL, Scotland, UK*

[3]*Department of Civil Engineering, Muğla Sıtkı Koçman University Muğla, Turkey*

Corresponding Author E-mail: ctopkaya@metu.edu.tr

Keywords

Silo,

Ring beam,

Discrete supports,

Vlasov theory,

Closed-form solution,

Cylindrical shell.

Abstract

Silos in the form of a cylindrical metal shell are often supported on a ring beam which rests on discrete column supports. The function of the ring beam is twofold. First, the ring beam is required to carry circumferential forces to maintain equilibrium at the transition junction between the cylinder and hopper. Second, the ring beam plays an important role in redistributing the majority of the discrete forces from the column supports into a more uniform stress state in the cylindrical wall. The Eurocode EN 1993-4-1 only provides design equations for stress resultants produced in the isolated ring beam under uniform transverse loading. This paper explores the extent to which a practical silo shell causes these stress resultants to be reduced when the ring beam has only practical stiffness. The behaviour of a ring beam which interacts with the silo shell is much more complex than that of an isolated ring beam. In traditional design treatments, it is assumed that the discrete support forces are redistributed entirely by the ring beam to provide circumferentially uniform axial membrane stresses in the silo shell. But this assumption is only even approximately valid if the ring beam is much stiffer than the silo shell. Since the cylindrical shell is very stiff in its own plane, the ring beam that is subject to flexure and twisting must be remarkably stiff to be stiffer than the shell. A ring beam stiffness ratio was previously developed by the authors to find the requirement for the ring beam stiffness to meet this traditional role. This paper presents a new study to explore the ring beam stress resultants when lower stiffness closed section ring beams of practical dimensions are used. A finite element parametric study is undertaken to explore the stress resultants and displacements in more flexible ring beams connected to a silo shell. The results show that the level of reduction from the isolated ring beam values can be directly related to the ring beam stiffness ratio.

PACE-2023

The Second International Congress on the Phenomenological Aspects of Civil Engineering

Keynote

20-23 June 2023

Behavior of Reinforced Concrete Columns and Buildings Under Seismic and Other Extreme Loads

Halil Sezen

Professor, Ohio State University, USA

Corresponding Author E-mail: sezen.1@osu.edu

Keywords

Important of reinforcement,

Kahramanmaras earthquakes,

Failure,

Lateral and gravity load.

Abstract

Major factors contributing to collapse of building structures under lateral and gravity loads will be presented. While the ductility and redundancy are critical for the transfer and redistribution of loads after the failure of a member, one of the main reasons for the collapse of buildings is insufficient design and detailing of columns. Shear failure and gravity load collapse of concrete columns with poor seismic details will be discussed. Experimental evidence from laboratory tests of columns and examples from the field (especially 2023 Kahramanmaras, Turkey earthquakes) will be shown to demonstrate the importance of reinforcement detailing in earthquake resistant design.

PACE-2023

The Second International Congress on the Phenomenological Aspects of Civil Engineering

Keynote

20-23 June 2023

Application of Hybrid Artificial Intelligence in Civil Engineering

Pijush Samui

Professor, Department of Civil Engineering, NIT Patna, INDIA;

Guest Professor, USTB Beijing; Title of Docent, Tampere University, INDIA

Corresponding Author E-mail: pijush.phd@gmail.com

Keywords

Machine learning,

Hybrid Model,

BIG Data.

Abstract

Need of Machine learning

Concept of Hybrid Model

Sample Application

Concept of BIG Data

Conclusion

1. Introduction

Outline of work:

- Need of Machine learning
- Concept of Hybrid Model
- Sample Application
- Concept of BIG Data
- Conclusion

2. Need of Machine Learning

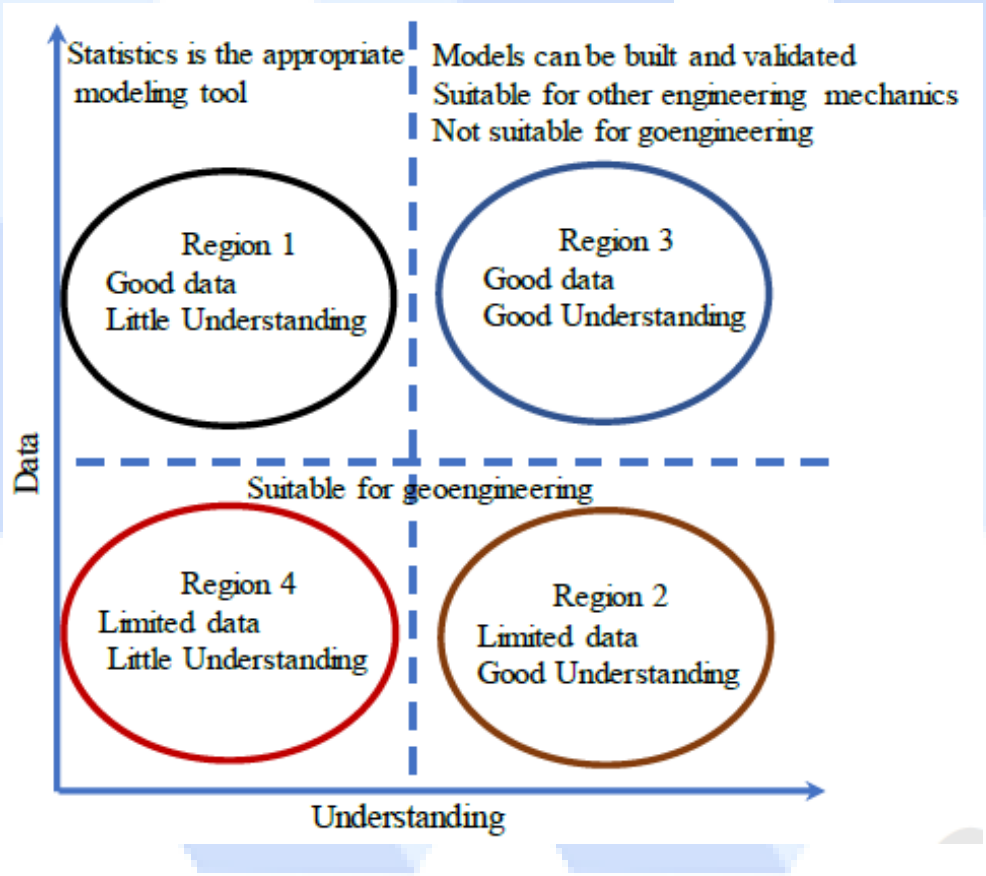

Figure 1. Data – Understanding (Holling-1978)

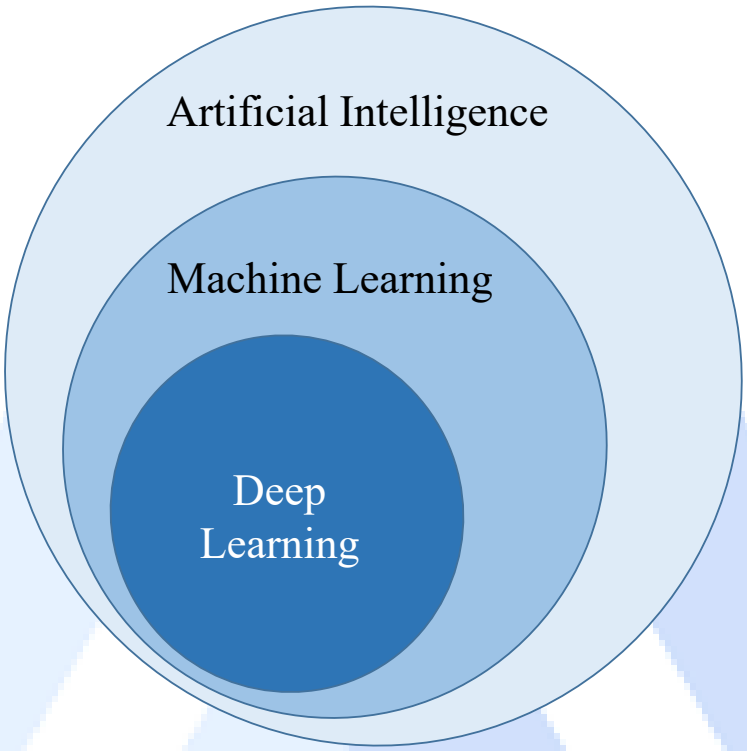

Figure 2. Learning

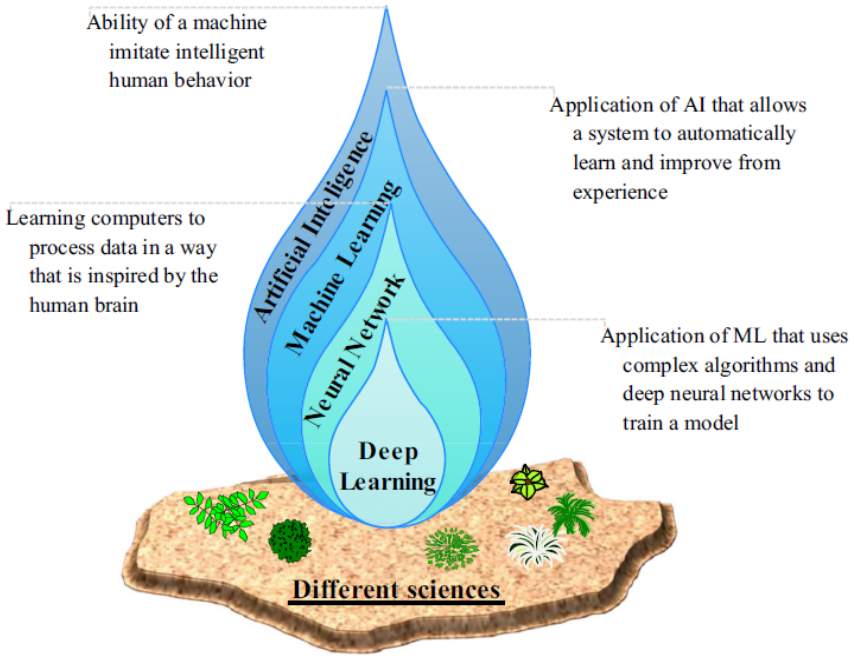

Figure 3. Different Sciences

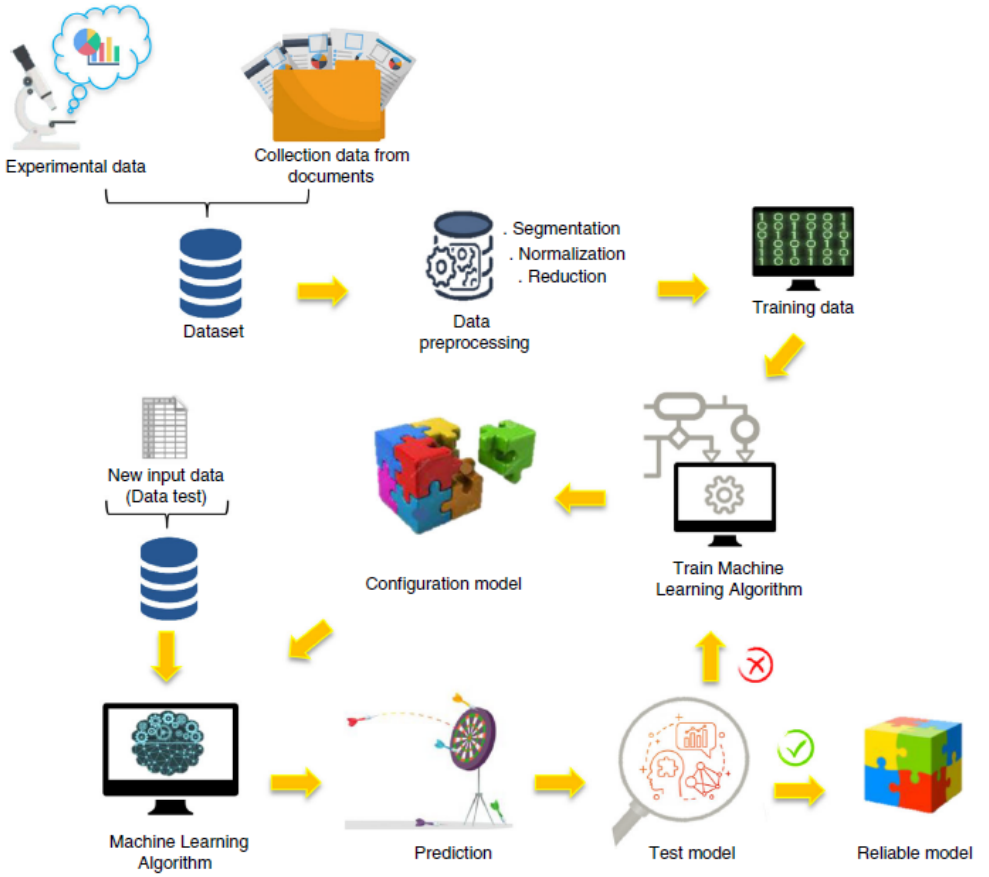

Figure 4. Data

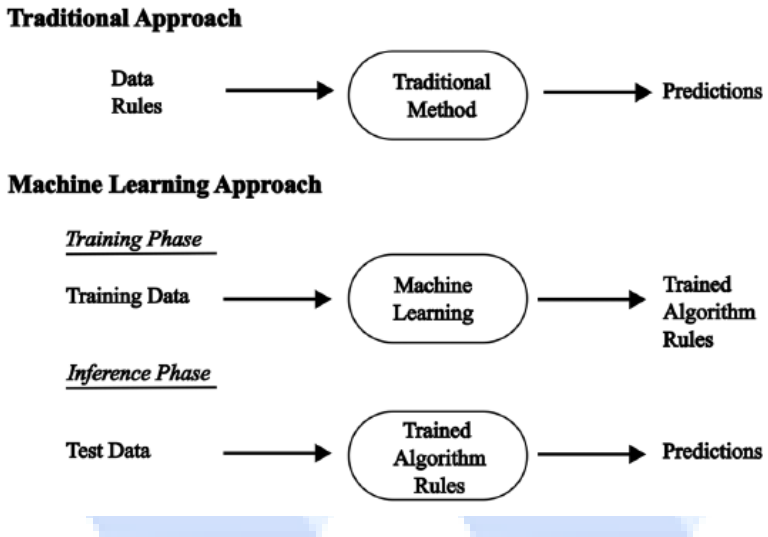

Figure 5. Difference between traditional methods and ML

2.1. Supervised machine learning

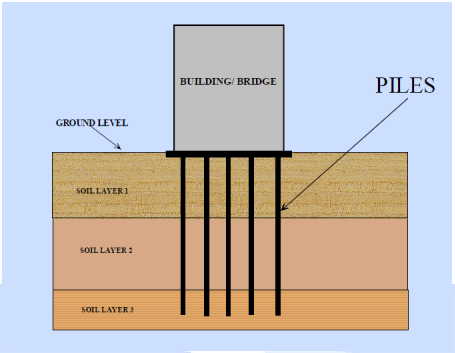

Figure 6. Supervised machine learning

Table1.

L(m)	D (cm)	σ_{vo} (kPa)	σ'_{vo} (kPa)	F_a(kPa)
14.1	15	96	26	27
13	15	102	15	26
11.7	20	54	23	14
17.5	14.3	87	23	26
15.9	15	49	17	12
8.1	13.5	37	13	11
7.7	16.5	32	15	9
10	13.5	33	10	12
12	15.5	39	12	10
10.2	22	19	15	8
24.2	15	146	19	29
17.1	15	109	57	24
12.7	23.2	38	19	17
10	17	82	36	28
14.3	26	89	22	22
22.5	47	60	45	23
5.5	30.5	44	30	38
19.2	61	142	31	30.2
15.2	35.6	448	104	109.2
15.2	35.6	718	162	162

Table 2.

Name	Description	Advantages	Disadvantages
Random forest 	• A group of decision trees. Each tree is a hierarchy of decisions which divide samples into two groups depending on the value of a single feature at a time	• Less susceptible to noise • Can handle large numbers of training samples	• A decision tree's disadvantage is high variance in its results, however random forests solve this problem by averaging many trees. The drawback: as you average many decision trees, it might be hard to interpret the results • Slower than other methods in the testing phase
Gradient boosting 	• Similar to random forests, but trains each tree sequentially. The samples which have the highest uncertainty according to the results of the previous iteration are prioritized	• Studies suggest it can be more accurate than random forests	• It is more challenging to train the algorithm
Support vector Machine	• Uses kernel functions (a class of algorithms used for pattern analysis) to describe the nonlinear	More suitable for situations with limited reference points	• Computational complexity when there is a large training set

	differences between training samples	• Can easily handle large numbers of input features • Can learn non-linear relations between features	• Sensitive to noisy data
Naive Bayes	• A graphical model describing the probabilistic relations between feature values and class labels	• Simple to implement • Scales easily • Feature importance is easy to interpret	• Assumes all features to be independent from each other, which is often not the case in real-world applications

2.2. Unsupervised Machine Learning

Figure 7. Liquefaction Damage, Adapazari, Turkey, 1999

Table 3.

Z(m)	$(N_1)_{60}$	FC	σ_{vo} (kPa)	σ'_{vo} (kPa)	amax (g)	Mw
1	6	90	16.3	14	0.4	7.4
1.8	8	94	30.9	20.6	0.4	7.4
2.6	7	100	45.6	27.3	0.4	7.4
3.4	5	87	60.3	34	0.4	7.4
4.2	5	74	75.8	41.5	0.4	7.4
5	3	92	90.1	47.8	0.4	7.4
6	3	97	108.2	55.9	0.4	7.4
7	19	70	127.9	65.6	0.4	7.4
8	26	58	147.5	75.2	0.4	7.4
1	3	74	18	15.8	0.4	7.4
1.8	5	86	32.8	22.6	0.4	7.4
3.4	2	85	62.4	36.2	0.4	7.4
4.2	10	93	77.4	43.2	0.4	7.4

6	4	99	109.5	57.3	0.4	7.4

Table 4.

Name	Description	Advantages	Disadvantages
K-means clustering 	• A clustering technique which iteratively calculates the "average value" (e.g., centroid) of each cluster and assigns each sample to the nearest cluster	• Simple implementation, performs well • Distance metric can be defined by the user	• User must define number of classes
Principal component Analysis 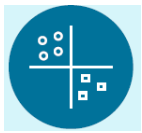	• Transforms the data to features which maximize the variance (differences) between samples	• Can be used to retain the relevant information while decreasing data dimensionality	• Resulting features are difficult to interpret
t-SNE 	• Nonlinear data dimensionality reduction technique suitable for visualization purposes	• Helps understand patterns by visualizing similar groups • Captures complex similarities	• Sensitive to hyperparameters • Computational complexity

2..3. Landslide/Slope failure

Stability(s) of slope depends on the following parameter:

- Slope angle(b)
- Height of slope(H)
- Cohesion(c)
- Unit weight of soil(g)
- Pore water pressure coefficient(ru)
- Angle of internal friction(f)

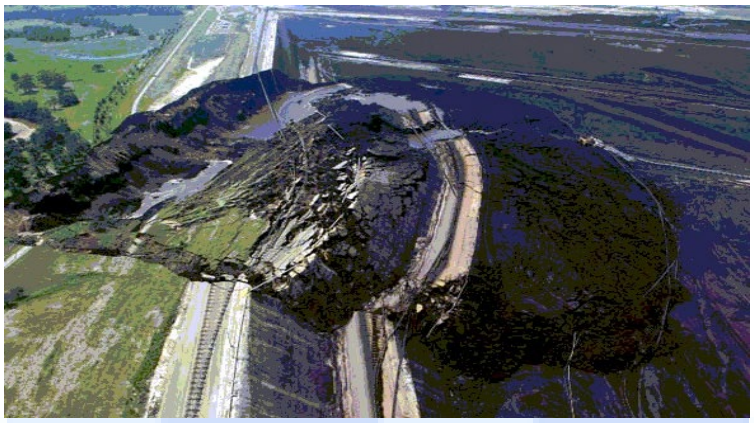

Figure 8. Slope failure in Australia

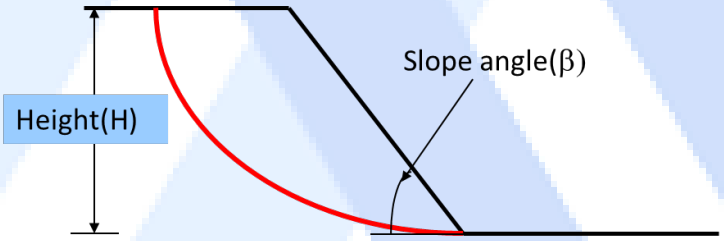

Figure 9.

2.4. Support Vector Machine(SVM)

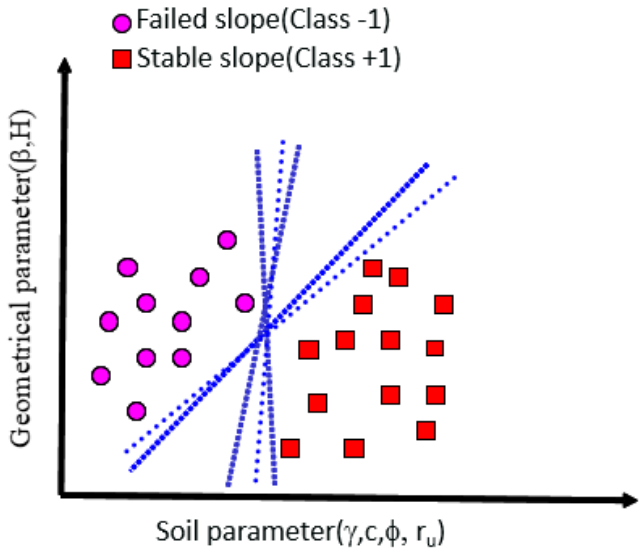

Figure 10.

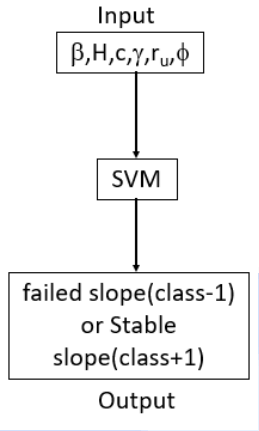

Figure 11. Failed and Stable Slope

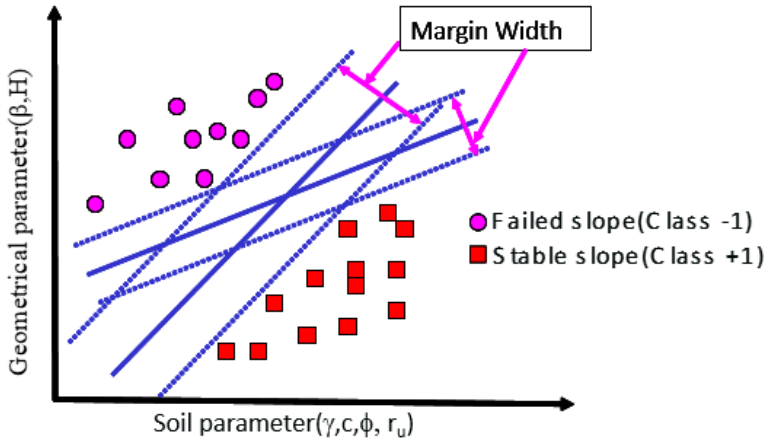

Figure 12. SVM: maximizing the margin (Samui, 2008 in Enviromental Geology)

2.5. Formulation of SVM for slope stability

Training vector:

$D = \{(x^1, y^1), \dots, (x^1, y^1)\}$ $y \in \{-1,1\}$ -1: Failed slope

+1: Stable slope

x= [β, H, c,γ, r_u, ϕ]

A Linear hyperplane:

f(x) = w.x + b = 0

w = an adjustable weight vector and b =scalar threshold.

A separating hyperplane can be defined for the two classes as

w. x_i + b ≥ 1 For y_i= 1

$$y_i(w.x_i + b) \geq 1 - \varepsilon_i$$ ε_i = Slack variable

w. x_i+ b ≤ 1 For y_i= -1

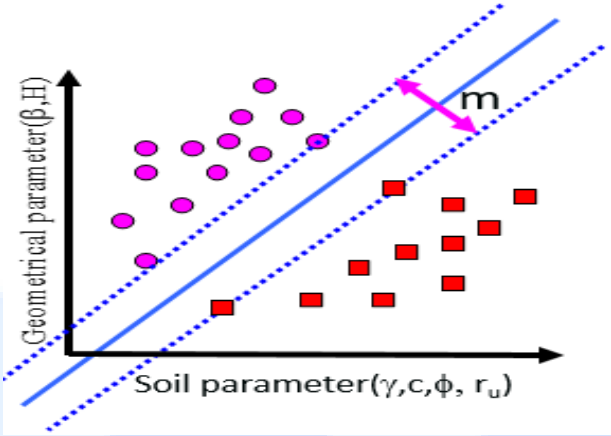

Figure 13. Optimization problem

$m = \frac{2}{|w|}$

Minimize: $\frac{1}{2}|w|^2 + C\sum_{i=1}^{1}\varepsilon_i$

Subjected to: $y_i(w.\ x_i + b\ ) \geq 1 - \varepsilon_i$

2.6. Details of SVM

12 from Australia, 8 from UK, 8 from China, 6 from Canada, 5 from India, 3 from USA, 1 from Japan, 1 from France, 1 from Spain, 1 from Greece, 1 from Italy

Input=x={β,H,c,γ,r_u,ϕ}

Output=y={+1(stable slope), -1(failed slope)}

Training dataset: This is required to construct the model. In this study, 23 out of the 32 data are considered for training dataset.

Testing dataset: This is required to estimate the model performance. The remaining 9 data is considered as testing dataset.

2.7. Equation for stability(s) determination of slope

S = sign $(\sum_{i=1}^{23}\alpha_i y_i K(x_i.x))$

K (x_i ,x) is kernel function(spline). Sign is signum function. It gives +1(stable slope) if the element is greater than or equal to zero and -1(failed slope) if it is less than zero. a_k Lagrange multipliers.

This equation has been used on the remaining 15 datasets and it has been shown that only one data has been misclassified

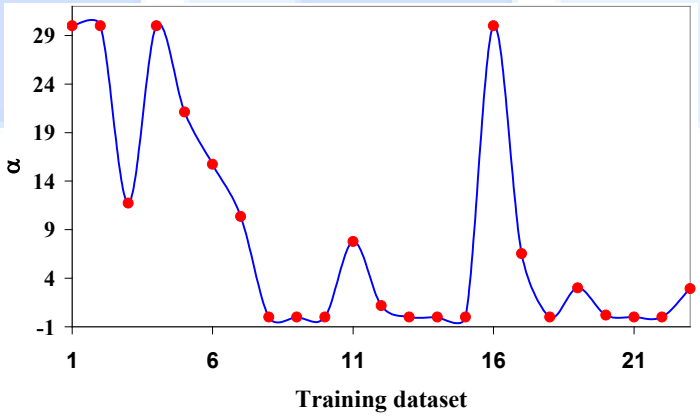

Figure 14. α – Training dataset Diagram (Samui, 2012- in Geomatics, Natural Hazards and Risk)

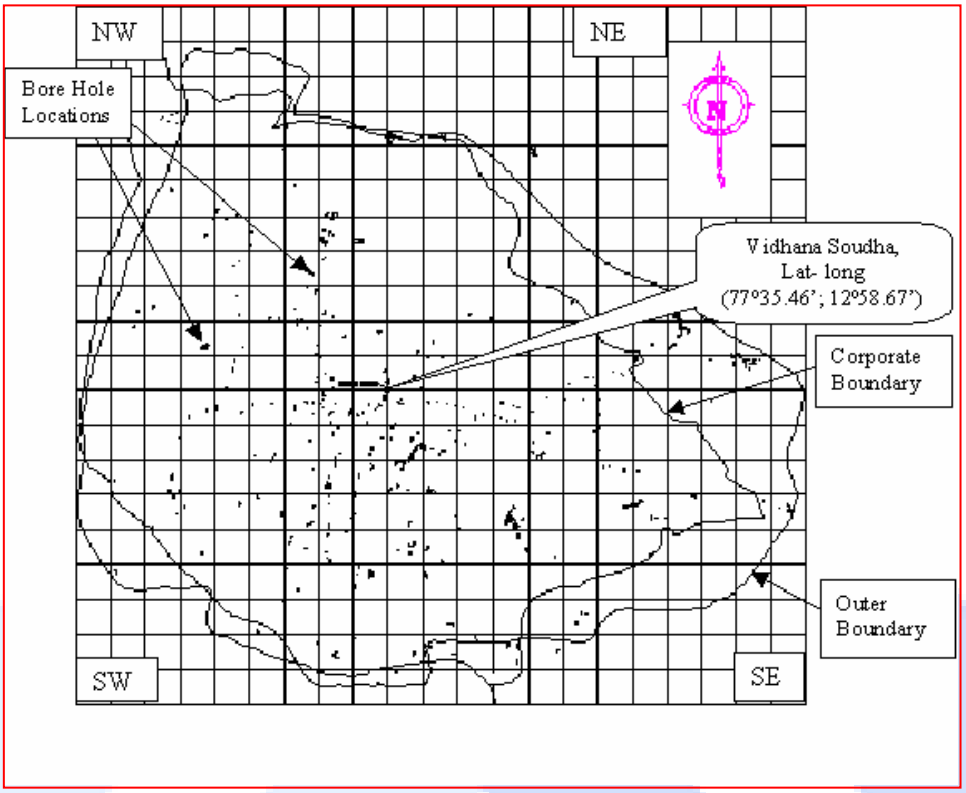

Figure 15. Site characterization of Bangalore

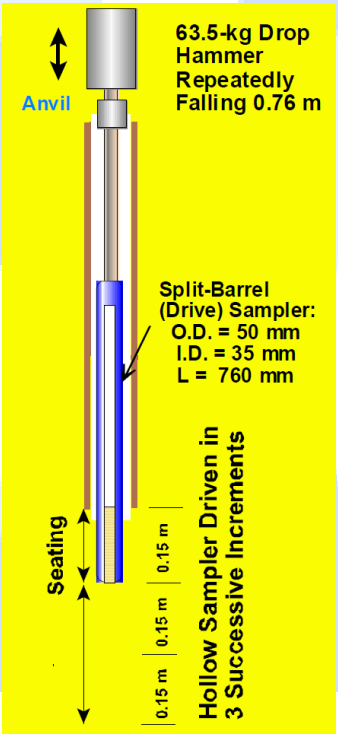

Figure 16. SPT(N)

Function N = f(X, Y, Z) is approximated with which N value at any half-space point in Bangalore can be determined.

2.7. Database

- Integrated with Digitized Bangalore map having around 12 layers of information on scale of 1:20000
- 766 boreholes located on GIS.
- Creation of datasheets with maximum geotechnical data for all 766 boreholes.
- Developed 3-D views of boreholes with geotechnical data attached at every 0.5m interval.
- Linking of data in 2-D view for standard reporting of bore log information.

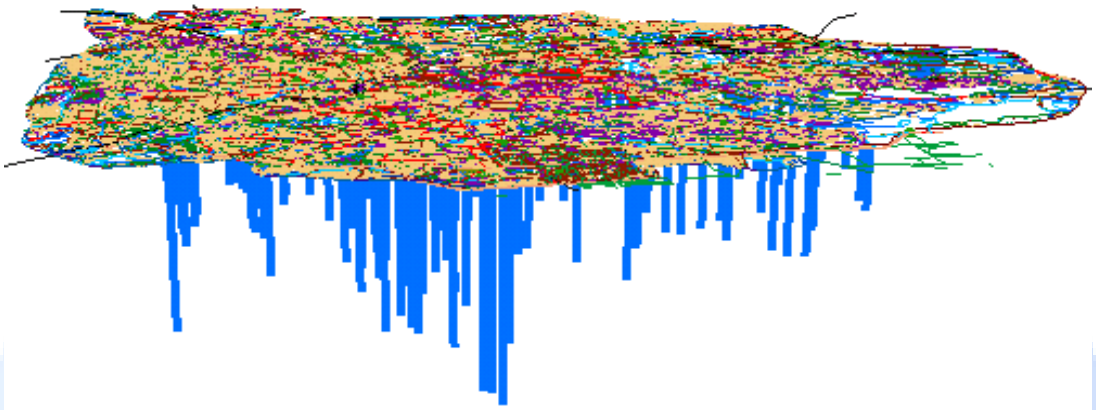

Figure 17. Database

2.8. Artificial Neural Network

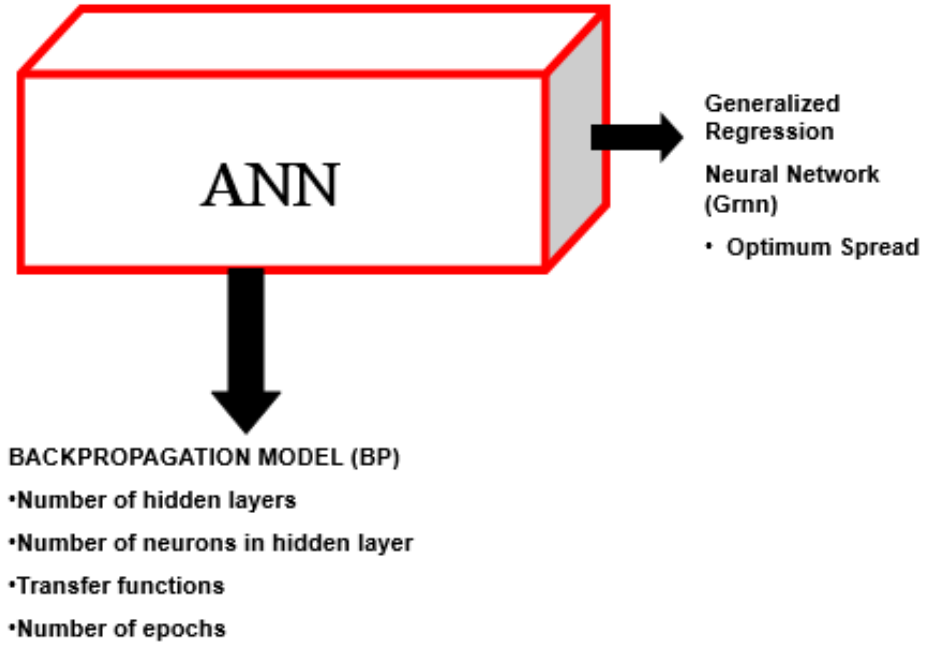

Figure 18. Artificial neural network

I. Backpropagation(BP) Model –Data division and Normalization

- Levenberg-Marquardt Algorithm
- Training Dataset: 2722 SPT values (90% of total boreholes – 689 / 767)
- Testing Dataset:293 SPT values (10% of total boreholes)
- Normalized the data against their maximum values
- Four-layer feed forward network
- Transfer function of First hidden layer: Tansig (-1 to +1)
- Transfer function of second hidden layer: Logsig (0-1)
- Transfer function of output layer: Logsig
- Epochs= 3000

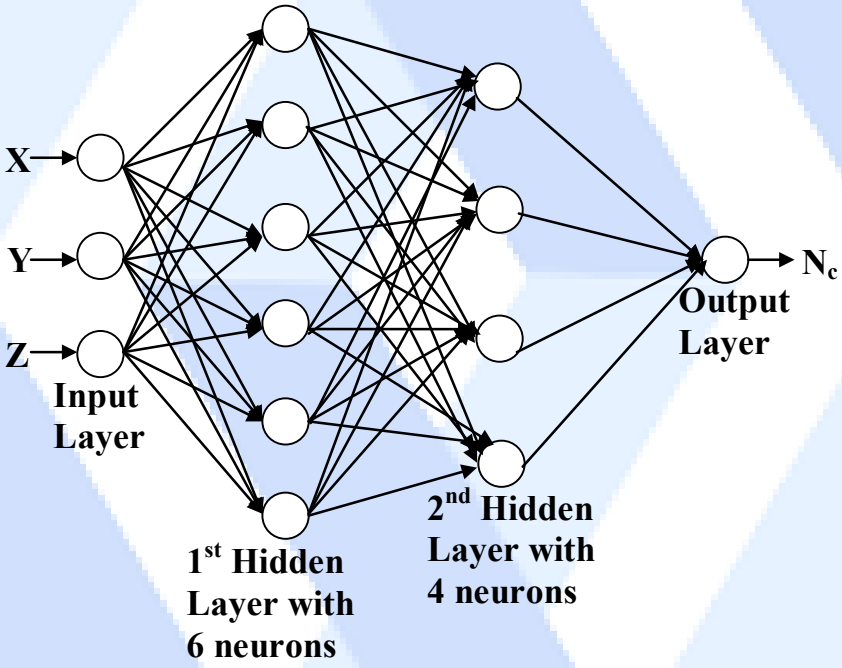

Figure 19. BP Architecture

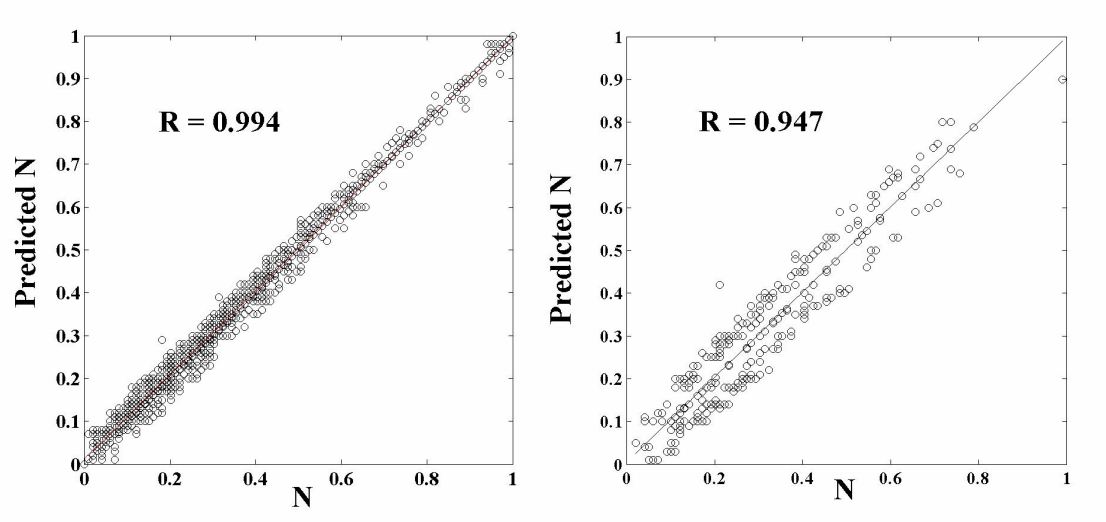

a) Training Dataset -2722 data points

b) Testing Dataset -293 data points

Figure 20. Performance of BP

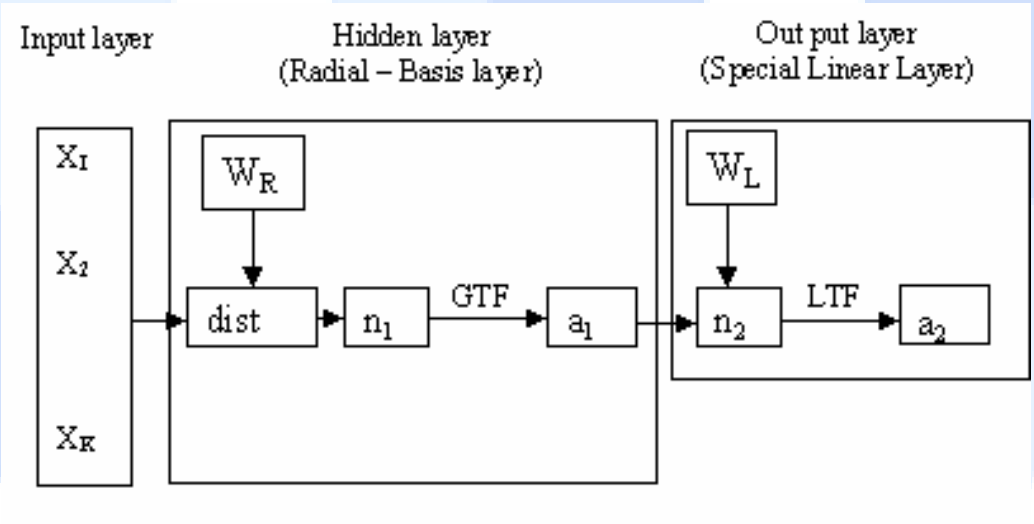

Figure 21. Generalized Regression Neural Network(GRNN)

Same training dataset, testing dataset and normalization technique

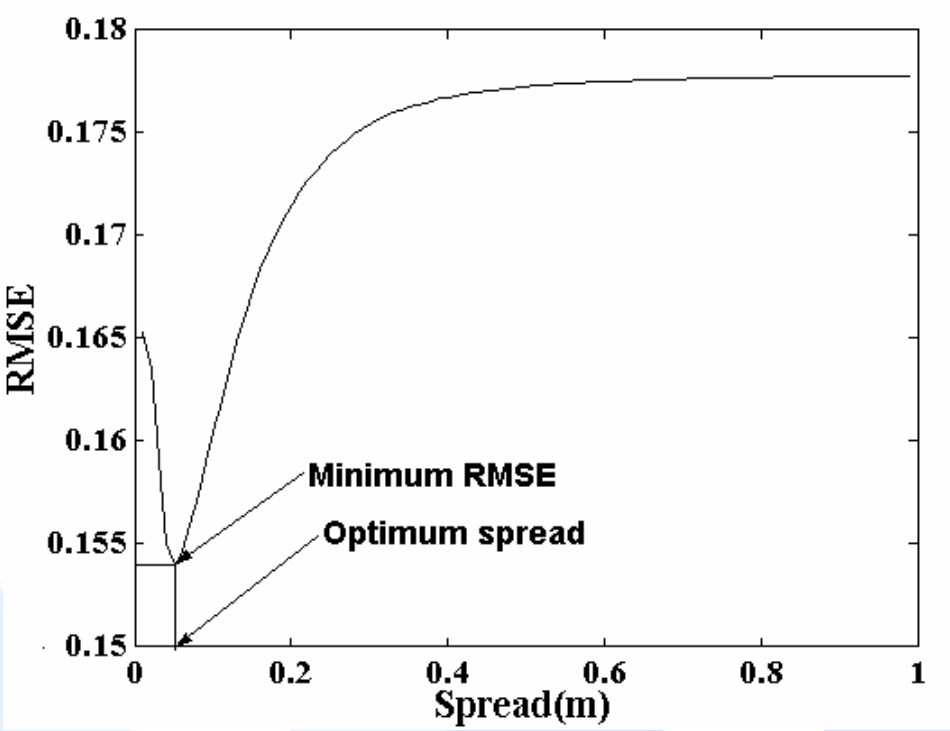

Figure 22. Optimum Spread

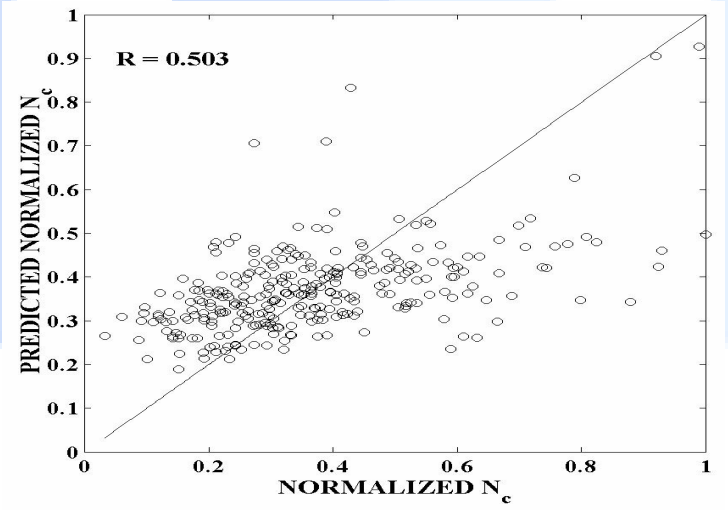

Figure 23. Performance of GRNN

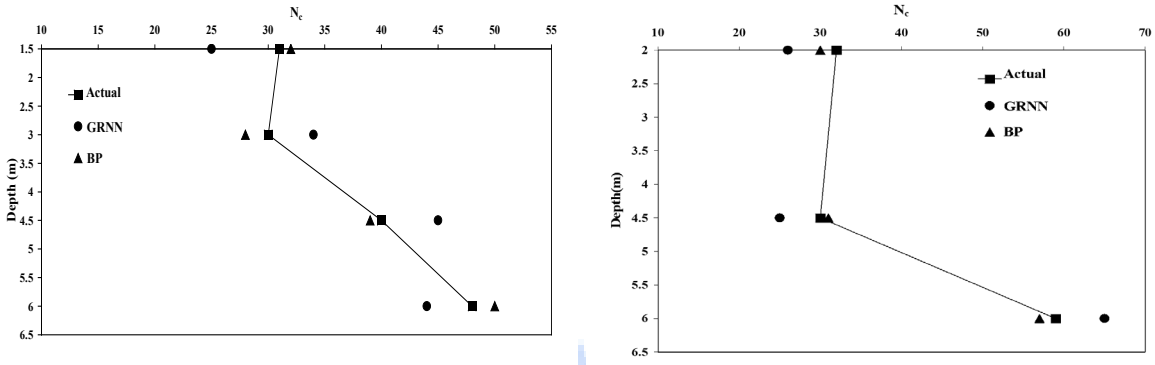

BH 71-1 BH 276-2

Figure 24. Predicted N_c for bore logs

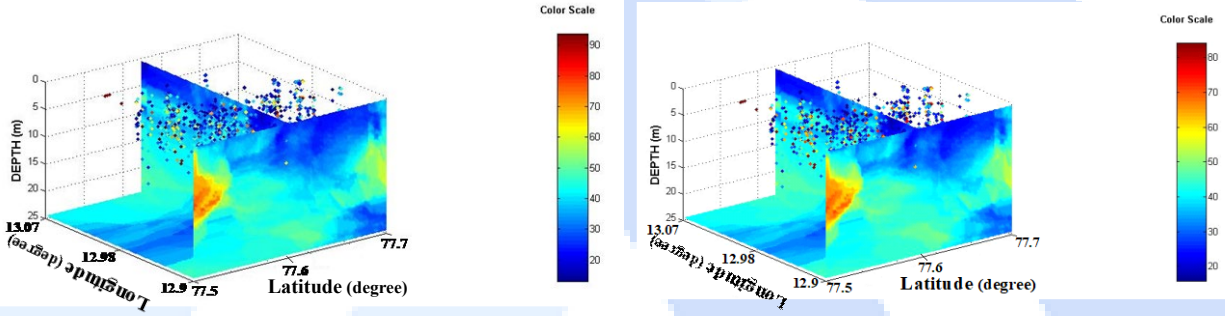

BP GRNN

Figure 25. Spatial and depth variation of N value

2.9. Limitation of classical optimization algorithms

It does not give suitable solution for large problem.

3. Concept of Hybrid ML

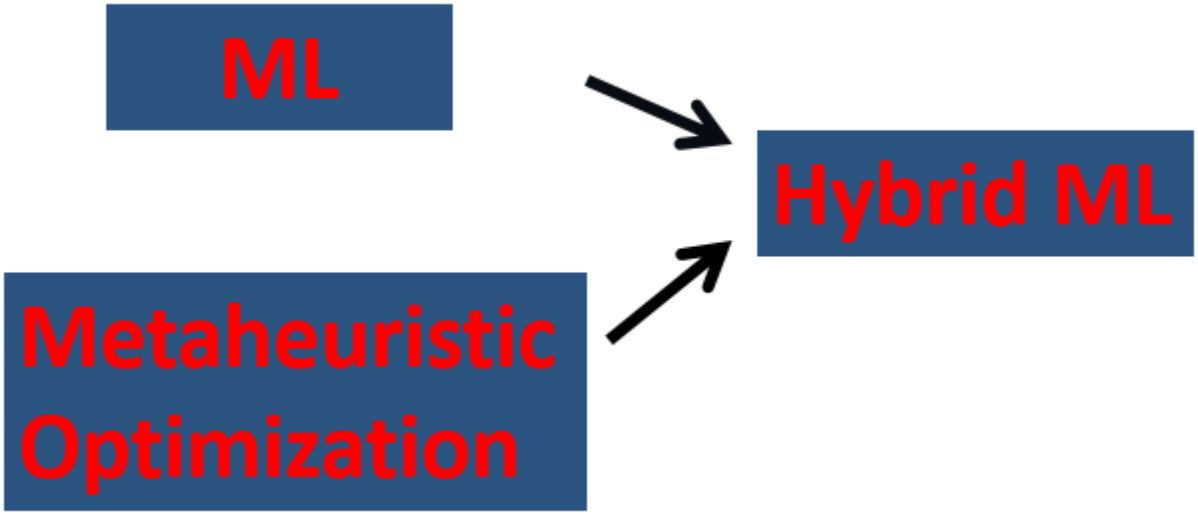

3.1. Choice of Algorithms

For a given type of problem, what is the best algorithm to use?

For a given algorithm, what kinds of problems can it solve?

3.2. Nature-Inspired Metaheuristics

Heuristics are techniques which seek good (near-optimal) solutions at a reasonable computational cost without being able to guarantee either feasibility or optimality, or even in many cases to state how close to optimality a particular feasible solution is." (Russell and Norvig,1995)

3.2.1. Components of Metaheuristic Algorithms

Exploitation: To focus on the search in a local region by exploiting the information that a current good solution is found in this region

Exploration: To generate diverse solutions so as to explore the search space on a global scale

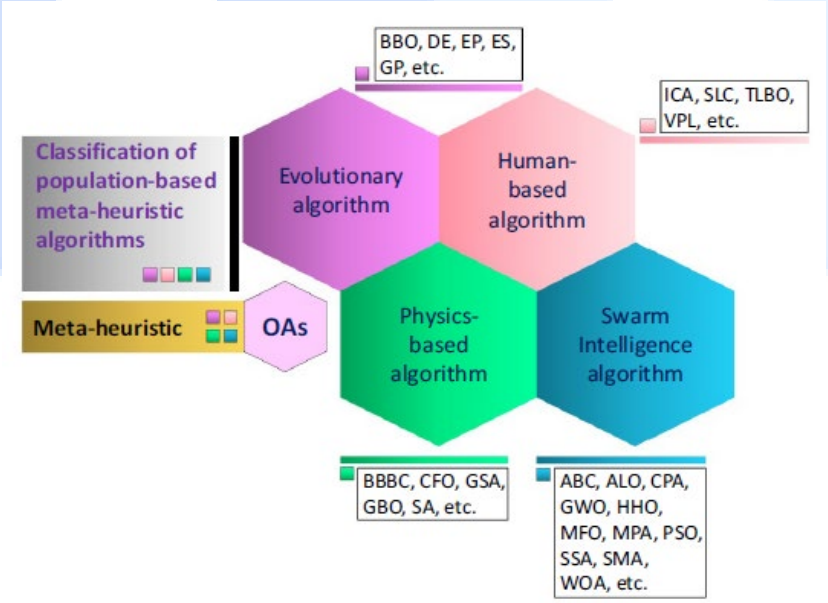

Figure 26. Classification of metaheuristic OA

4. Sample Application

4.1. Estimating Soil Compression Index

4.1.1. Study Area

A sum of 700 odometer test results was acquired from the mentioned section for predicting soil Cc. Besides consolidation test data, sub-soil data, grain size analysis results, plasticity characteristics, and other basic soil parameters were also collected.

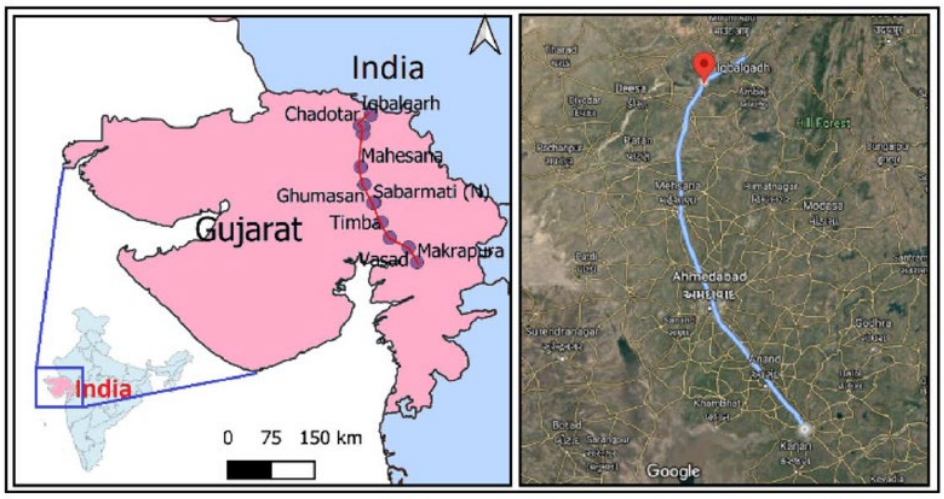

Figure 27. Study area

Table 5. Soil parameters

Parameters and description		Statistical particulars						
		Min	Avg	Max	Stnd. error	Stnd. dev	Kurtosis	Skewness
D	Depth of soil samples (m)	0.50	7.48	32.75	0.21	5.55	1.48	1.18
G	Gravel content (%)	0.00	3.42	18.00	0.14	3.67	1.58	1.32
CS	Coarse sand content (%)	0.00	2.15	11.00	0.07	1.89	2.35	1.21
MS	Medium sand content (%)	0.00	3.90	25.00	0.13	3.41	7.18	2.21
FS	Fine sand content (%)	1.00	26.40	62.00	0.47	12.45	-0.42	0.45
S	Total sand content (%)	3.00	32.45	68.00	0.46	12.24	-0.49	0.13
M	Silt content (%)	19.00	48.01	75.00	0.36	9.65	0.15	0.26
C	Clay content (%)	5.00	16.11	37.00	0.19	4.99	0.05	0.45
M&C	Silt and clay content (%)	28.00	64.13	97.00	0.46	12.28	-0.39	0.03
BD	Bulk density (gm/cm^3)	1.61	1.80	1.99	0.00	0.07	-0.30	0.15
DD	Dry density (gm/cm3)	1.46	1.59	1.71	0.00	0.05	0.12	-0.06
G_S	Sp. Gravity (-)	2.64	2.67	2.70	0.00	0.01	0.07	-0.08

LL	Liquid limit (%)	22.00	32.86	49.00	0.17	4.39	0.57	0.69
PL	Plastic limit (%)	12.00	18.84	26.00	0.07	1.76	1.97	-0.55
C_C	Compression index (-)	0.0700	0.1208	0.1676	0.0007	0.0198	0.1321	-0.4492

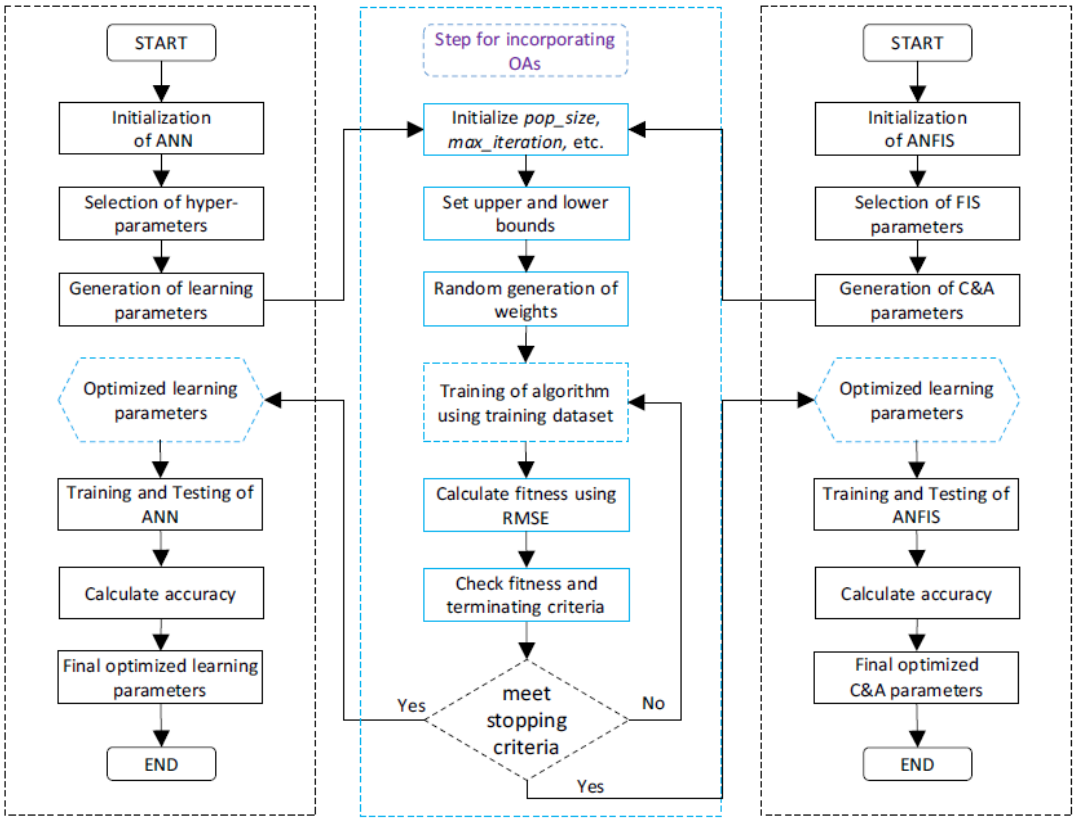

Figure 28. Flow chart

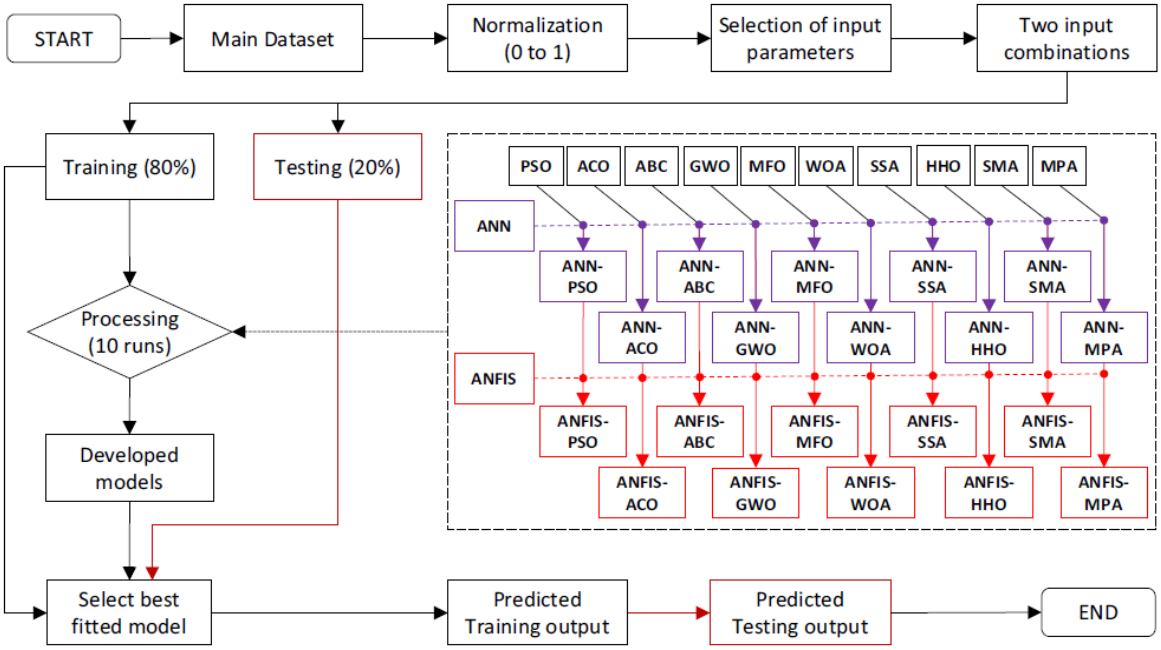

Figure 29. Date Processing & Model Development

4.2. Performance Parameters

$$NS = 1 - \frac{\sum_{i=1}^{n}(y_i - \hat{y}_i)^2}{\sum_{i=1}^{n}(y_i - y_{mean})^2}$$

$$R^2 = \frac{\sum_{i=1}^{n}(y_i - y_{mean})^2 - \sum_{i=1}^{n}(y_i - \hat{y}_i)^2}{\sum_{i=1}^{n}(y_i - y_{mean})^2}$$

$$PI = adj.R^2 + 0.01VAF - RMSE$$

$$WI = 1 - \left[\frac{\sum_{i=1}^{n}(y_i - \hat{y}_i)^2}{\sum_{i=1}^{n}\{|\hat{y}_i - y_{mean}| + |y_i - y_{mean}|\}^2}\right]$$

$$MAE = \frac{1}{n}\sum_{i=1}^{n}\left|(\hat{y}_i - y_i)\right|$$

$$RSR = \frac{RMSE}{\sqrt{\frac{1}{n}\sum_{i=1}^{n}(y_i - y_{mean})^2}}$$

$$RMSE = \sqrt{\frac{1}{n}\sum_{i=1}^{n}(y_i - \hat{y}_i)^2}$$

$$WMAPE = \frac{\sum_{i=1}^{n}\left|\frac{y_i - \hat{y}_i}{y_i}\right| \times y_i}{\sum_{i=1}^{n} y_i}$$

Models/Particulars		NS	R^2	PI	WI	MAE	RSR	RMSE	WMAPE	Total score
ANN-PSO	Value	0.8182	0.8489	1.5727	0.9574	0.0609	0.4263	0.0852	0.1115	19
	Score	2	3	2	2	3	2	2	3	
ANN-ACO	Value	0.9350	0.9374	1.8173	0.9837	0.0387	0.2550	0.0510	0.0704	54
	Score	7	7	7	7	6	7	7	6	
ANN-ABC	Value	0.7111	0.7560	1.3574	0.9268	0.0822	0.5375	0.1075	0.1484	8
	Score	1	1	1	1	1	1	1	1	
ANN-GWO	Value	**0.9500**	**0.9563**	**1.8594**	**0.9880**	**0.0324**	**0.2237**	**0.0447**	**0.0592**	**80**
	Score	**10**	**10**	**10**	**10**	**10**	**10**	**10**	**10**	
ANN-MFO	Value	0.8955	0.9105	1.7360	0.9752	0.0484	0.3233	0.0646	0.0889	32
	Score	4	4	4	4	4	4	4	4	
ANN-WOA	Value	0.9311	0.9331	1.8085	0.9823	0.0386	0.2626	0.0525	0.0696	44
	Score	5	5	5	5	7	5	5	7	
ANN-SSA	Value	0.9355	0.9403	1.8214	0.9842	0.0371	0.2540	0.0508	0.0683	64
	Score	8	8	8	8	8	8	8	8	
ANN-HHO	Value	0.8384	0.8439	1.5911	0.9578	0.0641	0.4020	0.0804	0.1180	21
	Score	3	2	3	3	2	3	3	2	
ANN-SMA	Value	0.9331	0.9365	1.8150	0.9832	0.0405	0.2586	0.0517	0.0729	46
	Score	6	6	6	6	5	6	6	5	
ANN-MPA	Value	0.9453	0.9519	1.8488	0.9868	0.0345	0.2339	0.0468	0.0639	72
	Score	9	9	9	9	9	9	9	9	

Figure 30. Testing Performance of ANN

Models/Particulars		NS	R^2	PI	WI	MAE	RSR	RMSE	WMAPE	Total score
ANN-PSO	Value	0.8182	0.8489	1.5727	0.9574	0.0609	0.4263	0.0852	0.1115	19
	Score	2	3	2	2	3	2	2	3	
ANN-ACO	Value	0.9350	0.9374	1.8173	0.9837	0.0387	0.2550	0.0510	0.0704	54
	Score	7	7	7	7	6	7	7	6	
ANN-ABC	Value	0.7111	0.7560	1.3574	0.9268	0.0822	0.5375	0.1075	0.1484	8
	Score	1	1	1	1	1	1	1	1	
ANN-GWO	Value	**0.9500**	**0.9563**	**1.8594**	**0.9880**	**0.0324**	**0.2237**	**0.0447**	**0.0592**	**80**
	Score	**10**	**10**	**10**	**10**	**10**	**10**	**10**	**10**	
ANN-MFO	Value	0.8955	0.9105	1.7360	0.9752	0.0484	0.3233	0.0646	0.0889	32
	Score	4	4	4	4	4	4	4	4	
ANN-WOA	Value	0.9311	0.9331	1.8085	0.9823	0.0386	0.2626	0.0525	0.0696	44
	Score	5	5	5	5	7	5	5	7	
ANN-SSA	Value	0.9355	0.9403	1.8214	0.9842	0.0371	0.2540	0.0508	0.0683	64
	Score	8	8	8	8	8	8	8	8	
ANN-HHO	Value	0.8384	0.8439	1.5911	0.9578	0.0641	0.4020	0.0804	0.1180	21
	Score	3	2	3	3	2	3	3	2	
ANN-SMA	Value	0.9331	0.9365	1.8150	0.9832	0.0405	0.2586	0.0517	0.0729	46
	Score	6	6	6	6	5	6	6	5	
ANN-MPA	Value	0.9453	0.9519	1.8488	0.9868	0.0345	0.2339	0.0468	0.0639	72
	Score	9	9	9	9	9	9	9	9	

Figure 31. Testing Performance of ANN

Models/Particulars		NS	R^2	PI	WI	MAE	RSR	RMSE	WMAPE	Total score
ANFIS-PSO	Value	**0.9700**	**0.9698**	**1.9039**	**0.9924**	**0.0217**	**0.1732**	**0.0353**	**0.0396**	**80**
	Score	**10**	**10**	**10**	**10**	**10**	**10**	**10**	**10**	
ANFIS-ACO	Value	0.9095	0.9257	1.7722	0.9726	0.0426	0.3009	0.0613	0.0768	34
	Score	3	6	5	3	5	3	3	6	
ANFIS-ABC	Value	0.8967	0.8975	1.7279	0.9718	0.0485	0.3214	0.0655	0.0894	12
	Score	2	1	1	2	1	2	2	1	
ANFIS-GWO	Value	0.8923	0.9074	1.7305	0.9670	0.0465	0.3282	0.0669	0.0833	12
	Score	1	2	2	1	2	1	1	2	
ANFIS-MFO	Value	0.9295	0.9315	1.8056	0.9823	0.0395	0.2656	0.0541	0.0725	56
	Score	7	7	7	7	7	7	7	7	
ANFIS-WOA	Value	0.9333	0.9330	1.8121	0.9827	0.0374	0.2582	0.0526	0.0685	65
	Score	8	8	8	9	8	8	8	8	
ANFIS-SSA	Value	0.9148	0.9145	1.7678	0.9769	0.0433	0.2919	0.0595	0.0790	30
	Score	4	3	3	4	4	4	4	4	
ANFIS-HHO	Value	0.9215	0.9213	1.7840	0.9796	0.0421	0.2801	0.0571	0.0770	46
	Score	6	5	6	6	6	6	6	5	
ANFIS-SMA	Value	0.9158	0.9152	1.7699	0.9775	0.0436	0.2902	0.0591	0.0798	34
	Score	5	4	4	5	3	5	5	3	
ANFIS-MPA	Value	0.9342	0.9342	1.8147	0.9824	0.0348	0.2566	0.0523	0.0631	71
	Score	9	9	9	8	9	9	9	9	

Figure 32. Training Performance of ANFIS

Models/Particulars		NS	R^2	PI	WI	MAE	RSR	RMSE	WMAPE	Total score
ANFIS-PSO	Value	**0.9635**	**0.9667**	**1.8906**	**0.9911**	**0.0265**	**0.1911**	**0.0382**	**0.0477**	**80**
	Score	**10**	**10**	**10**	**10**	**10**	**10**	**10**	**10**	
ANFIS-ACO	Value	0.9444	0.9497	1.8438	0.9865	0.0313	0.2359	0.0472	0.0572	65
	Score	8	7	8	8	9	8	8	9	
ANFIS-ABC	Value	0.9238	0.9284	1.7928	0.9811	0.0428	0.2760	0.0552	0.0781	9
	Score	1	1	1	2	1	1	1	1	
ANFIS-GWO	Value	0.9276	0.9372	1.8095	0.9794	0.0403	0.2691	0.0538	0.0718	15
	Score	2	2	2	1	2	2	2	2	
ANFIS-MFO	Value	0.9409	0.9488	1.8376	0.9859	0.0359	0.2431	0.0486	0.0658	48
	Score	6	6	6	6	6	6	6	6	
ANFIS-WOA	Value	0.9428	0.9502	1.8429	0.9863	0.0346	0.2393	0.0478	0.0633	57
	Score	7	8	7	7	7	7	7	7	
ANFIS-SSA	Value	0.9370	0.9408	1.8259	0.9842	0.0386	0.2509	0.0502	0.0705	35
	Score	5	4	4	4	4	5	5	4	
ANFIS-HHO	Value	0.9369	0.9426	1.8272	0.9845	0.0369	0.2512	0.0502	0.0676	37
	Score	4	5	5	5	5	4	4	5	
ANFIS-SMA	Value	0.9341	0.9405	1.8214	0.9839	0.0389	0.2567	0.0513	0.0713	24
	Score	3	3	3	3	3	3	3	3	
ANFIS-MPA	Value	0.9536	0.9575	1.8675	0.9885	0.0325	0.2153	0.0431	0.0592	70
	Score	9	9	9	9	8	9	9	8	

Figure 33. Training Performance of ANFIS

5. Concept of BIG Data

Data that is too large or too complex to be managed using traditional data processing, analysis, and storage techniques.

Volume
The amount of data

Variety
The types of data

Velocity
The frequency of data

Veracity
The quality of data

Figure 34. Prediction of Earthquake Magnitude using BIG Data (Cortes et al, 2-18, in Computer and Geoscience)

6. Conclusion

- ✓ The performance of ML is data specific
- ✓ The result of ML should be analyzed thoroughly and decision should be taken based on practical experience
- ✓ ML models can reduce the cost of project

ORAL PRESENTATIONS

PACE-2023
International Congress on the Phenomenological Aspects of Civil Engineering

PACE-2023
International Congress on Phenomenological Aspects in Civil Engineering

Research Article
20-23June 2023

Micro Friction and Adhesion Behavior of Coral Sands From South China Sea

Ji Zhou*,[1,2], Zhenyu Zhao[1,2], Zhengyu Fan[1,2], Yanhuai Ding*,[1,2]
[1]College of Civil and Environmental Engineering, Hunan University of Science and Engineering, Yongzhou, 425199, China
[2]School of Civil Engineering, Xiangtan University, Hunan 411105, China
Corresponding Author E-mail: hnkjxy_zhouji@163.com, yhding@xtu.edu.cn

Keywords

Coral sand,
Micro friction behavior,
South China Sea,
Interaction,
Particle-modified AFM tip.

Abstract

The investigation on the physical properties of coral sands is very important for their transportation and application. Here the micro friction and adhesion behavior of coral sands from South-China-Sea was investigated by atomic force microscopy (AFM). Variation of the friction coefficient was experimentally measured when a coral sand particle swept across different materials including mica, sapphire and SiO2. Besides, the interaction between coral sand particles and substrate was simulated by a finite element method (FEM).

1. Introduction

As specific marine bioclastic sediment, coral sands have not received much attention for a long time. Along with the population growth, the reduction of the resources and developing spaces stimulates the exploration of the coastal and marine resources. In this case, the construction of infrastructures at the coasts and islands is an urgent need. As a kind of calcareous sand with calcium carbonate content up to 90%, coral sands have the characteristics of fragility, irregular shape, large compressibility, and porosity [1-3]. Most of the research usually focuses on the engineering application of coral sand and the shear creep mechanical properties of coral sand particles. Many researchers have conducted research on the wide application of coral concrete in breakwaters, sand dykes, bank revetments, retaining walls, pavements, and building foundations [4, 5]. The coral sands can be used as raw materials for concrete, however, the concrete associated with coral-sand aggregate exhibited high porosity, large shrinkage, and low long-term strength compared to the ordinary concrete [6, 7].

Undoubtedly, the physical properties greatly impacted not only the application, but also the transportation and acquisition of coral-sands. As natural sources, the cost of coral sands was mainly constituted by the energy consumption during the exploiting, in which the friction behavior of the micro-sized coral sands is a crucial factor. Although the mechanical properties of coral sands have received much attention in recent years, however, there are few studies on the friction behavior of coral-sand particles with micron scale. In recent years, due to the high sensitivity of force detection, atomic force microscopy (AFM) has been widely used to characterize the interaction between nanostructures and nanomaterials [8-10]. Apart from AFM technology, finite element method (FEM) can effectively simulate the strain and stress in the nanomaterials [11, 12]. Thus, here we proposal a single method to evaluate the friction behavior of a single coral-sand particle towards different material surface with the assistance of AFM technology. The objective of this study was to gain better insight to improve the exploitation and transportation efficiency of coral sands.

2. Experimental

The coral sands were collected from Nansha islands in the South of China. X-ray powder diffraction (XRD) pattern of the coral sands was recorded on a Bruker D8 Advance powder X-ray diffractometer with Cu Kα (λ = 0.15406 nm). To perform the micro-friction experiment, a single coral sand was adhered to a commercial triangular cantilever according to the method reported in the literatures [13, 14]. The fabrication quality of the coral-sand modified AFM probe has been checked by scanning electron microscopy (SEM, Hitachi SU5000). Standard samples including mica, sapphire and SiO2 were purchased from Bruker company. The morphological features of the standard samples were measured by an atomic force microscopy (AFM, Bruker Multimode 8). Friction tests were performed by using the coral-sand modified AFM probe under contact mode. The interaction between the as-prepared AFM tip and the surface of the samples were simulated by finite element method (FEM). Based on the SEM image, MATLAB software was used to perform the morphological reconstruction of the particle-modified AFM tip. Firstly, edge detection of the SEM image was performed by the 'canny' operator in MATLAB software. Origin software was used to digitalize the profile curve from the edge detection result. Then Auto CAD software was employed to construct the calculation model of the coral sand particle. ABAQUS software was used to perform the FEM simulation with the parameters listed below:

Table 1. Calculation parameters in FEM simulation

	Elastic modulus (GPa)	Poisson's ratio
Coral sand particle	1000	0.4
Substrate	80	0.3

The size of the calculation model was presented in Fig.1.

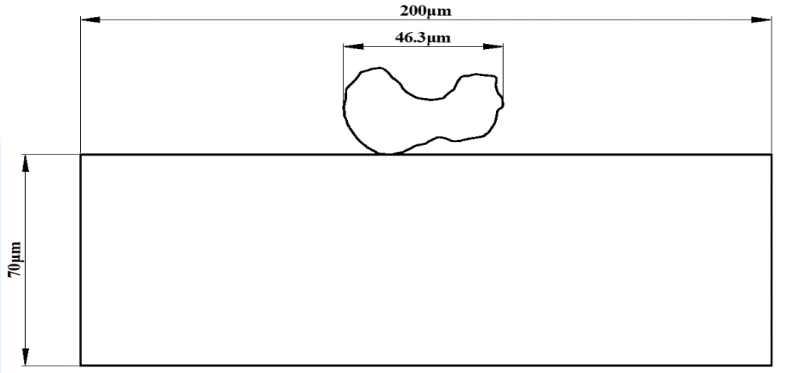

Figure 1. The size of the calculation model

3. Results and discussion

The XRD pattern of the coral sands is shown in Fig.2a. Most of the reflections can be indexed to the CaCO3 phases including calcite, aragonite, and vaterite [15, 16]. Apart from the CaCO3 phases, the XRD signal of SiO2 can be detected, which is originated from the Si substrate in the XRD characterization. The morphology of the selected coral sand was measured by SEM, as shown in Fig.2b. It can be found that a single coral sand was adhered to the edge of the cantilever. The lateral size of the coral sand is about 46 μm. However, the surface of the coral sand is not smooth. Thus, a digital technology was employed to reconstruct the real surface of the particle-modified AFM tip (presented in Supporting Information).

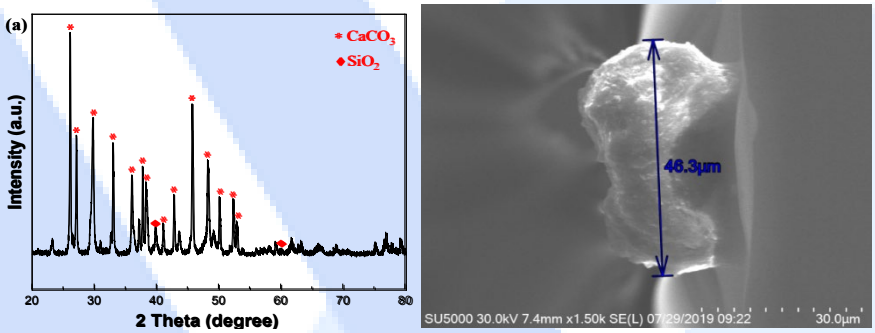

Figure 2. XRD pattern (a) of the coral sand powders. SEM image (b) of the particle-modified AFM tip.

When the coral sands contacted with the surface of the substrates, the deformation of the substrates can be calculated. Based on the saint venant principle [17], as shown in Fig.3, the function of stress at any point can be expressed as:

$$\varphi(\rho,\theta) = C_1\rho\,\mathrm{Cos}\,\theta + C_2\rho\,\mathrm{Sin}\,\theta - \frac{P}{\pi}\rho\theta\,\mathrm{Sin}\,\theta + C_3 \tag{1}$$

The function of displacement in the y and x directions:

$$u_r = -\frac{2P}{\pi E}\ln\rho\,\mathrm{Cos}\,\theta - \frac{(1-\mu)P}{\pi E}\theta\,\mathrm{Sin}\,\theta + C_1\,\mathrm{Cos}\,\theta \tag{2}$$

$$u_\theta = \frac{2P}{\pi E}\ln\rho\,\mathrm{Sin}\,\theta + \frac{(1+\mu)P}{\pi E}\mathrm{Sin}\,\theta - \frac{(1-\mu)P}{\pi E}\theta\,\mathrm{Cos}\,\theta - C_1\,\mathrm{Sin}\,\theta$$

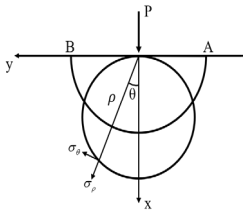

Figure 3. Scheme of the interaction between the coral sand and the substrate

The real stress and strain distributions during the contacting of substrates and modified AFM tip can be stimulated by the FEM. Compared with the conventionally reductive mode as shown in Fig.4a, reconstruction of the particle-modified AFM tip can greatly improve the analytic precision of the FEM. Based on the results of the FEM analysis, the real stress and strain distributions can be visualized. As shown in Fig.4b, the maximum stress appeared on the bottom of the coral sand particle. The stress distribution under the irregular particle is nonuniform. Based on the FEM analysis, the depth of the indentation under different level of loads can be simulated as presented in Fig.4c. With the increase of load, the indentation depth increases in both of the models. The FEM can effectively predict the deformation of the substrate's surface under different level of loads. Due to the irregular morphology, the depth of the indentation under the reconstructed coral-sand-particle tip is greater than that in the reductive model. With the increase of load, the difference of the depth between the two models becomes smaller.

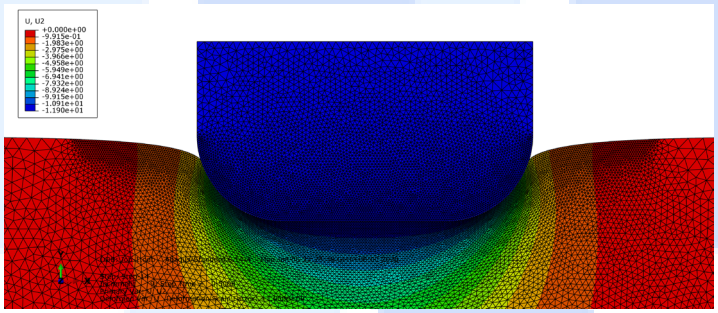

(a)

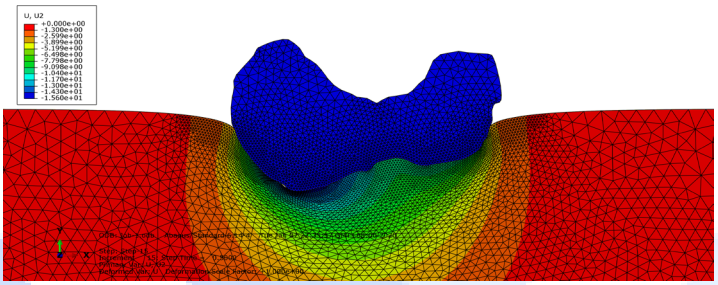

(b)

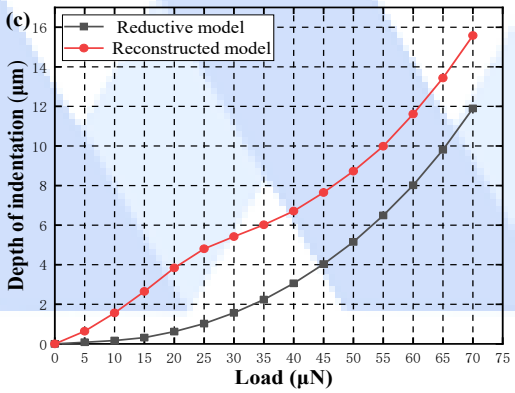

Figure 4. (a) Reductive model of the coral sand particle in FEM calculation; (b) The stress distribution under the coral sand simulated by FEM; (c) The change of the depth indentation with the increase of load

Variation of the friction coefficient was experimentally measured when a coral sand particle swept across different materials surface including mica, sapphire and SiO2. As shown in Fig.5a, the same coral-sand-particle modified tip exhibits different friction behaviors towards different

substrates. With the increase of normal force, the friction increases linearly. Very good linear relationships are observed for the three samples. The calculated friction coefficient on the three substrates is 0.096, 0.140 and 0.224, respectively. The roughness of the mica, sapphire and SiO2 samples are 0.92 nm, 3.5 nm and 1.9 nm. Thus, the roughness of the substrates may be a key factor affected the friction coefficient. The effect of the scanning rate on the friction has also been investigated. As presented in Fig.5b, the results show that relationship between friction and scanning rate did not follow any pattern. It indicates the effect of sliding velocity on the friction can be ignored.

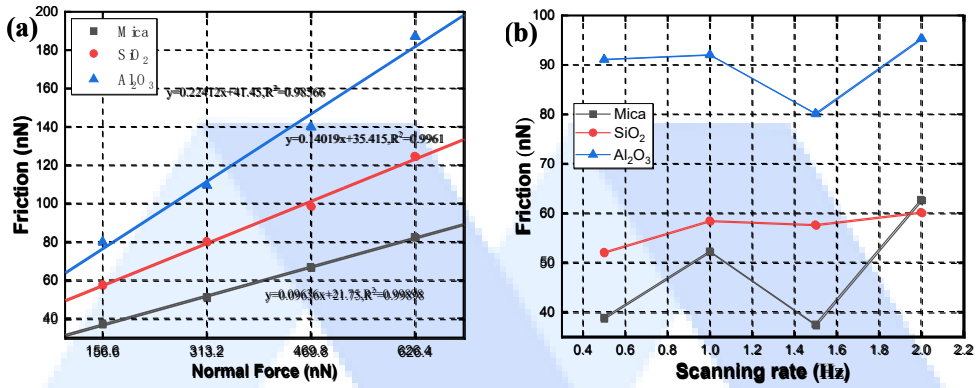

Figure 5. (a) Calculated friction coefficients of coral-sand-particle modified AFM tip on different substrates. (2) Effect of scanning rates on the friction between AFM tip and substrates

4. Conclusions

In summary, a particle modified AFM tip has been assembled to evaluate the micro- friction behavior of coral sand towards different materials including mica, SiO2 and Al2O3. The interaction between coral sand and the material surface was simulated by FEM. The calculated friction coefficient on the three substrates is 0.096, 0.140 and 0.224, respectively. The results show that the effect of scanning rate on the value of friction can be ignored.

Funding

This work was financially supported by the High-level Talent Gathering Project in Hunan Province (2019RS1059).

Availability of data and material

All data generated or analyzed during this study are included in this published article.

Declaration of Conflict of Interests

The authors declare that there is no conflict of interest.

References

[1.] Rashidian, V. and M. Hassanlourad, Predicting the Shear Behavior of Cemented and Uncemented Carbonate Sands Using a Genetic Algorithm-Based Artificial Neural Network. Geotechnical and Geological Engineering, 2013. 31(4): p. 1231-1248.

[2.] Tang, J., et al., Development of properties and microstructure of concrete with coral reef sand under sulphate attack and drying-wetting cycles. Construction and Building Materials, 2018. 165: p. 647-654.

[3.] Xu, Q., et al., Preliminary investigation of artificial reef concrete with sulphoaluminate cement, marine sand and sea water. Construction and Building Materials, 2019. 211: p. 837-846.

[4.] Yang, S., et al., Mechanical properties of alkali-activated slag concrete mixed by seawater and sea sand. Construction and Building Materials, 2019. 196: p. 395-410.

[5.] Ding, L., et al., Bond behavior between basalt fiber-reinforced polymer rebars and coral-reef-sand concrete conditioned in saline solution. Structural Concrete, 2020. 21(2): p. 659-672.

[6.] Cheng, S., et al., Durability and microstructure of coral sand concrete incorporating supplementary cementitious materials. Construction and Building Materials, 2018. 171: p. 44-53.

[7.] Martin, B.E. and O. Cazacu, Experimental and theoretical investigation of the high-pressure, undrained response of a cohesionless sand. International Journal for Numerical and Analytical Methods in Geomechanics, 2013. 37(14): p. 2321-2347.

[8.] Ding, Y., et al., AFM characterization and electrochemical property of Ag nanowires by modified AAO template method. Journal of Alloys and Compounds, 2008. 466(1): p. 479-482.

[9.] Ding, Y.H., et al., Nanoscale mechanical characterization of PMMA by AFM nanoindentation: a theoretical study on the time-dependent viscoelastic recovery. Journal of Materials Science, 2013. 48(9): p. 3479-3485.

[10.] Jin, H., et al., Designable and dynamic single-walled stiff nanotubes assembled from sequence-defined peptoids. Nature Communications, 2018. 9(1): p. 270.

[11.] Liu, X., et al., Mechanical properties of individual core-shell-structured SnO2@C nanofibers investigated by atomic force microscopy and finite element method. Science China Technological Sciences, 2018. 61(8): p. 1144-1149.

[12.] Liu, B., et al., The atomic-scale finite element method. Computer Methods in Applied Mechanics and Engineering, 2004. 193(17): p. 1849-1864.

[13.] Ma, W., et al., Atomic force microscope study of the aging/rejuvenating effect on asphalt morphology and adhesion performance. Construction and Building Materials, 2019. 205: p. 642-655.

[14.] Ma, W.B., et al., Adhesion force measurements between deep-sea soil particles and metals by in situ AFM. Applied Clay Science, 2017. 148: p. 118-122.

[15.] 1Kontoyannis, C.G. and N.V. Vagenas, Calcium carbonate phase analysis using XRD and FT-Raman spectroscopy. Analyst, 2000. 125(2): p. 251-255.

[16.] Ševčí, R., P. Šašek, and A. Viani, Physical and nanomechanical properties of the synthetic anhydrous crystalline CaCO3 polymorphs: vaterite, aragonite and calcite. Journal of Materials Science, 2017.

[17.] Horgan, C.O., Recent Developments Concerning Saint-Venant's Principle: A Second Update. Applied Mechanics Reviews, 1996.

PACE-2023
International Congress on Phenomenological Aspects in Civil Engineering

Research Article 20-23June 2023

Preparation of Sepiolite-Based Foam Concrete and Its Adsorption Properties

Yanhuai Ding*,[1], Zhenyu Zhao[1], Ji Zhou*,[1,2], Zhimin Zou[3]
[1]*Institute of Rheological Mechanics, Xiangtan University, Xiangtan, Hunan 411105, China*
[2]*College of Civil and Environmental Engineering, Hunan University of Science and Engineering, Yongzhou, Hunan 425199, China*
[3]*Hunan Expressway Group Co. LTD, Changsha, Hunan 410008, China*
Corresponding Author E-mail: yhding@xtu.edu.cn

Keywords

Sepiolite,
Concrete,
Adsorption capacity,
Methanol,
Heavy metal ions.

Abstract

Due to the unique physical properties including high specific surface area, high thermal stability and excellent adsorption capacity, sepiolite shows great potential for application in building and construction materials. In this paper, porous sepiolite/concrete composite has been prepared by a physical foaming technology. The adsorption capacity of the composite concrete towards methanal, ammonia and heavy metal ions has been investigated. The results show that the porous sepiolite/concrete with a high specific surface area can be used as functional concrete, which exhibits impressive adsorption capacity towards noxious gas and heavy metal ions.

1. Introduction

With the ever-increasing development of industrial technology, the energy crisis and environmental problems caused by the shortage of fossil energy have been a growing headache [1]. Therefore, it is urgently important to develop energy-saving products in the construction industry. Foam concrete has been recognized as a versatile construction material that is environmentally friendly and technically efficient [2, 3]. Due to its low density, thermal insulation and temperature regulation function, foam concrete has become more prevalent [4, 5]. Besides, foam concrete is of great advantage of convenient construction and convenient transportation in engineering applications. In recent years, the functions of foam concrete have been widely explored [6, 7].

Sepiolite is an abundant, natural and nontoxic phyllosilicate with a compositional formula of $Mg8Si12O30(OH2)4{\cdot}8H2O$ [8]. The fibrous structure of sepiolite has attracted much attention in recent years [9-12]. Compared with the nanoparticles, the fibrous sepiolite shows high dispersity in the matrix. Thus, sepiolite has been widely used to fabricate composites, which inherits the advantages of both sepiolite and matrix. In the construction industry, fiber-reinforced precast concrete has been fulfilling an important role by offering technical convenience [13-15]. Considering the prominent physical properties of the sepiolite material, Kavas et al. used sepiolite to produce cement [16]. The results indicate that the addition of sepiolite can greatly improve both the compressive and bending strengths of the mortar. In recent years, sepiolite materials have been widely used to prepare cement pastes and concretes [17, 18]. As a potential cement replacement material, sepiolite can increase the mechanical properties of the specimens, however, it has an adverse effect on the rheological behavior of slurry [18, 19]. Besides, the incorporation of sepiolite can to some extent improve the carbonation resistance of the modified mortar as well as the chloride resistance. Owing to the high adsorption properties towards gaseous pollutants and heavy metal ions in wastewater, many attempts have been made to prepare sepiolite-modified construction materials for application in the field of environmental decontamination [20, 21]. Compared with the conventional concretes, foam concretes are beneficial to facilitate the sepiolite-use efficiency in which the sepiolite fibers are exposed at the surface of the concretes.

Based on the issues mentioned above, the present work attempted to fabricate sepiolite-modified foam concretes by a physical foaming technology. The adsorption capacity of the composite concretes towards methanal, ammonia and heavy metal ions has been investigated.

2. Experimental

Santa Maria Church is a unique historical structure located in Trabzon, Turkey. The church building is one of the important historical structure of the Trabzon province, and it is still in use. It is known that it was built between 1869 and 1874 according to historical records. Fig. 1 depicts location and plan view of the church building.

2.1. Materials and chemicals

Sepiolite powders were provided by Xiangtan Sepiolite Technology Co. (Xiangtan, China). Ordinary Portland cement (OPC, 32.5 N) was used to prepare foam concrete. Sodium dodecyl sulfate, dodecanol and anhydrous calcium chloride were purchased from Sinopharm Chemical Reagent Co. Ltd.

2.2. Preparation of foam concretes

In a typical procedure, a certain proportion of sepiolite, OPC powders, calcium chloride and water were mixed to prepare the cement mortar. 4.0 g sodium dodecyl sulfate and 2.0 g dodecanol were added into 1000 ml water under stirring. 100 ml of as-prepared solution was treated by an agitator with strong stirring. Then the obtained foam was added into the cement mortar with strong stirring. Finally, the mixture was poured into the molds. After 72 h of maintenance, the mold was removed and continued to be maintained under standard curing conditions for 7 days.

2.3. Characterization of the foam concretes

The mechanical properties of the foam concrete were characterized by microcomputer-controlled electronic universal testing machine (HD-B615-S). Each piece of data is the mean value of five experiments performed. The structural features of the foam concrete were studied by scanning electron microscopy (SEM, JSM-6610LV). The crystal structure of the samples was studied by X-ray diffraction (XRD) technology (Bruker D8 Advance). The infrared thermal images were collected by an infrared camera. The adsorption capacity of the foam concrete towards methanol, ammonia and heavy metal ions was tested according to the Chinese standards as shown in Figure S1.

3. Results and discussion

The mechanical performance is one of the crucial parameters of foam concretes for their practical application. Therefore, the effects of the water-cement ratio, sepiolite content, and heat-treatment temperature of the sepiolite powders on the mechanical properties of the composite concrete have been investigated. Firstly, the sepiolite powders were heat-treated at 100℃, 200℃, 300℃ and 400℃. The XRD patterns of the heat-treated sepiolite are presented in Figure 1. Sepiolite powders have been employed to improve the physical properties of concrete previously. However, the effect of heat-treatment on the performance of the sepiolite did not cause attention. In this case, the intent of the introduction of the heat-treatment is to enhance the adsorption capability of sepiolite-based concrete. The water molecules in the channels of sepiolite can be partly eliminated by the heat-treatment at relatively low temperatures. Moreover, the heat-treatment is in favor of improvement of the activation of the sepiolite. In the XRD patterns of the sepiolite, a series of diffraction peaks can be observed, which can be ascribed to the feature peaks of sepiolite. The increase in the heat-treated temperature did not bring out a significant change in the XRD patterns. Generally, the diffraction peak at 2θ=7.26° corresponds to the (110) facet of sepiolite [22]. In the range of 100℃-400℃, the crystal structure of the sepiolite can be maintained after the heat-treatment. The morphological features of the sepiolite treated at different temperatures are shown in Figure 2. The fibrous structure of the sepiolite powders can be identified in all images. The sepiolite fibers are uniform in size and have an average diameter of 30 nm. Due to the complex chemical and crystalline composition, some nanoparticles can also be found in the sepiolite samples. The SEM analysis indicates that the number of the nanoparticles remarkably decreased with the increase in the heat-treatment temperatures.

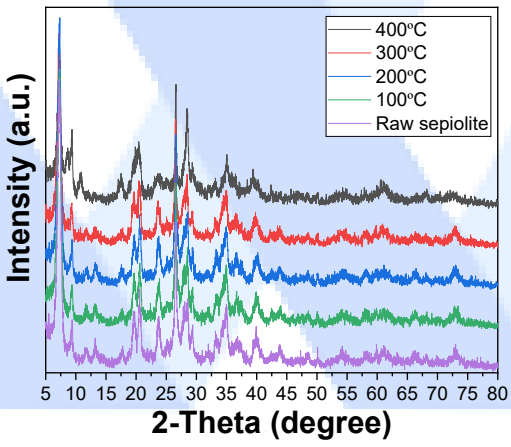

Figure 1. XRD patterns of the heat-treated sepiolite at different temperatures

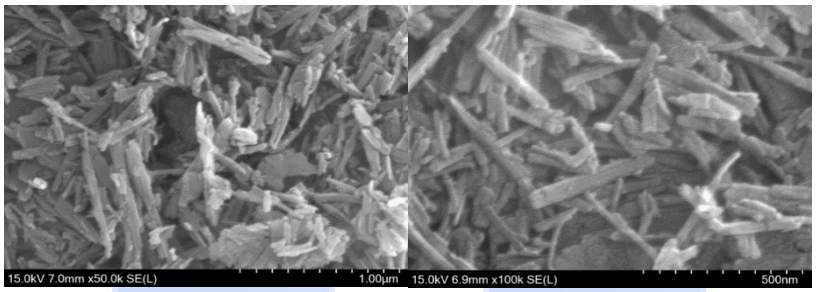

(a)

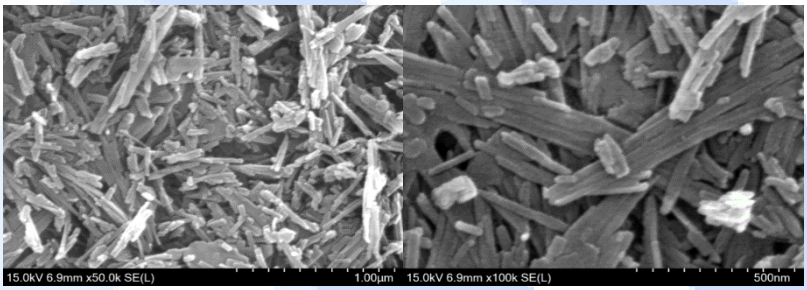

(b)

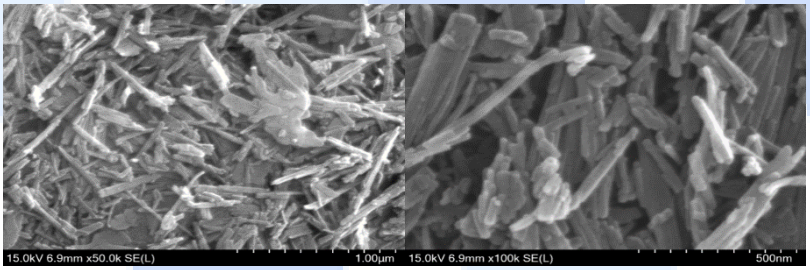

(c)

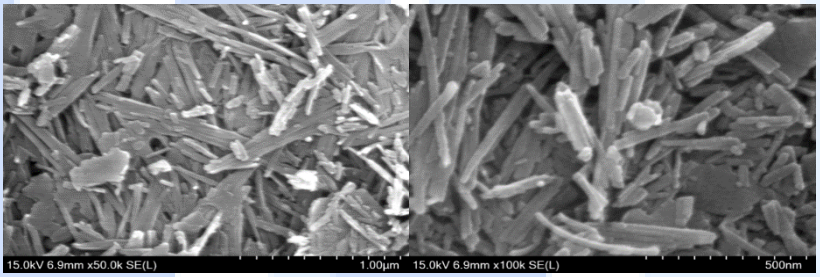

(d)

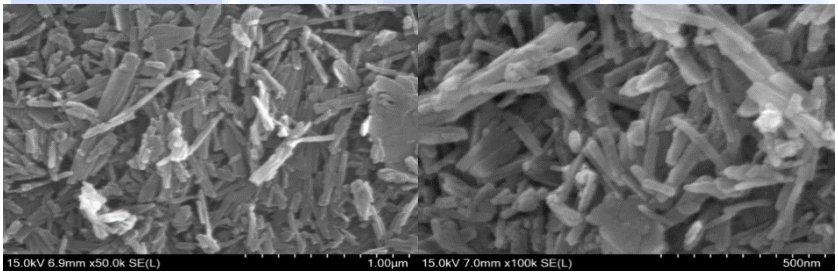

(e)

Figure 2. SEM images of the heat-treated sepiolite at different temperatures. (a) raw sepiolite; (b) 100°C; (c) 200°C; (d) 300°C; (e) 400°C

The effect of heat-treatment temperature on the mechanical properties of the foam concrete has been studied. The concrete mix design was listed in Table S1. The compressive strength of the foam concrete is shown in Figure 3a. With increasing heat-treatment temperature, the compressive strength of the foam concrete gradually increases except for the case of 400°C. Purification of the sepiolite can improve the mechanical properties of the sepiolite fibers, however, high treatment temperature would destroy the channel structures of sepiolite [23]. Thus, the 7-days compressive strength of the foam concrete firstly increased from 0.55 MPa to 0.68 MPa, and then decreased to 0.57 MPa. Besides, the effect of sepiolite content on the mechanical properties of the foam concrete has been studied. The concrete mix design of the composite concrete was listed in Table S2. With the ratio of sepiolite/cement was fixed at 2:3, the compressive strength reaches the maximum value. Besides, the effect of the water/cement ratio on the mechanical properties of the composite concrete has been investigated. The optimized water/cement ratio was set at 1:1. Due to the high water adsorption capacity of the sepiolite, the water/cement ratio of the foam concrete is much higher than that of the common concrete. All the results indicate that the composite concrete shows relatively low compressive strength (< 1.0 MPa). Thus, the use of this kind of foam concrete alone is limited to non-load-bearing sites. The digital image of the foam concrete with sepiolite content at 40% is shown in Figure 3b. Plenty of small pores can be found on the surface of the foam concrete. The pores are homogeneously distributed. The inner structure of the foam concrete has been investigated by SEM analysis as shown in Figure 3c-e. The results indicate that the foam concrete possesses numerous internal pores and the diameter is in the range of 10-200 μm. The enlarged SEM image shows that a large number of pores with much smaller diameters are distributed in the wall of the micropores. The nanosized porous structure in the wall can greatly improve gas diffusion. Besides, sepiolite fibers can be observed in the wall. Adequate exposure of the sepiolite fibers is essential to the adsorption function of the foam concrete.

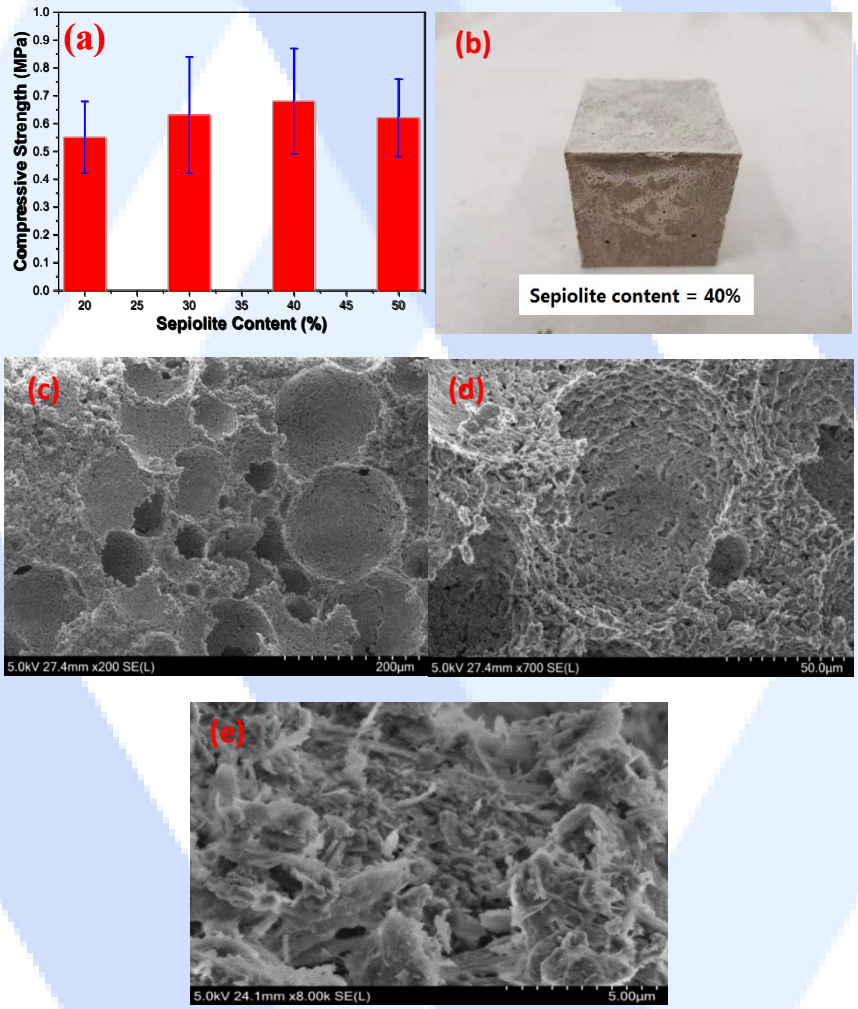

Figure 3. XRD patterns and morphology of the as-prepared foam concrete. (a) XRD pattern; (b) digital image; (c-e) SEM images

The effect of sepiolite content on the thermal conductivity of the foam concrete was studied as shown in Figure 4a. The sepiolite has been employed to improve the thermal stability and thermal insulation performance of the composites [24, 25]. From the figure, the sepiolite-based foam concrete with a sepiolite content of 40% shows the lowest thermal conductivity coefficient of 0.072 W/mK. The foam concretes with 0% and 40% of sepiolite content were placed on the surface of a heating console where the temperature reaches 100°C. The infrared thermal images of the foam concretes were measured as shown in Figure 4b-c. Due to the unique structure of the foam concretes, the thermal conduction in the foam concrete has been reduced significantly.

The adsorption capacities of the foam concrete towards methanal and ammonia were tested based on the JC/T1074-2008 and GT18582-2008 standards in China. With the mass ratio of sepiolite/cement fixed at 1:1, the adsorption capacities towards methanal and ammonia are presented in Figure 5. The adsorption capacity increases gradually and then reach the maximum value as the adsorption time increased. In the case of ammonia, the foam concrete exhibits similar adsorption behavior. After 25h, the adsorption capacities of methanal and ammonia are 10.77 mg/g and 2.28mg/g, respectively. The ammonia-adsorption capacity of the foam concrete was lower than in the case of methanal. It indicates that the sepiolite exhibits good selectivity towards methanal gas, which favors in-door air purification.

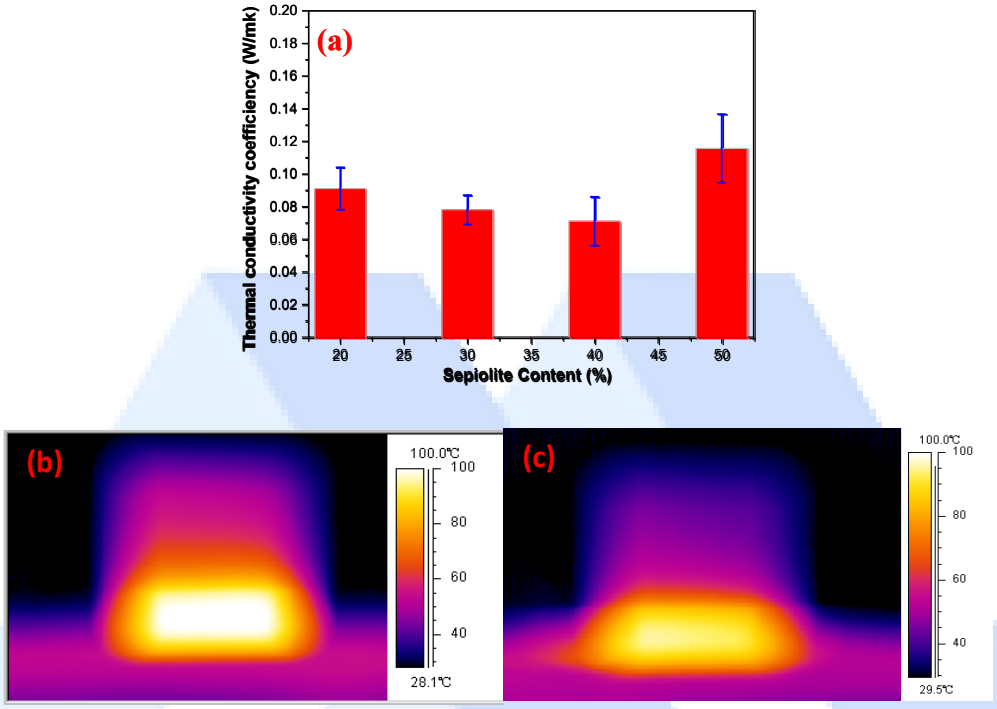

Figure 4. (a) thermal conductivity of the foam concrete with different sepiolite content; (b, c) infrared thermal images of the foam concretes

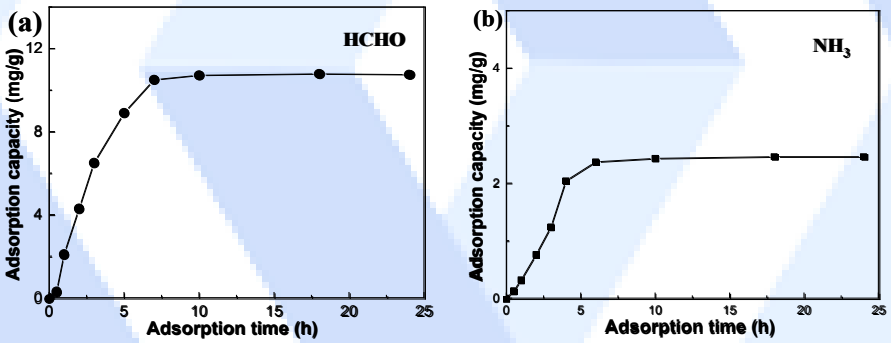

Figure 5. Adsorption capacities of foam concrete towards (a) methanal and (b) ammonia

The intoxication of the environment by heavy metal ions is one of the serious ecological problems [26]. Due to the huge usage of construction and building materials, functional concretes have the potential to play an important role in geoecoprotection. Foam concretes have been used for the removal of heavy metal ions [26, 27]. The adsorption of heavy metal ions can be greatly improved by construction of a multi-hierarchical pore structure in the foam concrete. Based on the results mentioned above, the addition of sepiolite results in a microporous structure in the foam concrete. Thus, sepiolite-based foam concrete can provide more adsorption active sites owing to the high adsorption capacity of raw sepiolite. The adsorption capacity of foam concrete towards Mn, Cd, Cr, As and Pb with the adsorption time is presented in Figure 6a-e. Among them, the composite concrete shows the highest adsorption capacity towards Mn. The capacity reaches a relatively stable value within 8h. A high adsorption capacity (~115.3 mg/g) for Mn ions can be obtained. The adsorption ability of the foam concrete follows this order: Mn^{2+}>Cd^{2+}>Cr^{3+}>As^{3+}>Pb^{2+}. The morphology of the foam concrete after adsorption of Mn ions is shown in Figure 6f. The porous structure in the foam concrete can be mainly maintained, indicating the high structural stability of the sepiolite-based concrete. Thus, the sepiolite-based foam concrete shows great potential for heavy-metal-ion removal, as well as indoor gas purification.

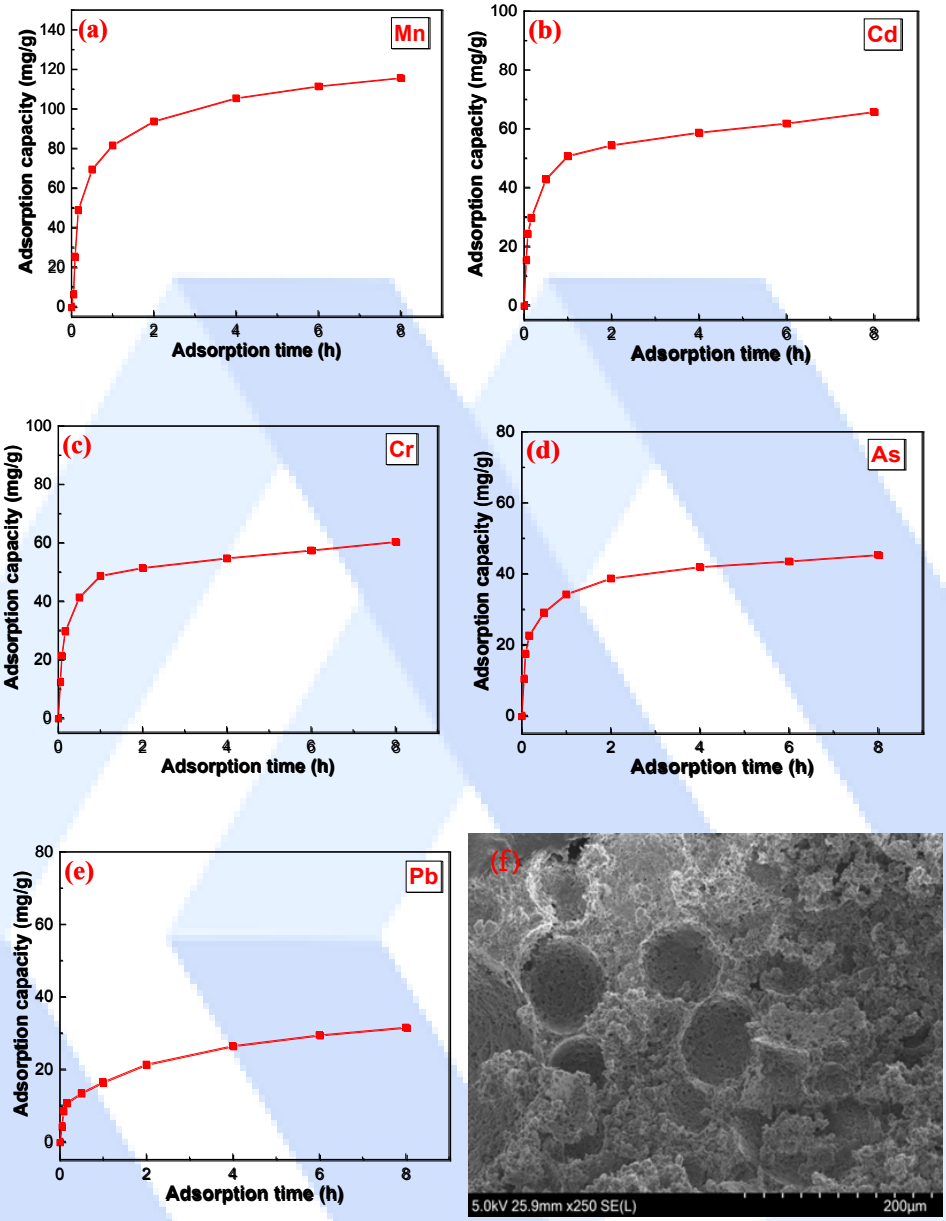

Figure 6. (a-e) Adsorption capacity of foam concrete towards Mn, Cd, Cr, As and Pb; (f) Morphology of the foam concrete after adsorption of Mn ions

4. Conclusions

In summary, sepiolite-based foam concrete has been successfully prepared by a simple physical foaming technology. This kind of composite concrete with high sepiolite content up to 50% shows great potential for in-door contaminant purification. The adsorption capacities of methanal and ammonia are 10.77 mg/g and 2.28mg/g, respectively. The low thermal conductivity coefficient guarantees the thermal insulation performance of the foam concrete. Besides, the composite concrete shows a high adsorption capacity towards Mn ions. Thus, this kind of sepiolite-based foam concrete can be employed as a multi-functional material in building and construction industry.

Acknowledgments

This work was financially supported by High-level Talent Gathering Project in Hunan Province (No.2019RS1059).

Data availability statement

All data generated or analyzed during this study are included in this published article and its supplementary information files.

Declaration of Conflict of Interests

The authors declare that there is no conflict of interest.

References

[1.] Meng M, Fu Y and Wang X 2018 J. Clean. Prod. 177 752

[2.] Zhang Z, Provis J L, Reid A and Wang H 2014 Constr. Build. Mater. 56 113

[3.] Fu Y, Wang X, Wang L and Li Y 2020 Adv. Mater. Sci. Eng. 2020 6153602

[4.] Lesovik V, Voronov V, Glagolev E, Fediuk R, Alaskhanov A, Amran YM et al 2020 J. Build. Eng. 31 101414

[5.] Raj B, Sathyan D, Madhavan M K and Raj A 2020 Constr. Build. Mater. 245 118373

[6.] Markin V, Krause M, Otto J, Schröfl C and Mechtcherine V 2021 J. Build. Eng 43 102870

[7.] Xingjun L, Mingli C, Yan L, Xin L, Qian L, Rong T et al 2015 Adv. Concr. constr. 3 103

[8.] Jiang W, Jiang Y, Zhao S, Peng J, Qin W, Ouyang D et al 2020 Energy Technol. 8 1901262

[9.] Deng C, Jiang Y, Fan Z, Zhao S, Ouyang D, Tan J et al 2019 Appl. Surf. Sci. 484 446

[10.] Jiang W, Han Y, Jiang Y, Xu F, Ouyang D, Sun J et al 2021 Appl. Clay Sci. 203 106020

[11.] Jiang W, Han Y and Ding Y 2022 Nanotechnol. 33 425601

[12.] Zhou J, Jiang W, Peng J and Ding Y 2022 Ionics 28 1091.

[13.] Huang J Q and Dai J G 2019 Compos. Struct. 207 136

[14.] Lima P R, Barros J A, Roque A B, Fontes C M and Lima J M 2018 Constr. Build. Mater. 187 620

[15.] Ghosh D, Abd-Elssamd A, Ma Z J and Hun D 2021 Constr. Build. Mater. 266 121051

[16.] Kavas T, Sabah E and Çelik M S 2004 Cement Concrete Res. 34 2135

[17.] Wu C-R, Hong Z-Q, Zhan B-J, Cui S-C and Kou S-C 2021 Constr. Build. Mater. 309 125076

[18.] Wu C and Kou S 2019 Constr. Build. Mater. 196 105

[19.] Wang C, Sun K, Niu H, Sun G, Zhang Z and Kong L 2021 Constr. Build. Mater. 279 122509

[20.] Song N, Hursthouse A, McLellan I and Wang Z 2020 Environ. Geochem. Hlth 43 2679

[21.] Wu C-R, Hong Z-Q, Zhan B-J, Tang W, Cui S-C and Kou S-C. 2022 Constr. Build. Mater. 316 125860

[22.] González del Campo MM, Darder M, Aranda P, Akkari M, Huttel Y, Mayoral A et al. 2018 Adv. Funct. Mater. 28 1703048

[23.] Zhou F, Yan C, Wang H, Zhou S and Komarneni S 2017 Appl. Clay Sci. 146 246

[24.] Wang F, Liang J, Tang Q, Chen C and Chen Y 2014 J. Nanosci. Nanotechnol. 14 3937

[25.] Shafiq M, Yasin T and Saeed S 2012 J. Appl. Poly. Sci. 123 1718

[26.] Svatovskaya L, Shershneva M, Baydarashvily M, Sychova A, Sychov M and Gravit M 2015 Procedia Eng. 117 345

[27.] Sychova A, Sychov M and Rusanova E 2017 Procedia Eng. 189 681

PACE-2023
International Congress on the Phenomenological Aspects of Civil Engineering

PACE-2023
International Congress on Phenomenological Aspects in Civil Engineering

Research Article 20-23June 2023

Sound Intensity Geo Referenced Maps: A Tool for Engineers Urban Planning and Urban Designers

Seyed Sobhan Alvani[1], Mohammad Gohari[*,2], Mona Tahmasebi[3]
[1]*Master Student at Urban Design Department, Bu-Ali Sina University, Iran*
[2]*Assistant Professor, Arak University of Technology, Iran*
[3]*Professor Assistant, Agricultural Engineering Research Department, Markazi Agricultural and Natural Resources Research and Education Center, Agricultural Research, Education and Extension Organization (AREEO), Arak, Iran*
Corresponding Author E-mail: moh-gohari@arakut.ac.ir

Keywords

Sound level map,
Urban management,
GIS,
Land base.

Abstract

Preparing a map of sound and noise levels as a land base is very important and is used by urban planners and development experts. In Iran, the preparation of this map has received less attention, and it needs to be looked at again by geographic information systems experts GIS, these maps are usually prepared by coordinate data collection and can be drawn by various software after pre-processing. The sound level map can be entered as an information layer in GIS and in the post-processing stages it can be combined with other base maps and new data can be extracted. According to the needs of planners and experts in the field of urban management, the existence of a noise pollution map of the big cities of Hamedan and Arak seemed necessary. In this research, an attempt was made to prepare a spatial map of sound intensity distribution and zoning the areas. The results of data collection and map drawing indicate that certain areas of both cities have the highest level of sound intensity, but in Hamedan city, the use of urban green spaces along with areas of high sound intensity has reduced its effect in residential areas. These maps can be used for decision-making and location systems based on GIS of urban facilities such as hospitals and educational places that require a low level of sound intensity.

5. Introduction

At the airport, more than other children are under threat. Increased heart rate, disturbance in the nervous and behavioral system are among the important harms of noise pollution that have occurred in the citizens of these areas, the air quality control company announced in a report; Most of the citizens of Tehran suffer from noise pollution. Surveys show that most of the citizens of Tehran live in areas where the noise in those areas exceeds the set standards, for example, in the south of Tehran, in addition to the noise from the traffic, the noise from the airport and the railway has also polluted this area in terms of sound [1].

The World Health Organization (WHO) considers noise pollution a serious threat to their health Sun has known that it is one of the most widespread risks to human health due to the diversity of traffic sources, industry, workplace and neighborhood. In Europe, 40% of the population is exposed to sound levels that are potentially dangerous to health. The treatment and elimination of the effects of noise pollution is interesting. For example, no measure and scale can be used to calculate the psychological pain and discomfort caused by exposure to noise pollution. However, the accuracy of the resulting figures is not without grace. For example, a calculation made in Norway in 1992 estimated the cost of noise pollution to be 88 to 541 dollars per capita per year, and the social costs of noise pollution in the European Union (when it had 15 members) was 42 billion euros, which according to The increase in the number of members to 27 members is being reconsidered. Sound intensity reference maps have recently been developed in Europe so that they can be used in the management and design of urban spaces and even decision-making models by combining with other GIS maps.

Preparing a map of noise levels as a land base is very important and is used by urban planners and development experts. In Iran, the preparation of this map has received less attention and needs to be reviewed by an expert. These maps are prepared based on geographic information systems by coordinate data collection and can be drawn by various software after pre-processing. Sound levels can be mapped as a layer Information is entered in GIS and in the post-processing stages, it can be combined with other base maps (overlay) and extract new data. One of the applications can be to determine the location of hospital, university and school and other places that require low noise levels or to plan the future of the city and its development based on the physiological health standards according to these maps. The recorded sound level is also a criterion for traffic measurement [2]. [Although the sound level and its intensity are not only due to the traffic caused by the traffic of cars, but it is a function of the traffic [3].

Dozens of noise levels in different parts of the city are collected during the peak hours of noise and traffic in the city, and a ground map based on volume levels of noise is obtained.

6. Research Methodology

In this stage of the research, different places of Arak and Hamadan cities, which are important commercial, traffic, traffic, social places such as places near squares, bus stations, markets, railway station, terminal and airport were selected. The data collection groups equipped with the measurement system were deployed at these points at 6 o'clock in the evening at the same time and performed data collection for 15 minutes according to the given instructions [4, 5, 6]. This range included almost the main points of Arak and Hamedan with different population concentration. The measurement system was equipped with the Sound Meter App2013 Android program and recorded the sound volume in decibels (Sound Volume Level) with a data sampling rate of 1 second [8]. Figure 1 shows the geographical map of Arak and data collection points. In the data processing stage, the average sound intensity in decibels was calculated for 15 minutes at each data collection point. Also, the exact coordinates of the location were recorded through the GPS of the data collection device. Spatial attributes of the points and the measured sound volume were entered into the Winsurf10 software [7 and9]. The data were first gridded and then the kriging technique was used for spatial interpolation. In the next step, the contour map of equal sound intensity was obtained based on geographic coordinates, as well as the three-dimensional graph of the sound intensity procedure [10]. In the last step, the Geospatial Sound Volume map was zoned to classify different areas according to sound intensity.

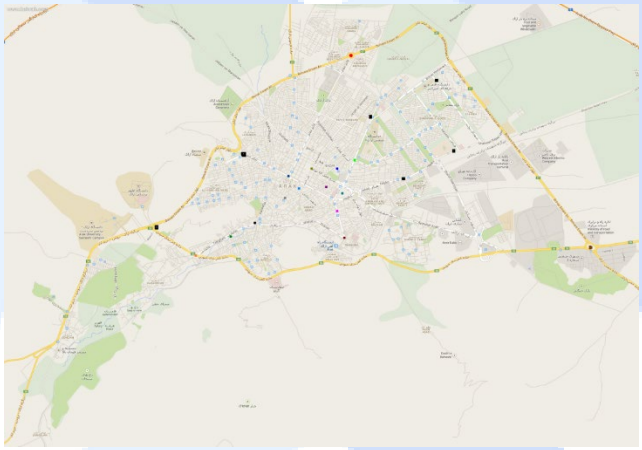

Figure 1. Sampling points in Arak City

7. Results

The map of equal sound intensity contours in decibels of Arak city is shown in Figure 2. The yellow points have the lowest sound intensity and the red points have the highest sound volume level. In this map, the area of Shariati Square has the highest level of urban noise pollution and the area of Baath Town has the lowest noise level. In Figure 3, the topographical map of the sound intensity of Arak city is given for a better understanding of urban planning experts and planners.

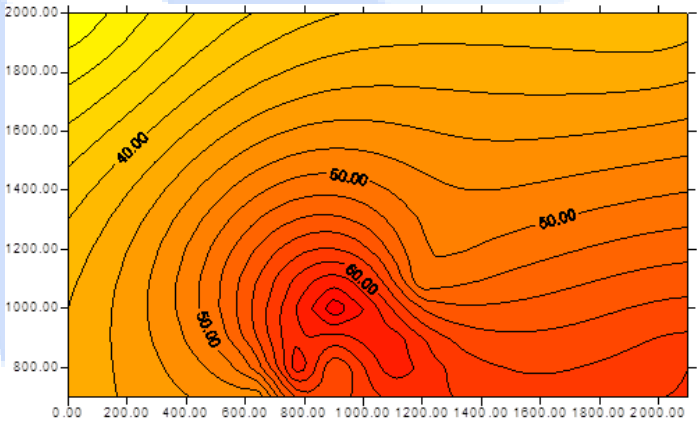

Figure 2. The Geo-referenced map of sound level in Arak City

Also, Figure 3 shows the 3D map of sound level. In Figure 4, the sound intensity ranges were divided. This map can be used as an information layer in GIS (Geographic Information System) software. In general, by using the sound intensity city map of Arak, it can be seen that there is no dangerous range in terms of human hearing physiology, and it is not high in terms of noise pollution, but it is suitable for the location of hospitals, schools and parks.

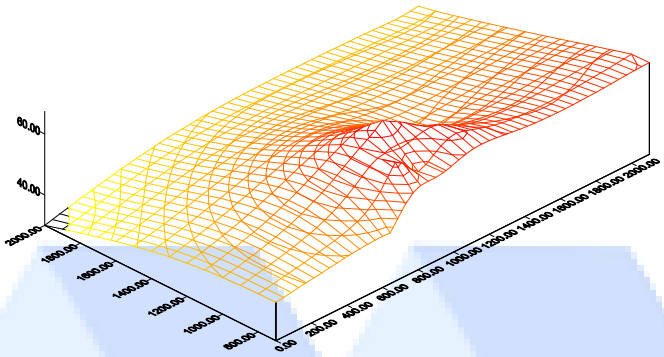

Figure 3. Sound level by 3D map

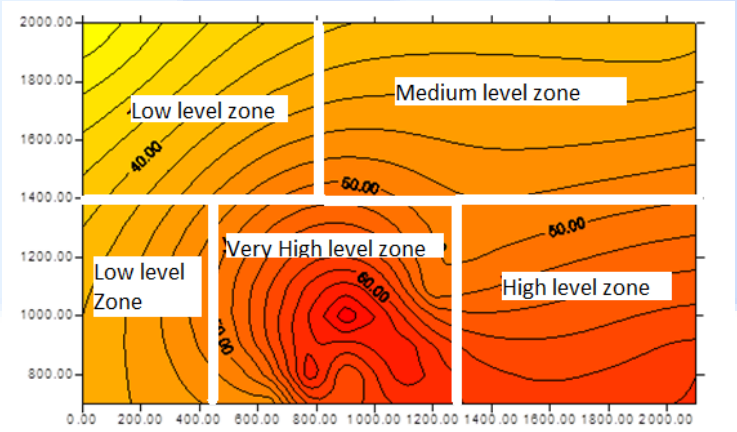

Figure 4. The zoning map of sound level intensity

Figure 5 shows the sound intensity map of Hamadan city and the sound distribution in the target area. Also, Figure 6 shows the topographical map of the sound intensity of Hamadan city. As in the right corner of the map, there is a point of high sound intensity of about 65 decibels, while the quiet area is seen at about 30 decibels, which is due to the presence of a park in this area. This shows that with the construction of parks, gardens and urban green spaces, healthier urban areas can be created in terms of sound.

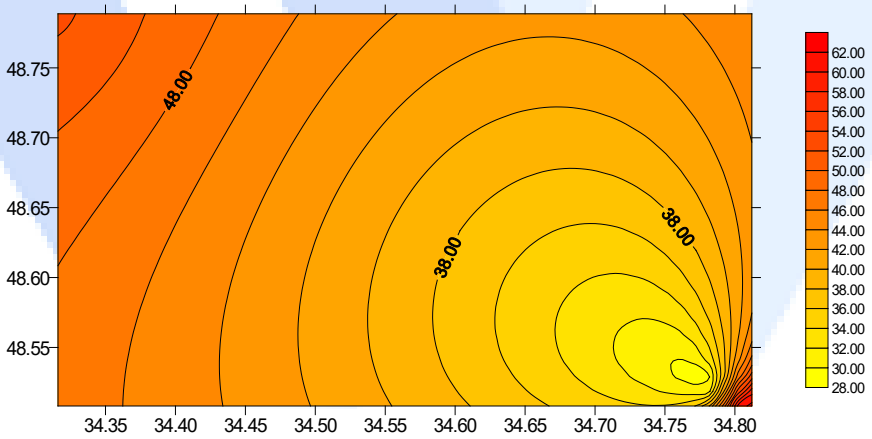

Figure 5. The Geo-referenced map of sound level of Hamadan City

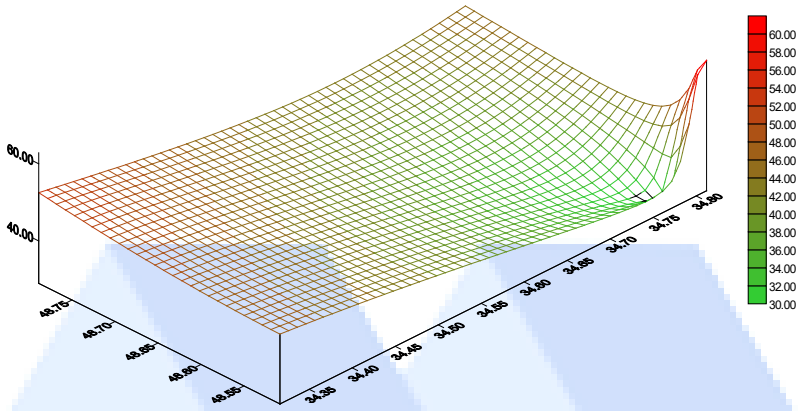

Figure 6. Sound level of Hamadan by 3D map

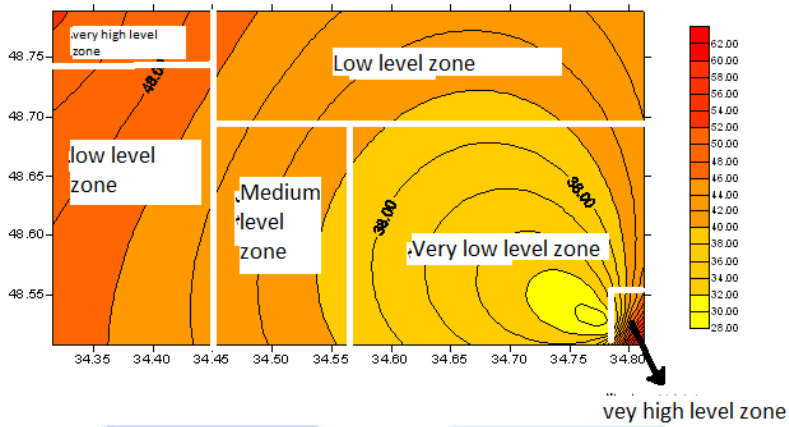

Figure 7. The zoning map of sound level intensity

8. Conclusion

According to the needs of planners and experts in the field of urban management, the existence of a noise pollution map of big cities like Arak and Hamedan seemed necessary. In this research, an attempt was made to prepare a spatial map of sound intensity distribution and zoning the areas. The results of data collection and map drawing indicate that in Arak, Shariati Square area has the highest sound intensity level, and in Hamadan city, Cheragh Red Light area and Amamzadeh Abdullah Square have the highest sound intensity level. This map can be used for decision-making and location systems based on GIS of urban facilities such as hospitals and educational places that require a low level of sound intensity. Also, urban areas that need to install noise reduction facilities will be identified.

Declaration of Conflict of Interests

The authors declare that there is no conflict of interest. They have no known competing financial interests or personal relationships that could have appeared to influence the work reported in this paper.

References

[1.] Farber, G. S., & Wang, L. M. (2017, December). Analyses of crowd-sourced sound levels of restaurants and bars in New York City. In Proceedings of Meetings on Acoustics 174ASA (Vol. 31, No. 1, p. 040003). Acoustical Society of America.

[2.] Hinton, J., Howell, K., et. al. (2005). BUMP-The Birmingham updated noise mapping [J]. Acta Acustica united with Scustica, 2005(1): 66-68.

[3.] Jia, X. P. (1995). Study on assessmentmethod of urban environmental noise [J]. Arid Environment Monitoring, 9 (4):236-2531 Engineering Acoustics. Edition 1.0 30th April 2006. Engineering Acoustics from Wikibooks, the open-content textbooks collection.

[4.] Foundations of Engineering Acoustics. Institute of Sound and Vibration Research,University of Southampton, Southampton, UK,2003.

[5.] Fundamentals of Acoustics. Michel Bruneau. British Library Cataloguing-in Publication Data. 2006.

[6.] Aumond, P., Can, A., Mallet, V., De Coensel, B., Ribeiro, C., Botteldooren, D., & Lavandier, C. (2018). Kriging-based spatial interpolation from measurements for sound level mapping in urban areas. The journal of the acoustical society of America, 143(5), 2847-2857.

[7.] Murphy, E., & King, E. A. (2016). Smartphone-based noise mapping: Integrating sound level meter app data into the strategic noise mapping process. Science of The Total Environment, 562, 852-859.

[8.] Kanjo, E. (2010). Noisespy: A real-time mobile phone platform for urban noise monitoring and mapping. Mobile Networks and Applications, 15, 562-574.

[9.] Rey Gozalo, G., Barrigon Morillas, J. M., & Prieto Gajardo, C. (2015). Urban noise functional stratification for estimating average annual sound level. The Journal of the Acoustical Society of America, 137(6), 3198-3208.

PACE-2023
International Congress on the Phenomenological Aspects of Civil Engineering

PACE-2023
International Congress on Phenomenological Aspects in Civil Engineering

Research Article
20-23 June 2023

Research Basis on The Potentials of The Saw-Cut Technique Applied to Prestressed Concrete

José R. Martí-Vargas*,[1], Juan Navarro-Gregori[1], Pedro Serna[1], Ester Giménez-Carbó[1], M. Carmen Castro-Bugallo[1], Juan A. Mateu-Sánchez[1]
[1]*Institute of Concrete Science and Technology (ICITECH), Universitat Politècnica de València*
Camino de Vera s/n, 46022, València, Spain
Corresponding Author E-mail: jrmarti@cst.upv.es

Keywords

Concrete,
Structure,
Prestress,
Loss,
Test,
Cut,
Assessment.

Abstract

In the prestressing design, the designer must set the prestressing force introduced to the concrete member and estimate both the short- and the long-term prestress losses, so that the structure meets its requirements over its service life. Since construction practice has commonly not considered the use of devices for monitoring after casting, prestress losses are usually unknown, and therefore the residual prestressing force. Hence, this paper presents the basis of a research project motivated by the need to formulate reliable assessments in the field of existing prestressed concrete structures (EPCSs. The project aims the implementation of a specific methodology for the diagnosis of the residual stress-deformational state of EPCSs, and is based on the potential synergy of the Isolated Concrete Block Method (ICBM) as an empirical basis and a multi-level structural modelling strategy following the latest trends. With a schedule developed through six tasks, it is intended to follow a working methodology that integrates the design/modelling and experimental aspects, so that there is an almost continuous feedback between both. According to the expected impact of results, the ICBM, which has a clear potential to become a reference non-destructive, practical, economical and reliable method, is suitable to promote an active approach to EPCSs maintenance.

1. Introduction

The accurate determination of the residual prestressing force is essential within the context of the assessment of existing prestressed concrete structures (EPCSs), since the effect of prestressing has a major impact on the stress-deformation responses and capacities of such structures under both serviceability and ultimate conditions. The de-sign of concrete prestressing is usually approached under stress criteria (allowable stresses in the elastic-linear re-gime) in accordance with the limitations imposed by codes and regulations, taking into account both geometrical limitations, derived from the minimum tendon cover requirements, and technological constraints (e.g. prestressed or post-tensioned reinforcement, internal or external prestressing, ...) and the subsequent variations of the prestressing force throughout the service life of the structure.

The prestressing of concrete by means of reinforcement requires the reinforcement to be stressed. The need to con-form to the design and the regulatory requirements for quality control require that the value of the "prestressing force" is known and documented, usually from the measuring devices (pressure sensors) of the hydraulic actuators used. Afterwards, with the transmission or introduction of the prestressing into the concrete, either by detensioning in the case of pre-stressed reinforcement or by anchoring in the case of post-stressed reinforcement, the resulting tensile force in the active reinforcement is the so-called "prestressing force", a force which is not usually known and which has different values both along the tendon and over time. Thus, "prestressing loss" is defined as the difference between the “prestressing force” and the "residual prestressing force" (prestressing force in a section of the structural member at a given time). Prestressing losses can be of different origin, and are usually classified as follows:

- Instantaneous: by penetration of anchor wedges, by elastic shortening of the concrete, and also, in the case of post-stressed reinforcement, by friction with the sheaths, and in the case of pre-stressed reinforcement, by re-laxation of the reinforcement, by thermal expansion and by shrinkage of the concrete up to the instant of pre-stress transfer.
- Deferred: by shrinkage and creep of the concrete and by relaxation of the active reinforcement.

In the design of the prestressing, the designer sets the prestressing force and makes an estimate of the prestressing losses, so that the final value of the prestressing force is equal to or greater than that required for the structure to meet its requirements throughout its service life. However, prestressing losses are not usually known, and therefore neither is the residual prestressing force, since the usual construction practice to date has not considered the incorporation of measuring devices in concrete structures to monitor them over time. Therefore, there

is a great deal of uncertainty when it comes to assessing the extensive stock of EPCSs, as it is increasingly necessary to have information on the condition of the structures: maintenance plans, service life prediction tools, decision-making criteria in the event of extraordinary events, etc., are undoubtedly elements that enhance sustainability in the field of infra-structure management.

For a large number of existing structures, the design life has been or will be reached in the near future, as highlighted in FIB bulletin no. 80(2016) [1]. This is because a large part of the existing structures was built in the 1960s, and may need a comprehensive assessment from a risk and reliability point of view. In this context, several studies [2-5] carried out on EPCSs (in service between 25 and 40 years) have found an appreciable deviation between the measured prestressing losses and the losses predicted by the models provided in the codes. Thus, it is clear that there are difficulties in determining the residual prestressing forces using the models provided by the codes. These difficulties are related to factors including (among others) assumptions about the characteristics of the prestressing system and time-dependent phenomena, as well as the possible development of degradation processes. Uncertainties associated with prestressing have on occasion led several prestressed concrete bridges to structural collapse [6,7]. Consequently, and as stated in the Strategic Plan 2020-2023 of the World Road Association (PIARC) [8], the scientific method and state-of-the-art knowledge for the assessment of existing structures should be promoted.

2. Current status

Despite the above uncertainties, there are few empirical methods to assess the condition of prestressed members, and their application is not always feasible. Destructive methods include [5]:

- Cracking moment (crack initiation).
- Concrete decompression (crack re-opening).
- Tendon cutting.

Destructive methods inevitably cause structural damage and are therefore unsuitable for application to in-service structures, hence the interest in developing non-destructive methods (or with conditions that only require aesthetic restitution) such as:

- Tendon deformation (exposed tendon) [9].
- Hole drilling [2].
- Saw-cuts [10].

On the other hand, although reliability-based assessment of existing concrete structures has been the subject of research over the past decades, a coherent structural assessment framework and a practical approach compatible with Eurocodes and applicable to existing concrete structures is currently lacking. Trends point towards multilevel structural modelling strategies [12-13]. The idea is as follows: with different design expressions and methods, the higher the level of approximation and the more sophisticated the analysis, the more realistic the safety estimation will be and the more possibilities there will be to find "hidden" structural capacities, so that the likelihood of avoiding overly conservative assessments and of incurring unnecessary costs resulting from decisions taken after assessment will also be higher.

The Model Code [14] has taken an important step in providing safety formats to be used in connection with non-linear finite element analysis. These safety formats define safety factors for material properties and overall structural strength. However, the development of specifications on how to perform the analyses has not kept pace with the development of the safety formats. There is no doubt that results using non-linear finite element analysis can be substantially influenced by the model and human factors arising from the skill of the analyst. In this respect, the recent (2020) guidelines promoted by the Dutch Ministry of Infrastructure [15] constitute a very advanced body of documentation that allows clear and common criteria for the analysis of existing structures to be established. Multilevel structural modelling strategies usually work by applying different degrees of modelling refinement, e.g. [12]:

- Level I: simplified linear analysis
- Level II: linear finite element analysis
- Level III: 2D non-linear finite element analysis
- Level IV: 3D finite element non-linear analysis, with perfect bond
- Level V: 3D non-linear finite element analysis, with bond constitutive laws.

With all this, the evaluation strategy using multilevel structural modelling must be "fed" with experimental results, with the saw-cut method [10] being the one addressed in this Project, as it is still far from being developed and validated for a reliable application. With this method, the residual prestressing force is obtained from the response of a concrete block formed by making surface cuts with a circular saw. These cuts are made perpendicular to the prestressing direction, defining a concrete block between two cuts which is isolated from the effect of the prestressing; the concrete in the block is decompressed. The deformations on the surface of the isolated block are obtained by comparison with the pre-cut state. Once the deformations are known, the stresses are computed and entered into a calculation model to determine the residual prestressing force.

Among the few documented realisations of this method it can be found a study carried out with beams from the Logan Canyon Bridge (Utah, USA) [16], and the evaluation of the Kiruna Bridge (Sweden) [10]. In both cases the method was used in conjunction with other destructive methods, and in neither case was the prestressing force monitored, so the residual prestressing force estimate was obtained from indirect measurements. Consequently, it is of the utmost interest to carry out an experimental investigation to materialise the saw-cut or isolated Concrete Block Method (ICBM) with prestressing force monitoring, in order to know the sensitivity of the method to different parameters (e.g. strip width between cuts, cut depth, stress level, ...) and to be certain about the actual prestressing force acting.

3. Justification for the proposal

Existing infrastructure and the built environment represent approximately 50% of national wealth in most developed countries [12], and the costs associated with their maintenance constitute about 50% (and tending to increase) of the total construction sector [17]. In Spain, the State

Road Network has more than 15,000 crossing structures with spans of at least 10 m in length, technically known as "bridges". Given these orders of magnitude, it is necessary that the decisions to be taken regarding the potential actions to be carried out for the adequate preservation of a structure (e.g. repair, reinforcement, limitation of actions, ...) are supported by adequate diagnoses, which will be all the more accurate to the extent that they are based on an adequate determination of the stress-strain state of the structure. In turn, the stress-strain state must be properly contextualized in the life cycle of the structure, in order to take into account for the interrelationships between the phases that make up this cycle, taking as initial reference the project phase (e.g. design methods and values), the specificities inherent to the construction phase (e.g. properties of the materials supplied) and the "clinical history" (e.g. previous inspections) corresponding to the service life phase.

Therefore, the need to formulate reliable diagnostics in the field of the assessment of existing prestressed concrete structures, in a context of a regulatory vacuum that makes it necessary to advance at the frontier of knowledge with the support of recently published reference documents, together with the large number of structures susceptible to assessment, justify this R&D&I Project based on the synergy of a new non-destructive method as an empirical basis and a multilevel strategy for structural assessment.

4. Research objectives

The general objective of the Project is to implement a specific methodology for the diagnosis of the residual stress-strain state of existing prestressed concrete structures. This general objective involves achieving the following specific objectives:

- To develop prediction models of the residual stress-strain state.
- Set up a guide for the application of the ICBM.
- To develop a modelling tool for structural assessment based on the residual state.
- To establish a guide to the application of multilevel structural analysis based on the residual stress-strain state.

5. Work packages

It is intended to follow a work methodology that integrates the aspects of design/modelling and experimentation, so that there is almost continuous feedback between the two throughout the development of the project. All the elements (beams and slabs) under study will have an initial design, as well as a pre-modelling and a post-modelling of their behaviour in a computer laboratory. The pre-modelling will be the simulation carried out with the available data before the element is tested in the experimental laboratory, while the post-modelling will correspond to the simulation incorporating the information obtained from the observation and the results obtained in the experimental laboratory. Under this premise, the development by stages, and additionally the sequential study foreseen in Stages 1 and 2, will allow progressing towards a progressive refinement of the pre- and post-modelling. In this way, the pre-modelling of element "i" will incorporate the aspects already known and introduced in the post-modelling of element "i-1"; in turn, once element "i" has been tested in the experimental laboratory, it will be post-modelled and the advances obtained will be incorporated into the pre-modelling of element "i+1". Based on this concept, the work plan is detailed, which includes the following tasks and milestones:

5.1. Task 1. Design and modelling of elements to be tested (beams and slabs).

The initial design will be approached according to simplified methods usually applied to prestressed concrete structural elements, for different combinations of parameters (concrete strength, prestressing force, prestressing eccentricity, cross-section, and distribution of transverse reinforcement). It is estimated that elements of 3-4 m length and rectangular cross-section will be optimal in terms of representativeness of the phenomena to be studied, consumption of resources and equipment required. Preferably, Y 1860 S7 prestressing steel strands will be used. All the elements designed will be pre-modelled in 2D with non-linear behaviour, using the DIANA FEA software.

A collection of designs shall be available from:

a) In the case of beams:

- 2 class of concrete (HP-40 and HP-70).
- 3 levels of prestressing force (75%, 60% and 50% of the maximum prestressing force allowed by the Spanish Structural Code and Eurocode 2).
- 2 depth (cross-section).
- 2 eccentricities (sectional positioning of the prestressing force).
- 2 transverse reinforcement distributions.

It should be noted that the combination of 2 concretes, 3 prestress levels, 2 depths and 2 eccentricities results in 24 different stress-strain states.

b) In the case of slabs: a single combination of concrete type-prestressing force, varying the distance between prestressing tendons. The aim is to see how the spacing between tendons affects the strip width between cuts, for different cut lengths and with different degree of interception in terms of number of tendons.

Milestones:

- 1.1. Design of the structural elements to be tested.
- 1.2. Initial behavioral models.

5.2. Task 2. Characterisation of materials (concrete and prestressing reinforcement): mechanical and bonding properties.

Obtention and characteriation of standard concretes based on the design of the corresponding mixtures; the compressive and flexural strengths and deformation moduli of the concretes to be used in the manufacture of the elements will be determined, analysing the evolution of these properties with age.

With regard to the prestressing reinforcement, the characteristics certificate shall be requested from the supplier, and tensile samples shall be tested.

The bonded concrete-strand interaction shall be studied by determining the transmission lengths. Note that the ICBM should be applied in region B (Bernouilli) of the structural element, as shown in Figure 1:

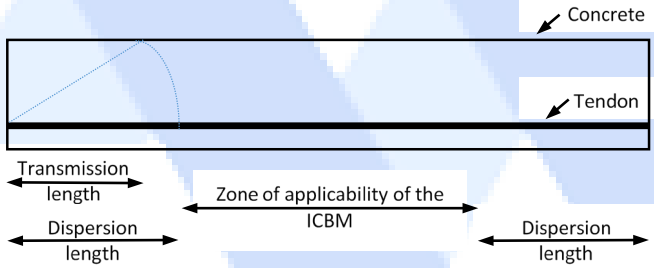

Figure 1. Idealisation of the zone of applicability of the ICBM

Milestones:

- 2.1. Test results of mechanical properties of concrete.
- 2.2. Results of tendon mechanical properties tests.
- 2.3. Definition of the area of applicability of ICBM.

5.3. Task 3. Development of Stage 1: ICBM tuning in beams.

Starting from the designs and models resulting from Task 1, with the materials characterised in Task 2, the ICBM will be developed through the sequential study of 5 type beams.

BEAM 1: positioning of cuts. The area of application of the ICBM will be instrumented on its most stressed face with strain gages arranged longitudinally (in the pre-stressing direction), foreseeing the practice of 6 cuts (Figure 2). To set the positions of the cuts (1 to 6), the simulation of the response will be based on the pre-modelling of the beam including the effect of the cuts, and the length of the strain gage to be used (estimated at 5-6 times the maximum size of the aggregate) and the spacing of the guard so that the instrumentation is protected from the cuts will be determining factors. For the same cutting position, the cut will be made progressively, advancing in steps (tentatively with a depth of 5 mm). First, cuts shall be made at positions 1 and 6, and the response detected by the strain gage assembly shall be observed. It will be crucial to analyse how the prestressing develops in the vicinity of the cuts. Once the maximum depth of cut at positions 1 and 6 has been exhausted, the same procedure shall be followed for positions 2 and 5, and then for positions 3 and 4.

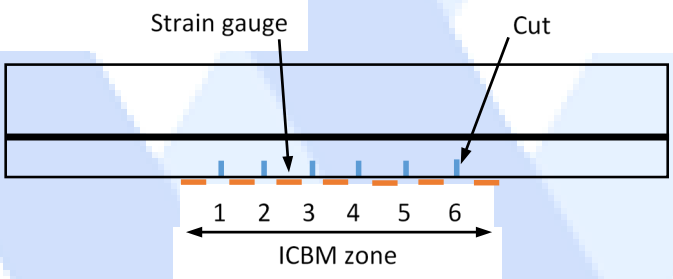

Figure 2. Layout of cuts and strain gauges in BEAM 1

BEAM 2: repositioning of the neutral fibre. Based on the results of BEAM 1 and a new modelling, another 6 shear positions will be set, in this case to form 3 ICBs that will be analysed: ICB 1-2, ICB 3-4 and ICB 5-6 (Figure 3). The most stressed face will be instrumented in the same way and strain gages will also be placed along the edge of the beam to analyse the effects of the cuts on the deformation profile.

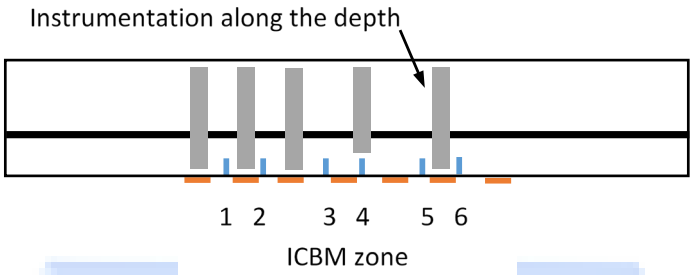

Figure 3. Layout of cuts and strain gauges in BEAM 2

BEAM 3: influence of transverse reinforcement. The starting point will be a beam design incorporating transverse reinforcement, so that given its spacing, the response of ICBs positioned in correspondence and in alternation with respect to the transverse reinforcement distribution will be analysed. The instrumentation scheme shall follow the guidelines of BEAM 2.

BEAM 4: sensitivity to stress Level-I. All the knowledge acquired with regard to ICBM will be used and a new BEAM 1 will be studied, in this case by instrumenting and cutting the less stressed face.

BEAM 5: sensitivity to stress level-II and pilot destructive test. A beam similar to BEAM 1 will be studied, with a different edge, which will have the most advanced pre-modelling in this Stage; it will be instrumented in an optimised way in terms of the number of ICBs (1 or 2) on the most stressed face, avoiding cuts in the central section of the ICBM zone with the idea of carrying out a pilot destructive test of great interest for Stage 3. This destructive test will be carried out in a 4-point load/reaction configuration, so that experimental information will be obtained on the cracking moment, the extent of the cracked zone and the exhaustion. These results will be used to contrast with traditional empirical methods (crack initiation and crack re-opening) and post-modelling of BEAM 5 will provide an excellent starting point for pre-modelling and possible revision of Stage 3 beam designs.

Milestones:

- 3.1. Characterisation of the extent of stress release in ICB concrete in beams (ICB length = element width).
- 3.2. Definition of the ICB: width, depth and shear progression, and positioning with respect to the transverse reinforcement.
- 3.3. Sectional impact of the ICB.
- 3.4. Additional recording of deferred losses in beams.
- 3.5. Pilot destructive testing.

5.4. Task 4. Development of Stage 2: application of ICBM on slabs.

The study of 2 slabs will be carried out. The prestressing will be introduced differently in each slab by varying the distance between prestressing tendons. Isolated concrete blocks (ICBs) of different lengths, intercepting a certain number of tendons as well as differentiated zones of influence of the tendons (Figure 4 shows some examples). Strain gages shall be arranged in and around the ICBs, considering coincidence and alternation of tendon positions. Based on the arrangement and configuration of the different ICBs in the 2 slabs, the possible effects due to the spacing between tendons will be analysed and the requirements to be met in terms of ICB length will be determined, as well as the convenience of forming a ICB by means of 4 parallel cuts two by two.

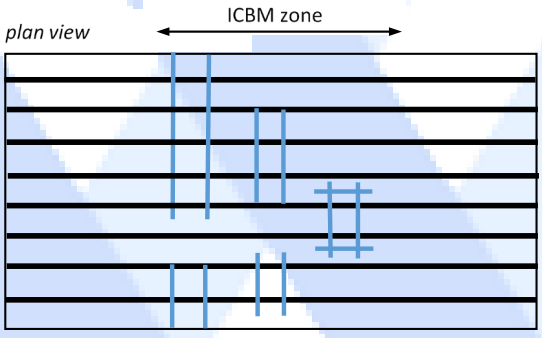

Figure 4. Layout of proposed cuts in a slab

The slabs will be placed under different environmental conditions in order to obtain records of the evolution of deferred prestressing losses.

Milestones:

- 4.1. Characterisation of the extent of stress release in ICBs in slabs (ICB length ≤ element width).
- 4.2. Definition of the ICB to be tested: length and transverse positioning.
- 4.3. Additional recording of deferred losses in slabs.

5.5. Task 5. Development of Stage 3: diagnosis of beams with ICBM.

In this task, a study campaign will be carried out with the 24 stress-strain states defined in Task 1. The initial designs may be subject to revision, and the highest possible multilevel structural analysis representing the detected effects of greatest impact will be applied. The computer laboratory and experimental laboratory work will go hand in hand for each element: (1) pre-modelling, (2) application of ICBM and diagnosis of the residual stress-strain state, and (3) post-modelling. The pre-modelling will focus on the prediction of the residual stress-strain state, while the post-modelling will focus on the reproduction of the diagnosis obtained. The different prestress levels introduced in the beams will be representative of 3 time instants that will be contextualised in the lifetime of the structure. The guidelines on instrumentation, positioning and materialisation of the ICBs will be in accordance with Task 3.

Milestones:

- 5.1. ICBM application protocol.
- 5.2. Prestressing loss recording.
- 5.3. Prediction of diagnostics in computer laboratory.
- 5.4. Obtaining diagnostics in experimental laboratory.

5.6. Task 6. Pilot testing and implementation of guidelines for structural assessment.

Based on the scientific-technical knowledge gathered throughout the Project, the drafting of documents will be undertaken that include the guidelines, recommendations and contextualisation of both the potential application of ICBM in the field of maintenance and assessment of prestressed concrete structures, and the suitability of considering approaches based on a multilevel structural modelling strategy in this field. Likewise, possible proposals for adjusting the design methods related to the estimation of prestressing losses will be implemented, in order to finally carry out pilot tests for the application of ICBM and multilevel structural modelling on beams manufactured on a real scale by a precast prestressed concrete company in the area.

Milestones:

- 6.1. ICBM application guide: diagnosis of the residual stress-strain state.
- 6.2. Guide to the application of multilevel structural analysis of the residual stress-strain state.
- 6.3. Review of prestress loss estimation design methods.
- 6.4. Pilot testing of real beams under controlled conditions.

6. Schedule

Figure 5 summaries the schedule for the Project Work Packages.

	Execution period (quarters)											
	Year 1				Year 2				Year 3			
Work Package	1	2	3	4	1	2	3	4	1	2	3	4
1												
2												
3												
4												
5												
6												

Figure 5. Schedule for the Project Work Packages

7. Conclusions, expected impact of results

The results of the Project will represent a significant advance in the frontier of knowledge, which will have a scientific-technical impact that will be reflected in:

- Promotion of the scientific method and state-of-the-art knowledge oriented to the evaluation of EPCSs.
- Contribution to overcoming the existing regulatory vacuum in the field of the assessment of EPCS.
- Technological, competitive and functional improvement, with the development of a new non-destructive test method capable of providing more reliable diagnostics of the stress-strain state of EPCSs.
- Development of advanced specifications on how to perform structural analysis with varying degrees of modelling refinement.
- Updating of design methods for estimating prestressing losses by reducing uncertainties in the determination of the residual prestressing force, which will allow the design of more resilient structures in the future.

Regarding the socio-economic impact, it is noted that:

- The Project has a preventive impact, in order to avoid or delay the appearance of problems that, if postponed, would be more complicated and costly to solve.
- The potential practicality, cost and reliability of the ICBM make it a non-destructive method of reference for the evaluation of prestressed concrete structures, which will make it possible to "popularise" the carrying out of a greater number of evaluations.
- The Project contributes to the Sustainable Development Goals: SDG 9 "Industry, Innovation and Infrastructure", SDG 12 "Responsible Consumption and Production" and SDG 13 "Climate Action", as the experimental and modelling tools resulting from the Project for the development of diagnostics will support decision-making criteria on the extension of the useful life of structures.

Acknowledgements

This work forms part of the Project "Looking for the lost prestress: multilevel strategy and non-destructive method for diagnosis of existing concrete structures" funded by the Agencia Estatal de Investigación (State Research Agency) of Spain (competitive research project PID2020-118495RB-I00 and human resources funding PRE2021-098777). The authors would also like to thank the ICITECH technical staff, Francisco J. Martorell and Daniel Tasquer, for their valuable contributions and involvement in the development of the experimental work.

Declaration of Conflict of Interests

The authors declare that there is no conflict of interest. They have no known competing financial interests or personal relationships that could have appeared to influence the work reported in this paper.

References

[1.] FIB (2016) Bulletin nº 80: Partial factor methods for existing concrete structures. Lausanne: Fédération Internationale du Béton.

[2.] Azizinamini, A.; Keeler, B.J.; Rohde, J.; Mehrabi A.B. (1996) Application of a new nondestructive evaluation technique to a 25-year-old prestressed concrete girder. PCI J 41, pp. 82–95.

[3.] Pessiki, S.; Kaczinski, M.; Wescott, H.H. (1996) Evaluation of effective prestress force in 28-year-old prestressed concrete bridge beams. PCI J 41, pp. 78–89.

[4.] Osborn, G.P.; Barr, P.J.; Petty, D.A.; Halling, M.W.; Brackus, T.R. (2012) Residual prestress forces and shear capacity of salvaged prestressed concrete bridge girders. J Bridge Eng 17, pp. 302–309.

[5.] Halsey, J.T.; Miller, R. (1996) Destructive testing of two forty-year-old prestressed concrete bridge beams. PCI J 41, pp. 84–93.

[6.] De Schutter, G. (2012) Damage to concrete structures. Boca Raton, FL, USA: CRC Press.

[7.] Blackler, M.J.; Cooke, R.S.; Besses, O.'Th. (1995) Barn bridge: inspection and testing of a segmental post-tensioned concrete bridge. Proc Inst Civ Eng: Struct Build 110, pp. 19–27.

[8.] PIARC (2020) Strategic Plan 2020-2023. La Défense cedex, France: World Road Association.

[9.] Civjan, S.A.; Jirsa, J.O.; Carrasquillo, R.L.; Fowler, D.W. (1998) Instrument to evaluate remaining prestress in damaged prestressed concrete bridge girders. PCI J 43, pp. 62–69.

[10.] Bagge, N.; Nilimaa, J; Elfgren, L. (2017) In-situ methods to determine residual prestress forces in concrete bridges. Eng Struct 135, pp. 41–52.

[11.] Biswal, S.; Ramaswamy, A. (2016) Measurement of existing prestressing force in concrete structures through an embedded vibrating beam strain gauge. Measurement 83, pp. 10–19.

[12.] Plos, M.; Shu, J.; Zandi, K.; Lundgren, K. (2017) A multilevel structural assessment strategy for reinforced concrete bridge deck slabs. Struct and Infrastr Eng 13, 2, pp. 223–241.

[13.] Bagge, N.; Plos, M.; Popescu, C. (2019) A multi-level strategy for successively improved structural analysis of existing concrete bridges:examination using a prestressed concrete bridge tested to failure. Struct and Infrastr Eng 15, 1, pp. 27–53.

[14.] FIB (2013) Model Code for Concrete Structures 2010. Berlin: Ernst & Sohn.

[15.] Rijkswaterstaat Centre for Infrastructure (2020) Guidelines for Nonlinear Finite Element Analysis of Concrete Structures Version: 2.2 RTD: 1016-1:2020 Status: Final. The Netherlands.

[16.] Kukay, B.; Barr, P.J.; Halling, M.W.; Womack, K. (2010) Determination of the residual prestress force of in-service girders using non-destructive testing. Structures Congress 2010. Orlando, FL, United States, pp. 709–716.

[17.] Long, A.E.; Henderson, G, D, Montgomery, F.R. (2001) Why assess the properties of near-surface concrete? Constr Building Mat 15, pp. 65–79.

PACE-2023
International Congress on the Phenomenological Aspects of Civil Engineering

PACE-2023
International Congress on Phenomenological Aspects in Civil Engineering

Research Article
20-23 June 2023

Structural Code Requirements on Inspection and Maintenance of Concrete Structures: The Spanish Case

José R. Martí-Vargas*[1], Juan Navarro-Gregori[1], M. Carmen Castro-Bugallo[1], Juan A. Mateu-Sánchez[1]
[1]*Institute of Concrete Science and Technology (ICITECH), Universitat Politècnica de València*
Camino de Vera s/n, 46022, València, Spain
Corresponding Author E-mail: jrmarti@cst.upv.es

Keywords

Concrete,
Structure,
Inspection,
Maintenance,
Assessment,
Code,
Guide.

Abstract

The maintenance needs of concrete structures have often resulted in costly interventions, not only due to the absence or lack of an adequate inspection and maintenance plan, but also as consequence of a common practice in the design-build process focused on solving requirements under "instantaneous" economic conditions. This situation is not compatible with the new paradigm of environmental, social and economic sustainability, so the planning of inspections and maintenance takes special relevance by considering economic conditioning factors of "deferred" scope. In this context, this paper presents an historical perspective of the main Spanish documentary references that, in the form of regulations and guides, have been conceived to establish mandatory specifications and/or provide tools to facilitate the inspection and maintenance of concrete structures. It is stated that, in the case of Spain, there have been no specific project provisions and practical guides for concrete structures oriented to facilitate their inspection and maintenance until well into the twenty-first century. The first requirements on maintenance of concrete structures appeared in the Structural Concrete Code approved in 2008, which considered the need of a complete documentary archive and the performance of inspections at different levels (routine, major and special). Afterwards, the new Structural Code 2022 introduced an extended approach within the aforementioned “deferred” scope which includes additional prescriptions focused on the Maintenance Plan, the assessment of existing structures and the management of concrete structures during their service life.

1. Introduction

For the case of concrete structures, and in view of the new paradigms of sustainability, the development of a maintenance plan conceived from the design phase of the structure should not be missing in new structures. In Spain, the first inventory of road bridges was carried out in 1985 [1], and more than 15,000 structures with spans of at least 10 m in length —technically "bridges"— were identified in 2010. So that, the time dimension should not be forgotten, as has often been the case with existing structures, to which little technical and regulatory attention has been devoted from the maintenance point of view, in contrast to the deserved recognition of maintenance in areas as different as the automotive or aviation sectors.

In view of these orders of magnitude, infrastructure maintenance should not only involve repairing what has deteriorated (reactive approach), but also prevention through maintenance plans (active approach), in order to avoid or delay the appearance of problems that would otherwise be more complicated to solve and would cost much more money. Concrete structures are a valuable asset for a society as a whole that is evolving towards higher levels of demand and commitment from the perspective of sustainability. Proof of this is the new benchmark: The Sustainable Development Goals (SDGs) as part of the 2030 Agenda [3].

In the case of new structures, current trends are oriented towards improving inspection and maintenance tasks right from the design phase of structures [4]. In the case of existing structures, there is a long way to go to implement measures aimed at achieving the SDGs, because although the first maintenance plans for structures in Spain date back several decades, their number is very low due to the absence of regulations that would require them to be drafted and carried out. Therefore, the purpose of this paper is to offer an historical perspective and to analyse the main Spanish documentary references that, in the form of regulations and guides, have been conceived to establish mandatory specifications and/or provide tools to facilitate the inspection and maintenance of concrete structures.

2. Background

Many existing structures have not had maintenance plans from the moment they were put into service, nor have they been instrumented in such a way as to allow monitoring of their behaviour over time. One of the reasons for the scarce proliferation of maintenance plans is probably the absence of reference documents that could serve as a guide for designers and those responsible for inspection and maintenance. It has been shown that in the case of Spain there are no project provisions and practical guides for structures oriented to facilitate their inspection and maintenance in crucial aspects such as structural scheme, selection of materials, dimensions, necessary instrumentation or prestressing elements [4]. In this respect, it is noteworthy the recent contribution of the ATC-PIARC Bridge Committee and the Working Group 4/4 of ACHE Commission 4 in the form of a monograph [5].

The design and construction phases are very important because they require, among other things, a large economic outlay, although their time span is, especially nowadays, very short compared to the useful life (e.g. 100 years). The lifetime phase is the longest, so that the maintenance of a structure covers almost its entire life cycle, and therefore the reasons that invite to a structural assessment respond to several aspects, either according to the activities carried out in the maintenance plans -intrinsic causes to the structure-, such as the detection of cracking and/or excessive deflections, degradation due to corrosion of the reinforcement or chemical alterations of the concrete components, ... or due to other (extrinsic) causes such as, for example, change of use, adaptation to new regulations, extraordinary events (impact, fire, etc.), effects of nearby works, etc. For a large number of existing bridges, the design life has been or will be reached in the near future, as highlighted in FIB bulletin no. 80 "Partial factor methods for existing concrete structures" (2016) [6].

A great deal of effort has been devoted to these design and construction phases in terms of teaching (this is what has been taught in universities), standardisation (structural codes have been designed to regulate the design and construction of new works, not to maintain existing ones) and economics, and consequently much of the efforts of designers, builders and administrations are focused on the feasibility of construction and the economic optimisation of the resources that lead to the "putting up" of the structure. However, procedures and regulations up for the inspections along the service life phase of the structure have only recently been developed [7-8].

3. Spanish Structural Concrete Codes

The first Spanish Code for plain and reinforced concrete (H-39) began to be drafted in March 1938 and was officially published in February 1939. Afterwards, the Code was revised (H-44). The HA-61 was significant since it was conceived by E. Torroja from a strong structural perspective focused on reinforced concrete. With this format, several evolutions and actualisations were made until 1991. Figure 1 shows the chronological development of Spanish Concrete Codes (or Official Standards). In this figure: (a) each rectangle corresponds to an approved official code, which is designed using the abbreviations detailed in the Nomenclature section; (b) the number following the abbreviation is the year of publication; (c) the vertical arrows mean the sequential evolution through time; and (d) the arrows with horizontal layout mean the integration or assimilation of a code in a subsequent code.

Regarding prestressed concrete, the first Code appeared in 1977 (EP-77), and several evolutions and actualisations were made until 1993. Taking into account that: (a) both EH-91 (Reinforced Concrete) and EP-93 (Prestressed Concrete) were coincident in some points of their content; (b) in numerous infrastructures, structural elements coexist that are studied and designed in both reinforced and prestressed concrete; and (c) the treatment that, both in technical texts related to concrete and in European and international technical regulations, is made of this material, it was considered appropriate to draft a single Code related to the design and execution of concrete constructions, both in mass and reinforced or prestressed, merging in it the two Codes mentioned above. Thus, through the EHE-98, the treatment of concrete was unified and, in this way, the design and execution of these constructions was regulated by a single official provision.

Other related Codes are also shown in Figure 1, which focused on aspects such as ready-mixed concrete, one-way reinforced or prestressed concrete floors, precast members, and road pavements (PG series, General Specifications for roads). Except the PG series, all of the remaining were integrated and merged at some point in time. The EHE was revised in 2008 [9] and was pioneer in including explicitly specific provisions regarding maintenance aspects of concrete structures. The current Spanish main code [10] includes not only structural aspects for concrete, but also for steel structures and composite structures. This main code, which has been conceived within the framework of the Eurocodes, introduces new regulations regarding the management of existing structures during their service life, which was outside the scope of the previous concrete and steel Codes, and systems for the protection, repair and strengthening of concrete structures.

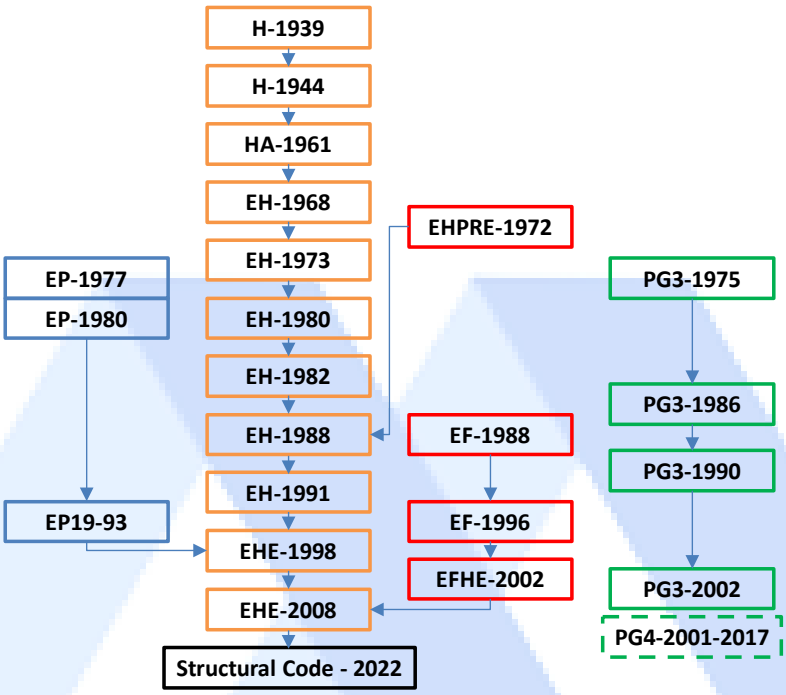

Figure 1. Chronological development of Spanish Concrete Codes

4. Pioneering requirements on maintenance of concrete structures (EHE-08) [9]

Maintenance is considered a preventive activity, which avoids or delays the appearance of problems that would otherwise be more complicated to solve and cost much more money. To this end, from the entry into service of the structure, the Owner must schedule and carry out maintenance activities in a consistent manner with the criteria adopted in the project. EHE-08 establishes that it is the responsibility of the Owner to organise the maintenance tasks around the indicated lines of action in order to have, at all times, information about the level of performance of the structure. According to the definition of "maintenance" in EHE-08 [9], maintenance of a structure means the set of activities necessary to ensure that the level of performance for which it was designed does not fall below a certain threshold during its design life, linked to its mechanical strength, durability, functionality and with appropriate aesthetic characteristics. The activities related to the maintenance of the structure are part of a broader overall context which can be referred to as the "structure management system". These activities are of great responsibility and require to be carried out by appropriately trained and equipped personnel. From an operational point of view, such a management system includes the following elements:

- Complete documentary archiving of the structure. It is the responsibility of the Owner to keep the complete Construction Project, as well as the projects, reports or reports that may eventually succeed it by virtue of repairs, reinforcements, extensions, etc., linked to the history of the structure.
- Routine inspections. It is also the responsibility of the Owner to carry out routine inspections to ensure the correct functioning of the elements linked to the operation and durability of the structure (e.g. auxiliary, non-structural elements with a useful life shorter than that of the structure and whose degradation may negatively affect the structure, such as drains, waterproofing, joints, etc.). The frequency of these inspections shall be established by the Author of the Project, depending on the operational and seasonal conditions.
- Major inspections. Carried out at the request of the Owner by technicians with training, means and accredited experience in this type of work, they constitute the set of technical activities which, in accordance with a prior plan, allow the detection, where appropriate, of damage to the structure, its conditions of functionality, durability and safety of the user, as well as estimating its future behaviour.
- Special inspections and load tests, which require specific auscultation of the structure and its subsequent analytical assessment for the formulation of diagnoses.

The design of all types of structures shall be required to include an Inspection and Maintenance Plan defining the actions to be carried out throughout their useful life and specifying, at least, the following points:

- Description of the structure and the exposure classes of its elements.
- Considered useful life.
- Critical points of the structure, requiring special attention for the purposes of inspection and maintenance.
- Frequency of inspections.
- Auxiliary means for access to the different areas of the structure, where appropriate.
- Recommended inspection techniques and criteria.
- Identification and description, with the appropriate level of detail, of the recommended maintenance technique, where such a need is foreseen.

The process begins with the performance of a first main, initial or "state 0" inspection, which will be the result of the control of the constructed element. From then on, with varying frequency, successive major inspections will be carried out, which will give an account of the evolution of the state of the structure. Having assessed the state of the structure and, where appropriate, its rate of deterioration by comparison with previous inspections, it shall be specified whether a special inspection is to be undertaken or whether, on the contrary, it can wait for the next scheduled major inspection in accordance with the protocol established by the Author of the Project or, where appropriate, by the Owner. The frequency of carrying out major inspections shall be defined by the Project Owner in the corresponding Inspection and Maintenance Plan and shall not be less than that established by the Owner, if applicable.

5. Structural Code-22 versus EHE-08

In general terms, the definition and the maintenance strategy described in [10] coincide with [9], even with the same words in many cases. Among the differences that the current Structural Code [10] presents with respect to the previous Code EHE-08 [9], there are:

- Explicit consideration of new construction and the cases of repair or strengthening of an existing structure.
- Use of the term "additional" life.
- Different descriptions of points to be included in a Maintenance Plan.
- Additional prescriptions focused on Maintenance Plan after completion of the execution of the construction works.
- Additional prescriptions focused on assessment of existing structures.
- Additional prescriptions focused on management of concrete structures during their service life.
- New regulations regarding structural interventions such as repair and strengthening of concrete structures, with particular reference to the respective Inspection and Maintenance plans.

6. Current requirements on inspection and maintenance of concrete structures (Structural Code) [10]

According to [10], the project, whether for new construction or for the repair or strengthening of an existing structure, shall include a maintenance plan which reflects the maintenance strategy and defines the maintenance actions to be carried out throughout the useful life of the project, which starts from zero in the case of new structures and should be understood as "additional" life to that already satisfied by an existing structure.

The maintenance plan shall contain a precise definition of at least the following points:

- Description of the structure and the exposure classes of its elements.
- Considered service life of the structure and of its constituent elements, given that some components of the construction will have shorter service lives (drainage systems, defences, support apparatus, paints, coatings, corrosion protection systems, etc.).
- Critical points of the structure, which require special attention for the purposes of their conservation and therefore for inspection and maintenance purposes. The plan shall establish the points to be inspected in both basic and major inspections.
- Periodicity of both basic or routine inspections and major inspections.
- Auxiliary means for access to the different areas of the structure, where appropriate.
- Recommended inspection techniques and criteria.
- Identification and description, with the appropriate level of detail, of the recommended maintenance operations, where such need is foreseen, including, where appropriate, frequency of action.

It should be borne in mind that the maintenance activity occupies practically the entire life cycle of a structure, so it is highly recommended that the maintenance plan includes an approximate assessment of the activities it contemplates. This assessment during the project is of great importance as it can lead to reconsideration of aspects and details of the project that may lead to exaggerated maintenance costs during the lifetime of the structure. Incidents arising during construction, as well as any design faults detected, will be included in a revision of the inspection and maintenance plan of the project, which will be drafted at the end of the execution of the works, whether they are of new construction or of repair or strengthening.

The inspection and maintenance plan drawn up after completion of the work must be made available to the responsible for the operation of the structure. Based on this maintenance plan, which replaces that of the project, and taking into account the indications of the project manager, the owner will be responsible for the elaboration of the maintenance program.

7. Maintenance Strategy Vs Assessment

The Maintenance Strategy is related to the structural assessment process of an existing structure, which shall normally be carried out by means of a quantitative verification of its bearing capacity and, where appropriate, its serviceability, taking into account possible deterioration processes. In fact, the Structural Code [10] defines the basis and procedures for the assessment of the structural capacity and residual service life of existing constructions, in accordance with the principles of structural safety analysis and durability prognosis.

A step-by-step assessment procedure can be adopted, since the process of structural assessment of an existing structure should be progressive, i.e. it starts from simple assessment procedures, associated with few data, and then, if necessary, using more sophisticated and more demanding formulations in terms of the amount of information, until it is possible to give an opinion about the suitability of the structure to accept defined actions with sufficient certainty. The following phases have to be considered: preliminary, detailed and advanced assessments. In particular: (a)

An initial inspection and the compilation and review of available documentation, including actions arising from the inspection and maintenance program, constitutes a first step in a preliminary assessment; and (b) The determination of the condition of the structure by means of a special inspection, including quantification of possible damage in the form of damage mapping, is required in a detailed assessment. Moreover, a special inspection (together auscultation and/or load testing) is considered in the Level 3 of the structural analysis defined in the assessment framework, which is aimed to carry verifications in a semi-probabilistic context, but using updated information in the form of residual/deduced strength properties and applying partial coefficients adjusted in order to obtain the same reliability as for new construction.

According to the prescriptions about management and assessment of existing structures [10], the determination of the residual service life of a concrete consists of deducting the period of time, from the instant of assessment, during which it takes for the structure or any part of it to reach one of the SLS or ULS identified either at the design stage or at the time of assessment. On the other hand, a 'qualitative validation' is possible in the case of structures for which there are no sanctioned procedures for quantitative structural analysis, no performance increments are required and have exhibited previous positive performance. Regarding load-bearing capacity, a major inspection must confirm the static scheme, must not disclose significant damage or deterioration, and the foreseeable deterioration of the structure shall not jeopardise structural safety, at least until the next scheduled major inspection.

Regarding serviceability, a major inspection must not show any signs of damage or deterioration, or of excessive deformation, displacement or vibration, whereas taking into account the foreseeable deterioration, as well as the planned maintenance schedule, an adequate durability must be ensured. Acceptance thresholds, for both SLS and ULS are implicit in the project basis and, where applicable, in the Inspection and Maintenance Program. Thus, the implication of an Inspection and Maintenance Program in the assessment is inevitable.

It should be taken into consideration that the assessment of the condition of structures is a highly complex issue that requires criteria and guidelines for action, well-trained teams and continuity over time to detect the speed of changes in the level of deterioration or performance of the structures and the related risks [11]. From the outset, the task of assessing a structure is always more complex than that of designing it, as the technician who is faced with it does not have the same idea as the original designer about its resistance scheme, and it is very likely that he does not have exhaustive information about the material properties, reinforcement layout, etc. In fact, the use of design-oriented methods to assess existing structures often leads to a high degree of conservatism [12]. Therefore, there is a regulatory vacuum in this area: there is currently no specific regulation that provides a clear and unequivocal methodology to address the assessment of a concrete structure with the same range and level of detail as that achieved for its design, as indicated in the document "Assessment of Reinforced Concrete Structures" (2019) [13], prepared by Working Group 4/1 of ACHE Commission 4, which at the same time emphasises the lack of sufficient research on crucial aspects such as the methodology to be followed to address the safety treatment of existing constructions. Moreover, as stated in [14], the scientific method and state-of-the-art knowledge for the assessment of existing structures should be promoted.

8. Conclusions

It has been offered a practical overview of the main Spanish documentary references that, in the form of regulations and guides, establish mandatory specifications and/or provide tools to facilitate the inspection and maintenance of concrete structures. The main conclusions are:

- Structures should be designed so that they can be properly and easily inspected and maintained. This requires that inspections and maintenance be an integral consideration in the design rather than treated as an afterthought.
- In the past, the principle of designing structures with future inspections and maintenance in mind has been overlooked. In the case of Spain, there have been no specific project provisions and practical guides for concrete structures oriented to facilitate their inspection and maintenance until well into the twenty-first century.
- The first requirements on maintenance of concrete structures appeared in the Structural Concrete Code approved in 2008, which considered the need of a complete documentary archive and the performance of inspections at different levels (routine, major and special).
- In many cases, the design approach focused on satisfying only the initial structural requirements (i.e. safety and serviceability)- and then minimizing the initial costs has resulted in costly future maintenance that has far outweighed the initial capital savings based on disregarding inspection and maintenance issues.
- The current Spanish Structural Code 2022 presents a complete treatment on Inspection and Maintenance of concrete structures based on an extended approach under not only instantaneous economic conditions but also under deferred considerations including additional prescriptions focused on the Maintenance Plan, the assessment of existing structures and the management of concrete structures during their service life.

Acknowledgements

This work forms part of the Project "Looking for the lost prestress: multi-level strategy and non-destructive method for diagnosis of existing concrete structures" funded by the Agencia Estatal de Investigación (State Research Agency) of Spain (competitive research project PID2020-118495RB-I00 and human resources funding PRE2021-098777). The authors would also like to thank the ICITECH technical staff, Francisco J. Martorell Romero and Daniel Tasquer Val, for their valuable contributions and involvement in the development of the experimental work.

Nomenclature

ACHE: Asociación Científico-Técnica del Hormigón Estructural (Scientific-Technical Association for Structural Concrete)

ATC: Asociación Técnica de la Carretera (Road Technical Association)

EH: Instrucción para el proyecto y la ejecución de obras de hormigón en masa o armado (Code for the design and execution of plain or reinforced concrete constructions)

EHE: Instrucción de Hormigón Estructural (Structural Concrete Code)

EHPRE: Instrucción para la fabricación y suministro de hormigón preparado (Code for the manufacture and delivery of ready-mixed concrete)

EF: Instrucción para el proyecto y la ejecución de forjados unidireccionales de hormigón armado o pretensado (Code for design and execution of oneway reinforced or prestressed concrete floors)

EFHE: Instrucción para el proyecto y la ejecución de forjados unidireccionales de hormigón estructural realizados con elementos prefabricados (Code for the design and execution of unidirectional structural concrete floors made with precast elements)

EP: Instrucción para el proyecto y la ejecución de obras de hormigón pretensado (Code for the design and execution of prestressed concrete)

FIB: Fédération Internationale du Béton (International Federation for Structural Concrete)

H: Instrucción para el proyecto y ejecución de obras de hormigón (Code for the design and execution of concrete constructions)

HA: idem EH

PG: Pliego de Prescripciones Técnicas Generales para obras de carreteras y puentes (General Technical Specifications for Road Works and Bridges)

PIARC: Permanent International Association of Road Congresses (also World Road Association)

SDG: Sustainable Development Goal

SLS: Serviceability Limit State

ULS: Ultimate Limit State

Declaration of Conflict of Interests

The authors declare that there is no conflict of interest. They have no known competing financial interests or personal relationships that could have appeared to influence the work reported in this paper.

References

[1.] Spanish Governement (2010) Guia para la realización del inventario de obras de paso. Madrid: Ministerio de Fomento.

[2.] United Nations (2015) A/RES/70/1: Transforming our world: the 2030 Agenda for Sustainable Development. United Nations, Treaty Series, 1771, No. 30822.

[3.] Long, A.E.; Henderson, G, D, Montgomery, F.R. (2001) Why assess the properties of near-surface concrete? Constr Building Mat 15, pp. 65–79.

[4.] PIARC (2019) 2019R37: Bridge design towards improved inspection and maintenance. La Défense Cedex, France: World Road Association.

[5.] ACHE (2015) M27: Guía para la Redacción del Plan de Mantenimiento en Puentes. Madrid: Asociación Científico-Técnica del Hormigón Estructural.

[6.] FIB (2016) Bulletin nº 80: Partial factor methods for existing concrete structures. Lausanne: Fédération Internationale du Béton.

[7.] Spanish Governement (2012) Guía para la realización de inspecciones principales de obras de paso en la Red de Carreteras del Estado. Madrid: Ministerio de Fomento.

[8.] PIARC (2022) 2022R20: Advancement of inspection techniques/technologies as a part of bridge management systems. La Défense Cedex, France: World Road Association.

[9.] Spanish Governement (2008) Real Decreto 1247/2008, de 18 de julio. por el que se aprueba la instrucción de hormigón estructural (EHE-08). Madrid: Ministerio de la Presidencia.

[10.] Spanish Governement (2021) Real Decreto 470/2021, de 29 de junio, por el que se aprueba el Código Estructural. Madrid: Ministerio de la Presidencia, Relaciones con las Cortes y Memoria Democrática.

[11.] PIARC (2011) 2011R07: Inspector Accreditation, Non-destructive Testing and Condition Assessment for Bridges. La Défense Cedex, France: World Road Association.

[12.] PIARC (2016) 2016R05: Risk-based management of the bridge stock. La Défense Cedex, France: World Road Association.

[13.] ACHE (2019) M-33: Evaluación de Estructuras de Hormigón Armado. Madrid: Asociación Científico-Técnica del Hormigón Estructural.

[14.] PIARC (2020) Strategic Plan 2020-2023. La Défense Cedex, France: World Road Association.

PACE-2023
International Congress on Phenomenological Aspects in Civil Engineering

Research Article 20-23June 2023

Stability Analysis of High Slopes in Mines Based on Slide and Midas

Maoxuan Wang*,[1]
[1]School of Civil Engineering, Chongqing University, Chongqing 400045, China
Corresponding Author E-mail: 1556522351@qq.com

Keywords

Midas,
Slide,
Rocky slope,
Rainfall seepage,
Seismic force,

Abstract

A stable high slope of a mine is a prerequisite for sustainable and efficient mining. In order to analyze the stability of slopes under different working conditions, a high slope of a mine in Chongqing is used as the research object, and the limit balance method in Slide software is used to analyze the slope stability of mine slopes under three working conditions, and the

Stability analysis. corresponding slope stability coefficients are derived, and then the stability analysis of slopes under three working conditions is carried out by Midas software with strength reduction method. The results show that the safety coefficients of the slopes under the three working conditions are higher than the design safety coefficients under the corresponding working conditions, indicating that the slopes are stable and safe under the three working conditions, and at the same time, the weak parts of the slopes are clarified according to the numerical simulation results, providing experience for the stability analysis of similar slopes.

9. Introduction

Mining work is a very important work in the energy mining in our country, during construction, the phenomenon of mine slope will also appear [1]. The safety and stability of mine slope is directly related to the production safety of mine, especially the geological condition of mine high slope is complex, and its stability analysis has been the focus of research. In recent years, computers have been widely used in rock slope stability evaluation and failure mode analysis, and some numerical simulation methods have incomparable advantages over many traditional analysis methods [2].

At present, limit equilibrium method is the most widely used slope stability analysis method at home and abroad, as well as the representative of traditional slope stability analysis methods [3]. Lu Lu [4] analyzed and judged the stability of the landslide under different working conditions by using the limit equilibrium method. As a typical numerical analysis method, finite element strength reduction method is also the most widely used numerical analysis method [5]. Nie Gaobo [4] used the finite element software ABAQUS to study the stability of slope under multiple working conditions by strength reduction method, and confirmed the feasibility of using this method to analyze the stability of slope.

This paper takes the high slope of a mine as an example, the mine slope is located in the northern axis of the Taodanganticline, the anticline axis extends in the direction of N20°E within the mining area, the ore layer is distributed in strip shape within the mining area, the northwest wing stratum occurrence of 280 ~ 315° Angle 18 ~ 53°, the southeast wing stratum occurrence of 95 ~ 114° Angle 11 ~ 33°. The exposed strata of the mining area and its surrounding area are mainly Quaternary (Q4) and Lower Triassic Jialingjiang Formation (T1j) strata. The mine mainly mines the third member of the Lower Triassic Jialingjiang Formation (T1j3) with a thickness of 180 ~ 210m.

Based on engineering geological survey data, Slide software (limit equilibrium method) and Midas software (strength reduction method) are used to analyze the stability of high slope under three different working conditions, and the corresponding safety factor is obtained. Based on the calculation results, the development trend of slope deformation and failure under different working conditions is analyzed, and effective suggestions are put forward from the perspective of finite element analysis.

10. Mechanical parameters of rock mass and load parameters under working conditions

2.1. Determination of mechanical parameters of rock mass

The physical and mechanical parameters of the high slope rock mass in the mine are listed in Table 2 according to the geotechnical physical and mechanical test report, Technical Specifications for Slope Engineering of Non-coal open-pit Mine (GB51016 ~ 2014) (Table 1) and related research literature.

Table 1. Suggested values of physical and mechanical parameters of slope rock mass

Basic quality level of rock mass	γ (kN/m3)	Peak shear strength		E (GPa)	μ
		ϕ (°)	c (MPa)		
Ⅰ	>26.5	>60	>2.1	>33	<0.2
Ⅱ		60~50	2.1~1.5	33~20	0.2~0.5
Ⅲ	26.5~24.5	50~39	1.5~0.7	20~6	0.25~0.3
Ⅳ	24.5~22.5	39~27	0.7~0.2	6~1.3	0.3~0.35
Ⅴ	<22.5	<27	<0.2	<1.3	>0.35

Table 2. Selected physical and mechanical parameters of slope rock mass

Rock mass	γ (kN/m3)	Compressive strength	E（GPa）	μ	c（MPa）	ϕ (°)

		saturated - natural				
Dolomitic limestone T1j2	27	39-42	2.1	0.33	0.42	34
Limestone T1J3	27	47-57	2.2	0.30	0.50	37
Argillaceous limestone T1J3	24	/	1.6	0.33	0.35	36
Karst breccia T1J2	25	2.1-3.2	1.2	0.40	0.26	26

2.2. Value of load parameter in working condition

2.2.1. Value of the seismic force parameter

According to China Ground Motion Parameter Zoning Map (GB18306-2015) and Code for Seismic Design of Buildings (GB50011-2010 (2016 edition)), the peak acceleration of ground motion in this area is 0.05g, the characteristic period of seismic response spectrum is 0.35s, and the basic intensity of earthquake is Ⅵ. No strong seismic activity has been found in this area and its adjacent areas in recent years. The mining area is an earthquake-free area with good regional stability.

2.2.2. Rainstorm parameter value

According to the relevant meteorological data, the mining area belongs to the subtropical monsoon climate zone of Sichuan Basin. The area has abundant rainfall, with annual average rainfall of 1049.3mm, annual maximum rainfall of 1356mm, monthly maximum rainfall of 445.9mm (September 1997) and daily maximum rainfall of 141.4mm (May 24, 1964). The distribution of rainfall in a year is uneven. The concentrated rainfall is distributed from May to September, accounting for 68.8% of the whole year. The dry season is distributed in January, February and December, accounting for only 4.3% of the whole year. When simulating the working conditions under the condition of rainstorm, the mechanical properties of rock under the extreme condition of rainstorm, namely saturation strength, are used as the basis for calculation.

2.2.3. Safety factor value of slope

According to "non-coal open-pit Mine slope Engineering Technical Code" (GB51016 ~ 2014), safety factor Fs is an important parameter of slope stability criterion, is an important threshold to judge the slope stability state. The stability coefficient Fs, the ratio of the comprehensive anti-sliding force to the comprehensive sliding force on the potential sliding surface, is calculated. The value of Fs is used to evaluate the geotechnical stability of the slope. Fs≥Fst is the stable state, and Fs<Fst is the unstable state.

According to "non-coal open-pit mine slope engineering Technical Specification" (GB51016 ~ 2014), the overall safety grade of the mine slope is Ⅱ. The values of slope safety factor under three working conditions are shown in Table 3.

Table 3. Selection of mine slope safety factor value table

Grade of slope safety engineering	Safety factor of slope engineering design		
	Combination Ⅰ (dead weight + groundwater)	Combination Ⅱ (Dead weight + groundwater + blasting)	Combination Ⅲ (dead weight + groundwater + seismic force)
Ⅱ	1.20	1.18	1.15

11. Stability analysis of slope by limit equilibrium method

3.1. The solution principle of Slide stability analysis

Limit equilibrium method is the traditional method of slope stability analysis. It evaluates the stability of slope quantitatively through the safety factor. Because the safety factor is intuitive, it is widely used in engineering field. Based on the rigid plastic theory, this method only focuses on the deformation mechanism of soil at the moment of failure, but does not care about the deformation process of soil. It only requires the balance of force and moment, and the Mohr-Coulomb criterion. The basic idea of the analysis problem is as follows: Firstly, a sliding surface of possible shape is presupposed according to experience and theory, and then the slope stability process of soil mass under its own load is calculated by analyzing the balance between the external force of soil mass and the resistance provided by the internal strength in the case of near failure.

The limit equilibrium method does not introduce the stress-strain relation to solve the essentially statically indeterminate problem like the traditional elastic-plastic mechanics, but directly assumes some unknown quantities, making the number of equations equal to the number of unknowns, so that the problem becomes statically indeterminate and solvable. According to the boundary conditions of slope failure, using the method of mechanical analysis, theoretical calculation and mechanical analysis of the sliding surface which may occur under various loads are carried out. Through repeated calculation and analysis, the stability coefficients of possible sliding surfaces are given.

3.2. Current slope profile selection

According to the reserves report of Baiyangwanshe limestone mine for building stone in Huaiyuan Village, Jiangjia Town, Banan District, Chongqing in the first half of 2022, the most unfavorable section 2-2' is selected as the analysis section (Fig 1), and the slope analysis model established accordingly is shown in Fig 2.

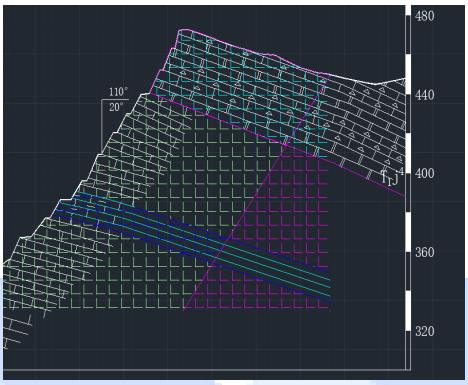

Figure 1. Schematic diagram of Section 2-2'

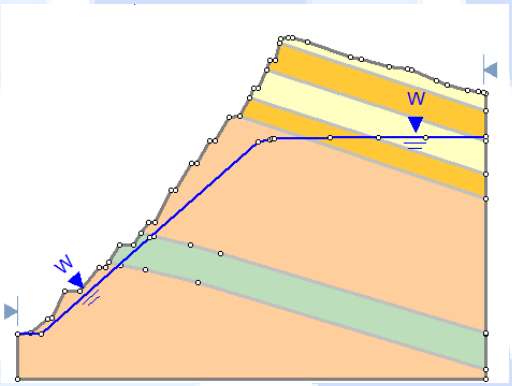

Figure 2. Slope analysis model

3.3. Current slope calculation results

The calculated results of slope stability coefficient of section 2-2' under the comprehensive conditions of dead weight + groundwater, dead weight + groundwater + blasting vibration force, dead weight + groundwater + seismic force are shown in Table 4.

Table 4. Stability calculation results of 2-2' profile under three working conditions

Selected profile		Minimum safety factor	Allowable safety factor	Analytical method
2-2' profile	Combination Ⅰ	1.772	1.20	Bishop
		1.670		Janbu
	Combination Ⅱ	1.702	1.18	Bishop
		1.589		Janbu
	Combination Ⅲ	1.657	1.15	Bishop
		1.538		Janbu

12. Stability analysis of current slope strength reduction method

In Chapter 3, based on the study of Slide limit equilibrium method, GTS-NX (strength reduction method) numerical simulation technology of Midas Company is used to analyze the stability of the current slope of 2-2' profile.

4.1. MIDAS GTS NX Basic principles and judgment basis

Strength reduction method is used in the calculation of MIDAS/GTS NX slope stability system. The principle of strength reduction method is to reduce the strength index of rock and soil mass in the ideal elastic-plastic constitutive model. Through continuous reduction, different values c and φ are obtained until the rock and soil mass is damaged. At this time, the reduction coefficient obtained is the stability coefficient. The strength index is reduced in accordance with equations (4.1) and (4.2).

$$c_f = c / F \tag{4.1}$$

$$\varphi_f = \arctan\left(\frac{\tan\varphi}{F}\right) \tag{4.2}$$

In formula, c and φ are the cohesion and internal friction angles of rock mass respectively. c_f and φ_f are respectively the cohesion and internal friction angles of the reduced rock mass. F is the reduction coefficient. The stability coefficient and the calculation nonconvergence of all elements are used as the criterion of slope stability.

4.2. The establishment of numerical analysis model

This paper plans to select the 2-2' section of the mine to conduct numerical simulation analysis and research on the stability. According to the geological prospecting report and the actual soil layer distribution, the slope model is divided into four rock and soil layers. The upper four layers are cross-distributed dolomite and karst breccia, and the lower three layers are limestone rock layers, among which a soft layer of argillaceous limestone is mixed. The profile was imported into Midas software. During mesh division, the element type was triangle + quadrilateral. The mesh division was slightly dense at the position of slope surface landslide with a mesh size of 2m, while the mesh division was slightly sparse at other boundaries with a mesh size of 2.5m. After the establishment of the model, the overall slope height is 142m, the length is 195m, the number of nodes is 3941, and the number of units is 3830.

The reaction more truly reflects the situation of mine slope, so it is necessary to consider the initial pore water pressure distribution of slope; In Midas percolation/consolidation module, the left and right head boundaries of the model are set according to the height of the water line at the left and right boundaries, and the numerical calculation model finally established is shown in Fig 3.

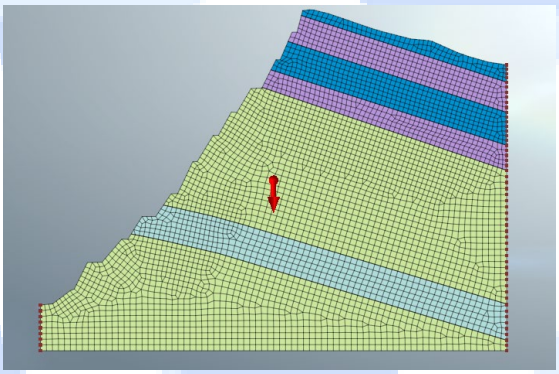

Figure 3. Numerical model of 2-2' profile

4.3. Current slope calculation results

4.3.1. Stability analysis under self-weight

The selected calculation method is strength reduction method, which has been verified by Chen Jianhong [6] and Wang Hongmei [7] in the search of plastic zone of rock slope. In order to simulate the deformation stress of the slope under the condition of dead weight and consider the occurrence of groundwater, the displacement strain nebulae of the slope under the condition of dead weight is solved.

Through simulation calculation, the effective plastic strain nephogram of the slope under the condition of dead weight is shown in Fig 4. The effective plastic strain of the slope is located at the foot of the slope, so it is necessary to strengthen the inspection and pay attention to the deformation of the slope foot.

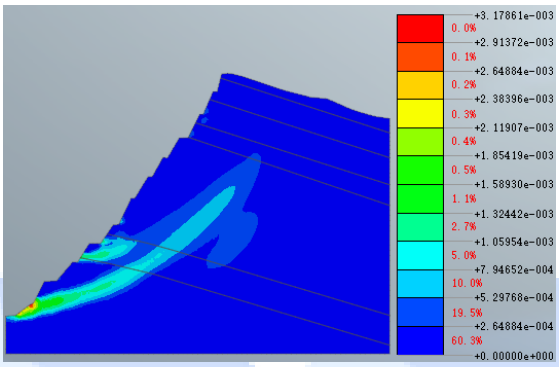

Figure 4. Effective plastic strain nephogram under dead weight condition

4.3.2. Stability analysis considering rainstorm condition

Rainfall is one of the common factors that lead to slope deformation and failure [8]. In this section, the influence of rainstorm conditions on the stability of mine high slope is considered. In order to facilitate the comparison with slope stability under self-weight condition, the numerical simulation model of slope is adopted which is consistent with the previous section, and the grid division and physical parameters are consistent with it. In order to avoid the impact of errors caused by unit division on the results.

Since the slope is a rock slope, it has little influence on the unsaturated characteristics of rainfall infiltration compared with soil. At this time, the saturated bulk density of various rocks is used for simulation calculation. The initial water level is consistent with the dead weight condition. Since this paper only considers the stability state of the slope under the condition of rainfall, the most unfavorable condition with the maximum daily rainfall of 141.4mm is selected according to the local meteorological data, and the working condition of continuous rainfall for two days is designed. According to the calculation results, the slope effective plastic strain nephogram under rainstorm condition is shown in Fig 5.

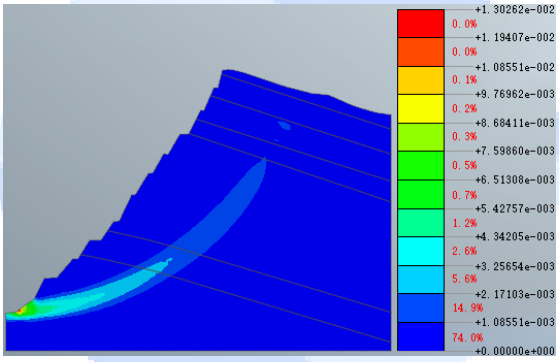

Figure 5. Effective plastic strain cloud map under rainstorm condition

By comparing the cloud map of effective plastic strain under the two conditions, it can be seen that the value of effective plastic strain increases somewhat under the condition of rainfall, but the position of the plastic zone does not change significantly, and the maximum effective plastic strain is still located at the foot of the slope.

4.3.3. Stability analysis considering seismic forces

The dynamic load is generated on the slope under the action of earthquake. Under the dynamic load, the slope soil generates inertial force and cyclic degradation, and the shear strength further decreases and the slope sliding force increases. Finally, the original stability of the slope is broken and the safety factor decreases under the action of earthquake, which may result in the slope instability [9].

In order to compare with the slope stability under the condition of dead weight, the calculation model still adopts the model under the condition of dead weight. On this basis, the horizontal component of El-Centro seismic wave is used as the load on the slope under earthquake conditions in the analysis. After investigation, the seismic intensity of the mine slope is level Ⅵ and the peak acceleration of ground motion is 0.05g, so the seismic wave must be reduced. The known peak acceleration of the seismic wave is 0.3569g (time=2.14s), and the proportional coefficient is set as 0.14. The final seismic waveform is shown in Fig 6. The linear time history analysis method in Midas-GTS + equivalent node force analysis method is adopted. Firstly, grid point force is checked in the output control during the linear time history analysis. Since the seismic wave reaches the peak acceleration at 2.14s, the maximum displacement of slope occurs near this time, so it is necessary to analyze the force situation of slope at this time. From the results of linear time history analysis calculation, the equivalent node force corresponding to 2.14s was extracted, and the equivalent node force was applied to the slope model, and the SRM stability analysis of the slope was carried out.

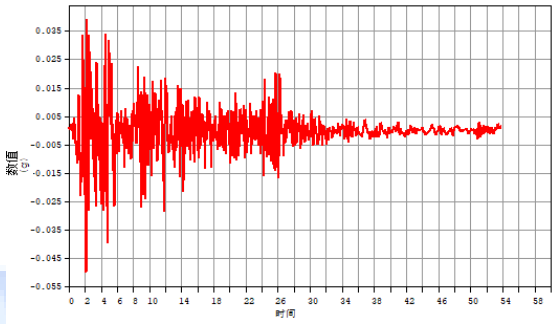

Figure 6. Modified time-history curve of ground motion acceleration of El-Centro seismic waves

Fig 7 shows the effective plastic strain cloud map of the slope under earthquake conditions. Compared with the cloud map of effective plastic strain under the previous two conditions, the value of effective plastic strain increases somewhat under the earthquake condition, and the location of the plastic zone is concentrated on the surface of the soft sandwich, and the plastic zone has no obvious zonal distribution. The reason why the flat failure area is concentrated near the weak interlayer is that the tensile strength of rock mass has a great influence on the stability of slope under the action of earthquake, and the tensile strength of argillous limestone in the weak interlayer is low. Tensile stress and shear stress also exist between rock masses under the action of earthquake. When the tensile stress and shear stress exceed the shear strength of rock, the rock mass will be damaged. In practical engineering, large displacement occurs, so the slope under earthquake action has obvious displacement and deformation at the weak interlayer.

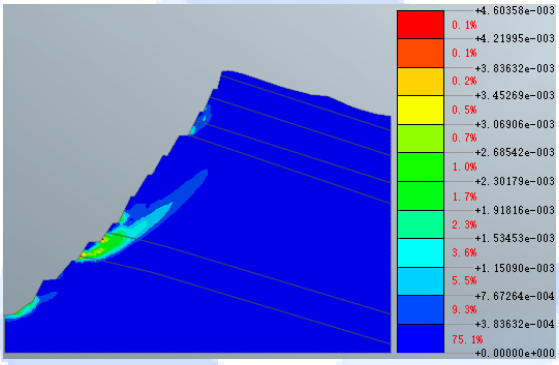

Figure 7. Cloud map of effective plastic strain under seismic conditions

4.3.4. Comparison of three working conditions

It can be seen from Fig 8 that the maximum horizontal displacement and vertical displacement of slope change under the three working conditions. In combination two (rainstorm) working conditions, the maximum horizontal displacement increases significantly, while the maximum vertical displacement changes little. In combination three (earthquake) condition, the maximum vertical displacement increases significantly compared with the dead weight condition, while the horizontal displacement does not change significantly.

The maximum values of displacement and stress-strain on the slope can be read directly through the result label display function of Midas software post-processing system. Under the condition of dead weight, the maximum horizontal displacement is 4.54cm, which is located at the bottom of the slope argillaceous limestone. Therefore, attention should be paid to the deformation monitoring of argillaceous limestone section and timely feedback information. The maximum vertical displacement is 9.1cm, which is located at the boundary between the uppermost karst breccia and dolomite at the top of the slope. Under the condition of rainstorm, the maximum horizontal displacement is no longer located at the bottom of the weak interlayer (argillous limestone), but widely distributed in the lower part of the circular landslide body. The maximum horizontal displacement is 8.02cm, which is located at the bottom of the landslide body, roughly at the foot of the slope. Compared with the deformation condition of dead weight, the vertical displacement at the top of the slope has no obvious change, but the vertical displacement value and distribution area of the slope below the weak rock stratum are significantly larger than the dead weight condition, the maximum vertical displacement is 9.17cm, and the obvious extrusion deformation can be found at the foot of the slope. The reason for the change of displacement in the second condition is the decrease of rainfall and the increase of seepage velocity under the rainstorm condition. When the rain water infiltrates into the weak interlayer, due to the poor permeability of the muddy limestone in the interlayer, the seepage path will be affected, which will lead to the obvious change of the displacement of the weak interlayer and the downhill body, which may bring security risks to the slope. Under seismic conditions, the maximum horizontal displacement is concentrated near the weak interlayer, and the maximum value is 6.12cm. The maximum vertical displacement is similar to the dead weight condition, both of which appear at the top of the slope, and the maximum value is 16.67cm.

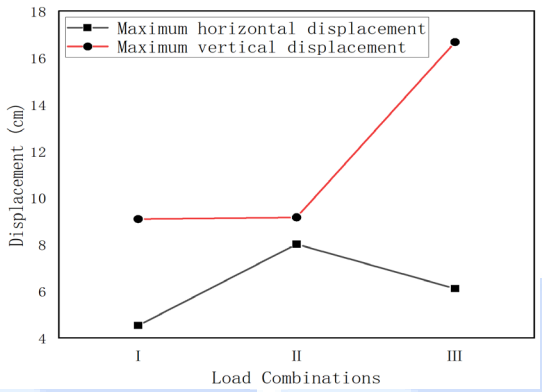

Figure 8. Maximum displacement under three working conditions

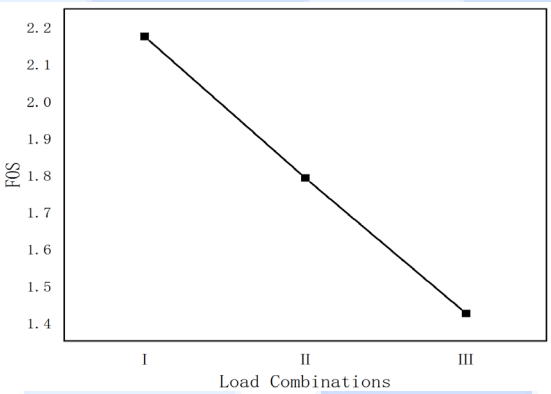

Figure 9. Safety factor of three working conditions

The stability coefficient can be read directly in the post-processing of the calculated results. As can be seen from Fig 9, the safety factor decreases successively under the three working conditions, indicating that the slope of load combination II (rainstorm) is relatively dangerous, while the slope of load combination III (earthquake) is the most dangerous. The results show that the slope stability coefficients under the three conditions are 2.075, 1.7918 and 1.425, respectively. According to Chapter 3, the minimum safety coefficients of load combination Ⅰ, Ⅱ and Ⅲ are 1.2, 1.18 and 1.15, respectively. It can be known that the slope is in a stable state under the three conditions.

5. Conclusion

In this paper, two analysis modules, the limit balance method provided by slide software and the strength reduction method provided by midas/GTS software, are used for quantitative analysis of the stability of the mine high slope. The analysis and simulation results show that the mine slope can be in a stable state under the three conditions of dead weight, rainstorm and seismic force, but the safety factor decreases under the latter two conditions. Moreover, attention should be paid to the displacement of weak interlayer and slope foot, and prevention should be strengthened in the future engineering design and management.

Declaration of Conflict of Interests

The authors declare that there is no conflict of interest. They have no known competing financial interests or personal relationships that could have appeared to influence the work reported in this paper.

References

[1.] Chen Qilin, Yao Luo. Stability analysis and landslide warning technology of mine high and steep slope [J]. World Nonferrous Metals,2021.

[2.] Yang Jianhua, Zhao Donglei, Deng Jiewen, Zhang Junjian, Gan Xiaoying. Stability analysis and support scheme of rock slope based on Midas/GTS software [J]. Electric Power Survey and Design,2022.

[3.] Wang Yu, Yu Hongming, Fan Tao, Tian Hao. Uniform design and numerical simulation of influence factors of cutting slope stability [J]. Coal Geology & Exploration,2011.

[4.] NIE Gaobo. Study on Stability of Soil Slope Based on Strength Reduction Method [D]. Henan University,2020.

[5.] Wu Changzhen, Wu Shaolong. Stability analysis of the end slope of a cement raw material open-pit mine [J]. Cement Engineering,2022.

[6.] Chen Jianhong, Zhong Fusheng, Yang Shan. Stability analysis of rock slope based on Finite element reduced strength method and limit equilibrium method [J]. Science and Technology Review,2012.

[7.] WANG Hongmei. Study on Stability analysis and evaluation of High rock slope [D]. Coal Research Institute,2004.

[8.] Lin Guocai, Xie Xinghua, Ruan Huining, Zhu Zhende, Lu Bin, Xu Chencheng, Lu Xiaogang. of Water Conservancy and Water Transport Engineering,2019.

[9.] WEI Gangqiang. Stability analysis of carbon shale cutting slope under rainfall and earthquake [D]. Changsha University of Science and Technology,2020.

PACE-2023

International Congress on the Phenomenological Aspects of Civil Engineering

Research Article

20-23 June 2023

The Earthquake Activity Observed in the Aziziye-Erzurum Region After the Devastating 2023 Kahramanmaraş Earthquakes (Mw 7.7 and 7.6)

Çaglar Özer*[1,2], Erdem Bayrak[1,2], Şukran Perk[1]

[1]*Earthquake Research Centre, Ataturk University, 25240 Erzurum, Turkey*
[2]*Department of Civil Engineering, Engineering Faculty, Ataturk University, 25240 Erzurum, Turkey*
Corresponding Author E-mail: caglarozer@atauni.edu.tr

Keywords

Aziziye earthquake,
Earthquake,
Aziziye,
Erzurum

Abstract

The devastating earthquakes with moment magnitudes of 7.7 and 7.6 occurred in Pazarcık and Elbistan districts of Kahramanmaraş on February 06, 2023 according to the data of the Earthquake Department of Disaster and Emergency Management (AFAD). The loss of life in these earthquakes exceeded 50,000 people and eleven provinces suffered loss of life and property. After these earthquakes, seismic activity increased in some regions and even some damaging triggering earthquakes occurred. An earthquake with a magnitude of Mw 6.4 occurred in Hatay province, located southwest of the 2023 Kahramanmaraş earthquakes on February 21, 2023, while seismic activity increased unusually in the northeastern part of the 2023 Kahramanmaraş earthquakes. The 2023 Kahramanmaraş earthquakes ruptured about 400 km of the Eastern Anatolian Fault Zone and changed the stress conditions in the region. Earthquake activity also increased in and around Erzurum province after February 6, 2023. Lastly, on 13.04.2023, more than 10 earthquakes, the largest of which was 3.9, occurred in Aziziye district of Erzurum province as of 00:00 on 14.04.2023. Since these earthquakes occurred in the residential areas of the city, they caused an echo in the city. At the same time, the citizens living in this region felt the earthquake more intensely due to the high liquefaction potential of Aziziye district related to the fact that the underground water level is very close to the surface of the surface and the soil bearing strength is low due to the thick alluvium. In this study, a series of statistical analysis on Aziziye earthquakes were conducted. At the same time, the damaged buildings in Söğütlü village of Aziziye district, the epicenter of the earthquake, were examined.

1. Intoduction

Erzurum, which is approximately 75 km from the Karlıova region, the junction area of the North Anatolian Fault Zone (NAFZ) and the East Anatolian Fault Zone (EAFZ), is a province with a high seismic hazard. In addition to its proximity to the NAFZ [1, 2], DAFZ [3-6] and Karlıova region [7], Erzurum is surrounded by important local faults, many of which pass through the city. From west to east, these faults are Aşkale Fault Zone, Başköy Kandilli Fault Zone, Palandöken Fault Zone, Erzurum-Dumlu Fault Zone and Northeast Anatolian Fault Zone [8]. In order to

monitor Erzurum province, which has active fault zones, Atatürk University Earthquake Research Center (ATA-DAM) and Disaster and Emergency Management (AFAD) Earthquake Department operate earthquake stations together (Figure 1).

Founded in 1989, ATA-DAM and AFAD Erzurum Earthquake Monitoring Network (ATANET) conduct seismological research in the Eastern Anatolia region [9]. In the historical period, earthquakes of up to ten magnitudes were reported in Erzurum and its immediate surroundings [9-10], while today, the AFAD Turkey Earthquake Hazard Map [11] predicts a value of more than 0.5g based on a 475-year return period. Geologically, the city is surrounded by terrestrial clastics in the west, andesites in the southwest, ophiolitic melange in the area covered by Palandöken Mountain in the south, and volcanites in the north and northwest [8, 9, 17]. The results of Coulomb stress analysis in and around Erzurum show the active stress character of the region [14].

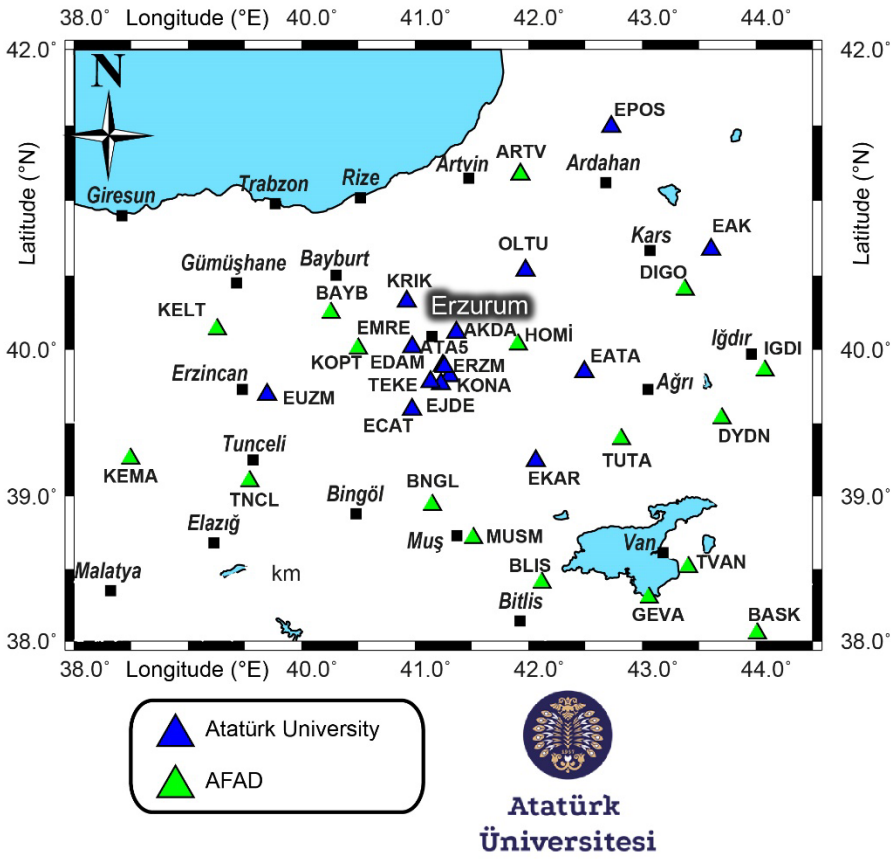

Figure 1. Atatürk University Earthquake Research Center seismic network distribution.

2. Aziziye Earthquakes

A series of earthquakes with a magnitude of 3.9 occurred in Aziziye district of Erzurum province on 13.04.2023. These earthquakes, called as this study Aziziye earthquakes, were also recorded by ATA-DAM stations (Figure 2-5). Figures 6-7-8 show that Erzurum and its vicinity has always been seismically active, not only today [14]. Figures 6 and 8 show that Erzurum and its vicinity was seismically active after the 06.02.2023 Pazarcık and Elbistan earthquakes [15-16]. Most of the earthquakes are located on the main tectonic lines (Figure 6). The focal depth of the earthquakes is shallow compared to the Eastern Anatolia region (Figure 7). Most of the earthquakes in the last 30 years are medium-sized earthquakes (Figure 8). After the February 6, 2023 Kahramanmaraş earthquakes, it is observed that the earthquake activity in and around Erzurum has increased compared to the normal period. Especially the tectonic lines passing through the city were observed to be seismically active (Figure 9). However, the majority of these earthquakes are small-magnitude earthquakes (Figure 10).

A team of researchers from Atatürk University Earthquake Research Center conducted a series of field observations in Aziziye district and especially around Söğütlü village on 14.04.2023. The damages were observed in some non-engineered structures and some walls in and around Söğütlü village (Figures 11-14). The fact that even in a small earthquake, structures can be damaged and even rendered unusable shows that the idea of disaster-resilient cities needs to be realized as soon as possible.

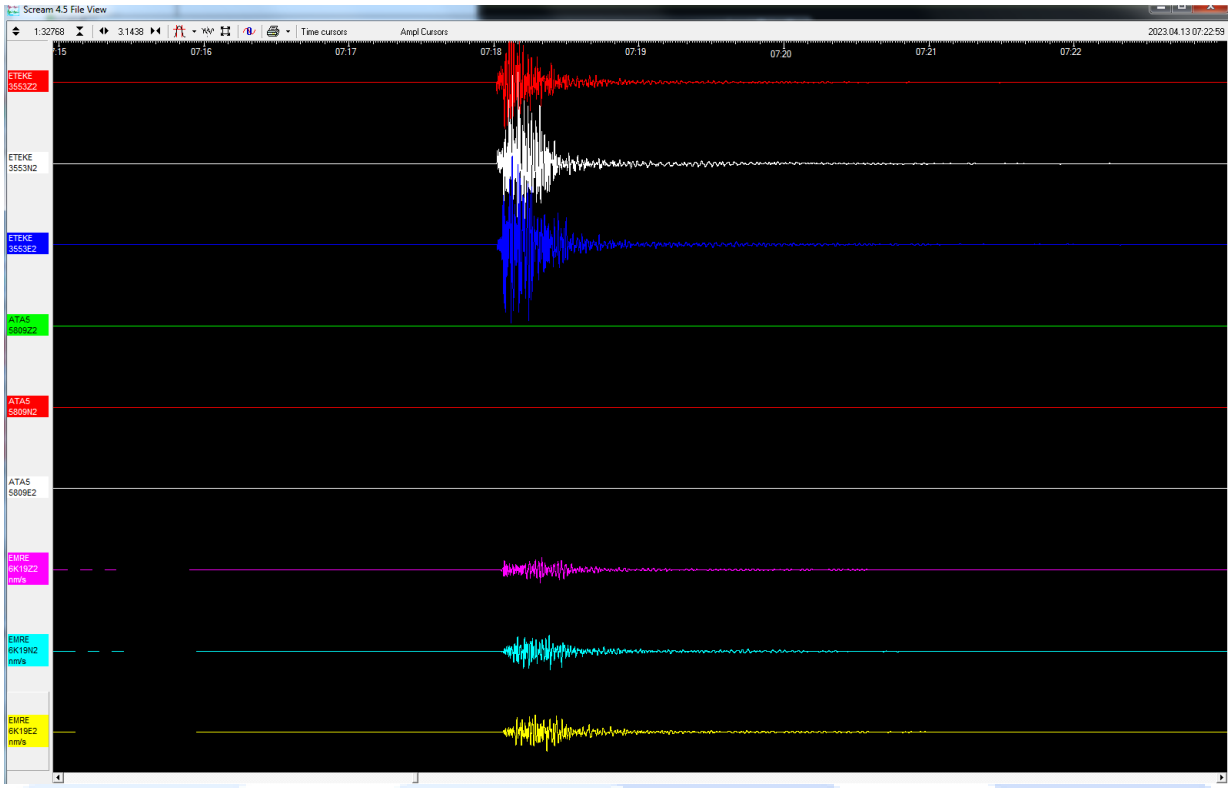

Figure 2. Scream earthquake monitoring software image of Erzurum-Aziziye (Mw 3.9) earthquake recorded by ATA-DAM stations

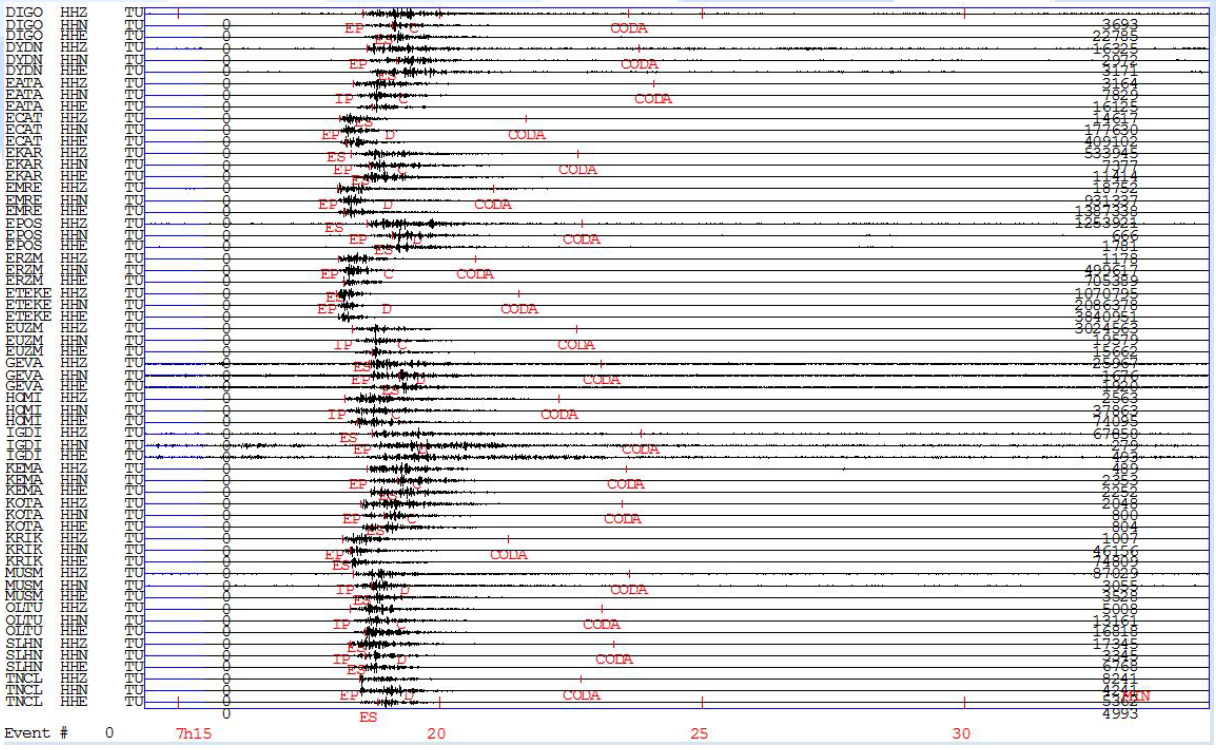

Figure 3. Location solution of Erzurum-Aziziye (Mw 3.9) earthquake recorded by ATA-DAM and AFAD Stations with SEISAN program

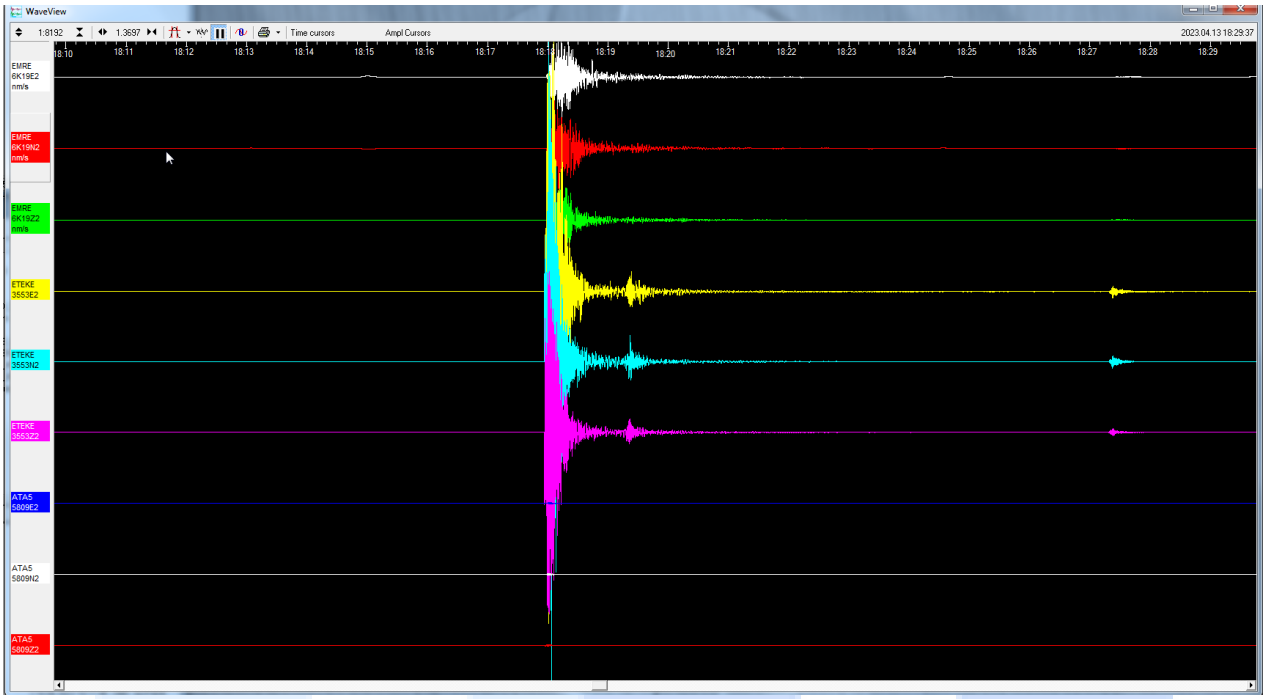

Figure 4. Scream earthquake monitoring software image of Erzurum-Aziziye (ML 3.4) earthquake recorded by ATA-DAM stations

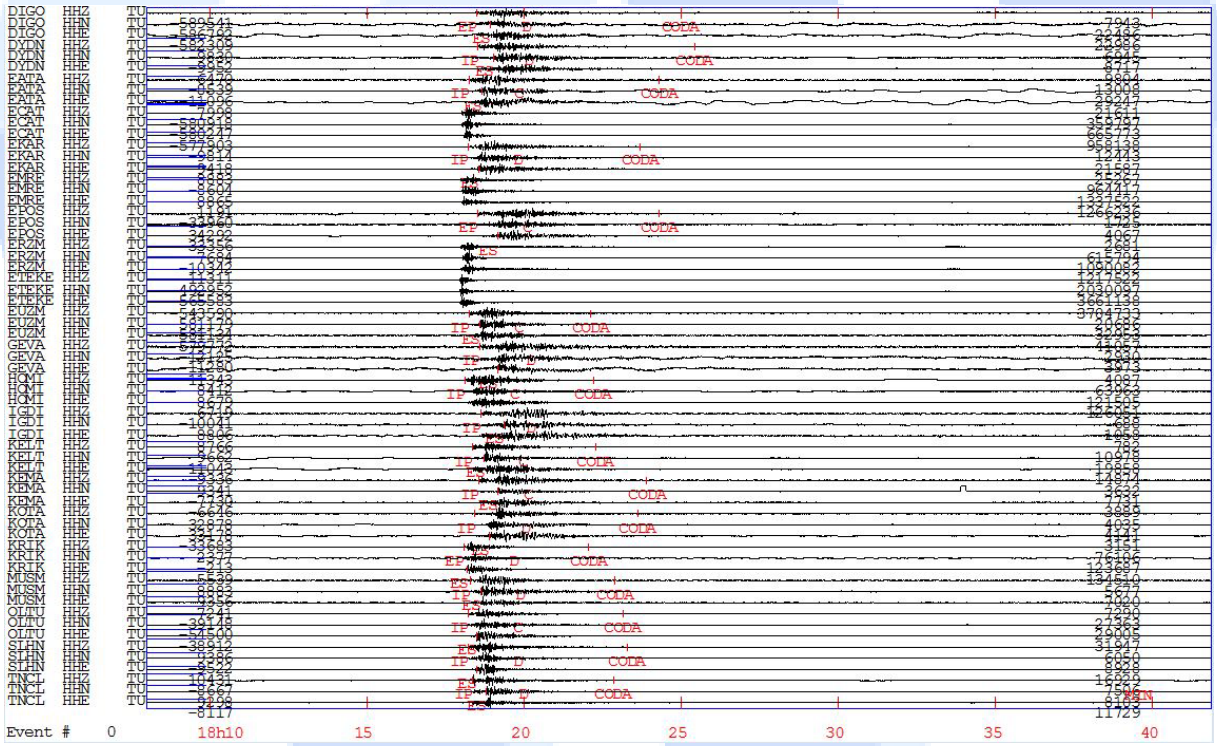

Figure 5. Location solution of Erzurum-Aziziye (ML 3.4) earthquake recorded by ATA-DAM and AFAD Stations with SEISAN program

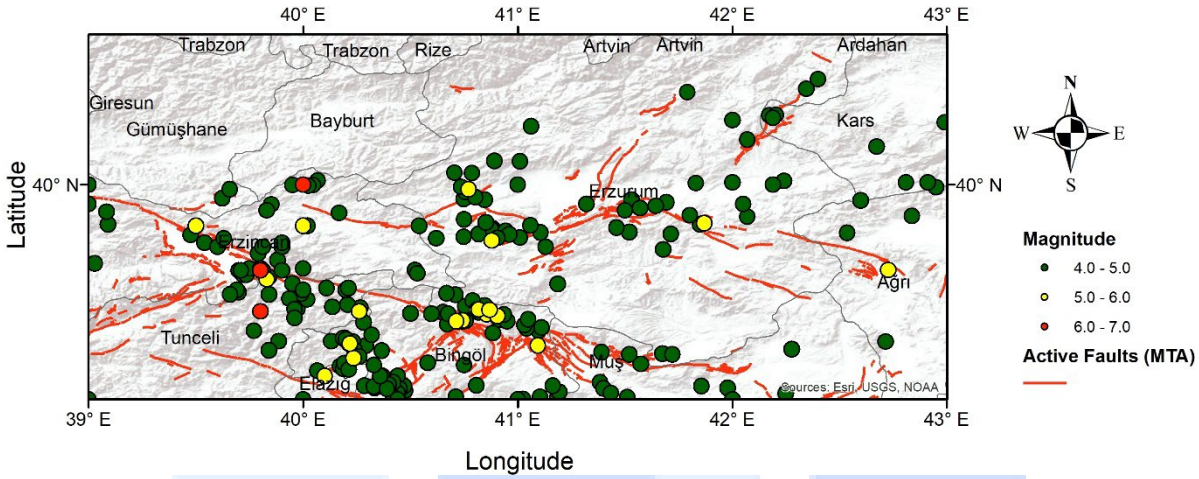

Figure 6. Distribution of Mw ≥ 4.0 epicenters that occurred between 1990 and 2023 in Erzurum and its vicinity. Earthquake epicenters [10] are shown with a circle symbol while red lines indicate fault zones [12, 13].

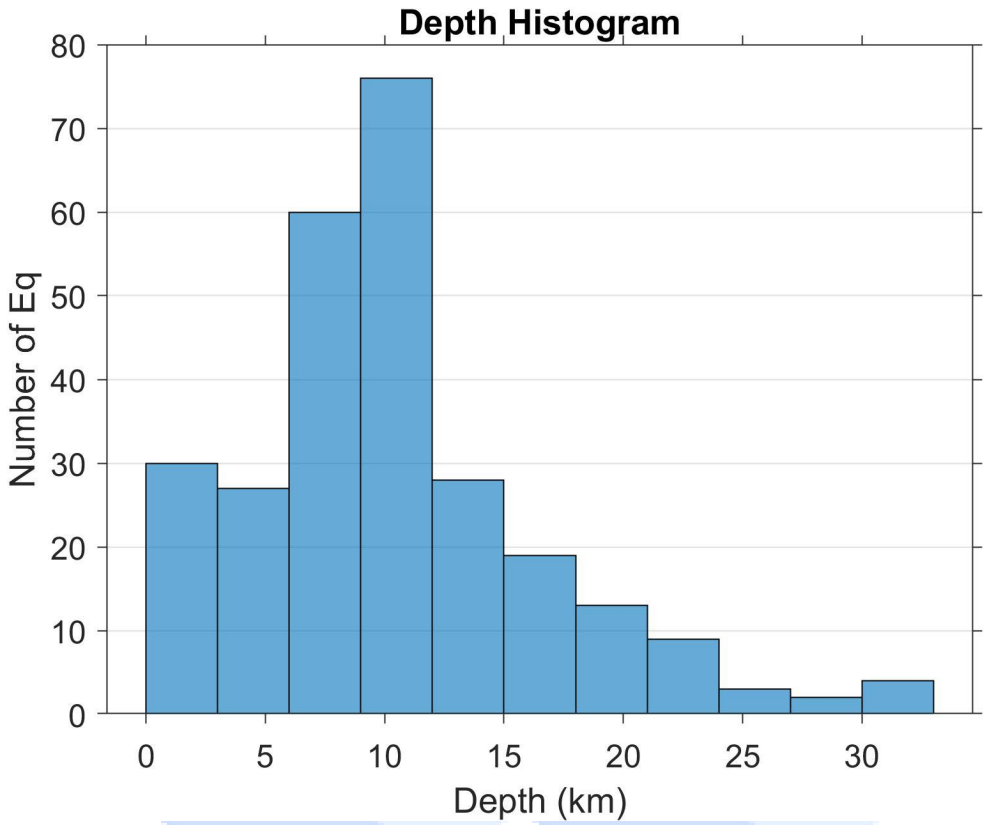

Figure 7. The depth-number of earthquakes (Mw ≥ 4.0) occurring between 1990 and 2023 in Erzurum and its vicinity (Earthquake data obtained from AFAD [10]).

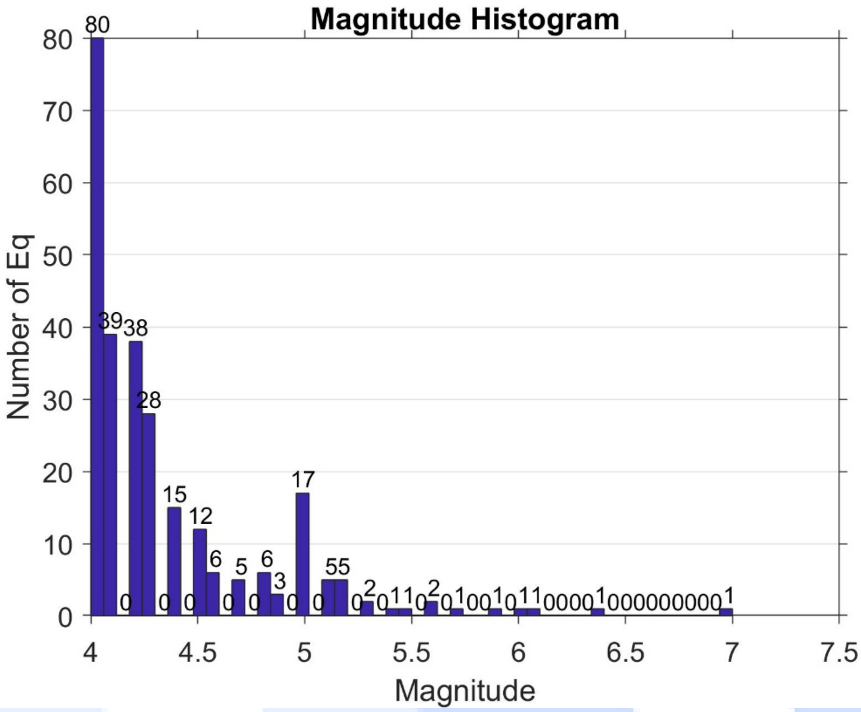

Figure 8. The magnitude-number of earthquakes (Mw ≥ 4.0) occurring between 1990 and 2023 in Erzurum and its vicinity (Earthquake data obtained from AFAD [10]).

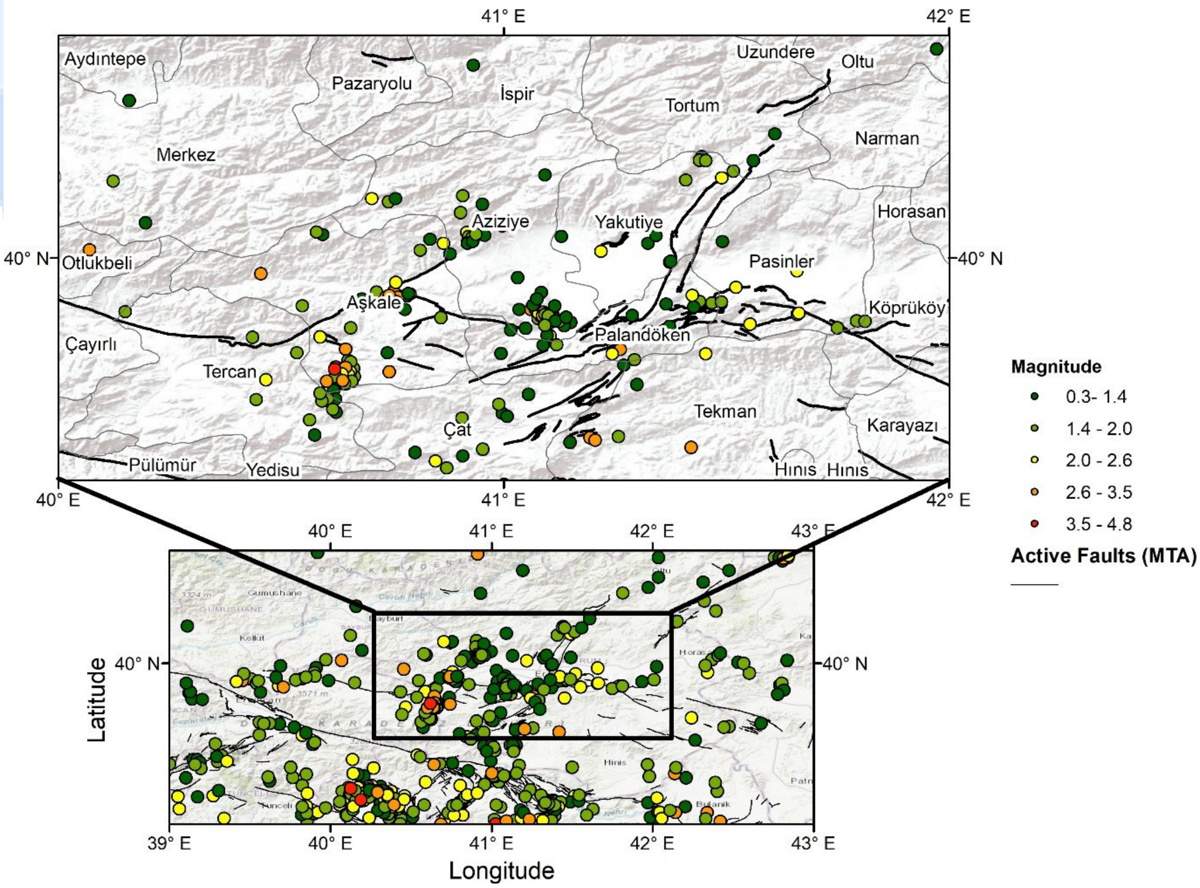

Figure 9. Epicentral distribution of earthquakes that occurred between 06.02.2023-14.04.2023. Earthquake epicenters [10] are shown with a circle symbol while black lines indicate fault zones [12, 13].

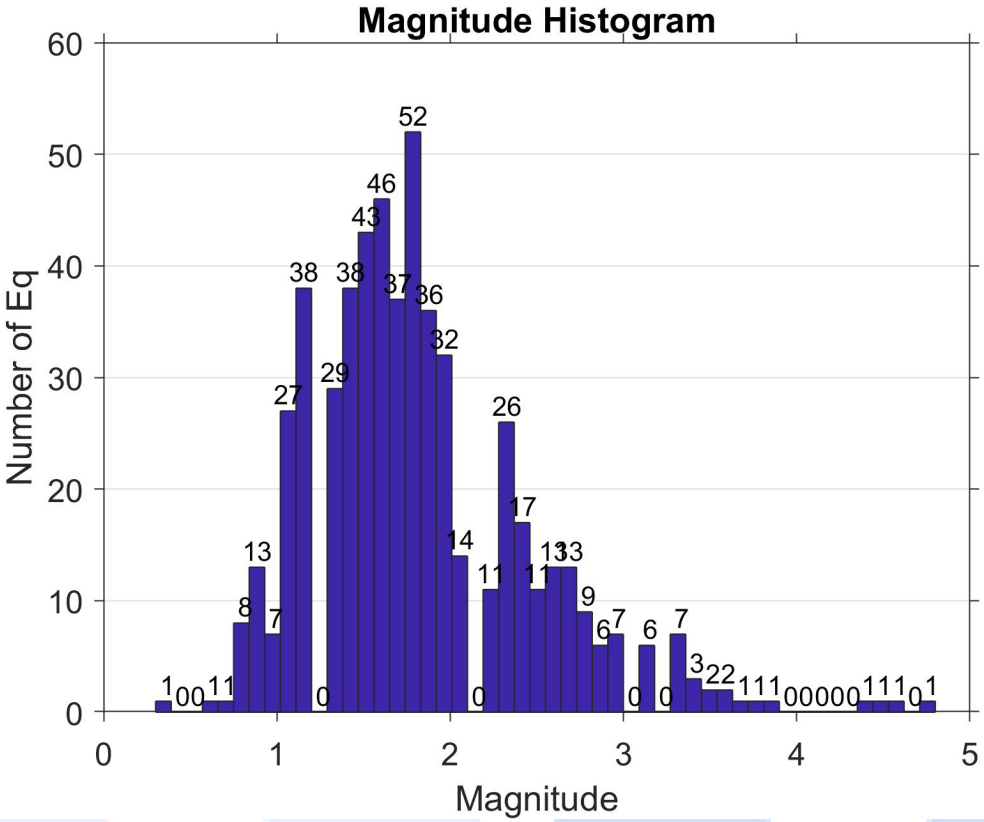

Figure 10. Magnitude-number of earthquakes between 06.02.2023-14.04.2023 (Earthquake data obtained from AFAD [10]).

Figure 11. An example of the damage observed after the April 13, 2023 Aziziye Earthquakes

Figure 12. An example of the damage observed after the April 13, 2023 Aziziye Earthquakes

Figure 13. An example of the damage observed after the April 13, 2023 Aziziye Earthquakes

Figure 14. An example of the damage observed after the April 13, 2023 Aziziye Earthquakes

3. Results

Erzurum province has an active tectonic structure and the recent small-scale earthquakes in Erzurum province, which have been felt in a wide area, have once again revealed the importance of housing in buildings designed to be earthquake resistant by taking into account the soil dynamic properties. Erzurum and its surroundings are surrounded by active tectonic zones and are among the provinces with high seismic hazard. For this reason, the occurrence of small and medium-scale earthquakes is a natural requirement of the tectonic conditions in the region. However, it should not be forgotten that there are many active tectonic units in Erzurum province that can produce destructive earthquakes in the future. In this respect, it is essential to design Erzurum a disaster-resilient city.

Acknowledgment

We would like to thank AFAD Earthquake Department for providing earthquake location and online data access [10]. The fault information was digitized from MTA drawing editor [12, 13]. Figures were prepared using GMT algorithm [18], SEISAN [19] and ArcGIS program. SeisComP software (https://www.seiscomp3.org/) was used for data transfer. The authors would like to thank the Rectorate of Atatürk University for providing logistical support for field observations [20].

Declaration of Conflict of Interests

The author(s) declare(s) that there is no conflict of interest. They have no known competing financial interests or personal relationships that could have appeared to influence the work reported in this paper.

References

[1.] Barka, A., The North Anatolian fault zone. Ann Tectonicae 6(1992)164–195.

[2.] Hubert-Ferrari, A., Armijo, R., King, G., Bertrand, M., Barka, A., Morphology, displacement, and slip rates along the North Anatolian Fault. Turkish Journal of Earth Sciences 107(2002) 2235.

[3.] Arpat, E., Şaroğlu, F., The East Anatolian Fault System: thoughts on its development. Journal of Mineral Research and Exploration 78(1972) 33-39.

[4.] Şaroglu, F., Emre, O., Kuşçu, I., The East Anatolian fault zone of Turkey. Annales Tectonicae 6 (1992) 99–125.

[5.] Herece, E., Atlas of East Anatolian fault-special publication series. 13. General Directorate of Mineral Research and Exploration (MTA) Turkey Ankara (2008).

[6.] Duman, T.Y., Emre, Ö., The East Anatolian Fault: geometry, segmentation and jog characteristics. Geological Society London Special Publications 372(2013) 495-529.

[7.] Karaoğlu, Ö., Selçuk, A. S., Gudmundsson, A., Tectonic controls on the Karlıova triple junction (Turkey): Implications for tectonic inversion and the initiation of volcanism. Tectonophysics 694(2017) 368-384.

[8.] Koçyiğit, A., Canoğlu, M.C., Neotectonics and Seismicity of Erzurum Pull-apart Basin, East Turkey. Russian Geology and Geophysics 58(2017) 99-122.

[9.] Ozer, C., Kocadagistan, M. E., Perk, S., Earthquake monitoring network of Erzurum: ATANET. International Journal of Scientific and Technological Research 5(8) (2019) 35-47.

[10.] AFAD, AFAD Earthquake Catalog. Ankara, Turkey (2023) https://deprem.afad.gov.tr/last-earthquakes.html (Access Date: 13 April 2023).

[11.] AFAD, Turkey Earthquake Hazard Map. Ankara, Turkey (2019) https://deprem.afad.gov.tr/deprem-tehlike-haritasi (Access Date: 23 November 2022).

[12.] Emre, Ö., Duman, T.Y., Özalp, S., Elmacı, H., Olgun, Ş. ve Şaroğlu, F., Annotated Turkey Active Fault Map (in Turkish). Scale 1:1.250.000 General Directorate of Mineral Research and Exploration Special Publication Series-30 (2013) Ankara-Turkey, ISBN: 978-605-5310-56-1.

[13.] Emre O., Duman T.Y, Ozalp, S., Saroglu, F., Olgun, S., Elmaci, H., Can, T., Active fault database of Turkey. Bulletin of Earthquake Engineering 16(2018) 3229–3275.

[14.] Bayrak, E., Özer, C., Perk, S., Stress Tensor and Coulomb Analyses for Erzurum and its Surroundings (in Turkish). Turkish Journal of Earthquake Research 2(1) (2020) 101-114.

[15.] AFAD-Kahramanmaraş February 06, 2023 Pazarcık (Kahramanmaraş) Mw 7.7 Elbistan (Kahramanmaraş) Mw 7.6 Earthquakes Preliminary Assessment Report (in Turkish). (2023) https://deprem.afad.gov.tr/assets/pdf/Kahramanmaras%20%20Depremleri_%20On%20Degerlendirme%20Raporu.pdf (Access Date: 01 May, 2023).

[16.] Karabacak, V., Özkaymak, Ç., Sözbilir, H., Tatar, O., Aktuğ, B., Özdağ, Ö. C., Çakir, R., Aksoy, E., Koçbulut, F., Softa, M., Akgün, E., Demir, A., Arslan, G., The 2023 Pazarcık (Kahramanmaraş, Türkiye) earthquake (Mw 7.7): implications for surface rupture dynamics along the East Anatolian Fault Zone. Journal of the Geological Society 180(3) (2023).

[17.] Akbaş, B., Akdeniz, N., Aksay, A., Altun, İ.E., Balcı, V., Bilginer, E., Bilgiç, T., Duru, M., Ercan, T., Gedik, İ., Günay, Y., Güven, İ.H., Hakyemez, H.Y., Konak, N., Papak, İ., Pehlivan, Ş., Sevin, M., Şenel, M., Tarhan, N., Turhan, N., Türkecan, A., Ulu, Ü., Uğuz, M.F., Yurtsever, A. ve diğerleri, (2011), 1:1.250.000 scale Geological Map of Turkey (in Turkish). Publication of General Directorate of Mineral Research and Exploration, Ankara-Turkey.

[18.] Wessel, P., Smith, W. H. F., Scharroo, R., Luis, J. F., Wobbe, F., Generic Mapping Tools: Improved version released. EOS Transactions American Geophysical Union 94(2013) 409-410.

[19.] Havskov, J., Ottemoller, L., SeisAn Earthquake analysis software. Seismological Research Letters 70(1999).

[20.] Ozer, C., Bayrak, E., Perk, S., Aziziye Earthquakes Preliminary Scientific Investigation Report (in Turkish). Erzurum, Turkey (unpublished) (2023).

PACE-2023
International Congress on the Phenomenological Aspects of Civil Engineering

PACE-2023
International Congress on Phenomenological Aspects in Civil Engineering

Research Article
20-23 June 2023

Investigation of Foreshock and Aftershock Earthquake Distribution of Devastating Events in Turkey

Çaglar Özer*,[1,2]

[1]*Earthquake Research Centre, Ataturk University, 25240 Erzurum, Turkey*
[2]*Department of Civil Engineering, Engineering Faculty, Ataturk University, 25240 Erzurum, Turkey*
**Corresponding Author E-mail: caglarozer@atauni.edu.tr*

Keywords

Earthquake, Foreshock, Aftershock, Seismicity, Turkey.

Abstract

It is important to examine earthquake distributions before and after major earthquakes and investigate the relationship between regional stress and earthquake activity. In the past 20 years, aside from the Kahramanmaraş earthquakes (Mw 7.7 and 7.6), Turkey has experienced four other important earthquakes with magnitudes greater than 6.5 that resulted in loss of life and property. These earthquakes are the 03 February 2002 Sultandağı-Afyon earthquake (Mw 6.5), 23 October 2011 Van earthquake (Mw 7.1), 24 January 2020 Sivrice-Elazığ earthquake (Mw 6.8), and 30 October 2020 Aegean Sea earthquake (Mw 6.6). This study investigates the foreshock and aftershock distributions of these four earthquakes using the Disaster and Emergency Management Authority (AFAD) weak ground motion earthquake data catalog. The study discusses whether earthquake activity before devastating earthquakes can provide information about major earthquakes that may occur in the future. Additionally, by examining aftershock distribution, the potential magnitudes and duration of aftershocks are investigated.

1. Introduction

The Omori law [1,2] has been used in the field of seismology for many years to define the earthquake number-magnitude distribution [3] and the reduction rate of aftershocks. Determining the magnitude of aftershocks is one of the most important questions that needs to be addressed due to the potential for new damage to heavily damaged structures after the largest aftershock [4,5,6]. Mogi [7] proposed three types of earthquake distributions: mainshock with foreshocks and aftershocks, mainshock and aftershock without foreshock, and earthquake accumulation without mainshock. The question of whether foreshocks provide information about the triggering of large earthquakes is still a matter of debate [8,9]. Bath's law [10] states that the largest aftershock is typically 1.2 magnitudes less than the mainshock magnitude. Additionally, Helmstetter [11] claimed that there is no physical difference between foreshocks, aftershocks, and mainshocks.

Aside from the Kahramanmaraş earthquakes (Mw 7.7 and 7.6) in Turkey, four destructive earthquakes with a magnitude greater than 6.5 have occurred in the last 20 years. These are respectively 03 February 2002 Sultandağı-Afyon (Mw 6.5), 23 October 2011 Van (Mw 7.1), 24 January 2020 Sivrice-Elazig (Mw 6.8), and 30 October 2020 the Aegean Sea (Mw 6.6) earthquakes (Figure 1).

The earthquake distributions before and after these four earthquakes were examined in this study. The foreshock, mainshock, and aftershock distribution of earthquake locations controlled by different tectonic conditions were investigated with this motivation.

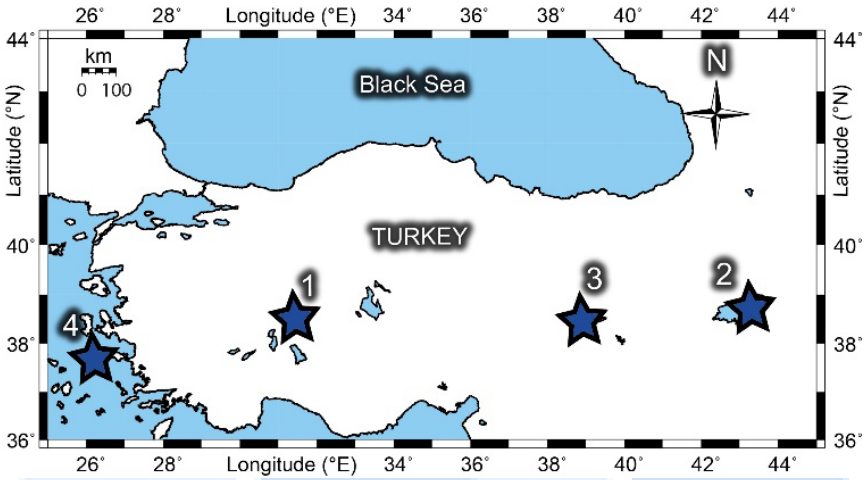

Figure 1. Devastating earthquakes of the study area during the period from 2002 to 2021 (M ≥6.5). The numbers are designed in chronological order of events.

2. Data

Figure 2a shows that one year before the 03 February 2002 Sultandağı earthquake (hereafter referred to as the Sultandağı earthquake), there were 34 seismic events. In the week prior to the Sultandağı earthquake, only one event was recorded (Figure 2b). Figure 2c shows that one month after the mainshock, 348 events occurred between 03 February 2002 and 03 March 2002. Between 03 March 2002 and 03 August 2002, 146 earthquakes were recorded (Figure 2d), and 28 events occurred between 03 August 2002 and 03 February 2003 (Figure 2e).

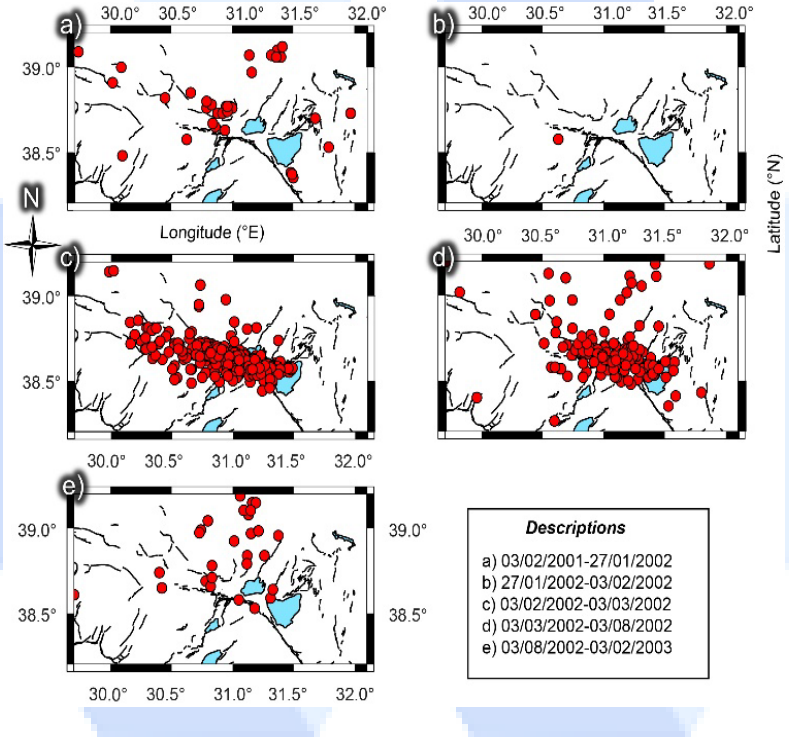

Figure 2. 03 February 2002 Sultandağı-Afyon (Mw 6.5) earthquake foreshock, mainshock and aftershock distribution. Earthquake epicenters [12] are shown with a circle symbol while black lines indicate fault zones [13, 14].

One year before the Van earthquake on October 23, 2011 (hereafter referred to as the Van earthquake), there were 499 earthquakes (Figure 3a). Only six earthquakes (Figure 3b) were recorded in the week leading up to the Van earthquake. One month after the mainshock (Figure 3c), 5233 earthquakes were detected between October 23, 2011, and November 23, 2011. From November 23, 2011, to April 23, 2012, 4854 events were recorded (Figure 3d). Between April 23, 2012, and October 23, 2012, there were 1548 earthquakes (Figure 3e). The earthquake distributions have been monitored since then due to ongoing tectonic activity in the region. In the following one-year periods - 10/2012-10/2013 (Figure 4a), 10/2013-10/2014 (Figure.4b), 10/2014-10/2015 (Figure 4c), 10/2015-10/2016 (Figure 4d), 10/2016-10/2017 (Figure 4e), 10/2018-10/2019 (Figure 4f), 2279 on 10/2019-10/2020 (Figure 4g), and 10/2020-09/2021 (Figure 4h) - there were 1167, 1235, 886, 795, 728, 532, 558, and 413 earthquakes, respectively.

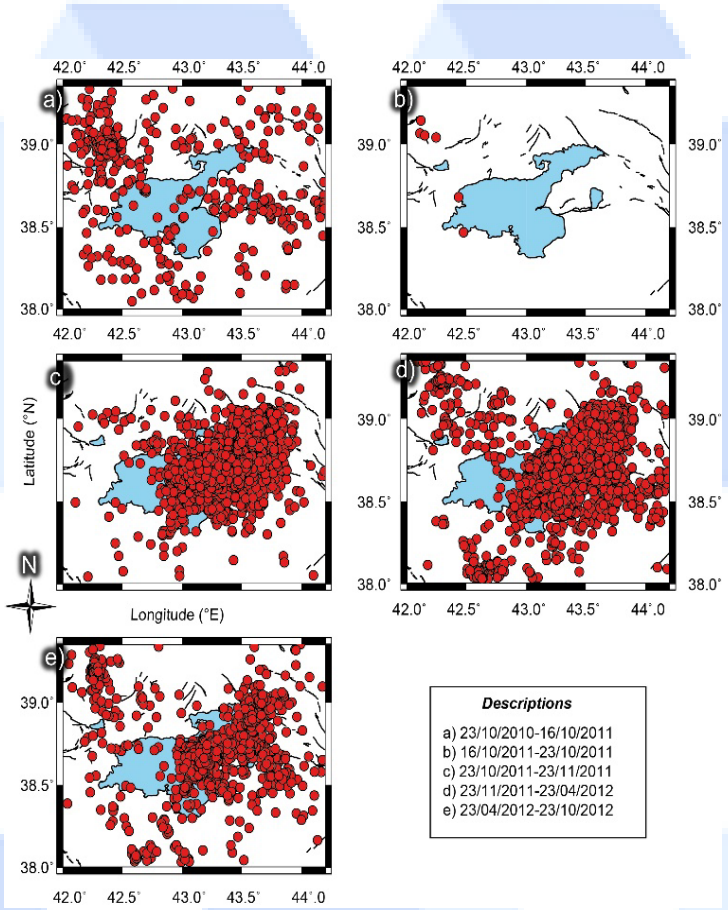

Figure 3. 23 October 2011 Van (Mw 7.1) earthquake foreshock, mainshock and aftershock distribution. Earthquake epicenters [12] are shown with a circle symbol while black lines indicate fault zones [14, 15].

There were 1,812 events recorded one year before the Sivrice earthquake that occurred on January 24, 2020 (hereafter referred to as the Sivrice earthquake) (Figure 5a). Thirteen earthquakes were recorded in the week leading up to the Sivrice earthquake (Figure 5b). One month after the mainshock (Figure 5c), there were 3,056 events recorded between January 24, 2020, and February 24, 2020. Between February 24, 2020, and July 24, 2020, 1,923 earthquakes were detected (Figure 5d). From July 24, 2020, to January 24, 2021, 1,663 earthquakes were recorded (Figure 5e).

There were 269 events one year before the 30 October 2020 Aegean Sea earthquake (hereafter referred to as the Aegean Sea earthquake) (Figure 6a) Two earthquakes occurred one week before the Aegean Sea earthquakes (Figure 6b). One month after the mainshock, 4517 earthquakes were traced between 30/10/2020 and 30/11/2020 (Figure 6c). The 2286 events monitored from 30/11/2020 to 29/04/2021 (Figure 6d). The 884 events were detected from 29/04/2021 to 07/09/2021 (Figure 6e).

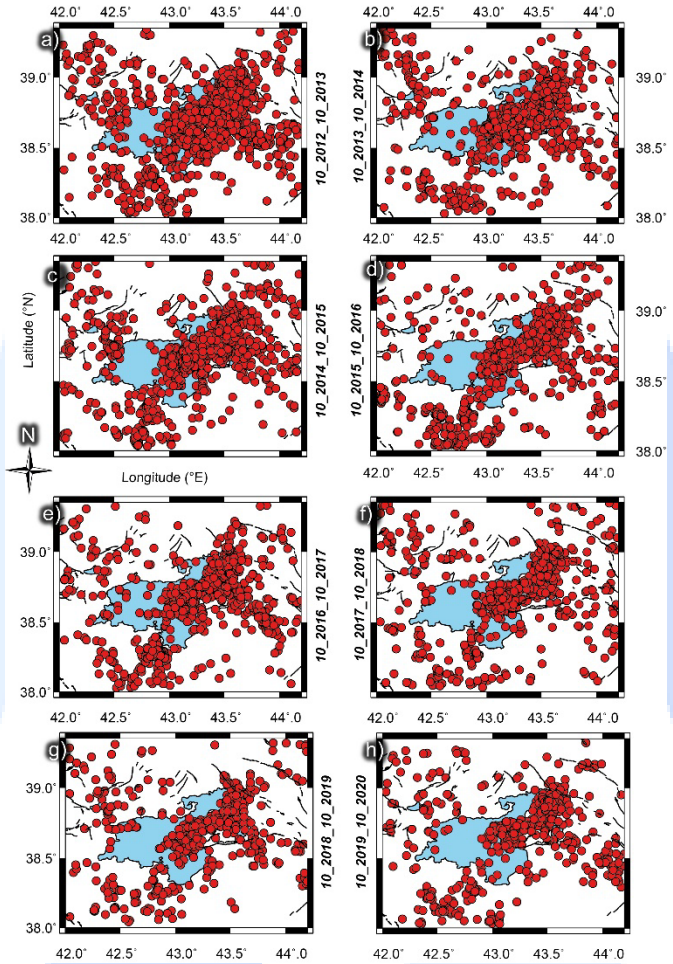

Figure 4. Seismic activity of Lake Van from 2012 to 2020. Earthquake epicenters [12] are shown with a circle symbol while black lines indicate fault zones [14, 15].

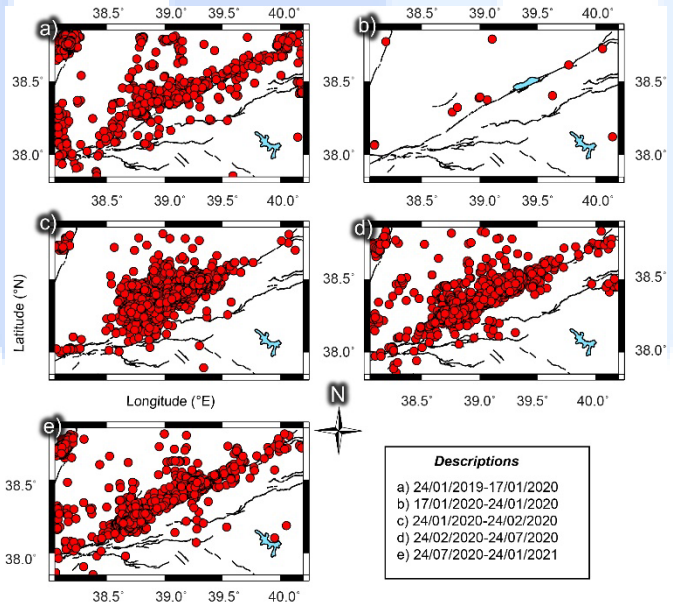

Figure 5. 24 January 2020 Sivrice-Elazig (Mw 6.8) earthquake foreshock, mainshock, and aftershock distribution. Earthquake epicenters [12] are shown with a circle symbol while black lines indicate fault zones [14, 15].

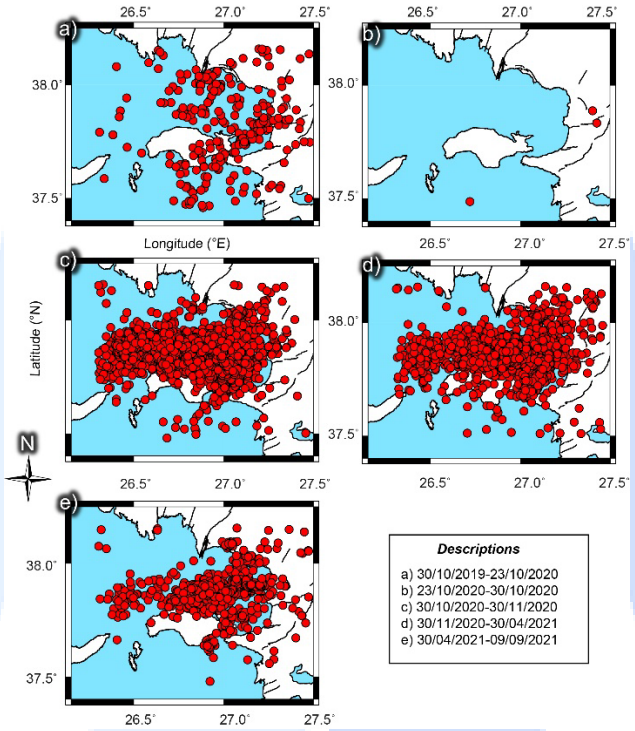

Figure 6. 30 October 2020 Aegean Sea (Mw 6.6) earthquake foreshock, mainshock and aftershock distribution. Earthquake epicenters [12] are shown with a circle symbol while black lines indicate fault zones [14, 15].

4. Results

No clear linearity can be detected prior to the mainshock of the Sultandağı earthquake. However, after the mainshock, a linearity extending in the East-West direction was observed, with bilateral propagation of aftershocks. The aftershocks continued for approximately six months after the mainshock, but subsequent distributions suggest that they have since ceased.

When observing the earthquake activity in the year leading up to the Van earthquake, there is no discernible pattern that correlates with the distribution observed after the mainshock. Furthermore, there were no notable earthquake activities one week prior to the mainshock. The earthquake activity that followed after the mainshock displayed a distribution in the NE-SW direction, and this pattern persisted for approximately one year after the mainshock. It is notable that this NE-SW direction earthquake distribution continued along the tectonic line where the mainshock occurred for the 10 years following the earthquake.

In the year preceding the Sivrice earthquake, there was notable earthquake activity in the region encompassing the Hazar-Sincik segment. However, there was no significant seismicity pattern that could have indicated the Sivrice earthquake one week prior to the main event. Aftershocks were observed to continue in the Hazar-Sincik segment for one year after the mainshock.

The earthquakes that occurred in the year before the Aegean Sea earthquake can be seen as the continuation and distribution of the tectonic units in the sea that control the Tuzla Fault and the Büyük Menderes Graben. One week before the earthquake, there was very little seismic activity. Following the earthquake, there was a strong distribution of East-West aftershocks in the first six months, which gradually decreased over the following six months.

5. Conclusion

In this study, we analyzed other four major earthquakes that have occurred in Turkey in the last 20 years aside from the Kahramanmaraş earthquakes (Mw 7.7 and 7.6) and had a magnitude greater than 6.5, resulting in significant damage. The seismic activity before these earthquakes did not exhibit any significant patterns except for the Sivrice earthquake, where there was noteworthy earthquake activity in the one year before the mainshock. The earthquake distributions after the mainshocks revealed that the number of aftershocks decreased considerably over a one-year period. However, tectonic activity has been ongoing in the region of the Van earthquake for the last 10 years. Although the magnitude of the aftershocks is consistent with Bath's law, it is important to note that the calculation of the largest aftershock may vary depending on the tectonic conditions in the area and the size distribution of aftershocks for each event.

Acknowledgment

The earthquake data was obtained from the AFAD (Earthquake Department of the Disaster and Emergency Management Presidency, Ankara-Turkey) [12]. All images were generated using the GMT software [15]. The tectonic units were digitized using a geoscience map viewer and drawing editor licensed to the General Directorate of Mineral Research and Exploration (MTA) [13,14].

Declaration of Conflict of Interests

The author declares that there is no conflict of interest. They have no known competing financial interests or personal relationships that could have appeared to influence the work reported in this paper.

References

[1.] Utsu, T. Magnitude of earthquakes and occurrence of their aftershocks. Zisin 2(10) (1957) 35-45.

[2.] Utsu, T., Ogata, Y. Matsuuara, R.S. The centenary of the Omori formula for decay law of aftershock activity. Journal of Physics of the Earth 43 (1995) 1-33.

[3.] Gutenberg, B., Richter, C.F. Frequency of Earthquakes in California. Bulletin of the Seismological Society of America 34 (1944) 185-188.

[4.] Shearer, P.M. Self-similar earthquake triggering, Båth's law, and foreshock/aftershock magnitudes: Simulations, theory, and results for southern California. Journal of Geophysical Research: Solid Earth 117(B6) (2012).

[5.] Shcherbakov, R., Zhuang, J., Ogata, Y. Constraining the magnitude of the largest event in a foreshock–main shock–aftershock sequence. Geophysical Journal International 212(1) (2018) 1-13.

[6.] Shcherbakov, R. Statistics and forecasting of aftershocks during the 2019 Ridgecrest, California, earthquake sequence. Journal of Geophysical Research: Solid Earth 126 (2021).

[7.] Mogi, K. Some discussions on aftershocks, foreshocks and earthquake swarms - the fracture of a semi-infinite body casued by an inner stress origin and its relation to the earthquake phenomena. Bulletin of the Earthquake Research Institute 41 (1963) 615–658.

[8.] Chen, X. Shearer, P.M. Analysis of foreshock sequences in California and implications for earthquake triggering. Pure and Applied Geophysics 173(1) (2016) 133-152.

[9.] Chang, Y.H., Hung, S.H., Chen, Y.L. A fast algorithm for automatic phase picker and event location: Application to the 2018 Hualien earthquake sequences. Terrestrial Atmospheric and Oceanic Sciences 30 (2019) 435-448.

[10.] Bath, M. Lateral inhomogeneities of the upper mantle. Tectonophysics 2 (776) (1965) 483-514.

[11.] Helmstetter, A., Sornette, D., Grasso, J.R. Mainshocks are aftershocks of conditional foreshocks: How do foreshock statistical properties emerge from aftershock laws. Journal of Geophysical Research: Solid Earth 108(B1) (2003).

[12.] AFAD, AFAD Earthquake Catalog. Ankara, Turkey (2023) https://deprem.afad.gov.tr/last-earthquakes.html (Access Date: 13 April 2023).

[13.] Emre, O., Duman, T.Y., Ozalp, S., Elmaci, H., Olgun, S., Saroglu, F. 1/1.250.000 scaled Turkey active fault map"-General Directorate of Mineral Research and Exploration Special Publication. http://www.mta. gov.tr/. Accessed 24 January 2021 (2013).

[14.] Emre, O., Duman, T.Y., Ozalp, S., Saroglu, F., Olgun, S., Elmaci, H., Can, T. Active fault database of Turkey. Bulletin of Earthquake Engineering 16 (2018) 3229-3275.

[15.] Wessel, P., Smith, W.H.F. GMT Version 5.1 Generic mapping tools graphics. Laboratory for Satellite Altimetry NOAA/NESDIS/NODC 123 (2004).

PACE-2023
International Congress on the Phenomenological Aspects of Civil Engineering

PACE-2023
International Congress on Phenomenological Aspects in Civil Engineering

Research Article
20-23 June 2023

An Overview on Tools for Assessment of Cost Overrun Factors in Construction Projects

Muhammad Hamza Zahoor*[1], Nafeesa Shaheen[2], Majid Ali[3]
[1,2,3] *Capital University of Science and Technology, Islamabad, Pakistan*
Corresponding Author E-mail: hamza.malik40755@gmail.com

Keywords

Cost Overrun,
Assessment Tools,
Project Success,
Management Factors,
Construction Industry.

Abstract

This study investigated the significant reasons for cost overruns in construction projects, the critical success factors, and various tools that are helping to avoid cost overruns. This study aims to determine the significant factors that make a project successful or fail. The factors that cause cost overrun and the tools that can be used in the cost overrun projects in Pakistan's construction industry so that future efforts can be directed to mitigate them. Numerous reasons for cost overruns in the global construction sector were realized after a comprehensive literature study. The top ten cost overrun variables identified were fluctuating raw material prices, expensive machinery, lowest bidder cost, poor project management, poor cost control, delays between design and procurement phases and inappropriate cost estimation methods. Questionnaire surveys, structure equation modelling, the Delphi method, regression-based model, statistical assessment, fuzzy-analytical network processing, fuzzy artificial neural network, and fuzzy simulation have been widely used and dominated the literature because they can quantify the intricacy and unpredictability of the cost overrun factors. A statistical method was determined to estimate the ranking of cost overrun factors. Therefore, the objective of the present literature study is to conduct a thorough analysis of the literature about the fundamental causes of cost overrun factors and various cost-controlling techniques used. This is done by focusing on articles published in highly reputable journals in the last decade.

1. Introduction

The hidden changes in the project result are increasing the overall cost and budget of the project. This hidden cost is known as overrun. Poor cost performance has therefore been regarded as one of the most critical problems in Pakistan projects [1]. The factors that have a success/failure on a project's result are called attributes. These attributes focus on people, resources, technology, working conditions, systems, and assigned tasks [2]. It is often regarded as successful when a construction project is finished on schedule, without cost overruns, and in line with specifications. The three factors have been utilized in literature studies to assess project performance [2], [3]. The iron triangle refers to these three requirements in project management. Some studies have employed other factors to gauge the success of projects, including stakeholder satisfaction, safety performance, and conflict resolution [1], [4]. This literature shows that project financing is the primary factor that should be considered, and a practical plan can avert the risk of cost overrun. It also shows that a good management project eliminates the project's risks.

Cost overrun in the construction plans can be based upon a different number of factors as there is no particular cause or reason. A study established that the delays occurred due to additional work and changes required at the last minute, and pricing fluctuations were the reason for the cost overrun. Lack of expertise in site workers, defects in the building, and incomplete drawings were known as failure factors worldwide [5]. The literature study identified the following critical failure factors: disagreements among project participants, ignorance and a lack of knowledge, the presence of poor project-specific characteristics and a lack of cooperation, unfavourable socioeconomic and climatic conditions, reluctance to make timely decisions, aggressive competition at the tender stage, and a lack of time for bid preparation [2]. The project's timely and cost-effective completion is the primary objective shared by the customer and the contractor. Due to the enormous aggregates that are held up and cause a delay in completion, costs would increase [3].

Success can be achieved when the project is completed within the time and reasonable budget and for the proposed cost. As long as the project's cash flow management during the implementation stage, proficiency in coordinating the project resources, and project controls are satisfactory, and there would be no cost overruns that can hurt the worker. This requires high capability, knowledge, and experience [5], [6]. According to the survey results, poor communication between the respondents and the contractor's financial limitations were the most crucial cost overrun factors [7]. *Fuzzy logic* is an analytical computing method designed to present vagueness and standardize fuzziness. It also makes it easier to

get a definite conclusion based on unclear, vague, noisy, and missing input. This research demonstrates that the tools help avert cost overruns like fuzzy logic and other tools for building information modelling (BIM) [1].

To the best of the author's knowledge, the most critical variables various techniques for reducing cost overruns and factors influencing the success or failure of construction projects. This review paper investigates the cost overrun factors and cost-controlling strategies mentioned in the literature. To do this, publications over the previous twenty years that were published in respected journals underwent a thorough review process to compile all available data on the causes and methods of cost overruns. The causes of success and failure are covered first. Then, the essential variables and methods are examined. Finally, numerous approaches for cost overrun are investigated.

6. Success/failure of construction projects

Gates et al. [8] found that schedule delays, frequent design changes, additional work and changes requested by the owner at the last minute, flaws in the design, insufficient planning and timelines, fluctuations in the prices, changes in the owner's scope of work, drawing that were incomplete or detailed designs at the time of presenting. Lack of expert site staff, construction defects, and failure in work are the major causes of cost overruns in construction projects worldwide. Herrando et al. [9] observed that they should have considered the significance of the project planning process, lack of experience executing a complicated task, poor design capacity, and frequent design changes. Cost overruns in the construction phase of projects have reportedly been attributed to factors including "insufficient site management and monitoring, slow decision-making, and client-initiated variations". The estimator and the parties that are involved in the construction project must be able to identify the cost overruns element.

Khodeir et al. [10] reported a quantitative questionnaire survey to analyze project failure factors. Their study revealed poor risk management, budget overruns, poor communication management, schedule delays, and poor estimation practices as the top five failure factors. According to studies by Alsolami [2] and Odeck [11], cost overrun-related factors and contractors' site management were critical factors affecting cost performance. According to Paraskevopoulou et al. [12], clear and realistic project goals, project planning, the project manager's competency & relevant experience the project management, the competency of the project management, clear and precise goals of the client, the project's value, complexity, and uniqueness, the project manager's experience, and the client's ability to make timely decisions are the top-ranking CSFs for construction projects. The three factors have been utilized in literature studies to assess project performance.

Figure 1. Importance of cost in iron triangle

In the future, the evaluation of success or failure in construction projects will be enhanced through various approaches. Advanced data analysis techniques, including artificial intelligence and machine learning, will play a crucial role in analyzing vast amounts of project-related data. By identifying patterns and predicting potential issues, these technologies will enable proactive measures to prevent failures and optimize project success. Additionally, there will be a greater emphasis on improved risk management, with the development of more sophisticated risk assessment models that consider a broader range of factors and incorporate real-time data. Effective stakeholder engagement and communication strategies will also be prioritized, recognizing the significance of involving stakeholders throughout the construction process to ensure project success. By addressing these areas, future work aims to enhance project evaluation methodologies and contribute to more successful and efficient construction projects.

7. Different Cost overrun factors

Paraskevopoulou et al. [12] studied that showed the cost and time management of construction projects that revealed the primary sources of cost and time overrun, which included changes in design, risks and doubts, wrong estimations of task time and length, complications, and poor performance of subcontractors. Sepasgozar et al. [13] studied the most important aspects determining building cost project features, attributes of the contractors, and conditions of the external market, according to research on the factors that influence the construction cost of Industrialized Building Systems (IBS) plans. Shah et al. [14] revealed that variations in material prices, cash flow and financial experiments faced by contractors, a lack of site labour, lack of communication between different parties, improper planning and arrangement by contractors, and frequent design changes are the factors that have the most negligible impact on the project's construction costs.

Herrando et al. [9] studied that the cost of building includes the cost of materials and labour. The survey's top three concerns include fluctuating raw material prices, unstable manufacturing material costs, and high machinery costs. Alsolami [2] studied that prices may fluctuate virtually daily, and they sometimes do. In many circumstances, these quick changes make it difficult for suppliers to commit to a single fixed pricing. Dikmen et al. [6] studied several reasons construction projects exceed the budget. Each factor of a cost overrun occurs at a different pace and has a distinct effect on the final project cost. While some specific factors appear, their impact on cost may be less severe. According to the literature study, several variables influence cost overruns in the construction industry. The top 10 factors are identified below:

Table 1. Identified Cost Overrun Factors

Author	Year	Factors	Findings
Khodeir et al. [10]	2019	Inadequate Estimation	Inaccurate cost estimates result in financial loss and increased claims and disputes. The Client will be in a financial crisis if the project estimate is insufficient.
Amini et al. [3]	2022	Inflation	The cost of materials, equipment, and labor varies due to inflation. Change in market prices of construction materials leads to loss if price adjustment terms are not considered in the project cost.
Wyke et al. [15]	2023	Improper Planning	Inadequate planning of the project, poor management experience, and adequate resources will result in faster project progress and longer project completion time, which increases indirect project costs.
Shehu et al. [16]	2014	Frequent Design Changes	Allot adequate time and resources for precise budget and schedule estimates in the preconstruction stage. Changes in design in the construction phase could lead to cost overrun.
Zhong et al. [17]	2022	Poor site management and supervision	Inexperienced subcontractors may make expensive errors and delay projects. Proper micro-level Management of the resources deployed on-site will result in early project completion and will avoid an increase in the budget.
Yun et al. [18]	2022	Inadequate Resources	If deployed at the site, inadequate equipment, tools, and plants will lead to delays. The project will suffer cost overruns.
Alekhya et al. [1]	2022	Unforeseen Site Conditions	The unforeseen site conditions involve risks like revolution, pandemic, thunderstorms, fire earthquakes, and other force majeure actions; when they do happen, projects typically experience significant delays and cost overruns.
Alsolami [2]	2022	Inadequate Design	The preliminary design will disrupt the progress during the execution and end in cost overruns.
Araskevopoulou et al. [12]	2022	Contractual claims	Initiating unnecessary contractual claims by both parties of the contract will affect the end delivery of the project. It may lead to cost overrun if claims were valid and their cost needed to be considered in the initial estimate of the project.
Wang et al. [19]	2022	Non-BOQ items	Various Non-BOQ items are incurred due to site requirements and other factors for which no budget is allocated in the initial estimate. Execution of Non-BOQ Items will always lead to cost overrun via variation orders.

In the future, further research and work on identifying and addressing cost overrun factors in construction projects will be crucial. One aspect of future work involves examining the role of project planning and design in cost overruns. By analyzing historical data and conducting comprehensive studies, researchers can identify common design-related factors that contribute to cost overruns and develop strategies to mitigate them. Additionally, enhancing risk management practices will be essential in addressing cost overruns. Future efforts may focus on developing robust risk identification and mitigation strategies, leveraging historical data and lessons learned from past projects. This could involve the use of advanced analytics to assess project risks, simulate various scenarios, and implement effective risk response plans.

8. Tools for Assessment

Cost control is a comprehensive set of cost analysis methods and managing techniques to improve cost efficiency using various techniques. Shah et al. studied that [14] construction risks and complexity are still assessed based on expert opinion. Therefore, the information for risk has quantitative. The chance of occurrence and severity of the risk are the starting points for measuring project risk and complexity, which are then converted into quantitative metrics to address the interdependencies for project cost [6]. These quantitative tools are built using various linear and non-linear methods. Non-linear probabilistic because the majority of construction projects display stochastic behaviour. According to the literature, several tools identify cost overruns factors to make construction sustainable. The top 9 tools are identified.

Khodier et al. [10] analyzed fuzzy approaches that have been widely used as hybridized techniques for construction risk assessment during the last ten years. They are very effective in stimulating the vulnerabilities faced in experts' judgments. Some questions about network interdependency have been highlighted by using structural equation modelling. Wang et al. [19] recommended that these approaches have limited uses in construction projects where system complexity and unpredictability are significant. A short discussion of probabilistic methods and their use in construction projects.

In the future, there will be continued efforts to develop and refine tools for assessing construction projects. These tools will aim to provide a comprehensive and standardized approach to evaluating various aspects of a project's performance. One area of future work involves the development of advanced performance measurement frameworks that consider not only traditional metrics such as cost and schedule but also factors like sustainability, quality, and stakeholder satisfaction. These frameworks will help project stakeholders gain a holistic view of project performance and enable more informed decision-making.

Table 2. Assessment of different tools for literature review

Author	Year	Tools	Advantage/Disadvantage
Dikmen et al. [6]	2022	Questionnaire Survey (Expert Judgment)	Data can be sent fast, and coming back time can be reasonable and can instantly connect with the audience. Online surveys are free of cost. Laying may be a problem. Respondents do not provide honest replies.

Khodeir et al. [10]	2019	Fuzzy Synthetic Evaluation	Fuzzy synthetic evaluation offers benefits in managing complex evaluations with various criteria and levels. Fuzzy logic cannot be used to answer all problems in a single, organized way and relies on human knowledge.
Herrando et al. [9]	2023	Structural Equational modelling	The modelling of measurement errors and unexplained variances are benefits of using SEM. SEM has several drawbacks, including selecting and utilizing variables.
Shah et al. [14]	2022	Delphi-SWARA method	Delphi is beneficial for creating estimations or forecasts. Lowers noise among group members based on other rankings by offering regulated feedback. There is no right or incorrect answer produced.
Ammar et al. [4]	2022	Regression Based Model	Regression models provide an algebraic equation, correlation coefficients, and other statistical metrics. Regression models become less reliable as variables rise and do not handle nonlinearity. The user must consider different variables to enhance the regression model.
Awodie et al. [5]	2023	Fuzzy group decision-making approach (FGDMA)	Factors causing cost overruns are assessed as the fuzzy probability of the independent risk. FGDMA computes the defusing scores of the non-conformities. The limits of expert assessments are addressed by disobeying scores by connecting them to relevant fuzzy numbers.
Shoar et al. [20]	2022	Computer Based Contingency Estimation	The contingency estimating system was developed utilizing contingency estimation modelling to solve a cost overrun. This system is based on the study of the present state of contract modification requests and the findings of the identification and analysis of risk.
Sepasgozar et al. [13]	2022	Statistical Method (Relative Importance Index)	The project risk variables were ranked using the relative relevance index technique. Reliability and correlation coefficient tests were also conducted.

9. Conclusion & Future Recommendation

This review paper examines the most critical factors contributing to cost overruns in the construction industry in developed countries, as reported in articles published in highly reputable journals in the last two decades. The current effort is to compose all published information related to factors, tools and techniques used in cost overrun. Based on this literature research, the following are the conclusions:

- Construction industry experts should constantly conduct accurate planning, estimating, management, and cost control in their projects to achieve sustainability.
- The most crucial aspects were the requirements of scope, cost, time, quality, resources, and management. Furthermore, unrealistic expectations, lack of resources, and lack of executive backing are the leading causes of project failures.
- By providing new tools for organizing, interpreting, and presenting data sets, statistical analysis often enables users to do more detailed analyses.

This study examined the factors that influence cost overruns, the ranking of these factors, and techniques that will be used in cost control to achieve sustainability in construction projects, which can help minimizing the impact cost overruns.

Acknowledgment

The authors would like everyone who helps them throughout this literature research.

Declaration of Conflict of Interests

The authors declare that there is no conflict of interest.

References

[1.] Alekhya, G., K. Shashikanth, and M.A. Prasad, Risk assessment of cost overrun using fuzzy logic model. Materials Today: Proceedings, 2022. 62: p. 1803-1810.

[2.] Alsolami, B.M., Identifying and assessing critical success factors of value management implementation in Saudi Arabia building construction industry. Ain Shams Engineering Journal, 2022. 13(6): p. 101804.

[3.] Amini, S., et al., Causes of cost overruns in building construction projects in Asian countries; Iran as a case study. Engineering, Construction and Architectural Management, 2022(ahead-of-print).

[4.] Ammar, T., M. Abdel-Monem, and K. El-Dash, Risk factors causing cost overruns in road networks. Ain Shams Engineering Journal, 2022. 13(5): p. 101720.

[5.] Awodi, N.J., et al., Fuzzy TOPSIS-based risk assessment model for effective nuclear decommissioning risk management. Progress in Nuclear Energy, 2023. 155: p. 104524.

[6.] Dikmen, I., et al., A decision-support tool for risk and complexity assessment and visualization in construction projects. Computers in Industry, 2022. 141: p. 103694.

[7.] Dikmen, I., M.T. Birgonul, and S. Han, Using fuzzy risk assessment to rate cost overrun risk in international construction projects. International journal of project management, 2007. 25(5): p. 494-505.

[8.] Eash-Gates, P., et al., Sources of cost overrun in nuclear power plant construction call for a new approach to engineering design. Joule, 2020. 4(11): p. 2348-2373.

[9.] Herrando, M., et al., The cost overrun of depopulation to improve energy efficiency in buildings: A case study in the Mediterranean Region. Sustainable Energy Technologies and Assessments, 2023. 55: p. 102985.

[10.] Khodeir, L.M. and A. El Ghandour, Examining the role of value management in controlling cost overrun [application on residential construction projects in Egypt]. Ain Shams Engineering Journal, 2019. 10(3): p. 471-479.

[11.] Odeck, J., Cost overruns in road construction—what are their sizes and determinants? Transport policy, 2004. 11(1): p. 43-53.

[12.] Paraskevopoulou, C., et al., Assessing the failure potential of tunnels and the impacts on cost overruns and project delays. Tunnelling and Underground Space Technology, 2022. 123: p. 104443.

[13.] Sepasgozar, S.M., et al., BIM and Digital Tools for State-of-the-Art Construction Cost Management. Buildings, 2022. 12(4): p. 396.

[14.] Shah, P. and A.A. Chandragade, Application of project management tool in construction for Planning, Scheduling and Optimization. Materials Today: Proceedings, 2022.

[15.] Wyke, S., S.M. Lindhard, and J.K. Larsen, Using principal component analysis to identify latent factors affecting cost and time overrun in public construction projects. Engineering, Construction and Architectural Management, 2023(ahead-of-print).

[16.] Shehu, Z., et al., Cost overrun in the Malaysian construction industry projects: A deeper insight. International journal of project management, 2014. 32(8): p. 1471-1480.

[17.] Zhong, S., H. Elhegazy, and H. Elzarka, Key factors affecting the decision-making process for buildings projects in Egypt. Ain Shams Engineering Journal, 2022. 13(3): p. 101597.

[18.] Yun, J., K.R. Ryu, and S. Ham, Spatial analysis leveraging machine learning and GIS of socio-geographic factors affecting cost overrun occurrence in roadway projects. Automation in Construction, 2022. 133: p. 104007.

[19.] Wang, R., et al., Assessing effects of economic factors on construction cost estimation using deep neural networks. Automation in Construction, 2022. 134: p. 104080.

[20.] Shoar, S., N. Chileshe, and J.D. Edwards, Machine learning-aided engineering services' cost overruns prediction in high-rise residential building projects: Application of random forest regression. Journal of Building Engineering, 2022. 50: p. 104102.

PACE-2023
International Congress on the Phenomenological Aspects of Civil Engineering

PACE-2023
International Congress on Phenomenological Aspects in Civil Engineering

Research Article
20-23 June 2023

Simulating the Behavior and Reinforcing Corroded Concrete Beams Using Carbon Fiber Polymer Sheets

Mohammed Kusay Ebrahım Al-Dulayme [*,1], Ahmct Budak[2]
[1]*Department of Civil Engineering, Atatürk University, Erzurum, Turkey*
[2]*Associate Professor, Department of Civil Engineering, Atatürk University, Erzurum, Turkey*
**Corresponding Author E-mail: mhmdlord94@gmail.com , abudak@atauni.edu.tr*

Keywords

Corroded concrete beam,
Reinforced concrete,
Corrosion damage,
Finite element analysis,
Carbon fiber polymer sheets,
Strengthening techniques,
Bearing capacity,
Strength restoration,
Performance enhancement,
Corrosion mitigation.

Abstract

This study focuses on understanding how to simulate the behavior of a reinforced concrete beam that has been damaged by corrosion. The researchers used ABAQUS software for finite element analysis of concrete beams. They also explored the use of carbon fiber polymer sheets to strengthen the beam by applying them to the lower part where corrosion occurs. The study found that the beam weakened significantly due to corrosion. However, by using carbon fiber polymer sheets, the researchers were able to strengthen the beam and provide a viable alternative for the repair process. This means that the sheets were effective in restoring a lot of the strength of the beam that was affected by corrosion.

1. Introduction

Reinforced concrete structures are susceptible to steel corrosion, which can lead to costly repairs. To address this issue, researchers have turned to evaluating Fiber Reinforced Polymers as an alternative to steel for concrete reinforcement. Carbon Fiber Sheets Polymers are particularly attractive due to their high strength-to-weight ratio and non-corrosive nature. When applied to a concrete beam, carbon fiber sheets made from carbon fiber-reinforced polymer provide additional strength and stiffness, helping to reduce damage. The process of applying carbon fiber sheets to a concrete beam involves preparing the surface by removing any loose debris or contaminants, cutting the sheets to the appropriate size and shape, and using a specialized adhesive to apply them to the beam's surface. Compared to traditional reinforcing materials like steel, carbon fiber sheets are much lighter and easier to handle due to their high strength-to-weight ratio. As such, they are well-suited for use in industries where weight is a concern, such as aerospace or automotive industries (Saeed, 2016). Despite their advantages, it is important to notice that the cost of carbon fiber sheets is typically higher than other reinforcing materials. In this study, the researchers aimed to understand how to model a reinforced concrete beam that has been damaged by corrosion. They used carbon fiber polymer sheets for the reinforcement and compared the results with a normal beam. The goal was to see how effective the carbon fiber sheets are in strengthening the corroded beam compared to a regular beam. then we wanted to find how much strength would be restored for the corroded beam using carbon fiber sheets (Mohammad, 2011).

2. General Properties of Method

The aim here is to investigate the performance of a concrete beam that has been reinforced with carbon fiber sheets. To conduct the analysis, we will utilize the finite element method and test the subject. Below is a summary of the finite element method.

2.1. Finite Element Method (FEM)

The Finite Element Method is a numerical analysis technique used in engineering and physics to approximate and solve complex physical problems. It involves dividing a complex system into smaller, simpler parts, known as finite elements, and then analyzing the behavior of each element using mathematical equations. By solving these equations for each element and assembling them into a larger system, the overall behavior of the complex system can be approximated and analyzed. The method is widely used in fields such as structural engineering, heat transfer analysis, fluid mechanics, and electromagnetics (Reddy, 2019). (Asheghabadi and Matinmanesh, 2011)

2.2. Materials and Their Properties

2.2.1. Concrete

Concrete is a composite material that is strong in compression but weak in tension. When subjected to a load, it experiences both compressive and tensile stresses, which can cause different types of damage. Compressive damage occurs when compressive stresses exceed the compressive strength of the concrete, leading to crushing or cracking of the concrete. Tensile damage occurs when tensile stresses exceed the tensile strength of the concrete, resulting in cracking or splitting of the concrete, which can propagate and lead to failure of the structure. To address the issue of concrete tensile damage, reinforcement is often used, to provide additional strength and stiffness to the structure and distribute tensile stresses more evenly.

Table 1. Properties of concrete that are used in the modeling. (Neville, 1995)

Property	Magnitude	Pref explain if needed
Density	2.4E-009	density of concrete
Elastic (Young's Modulus)	23900	Elastic is a property of the material that tells us how easily it can stretch and deform
Elastic (Poisson's Ratio)	0.2	Poisson's Ratio the phenomenon in which a material tends to expand in directions perpendicular to the direction of compression
Concrete damaged Plasticity (Dilation Angle)	30	Concrete Damaged Plasticity (CDP) is a mathematical model that combines plasticity and damage mechanics to simulate the behavior of concrete structures under loading. CDP takes into account the damage level of the material and its ability to deform plastically, as well as the triaxial state of stress, strain rates, and loading history, to predict the behavior of concrete structures accurately.
Concrete damaged Plasticity (Eccentricity)	0.1	
Concrete damaged Plasticity (fb0/fc0)	1.16	
Concrete damaged Plasticity(K)	0.667	
Concrete damaged Plasticity (Viscosity Parameter)	0.0005	

2.2.2 Carbon Fiber Sheets (See Fig. 1.)

Fiber Reinforced Polymer is an attractive material for structural engineers because it has high tensile strength and is lightweight, corrosion-resistant, non-magnetic, and not sensitive to electricity. It has a higher strength-to-weight ratio, stiffness-to-weight ratio, and lower life cycle costs than steel, but its initial cost is higher. However, FRP has some drawbacks, including its weakness in the transverse direction and lack of ductility, which leads to non-preferred performance for concrete elements reinforced or prestressed with FRP rods. FRP is also more expensive than steel. The stress-strain relationship for steel and different types of FRP are presented as shown in Fig. 2. and listed in Table 2. (Saeed, 2016)

Figure 1. Carbon fiber sheets

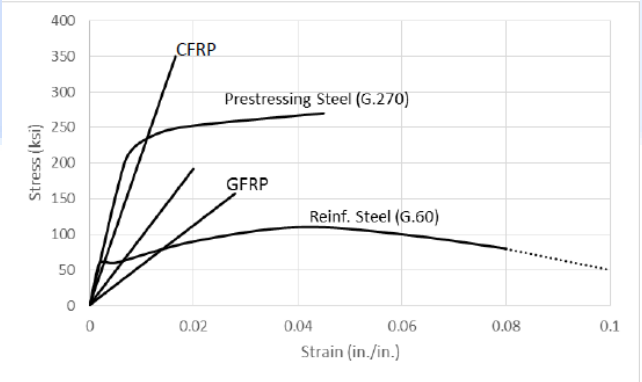

Figure 2. Typical stress-strain curves for steel and FRP composite bars (Saeed, 2016)

Table 2. Carbon fiber sheets properties

Property	Magnitude	Pref explain if needed
Hashing Damage (Density)	1.56E-009	Hashing Damage Model is a constitutive model used to simulate the behavior of materials under loading. The model is based on the theory of continuum damage mechanics and is commonly used in the analysis and design of composite materials. The Hashing model accounts for the damage and failure mechanisms that occur in the material by considering the damage to the material in terms of the number of broken fibers or cracks that have occurred within the material. The model considers both the tensile and compressive behavior of the material and is capable of predicting the stiffness reduction and the change in the failure mode of the material as damage accumulates.
Hashing Damage (Elastic) (E1)	13000	
Hashing Damage (Elastic) (E2)	800	
Hashing Damage (Elastic) (Nu12)	0.28	
Hashing Damage (Elastic) (G12)	4500	
Hashing Damage (Elastic) (G13)	4500	
Hashing Damage (Elastic) (G23)	4500	

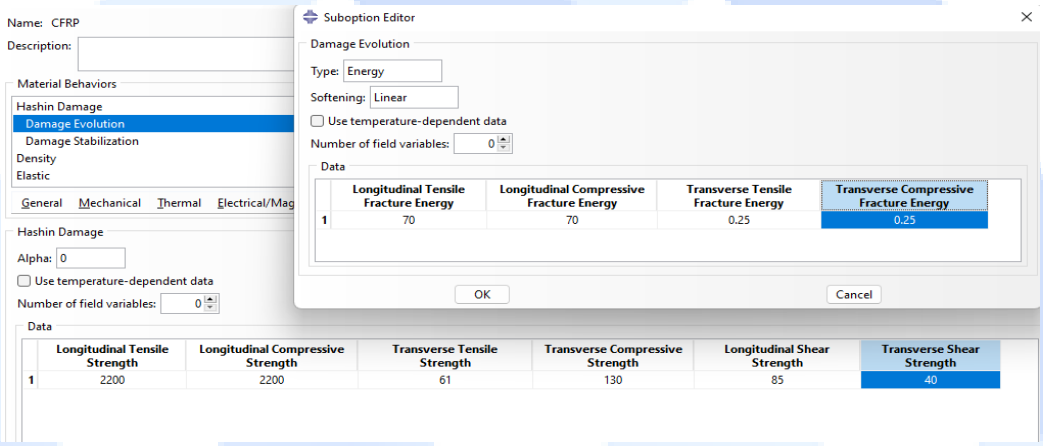

Figure 3. Carbon fiber sheets properties

2.2.3. Steel Bars

The steel bars used in this study have standard properties as indicated below, but the focus of our research is to investigate the effects of corrosion on them. As a result, we will analyze the impact of corrosion, explore approaches to incorporate it into our study, and model the potential consequences of corrosion on the steel bars. as shown in Fig. 4. and listed in Table 3. (Malvar, 1998)

Table 3. Steel bars properties that are used in the testing

Property	Magnitude	Pref explain if needed
Density	7.85E-009	Normal proportion of steel bars
Elastic (Young's Modulus)	199000	
Elastic (Poisson's Ratio)	0.3	

3. Applications

In this study, our goal is to create a model of a beam that has been damaged by corrosion. To do that, we need to understand how corrosion affects the reinforced concrete. Previous studies have shown that corrosion mainly affects the cross-section area of the steel parts of the beam, resulting in a loss of strength in those areas. This loss of strength is due to the reduction in the bond between the concrete and the steel parts of the beam (Almassri et al., 2016; Nasser et al., 2019). A key aspect of the research involved determining the most appropriate method for modeling a concrete beam affected by corrosion. Extensive research was conducted by referring to journals and gathering information. The optimal approach was to reduce the cross-sectional area of the steel bars by a percentage between 10% to 30%. For this study, the reduction was set at 20%. To mimic a corroded reinforced concrete beam, connections were only made between the steel parts and the concrete at certain places across the beam to mimic the corrosion effect. The study goes into greater detail about the tests conducted. (Zhang et al., 2021, 2014).

The evaluation of corrosion-damaged steel-reinforced concrete structures. Visual inspections may not show the actual structural performance, and finite element (FE) analysis is used to determine the impact of corrosion damage on the capacity for shear critical beams. The study found that corrosion damage reduced stiffness, load-carrying capacity, and deformation capacity of reinforced concrete beam specimens. Different types of corrosion damage components were analyzed, including concrete section loss, rebar cross-sectional loss, and debonding of corrosion-damaged stirrups from the concrete. The combination of different damage parameters effectively represented the experimental specimen in the most severe corrosion damage state.(Potisuk et al., 2011)No clear

To begin with, we started modeling the concrete beam. It had dimensions of 300 mm by 600 mm and a length of 4000 mm. We used steel bars that were 16 mm in diameter and strips that were 8 mm in diameter. The spacing between the strips was different depending on whether it was in the middle or on the sides of the beam. On the sides, the spacing was approximately 150 mm, while in the middle part, it was around 250 mm. The middle part, with a width of 2000 mm, was the specific area we focused on because it was considered to be the part most affected by corrosion. Table 4 shows the steel bars strips and the effect of corrosion on them.

Table 4. Area and radius of steel bars and the amount that is being reduced by corrosion

Section	Total Cross – Section (A)	R
Longitudinal Bar	201.056	8
Stirrups	28.2735	3
% Area Lost	20%	
% Remaining Area	80%	
Section	Total Cross – Section (A)	
Longitudinal Bar	160.8448	7.16
Stirrups	22.6188	2.68

During the modeling process, we made adjustments to the middle part of the concrete beam. We reduced the area of the steel bars and strips according to percentages shown in table 4 then removed the concrete cover only in the lower section of the middle part, as show in Fig. 4. The exposed area where the concrete cover was removed was connected to the remaining steel bars as show in Fig. 4.

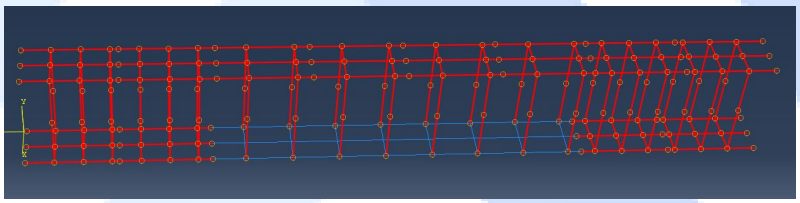

Figure 4. The connection between the bars and concrete for the corroded beam

Figure 5. Corrosion in the middle lower part of the concrete beam

We added four steel pads to apply the force and the boundary condition as shown in Fig. 6. and we use the static general analysis step in ABAQUS which involves solving equilibrium equations to analyze a structure under external loads and boundary conditions. It calculates displacements, stresses, and strains using the finite element method. The analysis applies prescribed loads and constraints, solves the equations iteratively for convergence, and provides results for evaluating structural behavior and making design decisions.

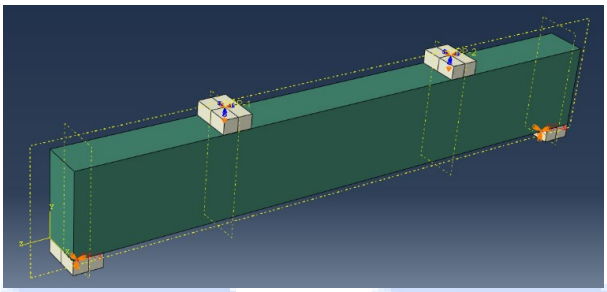

Figure 6. Showing how the load and boundary condition be applied

To create the mesh for the beam, we used different types of elements. For the concrete part, we used 3D stress C3D8R, which is an 8-node linear brick element. This element helps to represent the concrete accurately. For the steel elements, we used T3D2, a 2-node linear 3-D truss element, which is suitable for modeling steel components. Lastly, for the carbon fiber sheets, we used S4R, a 4-node doubly curved thin or thick shell element, which is ideal for representing the behavior of the carbon fiber sheets. See Fig. 7.

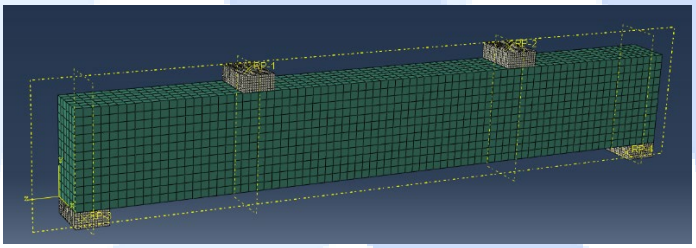

Figure 7. The meshing process of the beam

We focused on the lower part of the beam, which is most affected. To counteract the corrosion damage, we applied the carbon fiber sheet specifically to this area. This is shown in Fig. 8, showing the targeted application of the carbon fiber sheet on the lower part of the beam. The process of applying carbon fiber sheets to a concrete beam affected by corrosion involves the following steps (Duthinh and Starnes, 2001; Soudki and Alkhrdaji, 2005):

- Surface preparation: The affected area of the concrete beam needs to be thoroughly cleaned and prepared before applying the carbon fiber sheets. This includes removing any loose debris, rust, or contaminants from the surface.
- Adhesive application: A suitable adhesive or epoxy is applied to the cleaned surface of the concrete beam. This adhesive acts as a bonding agent between the carbon fiber sheets and the concrete surface.
- Carbon fiber sheet placement: The carbon fiber sheets, which are usually available in the form of rolls or sheets, are carefully positioned over the affected area of the concrete beam. The sheets should be pressed firmly onto the adhesive to ensure proper adhesion and contact with the concrete surface.
- Resin application: To enhance the strength and rigidity of the carbon fiber sheets, a resin is often applied on top of the sheets. This resin helps to bond the individual carbon fibers together and provides additional reinforcement.
- Curing and strengthening: Once the carbon fiber sheets and resin are applied, they need to be allowed to cure and harden. This process typically involves a specific duration of time, during which the carbon fiber sheets and resin chemically react and form a strong composite structure.

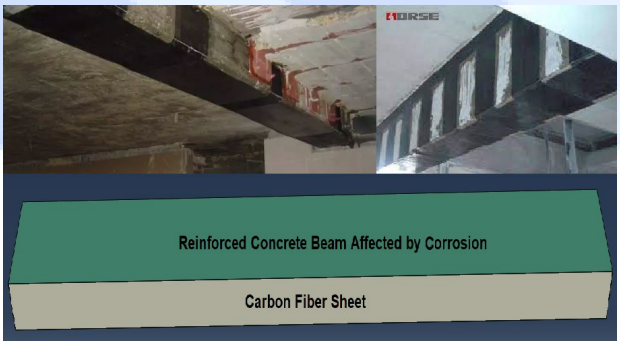

Figure 8. Shows the part that are covered with carbon fiber sheets with live examples

4. Conclusions

After the analysis and extracting the result as shown in fig. 9. we conclude the following:

- After conducting the analysis and evaluating the results, it was observed that the concrete beam affected by corrosion experienced a significant loss of bearing capacity. Specifically, it lost 61.7% of its original strength when compared to a similar concrete beam in normal conditions.
- However, when carbon fiber sheets were applied to the corroded area of the concrete beam, a improvement was observed. The beam's bearing capacity lost was only 35.8% of the concrete beam in normal conditions. This reduction was lower than the case without the carbon fiber sheets.
- It is important to note that over time, the concrete beam reinforced with carbon fiber sheets has the potential to gain even more strength. This makes it a viable and cost-effective alternative to the traditional approach of demolishing the entire concrete beam and replacing it with a new one.

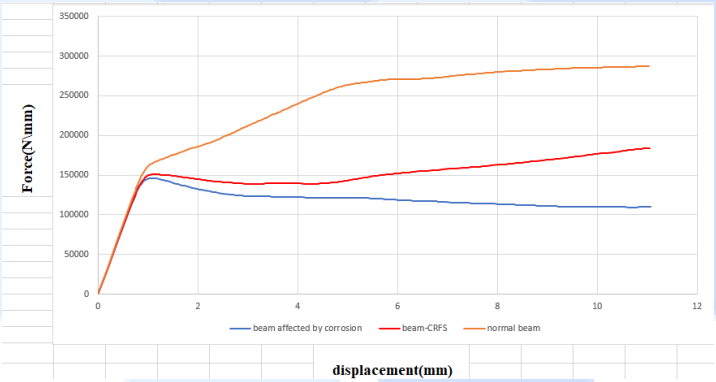

Figure 9. The analysis results were compared for three situations involving the concrete beam

By utilizing carbon fiber sheets in the specific area affected by corrosion, the overall structural integrity and performance of the concrete beam can be effectively restored. This finding highlights the potential of carbon fiber sheets as a reliable solution for reinforcing corroded concrete structures without the need for extensive demolition and reconstruction.

Lastly, it's worth noting that in this study, we used a small quantity of carbon fiber sheets, specifically applied to the lower part of the concrete beam. However, it was observed that if we partially or fully cover the sides of the concrete beam with carbon fiber sheets, it would provide even greater benefits for the overall strengthening process.

Acknowledgment

The earthquake data was obtained from the AFAD (Earthquake Department of the Disaster and Emergency Management Presidency, Ankara-Turkey) [12]. All images were generated using the GMT software [15]. The tectonic units were digitized using a geoscience map viewer and drawing editor licensed to the General Directorate of Mineral Research and Exploration (MTA) [13,14].

Declaration of Conflict of Interests

The author declares that there is no conflict of interest. They have no known competing financial interests or personal relationships that could have appeared to influence the work reported in this paper.

References

[1.] Almassri, B., Al Mahmoud, F., and Francois, R. (2016). Behaviour of corroded reinforced concrete beams repaired with NSM CFRP rods, experimental and finite element study. *Composites Part B: Engineering*, *92*, 477-488.

[2.] Asheghabadi, M. S., and Matinmanesh, H. (2011). Finite element seismic analysis of cylindrical tunnel in sandy soils with consideration of soil-tunnel interaction. *Procedia engineering*, *14*, 3162-3169.

[3.] Duthinh, D., and Starnes, M. A. (2001). Strengthening of reinforced concrete beams with carbon FRP.

[4.] Malvar, L. J. (1998). Review of static and dynamic properties of steel reinforcing bars. *Materials Journal*, *95*(5), 609-616.

[5.] Mohammad, K. I. (2011). *Behavior of RC Beams Strengthened with CFRP Under Combined Actions* College of Engineering Civil Engineering Department BEHAVIOR OF RC BEAMS ...].

[6.] Nasser, H., Van Steen, C., Vrijdaghs, R., TORRESACOSTA, A. A., Vandewalle, L., and Verstrynge, E. (2019). Numerical modelling of corroded reinforced concrete beams based on visual inspection data. Fifth SMAR Conference, Potsdam, Germany, August,

[7.] Neville, A. M. (1995). *Properties of concrete* (Vol. 4). Longman London.

[8.] Potisuk, T., Higgins, C. C., Miller, T. H., and Yim, S. C. (2011). Finite element analysis of reinforced concrete beams with corrosion subjected to shear. *Advances in civil engineering*, *2011*.

[9.] Reddy, J. N. (2019). *Introduction to the finite element method*. McGraw-Hill Education.

[10.] Saeed, Y. M. (2016). *Behavior of prestressed concrete beams with CFRP strands* Portland State University].

[11.] Soudki, K., and Alkhrdaji, T. (2005). Guide for the design and construction of externally bonded FRP systems for strengthening concrete structures (ACI 440.2 R-02). Structures Congress 2005: Metropolis and Beyond,

[12.] Zhang, T., Xu, L., Li, P., and Chen, H. (2021). Numerical Simulation Analysis for Mechanical Properties of Corroded Reinforced Concrete Beams. *Academic Journal of Engineering and Technology Science*, *4*(7), 44-50.

[13.] Zhang, W., Zhou, B., Gu, X., and Dai, H. (2014). Probability distribution model for cross-sectional area of corroded reinforcing steel bars. *Journal of Materials in Civil Engineering*, *26*(5), 822-832.

PACE-2023

International Congress on the Phenomenological Aspects of Civil Engineering

PACE-2023

International Congress on Phenomenological Aspects in Civil Engineering

Research Article 20-23 June 2023

A New Insight from Literature on Microbe-Assisted Self-Healing of Concrete Micro Cracks

Zeenat Khan*,[1], Majid Ali[2]

[1]*Department of Biotechnology, Capital University of Science & Technology, Islamabad, Pakistan.*

[2]*Department of Civil Engineering, Capital University of Science & Technology, Islamabad, Pakistan.*

Corresponding Author E-mail:khanzeenat2611@gmail.com, majid.ali@cust.edu.pk

Keywords

Bacteria,
Concrete,
Calcium carbonate,
Crack repairing.

Abstract

In this modern world, concrete is still the prime construction material, and cracks are the intrinsic weakness of concrete. These cracks cause seepage of water, which leads to corrosion and thus weakens the structural strength. Many techniques are available in civil engineering to repair these cracks, but these require a high cost of implementation. At the same time, majority of these frequently adopted techniques (i.e., chemicals, resins, polymers etc.) are not environment friendly. In last two decades, bacteria (when directly or indirectly mixed in concrete) have been reported for automatic crack repair. Thus, the goal of this literature research is to provide a comprehensive review of the potential of bacteria for self-healing of concrete. The articles published in highly reputable journals in the last decade are considered. First, cracks, its causes and recommended solutions are discussed in detail. And then, philosophy involved in
concrete self-healing with focus on bacteria and its mixing techniques in concrete are elaborated. Based on this, suitable bacteria are recommended as environment friendly and cheap approach for self- healing of concrete. Finally, the adoptability of bio concrete in developing countries is debated, considering its pros and cons. Bio concrete can be used in real life structures after its in-depth investigation for global behavior.

1. Introduction

Concrete plays a vital role in construction, and cracks in it hold significant importance. A developing biological self-healing technique aims to resolve this issue of concrete cracking. Concrete suffers from physical, chemical, and biological conditions. Experimental results have shown that concrete is strong in compressive loading but weak in tension. To address this weakness in tension, steel reinforcement is introduced to

counter the load when concrete fails [1]. This weakness of concrete causes cracking, which can be either micro or macro in nature. Concrete cracks result from factors like tension, freeze-thaw cycles, shrinkage, indicating diverse causes. Cracking can also occur during the hardening of concrete, ultimately leading to structural failure. Loading beyond the limit causes macro cracks, while various factors lead to micro cracks. Sometimes these cracks are noticeable, but often they are ignored [2]. Water droplets may enter concrete cracks over time, depending on their location and the situation. Water permeability enlarges cracks, leading to increased volume and corrosion of steel reinforcement in concrete. Cracks manifest in various types (from various causes) and introduce themselves as potential threats. Cracks in concrete are crucial as they jeopardize structural integrity and elicit negative responses to tensile stress.

To heal cracks, there are several ways that can be either automatic or non-automatic. Non-automatic methods require human efforts, which are not only time-consuming but also costly. Automatic methods utilize self- healing processes where a healing agent autonomously repairs concrete cracks. Self-healing can be achieved through various means, including the use of chemicals and minerals. However, these methods can have a significant impact on the environment and human life. Microorganisms are the favored choice in civil engineering for crack repair, as proposed by biotechnology [2]. Bacteria, a well-known organism for precipitating calcium carbonate, is used for sealing cracks. $CaCO_3$ precipitation done by a process called bio-mineralization. It typically involves two pathways for the formation of this compound [3]. The choice of pathway depends on how bacteria are mixed into the concrete mixture. Autotrophic pathways directly add bacteria, while heterotrophic pathways encapsulate and modify bacteria for nutrients addition [4]. Ureolytic strains thrive in high pH and facultative anaerobic environments, making them resilient and preferred for their longevity. The selection of bacteria is also based on these characteristics. The suitability of bacteria for long-term use is examined by various researchers and reported in literature reviews. Assessing the extent of crack repair is crucial as concrete cracks directly impact the structural integrity. Bacteria-based concrete is one of the most suitable methods for maximizing crack repair in concrete. Optimal conditions for crack repair involve bacteria selection, concentration, survival conditions, concrete mixing, and calcium carbonate precipitation.

Bio-concrete is a promising, eco-friendly, cost-effective approach. But its adaptability is limited due to challenges, cost of implementation, and time constraints. Bio mineralization is an ancient technique, while concrete is an invention of the 19th century. Researchers aim to attain desired concrete properties through experimentation, with bio-concrete displaying great potential for self-healing micro cracks [5, 6]. Finding suitable bacteria, proper nutrients, and effective mixing methods are crucial for cost reduction and optimal outcomes. Mixing bacteria with concrete is simple in a controlled lab, but skilled labor is necessary for field applications. This presents a significant hurdle for the widespread usage of bio concrete at the industrial level. However, promising results have been observed in experiments comparing bio concrete with other chemical methods for crack repair. Since cracks directly affect the stability of structures, bio concrete is seen as a valuable solution. Success hinges on employing bacteria with crack repair traits and addressing factors to mitigate micro cracks under stress [7]. However, the challenge lies in achieving adaptability at an industrial level. Bio-concrete encounters obstacles in industry adoption, but experimentation and skill development programs can overcome these challenges.

Keeping in view the extensive usage of concrete in today's world, damage to concrete is unavoidable [1, 2]. To address this issue, it is crucial to focus on potential solutions, and among them, bio concrete emerges as the best option. Micro cracks are hair-like cracks that just begin to start. Bio concrete is primarily designed to heal these micro cracks. Because, when micro cracks will be healed, formation of macro cracks will be prevented [8]. To achieve this objective, various articles published in highly reputable journals over the past decade have been studied. At start, concrete, cracks, its types emerged from various causes are studied. Phenomenological aspects of bio concrete are explained by shedding light on healing agent's formation pathways and techniques. The preference to bio concrete is also explained on the basis of cost and environmental effects. After in depth study of bio concrete suitable bacteria are suggested by overviewing the experimental results. At last, adaptability of bio concrete is argued with focus on developing countries.

2. Cracks, its causes and available solutions

Different cracks are formed due to various causes. Multiple repair techniques exist, but employing bacteria is regarded as a superior approach for concrete repair. The presence and size of cracks greatly impact the overall structure of concrete. These cracks are a result of tensile stress during execution and external factors such as loads and stresses. Cracks expose steel to the environment and causes water penetration, reduced structural capacity, corrosion, and diminish durability. In reinforced concrete structures, cracks indicate the ingress of harmful elements. Cracks in concrete also contribute to the reduction of carbonation resistance. Water penetration through cracks subjects the concrete to freeze and thaw cycles, leading to structural deterioration. Cracks become incurable once hardened, emphasizing the need to extensively minimize and manage them during the plastic state. Despite meticulous care and controlled conditions, numerous factors can cause cracks in concrete and structures. These causes include elastic deformation occurring at material junctions within the concrete, thermal movements resulting from temperature fluctuations, shrinkage and expansion, settlement and foundation movements, segregation, roots growing near the foundation, the formation of weak zones (interfacial transition zones) at the interaction between cement and coarse aggregate, autonomous shrinkage due to low water-cement (w/c) ratio, subgrade movements before concrete hardening, creep (slow elastic deformation), and formwork movements [9]. Concrete can be categorized into pre-hardening and post-hardening states, each associated with different types of cracks (Table 1). Exploring various crack types help to understand their formation mechanisms, as they can result in structural damage and failure. The solutions for repairing these cracks are generally cost-effective but require significant human effort.

Bacteria surpasses other techniques by addressing strength reduction caused by water-filled cracks and pores in concrete. There are several methods available to repair these cracks (Table 1). However, these methods are expensive, labor-intensive, and environmental unfriendly. Biotechnology, when integrated with other domains, offers cost-effective solutions for diverse issues, such as concrete crack repair. While concrete and its cracks are typically linked to civil engineering, biotechnological approaches provide cost-effective and eco-friendly solutions. Research and ancient techniques highlight bacteria's role in forming calcium carbonate precipitates to seal concrete cracks [10]. Bio-mineralization is a self-healing process where bacteria catalyze the reaction, forming calcium carbonate in concrete. The pathways for calcium carbonate formation vary based on bacteria, their nutritional needs, and crack locations. The exothermic energy during concrete formation and freeze-thaw cycles increase the likelihood of crack formation in regular concrete. Bacteria can survive harsh conditions and aid in maintaining favorable conditions to prevent concrete cracking. Repairing these cracks using alternative techniques can be costly and have adverse environmental impacts.

Table 1. Types of Cracks and their solutions [1, 3, 9]

Sr. No.	Type of Cracks.	Reasons.	Solutions.
1	Offset Cracking	When few parts in concrete are broken due to difference in heights offset crack occurs.	Resurfacing, crack sealing, reconstruction.
2	D-Cracking	Inability of concrete to sustain during freeze and thaw condition causes D-Cracking.	Drainage, surface sealing, epoxy resins.
3	Plastic Shrinkage	Occurs in a very small length but runs to the mid of concrete and spread in all parts.	Water curing, fogging, plastic sheets, joint placement.
4	Spalling	Moves along the rebar and have higher depression than cracks and scaling.	Expansion joints, protective coating, drainage.
5	Hairline Cracking	Occurs because of variation in temperature and is very thin and deep.	Sealants, crack injections, joint installation.
6	Map Cracking	Extends in 1200 angle from surface and is fine and shallow.	Chemicals, epoxy, sealants.
7	Scaling	The disclosure of outer aggregates occurs because of the loss of outer surface.	Sealants, chemicals, resins.
8	Pop-Outs	Because of low humidity aggregates with high pores absorbs water and these type of cracks occurs.	Non-reactive aggregates, control moisture, adequate curing.

3. Self-healing of concrete

Self-healing is a great way to fix cracks, with two types: passive and active methods [11, 12]. Passive cracks are visible on the concrete surface and are typically repaired by human intervention. They mainly address exterior cracks and sometimes interior cracks connected to the exterior. Passive treatments include coatings, sealers, and concrete chipping to repair cracks with chemicals or epoxy resins. These methods are often expensive and not environmental friendly. On the other hand, active treatment is a method of addressing cracks as soon as they appear. It can address both interior and exterior cracks. Active treatment options for crack repair include polymers, auxiliary cementing materials, and natural or bacterial self-healing methods. Chemical-based active treatments are not only costly but also harmful to the environment. Therefore, it is recommended to utilize biological self-healing techniques. Self-healing techniques do not require human intervention and involve the use of cementitious materials. These methods boost structural strength, lifespan, and prevent corrosion, minimizing crack occurrence and enhancing structural integrity. A strong healing material is essential for effective self-healing crack repair, capable of enduring concrete's mechanical stress [2]. The proposed strategies aim to overcome the limitations of other techniques.

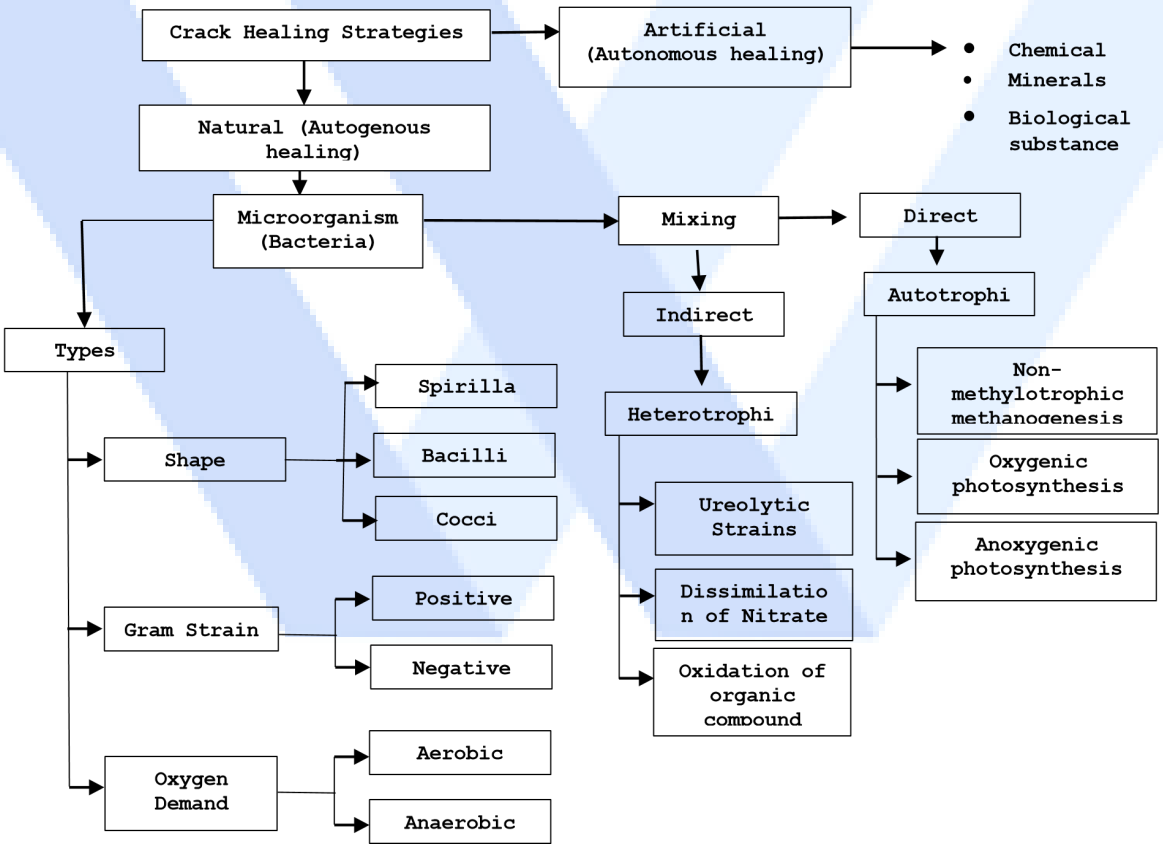

Figure 1. Crack healing strategies as depicted from [10, 11, 13,18]

Two strategies commonly used for self-healing in concrete are autonomous healing (artificial method) and autogenous healing (natural method). Autonomous healing repairs concrete cracks by adding external materials such as chemicals, minerals, or biological substances. Dispersion of these mixtures in different parts of the concrete leads to improve results. The healing agent activates only the necessary substances for healing, minimizing their usage. Limited quantities are used to prevent any impact on the mechanical properties of cement. For self-healing, bacterial growth in concrete requires prerequisites and chemicals, which can compromise its mechanical properties (25 g) [11]. Autogenous healing is a natural process in concrete where cracks can partially or completely close over time. The process of autogenous healing allows for the recovery of physical, mechanical properties, and initial durability in concrete. Autogenous healing involves crack carbonation, converting Ca(OH)2 into calcium carbonate to seal cracks, and unhydrated material hydration. This technique can repair cracks with widths ranging from 0.2 mm to 0.3 mm. Both strategies exhibit high efficiency in terms of the percentage of recovery achieved. The choice of mixing method (direct or indirect) depends on the bacteria's nature and their ability to precipitate calcium carbonate.

Table 2. Pathways for calcium carbonate precipitation, [19-23]

Pathways of calcium carbonate precipitation						
Types	Autotrophic			Heterotrophic		
Methodology	nonmethylo-trophic methano-genesis	Oxygenic Photosynthesis	anoxygenic photosynthesis	Ureolytic Strains (MICP pathway)	Dissimilation of Nitrate	Oxidation of organic compounds
Nutrients	Organic matter	Organic matter	Organic matter	Ammonia	Nitrogen & Carbonic acid	Organic matter
Ions formation	Nil	Nil	Nil	CO32-	3HCO3- & 2CO32-	5Ca (OH)2
pH level	6.5 - 8.5	7.0 - 9.0	6.5 - 8.5	7.0 - 9.5	7.0 - 8.5	6.5 - 8.5
Oxygen level	Zero	High	Zero	Moderate	Zero	Moderate
Chemical Compounds	Methanogens	Organic compounds	Depends on the type of bacteria used.	Urea	Formic Acid	Calcium Lactate
Examples	Methanobacterium specie.	Cynobacterium genus	Halobacterium and Heliobacterium species	Bacillus Sphaericus, Bacillus pasteurii, and Bacillus subtilis	Denitobacilus, Thiobacilus, Alcaligenes, Pseudomonas, Spirilium, Achromobacteri, and Micrococcus species	Bacillus pseudofirmus, Bacillus subtilis, Bacillus cohnii, Bacillus alkalinitrilicus, Bacillus thuringiensis, and Bacillus halodurans
Preferable	Less than other two	Preferred due to high pH.	Less as compare to oxygenic	Preferred due to high pH. and nutrients	Less as compare to urea	Less than other two

3.1. Bacteria and its mixing techniques in concrete

Incorporating microorganisms into cement-based materials poses a significant challenge in construction research and development. Introducing bacteria into concrete enables the unique self-healing method of calcite precipitation to occur. Bacteria are defined as single-celled organisms and are classified based on their characteristics, mainly into three categories (Figure 1). Through bio mineralization, bacteria can decompose calcium and urea, generating calcium carbonate and enabling concrete self-healing. Several studies have shown that cracks with widths up to 0.97mm can be repaired using bacterial self-healing techniques [11]. This chemical reaction occurs in the presence of catalysts, which can be either chemical or biological substances. The catalyst plays a crucial role in the formation of the crack filling material. Bacterial catalysts are essential in the active chemical reaction that forms calcium carbonate, acting as crack filling material. Historical research confirms calcium carbonate's efficacy for stone preservation and its positive influence on concrete. The selection of the bacterial catalyst is crucial in determining the amount of calcium carbonate formed.

Direct mixing is the easiest way, while indirect mixing is a slightly more complex method. In direct mixing, bacterial cells are directly added to the water. Bacteria strains capable of thriving in highly alkaline environments with limited nutrients are identified when added to cement [13].

Encapsulating bacterial concrete eliminates the need for water regulation, making it a more effective method for self-healing. Indirect mixing is a versatile technique for various purposes, including three general methods of immobilization: (1) pellets and flakes, (2) microencapsulation in gels, and (3) encapsulation in porous solids [14]. Encapsulating calcium lactate and yeast extracts in quantities less than 6% and 0.1% of aggregate mass aids self-healing [15, 16]. Bacteria are vital for calcium carbonate precipitation, necessary for crack repair in concrete when mixed under suitable conditions [17]. Bio mineralization is the phenomenon of converting organic matter into inorganic matter with the help of living organisms. This phenomenon aids the civil engineering department in addressing various construction issues, including crack repair through calcite precipitation. The precipitation of calcium carbonate results in the formation of three minerals: aragonite, vaterite, and calcite. However, research has shown that calcite is preferred by bacteria for self-healing due to its thermodynamic stability. For bacteria-induced CaCO3 precipitation in crack healing, two main types of methods, with various techniques, are employed. And MICP (Ureolytic strains) pathway is considered to be best for CaCO3 precipitation.

Table 3. Literature Review on most commonly used Bacillus specie of bacteria in concrete

Sr. No.	Bacteria	Mechanical Test	Monitorin g technique	Caco3 precipitati on technique	Aerobic / anaerobic	Nutrients	Result	Ref.
1	Bacillus pasteurii Bacillus sphaericus	Compressive and Flexural	SEM, EDAX, and DTA	Ureolytic Hydrolysis	Aerobic facultati ve anaerobic	Phosphate, Ammonia, Acetate	At optimum conditions were 0.25% of B. sphaericus or 0.50% of B. pasteurii with 0.125% of calcium lactate, showed flexural strength restoration up to 2.3 and 2.6 folds	[27]
2	Bacillus subtilis	Compressive strength and Water absobtion	XRD, FTIR, SEM, and EDX)	Urea Hydrolysis	Aerobic or facultati vely anaerobic.	Amino acids & 109 cells/mL	The bio (glutamine concrete with glutamate) (BC-9) of Bacillus subtilis shows a 25.9% increase in compressive strength	[21]
3	B.cohnii B.halodurans B. pseudofirmus	Non	ESEM	Urea Hydrolysis	Aerobic	KH, P0, /Na2HP04 buffer.PH 7-2.15 mMammonium sulphate, Sodium acetate	bacteria incorporated in high numbers (109 cm-3) do not affect concrete strength, that a substantial number of added bacteria remain viable	[28]
4	Bacillus. Cereus	water and chloride permeabilit y	SEM	Urea Hydrolysis	Obligate Aerobes	Glucose, Malate, Simple sugars, Dipotassiu m phosphate, Citric acid	The water absorption and chloride permeability of the specimens treated in this way were 12% and 10.9% lower than those of the reference specimens, respectively	[22]

5	Bacillus safensis Bacillus pumilus	Compressive test and UPV	SEM, XRD and analysis	Urea and TG Hydrolysis	Facultati vely anaerobic	Calcium yeast extract 86 %	47 % effectivenes s by UPV test	healing	[20] lactate and and strength recovery index endorse the viability of bacterial strains in alkaline cementitious environment

3.2. Suitable bacteria for concrete self-healing and its role in concrete strength improvement

Factors like scale-up, cost-effectiveness, and practicality need to be considered. To ensure the suitability of bacteria-based self-healing techniques for real-world applications. The suitability of bacteria depends on their nutritional requirements, food-making nature, and oxygen demand, impacting strength changes. Different bacteria can boost calcium carbonate precipitation. The focus is on selecting bacteria with positive impacts and minimal harm to humans. Many bacterial strains have been studied and employed for concrete self-healing. Bacillus specie (gram positive, rod shape, heterotrophic) excel with eco-friendliness, soil availability, rapid healing, urease production, and resistance, enhancing effectiveness [18]. Bacillus pasteurii is highly suitable among Bacillus specie, with a 30% calcium carbonate formation rate. Bacillus safensis is unsuitable, showing minimal calcium carbonate production. It has negligible impact on concrete strength based on multiple studies conducted over 28 days [24]. Various Bacillus subtypes are used for concrete self-healing, based on their nutritional needs and survival conditions (Table 3). They are ranked according to their percentage of calcium carbonate production and strength improvement.

Bacteria can enhance the strength of a structure by directly improving the concrete composition. Experimental results have shown that bacteria outperform other strategies for repairing micro cracks. Bacteria itself does not directly heal the cracks. Bacteria plays a crucial role in the chemical reaction that leads to the formation of calcium carbonate. And cracks are filled by calcium carbonate. The strength of the concrete depends on the bacteria because the precipitation of $CaCO3$ relies on bacterial activity. The crack filling is determined by the bacteria concentration (CFU) and affects the percentage of concrete strength improvement. Suitability is assessed by considering the duration of healing after activating the healing agent [25, 26]. Literature highlights that concrete cracks can be filled, enhancing strength, through $CaCO3$ precipitation facilitated by diverse bacterial species. Optimal improvement occurs when specific bacterial species are present in the right concentration and meet their nutritional needs. Monitoring the behavior of concrete and the response of bacteria are two key aspects to consider. Both will be monitored according to their properties to achieve the desired results. This study analyzes literature (Table 3) on bacteria-mixed concrete experiments, emphasizing bacteria type, strength tests, and monitoring techniques. The results obtained from mixing bacteria in concrete under various conditions [12]. Suitability and strength improvement depend on selecting bacteria with appropriate requirements and considering their environmental effects. Bacillus species are favorable for high calcite precipitation percentage via the MICP (Ureolytic strains) pathway. Most common techniques for monitoring results include SEM, EDAX, and DTA.

4. Adaptability of bio concrete in developing countries

Bio concrete is the fastest healing technique. While holding potential benefits for developed and underdeveloped nations, widespread usage of bacteria-mixed concrete remains experimental and unobserved [29]. Bio-concrete has the advantage of reactivating bacteria automatically when cracks appear, eliminating the need for human intervention. Moreover, it generates less waste during the repair process and requires skilled labor. It can also cause damage to human life if not handled carefully. Developing countries face limitations in adopting bio-concrete. Due to factors like high cost, limited resources, and specialized skills for handling living organism. Although environmental friendly, bacteria are used in bio-concrete. They can pose health risks if mishandled, due to their potential of causing diseases [30, 31]. Producing bio-concrete in developing countries can be hindered by skill requirements, limited bacteria availability, and higher costs relative to traditional concrete. Therefore, bio-concrete is not widely adopted in developing countries.

Research, experiments, skill development, resource availability, and adequate equipment are vital for potential adoption of bio-concrete in developing countries. Bio-concrete has been implemented on a limited scale in various research and experimental projects. While it has shown promising results, widespread implementation on a large scale is still in the early stages and not yet in common practice. It has been assumed that living in bio-concrete may not be safe from a physiological perspective. If bacteria are manually mixed with the concrete, despite its environmental benefits [32]. This ancient technique has gained recent popularity in collaboration with civil engineering to preserve concrete and prevent cracks. Insufficient laborers' awareness about handling living organisms hampers the wide adoption of bio-concrete in the industrial sector. Suitable bacteria are available freely, but manual mixing poses health hazards due to the lack of awareness. Raising awareness, conducting research, and skill development can enhance adaptability, if cost is not a major concern. However, cost remains a significant obstacle until research is completed, requiring sufficient funding for conducting research. Once the research is being completed cost will not remain an issue. Keeping in view the cost of repairing cracks with other technique, the implementation cost of bio-concrete is avoidable. Bio-concrete's global potential for self-healing is limited to research in developed countries; challenges in cost, resources, skills, and health risks must be addressed for adoption in developing nations.

Table 4. Merits and Demerits of Bio concrete [33]

Merits of Bio concrete.	Demerits of Bio concrete.
Compressive strength and stiffness increases to a significant level.	Cost is 7-28% higher than normal concrete but it can reduce the repairing cost in future.
Towards freeze and thaw reactions a good resistance in provided by chemical reactions of bacteria.	Bacteria can cause damage to human health so it should not be used near human life.
Amount of carbonation is directly proportional to the decrease in permeability and porosity	No standards have been made yet for bacterial concrete and suitability changes according to type of bacteria and its applications.

5. Conclusions

This review paper explores the potential of bacteria for CaCO3 precipitation in concrete. By focusing on articles published in highly reputable journals in last one decade. The current effort is to compose all published information related to bacterial specie used in self-healing of concrete cracks. Following conclusions are drawn from the conducted study:

- Concrete is the backbone of construction, but the major challenge lies in the minimization of cracks. Cracks are fractures that result from various causes and take different forms, making them inevitable. Numerous techniques, including self-healing methods, have been developed to address these cracks, achieving some success. However, these techniques often have detrimental environmental impacts and require significant financial investment. On the other hand, the utilization of bacteria as a crack repair technique offers a superior solution compared to other methods.
- Self-healing of concrete is an environment friendly technique. This technique automatically repairs the cracks without human intervention. This self-healing process can occur actively or passively. Active healing by bacteria is considered superior to others. It allows the precipitation of calcium carbonate following different pathways, which seals the cracks.
    - Bacteria is considered to be environment friendly unicellular organism. The most environmental friendly bacteria from Bacillus specie (i.e. B. Pasteurii) is suggested to be suitable for calcite precipitation if mixed with concrete indirectly via encapsulation. This bacteria can achieve maximum percentage of crack repairing by bio mineralization process following MICP pathway for CaCO3 precipitation.
    - Bacteria can improve concrete strength up to a high number. To evaluate the results, numerous tests and monitoring techniques are available with respect to area of interest. SEM, EDAX, and DTA techniques are commonly used techniques to evaluate the results of bio concrete self-healing.
- Bio-concrete has global potential for fast healing. But its widespread use is currently limited to research in developed countries. To expand adoption in developing nations, challenges like cost, resources, skills, and health risks need to be addressed through research and skill development.

The above outcome is favorable indicating the exploration of its in-depth behavior at large scale. Complete investigation and experimental research can make implementation of bio concrete successful in real-life structures. The issue of cost (a major hurdle in the application of bio concrete) can be overcome, once the experimental research will be completed.

Declaration of Conflict of Interests

The authors would like to thank every person/department who helped throughout the research work.

References

[1.] M. K. Akhtar, M. Kanwal, R. A. Khushnood, and M. B. E. Khan, Assessment of mechanical attributes and microstructural densification of self-healing recycled coarse aggregate concrete using various bacterial immobilizers. Journal of Building Engineering. 69 (2023) 106229.

[2.] G. F. Huseien, M. L. Nehdi, I. Faridmehr, S. K. Ghoshal, H. K. Hamzah, O. Benjeddou, and F. Alrshoudi, Smart Bio-Agents-Activated Sustainable Self-Healing Cementitious Materials: An All-Inclusive Overview on Progress, Benefits and Challenges. Sustainability. 14 (2022).

[3.] M. Wu, B. Johannesson, and M. Geiker, A review: Self-healing in cementitious materials and engineered cementitious composite as a self-healing material. Construction and Building Materials. 28 (2012) 571-583.

[4.] J. Y. Wang, H. Soens, W. Verstraete, and N. De Belie, Self-healing concrete by use of microencapsulated bacterial spores. Cement and Concrete Research. 56 (2014) 139-152.

[5.] J. Qiu, D. Q. S. Tng, and E.-H. Yang, Surface treatment of recycled concrete aggregates through microbial carbonate precipitation. Construction and Building Materials. 57 (2014) 144-150.

[6.] M. Nodehi, T. Ozbakkaloglu, and A. Gholampour, a systematic review of bacteria-based self-healing concrete: Biomineralization, mechanical, and durability properties. Journal of Building Engineering. 49 (2022) 104038.

[7.] N. De Belie, E. Gruyaert, A. Al Tabbaa, P. Antonaci, C. Baera, D. Bajare, A. Darquennes, R. Davies, L. Ferrara, and T. Jefferson, A review of self-healing concrete for damage management of structures. Advanced Materials Interfaces. 5 (2018) 1800074.

[8.] B. A. C. Roque, P. P. F. Brasileiro, Y. B. Brandão, A. A. Casazza, A. Converti, M. Benachour, and L. A. Sarubbo, Self-Healing Concrete: Concepts, Energy Saving and Sustainability. Energies. 16 (2023) 1650.

[9.] G. L. Golewski, The Phenomenon of Cracking in Cement Concretes and Reinforced Concrete Structures: The Mechanism of Cracks Formation, Causes of Their Initiation, Types and Places of Occurrence, and Methods of Detection—A Review. Buildings. 13 (2023) 765.

[10.] O. Šovljanski, A. Tomić, and S. Markov, Relationship between Bacterial Contribution and SelfHealing Effect of Cement-Based Materials. Microorganisms. 10 (2022) 7.

[11.] W. Khaliq, and M. B. Ehsan, Crack healing in concrete using various bio influenced selfhealing techniques. Construction and Building Materials. 102 (2016) 349-357.

[12.] W. Du, C. Qian, and Y. Xie, Demonstration application of microbial self-healing concrete in sidewall of underground engineering: A case study. Journal of Building Engineering. 63 (2023) 105512. [13] M. M. Meraz, N. J. Mim, M. T. Mehedi, B. Bhattacharya, M. R. Aftab, M. M. Billah, and M. M. Meraz, Self-healing concrete: Fabrication, advancement, and effectiveness for long-term integrity of concrete infrastructures. Alexandria Engineering Journal. 73 (2023) 665-694.

[13.] J. Y. Wang, D. Snoeck, S. Van Vlierberghe, W. Verstraete, and N. De Belie, Application of hydrogel encapsulated carbonate precipitating bacteria for approaching a realistic self-healing in concret. Construction and Building Materials. 68 (2014) 110-119.

[14.] X. Xiao, C. Unluer, S. Chu, and E.-H. Yang, Single bacteria spore encapsulation through layer-by-layer self-assembly of poly (dimethyldiallyl ammonium chloride) and silica nanoparticles for self-healing concrete. Cement and Concrete Composites. 140 (2023) 105.

[15.] J. Wang, A. Mignon, D. Snoeck, V. Wiktor, S. Van Vliergerghe, N. Boon, and N. De Belie, Application of modified-alginate encapsulated carbonate producing bacteria in concrete: a promising strategy for crack self-healing. Frontiers in Microbiology. 6 (2015).

[16.] O. A.-O. Šovljanski, A. A.-O. X. Tomić, and S. Markov, Relationship between Bacterial Contribution and Self-Healing Effect of Cement-Based Materials. Microorganisms. (2023) 2076-2607.

[17.] S. Mondal, and A. Ghosh, Biomineralization, bacterial selection and properties of microbial concrete: A review. Journal of Building Engineering. 73 (2023) 106695.

[18.] R. Garg, R. Garg, and N. O. Eddy, Microbial induced calcite precipitation for self-healing of concrete: a review. Journal of Sustainable Cement-Based Materials. 12 (2023) 317-330.

[19.] N. Shaheen, R. A. Khushnood, S. A. Memon, and F. Adnan, Feasibility assessment of newly isolated calcifying bacterial strains in self-healing concrete. Construction and Building Materials, vol. 362, pp. 129662, 2023.

[20.] F. Mahmood, S. Kashif Ur Rehman, M. Jameel, N. Riaz, M. F. Javed, A. Salmi, and Y. A. Awad, Self-Healing Bio-Concrete Using Bacillus subtilis Encapsulated in Iron Oxide Nanoparticles. Materials. vol. 15 (2022) 7731.

[21.] M. Wu, X. Hu, Q. Zhang, D. Xue, and Y. Zhao, Growth environment optimization for inducing bacterial mineralization and its application in concrete healing. Construction and Building Materials. 209 (2019) 631-643.

[22.] H. A. Algaifi, S. A. Bakar, A. R. M. Sam, A. R. Z. Abidin, S. Shahir, and W. A. H. AL-Towayti, Numerical modeling for crack self-healing concrete by microbial calcium carbonate. Construction and Building Materials. 189 (2018) 816-824.

[23.] M. Bagga, C. Hamley-Bennett, A. Alex, B. L. Freeman, I. Justo-Reinoso, I. C. Mihai, S. Gebhard, K. Paine, A. D. Jefferson, and E. Masoero, Advancements in bacteria based self-healing concrete and the promise of modelling. Construction and Building Materials. 358 (2022) 129412.

[24.] K. W. Shah, and G. F. Huseien, Bond strength performance of ceramic, fly ash and GBFS ternary wastes combined alkali-activated mortars exposed to aggressive environment. Construction and Building Materials. 251 (2020) 119088.

[25.] T. C. S. Reddy, and A. Ravitheja, Macro mechanical properties of self-healing concrete with crystalline admixture under different environments. Ain Shams Engineering Journal, vol. 10, no. 1, pp. 23-32, 2019.

[26.] A. A. Nasser, N. M. Sorour, M. A. Saafan, and R. N. Abbas, Microbially-Induced-CalcitePrecipitation (MICP): A biotechnological approach to enhance the durability of concrete using Bacillus pasteurii and Bacillus sphaericus. Heliyon. 8 (2022) e09879.

[27.] O. Šovljanski, A. Tomić, and S. Markov, Relationship between Bacterial Contribution and SelfHealing Effect of Cement-Based Materials. Microorganisms. 10 (2022).

[28.] A. Raza, M. H. El Ouni, Q. u. Z. Khan, M. Azab, D. Khan, K. M. Elhadi, and Y. Alashker, Sustainability assessment, structural performance and challenges of self-healing bio-mineralized concrete: A systematic review for built environment applications. Journal of Building Engineering. 66 (2023) 105839.

[29.] G. F. Huseien, A. R. M. Sam, H. A. Algaifi, and R. Alyousef, Development of a sustainable concrete incorporated with effective microorganism and fly Ash: Characteristics and modeling studies. Construction and Building Materials. 285 (2021) 122899.

[30.] Y. Guo, X. Wang, Z. Yan, and H. Zhong, Current progress on biological self-healing concrete. Materials Research Innovations. 19 (2015) 750-753.

[31.] V. Wiktor, and H. Jonkers, Bacteria-based concrete: From concept to market. Smart Materials and Structures. 25 (2016) 084006.

[32.] E. Tziviloglou, V. Wiktor, H. Jonkers, and E. Schlangen, Bacteria-based self-healing concrete to increase liquid tightness of cracks. Construction and Building Materials. 122 (2016) 118-125.

PACE-2023

International Congress on the Phenomenological Aspects of Civil Engineering

PACE-2023

International Congress on Phenomenological Aspects in Civil Engineering

Research Article

20-23 June 2023

Circular Economy Practices in Construction Industry – A Critical Review

Muhammad Usman Shahid*,[1], Majid Ali[1]

[1]*Capital University of Science and Technology, Islamabad, Pakistan*

Corresponding Author E-mail: usman.shahid987@gmail.com

Keywords

Circular economy (CE),
Construction waste,
Barriers of CE,
Enablers of CE.

Abstract

There is a growing need for construction projects to upgrade and create new infrastructures, not only in developing but also in developed countries. During this development process, substantial amount of natural resources is being used. But such developments do not come cheap. During this process, significant amount of material waste is produced. Therefore, circular economy culture is inevitable to avoid the depletion of natural resources. But the culture of circular economy is yet to develop in construction industry. In order to dig out the barriers in circular economy and its enablers, a comprehensive literature review was conducted. After going through a filtering process, around fifty (50) different research papers are consulted. Major barriers identified through literature include non-availability of environmental bylaws, governmental preferences, lack of recycling materials market and worker's behaviour in waste control. Further, major strategies to promote circular economy are development of business models for wasted materials, formulation of bylaws to implement waste control strategies on construction sites, financial support from governments in the form of subsidize. In the end, usage of latest tools such as building information modelling, radio frequency identification and global positioning system for different waste control processes are described.

1. Introduction

The construction sector is well renowned for its ability to boost a nation's economy. It contributes 5–15% on average to a nation's GDP [1, 2]. However, such an output is not that much cheap, because construction sector is one of the biggest resource consumers. According to[3], around 40% of the materials in construction sector is being utilized by buildings. Construction industry is considered as one of the most waste generation sector [4]. As a result, the construction sector has a detrimental influence on the environment [5]. Construction related waste accounts for a startling 40% of all waste produced globally, closely followed by domestic waste (36.73%) and market and commercial waste (21.54%)[6]. So, all this waste generation is due to the practices of philosophy of using materials in linear way. It means materials are produced, transported, used and then thrown away to the construction sites or illegal dumping sites. Therefore, circular economy is an effective way to deal with such problems. In circular economy, construction materials are produced, used and then again recycled to use them again. This way, efficiency and utilization of materials is maximized. But such practices are not being followed by construction industry stakeholder due to

number of reasons. Major barriers due to which circular economy is not being practices up to the required level are non-availability of rules, regulations, non-availability of market for recycled materials, lack of support from governments, lack of funding, non-availability of technical expertise, etc. [7], [8]. So, there is severe need to tackle these barriers to introduce the true concept of circular economy in any construction industry. In this regard, strategies are being formulated and reported in number of studies. These strategies include development of environmental bylaws, support from governments in terms of subsidize, building market for recycled materials, etc. Further, usage of latest tools and techniques such as building information modelling (BIM) at design and construction phases of a project, usage of radio frequency identification (RFID)for materials and human resource tracking and global positioning system (GPS) for landfill sites location have also been an effective tools to promote circular economy practices.

In this regard, a formal retrieval procedure for research papers was employed to conduct an extensive assessment of the literature on the situation of circular economy practices. For this, papers from 2009 to 2022 are consulted. Major journal, from where papers were retrieved include “Journal of Cleaner Production”, “Waste Management”, “Waste Management and Research”, “Automation in Construction”, “Resources, Conservation and Recycling”, and “Building and Environment” ranking as the most significant journals in the field of construction management. Initially, more than 100 papers were found by searching for keywords in the title and abstract; however, some of these papers were related to other wastes such as food waste, medical wastes, etc. Thus a filtering procedure was used. About fifty (50) papers that were directly related to the barriers of CE, enablers of CE and usage of latest tools for waste control. The following sections present the study's findings.

2. Circular Economy Principles

The concept of circular economy is very much wider when it is discussed in different construction industries. It is not being adopted by only construction industry but almost every industry including food, manufacturing, pharmaceuticals, etc., are following this method to control waste, pollution and save resources [9-11]. So, basic principles of CE vary across the industries as well as within the same industry. In Table 1, different principles for CE are given which had been reported in different research studies. These principles vary from 3R to 10R. If these principles are analyzed, it will be very clear that the basic principle of CE is the 3R, while all other from 4R to 10R are just the detailed bifurcation or subdivision of these processes which are given in 3R’s. [12] reported the meaning of each of these processes in details as shown in Figure 1.

Table 1. Circular economy principles

Sr. No	Core Principle	Details	Reference
01.	3 R’s	Reduce, reuse and recycle.	[13]
02.	4 R’s	Reduce, reuse, recycle and recover.	[12]
03.	5 R’s	Refuse, reduce, reuse, repurpose and recycle	[14]
04.	7 R’s	Redesign, reduce, reuse, repair, renovate, recycle and recover	[13]
05.	10 R’s	Refuse, rethink, reduce, reuse, repair, refurbish, remanufacturer, repurpose, recycle and recover	[12]

So, it can be concluded over here, that the processes of controlling materials or resources can be outlined in details through 10R principle (refuse, rethink, reduce, reuse, repair, refurbish, remanufacturer, repurpose, recycle and recover) but the basic principle which generally cover all these processes is based on 3R (reduce, reuse and recycle).

R0 Refuse	Make product redundant by abandoning its function or by offering the same function with a radically different product
R1 Rethink	Make product use more intensive (e.g. by sharing product)
R2 Reduce	Increase efficiency in product manufacture or use by consuming fewer natural resources and materials
R3 Reuse	Reuse by another consumer of discarded product which is still in good condition and fulfils its original function
R4 Repair	Repair and maintenance of defective product so it can be used with its original function
R5 Refurbish	Restore an old product and bring it up to date
R6 Remanufacture	Use parts of discarded product in a new product with the same function
R7 Repurpose	Use discarded product or its parts in a new product with a different function
R8 Recycle	Process materials to obtain the same (high grade) or lower (low grade) quality
R9 Recover	Incineration of material with energy recovery

Figure 1. 10R Principle of CE

3. Barriers in Circular Economy

Circular economy faces number of barriers which hinders its implementation on construction sites. Most of these barriers are related to national policies and governmental preferences as shown in Table 2. So, lack of support from governments in financial terms like giving subsidize to those contractors, who are using recycled materials on construction sites and giving preference to these contractors during bidding procedure. Then comes the non-availability of environmental laws and regulations which bound the contractors to reuse and recycle materials rather than dumping them at illegal dumping sites. At industrial level, lack of operational weaknesses, non-availability of recycling plants, high upfront cost in implementing CE strategies, lack of availability of skilled labour and technical experts and poor awareness and education in terms of CE are the major reasons for poor CE implementations in construction industry [7]. With respect to investors' perspective, high upfront costs of establishing recycling plant and non-availability of recycled materials market are the major reasons which discourage the businesses of reused and recycled materials.

Table 2. Barriers in CE Practices

Sr. No.	Barriers Name	Details of Barrier	References
1	Financial issues	Lack of funding from governments, Insufficient financial support from client	[15], [7, 16-20]
2	Operational weaknesses	Lack of tracking of dumping sites, deficiency of dumping machines	[7, 16-18], [20]
3	Inappropriate regulations	Non-availability of environmental regulations, Absence of waste management policies	[16, 17]
4	Lack of awareness	Lack of training and education	[15], [20], [21]
5	Lack of standards	Absence of waste management policies	[16-18], [21]
6	Lack of collaboration	Poor communication among different departments	[17], [22]
7	Low virgin materials	Virgin material availability is limited	[17, 18], [21]
8	Costly recycled material	Recycled materials are more costly than virgin materials due to operational cost	[18], [23]

9	Lack of education and training	Training and education is limited	[19, 20, 23], [24]
10	High upfront cost	Capital cost of investment for recycled materials is very high	[18]
11	Lack of support from Governments	No subsidize from governments for following waste management policies	[7], [8]
12	Lack of environmental standards	Few environmental regulations for waste control	[7], [23], [25]
13	Health and Safety issues	Non-inert materials such as concrete can be harmful for environment through leaching	[24]
14	Lack of consumer interest in the environment	User motivation to reduce waste of materials	[7]
15	Lack of qualified professional's in environmental management	Low qualification of employees working in environmental departments	[7]
16	Lack of legal enforcement	Less implementation of bylaws	[15]
17	Operating in linear economy	Use and throw away policy	[17]
18	Lack of economically-viable facilities for waste management	Costly arrangements for waste management techniques	[15]
19	Low cost for waste disposal	Fines for waste dumping are very low	[20]
20	Cultural Issues	Industry preference Issues	[26]

Therefore, it is synthesized that barriers of CE exist at all levels. But initiatives from governmental and industrial level would have more substantial impacts to implement CE culture in construction industry. The reason is most of these barriers would require usage of resources and capital investment, so governmental and industrial stakeholders seriousness is important to remove these barriers from the top.

4. Enablers of Circular Economy

CE which is based on the 3 R's principle (reduce, reuse and recycle) follows the process as shown in Figure 1. It can be observed that material is manufactured then it goes to the supplier, where it is sold out to the consumers. Consumers used these materials and wasted materials go to the recycling plants where they're recycled. These recycled materials are again sent back to the market for selling. This way, material follows the circular loop, that's why, it is named as circular economy strategy. So the strategies which promotes the adaptation of CE in construction industry are shown in Table 3. These strategies mainly deal the barriers which were found in different studies worldwide. First of all, business models should be such that it has some profit margin for suppliers of recycled materials. Bylaws, legislation, policies and standard operating procedures should be formulated by governments [27],[16].

Table 3. Strategies for CE

Sr. No	Strategy	Details	References
01	Business Model	Business models to support the recycled materials	[28, 29]
02	Governmental Support	Facilitating policies	[30]
03	SOPs	Standard Operating Procedures for waste management	[27], [16]
04	Incentives for recycled materials	To make them cheap	[31]
05	Green behavior	Through incentive reward programs (IRP)	[32, 33]
06	Education and training	For awareness of benefits	[34, 35]
07	Public Private Partnership Programs	For financial support of governmental projects	[36]

08	Environmental Management System	To save depletion of resources	[37]
9	An advanced research and developments	For more details and smooth running	[38]
10	Legislation and policies	Define rules and regulations for CE practices	[39]
11.	Education on sustainable development	To promote environmental friendly practices and saving of natural reserves	[23]
12.	Financial support for circular economy research	Research projects should be funded	[23]
13.	Provide subsidize on CE projects	Subsidize the projects with financial benefits who are following CE methods	[23]
14.	Policies for recycled materials	Recycled materials market should be established	[40]
15.	Designated public and landfilling areas	For inert and non-inert material separation	[40]

Further, at industrial level, skilled labour should be developed by proper training and education of the workers. It is observed that incentive reward program has substantial impact on changing the behavior of the workers [41]. Moreover, designated landfill and public filling sites can improve the process by facilitating to bifurcate the inert and non-inert materials. So these strategies could have significant impact on waste reduction and preservation of natural reserves of these materials. Ultimately, less waste means the less project cost.

4.1. Tools and Techniques for Circular Economy

The number of advanced tools which have been used and reported in different studies for waste control of materials are as follows:

4.1.1. Use of Building Information Modelling (BIM) in Circular Economy

Latest studies are focusing on management of these wastes with the help of advance technologies. In this regard, BIM has been proved a potential tool to design out waste at planning stage as well as during execution phase. BIM can reduce waste during planning and design stage by accurate estimation, better collaboration, feasibility analysis, using multiple possible design options, modular design, removing any clashes at early stage of project [42]. Further, it could reduce construction waste by 15% by using its characteristics of clash detection, identification of discrepancies and errors and omissions [43]. Moreover, BIM was used for planning of tiles by developing algorithm to design out waste through proper selection of cutting. Waste reduced almost from 5 to 15 % [44]. So importance of using BIM in controlling construction waste cannot emphasized enough. So, this 15% reduction in waste of different materials will improve the efficiency of these materials and reduce the burden on natural resources. Therefore, BIM can have large impacts to control material waste during design and execution phases of project. At the same time, it can have significant impact on cost reduction of a project.

4.1.2. Use of Radio Frequency Identification (RFID) for Circular Economy

RFID is a good data resource since it can record data accurately and deliver real-time information. At the exits and entrances of building sites, RFID readers or writers can be deployed. On objects like transport vehicles or other objects, RFID tags can be implanted. The RFID tags can store data such as the date and time of garbage disposal, the type of waste, the volume of waste being transported, and the location. Reading and writing happen automatically and without any lag time. As a result, there are fewer human errors and there is high efficiency. [45]reported that a system that employs RFID to record research data, including position, volume, weight, and inventory tracking as well as data on cargo container movement. The collected data can be entered into a management program to help decision-makers with analysis, planning, and tracking. The use of this system in a case study demonstrates the effectiveness of RFID technology in obtaining timely and accurate information, which is the foundation of this system. So, RFID technology can be used at execution as well as post construction phases of project to track and record keeping of materials and wastes.

4.1.3. Use of GPS-GIS for Circular Economy

GIS offers significant advantages for data collection, archival, correlation, processing, and analysis. GIS is a tool for environmental impact assessments in addition to its purpose for estimating the generated demolition waste. It is used to create a bottom-up material stock model that integrates with Life Cycle Assessment (LCA) to evaluate the environmental impact at the urban scale and integrates with GPS technology to provide real-time location information for the material and its arrival time at the construction site [46]. Recently, [47] used GIS to pinpoint the locations where C&D waste was illegally disposed. Further, [48] integrated GPS and GIS technology with M&E management system. Although there is little information now available on GPS applications in C&D waste management, the location system is crucial to the practice of C&D waste management. For instance, GPS can be integrated into the vehicles used for C&D waste transportation to allow for real-time monitoring. Therefore, Inclusion of latest tools during project design, construction and post construction phases can provide good results in waste control.

So, substantial amount of materials can be saved by following circular economic strategies along with latest tools and techniques at all levels of a project.

5. Conclusions

In order to move from linear economy practices to the circular economy, a review was required to highlight the major barriers and their solutions globally. For this a comprehensive literature review was conducted, where more than fifty (50) relevant papers were consulted. Major findings of this study are:

- Basic principle of circular economy includes 3R principle (reduce, reuse and recycle) while all other principles from 4R to 10R defines processes in more details but do not go out of the scope of 3R principle.
- Major barriers in circular economy are non-availability of rules and regulations, governmental preferences, non-availability of recycling materials market and worker's behaviour in waste control.

- Significant strategies for CE include the governmental support for developing business models and market of used materials, change of selection criteria for contractors during bidding, incentives reward programs to change the behaviour of the workers and designation of landfill and public filling areas.

- In terms of latest tools, BIM can be an effective tool for waste control at design and construction phases of a project, RFID can have potential impacts in material saving during construction and post construction phases and GPS-GIS can produce significant results in waste disposal and location of landfill and public filling sites.

Considering the above discussion, formulation of policy frameworks by removing the barriers of construction industry can produce significant results in waste control and preserving the natural resources.

Declaration of Conflict of Interests

The authors declare that there is no conflict of interest. They have no known competing financial interests or personal relationships that could have appeared to influence the work reported in this paper.

References

[1.] DTIE, U., Buildings and Climate Change: A Summary for decision makers: Paris, France. 2009.

[2.] Areias, I., et al., Could city sewage sludge be directly used into clay bricks for building construction? A comprehensive case study from Brazil. 2020. 31: p. 101374.

[3.] Norouzi, M., et al., Circular economy in the building and construction sector: A scientific evolution analysis. 2021. 44: p. 102704.

[4.] Kamali, M., et al., Conventional versus modular construction methods: A comparative cradle-to-gate LCA for residential buildings. 2019. 204: p. 109479.

[5.] Wu, G., et al., Role stress, job burnout, and job performance in construction project managers: the moderating role of career calling. 2019. 16(13): p. 2394.

[6.] Amaral, R.E., et al., Waste management and operational energy for sustainable buildings: a review. 2020. 12(13): p. 5337.

[7.] Ormazabal, M., et al., Circular economy in Spanish SMEs: challenges and opportunities. 2018. 185: p. 157-167.

[8.] Mura, M., M. Longo, and S.J.J.o.C.P. Zanni, Circular economy in Italian SMEs: A multi-method study. 2020. 245: p. 118821.

[9.] Adabre, M.A., et al., Facilitating a transition to a circular economy in construction projects: intermediate theoretical models based on the theory of planned behaviour. 2023. 51(1): p. 85-104.

[10.] Suhandi, V. and P.-S.J.J.o.C.P. Chen, Closed-loop supply chain inventory model in the pharmaceutical industry toward a circular economy. 2023. 383: p. 135474.

[11.] Zhang, Q., et al., Circular economy and the food sector: A systematic literature review. 2022.

[12.] Kirchherr, J., et al., Conceptualizing the circular economy: An analysis of 114 definitions. 2017. 127: p. 221-232.

[13.] Austin, A. and I.U.J.J.o.C.P. Rahman, A triple helix of market failures: Financing the 3Rs of the circular economy in European SMEs. 2022. 361: p. 132284.

[14.] Balwan, W.K., et al., 5R's of zero waste management to save our green planet: A narrative review. 2022. 10(1): p. 7-11.

[15.] Negash, Y.T., et al., Sustainable construction and demolition waste management in Somaliland: Regulatory barriers lead to technical and environmental barriers. 2021. 297: p. 126717.

[16.] Bui, T.D., et al., Identifying sustainable solid waste management barriers in practice using the fuzzy Delphi method. 2020. 154: p. 104625.

[17.] Hart, J., et al., Barriers and drivers in a circular economy: The case of the built environment. 2019. 80: p. 619-624.

[18.] Huang, B., et al., Construction and demolition waste management in China through the 3R principle. 2018. 129: p. 36-44.

[19.] Torgautov, B., et al., Circular economy: Challenges and opportunities in the construction sector of Kazakhstan. 2021. 11(11): p. 501.

[20.] Yuan, H., L. Shen, and J.J.F. Wang, Major obstacles to improving the performance of waste management in China's construction industry. 2011.

[21.] Menegaki, M., D.J.C.O.i.G. Damigos, and S. Chemistry, A review on current situation and challenges of construction and demolition waste management. 2018. 13: p. 8-15.

[22.] Salmenperä, H., et al., Critical factors for enhancing the circular economy in waste management. 2021. 280: p. 124339.

[23.] Bilal, M., et al., Current state and barriers to the circular economy in the building sector: Towards a mitigation framework. 2020. 276: p. 123250.

[24.] Low, J.K., et al., Encouraging circular waste economies for the New Zealand construction industry: Opportunities and barriers. 2020. 2: p. 35.

[25.] Yuan, H.J.J.o.C.P., Barriers and countermeasures for managing construction and demolition waste: A case of Shenzhen in China. 2017. 157: p. 84-93.

[26.] Pietzsch, N., J.L.D. Ribeiro, and J.F.J.W.M. de Medeiros, Benefits, challenges and critical factors of success for Zero Waste: A systematic literature review. 2017. 67: p. 324-353.

[27.] Blaisi, N.I.J.J.o.c.p., Construction and demolition waste management in Saudi Arabia: Current practice and roadmap for sustainable management. 2019. 221: p. 167-175.

[28.] Henry, M., et al., The battle of the buzzwords: A comparative review of the circular economy and the sharing economy concepts. 2021. 38: p. 1-21.

[29.] Jabłoński, A., et al., New economy business models in the concepts of big data, the sharing economy and the circular economy. 2020: p. 51-88.

[30.] Ferronato, N., et al., Introduction of the circular economy within developing regions: A comparative analysis of advantages and opportunities for waste valorization. 2019. 230: p. 366-378.

[31.] Hua, C., et al., Promoting construction and demolition waste recycling by using incentive policies in China. 2022. 29(35): p. 53844-53859.

[32.] Jain, S., et al., Construction and demolition waste recycling: Investigating the role of theory of planned behavior, institutional pressures and environmental consciousness. 2020. 263: p. 121405.

[33.] Long, H., et al., An evolutionary game theory study for construction and demolition waste recycling considering green development performance under the Chinese government's reward–penalty mechanism. 2020. 17(17): p. 6303.

[34.] Hartley, K., et al., Policies for transitioning towards a circular economy: Expectations from the European Union (EU). 2020. 155: p. 104634.

[35.] Torkayesh, A.E., B. Malmir, and M.R.J.W.M. Asadabadi, Sustainable waste disposal technology selection: The stratified best-worst multi-criteria decision-making method. 2021. 122: p. 100-112.

[36.] Dolla, T. and B.J.I.J.o.C.M. Laishram, Factors affecting public-private partnership preference in Indian municipal waste sector. 2020. 20(6): p. 567-584.

[37.] Ikram, M., et al., Do environmental management systems help improve corporate sustainable development? Evidence from manufacturing companies in Pakistan. 2019. 226: p. 628-641.

[38.] Umar, U.A., et al., A review on adoption of novel techniques in construction waste management and policy. 2017. 19: p. 1361-1373.

[39.] Khan, S. and A.J.I.J.o.S.E. Haleem, Investigation of circular economy practices in the context of emerging economies: a CoCoSo approach. 2021. 14(3): p. 357-367.

[40.] Hossain, M.U., et al., Circular economy and the construction industry: Existing trends, challenges and prospective framework for sustainable construction. 2020. 130: p. 109948.

[41.] Begum, R.A., et al., A benefit–cost analysis on the economic feasibility of construction waste minimisation: The case of Malaysia. 2006. 48(1): p. 86-98.

[42.] Mohammed, M., et al., Beneficial Effects of 3D BIM for Pre-Empting Waste during the Planning and Design Stage of Building and Waste Reduction Strategies. 2022. 14(6): p. 3410.

[43.] Zoghi, M. and S.J.S. Kim, Dynamic modeling for life cycle cost analysis of BIM-based construction waste management. 2020. 12(6): p. 2483.

[44.] Wu, S., et al., Intelligent optimal design of floor tiles: A goal-oriented approach based on BIM and parametric design platform. 2021. 299: p. 126754.

[45.] Li, C.Z., et al., Research trend of the application of information technologies in construction and demolition waste management. 2020. 263: p. 121458.

[46.] Ratnasabapathy, S., S. Perera, and A. Alashwal, A review of smart technology usage in construction and demolition waste management. 2019.

[47.] Paz, D.H.F.d., et al., GIS-based planning system for managing the flow of construction and demolition waste in Brazil. 2018. 36(6): p. 541-549.

[48.] Bansal, V.J.I.J.o.C.M., Application areas of GIS in construction projects and future research directions. 2012. 12(4): p. 17-36.

PACE-2023
International Congress on the Phenomenological Aspects of Civil Engineering

PACE-2023
International Congress on Phenomenological Aspects in Civil Engineering

Research Article 20-23June 2023

The Influence of Recycled Aggregates on The Physico-Mechanical Behavior of Concrete

Mounira Chadli[*,1], Messaouda Bensmail[2], Sara Rais[3], Mekki Mellas[4].
[1,4]*Laboratory of Civil Engineering, Department of Civil Engineering and Hydrology, University of Biskra, BP 145 RP, Biskra 07000, Algeria*
[2]*Laoratory of Civil Engineering at the University of Djelfa, POBox 3117, 17000 Djelfa - Algeria*
[3]*Research Laboratory in Civil Engineering, Hydraulics, Sustainable Development and Environment LARGHYDE, University of Biskra, 07000 Biskra, Algeria*
Corresponding Author E-mail: Mounira.chadli@univ-biskra.dz

Keywords

Recycled aggregate,
Concrete,
Property,
Strength,
Waste.

Abstract

The use of recycled aggregates in concrete reduces the environmental impact of the construction industry by reducing CO_2 emissions and ensuring rational use of natural resources. Several searches were led in many countries to develop the use of demolition waste as components of new concrete. In this context, an experimental program will be undertaken to contribute to the recovery of demolition waste in concrete. In the concrete mixes the ratios of concrete aggregate range from 0% to 100% with the increment of 25%. The specimens were tested for compression strength and splitting tensile strength. This research shows that increasing recycle concrete aggregate will decrease the compressive strength and bending tensile strength. The comparative study between different recycled concrete compositions showed acceptable physical and mechanical properties vis-à-vis the strength. Recycled aggregates can be a substitute material for natural aggregates.

1. Introduction

Concrete is a material characterized by a strong heterogeneity. It is often broken down into two constituents: cement paste and aggregates, knowing that cement paste can also include adjuvants or additions. From a physical point of view, concrete has different phases, in particular a solid phase comprising aggregates and cement paste, a liquid phase characterized by the presence of free and adsorbed water and finally a gaseous phase consisting of air and of water vapour.

Particular attention must be paid to the different constituents of concrete. Cement paste is usually the subject of most research. However, aggregates occupy a large part of the volume of concrete, and represent about 60-75% of its total volume [1]. The properties of a concrete are strongly linked to the aggregates [2]: these can limit the strength of the concrete, in particular the durability and the structural performance of the concrete.

The amount of waste from the construction industry used as filler or dumped illegally in the environment has increased over time. This has led to a growing shortage of landfill areas, along with increased costs in landfills. Therefore, waste handling has become one of the most important environmental issues in developed countries [3-4].

Sand and gravel can come from concrete waste and replace the original materials natural. Currently the construction sector consumes a large quantity of materials, such as which natural rocks, gravels and sands. However, these resources are not unlimited and can create critical situations locally [5].

In Algeria, over the last few years, the demand for aggregates has increased more and more to meet the needs of the major projects implemented. The ban on the extraction of alluvial materials, the depletion of certain natural deposits of aggregates and the difficulties of setting up new quarry operations make it necessary to seek new sources of supply of aggregates. However, the irregularity of the intrinsic characteristics, the weak physico-mechanical properties of recycled aggregates and the absence of standards in force hinder their popularization as basic materials in the formulation of concretes.

In addition, the depletion of available natural sources of aggregates, the strictest environmental protection laws in the world and the problems posed by the destruction of waste are all factors which favor the recycling of construction waste. According to bibliographical research, the recovery of demolition waste has passed the experimental stage throughout the world and is undergoing fairly significant development. In addition, the rate of recycling of construction and demolition debris has reached 80% in some countries (Japan, China, Europe...etc.).

The reuse of construction and demolition waste as aggregates in the manufacture of concrete has been the subject of work carried out by several researchers around the world. The reuse of recycled aggregates as a replacement for natural aggregates in the manufacture of concrete has still

remained limited despite its impact on the environment due to a few factors of technical problems; trade barriers (competition with natural aggregates); quality assurance and control issues lack of proper regulation and experience as well as poor image on recycled materials

The materials used and their characterizations

2.1. Cement

The cement used is Portland limestone cement CEM II/A-L 42.5R (Biskria) (Figure 1), conforming to the NA 442 standard [6], whose chemical and mineralogical compositions, as well as the physico-chemical characteristics are presented respectively in Table 1.

Table 1. Physico-mechanical characteristics of cement

Apparent volumetric mass (kg/m^3)	953
Absolute Density (Densitometer) (kg/m^3)	2980
Absolute density (liquid pycnometer)(kg/m^3)	2985
Consistency (%)	27.5
The start time of plug	2h:55

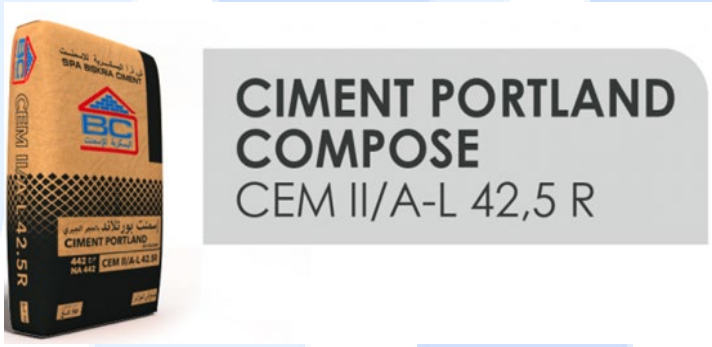

Figure 1. Cement Portland CEM II/A-L 42.5R (Biskria)

2.2. Aggregates

2.2.1. Preparation of aggregate

It was chosen for this study, to design three granular classes 0/5, 3/8 and 8/15, and this to have ternary concretes with a better granular extent and a formulation adapted to the desired requirements (Consistency and Resistance).

2.2.2. Crushed sand

The sand used comes from a large quarry in the region of Ain Touta (Batna, it is the National Company of Aggregates. This choice is dictated by the fact that this quarry mainly supplies the region due to its importance in production. The physical characteristics are shown respectively in Table 2.

Table 2. Physical characteristics of crushed sand

Apparent volumetric mass (g/cm^3)	1.46
Water content (%)	0.325
Water absorption degree (%)	2.79
Sand equivalent (%)	68

2.2.3. Gravel

2.2.3.1. Cleanliness of aggregates

Impurities can disturb the hydration of the cement or lead to defects in aggregate-paste adhesion, which can affect the strength of the concrete. Cleanliness reflects the absence of undesirable fine elements in the aggregates. It essentially designates the content of clay fines, the value of which must be limited. The aggregate cleanliness test consists of determining the percentage of elements less than 0.5 mm in accordance with standard NF P18-591 [7].

The physical and mechanical characteristics of gravel aggregates are shown respectively in Table 3.

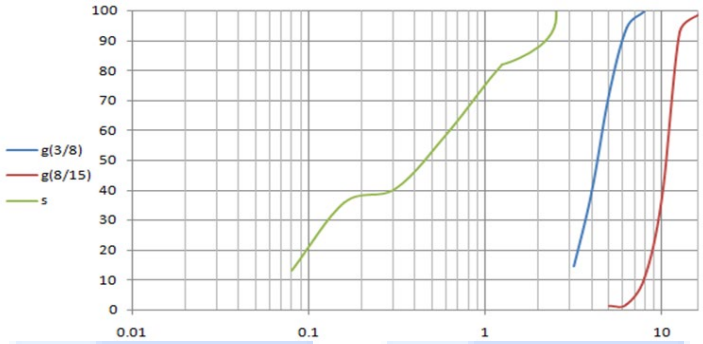

Figure 2. Particle size curves of the different aggregates used S, GN (3/8) and GN (8/15)

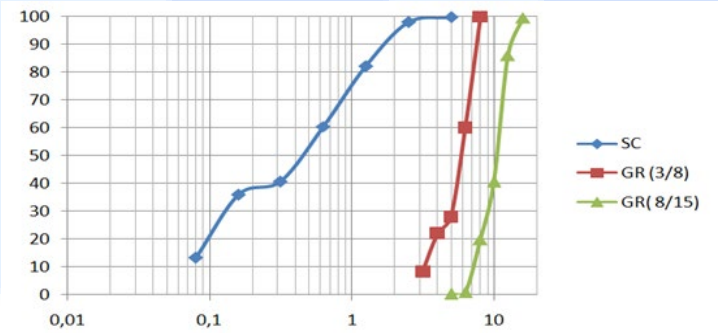

Figure 3. Particle size curves of the different aggregates used S, 100% GR (3/8) and 100% GR (8/15)

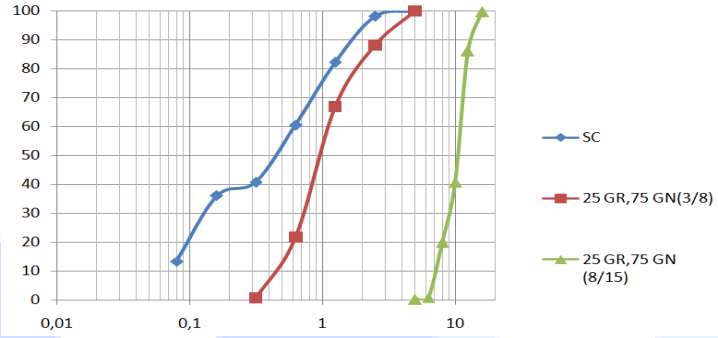

Figure 4. Particle size curves of the different aggregates used S, 25% GR (3/8) and 75% GR (8/15)

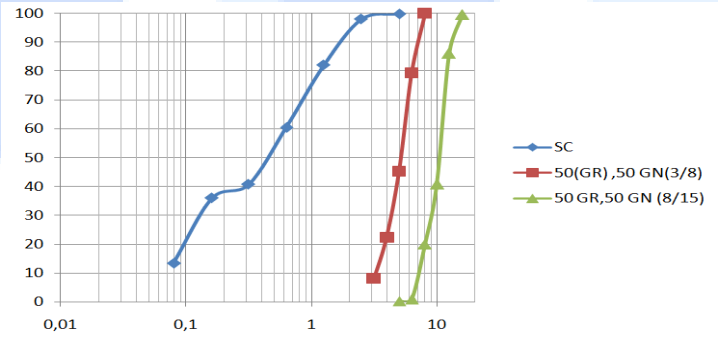

Figure 5. Particle size curves of the different aggregates used S, 50% GR (3/8) and 50% GR (8/15)

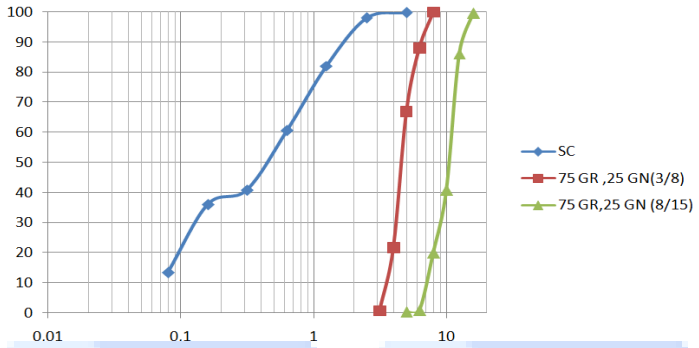

Figure 6. Particle size curves of the different aggregates used S, 50% GR (3/8) and 50% GR (8/15)

Table 3. Physical characteristics of crushed sand

Type of aggregate	GN (3/8)	GN (8/15)	GR (3/8)	GR (8/15)
Absolute density (g/cm^3)	2.60	2.53	2.45	2.41
Apparent volumetric mass (g/cm^3)	1.337	1.318	1.055	1.048
Los Angeles (%)	23	35.38	26.2	32.8

GN(3/8): Crushed natural gravel GN(8/15): Crushed natural gravel GR(3/8): Recycled gravel GR(8/15): Recycled gravel

2.3. Mixing and vibration

The mixing of the concretes was done in an electric cement mixer with inclined axis, capacity 30 liters. The mixing time is 05 minutes including 02 minutes of dry mixing. The concrete is placed on a vibrating table (external vibration), according to standard NF P18–421 [8].

2. Tests methods and procedures

3.1. Characterization of concrete in the fresh state

3.1.1. Subsidence The workability of the concrete

Is evaluated using the Abrams cone, in accordance with standard NF P 18-451 [9]. The test consists of introducing the fresh concrete into a frustoconical mold (D=20, d=10, H=30 cm) in three layers, where each undergoes 25 tapping strokes using a Q16 mm rod, then the mold is slowly removed and the sag measurement taken.

Figure 7. Concrete slump measurement at Abrams cone

3.2. Characterization of concrete in the hardened state

3.2.1. Compressive strength

The test for determining the compressive strength of the specimens is carried out in accordance with the requirements of the NA 427 standard [10]. The breaking stress is given directly by the testing machine (Figure 8.)

Figure 8. Compressive testing machine

3.2.2. Dynamic auscultation test (ultrasound)

Ultrasound monitoring is a non-destructive method intended to test the homogeneity of concrete, it consists of determining the speed of propagation of longitudinal (compression) waves through a concrete element in accordance with standard NF P 18-418 [11]. The principle of the method consists in measuring the time taken by a wave to travel a given distance. The relationship between the speed of propagation of ultrasonic waves and the compressive strength is affected by a number of variables such as the age of the concrete, the humidity conditions, the ratio between aggregates and cement, the type of aggregates and location of steels and cracks. Ultrasonic inspection makes it possible, without harming the integrity of a structure, to characterize the defects it contains and thus to pass judgment on the acceptance of the parts produced.

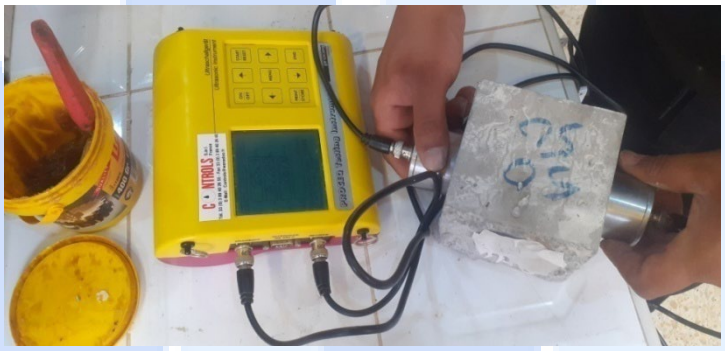

Figure 9. Calibrating the Ultrasound device

Table 4. Composition of concrete

Type of concrete	Cement (Kg/m^3)	Aggregates (kg/m^3)			Water (L/m^3)	W/C
		8/15	3/8	0/5		
B(100%GN)	350	905	200	670	180	0,55
B(100%GR)	350	905	200	670	280	0,8
B(75%GN+25%GR)	350	905	200	670	210	0,6
B(50%GN+50%GR)	350	905	200	670	227,5	0,65
B(GN25%+75%GR)	350	905	200	670	245	0,7

3. Results and discussion

4.1. Slump

We took a single slump reading for each formulation (test) and the results obtained are shown in Figure 10.

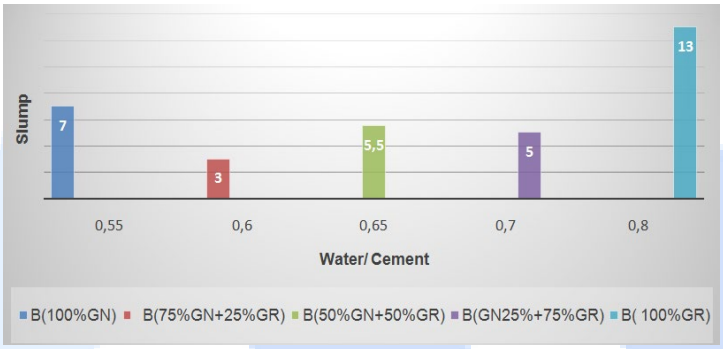

Figure 10. Variation of subsidence as a function of the percentage of aggregate at the age of 28 days

Initially for small subsidence, the water in the mix is both absorbed by the aggregates, wets the cement and the rest is used for the workability of the mix. The analysis of the results shows that for a high W/C ratio, the workability of a concrete made of 100% recycled aggregates (recycled concrete) is greater than that of a concrete made of natural aggregates due to the large quantity of water used.[12-15]. Bravo et al. (2015) [4] reported that it is necessary to increase the effective W/C ratio as the proportion of recycled aggregate increases. However, this increase is not identical in all families of mixtures with recycled aggregate. This can be explained by recycled concrete aggregates which are characterized by a high capacity to absorb water. In addition, it seems that the finer part of the recycled aggregates absorbs a higher quantity of water than the coarser elements [PAD 09].

4.2. Compressive strength

We carried out three measurements for each formulation (test) and the results obtained are recorded in Figure 11.

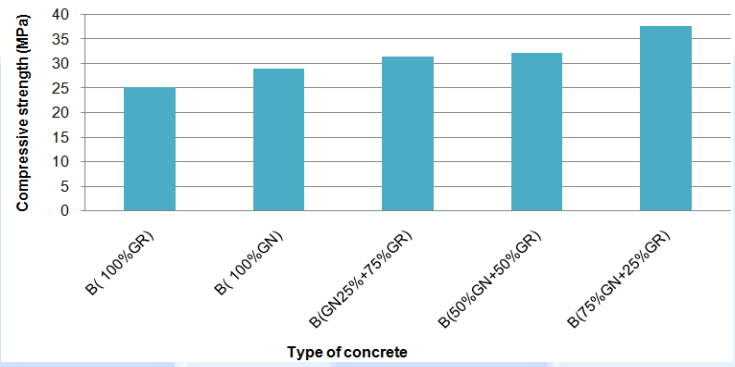

Figure 11. Variation in compressive strength as a function of the percentage of aggregate at 28 days of age

In all cases and at 28 days the compressive strength is affected by the replacement rate, we see a loss of around 13% of the compressive strength for the highest replacement rate of 100% (concrete recycled aggregate). This is mainly due to the high value of the W/C ratio. This strength loss value is within the upper limit of what is generally observed in the literature for similar concretes. A loss of compressive strength of 10 to 20% is generally observed [16-18] for the highest natural aggregate replacement rates (75% to 100%). In this study, the recycled concrete (with 25%, 50% and 75%) has a better compressive strength at 28 days than the corresponding control concrete (+ 30%, 11%, 8.4%) respectively. This particular case may result from the lower value of E due to the absorption of the aggregates but also from the greater quantity of cement used in the formulations of recycled concrete [19-20].

4.3. Non-destructive testing by ultrasound

For better precision, we repeated the test three times on each specimen, and we then calculated the average of the three measurements obtained on each concrete specimen. The averages thus obtained are summarized in Figure 12.

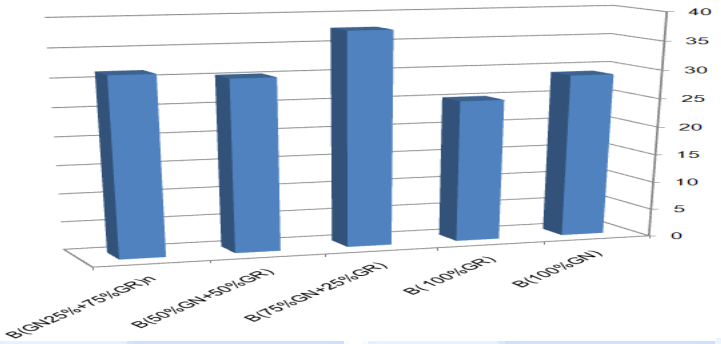

Figure 12. Non-destructive ultrasound test at 28 days

The results in Figure 12 show that the ultrasonic velocities for these concretes decrease with the increase in the percentage of recycled aggregates in the concretes. The more GRs there are, the slower the waves go. Thus, the speed goes from 4186 m/s for concrete with 75% GR to 4410 m/s for concrete with 25% GR. The Ultrasonic Pulse Velocity (UPV) value for natural aggregate concrete is 3983 m/s, this value is in the range 3500-4500 m/s where the concrete quality can be said to be good. The ultrasonic pulse velocity values of all samples were in the range of 4410 m/s to 4056 m/s.

4. Conclusion

From the analysis of the experimental results it can be concluded:

- Losses of resistance are greater for those based on recycled aggregate (100% GR). However, the concretes with a low percentage of recycled aggregates (B25%, B50% and B75%) show a compressive strength comparable to that of the natural control concrete, this is due to the W/C ratio effect. For all the experimental tests, the control concrete or ordinary concrete is based on ordinary crushed gravel.
- Recycled gravel is also crushed. In summary, the performance of concretes is primarily dominated by the W/C ratio. The relative absorption rate of recycled aggregate is greater than that of natural aggregate.
- This property is therefore important to consider when preparing concrete using recycled aggregates. It is possible to minimize or prevent the negative impact of recycled aggregates on the properties in the fresh state of the concrete by adding a phase of partial pre-saturation of the aggregates to the mixing protocol.
- Replacing 25% of natural aggregates with recycled concrete aggregate is also an interesting possibility to maximize the use of recycled aggregates while allowing a low impact on the properties of the concrete.
- The high absorption of the recycled aggregates used contributes to the development of the mechanical resistance of the recycled concretes of the W/C ratio = 0.6.
- It can be noted and from previous research on concrete made from recycled aggregates that the compressive strength is proportional to the speed of ultrasound and that the correlation is of the linear type: Rc = a (V) + b.

Nomenclature

CEM II/A-L 42.5R: Portland limestone cement
GN: Crushed natural gravel
GR: Recycled gravel
UPV: Ultrasonic Pulse Velocity
Rc: Compressive strength

Declaration of Conflict of Interests

The author declares that there is no conflict of interest. They have no known competing financial interests or personal relationships that could have appeared to influence the work reported in this paper.

References

[1.] Irina Ivanova and Viktor MechtcherineEffects of Volume Fraction and Surface Area of Aggregates on the Static Yield Stress and Structural Build-Up of Fresh ConcreteMaterials (Basel). 2020 Apr; 13(7): 1551. Published online 2020 Mar 27. Doi:10.3390/ma13071551

[2.] Adewumi John Babafemi, Branko Šavija,Suvash Chandra Paul, Vivi Anggraini,Engineering Properties of Concrete with Waste Recycled Plastic: A Review,*Sustainability* 2018, *10*(11), 3875; https://doi.org/10.3390/su10113875

[3.] Behera, M., Bhattacharyya, S. K., Minocha, A. K., Deoliya, R., Maiti, S., Recycled aggregate from C&D waste & its use in concrete–A breakthrough towards sustainability in construction sector: A review. *Construction and building materials 68* (2014) 501-516. https://doi.org/10.1016/j.conbuildmat.2014.07.003.

[4.] Bravo, M., de Brito, J., Pontes, J., Evangelista, L., Mechanical performance of concrete made with aggregates from construction and demolition waste recycling plants. Journal of Cleaner Production 99 (2015) 59–74. https://doi.org/10.1016/j.jclepro.2015.03.012.

[5.] NA 442 Algerian Standard, cement composition, specifications and conformity criteria for common cements, (2005).

[6.] NF P18-591 French Standard, "Cleanliness of coarse aggregates", (1990).

[7.] NF P18-421 French Standard, "Fresh concrete placed by micro vibrating table", (1981).

[8.] NF P18-451 French Standard, “fresh concrete cone slump tests”, 1981.

[9.] NA 427 Algerian Standard, concrete - determination of compression strength of specimens, (1989).

[10.] NF P18-418 French Standard, Concrete - Sonic auscultation - Measurement of the propagation time of sonic waves in concrete, (1989).

[11.] Boulay, V., Valorization of recycled granular materials in cement concrete for residential use. Université de Sherbrooke, (2014).

[12.] Chakradhara Rao, M., Bhattacharyya, S. K., Barai, S. V., Influence of field recycled coarse aggregate on properties of concrete. *Materials and structures 44* (2011) 205-220. https://doi.org/10.1617/s11527-010-9620-x

[13.] Butler, L., West, J. S., Tighe, S. L., The effect of recycled concrete aggregate properties on the bond strength between RCA concrete and steel reinforcement. Cement and Concrete Research 41.10 (2011) 1037–1049. http://doi.org/10.1016/j.cemconres.2011.06.004

[14.] López-Gayarre, F., Serna, P., Domingo-Cabo, A., Serrano-López, M. A., López-Colina, C., Influence of recycled aggregate quality and proportioning criteria on recycled concrete properties. *Waste management 29.12* (2009), 3022-3028. https://doi.org/10.1016/j.conbuildmat.2009.02.018

[15.] de Oliveira, M. B., Vazquez, E., The influence of retained moisture in aggregates from recycling on the properties of new hardened concrete. *Waste management 16.1-3* (1996), 113-117. https://doi.org/10.1016/S0956-053X(96)00033-5

[16.] Etxeberria, M., Marí, A. R., Vázquez, E., Recycled aggregate concrete as structural material. *Materials and structures 40* (2007) 529-541. https://doi.org/10.1617/s11527-006-9161-5

[17.] Rahal, K., Mechanical properties of concrete with recycled coarse aggregate. Building and environment 42.1 (2007), 407-415. https://doi.org/10.1016/j.buildenv.2005.07.033

[18.] Hansen, T.C., Recycling of Demolished Concrete and Masonry. Report of Technical Committee 37-DRC Demolition and Reuse of Concrete. RILEM, E & FN Spon, London, (1992). https://doi.org/10.1201/9781482267075

[19.] Xiao, J., Lu, D., Ying, J., Durability of recycled aggregate concrete: an overview. Journal of Advanced Concrete Technology 11.12 (2013), 347-359. https://doi.org/10.3151/jact.11.34

[20.] Chadli, M., Tebbal, N.,Mellas,M.Study of the mechanical behavior of a reactive powder concrete containing fibers . springer nature Switzerland. Proceedings of the 4th International Symposiumon Materials and Sustainable Development, Springer, (2020) Cham,pp.71-82.https://doi.org/10.1007/978-3-030-43211-9_7

[21.] Chadli, M., Tebbal, N., Mellas, M. Impact of elevated temperatures on the behavior and microstructure of reactive powder concrete. Construction and Building Materials, 300: 124031. (2021), https://doi.org/10.1016/j.conbuildmat.2021.124031

[22.] Mounira, C., Nadia, T., Mekki, M. Study of mechanical and elastic properties of reactive powder concrete. Algerian Journal of Engineering Research, (2021) 5(1): 11-17.

[23.] Chadli, M., Mellas, M., Mezghiche, B. Formulation and study of metal fiber-reinforced reactive powder concrete. MaterialsScience, WorldJournal of Engineering,(2018).,15:531-539.https://doi.org/10.1108/WJE-04-2017-0094

PACE-2023
International Congress on the Phenomenological Aspects of Civil Engineering

PACE-2023
International Congress on Phenomenological Aspects in Civil Engineering

Research Article
20-23 June 2023

The Use of Natural Resin and Natural Asphalt as A Substitution of Oil Asphalt in Pavement Flexible

La One*,[1], Edward Ngii[2], Rini Sriyani [3], Laode Muh Adhrian Syahputra Atodding[4]
[1,2,3]Civil Engineering, Engineering Faculty, Haluoleo University, Kendari-Indonesia
[4]student of Civil Engineering, Engineering Faculty, Haluoleo University, Kendari-Indonesia
Corresponding Author E-mail: laone@uho.ac.id

Keywords

Pine Resin,
Buton Natural Asphalt,
Marshall Stability,
Hot Mix Asphalt,
AC-WC.

Abstract

The objective of this study was to analyze the effect of using natural resin and natural asphalt on the performance of flexible road pavements. Natural resin and natural asphalt are local materials that are widely available in Indonesia as binders for flexible road pavements. This material has binding properties and can substitute some of the oil asphalt. This research is a laboratory experiment using Marshall cylinder Specimens. The material used in this study consisted of asphalt penetration 60/70, Buton Natural Asphalt B 50/30, pine resin, and standard aggregate. The Specimens were made using aggregate gradation for hot mix asphalt of Asphalt Concrete Wearing Course, bituminous content of 6.5%, natural asphalt as a substitute for asphalt pen 60/70 and fine aggregate as much as 10% of the total weight of Specimens, and pine resin as a substitute for oil asphalt with variations 0%, 2.5%, 5.0%, 7.5%, 10%, and 12.5%. The results showed that the use of 12.5% pine resin content and natural asphalt as much as 10% still met the requirements specified by Indonesia Standard with Marshall Stability is 2515 kg, flow is 2.0 mm, Marshall Quotient is 1,237 kg/mm, and Void in Mixture is 3.6%. Here shows that the use of 12.5% pine resin and 10% Buton Asphalt can substitute as much as 42.28% of oil asphalt. This research is expected to be applied to reduce dependence on the use of oil asphalt for flexible road pavement materials.

1. Introduction

Roads are basic infrastructure in supporting the economic growth and social welfare of a country. Road construction consists of rigid pavement, flexible pavement, and composite pavement (a combination of rigid pavement and flexible pavement). The quality of rigid pavements and composite pavements is higher than that of flexible pavements. However, the initial investment for rigid and composite pavements is more expensive than flexible pavements. Due to the limited funding for road construction and the high demand for road infrastructure in Indonesia, the selection of flexible pavement is a solution in the context of fulfilling road infrastructure. The main materials for flexible pavement construction are bitumen as a binder and aggregate.

Currently, the commonly used flexible pavement binders in Indonesia include oil asphalt and natural asphalt. Oil asphalt is obtained from the remaining processing of crude oil refining. Meanwhile, natural asphalt is found in the southern part of Buton Island from Sampolawa Bay to Lawele Bay, 75 km long. Asphalt sludge is located in the valleys under the slopes of the hills. Asphalt sludge deposits average 4 meters, with variations from 1–17 meters, below the soil surface. Asphalt content also varies from 10-50 percent. Natural asphalt is from the petroleum family, with long carbon chains. The color is dark black, and in it mixed various kinds of mineral grains [1].

The deposit of Buton natural asphalt is around 662 million tons. Here is equal to 340 million tons of bitumen. The asphalt deposit was discovered in the early 1920s. Until 1994, it was used very little as a binder material for flexible pavement. It does not reach 5 million tons. After that, the natural asphalt mining and processing industry was quiet and Indonesia was flooded with imported asphalt. This condition is very ironic with the incessant development of road infrastructure in Indonesia where the national asphalt demand reaches 4 to 5 million tons per year [1]. Here was triggered the results of processing natural asphalt did not provide a homogeneous asphalt content. So the performance of the road pavement does not meet the requirements both in terms of stability and durability.

Currently, in increasing the use of Buton natural asphalt, the Indonesian government has issued some policies for using Buton natural asphalt in roads construction, namely: the regulation of public work minister Number 18-2018 concerning technical references for using Buton asphalt, Regulation of Home affair minister Number 27-2021 concerning optimizing and increasing the use of Buton asphalt, and Regulation of Public work minister number 5-2021, which requires the use of Buton asphalt for the construction and preservation of provincial/ regency/ city roads, which is financed by the Special Allocation Fund. The existence of this policy is supported by an increase in the quality of processed Buton

asphalt products. PT. Wika Bitumen, a subsidiary of the State Enterprise-PT Wijaya Karya, continues to improve the quality of Buton asphalt processing. Some of the natural asphalt products include are Lawele Granular Asphalt (LGA), Asbuton Granular Filler (AGF) for high traffic, Asbuton Active Filler (AAF), and Asbuton Instant Concrete (AIC)[1].

Flexible road construction in Indonesia, apart from using oil asphalt as a binder, also uses natural asphalt. Natural asphalt which is often found in the Indonesian market is in the form of granules. This natural asphalt is commonly used as a partial substitution for oil asphalt.

There were many studies on the use of Buton natural asphalt showing that the natural asphalt product can be applied to high traffic. The use of Buton asphalt can protect the road distress due to bleeding problems and rutting, increase the Marshall stability and dynamic stability, increase tensile strength and unconfined compressive strength, and have sufficient flexibility. Meanwhile, the disadvantage of using Buton natural Asphalt, especially in formed granular, is the release of granules higher. The use of Buton granular asphalt in more contents could the mixture more brittle [2,3,4,5].

In encouraging the construction of green road pavements, one alternative is the use of renewable natural resources such as natural resins. One of which is pine resin. Pine Tree is one of the plants developed by PT. Perhutani, one of the state companies. PT. Perhutani processes pine resin into gondoruken and turpentine. Perhutani has 8 pine resin processing factories with a production capacity of 92,550 tons. Pine resin processing production in 2021 is 81,788 tons [6].

Several studies showed that the use of pine resin can improve the characteristics of asphalt mixtures. The addition of pine resin reduced the asphalt ductility and was resistant to water immersion (Yuniarti et al., 2021). The use of pine resin affects the increase in the value of stability, Cantabro Loss, Asphalt Flow Down, and Void in the Mixture [7,8,9].

2. Research Methodology

The research method used is a laboratory experiment. It was be conducted at the Civil Engineering Laboratory, Engineering Faculty of Halu Oleo University. The research began with the material preparation and testing of its physical characteristics. Then, prepare Marshall cylindrical specimens with a target specimen height of 63.5 mm. All the materials were mixed at a mixing temperature of 160oC and compacted with 3x75 blows at a temperature of 150oC. After that, the specimens were soaked for 24 hours to obtain a volumetric mixture. Then, the specimens were immersed in a water bath at 60oC for 30 minutes. Lastly, the Marshall Stability test was carried out using Marshall Stability Testing Machine. It is used to determine the maximum load and flow of the mixture. The apparatus used has a capacity of 50 KN with a load plate speed of 50.8 mm/minute.

3. Materials

Materials used to make the specimens of hot mix asphalt AC-WC consist of aggregate, asphalt pen 60/70, Buton natural asphalt grade B 50/30, and pine resin.

a. Aggregate b. Filler c. Asphalt Grade 60/70

b. Granular Asphalt e.Pine Resin

Figure 1. Materials used to make specimens of hot mix asphalt AC-WC

3.1. Aggregate and Filler

The aggregate and filler used in this study were taken from the Moramo Stone Crusher in Kendari. The physical characteristic of coarse aggregate, fine aggregate and filler meet The Indonesian National Standard. The physical characteristics of aggregate and filler are shown in Table 1.

Table 1. Physical Properties of Aggregate and Filler

Description	Unit	Testing Method	Specification	Testing Result
Course Aggregate	-	SNI 03-1969-2008	>2.5	2.65
Bulk Specific Gravity	-	SNI 03-1969-2008	>2.5	2.65
SSD Specific Gravity	-	SNI 03-1969-2008	>2.5	2.72
Apparent Specific Gravity	-	SNI 03-1969-2008	>2.5	2.78
Water Absorption	%	SNI 03-1969-2008	<3	1.27
Abrasion	%	SNI 03-2417-2008	<40	31.1
Material passed sieve No. 200	%	SNI 03-4142-1996	<1	0.73
Bulk Specific Gravity	-	SNI 03-1969-2008	>2.5	2.65
SSD Specific Gravity	-	SNI 03-1969-2008	>2.5	2.68
Apparent Specific Gravity	-	SNI 03-1969-2008	>2.5	2.74
Water Absorption	%	SNI 03-1969-2008	<3	1.24
Material passed sieve No. 200	%	SNI 03-4142-1996	<1	0.43
Filler				
Specific gravity	-	SNI 03-1969-2008	>2.5	2.56

Aggregate and filler were combined to meet well gradation for the Asphalt Concrete Wearing Course (AC-WC). It is presented in Figure 1 as follows.

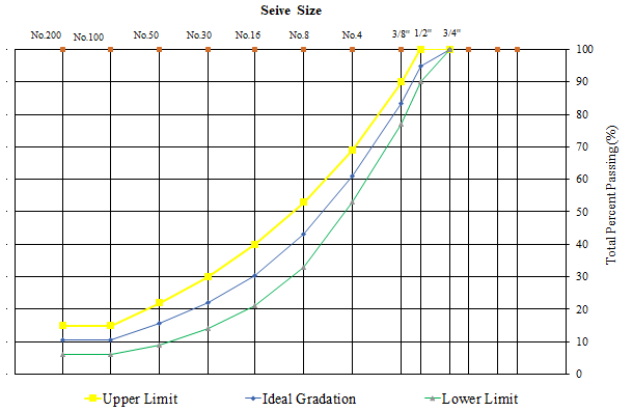

Figure 2. Combined Aggregate gradation for AC-WC

3.2. Oil Asphalt

The oil asphalt used in the study is asphalt grade 60/70. The physical properties of oil asphalt are 68.2 (0.1 mm) penetration, 1.02 specific gravity, and 146 cm ductility.

3.3. Natural Asphalt product

The tests carried out on the physical properties of LGA grade 50/30 were bitumen content, water content, and mineral gradation. The bitumen content of LGA was extracted with a reflux method. The bitumen content of LGA 50/30 is 22.12% and its water content is 0.64%. The mineral gradation of LGA grade 50/30 showed in Table 2.

Table 2. The Mineral Gradation of LGA grade 50/30

Sieve Size	3/8"	No.4	No.8	No.16	No.30	No.50	No.100	No. 200
% passed cumulative	100	95.5	79.3	68.2	58.4	52.6	28.91	18.29

3.4. Pine Resin

The tests carried out on the physical properties of pine resin were specific gravity and water content. The specific gravity of pine resin is 1.05 and the water content is 1.39%.

3.5. Asphalt grade 60/70 modified Pine Resin

Pine resin used as the partial substitution of oil asphalt was 2.5-12.5% interval 2.5%. The use of pine resin affected to physical characteristics of the modified asphalt. The More pine resin content used, the lower penetration on the modified asphalt. Here is shown in Table 3 as follows.

Table 3. The Physical characteristic of oil asphalt modified pine resin

Pine resin content	Ductility (cm)	Penetration (0,1 mm)
2.5%	>140	67.0
5.0%	>140	65.1
7.5%	>140	64.4
10.0%	>140	64.1
12.5%	>140	63.8

3.6. Material Composition of specimen

All specimens were made with 6.5% bitumen content, 10% LGA content, aggregate gradation for hot mix AC-WC, and pine resin variations of 0-12.5% of oil asphalt. Pine resin is used as a partial substitute for oil asphalt. The composition of materials used to make a Marshall cylindrical specimen is shown in Table 4 as follows.

Table 4. The material composition of AC-WC hot mix specimen

Specimen Code	Pine resin Content (%)	Oil Asphalt Content(%)	10% Natural Asphalt Content		Aggregate Content (%)	Total (%)
			Bitumen LGA (%)	Mineral LGA (%)		
P0	-	4.29	2.21	7.79	85.71	100
P2.5	0.11	4.18	2.21	7.79	85.71	100
P5.0	0.21	4.08	2.21	7.79	85.71	100
P7.5	0.32	3.97	2.21	7.79	85.71	100
P10.0	0.43	3.86	2.21	7.79	85.71	100
P12.5	0.54	3.75	2.21	7.79	85.71	100

4. Data Analysis

Data obtained from a volumetric test and Marshall Stability test was analyzed to find the Marshall characteristic consisting of density, void Mineral Aggregate (VMA), Void Filled Bitumen (VFB), Void in Mixture (VIM), Marshall Stability (MS), Flow, and Marshall Quotient (MQ). To analyze the Marshall characteristic used equations (1) -(6) as follows [10].

$$\gamma_d = \frac{w_d}{V} \quad (1)$$

$$VMA = \frac{100(G_{sb} - G_{mb}) + G_{mb} \cdot p_b}{G_{sb}} \quad (2)$$

$$VIM = \frac{G_{mm} - G_{mb}}{G_{mm}} \times 100 \quad (3)$$

$$VFB = \frac{(VMA - VIM)}{VMA} \times 100 \quad (4)$$

4.1. Marshall Stability

The Marshall stability indicates the strength of the asphalt mixture to withstand the maximum static load before deformation failure. It is calculated using equation (1).

$$MS = 100 S_d c_a c_v \quad (5)$$

4.2. Flow

Flow is the deformation ability of the asphalt mixture due to loading. The flow of the asphalt mixture identifies the ductility of the mixture. The higher the mixture flow, the more flexibility the mixture. Conversely, the lower the flow, the higher the stiffness of the mixture.

4.3. Marshall Quotient

The Marshall Quotient indicates the stiffness of the asphalt mixture. The higher the Marshall Quotient of the asphalt mixture, the stiffer the mixture is. Marshall Quotient is a comparison between the marshall stability with the flow.

$$MQ = \frac{MS}{F} \quad (6)$$

5. Discussion

5.1. Volumetric of Asphalt Mixture

5.1.1. Density

Density is usually used to determine the quality and quantity of pavement work. A density relates to the tonnage of the asphalt mixture. If the pavement thickness is known, referring to the density of the mixture, the tonnage of the work will be obtained. Density also is related to void in asphalt mixture.

The higher using of resin as the partial substitution of oil asphalt is effected to increase of the mixture density. The use of 1% pine resin as a substitution for oil asphalt increases 0.0023 gr/ml of the mixture density. The correlation between pine resin content and the density of asphalt mixture using natural asphalt is shown in Figure 3.

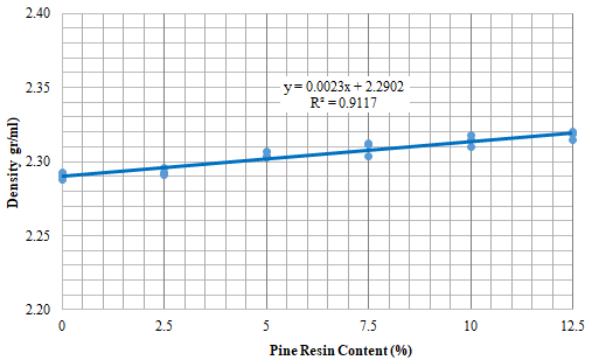

Figure 3. The correlation between pine resin content and the density of asphalt mixture

5.1.2. Void Mineral Aggregate

The use of 2.5-12.5% pine resin as a partial substitution for oil asphalt can reduce Void mineral aggregate. The VMA of a mixture of asphalt without pine resin was 18.1% and the use of 12.5% pine resin reduced the VMA to 16.9%. Here still meets the specifications required by Indonesia Standard, Bina Marga-2010, a minimum of 15% VMA [11]. The viscosity of pine resin at mixing temperature (160oC) and compaction temperature (150oC) is lower than oil bitumen. Pine resin as a partial substitute for oil asphalt can be more easily absorbed into void mineral aggregate. So that the void in mineral aggregate decreases. The correlation between pine resin content and VMA of asphalt mixture using natural asphalt grade B 50/30 is shown in Figure 4.

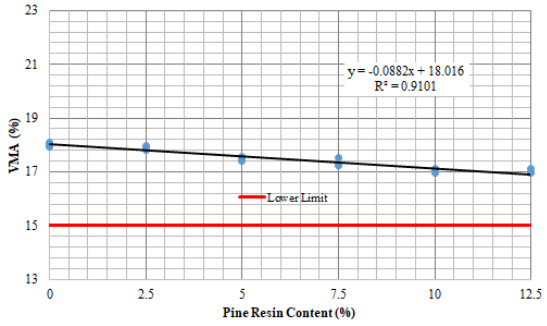

Figure 4. The correlation between pine resin content and VMA of asphalt mixture

At figure 4 above, it is shown that the higher using of pine resin as a partial substitution for oil asphalt influences to decrease of the void in mineral aggregate. The use of 1% pine resin as a substitution for oil asphalt can decrease 0.0882% VMA.

5.1.3. Void in Mixture

The VIM test result showed that the VIM of asphalt mixture without pine resin is 4.8% and the use of 12.5% pine resin produces a VIM of 3.5%. Based on Indonesia Standard, Highways specifications-2018, the VIM of asphalt mixture used 2.5-12.5% pine resin still meets the requirements, 3-4%. The decreasing of VIM was affected by the viscosity of pine resin which was lower than the viscosity of asphalt at mixing temperature and compaction temperature. This condition allows asphalt modified with pine resin to have the ability to fill more voids in asphalt mixing. The correlation between pine resin content and the VIM of asphalt mixture is shown in Figure 5.

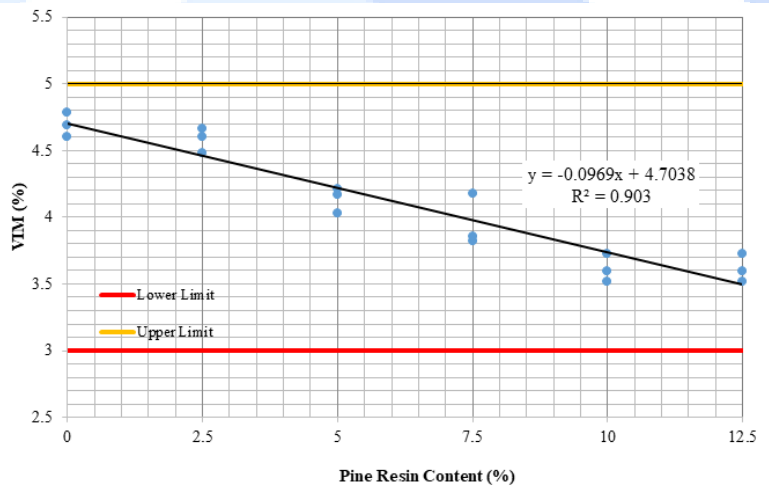

Figure 5. The correlation between pine resin content and VIM of asphalt mixture using natural asphalt

At figure 5 above, it is shown that the higher using of pine resin as a partial substitution for oil asphalt influences to decrease of the VIM of asphalt mixture. The use of 1% pine resin as a substitution for oil asphalt can decrease 0.0969 VIM.

5.1.4. Void Filled Bitumen

The VFB of Asphalt filled bitumen has a strong correlation to Void in Mixture. Increasing voids filled bitumen results in reduced voids in the mixture. The VFB test result showed that the VFB of asphalt mixture without pine resin is 73.6% and the use of 12.5% pine resin produces a VFB of 79.2%. Based on Indonesia Standard, Highways specifications-2018, the VFB of asphalt mixture used 2.5-12.5% pine resin still meets the requirements, more than 65% [11]. Increasing VFB was influenced by the viscosity of oil asphalt modified with pine resin at mixing temperature and compaction temperature lower than oil asphalt viscosity. Therefore, the more the use of pine resin the more voids filled bitumen. The correlation between pine resin content and the Void filled bitumen of asphalt mixture using natural asphalt grade 50/30 is shown in Figure 6.

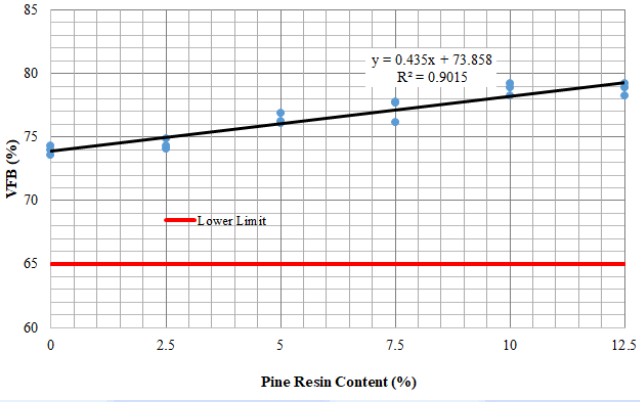

Figure 6. The correlation between pine resin content and VFB of asphalt mixture

At figure 6 above, it is shown that the higher using of pine resin as a partial substitution for oil asphalt is effected to increase of the voids filled bitumen. The use of 1% pine resin as a substitution for oil asphalt can increase VFB by 0.435 %.

5.2. Stability, Flow, and Marshall Quotient

5.2.1. Marshall Stability

The use of pine resin for hot mix AC-WC containing natural asphalt influences the Marshall criteria. Increasing the use of pine resin due to the decreasing of Marshall Stability. The stability of hot mix asphalt without pine resin is 3055 kg and the stability of hot mix asphalt with 12.5% pine resin is 2397 Kg. The use of pine resin up to 12.5% in asphalt mixtures containing natural asphalt produces Marshall Stability 2.4 times more than that designated in the Indonesian Standard, Highway Specifications-2018, which is more than 1000 kg [11]. The correlation between pine resin content and Marshall Stability is shown in Figure 7.

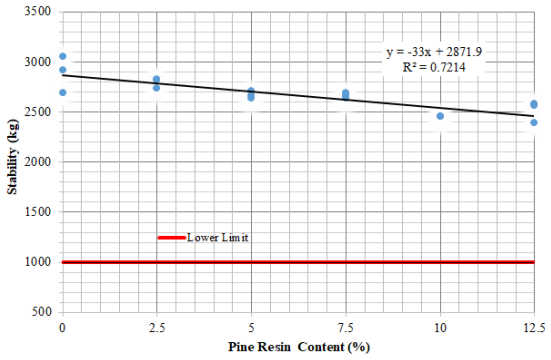

Figure 7. The correlation between pine resin content and stability of asphalt mixture

At figure 7 above, it is shown that the higher using of pine resin as a partial substitution for oil asphalt decreases the Marshall Stability. The use of 1% pine resin as a substitution for oil asphalt can decrease MS by 33 kg.

5.2.2. Flow

The addition of the use of pine resin as much as 2.5 -12.5% decreases the flow of the asphalt mixture. The flow of asphalt mixture without pine resin is 3.2 mm and the flow of asphalt mixture with 12.5% pine resin is 2.0 mm. These results indicate that the flow of asphalt mixture containing up to 12.5% pine resin still meets Indonesian standards, highway specifications-2018, namely 2-4 mm [11]. The reduced flow of asphalt mixture is caused by the penetration of asphalt modified with pine resin at room temperature which is lower than the penetration of oil asphalt. The correlation between the flow of asphalt mixture and the use of pine resin in hot mix A-WC containing natural asphalt is shown in Figure 8.

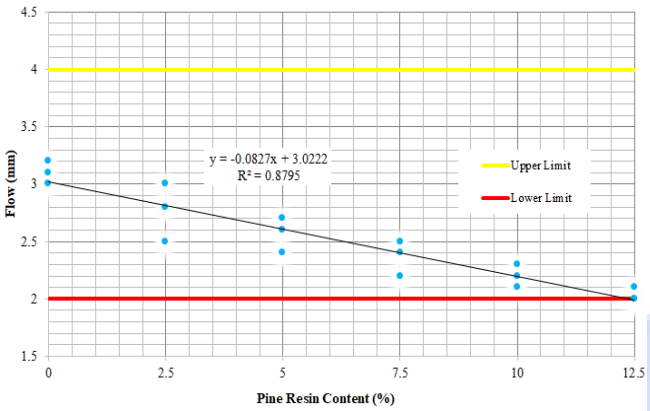

Figure 8. The correlation between pine resin content and flow of hot mix AC-WC using natural asphalt

At figure 8, it is shown that the higher use of pine resin as a partial substitution for oil asphalt can decrease Flow. The use of 1 % pine resin as a substitution for oil asphalt can decrease 0.0827 mm of Flow.

5.2.3. Marshall Quotient

The addition of pine resin with a variation of 2.5-12.5% has the effect of reducing the Marshall stability and the flow of the asphalt mixture. The Marshall question is the ratio between the stability of the marshall to the flow of the asphalt mixture. The greater the MQ of the asphalt mixture, it indicates that the mixture is stiffer. The MQ of asphalt mixture without pine resin is 840 kg/mm and The MQ of asphalt mixture containing 12.5% pine resin is 1,293 kg/mm. These MQ meet the Indonesian standard, Highway specification-2018, namely more than 250 kg/mm [11]. The correlation between the MQ of asphalt mixture and the use of pine resin in hot mix asphalt AC_WC containing natural asphalt is shown in Figure 9.

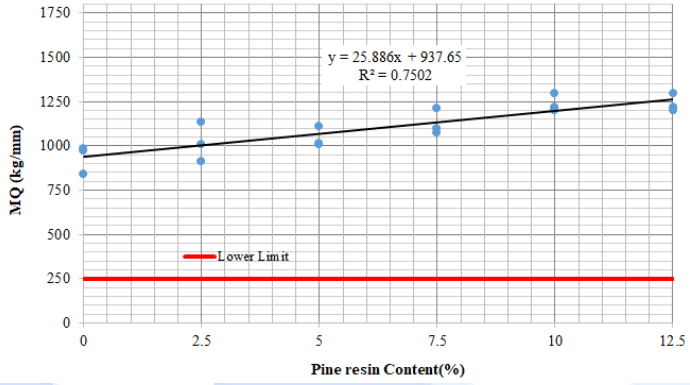

Figure 9. The correlation between pine resin content and MQ of asphalt mixture using natural asphalt

At figure 9 above is shown that the higher using of pine resin as partially substitution of oil asphalt is effected to increase of the Marshall Quotient. Using 1% of pine resin as substitution of oil asphalt can increase 25.89 kg/mm of MQ. At figure 9, it is shown that the higher use of pine resin as a partial substitution for oil asphalt can increase the Marshall Quotient. The use of 1% pine resin as a partial substitution for oil asphalt can increase MQ by 25.89 kg/mm.

In brief, the effect of using pine resin in the hot asphalt AC-WC containing natural asphalt on the Marshall criterion is shown in Table 5 below.

Table 5. The Marshall criterion of asphalt mixture containing natural asphalt and pine resin

Pine Resin Content (%)	**Density** (gr/ml)	**VMA** (%)	**VIM** (%)	**VFA** (%)	**Marshall Stability** (Kg)	**Flow** (mm)	**Marshall Quotient** (kg/mm)
0	2.290	18.0	4.7	73.9	2,889	3.1	908
2.5	2.293	17.9	4.6	74.4	2,796	2.8	1,017
5	2.304	17.5	4.1	76.4	2,672	2.6	1,043
7.5	2.309	17.3	4.0	77.0	2,664	2.4	1,128
10	2.314	17.2	3.8	78.1	2,570	2.2	1,099
12.5	2.318	17.0	3.6	78.8	2,515	2.0	1,237
Spesification	-	14	3-5	>65	1000	2-4	>250

6. Conclusion

Based on the discussion above, the use of pine resin as a partial substitute for oil asphalt in hot mix asphalt AC-WC containing natural asphalt greatly influences the Marshall criterion. The conclusions of this research are:

- ✓ The higher use of resin as a partial substitution of oil asphalt has an impact on increasing the density of the mixture, decreasing voids in the mixture, decreasing voids in the mixture, increasing voids filled with asphalt, decreasing Marshall Stability, decreasing Flow, and increasing Marshall Quotient.
- ✓ The use of 1% pine resin as a partial substitution for oil asphalt can increase 0.0023 gr/ml of the mixture density, decrease 0.0969 % of VIM, decrease 0.0969 % of VIM, increase 0.435 % of VFB, decreases 33 kg of MS, decreases 0.0827 mm of Flow, and increase 25.89 kg/mm of MQ.
- ✓ The use of up to 12.5% pine resin and 10% natural asphalt in the AC-WC asphalt mixture meets the requirements of the Indonesian Standard, Highway Specifications - 2018.
- ✓ The use of 12.5% pine resin and 10% natural asphalt can substitute as much as 42.28% of oil asphalt.

Future Work

Following up on the research that has been done, some research that needs to be continued in the future is as follow:

- The durability of the hot mix asphalt containing natural asphalt and pine resin.
- The characteristics of hot mix asphalt containing natural asphalt and pine resin due to cyclic loading.
- The contribution of using other natural resins as a substitute for oil asphalt in asphalt mixtures containing natural asphalt and pine resin.

Nomenclatures

c_a : apparatus calibration (KN)
c_v : correction on specimen volume.γ_d : dry density of specimen (gr/ml)
F : flow (mm)
G_{mb} : the bulk specific gravity of specimen(gr/ml)
G_{mm} : the maximum specific gravity of specimen (gr/ml)
G_{sb} : the bulk specific gravity of combined aggregate (gr/ml)
MS : Marshall stability (kg)
MQ : Marshall quotient (kg/mm),
V : the volume of specimen(ml)
VFB : void filled bitumen (%)
VIM : void in the mixture (%)
VMA: Void Mineral Aggregate (%)
w_d : the dry weight of specimen(gr)
S_d : stability dial needle display
p_b : proportion aggregate to the total weight of the specimen (%)
γ_d : density (gr/ml)

Declaration of Conflict of Interests

The authors declare that there is no conflict of interest. They have no known competing financial interests or personal relationships that could have appeared to influence the work reported in this paper.

References

[1.] Trihusodo, P. Beralih ke Aspal Buton. Portal Informasi Indonesia.Indonesia.go.id. Oktober 2022.

[2.] Affandi, F. Pengaruh Asbuton Semi Ekstrasi Pada Campuran Stone Mastic Asphalt, Puslitbang Jalan Dan Jembatan, Bandung. 2010.

[3.] One L, Tjaronge M.W, Irmawaty R, Hustim M. Effect of Buton Granular Asphalt Gradation and Cement as Filler on Performance of Cold Mix Asphalt Using Limestone Aggregate. Journal of Engoneering Science and Technology. Vol.16(1). Taylor's University. Malaysia. 2020.

[4.] One L, Tjaronge M.W, Irmawaty R, Hustim M. Effect of buton's granular asphalt gradation on marshall stability of cold emulsified asphalt mixtures under wet condition. IOP Conference Series: Earth and Environmental Science. Volume 419. The 3rd International Conference on Civil and Environmental Engineering (ICCEE 2019) Bali, Indonesia. 29–30 August 2019.

[5.] Ngii E, One L, Nasrul N, and Udo M.I. Effects of Dammar as the partial substitution of bitumen in HMA AC-WC containing Buton Asphalt. IOP Conference Series: Earth and Environmental Science. Volume 1065. The Fourth International Conference on Sustainable Infrastructure and Built Environment. Bogor. Indonesia. 2022.

[6.] PT. Perhutani. Rise and Growth (Bangkit dan Tumbuh). Laporan Tahunan/ annual report 2021. Jakarta – Inodenisia. 2022. https://drive.google.com/file/d/1XECYi4lh0DeamLAsTGo19X__IzLCl9e8/view.

[7.] Kencanawati C., Sugita I.K.G, Suardana N, and Suyasa, I.W.B. Karakteristik Dan Analisis Awal Getah Pinus Merkusii (Pine Resin) dengan Variasi Suhu Pemanasan sebagai Alternatif Resin Pada Komposit. Proceeding Seminar Nasional Tahunan Teknik Mesin (SNTTM). Surabaya-Indonesia.2017.

[8.] Maula A, Saleh S.M, and Mita F. Pemanfaatan Gondorukem Sebagai Bahan Substitusi ke Dalam Aspal Pen 60/70 pada Campuran Aspal Porus. 1(2), 93–99. 2019.

[9.] Perceka D.P, and Ing T.L. Pengaruh Getah Pinus Pada Stabilitas, Pelelehan, dan Durabilitas Lapis Pengikat Beton Aspal. 64–83. (2016).

[10.] Asphalt Institute. Manual Series No. 4 (MS 4). 1989.

[11.] Direktorat Jendral Bina Marga. Spesifikasi Umum 2018 Untuk Pekerjaan Jalan Dan Jembatan. Jakarta: Direktorat Jendral Bina Marga. 2018.

PACE-2023
International Congress on the Phenomenological Aspects of Civil Engineering

PACE-2023
International Congress on Phenomenological Aspects in Civil Engineering

Research Article
20-23 June 2023

An Overview on Role of Different Joints in Mortar-free Interlocking Structures

Shehryar Ahmed*,[1], Majid Ali[1]
[1]Capital University of Science and Technology, Islamabad, Pakistan
Corresponding Author E-mail: engr.shehryar@outlook.com

Keywords

Interlocking structures,
Mortar-free,
Interlocking blocks,
Connections,
Mortarless construction,
Energy dissipation.

Abstract

Mortar-free interlocking structures are being considered a viable replacement of conventional masonry structures due to their benefits like cost-effective, easy to build. But, the joints among the elements of interlocking structures still need a comprehensive methodology to provide feasible connection type due to use of various interlocking block shapes. Thus, the aim of this literature research is to comprehensively review the joint locations in interlocking structures and type of connections used in other structural systems. This is accomplished by focusing on articles published in highly reputable journals. Interlocking structures require adequate horizontal and vertical connecting mechanism at joint locations due to nature of interlocking block shape. These connections act as restraining elements when structure tends to deform due to lateral loading. The stress concentrations occur at the adjacent surfaces of blocks and at joining locations of elements which are further released in the form of dissipated energy. Interlocking block surfaces resist local failure by resisting sliding over leading to shape deformation. However, connections resist global displacement of structure by resisting lateral movement of individual interlocking block elements in the form of edge confining restraints or in the form of reinforcing rebars. Thus, the role of connecting mechanism in mortar-free interlocking structures is critical for the stability and robustness of the structure.

1. Introduction

To cope up with the increasing housing demand, developing nations are facing multiple challenges including limited finance, material shortage, labor unavailability and technological advancement, etc. Conventional masonry structures mainly use clay bricks or concrete blocks with mortar. They tend to perform poor in case of seismic hazard due to low lateral resistance. Modular construction has gained a lot of attention due to simplified assembling procedures contrary to masonry construction. These consist of off-site manufactured prefabricated parts which are joined together at site assembling a complete structure [1]. In addition to the concept of a modular construction, a relatively similar concept of assembling structures with interlocking modules has gained a lot of consideration in the past decade. These modules can be bricks/blocks of conventional materials like clay and concrete or sustainable materials like recycled aggregate concrete, autoclaved aerated concrete and stabilized soil [2]. Blocks are joined together to form interlocking structures without use of mortar. These interlocking blocks are easily stacked over another to construct mortar-free interlocking structures. The interlocking geometry of blocks assist the smooth stacking leading to mortar lessness. Advantages of mortar-free interlocking structures include low cost due to material saving in mortar and reduced labor cost due to easy assemblage. These advantages tend to elevate dominance of mortar-free interlocking structures over conventional masonry structures. In addition to economic benefits, the leading advantage of mortar-free interlocking structures is the resistance to lateral loading due to geometry of interlocking block. The shear keys of interlocking block resist the in-plane and out-of-plane movement of structural elements like walls and columns thus, reducing the lateral displacement of overall structure [3, 4]. Additionally, the application of the concept of confined masonry and reinforced masonry can further enhance the lateral stability of mortar-free interlocking structures. Edge restraints can be employed for the confinement of interlocking block walls and voids in interlocking block can be provided for reinforcing the walls.

Joints among structural elements are crucial for the stability of structure. Unlike conventional masonry structures, mortar-free interlocking structures require specialized arrangement at joint locations for adequate connecting mechanism. Structures have multiple joint locations including wall to wall joint, wall to foundation joint, wall to slab joint, wall opening peripheral joint, etc. These joints may need various type of connections as per the structural stability requirements [5-7]. Depending on the characteristics, the connections can be categorized as moment resisting connections and shear connections. However, the mechanism of joining units can be by welding, bolting, riveting or high strength adhesive epoxy resins. Confined masonry and reinforced masonry are some of the typical examples having adequate structural integrity mechanisms, but the details of confinement and reinforcing requirement are interlinked with the governing response of the structure [8, 9]. Structural stability requirement defines the necessity of either horizontal connections, vertical connections or both. In case of mortar-free interlocking structures, adequate anchorage from wall to foundation is crucial if lateral forces are governing. The overall height of the structure will control the requirement of embedment length of anchors in the foundation. The role of joints in controlling the horizontal displacement as well as vertical uplift is crucial when structure is subjected to seismic excitation. Though, the weight of structure can resist the vertical

component of an earthquake but the pull-out displacement at the wall foundation location may be critical if a light weight structure is subjected to wind loading. These requirements lead to comprehensive design of connections and anchorages of structural stability.

Excitation of a structure leads to stress origination with in the elements as well as at the joint locations among elements [10, 11]. These stresses initiate deformation at local level with in the block elements and displacement at the global level in the overall structure [12]. The adjacent surfaces of the interlocking blocks experience frictional stresses. Behavior of mortar-free interlocking structures is quite different in comparison to conventional masonry structures. The adjoining surfaces of the interlocking blocks experience the frictional resistance against sliding over another and dissipate energy, when subjected to lateral loading [13, 14]. In addition, controlled repetitive rocking motion at joints can help in energy dissipation, and enhancing seismic resistance. In confined masonry, the cumulative displacements of individual block elements are resisted by edge confining elements thus aiding the energy dissipation phenomenon. However, in reinforced masonry, the reinforcing rebars at equal intervals in the walls are the main source of keeping the structure intact through dissipation of energy at local level in the elements. The wall-foundation connection remains critical against lateral loading due the induced moment and its capacity to dissipate energy prior to failure.

To the best of author's knowledge, connecting mechanisms at joints in interlocking structures have not been reported in literature. Thus, the literature about the types of connections in various structural systems has been comprehensively reviewed. The study is limited to the literature produced in perspective of connections in steel modular buildings, interlocking structures and composite structures. Various types of connectors with their specified role at respective locations have been highlighted to corelate the joint requirements in mortar-free interlocking structures. Energy dissipation mechanism at joint locations is also reported to enhance the significance of this research.

2. Philosophy of interlocking structures

The concept of interlocking may be distinguished based on the type of bond between bricks/blocks. Researchers have employed interlocking mechanism both in the form of mortar induced interlocking and mortarless interlocking. Figure 1 shows various interlocking block shapes that have been employed to construct confined, unconfined and reinforced masonry elements and structures. Imai et al. (2015) [15] evaluated the seismic performance of concrete hollow block masonry (CHB) house models with bifurcation of engineered and non-engineered construction. The engineered model was constructed with compliance to standards whereas the non-engineered model had commonly used simple mortar mix with poorly compacted hollow block units. Models were connected with anchor bolts to reinforced concrete (RC) foundation. Both the models were subjected to the NS component of Kobe 1995 earthquake on a 1D shaking table. The gable walls between the triangular portion of roof were the most vulnerable ones exhibiting large displacements. The model engineered survived the seismic excitation with only minor damage whereas the non-engineered model exhibited consistent failure due to poor compaction in CHBs. Joyklad and Hussain (2019) [16] conducted an experimental study on axial compressive behavior of hollow brick masonry made of cement-clay mix. Brick masonry walls of 1000 mm x 1000 mm were tested under uniaxial compression. Walls were categorized into five types having dry stacking without any binding material, walls with grouting in circular holes of bricks, walls with grouting in square holes of bricks, walls with grouting & reinforcement in circular holes of bricks and walls with grouting & reinforcement in square holes of bricks. Th results demonstrated ductile failure pattern of reinforced masonry walls as compared to other types. Fig. 1 shows various shapes of interlocking blocks and their corresponding elements and structures reported by researchers.

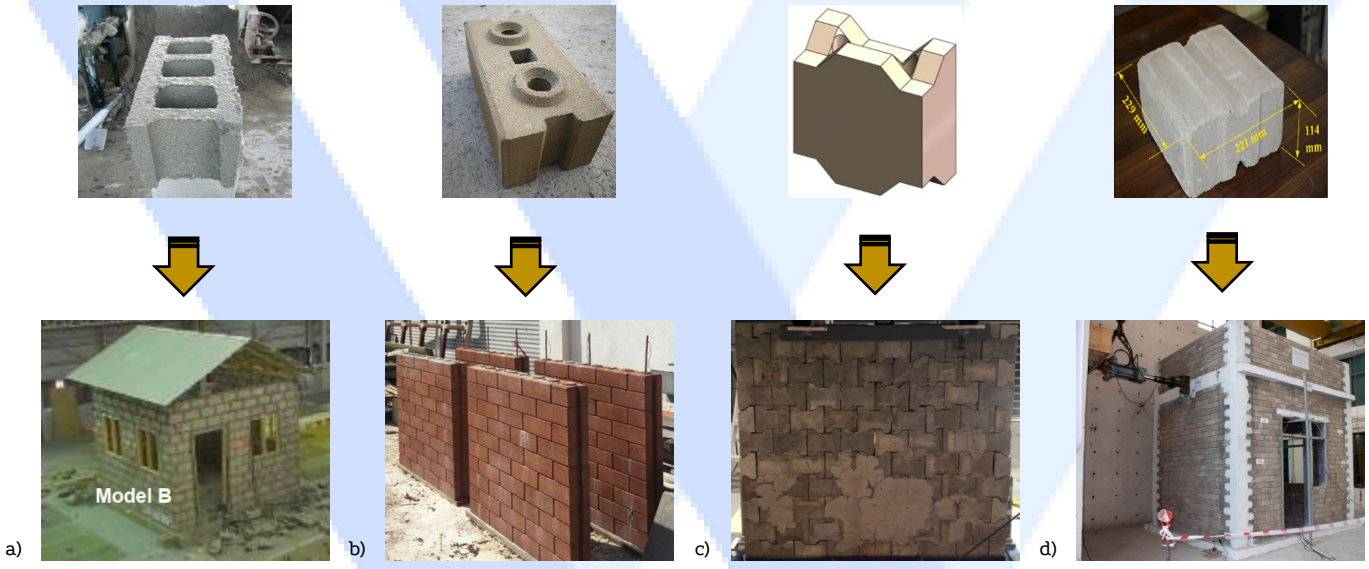

Figure 1. Block shape and corresponding element/structure; a) Imai et al. [15], b) Joyklad and Hussain [16], c) Xie et al. [17] and d) Gul et al. [18]

In addition to static, dynamic behavior of interlocking elements has a significant role in controlling the seismic response of interlocking structures. Xie et al. (2022) [17] performed shaking table tests on scaled down interlocking block reinforced masonry walls and investigated seismic response through failure modes and energy dissipation. For comparison, conventional masonry walls were considered as control specimens. Walls were subjected to uniaxial ground motion in the in-plane direction only. Against horizontal seismic excitation, the dominating response in terms of strength and deformation capacity was observed in interlocking block walls as compared to CM walls. Gul et al. (2023) [18] tested full-scale interlocking structure against quasi-static loading to evaluate the failure patterns, ductility, lateral load resistance capacity and stiffness. Interlocking blocks were manufactured using cement, soil and water. The sliding tolerance of blocks was limited to utilize the lateral strength of blocks to maximum level. After the utilization of lateral capacity, the failure moved to the confining concrete elements which indicates the potential to limit damage at local level by adopting high strength blocks. The structure exhibited better performance in out-of-plane walls due to the tolerance in the rotation of interlocking blocks leading to reduction in torsional shear failure. Past studies show that as

the strength enhancement moves from structural level to element level, the damage resistance can be optimized up to satisfactory level. This depicts the better structural response of reinforced masonry over confined masonry in mortar-free interlocking structures.

3. Different connection mechanisms in structures and their role

Loo et al. (2014) [19] investigated the feasibility of using brake lining and abrasion resistant steel as center-plate in slip-friction connectors. The evaluation majorly focused on the hysteresis behavior of the connector having mild steel external plates and center plate of abrasion resistant steel. Symmetric connectors exhibited better performance in terms of maintaining strength, stiffness, and hysteretic stability over a large number of cycles. Based on the findings, the slip friction connector was recommended as an energy dissipation device for steel moment resisting frames and braced frames. Zheng et al. (2019) [20] proposed notched perfobond shear connector as an alternate to conventional perforation of reinforcing bar through multi-rib perfobond shear connector. The suggested methodology included the cutting out the edge of circular hole prior to installation of perforating rebars. The objective was to determine the failure mode, shear capacity and slip behavior of the shear connectors. In addition to experimental investigation, the study also included non-linear finite element analysis to determine the effects of variables like diameter, distance, number of the hole, cut width, perfobond thickness, strength of concrete and rebar, and diameter of rebar. It was found that diameter of hole, cut width, diameter and strength of rebar had minimal effect on the shear capacity. However, the by increasing the hole distance by 300%, the shear capacity increased by 30%. In addition, increasing the number of holes led to decrease in shear capacity. Fig. 2 shows moment resisting slip friction connector, shear connector and bolted connection.

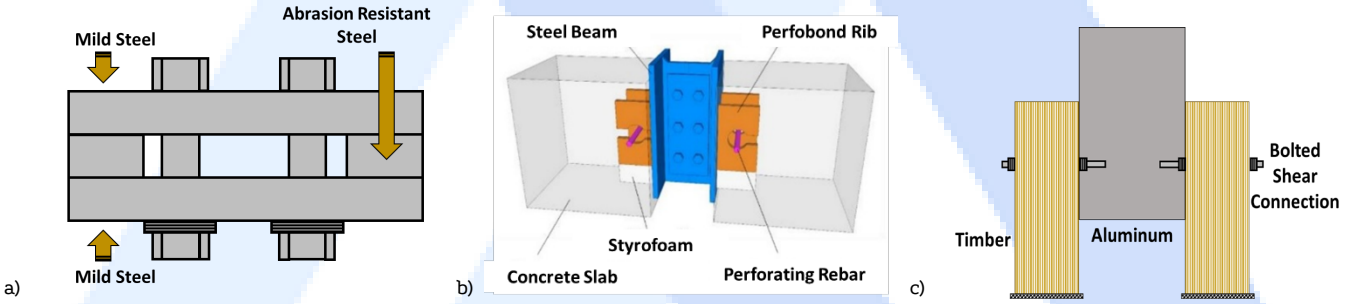

Figure 2. Types of connectors; a) slip-friction connector Loo et al. (2014) [19], b) notched shear connector Zheng et al. (2019) [20] and c) bolted connection Chybinski and Polus (2021) [21]

Leonetti et al. (2020) [22] experimentally and numerically investigated the clamping force of in-situ installed rivet connections in existing steel bridges. The bridges were serviceable from past 50 years and probability of imperfections and deterioration was higher. Rivet clamping force was found to be higher with increasing trend of grip length but this effect becomes less dominant due to imperfections. The lower inclination of clamping force was attributed towards mis-alignment of holes, eccentric head, hammering period and temperature profile. The mechanical and thermal behavior was well predicted by finite element model along with taking into account the grip length as a function of clamping force. The applicability of the conducted research was well aligned with the fatigue assessment of riveted connections. Chybinski and Polus (2021) [21] investigated bolted connection and screwed connection between aluminum beam and timber slab through push-out tests. Slip moduli, stiffness and load carrying capacity of connection were determined. Experimental output was compared with analytical results. A 10% decrease in ultimate load carrying capacity of composite beams with screwed connections was observed in comparison with bolted connections. In addition, 3% lower slip was observed in screwed connections than in bolted connections. By increasing the effective width of slab, a greater stiffness and lower deflection can be obtained in aluminum-timber composite beam.

4. Energy dissipation mechanism at joints/connections in structures

A major source of energy dissipation in interlocking structure is the sliding tolerance in masonry courses. Hossain et al. (2016) [23] investigated the frictional capacities of three types of interlocking brick surfaces through shear test. The comparison was made among bricks with dry surface, surface with linseed oil-based putty and surface with rubber foam tape. Brick surface with putty shows better coefficient of friction and seismic energy dissipation against both static and dynamic loading than other surfaces. However, dry surface had greater static friction coefficient than the dynamic friction coefficient. At higher pre-compression level, the panel were able to dissipate greater seismic energy. Wang et al. (2017) [24] investigated the seismic performance of confined masonry walls with conventionally constructed columns and confined masonry walls with precast interlocking block columns. The masonry infilled walls with interlocking block columns exhibited higher energy dissipation than infilled walls with conventional columns. In addition, the effect of over burden and wall openings on the lateral performance was reduced due to edge confinement. 11 experiments were performed to check the suitability of using concrete interlocking blocks for confining columns. After establishing the dominance of interlocking block columns over conventional columns for confinement, implementation of this technique was demonstrated through construction of 37 trial buildings. Table 1 shows different studies that demonstrate the mechanism of energy dissipation at joining locations.

Table 1. Performance of connection types at various joint locations

Reference	Connection Type	Joint Location	Structural System	Output
Hossain et al. (2016) [23]	Dry surface, surface with linseed oil-based putty and surface with rubber foam tape	Inter-brick joint	Interlocking brick masonry structure	Ability to dissipate seismic energy is greater in case of brick surface with putty than other surfaces.
Wang et al. (2017) [24]	Toothing connection	Wall-column joint	Confined masonry structure	Masonry infilled walls with interlocking block columns exhibited higher energy dissipation than infilled walls with conventional columns.
Chen et al. (2021) [25]	Self-locking moment connection	Beam-column joint	Modular steel structure	Energy dissipation in H-section beams was greater than HSS beams.
Gul et al. (2023) [18]	Toothing connection	Wall-column joint	Confined masonry structure	Average energy dissipation of dry stacked masonry was 50% greater than that of mortared confined masonry

Chen et al. (2021) [25] proposed an innovative self-locking inter-module connection at beam-column joint in a modular steel structure. Seismic behavior of connection types in the form of stiffness, ductility, energy dissipation and failure mode was investigated through cyclic tests. In addition, testing data was employed for a simplified finite element model for validation. The purpose of the study was to address the issue of limitations in installation of internal connections. Through analysis of hysteresis curves obtained from seismic tests, self-locking connection was found to be equally reliable in comparison to welded inter-module connection. The energy dissipation capacity of H-section beams was greater than HSS beams. Also, the rotational deformation was found to be less with greater moment transfer capacity as compared to plug-in self-lock joint and the rotary inter-module connection. The masonry infilled walls with interlocking block columns exhibited higher energy dissipation than infilled walls with conventional columns. Gul et al. (2023) [18] evaluated energy dissipation of a full-scale interlocking dry stacked masonry structure subjected to quasi-static loading. Energy dissipation in the form of slippage of interlocking blocks was observed at lower drift ratios that can be effective against lower to moderate earthquakes. The obtained energy absorption was 50% higher than a conventional mortared confined masonry structure.

5. Conclusions

Construction of mortar-free interlocking structures has gained a substantial admiration due to enhanced performance against seismic loading. However, the focus towards development of structural connections among various elements need detailed research program due to complexity at joints. In addition, complications may arise due to variety of interlocking block shapes. Thus, joint locations in mortar-free interlocking structures and connection types used in various structural systems have been reviewed and conclusions have been drawn in the light of energy dissipation mechanisms.

- Joint locations in mortar-free interlocking structures require adequate connecting mechanism with respect to block and joint geometry.
- The philosophy of shear and moment resisting connection design should be implemented to propose connections for mortar-free interlocking structures.
- The type of connection and its tolerance plays a crucial role in energy dissipation mechanism prior to failure.

Future researches should be oriented towards evolving the construction of mortar-free interlocking structures through comprehensive development of connections at various joint locations.

Acknowledgements

The authors would like to thank every person who supported in conducting this research.

Declaration of Conflict of Interests

The authors declare that there is no conflict of interest. They have no known competing financial interests or personal relationships that could have appeared to influence the work reported in this paper.

References

[1.] Agha, A., et al., *Modular construction in the United Kingdom housing sector: barriers and implications.* Journal of Architectural Engineering Technology, 2021. 10(2): p. 236.

[2.] Sarhosis, V., S. Garrity, and Y. Sheng, *Influence of brick–mortar interface on the mechanical behaviour of low bond strength masonry brickwork lintels.* Engineering Structures, 2015. 88: p. 1-11.

[3.] Shi, T., et al., *Experimental and numerical investigation on the compressive properties of interlocking blocks.* Engineering Structures, 2021. 228: p. 111561.

[4.] Shi, T., et al., *Experimental and numerical studies of the shear resistance capacities of interlocking blocks.* Journal of Building Engineering, 2021. 44: p. 103230.

[5.] Nasly, M. and A. Yassin. *Sustainable housing using an innovative interlocking block building system*. in *Proceedings of the Fifth National Conference on Civil Engineering (AWAM'09): Towards Sustainable Development, Kuala Lumpur, Malaysia*. 2009. Citeseer.

[6.] Thamboo, J.A., T. Zahra, and R. Dhanasekar, *Development of design methodology for mortarless masonry system: Case study–a resettlement housing colony*. Journal of Building Engineering, 2020. 27: p. 100973.

[7.] Li, J., et al., *Shear properties of a new type recycled aggregate concrete interlocking hollow block masonry with axial load*. Advances in Structural Engineering, 2021. 24(12): p. 2735-2747.

[8.] Gul, A., B. Alam, and K. Shahzada, *Seismic performance evaluation of unconfined dry stacked block masonry structure*. Engineering Structures, 2022. 265: p. 114529.

[9.] Kasinikota, P. and D.D. Tripura, *Flexural behavior of hollow interlocking compressed stabilized earth-block masonry walls under out-of-plane loading*. Journal of Building Engineering, 2022. 57: p. 104895.

[10.] Di Benedetto, S., et al., *Seismic behaviour of steel Moment Resisting Frames with traditional and innovative connections*. Procedia Structural Integrity, 2023. 44: p. 1901-1908.

[11.] Lan, G., et al., *Seismic performance of interlocking compressed-earth block composite walls*. Composite Structures, 2023: p. 116704.

[12.] Zahra, T. and M. Dhanasekar, *Characterisation and strategies for mitigation of the contact surface unevenness in dry-stack masonry*. Construction and Building Materials, 2018. 169: p. 612-628.

[13.] Dorji, S., et al., *Behaviour and material properties of versaloc semi-interlocking mortarless masonry*. Materials and Structures, 2023. 56(1): p. 17.

[14.] Sokairge, H., A. Rashad, and H. Elshafie, *Behavior of post-tensioned dry-stack interlocking masonry walls under out of plane loading*. Construction and Building Materials, 2017. 133: p. 348-357.

[15.] Imai, H., et al., *A full-scale shaking table test on philippine concrete hollow blocks (Chb) masonry houses*. Journal of Disaster Research, 2015. 10(1): p. 113-120.

[16.] Joyklad, P. and Q. Hussain, *Axial compressive response of grouted cement–clay interlocking hollow brick walls*. Asian Journal of Civil Engineering, 2019. 20: p. 733-744.

[17.] Xie, G., et al., *Response of reinforced mortar-less interlocking brick wall under seismic loading*. Bulletin of Earthquake Engineering, 2022. 20(11): p. 6129-6165.

[18.] Gul, A., et al., *Improving seismic capacity of dry stacked interlocking masonry structure through confinement at corners*. Soil Dynamics and Earthquake Engineering, 2023. 165: p. 107710.

[19.] Loo, W.Y., P. Quenneville, and N. Chouw, *A new type of symmetric slip-friction connector*. Journal of Constructional Steel Research, 2014. 94: p. 11-22.

[20.] Zheng, S., et al., *Experimental and numerical study on shear resistance of notched perfobond shear connector*. Materials, 2019. 12(3): p. 341.

[21.] Chybiński, M. and Ł. Polus. *Experimental and numerical investigations of aluminium-timber composite beams with bolted connections*. in *Structures*. 2021. Elsevier.

[22.] Leonetti, D., et al., *Rivet clamping force of as-built hot-riveted connections in steel bridges*. Journal of Constructional Steel Research, 2020. 167: p. 105955.

[23.] Hossain, M., Y. Totoev, and M. Masia. *Friction on mortar-less joints in semi interlocking masonry*. in *Proc. 16th International Brick and Block Masonry Conference (IBMAC 2016) Padova (Italy)*. 2016.

[24.] Wang, G., et al., *Testing and modelling the in-plane seismic response of clay brick masonry walls with boundary columns made of precast concrete interlocking blocks*. Engineering Structures, 2017. 131: p. 513-529.

[25.] Chen, Z., et al., *Seismic behavior and moment transfer capacity of an innovative self-locking inter-module connection for modular steel building*. Engineering Structures, 2021. 245: p. 112978.

A Review on Different Materials Composition of Engineered Cementious Composites, Micromechanics and Structural Applications

Amaan Sikandar*,[1], Majid Ali[2]
[1]Capital University of Science and Technology, Islamabad, Pakistan.
[2]Capital University of Science and Technology, Islamabad, Pakistan.
Corresponding Author E-mail:amaan.sikandar@gmail.com, majid.ali@cust.edu.pk

Keywords

Theoretical,
Theoretical,
ECC,
Bendable composite,
Polymer Fiber,
Strain Hardening,
Multiple cracking,
ECC material,
ECC applications.

Abstract

Concrete, a commonly used material in construction, has limitations such as brittleness, low tensile strength, and shrinkage cracks, which impact its sustainability. These limitations result in a brittle failure mechanism under load, highlighting the need for alternative solutions to enhance durability and address these challenges. Engineered Cementious Composite (ECC) is a fiber-reinforced concrete with high ductility, strain-hardening behavior, and multiple fine fractures. It offers improved impact strength and self-healing properties, making it a valuable material for enhancing structural performance. This study explores the application of bendable composite or engineered cementious composite (ECC) in building, transportation, and water resources infrastructure. Different researches from the developed countries has been studied and the parameters for the bendable composite are identified. It aims to provide insights for developing countries to produce and use ECC with local materials effectively in their infrastructure projects.

1. Introduction

Sustainability in construction is requirement of this modern time. Concrete being a material used widely in development has some flaws which puts a limit on its utilization and durability. Concrete used in construction has certain flaws like brittleness, weakness in tension and shrinkage cracks formation. Concrete exhibits brittle failure mechanism under load due to low tensile strength [1]. Concrete can have synthetic and polymer fibres added to it at specific ratios to increase the vital ductility behavior. Bendable composite also called ECC engineered cementious composite are fiber-reinforced composites with strain hardening behavior and multiple fractures development [1-2]. ECC may reach a strain capability of 3% and a fracture width under 100 micrometer in tension stress with correct micromechanics-based design, which gives structures remarkable ductility and robustness [1]. Many nations, including those in North America, Asia, Australia, Europe, South America, and South Africa, have created, developed, and deployed a variety of ECC mix designs in different structural elements [3].

Bendable composite or ECC consists in a classification of fiber reinforced composites that has high tensile strength and resilient tensile properties with many fine fractures of width less than 100 micrometer, then concrete having one large crack. Due to its outstanding strain-hardening capabilities and high mechanical performance, fibre reinforced cementious composites are frequently used to prevent the spread of fractures and reduce the brittle fracture of traditional cementious composites [2]. ECC has ability to heal these small cracks, when it comes in contact with water and air [3] [4]. Subjected to tensile and bending loads, typical ECC displayed good energy dissipation capability and formed a considerable number of fine fractures [5]. ECC, a specific class of fiber reinforced cementious composites, have been developed to increase the impact strength of structural materials [6]. The number and breadth of the crack, which distinguish the various cracking procedures of ECCs, are highly correlated with the higher flexibility and durability of ECC.

Local materials are favored for BC or ECC in large scale applications for both structure performance and economic reasons. In Germany and Brazil, ECCs made from regional raw materials and PVA fibres have been created successfully. ECCs made using local PVA fibers were also studied in China. Mechanical qualities and cost management, however, are still unacceptable. Hence, a better alternative fibre option has to be created. BC or ECC has been prepared with different material composition and fiber types. There have been several attempts to replace all or a portion of PVA fibres with less expensive synthetic fibres like polyethylene (PE), polypropylene (PP) and polycrylonitrile (PAN) fibres. Finding substitute fibers is crucial since the widespread use of ECC has been greatly constrained by the material performance and high cost of PVA fibers [11].

ECC application has been reported in three different types of infrastructure i.e Building infrastructure, Transportation and Water Resources infrastructure. Issues in Building, Transportation and water resources infrastructure are resolved using different qualities of ECC material [21]. This study is focused on the emerging new material that is bendable composite or engineered cementious composite with in the developed countries and how the developing countries can produce this material. Different papers have been studied in which ECC has been reported. BC or ECCs behavior, micromechanics design and its criteria's, along with the material used by the developed countries and followed by the practical applications in different infrastructure. The knowledge can be utilized by the developing countries for producing the bendable composite and utilizing it for solving various issues in different infrastructure projects.

2. Nature of BC and NC

Concrete has traditionally been used by structural engineers to support compressive loads. However in actual field circumstances, loads and environmental factors like shrinkage, chemical deterioration, and heat impacts can predispose concrete to tensile stresses. Concrete's tensile strength is only 10% as strong as its compressive strength. The fundamental drawback of concrete is that it is brittle, which leads to damage, degradation, and cracking, and necessitates frequent repair of the structural parts [7]. A composite known as bendable concrete or engineered cementious composite, which has properties with strain hardening effect of the reinforced fibre, is developed when synthetic polymer fibre from the textile industry of high tensile strength is combined with concrete ingredients less coarse aggregates, along with fly ash and super plasticizer. The composite is exceptionally durable, capable of self-healing, and highly resistant to shrinking, impact, and fire resistant [6]. Traditional concrete is limited in its ability to withstand tensile stresses due to its brittleness, leading to damage and frequent repairs. A

composite material called bendable concrete or engineered cementitious composite, combining high-tensile-strength synthetic polymer fibers with concrete ingredients, offers improved durability, self-healing properties, and resistance to shrinking, impact, and fire.

Bendable composite or (ECC) are fiber-reinforced materials with strain hardening behavior and multiple fracture development [8].ECC may reach a strain capacity of above 3\% and a fracture width under 100 um in tension with suitable micro mechanics-based design criteria. Due to their outstanding strain-hardening capabilities and high mechanical performance, fibre reinforced cementious composites have been widely used to stop the spread of fractures and reduce the brittle fracture of conventional cement-based materials [9]. Fibres are placed into concrete, which has great impact and abrasion resistance, to reduce cracking caused by dryness and plastic shrinkage [10]. The tensile strength of ECCs is approximately (4:12) MPa, and the range of the midpoint beam deflection is (4:7) mm. When compared to a regular concrete mix, it has a higher resistance to freeze-thaw [12]. Bendable composite materials, such as fiber-reinforced ECC, offer high strain capacity and narrow fracture widths, making them effective in preventing crack propagation and reducing brittleness in cement-based materials. By incorporating fibers, they improve impact resistance, reduce cracking, and exhibit enhanced freeze-thaw resistance compared to regular concrete mixes. Fig 1 shows the brittle nature of normal concrete, tension softening of FRC and strain hardening nature of ECC.

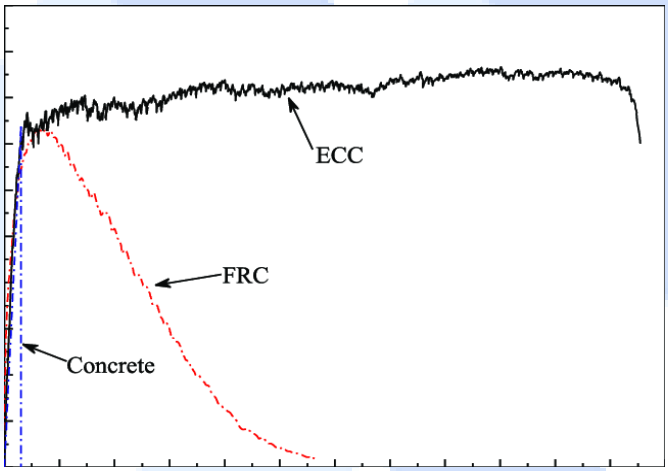

Figure 1. Tensile stress-strain curves of strain-hardening ECC, tension-softening FRC, and quasi-brittle concrete [11].

2.1. Bendable Composite Micro-Mechanics

To ensure crack initiation at multiple locations, the maximum fiber-bridging strength must be greater than the matrix rupture strength, while the complementary energy of the bridging fiber must surpass the peak of the crack toughness to ensure steady-state condition multiple cracking. These requirements are outlined in the ECC pseudo strain hardening criteria [3-12, 16-20]. According to the strength requirement, the ultimate crack-bridge stress must be greater than the matrix initial cracking strength. The energy criteria states that the fracture tip toughness of the matrix should be outperformed by the fibre bridging complementary energy. Fig 2 represents load crack opening relation of fiber reinforced ECC The likelihood of creating new fractures in an ECC specimen is more favorable with a higher bridging energy value [20-22]. Micro-crack initiation from flaw happens at cracking strength, and steady-state flat crack growth happens at steady-state stress. Multiple cracking occurs when both the strength conditions are satisfied, as seen by the ECC's tensile strain hardening effect presented in Fig 2. The ECC pseudo strain hardening characteristic state that maximum fiber bridging capacity strength must surpass the matrix rupture strength while the complementary energy of bridging fiber should surpass the peak of the crack toughness. ECC materials demonstrate a tensile strain hardening effect through multiple cracking when these strength conditions are met.

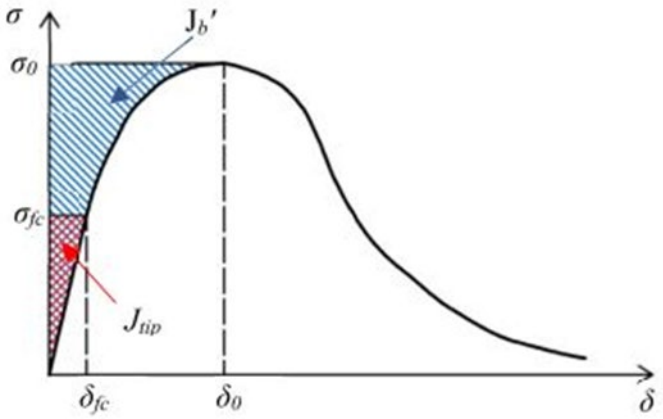

Figure 2. Represents the Stress vs crack opening relationship of bridging fibers in ECC [3]

2.2. Cracking Phenomena

Multiple cracks in steady state condition that develop after starting within fault locations and extending in the matrix under continuous ambient load—are reasoned for the ECC tensile behavior of strain-hardening [2-3]. The energy added from external effort less the energy of the fiber-bridging, which is referred to as the complementary energy of fiber-bridging. The need for steady-state cracking, according to physical interpretation, is that the system's net available energy be adequate to overcome the fracture tip toughness for indefinite crack expansion at an uninterrupted ambient load [5-7]. Another crucial requirement for the development of numerous steady state fractures in ECC is that the composites tensile fracturing strength must be larger than the fiber-bridging strength [18]. A strength-based crack formation criterion makes sure that fractures can start from a variety of rupture locations whereas the steady-state condition fracturing specifies the mechanism of crack propagation [9-10].

The addition of various fibre kinds and sizes can have various inhibitory impacts on the spread of fractures in concrete. When steel and polymer fibres were combined to create ECC, some researchers discovered that the hybrid fibres' synergistic impact allowed ECC to achieve substantially smaller fracture widths and less drying shrinkage [11]. Inner pores and the interaction among sand and cement mix in ECC are the main contributors to crack start and growth [14]. As the mid-crack gap expands endlessly with crack length in this crack development mode, fibres farther from the fracture tip can be dragged out or shatter. This phenomenon has the immediate effect of requiring an ambient load drop to maintain balance as the fracture widens, causing the material's sensitivity to strain to soften. The depletion of bridging fibres caused by the whole path of the propagating fracture will reduce the composite's ability to support loads. This crack propagation method, also known as Griffith form crack propagation, is undesirable for repeated cracking because it causes the specimen to continuously unload (soften) after a matrix first crack appears [15].

For cemetitious composites reinforced with fibres, a different flat crack growth pattern is proposed. In this pattern, the fracture is largely flat with a constant opening for cracks under a stable ambient load, with the exception of a tiny area around tip of the crack. This flat cracks mode beats the Griffith fracture propagation mode, if the following condition is satisfied: When a crack starts at a defect site, the maximal complimentary energy is necessary to surpass the matrix toughness for the flat crack development mode to must win over the Griffith crack development mode. This may be accomplished by restricting the matrix toughness, which is controlled by the matrix's material composition. For the ECC matrix, these considerations offer design recommendations. Alternately, raising will also encourage the spread of flat cracks and consequent multiple cracking. Standards of design for the fibre and ECC interface are provided by this factor. For this, a deeper comprehension of the stress crack opening connection is required [18-22].

3. Materials used in ECC and Normal Concrete

For producing plain cement composite (PC), OPC cement along with sand locally available and portable tape water are used. While making bendable composite OPC cement, Fly ash, Sand, Super plasticizer and portable water are used along with synthetic polymer fibers. When cracking begins in the matrix (post-cracking area), fibre crack bridging, which includes crack limiting and crack stabilization, becomes the principal role of the fibres in the matrix [12].ECC reinforced with PVA fibres having a tensile strength 1,600 MPa produced a tensile value of 4.5 MPa and tensile strain value of more than 4%. In contrast to PE fibres, which have a tensile strength in the range of 2500–3800 MPa, PVA fibres have a comparatively low tensile strength of 800-1600 MPa. Due to the high tensile strength, elastic modulus, and hydrophobic properties of PE fibers—all of which are crucial for the structural reliability performance—PE-ECC produces more robust tensile ductility than PVA-ECC, with a tensile strain capacity of over 4% [16-18]. The different material combinations which are used in different studies for making of ECC are represented in table 1.

The performance of the fibre and matrix interfaces determines the characteristics of ECC composites. The fibre component of ECC serves as coarse aggregate in part and boosts ductility by bridging crack forms. Recron 3s, a polyester fibre, was utilized in ECC, and it was discovered that it eliminates shrinkage cracks, hence reducing moisture infiltration. It produces homogeneous concrete, enhancing its capacity to absorb

more energy while also improving its mechanical characteristics, ductility, and flexural strength. Further research revealed that the steel, carbon, glass, and polyethylene (PE) fibres are also used in ECC as represented in Table 1. Because coarse aggregate is totally neglected in this composition, the part of powdered content is considerably larger than that of typical concrete. In order to make the paste for creating ECC concrete, several pozzolanic ingredients were added to cement in order to enhance powder content. Numerous studies were done to assess how well ECC combined with various mineral admixtures performed. Table 2 lists the different mineral admixture types and their impact on ECC.

Table 1. Different material composition used for ECC

Ref	Fiber/Length	Fiber Tensile Strength	Cement	Fly ash	Sand	Superplasticizer	W/B Ratio
[1]	PVA/ 12mm	950 MPa	OPC	Class F	Silica Sand	Polycarboxlate SP	0.30
	PET/ 12mm	900 MPa					
[2]	Steel/30mm	1570 MPa	OPC	-	Normal Sand	Polycarboxlate SP	0.35
[5]	PE/ 12mm	3000 MPa	OPC	Class F	Silica Sand	Polycarboxlate SP	0.30
[6]	PVA/ 12mm	1560 MPa	OPC	Class F	Silica sand	Polycarboxlate SP	0.28
[7]	PVA/ -	-	OPC	Class F	Silica sand	Polycarboxlate SP	0.30
[9]	PE/ 18mm	2400 MPa	OPC	-	Silica sand	Polycarboxlate SP	0.30
[11]	PE/ 12 mm	3000 MPa	OPC	Class F	Silica sand	Polycarboxlate SP	0.24
	Steel/ 13mm	2850 MPa					
[13]	PE/ 18mm	2900 MPa	OPC	Class F	Silica Sand	Polycarboxlate SP	0.32
[14]	PE/ 6mm	3000 MPa	OPC	Class F	Silica Sand	Polycarboxlate SP	0.26
[15]	PE/ 13mm	3200 MPa	OPC	-	Silica Sand	Polycarboxlate SP	0.38
[16]	PE/ 6mm	3000 MPa	OPC	Class F	Quartz sand	Polycarboxlate SP	0.26
[17]	PE/ 18mm	3000 MPa	OPC	Class F	Silica sand	Polycarboxlate SP	0.20
[18]	PVA/ 12mm	1631 MPa	OPC	Class F	Silica sand	Polycarboxlate SP	0.42
[22]	PVA/ 8mm	1620 MPa	OPC	Class F	Silica sand	Polycarboxlate SP	0.27
[23]	Basalt/ 9mm	2230 MPa	OPC	Class F	-	Polycarboxlate SP	0.20
[24]	PVA/ 8mm	1600 MPa	OPC	Class C	Silica sand	Polycarboxlate SP	0.25
[25]	PE/ 12mm	3000 MPa	OPC	-	Silica sand	Polycarboxlate SP	0.35
[26]	PE/ -	3000 MPa	OPC	Class F	Silica sand	Polycarboxlate SP	0.32
[27]	PVA/ 8mm	1600 MPa	OPC	Class F	Silica sand	Polycarboxlate SP	0.11
[28]	PVA/ 8mm	1600 MPa	OPC	Class F	River sand	Polycarboxlate SP	0.32

Table 2. Mineral admixtures types used in ECC

Reference	Mineral admixture type	Observation
[1,5,6,7,11,13,14,16,17 18,18,22,23,26,27,28]	Fly Ash Class F	increases the toughness, ductility, and workability
[9,15,25]	Silica Fume (SF)	Improve mechanical properties and Durability
[9]	(GGBS) Slag	Reduced permeability, increased toughness, Long term strength and reduced hydration Heat.

4. Application of ECC in Structural Elements

Without practical uses for the material, the making of Engineered Cementious Composites (ECC) would fall short. Applications for the field have several uses. First, it offers the chance to link fundamental material properties—in particular, the high tensile strain ductility of ECC—to improved structural performance. Second, field applications demonstrate the value of ECC's special qualities, which are not possible with regular concrete. Third, practical experience with ECC in structures offers a feedback channel for further material development and improvement.

Several large-scale applications in Japan, China Korea and the US in structural elements and problem solving. Some of the applications are listed in Table 3 below.

Table 3. ECC applications in infrastructures, [21].

Infrastructure	Application	Issue Solved	Property Utilized	Process Method
Building	Building Core Coupling Beams	ECC's damage tolerance enables rapid recovery from seismic occurrences while also reducing the need for repairs and replacements, cutting down on installation costs and time, and increasing useable floor space.	Damage tolerance, tensile ductility, energy absorption under stress, and fire resistance	manufactured precast
	External walls insulation	comply with governmental energy regulations; Reduce the cost, time, and labor of building Reduce the possibility of uneven building quality on the job site.	Resistance to drying and heat cycles	manufactured precast
	Retrofit of External walls to prevent concrete spalling	Reduce the likelihood of falling debris and the associated responsibility; accelerate retrofit; and increase reliability. Decrease installation time, weight, labor, and installation equipment.	durability in tropical climates and along coasts; capacity to hold spalling Crack resistance without steel reinforcement	Hand troweling at the spot
	Modular housing	Reduce the frequency and expense of maintaining the bridge deck; quiet down the traffic	Narrow crack width, tensile ductility to accommodate heat deformation, fatigue resistance, and wear resistance.	manufactured precast
Transportation	Retrofits to the bridge deck and the link slabs on the roads	Reduce the possibility of steel deck fatigue failure. Reduce the price and weight.	Tensile strength and fatigue resistance	Precasting or casting in situ
	Composite bridge deck	Reduce costs and labor. Reduce maintenance needs	Water tightness, carbonation resistance, freeze-thaw resistance, and tensile ductility	casting in situ
	Tunnel linings repair and retrofit	Extended service life and less chance of dam leaking	Water tightness; resistance to cracking and spalling	Spraying
	Retrofit of Mitakadam	Reduced chance of reflective cracking; lessening of water leakage	Tensile ductility Water tightness	Spraying
Water Resources	Repair of dam of hydraulic power plant	Prevent water loss; Reduce Maintenance frequency and cost	Water tightness; resistance to cracking and spalling	Spraying

	Irrigation channel repair	Hand troweling; spraying

5. Conclusions

Bendable Composite or ECC exhibits superior pseudo ductile behavior compared to normal concrete due to multiple cracking phenomena and resilient strain hardening nature. Single brittle crack in concrete is replaced my multiple small cracks which dissipates the energy in steady condition. ECC provides crack-resistant concrete for use in structural applications. Bendable composite is a fantastic material to employ in the construction sector due to enhanced mechanical qualities of concrete, which the normal concrete can doesn't have. The following findings are drawn in light of the assessment of the ECC concrete study:

- Utilization of ECC in flexural elements of all categories improved the load taking capacity and fracture performance. Flexural members composed of ECC exhibited enhanced ductility and dissipation of energy which were exceptionally excellent then conventional concrete.
- Bendable composite materials, like fiber-reinforced ECC, are effective in preventing crack propagation and reducing brittleness in cement-based materials.
    - The ECC tensile behavior of strain hardening is achieved through the development of multiple steady-state cracks.
    - The energy input exceeds the stored energy in fiber-bridging, and the composite's tensile fracturing strength must be greater than the fiber-bridging strength.
- For ECC concrete, PVA fibre is typically chosen. But the outcomes of other fibres, such those made of steel, glass, and (PE), are equivalent to those of PVA fibres. Because of strain hardening tendency of beams upon loading, fibre dosages within 1.5% and 2.0% had demonstrated greater flexural strength performance and ductility.
- ECC exhibits superior performance in buildings, transportation and water resources infrastructures. Various problems are solved through utilization of ECC qualities in terms of ductility, toughness, strain hardening behavior and durability.

The developing countries can utilize this emerging material properties to solve different issues. From materials prospective ECC made from local material is encouraged if the matrix exhibits behavior of similar nature. The tensile properties enhancement of concrete is mostly preferred. ECC application has predominantly been studied in large-scale infrastructures, while its presence in small-scale projects remains limited.

Nomenclature

BC: Bendable Composite
ECC: Engineered Cementious Composite
PVA: Poly vinyl alcohol
PE: Poly Ethylene

Declaration of Conflict of Interests

The authors declare that there is no conflict of interest. They have no known competing financial interests or personal relationships that could have appeared to influence the work reported in this paper.

Acknowledgement

The authors would like to thank all who helped in the literature research.

References

[1.] C. Lu, Z. Hao, H. Chu, Z. Lu, Investigation on performance of engineered cementitious composites (ECC) based on surface modification of PET fibers using graphene oxide (GO) and polydopamine (PDA). Construction and Building Materials 368(2023)130343.

[2.] K.Zhang, Q. Yaun, T. Haung, S. Zuo, H. Yao. Utilization of novel stranded steel fiber to enhance fiber–matrix interface of cementitious composites. Construction and Building Materials 369(2023)130525.

[3.] J. Li, J. Qiu, J. Weng, E. Yang. Micromechanics of engineered cementitious composites (ECC): A critical review and new insights. Construction and Building Materials 362(2023)129765.

[4.] R. Sun, L. Han, H.Zhang. Z. Ge, Y. Gaun, Y. Ling, E. Schlangen, B. Savija, Fatigue life and cracking characterization of engineered cementitious composites (ECC) under flexural cyclic load Construction and Building Materials 335(2022)127465.

[5.] H. Zhou, J. Wu, X. Wang, Y. Chen, X. Du, S. Yu. Performance of engineered cementitious composite (ECC) monolithic and composite slabs subjected to near-field blast. Engineering Structures 279(2023)115561.

[6.] M. Chen, Y. Wang, T. Zhang, M. Zhang. Behaviour of structural engineered cementitious composites under dynamic tensile loading and elevated temperatures. Engineering Structures 280(2023)115739.

[7.] Z. Hao, C. Lu, Z.Li. Highly accurate and automatic semantic segmentation of multiple cracks in engineered cementitious composites (ECC) under dual pre-modification deep-learning strategy. Cement and Concrete Research 165(2023)107066.

[8.] B.T. Haung, J.X. Zhu, K.F Weng, V.C Li, J.G Dai. Recent developments in Engineered/Strain-Hardening Cementitious Composites (ECC/SHCC) with high and ultra-high strength. Construction and Building Materails 129(2022)14464.

[9.] K. Yu, M. Lin, L. Tian, Y. Ding. Long-term stable and sustainable high-strength engineered cementitious composite incorporating limestone powder. Structures 47(2023)530-543.

[10.] S.Qian, J. Zhou, M.R Rooij, E. Schlangen, Breugel. Thangaraj, B. Shanmugam. Self-healing behavior of strain hardening cementitious composites incorporating local waste materials. Cement and Concrete Composites 31(2009)631-621.

[11.] D. Liu, J. Yu, F. Qin, K. Zhang, Z. Zhang. Ultra-high-strength engineered/strain-hardening cementitious composites (ECC/SHCC): Material design and effect of fiber hybridization Cement and Concrete Composite 18(2023) e01961.

[12.] H. Zhong, M. Chen, M. Zhang. Engineering properties of sustainable engineered cementitious composites with recycled tyre polymer fibres. Construction and Buildibg Materials 370(2023)130672.

[13.] M. Hou, D. Zhang, V.C. Li L. Li, D. Tan, M. Uddin, Z. Cai, K. Yu. Crack width control and mechanical properties of low carbon engineered cementitious composites (ECC). Construction and Buildibg Materials 348(2022)128692.

[14.] B. Zhu, J. Pan, M. Zhang, C, Leung. Predicting the strain-hardening behaviour of polyethylene fibre reinforced engineered cementitious composites accounting for fibre-matrix interaction. Cement and Concrete Composites 134(2022)104770.

[15.] J. Choi, S. Park, Y. Kim, K. Yang, Y. Kim, B. Lee. Highly ductile behavior and sustainability of engineered cementitious composites reinforced by PE based selvage fibers. Cement and Concrete Composites 134(2022)104729.

[16.] B. Zhu, J. Pan, J. Li, P. Wang, M. Zhang. Relationship between microstructure and strain-hardening behaviour of 3D printed engineered cementitious composites. Cement and Concrete Composites 133(2022)104677.

[17.] L. Xu, B. Haung, Q. Ping, J. Dai. Enhancing long-term tensile performance of Engineered Cementitious Composites (ECC) using sustainable artificial geopolymer aggregates. Cement and Concrete Composites 133(2022)104676.

[18.] V.C. Li, T. Horikoshi, A. Ogawa, S. Torigoe, T. Saito. Micromechanics-Based Durability Study of Polyvinyl Alcohol-Engineered Cementitious Composite. ACI Material Journal (2004)101-M27.

[19.] V.C. Li. Introduction to Engineered Cementitious Composites (ECC) Chaptar 1 . Springer-Verlag GmbH Germany, part of Springer Nature 2019.

[20.] V.C. Li. Micromechanics and Engineered Cementitious Composites (ECC) Design Basis Chaptar 2. Springer-Verlag GmbH Germany, part of Springer Nature 2019.

[21.] V.C. Li. Applications of Engineered Cementitious Composites (ECC) Chaptar 9. Springer-Verlag GmbH Germany, part of Springer Nature 2019.

[22.] M. Sahmaran, E. Ozbay, H. Yucel, M. Lachemi, V.C. Li. Frost resistance and microstructure of Engineered Cementitious Composites: Influence of fly ash and micro poly-vinyl-alcohol fiber. Cement & Concrete Composites 34(2012)156-165.

[23.] M. Xu, S. Song, L. Feng, J. Zhou, H. Li, V.C. Li. Development of basalt fiber engineered cementitious composites and its mechanical properties. Construction and Building Materials. 266(2021)121173.

[24.] T. Wang, D. Zhang, H. Zhu, B. Ma, V.C. Li. Durability and self-healing of engineered cementitious composites exposed to simulated sewage environments. Cement and Concrete Composites 129(2022)104500.

[25.] B. Ye, H. Wang, Y. Ma, P. Pan. Seismic performance of flexure-dominated reinforced-engineered cementitious composites coupled shear wall. Engineering Structures 272(2022)114992.

[26.] B. Deng, D.Tan, L. Li, Z. Zhang, Z. Cai, K. Yu. Flexural behavior of precast ultra-lightweight ECC-concrete composite slab with lattice girders. Engineering Structures 279(2023)115553.

[27.] H. Qian, Z. Li, J. Pei, L Kang, H. Li. Seismic performance of self-centering beam-column joints reinforced with superelastic shape memory alloy bars and engineering cementitious composites materials. Composite Structures 294(2022)115782.

[28.] S. Subedi, G. Arce, M.M. Hassan, M. Barbato, L.N. Mohammad, T. Rupnow. Feasibility of ECC with high contents of post-processed bagasse ash as partial cement replacement. Construction and Building Materials 319(2022)126023.

PACE-2023
International Congress on the Phenomenological Aspects of Civil Engineering

PACE-2023
International Congress on Phenomenological Aspects in Civil Engineering

Research Article
20-23 June 2023

Enhancing Mechanical Properties of Limestone Aggregates through Pasta Cement Coating

Edward Ngii[*,1], La One[2], Adris Ade Putra[3], Munansar[4]
[1,2,3,4] *Civil Engineering, Engineering Faculty, Universitas Halu Oleo, Kendari-Indonesia*
Corresponding Author E-mail: edward.ngii@uho.ac.id

Keywords

Limestone,
Aggregates,
Mechanical properties,
Pasta cement,
AIV,
Abrasion.

Abstract

Limestone is abundant in the archipelago and coastal regions of Indonesia, but its utilization as an aggregate is limited due to its low mechanical properties, restricting it to lightweight and simple construction applications. This study investigates the impact of coating on the mechanical properties of limestone aggregates after being covered with pasta cement. The limestone samples are crushed and filtered using various sieve sizes. The coating process, utilizing a water/cement ratio of 0.5, involves a 60-minute soaking period followed by 24 hours of drying. Abrasion testing (SNI 03-2417-1991) and Impact testing (BS 812: part 3: 1975) are conducted to evaluate the abrasion value and Aggregate Impact Value (AIV) after immersion. The results indicate a notable decrease in the abrasion value from 41.66% to 38.47% and the AIV value from 23.06% to 22.65%. These findings demonstrate the potential of pasta cement coating to enhance the strength of limestone aggregates, making them more suitable for diverse construction applications, particularly in coastal areas of Indonesia.

PACE-2023
International Congress on the Phenomenological Aspects of Civil Engineering

PACE-2023
International Congress on Phenomenological Aspects in Civil Engineering

Research Article
20-23 June 2023

Development of Effective Technique for Recycling Waste Plastic for Sustainable Building Products

Aaroon Joshua Das*,[1], Majid Ali[2]
[1]Ph.D. student, Department of Civil Engineering, Capital University of Science and Technology, Islamabad, Pakistan
[2]Professor, Department of Civil Engineering, Capital University of Science and Technology, Islamabad, Pakistan
Corresponding Author E-mail: ajodas@yahoo.com

Keywords

Waste plastic, Recycling, Construction.

Abstract

Thermoplastics are a set of materials that are in production with shortsightedness. Plastic is inert and durable; improper disposal after use accumulates and produces waste for water, land, and air. Many formulations are under speculation in the literature that entangles the reuse of plastic for sustainable development. The production of plastic is more than 400 million tons of plastic yearly. These stats require efficient recycling of plastic techniques for usage on a large scale. The overall aim of the research program is to recycle waste plastic and to produce products for the construction industry. The construction industry already has an appetite for large-scale material consumption. Conversely, the sector requires that the materials match the strengths and toughness standards. Previous studies indicate the possible use of waste plastic in pavement, concrete, and other products. The only problem is that the utilization index is minor. This study presents a work in process, with an efficient technique for recycling waste plastic for construction products. Studies are required to assess further the viability of recycled waste plastic for construction products, which shall target low-cost and lightweight housing.

1. Introduction

Virgin plastic in the construction industry accounts for only 19.70% of the materials utilized. Plastic creates panels, ceilings, doors, and other finishing items. However, the construction industry relies on various materials for load-bearing structural and aesthetic purposes. Plastic in construction is not so popular and typical for its aesthetic appeal, while materials like steel and concrete are for structural integrity. Ongoing efforts in research are to explore using plastic waste as fine aggregate in concrete composites. However, it is important to note that this approach does not significantly enhance the strength of the mixture; instead, it replaces a small portion, typically around 1 to 5% [1]. Other research highlights the potential use of waste plastic in pavement construction [2]. Despite these promising findings, the industry is still in the early stages of developing complete models for large-scale utilization of plastic waste. Therefore, raising societal awareness and considering the cost implications are crucial to encourage further exploration and reduce plastic waste in construction.

However, addressing potential challenges and concerns associated with using plastic waste in construction is essential. One such concern is plastic-based building materials' long-term durability and structural integrity. Extensive research and testing are necessary to ensure that the incorporation of waste plastic does not compromise the strength and stability of the constructed elements. Furthermore, it is crucial to establish proper guidelines and standards for collecting, sorting, and processing plastic waste to ensure its suitability for construction applications. Addressing these challenges through rigorous research, development, and collaboration among industry stakeholders will pave the way for a more sustainable and responsible use of plastic waste in the construction sector[3].

Additionally, plastic exhibits intriguing properties such as chemical inertness, making it resistant to external exposure. The production of plastic waste in different sectors results in various stages of contamination, leading to a significant environmental impact. By utilizing waste plastic, we reduce the burden on landfills and promote an incentivized circular economy. The significance of these efforts extends beyond waste management, as they can provide housing units for impoverished populations[4]. However, addressing the challenge requires a structured plan developed through comprehensive research. This plan should encompass the entire process, from the efficient collection at disposal points to synthesis, while addressing practical usage concerns related to strength and durability.

The increasing need for housing in major cities attributes to rapid urbanization. Many economically disadvantaged individuals resort to informal settlements due to the high house construction cost. The limited availability of inexpensive materials in the market further exacerbates the situation. However, reusing old materials offers a viable solution to reduce construction costs for building units significantly. Another factor to consider is the abundance of locally available materials. The accumulation of waste plastic reaching alarming levels presents a promising option to address housing needs. Attempt are being continued to employ recycling of waste plastic to produce building products such as rebars etc., [5].

By repurposing waste plastic as a construction material, we can divert a significant amount of plastic from ending up in already overburdened landfills. This analogy addresses the waste management issue and contributes to the conservation of natural resources. Plastic waste, when properly processed and incorporated into construction materials, can extend the material's lifespan and reduce the need for virgin resources. This sustainable approach aligns with the principles of a circular economy, where reusing, recycling, and reintegration into the production cycle makes resources valuable. This will minimize waste and environmental impact. Moreover, using waste plastic in construction can have positive social implications. In many regions, impoverished communities face a lack of adequate housing options. By incorporating waste plastic into affordable housing projects, we can provide a viable solution that meets the housing needs of these populations. The lower cost of using waste plastic as a construction material can make housing more accessible and affordable, particularly for economically disadvantaged individuals[6].

The literature discusses various formulations that explore the potential reuse of plastic for sustainable development. With plastic production is exponentially increasing annually [7], there is a pressing need for effective large-scale plastic recycling techniques. The research program aims to address this by recycling waste plastic and producing construction products. The construction industry, known for its substantial material consumption, seeks materials that meet standards of strength and durability. Previous studies have suggested the possible utilization of waste plastic in pavement, concrete, and other construction products [8]. However, the current utilization rate remains low. This study focuses on review of an ongoing effort to develop an efficient technique for recycling waste plastic into construction products. Further studies are necessary to assess the viability of recycled waste plastic, specifically for low-cost and lightweight housing solutions.

3. Waste Plastic and properties

Plastics have three main classes based on their molecular structure: thermoplastics, thermosets, and elastomers. Thermoplastics have non-cross-linked polymer chains, making them easily reheat-able and moldable. Examples include polyethylene terephthalate (PET) for beverage bottles and food packaging. Thermosets, conversely, have cross-linked molecular structures, providing improved heat resistance and strength. Elastomers have cross-linked chains that give them stretch ability [3].

Thermoplastics encompass various types, such as PET, known for its resistance to heat and chemical attacks and impermeability to carbon dioxide and oxygen. High-density polyethylene (HDPE) is rigid and robust, often used for water bottles and containers. Low-density polyethylene (LDPE) is a lower-grade HDPE version commonly found in plastic bags and wires. Polyvinyl chloride (PVC), available in un-plasticized and plasticized forms, is a versatile thermoplastic with applications in sanitary and plumbing systems (UPVC) and flexible products like garden hoses and blood bags. Polypropylene (PP) offers chemical and environmental resistance at a low cost, making it suitable for pipes, sheets, and containers. Polystyrene (PS) is a stern, high-clarity thermoplastic commonly used in toys and wall tiles[9].

Thermosets, including polyurethanes, phenols, and polyesters, undergo chemical changes when heated. One well-known thermoset is Bakelite; historically telephone production used this plastic [10]. Recycling thermoplastics presents technical challenges, especially during the initial sorting stage. Techniques for separating PP and PE plastics have evolved from studies, as they are widely used in households, and pose complexities in separation. HDPE and LDPE also present challenges due to their similar physical characteristics. Studies have suggested different recycling methods for various plastics, such as mechanical recycling for PET and PP, feedstock recycling for PVC and PS, chemical recycling for HDPE, and incineration with energy recovery for LDPE. These recycling approaches have the basis from the currently available matrix, and as the construction industry explores more options, the categorization of recycling methods will likely become more diverse[11].

The properties of different plastics, as classified by the Society of Plastic Industry, are presented in Table 1. Each type of plastic possesses its own unique set of properties and densities. The sorting process is based on these general properties and the physical appearance of each plastic. However, not all plastics are suitable for recycling due to contamination issues that may arise during their use. Mechanical methods, such as extrusion, are commonly employed for recycling each type of plastic. However, it is important to note that different temperatures are required for each plastic type. Exceeding these temperature limits can result in the degradation of the polymer, leading to a decrease in the overall properties of the material.

Table 1. Recyclable plastic as per SPI [12][10]

Plastic	General Properties	Recyclable	Density(gm/cm^3)
PETE	Hard, Solvent Resistance	Widely	1.38-1.40
HDPE	Impermeable, Chemical repellent	Widely	0.93-0.97
V	Chemical Repellent, Rigid	Not often because of contamination	1.10-1.45
LDPE	Waxy, Flexible	Not recycled	0.91-0.94
PP	Translucent High melting point	Rarely Recycled	0.90-0.92
PS	Glassy. Rigid, Brittle	Rarely	1.04-1.11
Others	Includes polyamides, ABS etc.,	Not recycled	varies

4. Mechanical Methods and Different molds developed for assessing properties of Waste plastic recycling

Comprehensive studies have been carried out to determine the methods of waste plastic recycling. Damayanti et al., (2022) [13] have provided different prospects of waste plastic treatment in the review studies and for different plastic material what techniques are best suited. The Chemical and mechanical methods are low cost techniques and are best suited for most of the plastic materials. Figure 1 presents a typical extrusion recycling setup along with different mold prepared for producing test samples in Figure 2.

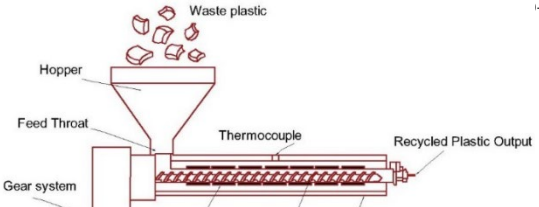

Figure 1. Extrusion molding setup

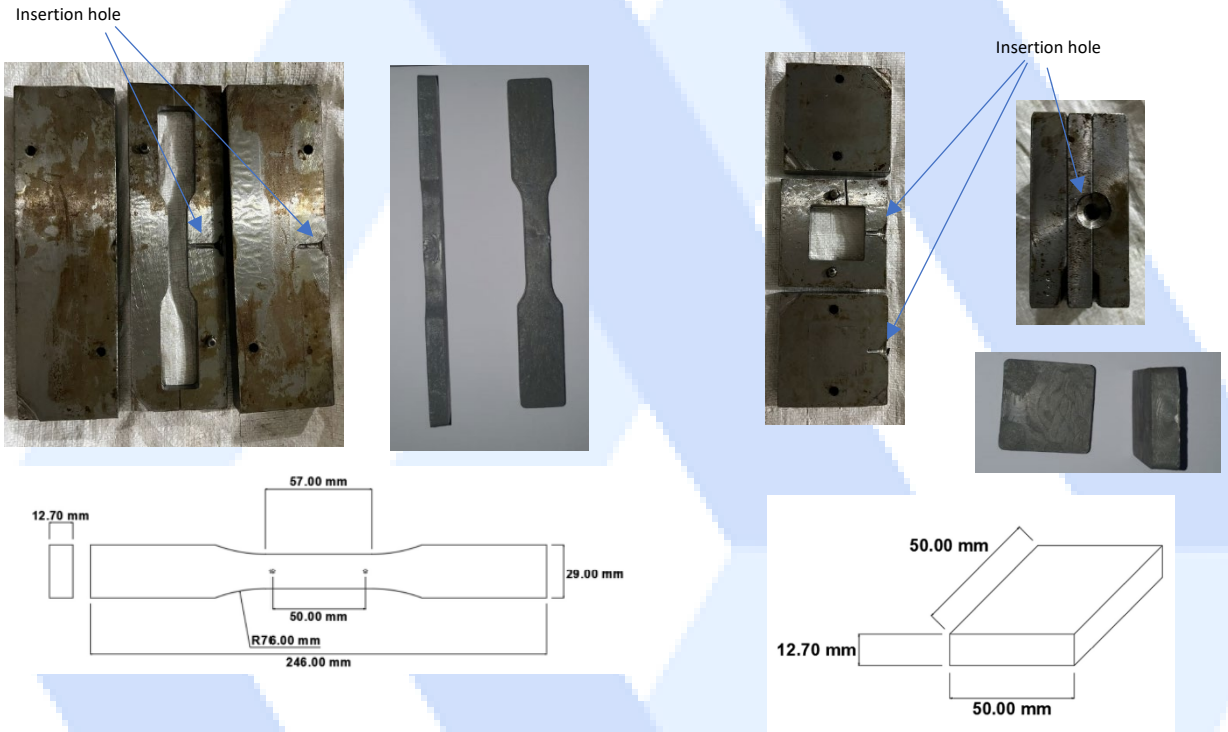

a. Molds prepared for ASTM D638

b. Molds prepared for ASTM D732

Figure 2. Molds for (a) Flexure strength and (b) shear strength for recycled plastic

The recycling of waste plastic and its use in construction industry requires assessment of proper properties of the recycled material for which comparable standards are available. In order to develop samples each set of plastic have different working temperature. Figure 2 shows the arrangement developed for assessing different properties of recycled plastic. These molds are attachable to the extrusion machine with a bench arrangement and are detachable. The simple extrusion machine is employed to reduce the cost of manufacturing. Although the gas emission is less in the extrusion process and the entire plastic is inside the worm. Additives and control of temperature is also used to control the emission of these gasses [14]. The extrusion machine uses thermocouples, which are attached with temperature controllers and speed controller for the motor. The extrusion method is employed for producing rebars and corrugated sheet in a different set of arrangements and properties of which are recorded [5][15]. This secondary method of recycling is best suited for developing construction products from waste plastic. It gives proper shape and uniformity to the recyclate.

5. Discussion

Improvements are required in the processes of recycling waste plastic. Using recycled plastic in the production of various products can lead to enhanced performance. It is crucial to discourage and discontinue high-time patent practices in the market in order to promote the use of sustainable materials in housing. The author aims to introduce environmentally friendly and eco-safe housing systems, such as rebars and green roofing. The implementation of corrosion-resistant and sustainable rebars, blocks, and other building elements has the potential to revolutionize the entire industry. The recycling of waste plastic and its utilization in the long-term construction industry has the potential to significantly, reduce landfill waste and marine plastic pollution.

6. Conclusion

Recycling of waste plastic requires further studies and its uses are limitless. The present study is under way and testing shall conclude in parts to assess different properties of waste plastic for use in construction. The following conclusions are drawn from studies and review.

- The Recycled plastic use in construction industry will provide as a sustainable solution of waste plastic.
- The cost of construction is increasing exponentially and low cost materials are required in order to control poverty elevation.
- The recycled plastic is a good contender being moldable and also having variation in aesthetics to be used in construction industry.

Future studies are required to explore the properties of waste plastic, its energy absorption capability for earthquake resistant low cost houses.

Declaration of Conflict of Interests

The authors declare that there is no conflict of interest. They have no known competing financial interests or personal relationships that could have appeared to influence the work reported in this paper.

References

[1.] Aldahdooh MAA, Jamrah A, Alnuaimi A, Martini MI, Ahmed MSR, Ahmed ASR, *Influence of various plastics-waste aggregates on properties of normal concrete*, J Build Eng [Internet]. 2018. 17:13–22. Available from: https://doi.org/10.1016/j.jobe.2018.01.014

[2.] Yaghoubi E, Arulrajah A, Wong YC, Horpibulsuk S, *Stiffness Properties of Recycled Concrete Aggregate with Polyethylene Plastic Granules in Unbound Pavement Applications*, J Mater Civ Eng. 2017. 29(4):04016271.

[3.] Awoyera PO, Adesina A, *Plastic wastes to construction products: Status, limitations and future perspective*, Case Stud Constr Mater [Internet]. 2020. 12:e00330. Available from: https://doi.org/10.1016/j.cscm.2020.e00330

[4.] Haque MS, *Sustainable use of plastic brick from waste PET plastic bottle as building block in Rohingya refugee camp: a review*, Environ Sci Pollut Res. 2019. 26(36):36163–83.

[5.] Das AJ, Ali M, *Energy absorption capabilities of recycled-plastic reinforcing bars for earthquake resistant housing construction*, In: Australian Earthquake Engineering Society, Virtual Conference 2021. 2021. p. 197–205.

[6.] Oyinlola M, Whitehead T, *Recycling of Plastics for Low Cost Construction*, Encycl Renew Sustain Mater. 2020. :555–60.

[7.] Hahladakis JN, Velis CA, Weber R, Iacovidou E, Purnell P, *An overview of chemical additives present in plastics: Migration, release, fate and environmental impact during their use, disposal and recycling*, J Hazard Mater [Internet]. 2018. 344:179–99. Available from: http://dx.doi.org/10.1016/j.jhazmat.2017.10.014

[8.] Almeshal I, Tayeh BA, Alyousef R, Alabduljabbar H, Mustafa Mohamed A, Alaskar A, *Use of recycled plastic as fine aggregate in cementitious composites: A review*, Constr Build Mater [Internet]. 2020. 253:119146. Available from: https://doi.org/10.1016/j.conbuildmat.2020.119146

[9.] Kutz M, *Applied plastics engineering handbook: processing and materials*, William Andrew; 2011.

[10.] Maris J, Bourdon S, Brossard JM, Cauret L, Fontaine L, Montembault V, *Mechanical recycling: Compatibilization of mixed thermoplastic wastes*, Polym Degrad Stab [Internet]. 2018. 147:245–66. Available from: https://doi.org/10.1016/j.polymdegradstab.2017.11.001

[11.] Hamad K, Kaseem M, Deri F, *Recycling of waste from polymer materials: An overview of the recent works*, Polym Degrad Stab [Internet]. 2013. 98(12):2801–12. Available from: http://dx.doi.org/10.1016/j.polymdegradstab.2013.09.025

[12.] Rahimi AR, Garciá JM, *Chemical recycling of waste plastics for new materials production*, Nat Rev Chem. 2017. 1:1–11.

[13.] Damayanti D, Saputri DR, Marpaung DSS, Yusupandi F, Sanjaya A, Simbolon YM, et al., *Current Prospects for Plastic Waste Treatment*, Polymers (Basel). 2022. 14(15).

[14.] Yamashita K, Kumagai K, Noguchi M, Yamamoto N, Ni Y, Mizukoshi A, et al., *VOC emissions from waste plastics during melting processes*, IAQVEC 2007 Proc - 6th Int Conf Indoor Air Qual Vent Energy Conserv Build Sustain Built Environ. 2007. 2(May 2014):407–12.

[15.] Das AJ, Ali M, *Flexural Capacity of Recycled Plastic Corrugated Sheet*, In: ICACEE 2022, UET Taxila. UET Taxila; 2022. p. 1–5.

PACE-2023

International Congress on Phenomenological Aspects in Civil Engineering

Research Article 20-23June 2023

Establishing a Web-Based Structural Health Monitoring Site to Assess The Existing Status of Structures

Fatih Yesevi Okur*,[1], Ahmet Can Altunışık*,[1]
[1]Karadeniz Technical University, Department of Civil Engineering
Corresponding Author E-mail: yesevi@ktu.edu.tr

Keywords

Algorithm, Baseline assesment, Structural Health Monitoring, Baseline assessment..

Abstract

Structural Health Monitoring is a system that aims to pre-detect damage or collapse that may occur when structural elements exceed their load carrying capacity and displacement limits under possible effects (excessive snowfall, earthquake, strong wind, etc.) by preserving the operational status of structures. This system, which aims to prevent loss of life and property in a possible situation with early intervention to the building, is widely used in many parts of the world, although it has just begun to be recognized in our country. Within the scope of the paper, studies were carried out to evaluate the current conditions of the buildings and to prepare the Structural Health Monitoring site, which allows to determine the possible damage/deterioration status by keeping them under observation 24/7. The Structural Health Monitoring system enables the collection, processing, storage, graphing of the raw signals obtained with the sensitive sensors placed in the structure and all data can be accessed 24/7. Since the raw data of the structures will require a lot of storage space, they are generally not stored after processing by the users. With the storage systems created on the website, the raw data of each structure will be stored, and interpretation will be provided by reprocessing with the new processing (interpretation) algorithms developed in the future. The storage of data belonging to various structures will also have the quality of a database that sets a precedent, as it will enable the creation of a building stock.

1. Introduction

In our country, the construction sector has been progressing very rapidly, especially in recent years, and is one of the sectors that are the locomotive of the economy. Many important engineering structures are being designed and built in our country and in the world. In the design phase, finite element package programs are used in order to reduce the processing volumes as manual analysis becomes impossible. However, it is a fact that many assumptions are made during the analysis and some uncertain parameters are chosen in order to obtain solutions. For this reason, the structural behavior taken into account during the project phase may have deviated from the levels/values envisaged at the project phase over time. In order to eliminate this uncertainty, it is necessary to determine the structural behavior of such important engineering structures by experimental methods.

Considering the geometry of the structures, its intended use and the external factors it is exposed to, data on the parameters reflecting the current state of the structure are obtained through appropriate sensors placed in the structure. With the interpretation and comparison of the experimental measurements taken on the structure at different time intervals, any change in the structural behavior (damage, crack, material deterioration, support collapse, fire effect, temperature effect, fatigue, etc.) can be evaluated quickly. It is of great importance to have measurement systems placed on these structures that record data continuously and to activate emergency warning systems in case of a possible danger for structures that have very high initial construction costs and can cause great loss of property and life when they are damaged and destroyed.

Although it is important and mandatory to monitor the structural safety of structures with strategic importance throughout the world, it has been made compulsory for high-rise buildings with the Turkish Building Earthquake Code-2018 (TBEC-2018) published in 2018 in our country [1]. Since the phrase "Article 13.8.2 - Owners of the building will be responsible for the maintenance and protection of the monitoring system" in TBEC-2018 creates the perception that the measurement system will be installed and delivered to the building owner in general, the processing, interpretation and follow-up of the data of these sensors is generally not done [1]. It will not be difficult or even healthy for people who do not have sufficient knowledge and experience, or the necessary tools and machines to take measurements, to determine the sensors to be placed in the building, to decide in which areas these sensors will be placed, and to interpret and monitor the data to be obtained from the sensors.

The Structural Health Monitoring method, which is made with non-destructive experimental methods and applied in many engineering branches, mainly includes monitoring based on sensor data. Sensors and sensor systems are allocated to a certain physical parameter such as sound, vibration, electromagnetism, temperature, light, and provide the opportunity to evaluate according to sensor data [2]. Vibration data is widely used in Structural Health Monitoring applications applied in civil engineering.

The purpose of monitoring the structures with non-destructive experimental methods is to detect, localize, measure and characterize the damage indicated by the changes in the measured vibration response of the structures [3]. This situation, which is often called damage assessment, forms the basis of the building health monitoring method. Damage detection methods are generally based on the variation of dynamic characteristics such as frequency, mode shape and damping ratio. Structures can be damaged due to various reasons over time. For this reason, the structural conditions of engineering structures should be monitored periodically or continuously by experimental methods and their damage should be determined early. In this way, it will be possible to prevent future destruction.

Experimental Modal Analysis method is widely used in determining the dynamic characteristics of engineering structures, called natural frequency, mode shape and damping ratio, depending on experimental measurement methods. In this method, sensitive accelerometers are placed on the structure to be studied, taking into account the modal motion points obtained as a result of finite element analysis. Vibration signals from accelerometers are collected with the help of data acquisition unit and dynamic characteristics are obtained by using up-to-date software. In experimental methods, the changes in the dynamic characteristics obtained as a result of the measurements made for the damaged and undamaged conditions of the structure are interpreted and the damage situations and regions are tried to be determined [4-6]. Since the response of the structure is measured directly with the sensitive sensors placed in the structure in experimental methods, more realistic results are obtained compared to numerical methods.

Within the scope of this study, it is aimed to create a web-based site, where experimental data is transferred, continuous signals are received, and this raw data is processed, interpreted and graphed, in order to access all the data belonging to the studies carried out for the purpose of Structural Health Monitoring 24/7 and to have information about the building at any time. Considering the issues explained above, together with the prepared web-based site;

- Continuous monitoring can be achieved with sensitive accelerometers to be placed in the structure,
- It is possible to transfer the signals coming from the structures to the main server, store them and evaluate the data by processing,
- It is possible to systematically display the processed data by date and hour and compare it with the new data received during the monitoring process,
- In the monitoring process, data processing algorithms found in the literature and widely used can be applied,
- In the structural monitoring process, instantaneous presentation of the changes in structural behavior and emergency response in extreme cases that may occur,
- Site members can access their structures at any time of the day with their special passwords, and emergency alerts can be reported via e-mail or sms.

2. Establishment of a Structural Health Monitoring Site

Damage can be defined as any deviation in the original structure geometry or material properties that can cause unwanted stresses, displacements or vibrations in structures. With the Structural Health Monitoring System, it is possible to determine the location and severity of the damage by means of sensitive sensors placed in the buildings (Figure 1). By detecting the presence, location and severity of damage in buildings, early intervention in the damage area will prevent the progression of the damage and causing further damage to the structure. The structure's useful life can be increased for less money while also increasing safety if the appropriate local reinforcement is applied to the damaged area.

With the Structural Health Monitoring Site, which is prepared on a web-based basis, it is possible to monitor the current status of engineering structures, which can change depending on many environmental factors such as ambient temperature, humidity and wind speed, to process, interpret, graph, report and easily access the data on the desired date. You can access the Web-based Structural Health Monitoring Site prepared within the scope of the study at http://www.yapisagligilab.com. The homepage screenshot of the site is given in Figure 2.

This site has a special page for each structure followed. Persons authorized by the requester will be able to access the page of the building with the password they define. On this page, it will be possible to access the graphics of the signals received 24/7 from the sensors placed in the structure, information about the current state of the structure and reports. Within the scope of the infrastructure project prepared within the body of Karadeniz Technical University, there are 7 structures that are actively monitored: Deriner Kemer Dam, 25-storey high structure, Trabzon Mosque Minaret, KTU Mosque Minaret, Historical Erzurum Double Minaret, Artvin Ortaköy and Berta Balanced Cantilever Bridges.

In the image in Figure 3, the page containing the raw signals obtained from the accelerometer sensors of a sample building (KTÜ mosque minaret) that is actively monitored and the graphics of the frequency values obtained by processing these data is seen. Figure 4 also shows the air temperature data for the day and time corresponding to the collected raw signals. The subheadings on the left panel of the image contain the grouped data and structure properties of the structure.

Many different sensors (accelerometer, strain gauge, displacement gauge, etc.) are used in Structural Health Monitoring. The data from the sensors can be evaluated on their own, or if different sensors are related to each other. Correlation Analysis is used to evaluate the relationship between different data types. If the Correlation Analysis is greater than 0.5, it is an indication that there is a fit between the data. In this study,

the relationship between the temperature and frequency values of the minaret is given and shown in Figure 5. In Figure 5, the relationship between all parameters was found to be greater than about 0.5.

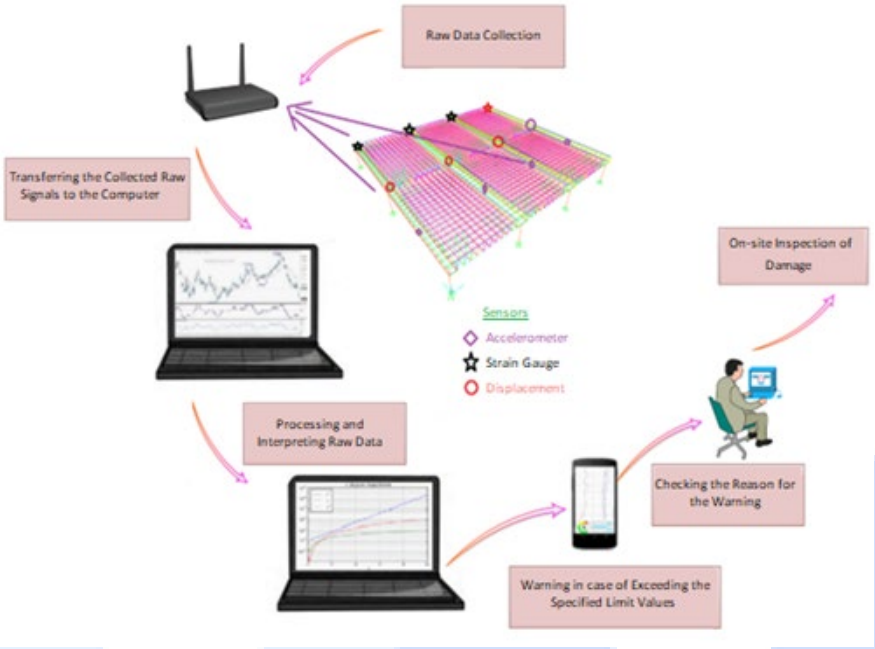

Figure 1. Flow chart of Structural Health Monitoring System

Figure 2. Homepage screenshot of the Web-based Structural Health Monitoring Site

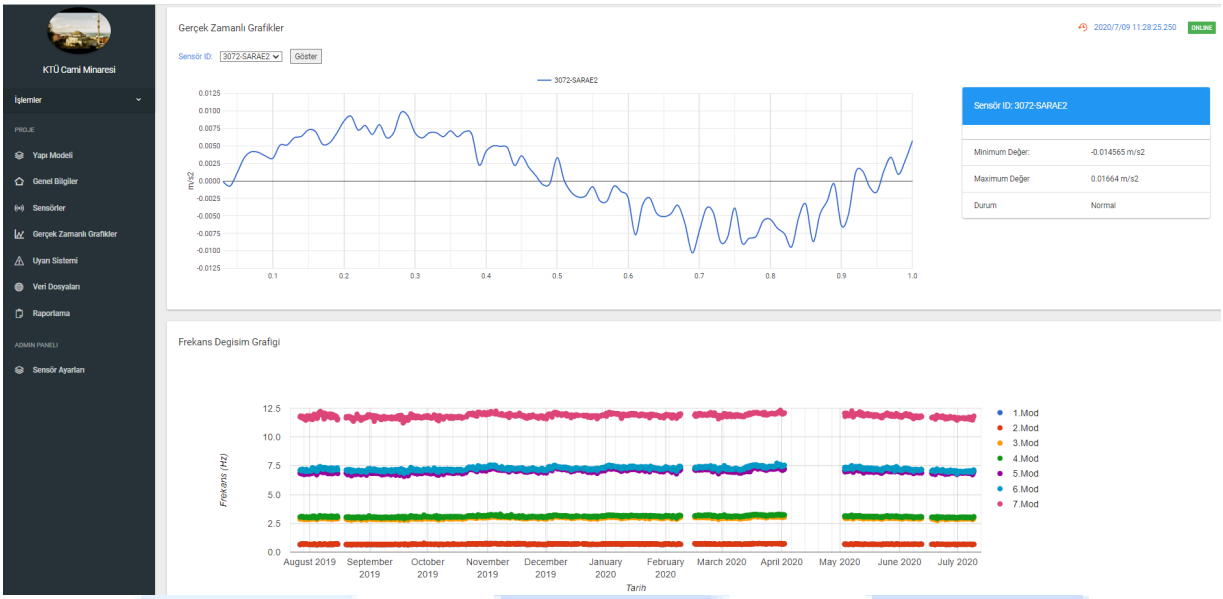

Figure 3. Vibration signals and frequency values of KTU Mosque Minaret

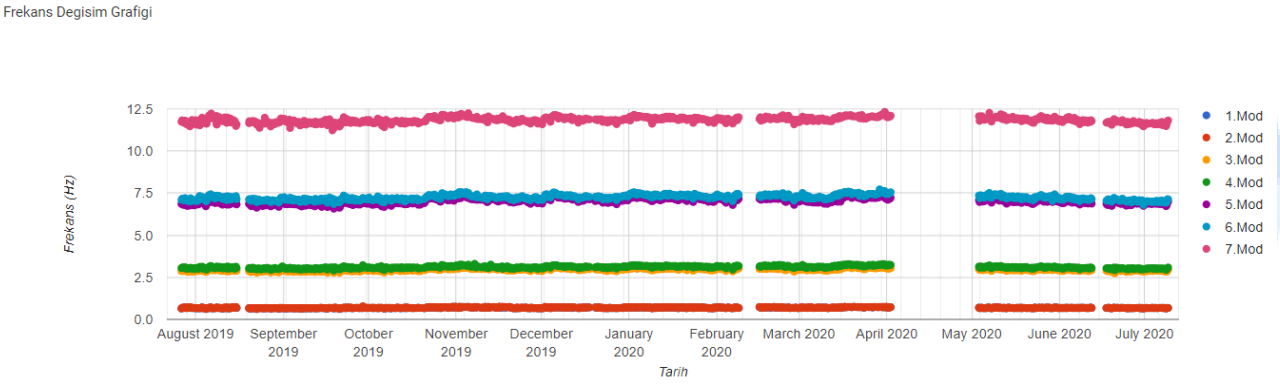

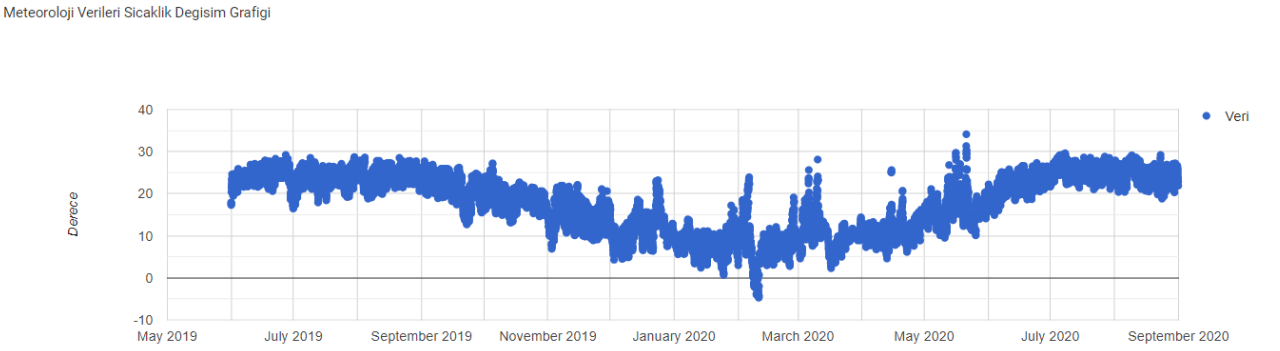

Figure 4. Frequency values and corresponding temperature data of KTU mosque minaret

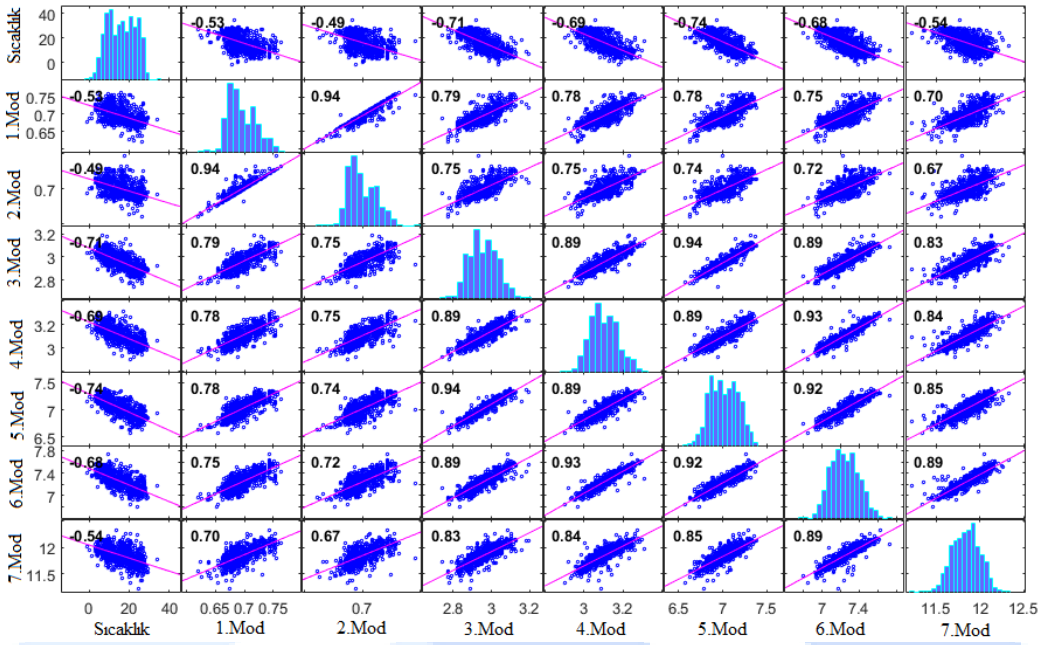

Figure 5. Graph of correlation distribution between temperature and frequency values of KTU Mosque Minaret

3. Conclusion

The Structural Health Monitoring system consists of various steps such as storing, processing and graphing the raw signals obtained with various sensors placed in the structures. The decision to be made at the interpretation stage, where knowledge and experience play an important role, will determine whether the structure is damaged, how much it is affected by external environmental factors, and how much these effects damage the useful life of the structure. For this reason, it is possible for the members to access the information about the structure without any difficulty by collecting the data of the buildings in the center and giving the members who want to access the right to log in via the website. In this way, more reliable information about the behavior of the structures can be obtained. These data will also make important contributions to the literature. With the storage systems to be created on the website, it will be possible to interpret by reprocessing it with the new algorithms developed in the future.

Declaration of Conflict of Interests

The authors declare that there is no conflict of interest. They have no known competing financial interests or personal relationships that could have appeared to influence the work reported in this paper.

Thanks

The first author would like to thank TÜBİTAK for their support within the scope of "2214/A Overseas Doctorate Research Scholarship Program" numbered 1059B141800930.

References

[1.] TBEC-2018, (Turkish Building Earthquake Code), Specifications for buildings to be built in seismic areas. Ministry of Public Works and .Settlement, Ankara, Turkey
[2.] Boller, C., Meyendorf, N., State-of-the-art in structural Health Monitoring for aeronautics. In Proceedings of the International Symposium on NDT in Aerospace, 3-5 December (2008), Fürth/Bavaria, Germany.
[3.] Çolak, H., Structural health monitoring condition assessment and seismic vulnerability estimation of highway bridges. Ms.C Thesis, Boğaziçi University (2016), Turkey.
[4.] Fritzen, C.P., Vibration-based structural health monitoring concepts and applications. Key Engineering Materials, 293 (2005), 3-20.
[5.] Montalvao, D., Maia, N.M.M., Ribeiro, A.M.R., A review of vibration-based structural health monitoring with special emphasis on composite materials. Shock and Vibration Digest, 38(4) (2006), 295-324.
[6.] Erazo, K., Sen, D., Nagarajaiah, S., Sun, L., Vibration-based structural health monitoring under changing environmental conditions using Kalman filtering. Mechanical Systems and Signal Processing, 117 (2019), 1-15.

PACE-2023
International Congress on the Phenomenological Aspects of Civil Engineering

PACE-2023
International Congress on Phenomenological Aspects in Civil Engineering

Research Article
20-23 June 2023

Near-Fault and Far-Fault Ground Motions Effects on Seismic Responses of Timber Bridges

Fezayil Sunca*,[1], Ahmet Can Altunışık*,[2]
[1]Sivas Cumhuriyet University, Faculty of Engineering, Department of Civil Engineering
[2]Karadeniz Technical University, Faculty of Engineering, Department of Civil Engineering
Corresponding Author E-mail: fsunca@cumhuriyet.edu.tr

Keywords

Dynamic analysis,
Far-fault record,
Near-fault record,
Timber bridge.

Abstract

This paper investigates the seismic behavior of historical timber bridges subjected to near-fault and far-fault ground motions. For this purpose, Buzlupınar Bridges located in the East Black Sea Region in Turkey were selected as an application. Acceleration records recorded in same event were applied to the orthogonal and vertical directions of the bridge. As a result of dynamic analysis, the distributions of maximum amplitudes under acceleration records with near-fault and far-fault were comparatively presented. All numerical results indicated that both the near-fault ground motions and their far-fault counterparts were played major roles in terms of seismic responses of selected historical timber bridge.

1. Introduction

Timber, one of the oldest structural materials, has been used in the construction of many equipment and structures such as buildings and bridges throughout human history. Timber has significant advantages compared to other masonry materials that are extensively used in historical structures. Therefore, timber has become one of the essential structural materials in many areas from past to present [1]. They were exposed to degradation and destruction due to various environmental effects. Among these effects, earthquakes are one of the main factors that can cause inheritance loss [2].

Linear or non-linear dynamic behaviors and seismic performances of structures are highly sensitive to the utilized ground motions characteristics. By examining the ground motions measured in the region where the earthquake occurred, it can be observed that the near-fault ground motions have many different properties compared to their far-fault counterparts [3]. In the literature, some investigations on the seismic assessments of historical structures considering the near-fault and/or far-fault ground motion effects have been handled in masonry arch bridges [4], masonry bell tower [5] and masonry building [6]. It can be seen from the literature review that the seismic assessments of historical timber structures have not been sufficiently investigated under near-fault and far-fault ground motions effects. Therefore, this paper comparatively investigated the seismic assessments of historical timber bridges under near-fault and far-fault ground motion effects.

2. Buzlupınar Bridge

Buzlupınar Bridge was built on the Madenli stream located in the Çayeli province of Rize city in northern Turkey. This bridge utilized for regional pedestrian, animal, and cargo transportations, is completely made of timber using rare construction techniques. The total bridge length and width are approximately 31.50m and 2.20m. The main span length between both abutments is 21.80m. It is formed the several structural elements. The main carrier system consists of simply supported three timber main beams of circular cross-section and timber studs with various rectangular cross-section areas from 90cm^2 to 238cm^2. Before the restoration process, the spans and diameters of main beams varied between 14.35m to 14.50m and 21.00cm to 25.00cm, respectively. The diameters of the main beams changed to 40cm, after the restoration process. The timber studs are connected and the deck of the bridge utilizing timber beams and L-shaped buttress. Other timber structural elements of the bridge are transverse bracings, deck plates, railings, and roof elements (purlins, rafters, etc.). Moreover, the main span of the bridge reduces by cantilever beams fixed to both abutments. Abutments have a total of 39 cantilever beams stabilized by perpendicular beams. The lengths, diameters, and horizontal angles of cantilever beams vary between 5.35m to 9.87m, 16.00cm to 32.00cm, and 5° and 20°, respectively. Fig. 1 presents some photographs of the general view of the bridge. The structural schemes in the plan views of the restoration project are given in Fig. 2

Figure 1. The Buzlupınar Bridge

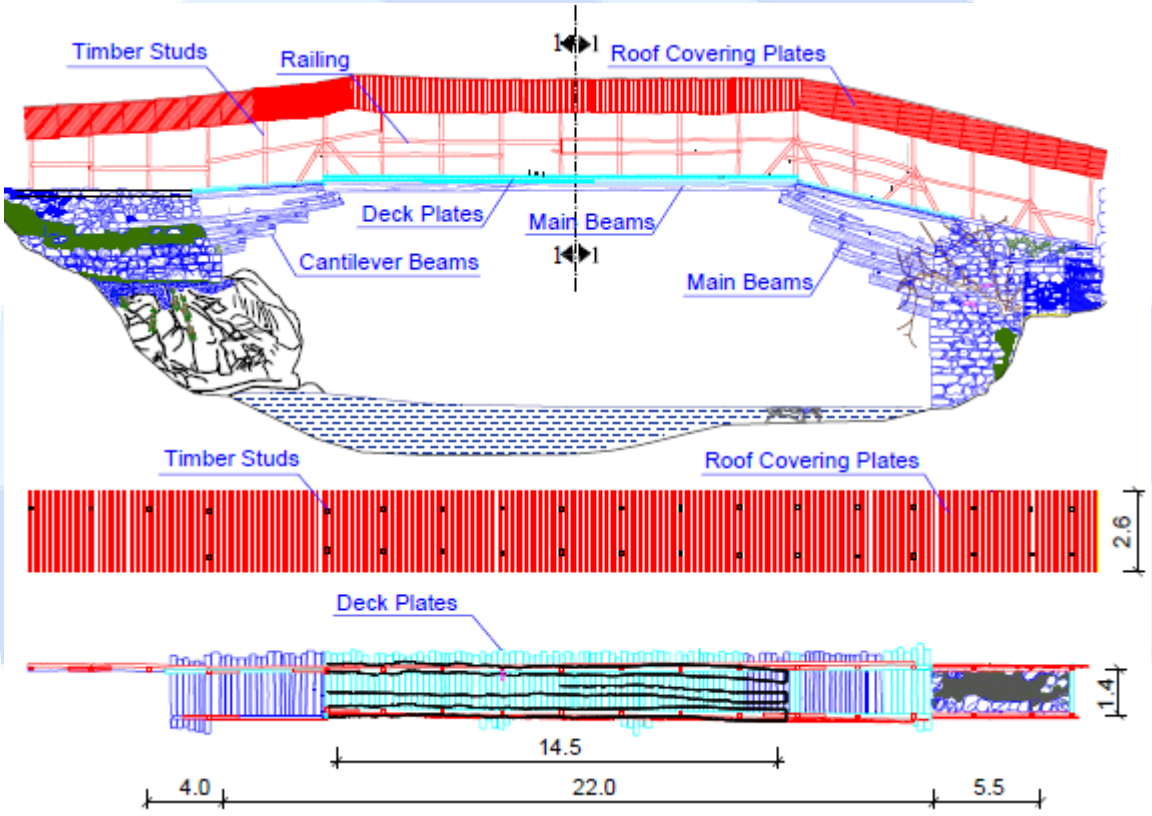

Figure 2. The geometric properties of the Buzlupınar Bridge

3. Finite Element Model

The finite element model of the bridge were developed using the SAP2000 software [7] based on the restoration project. Abutments, main beams, railings, roof elements, and studs were modeled by frame elements. Also, roof covering plates of the bridge were constituted by using shell elements. The finite element model of the Buzlupınar Bridge are presented in Fig. 3.

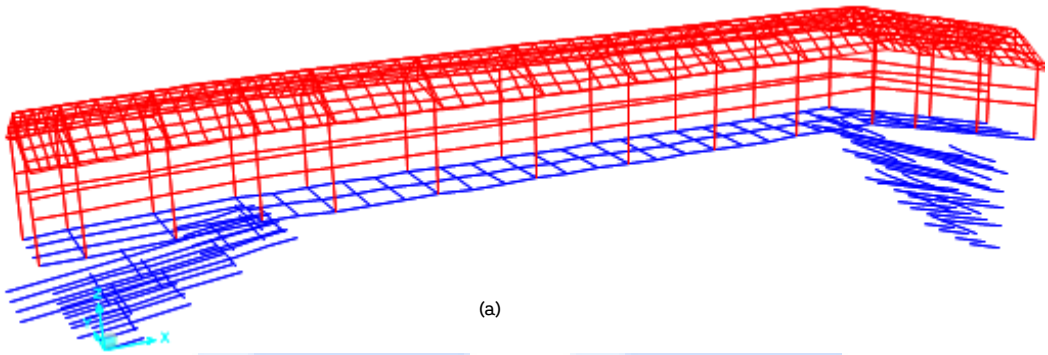

(a)

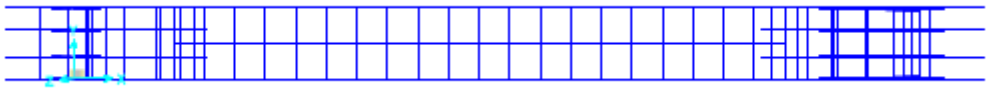

(b)

Figure 3. Numerical model of the Buzlupınar Bridge (a- three-dimensional view, b- plan view)

Table 1 briefs the mechanical properties of the main materials. The orthotropic material properties were used in the finite element models [8].

Table 1. Mechanical properties of the materials

Material Properties	Modulus of Elasticity (kN/m^2)			Poisson's Ratio (-)	Density (kN/m^3)
	E1	E2	E3		
Buzlupınar Bridge	5.701E6	1.710E5	1.710E5	0.04	5.00

4. Near-Fault and Far-Fault Ground Motions

The near-fault ground motions were decided according to the following three parameters: (i) the ratio of peak ground velocity (PGV) to peak ground acceleration (PGA) was larger than 0.1s, (ii) ground motion selected in the vicinity of a fault having apparent velocity pulse signals (velocity pulse duration (T_p) larger than 1.0s), (iii) Joyner-Boore distance (R_{jb}) of the ground motions less than 10km. The near-fault ground motions and their far-fault counterparts were chosen from the same seismic events to minimize the effects of earthquake characteristics on the results of the analyses. All components of ground motions were also considered.

The analyses were carried out by using scaled ground motion records with the same PGA values. The expected PGA value of the Buzlupınar Bridge is approximately 0.23g for the design base earthquake level. The PGA values of selected original ground motions were scaled considering expected PGA in order to compare the results more accurately. The properties of the selected ground motions are presented in Table 2.

Table 2. The selected ground motions

Earthquake	Type	Station	Code	Year	Mw	Mechanism	Rjb
Loma Prieta	Far-Fault	Gilroy Array #7	GMR000 GMR090 GMR-UP	1989	6.93	Reverse Oblique	22.35
	Near-Fault	Los Gatos - Lex. Dam	LEX000 LEX090 LEX-UP				3.22
Kobe	Far-Fault	Chihaya	CHY000 CHY090 CHY-UP	1995	6.9	Strike-Slip	49.91
	Near-Fault	Port Island	PRI000 PRI090 PRI-UP				3.31

5. Results and Discussions

Distributions of displacements along the deck and time-history of maximum vertical displacement at the midpoint of the bridge deck are comparatively given in Figs. 4-5. These displacements were compared, it could be seen the displacements had an increasing trend towards the midpoint of the bridge deck. By comparing these vertical displacements separately, it was seen that both the near-fault and far-fault ground motions might produce significant structural responses in terms of vertical displacements along the deck of the bridge.

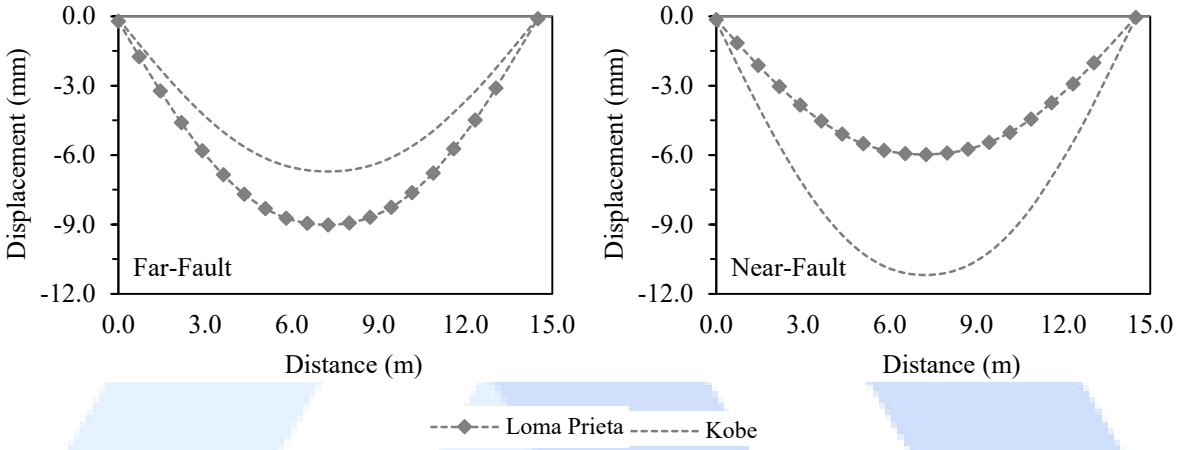

Figure 4. Distributions of displacements along to deck

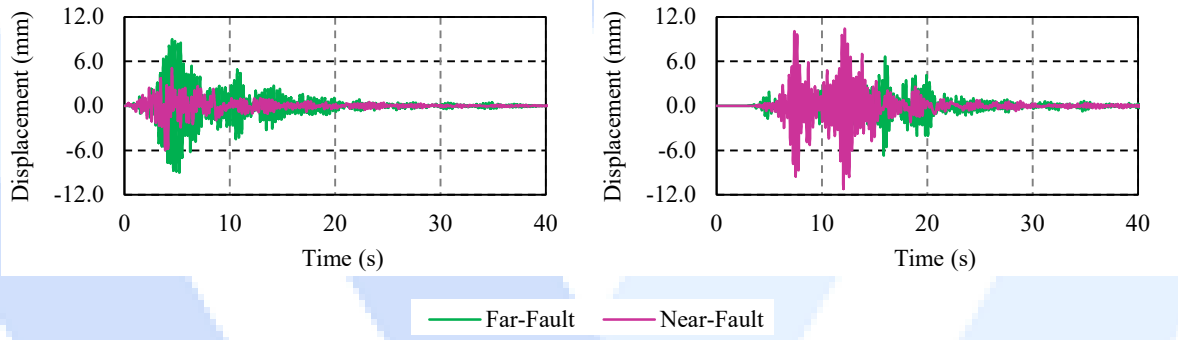

1989 Loma Prieta Earthquake 1995 Kobe Earthquake

Figure 5. Time-history of the maximum displacements at the midpoint of the bridge deck

Figs. 6-8 illustrates the time-history of maximum internal forces. For the near-fault and far-fault records of 1989 Loma Prieta and 1995 Kobe Earthquakes, the maximum axial forces were obtained as 0.80kN/2.23kN, 2.21kN/1.99kN; the maximum shear forces were obtained as 1.71kN/3.44kN, 1.82kN/0.91kN; and the maximum moments were determined as 7.19kNm/14.58kNm, 7.32kNm/3.53kNm, respectively.

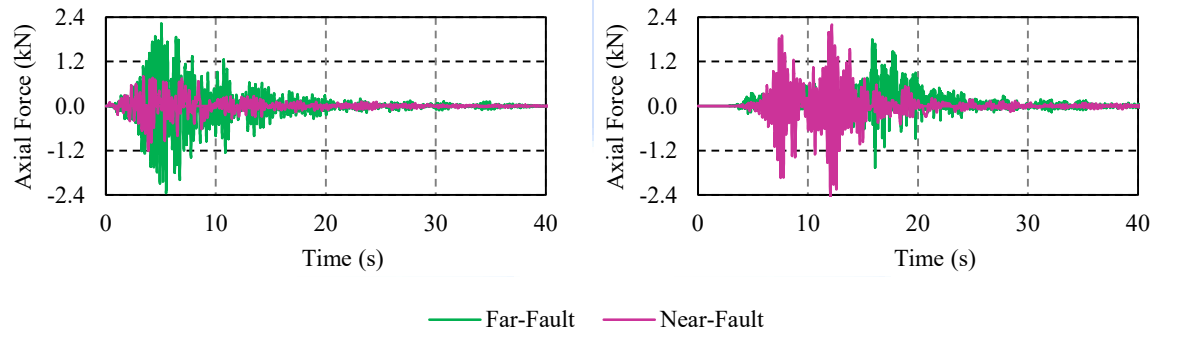

1989 Loma Prieta Earthquake 1995 Kobe Earthquake

Figure 6. Time-history of the maximum axial forces at the bridge deck

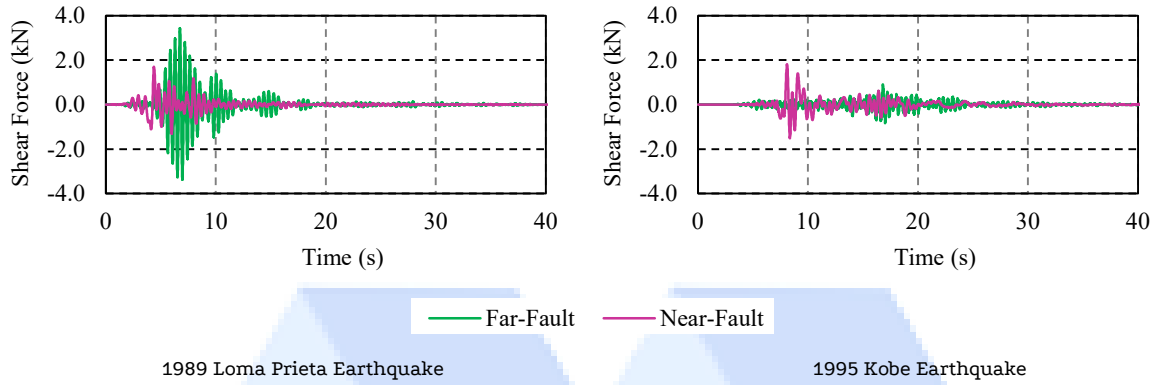

Figure 7. Time-history of the maximum shear forces at the bridge deck

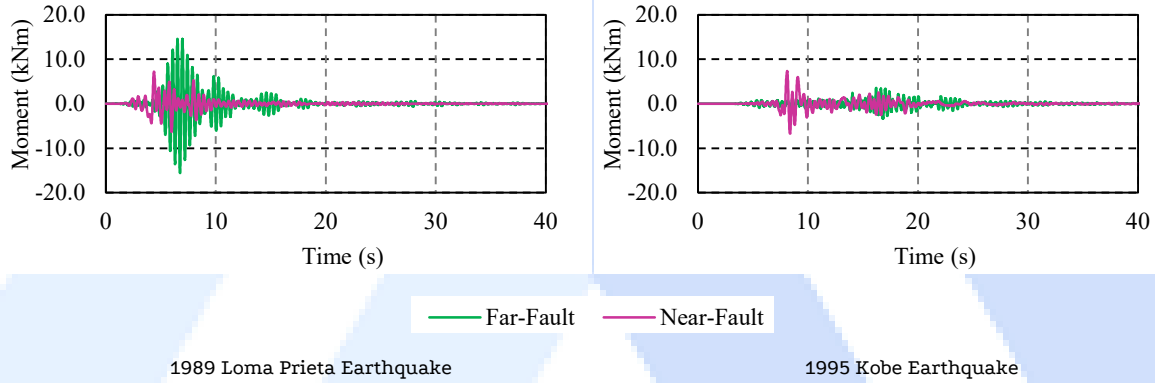

Figure 8. Time-history of the maximum bending moment at the bridge deck

6. Conclusion

This paper presents the seismic assessments of historical timber bridges under near-fault and far-fault ground motion effects. To this aim, a historical timber bridge was considered and linear time history analyses were performed. The studies conducted within the scope of the study reveal that amplitudes (displacement and internal forces) obtained from both the near-fault ground motions and their far-fault counterparts might be caused the critical results for selected historical timber bridges. This situation pointed out that they have undeniable effects on historical timber bridges. In the previous studies, this critical point was also emphasized for other historical bridges [4,9].

Declaration of Conflict of Interests

The authors declare that there is no conflict of interest. They have no known competing financial interests or personal relationships that could have appeared to influence the work reported in this paper.

References

[1.] Altunişik, A.C., Karahasan, O.Ş., Okur, F.Y., Kalkan, E., Ozgan, K., Finite element model updating and dynamic analysis of a restored historical timber mosque based on ambient vibration tests. Journal of Testing and Evaluation 47(5) (2018) 3533-3562.
[2.] Ramírez, E., Lourenço, P.B., D'Amato, M., Seismic assessment of the Matera Cathedral. Structural Analysis of Historical Constructions (2019) 1346-1354.
[3.] Adanur, S., Altunişik, A.C., Bayraktar, A., Akköse, M., Comparison of near-fault and far-fault ground motion effects on geometrically nonlinear earthquake behavior of suspension bridges. Natural Hazards 64(1) (2012) 593–614.
[4.] Simos, N., Manos, G.C., Kozikopoulos, E., Near-and far-field earthquake damage study of the Konitsa stone arch bridge. Engineering Structures 177 (2018) 256-267.
[5.] Habieb, A.B., Valente, M., Milani, G., Effectiveness of different base isolation systems for seismic protection: Numerical insights into an existing masonry bell tower. Soil Dynamics and Earthquake Engineering 125 (2019) 105752.
[6.] Chieffo, N., Formisano, A., Mosoarca, M., Lourenço, P.B., Seismic vulnerability assessment of a romanian historical building under near-field earthquake. XI International Conference on Structural Dynamics (2020) Greece.
[7.] SAP2000, Structural Analysis Program, Computers and Structures Inc. Version: 17.1.1 (2015) Berkeley California USA.
[8.] Altunişik, A.C., Kalkan, E., Okur, F.Y., Karahasan, O.Ş., Ozgan, K., Finite-element model updating and dynamic responses of reconstructed historical timber bridges using ambient vibration test results. Journal of Performance of Constructed Facilities 34(1) (2020) 04019085.

[9.] Sevim, B., Atamturktur, S., Altunişik, A.C., Bayraktar, A., Ambient vibration testing and seismic behavior of historical arch bridges under near and far fault ground motions. Bulletin of Earthquake Engineering 14(1) (2016) 241-259.

PACE-2023
International Congress on the Phenomenological Aspects of Civil Engineering

PACE-2023
International Congress on Phenomenological Aspects in Civil Engineering

Research Article 20-23June 2023

Ambient Vibration Based Model Updating of A Historical Masonry Church

Esin Ertürk Atmaca*,[1,2], Ali Fuat Genç[1], Ahmet Can Altunişik[1], Murat Günaydin[1], Fatih Yesevi Okur[1]
[1]*Department of Civil Engineering, Karadeniz Technical University, Trabzon, Turkey*
[2]*Department of Civil Engineering, Yalova University, Yalova, Turkey*
Corresponding Author E-mail: ahmetcan8284@hotmail.com

Keywords

Historical masonry structures,
FE model updating procedure,
Ambient vibration test,
Dynamic characteristics.

Abstract

This paper presents a finite element model updating procedure of historical Santa Maria Church in Trabzon, Turkey. This process involves ambient vibration method, which is non-destructive experimental measurement, and numerical evaluation using finite element method. Scope of paper, the experimental dynamic characteristics were identified of the church building and the initial finite element model was developed. To minimize the differences between numerical and experimental dynamic characteristics, the manual FE model updating procedure was used. The maximum difference of 34.81% between the numerical and experimental frequencies was reduced to 2.22% with the FE model updating procedure and structural behavior was tried to be determined as close to actual as possible.

1. Introduction

Historical masonry buildings are highly vulnerable to under external factors and experience deterioration in material characteristics and strength over time. Therefore, the finite element (FE) model updating procedure, which allows for the most accurate structural behavior predictions, is quite significant for historical masonry structures built with different construction techniques and materials.

Using the FE model updating procedure, it is possible to estimate the uncertain parameters such as material properties, geometrical characteristics, and boundary conditions in the FE model of structures and identify the structural behavior as close to actual as possible [1-2]. The FE model updating procedure can be classifying two procedures as manual or automated updating. The manual updating procedure is accomplished by trial and error. On the other hand, automated model updating procedure is performed by specialized software [3-4].

To determine the experimental dynamic characteristics, modal testing is used. The modal testing is conducted by two methods, forced vibration test (FVT) and the ambient vibration test (AVT). In AVT, which is non-destructive method to obtain the dynamic characteristics of a structure, the data are collected from the ambient vibrations of the structure and are then processed. On the other hand, modal tests are carried out with a known excitation force and structural response is measured. AVT is more appropriate method to identify the dynamic characteristics of historical structures compared to FVT because it is a totally non-destructive [5-6]. Also, there are many studies using AVT method historical structures [7-11].

In this paper, numerical and experimental dynamic characteristics of historical Santa Maria Church were investigated to show the requirement of the FE model updating procedure for a historical structure. While manual updating procedure was conducted in FE updating procedure, AVT method was employed to obtain the experimental dynamic characteristics of the church building.

2. Testing Process a Brief History of the Santa Maria Church

Santa Maria Church is a unique historical structure located in Trabzon, Turkey. The church building is one of the important historical structure of the Trabzon province, and it is still in use. It is known that it was built between 1869 and 1874 according to historical records. Fig. 1 depicts location and plan view of the church building.

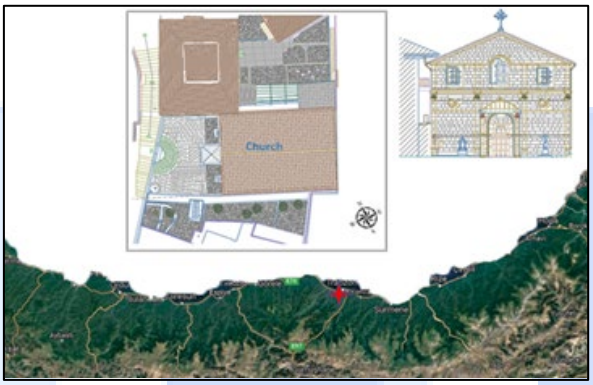

Figure 1. The location and plan view of the Santa Maria Church

The church building was constructed of stone masonry. The structure is 14x20m in size and has a square plan. The building's height is approximately 12.4m. Vaults and arches were used to cover the roof of the church, which features a wide courtyard. Fig. 2 shows views of the church building.

Figure 2. Views of the church building

3. Experimental Dynamic Characteristics of the Santa Maria Church

The AVT method was used to determine experimental dynamic properties such as natural frequencies, mode shapes, and damping ratios. AVTs measurement lasted 30 minutes and vibration signals were recorded using data from eight accelerometers situated on the top of the church building.

To process the data, several methods are used, including the Enhanced Frequency Domain Decomposition (EFDD) method in the frequency domain and the Stochastic Subspace Identification (SSI) method in the time domain. The modes in the EFDD method, which is an improved version of the FDD method based on the Fast Fourier Transform (FFT) analysis, are easily identified by picking the peaks in singular value decomposition plots produced from the spectral density spectra of the responses. The SSI method, on the other hand, is a general stochastic state space model. This method is suitable for defining a linear vibratory structure by experimental measurement [12, 13]. The EFDD and SSI methods were employed in this paper to determine dynamic characteristics. Fig. 3 shows the singular values of spectral density matrices (SVSDM) of the data set resulted in by the EFDD method and the stabilization diagram obtained by the SSI method. As can be observed Fig. 3, three natural frequencies were acquired between 0 and 15Hz. In addition, Fig. 4 shows the first three mode shapes for the church building. The first one is transverse mode, the second is longitudinal mode, and the third is torsional mode.

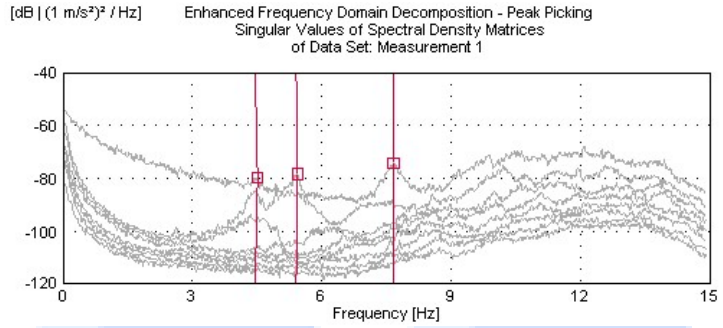

(a)

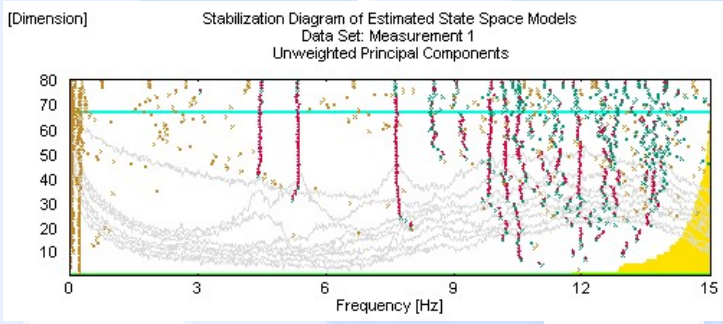

(b)

Figure 3. (a) SVSDM and (b) stabilization diagram

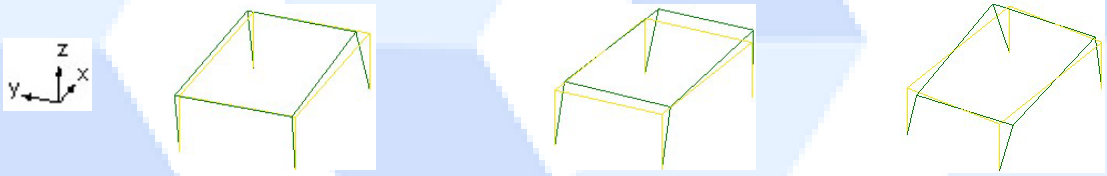

1st Mode (Transverse) | 2nd Mode (Longitudinal) | 3rd Mode (Torsional)

Figure 4. The first three experimental modes shapes

The experimental natural frequencies and damping ratios of the church building obtained from the EFDD and SSI methods are presented in Table 1. The natural frequencies were calculated within 4.46Hz-7.68Hz and the damping ratios were obtained between 1.36-3.17%. It can be seen that there is good agreement between the natural frequencies.

Table 1. Experimental natural frequencies and damping ratios obtained from EFDD and SSI method

Mode	Frequency (Hz)			Damping Ratios (%)	
	EFDD	Diff. (%)	SSI	EFDD	SSI
1	4.46	0.22	4.47	1.43	2.01
2	5.41	0.93	5.36	1.36	3.17
3	7.67	0.13	7.68	1.97	1.94

4. Initial FE Model and Numerical Dynamic Characteristics of the Santa Maria Church

The FE model of the church was developed using Abaqus software [14]. In the FE models, the masonry elements were represented by a linear tetrahedron C3D4 finite element with four nodes. Meshing size selected was 50cm. The base/support was assumed fixed as a boundary condition. Some views of the FE model are shown in Fig. 5. The major structural elements of the church are stone masonry walls, brick masonry walls, pillars, timber elements, RC elements, and vaults. Table 2 shows the elastic parameters considered in the initial FE model for these structural elements. These values were taken from the relevant literature for the masonry structures [15-18].

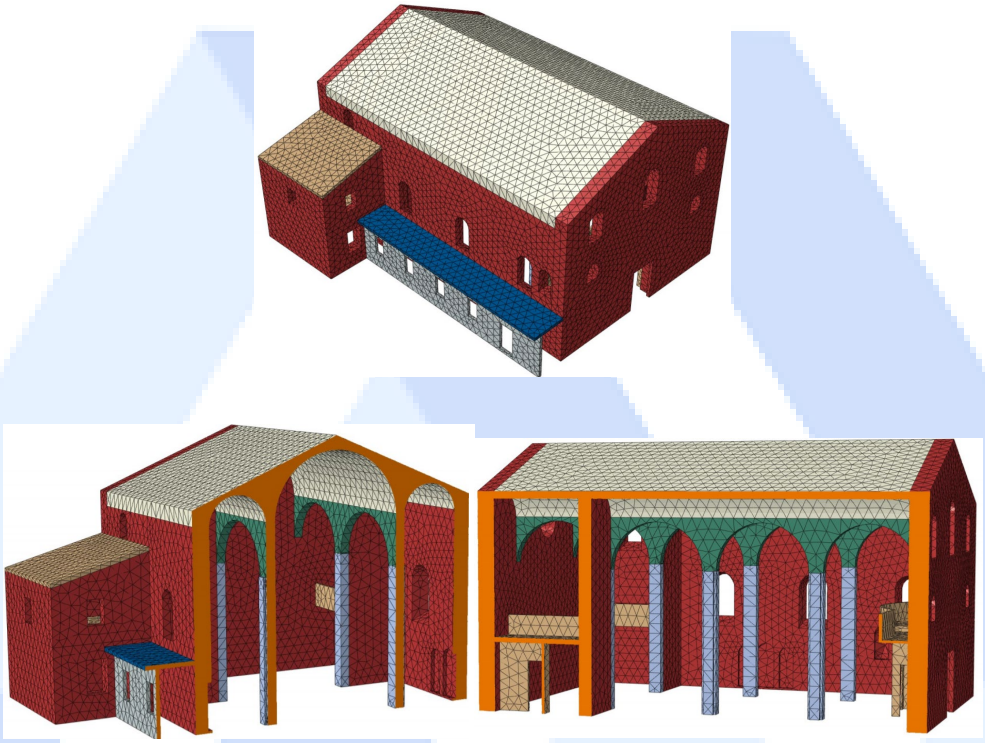

Figure 5. FE model of the Santa Maria Church

Table 2. Material properties included in the initial FE model

Elements	Young's modulus (N/m^2)	Poisson Ratio (-)	Material density (kg/m^3)
Stone Masonry Wall	2.0E9	0.2	2000
Brick Wall	2.0E9	0.2	1750
Timber Elements	1.0E9	0.2	500
Pillar	2.0E10	0.2	2400
RC Elements	2.0E10	0.2	2400

Modal analyses were carried out and the numerical dynamic characteristics were identified. Fig. 6 shows the first three mode shapes and corresponding natural frequencies for the church building. As can be seen, the mode shapes were obtained as transverse, longitudinal and torsional modes.

Table 3 includes differences of the numerical and experimental natural frequencies, and these differences indicates that there is not enough correlation between the numerical and experimental natural frequencies. The differences are more than the literature-recommended limit of 5% [3]. It should be noted that it is essential that the initial FE model should be updated to minimize the differences.

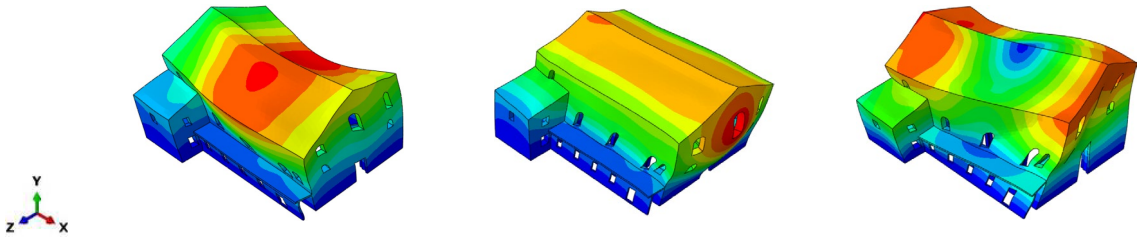

First Mode (Transverse) f1=5.90Hz | Second Mode (Longitudinal) f2=7.04Hz | Third Mode (Torsional) f3=10.34Hz

Figure 6. First three numerical mode shapes and natural frequencies for the initial FE model

Table 3. Comparison of experimental and initial FE model natural frequencies

Mode	Frequency (Hz)			
	EFDD	SSI	Initial Model	Max. Diff. (%)
1	4.46	4.47	5.90	32.28
2	5.41	5.36	7.04	30.13
3	7.67	7.68	10.34	34.81

5. FE Model Updating Procedure

To minimize the differences between numerical and experimental dynamic characteristics, the FE model updating procedure is used. As previously stated, the FE model updating procedure can be characterized as manual or automated. The manual model updating procedure was used in this paper to minimize the differences between numerical and experimental dynamic characteristics. Table 4 shows the final material properties of church building.

Table 4. The final material properties

Elements	Young's modulus (N/m2)	Poisson Ratio (-)	Material density (kg/m3)
Stone Masonry Wall	1.20E9	0.2	2300
Brick Wall	1.25E9	0.2	1750
Timber Elements	5.00E8	0.2	500
Pillar	2.0E10	0.2	2300
RC Elements	2.0E10	0.2	2400

Figure 7 depicts the first three mode shapes and corresponding natural frequencies for the church building. Also, Table 5 compares the experimental and updated natural frequencies. The greatest difference was calculated as 2.22%. The method used minimized the maximum difference from 34.81% to 2.22%. The authors thought that the updated FE model of the church building is more representative of the current behavior.

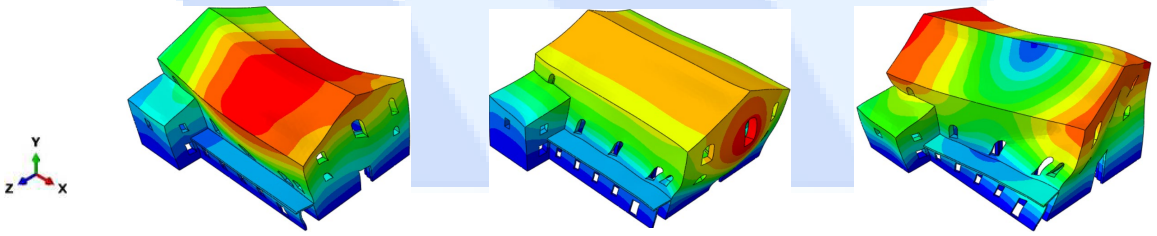

First Mode (Transverse) f1=4.54Hz | Second Mode (Longitudinal) f2=5.29Hz | Third Mode (Torsional) f3=7.73Hz

Figure 7. Final mode shapes and corresponding natural frequencies

Table 5. Comparison of experimental and updated natural frequencies

Mode	Frequency (Hz)			
	EFDD	SSI	Updated Model	Max. Diff. (%)
1	4.46	4.47	4.54	1.79
2	5.41	5.36	5.29	2.22
3	7.67	7.68	7.73	0.78

*The comparison was calculated in accordance with EFDD results

6. Conclusion

FE model updating procedure, which enable to make real structural behavior predictions as credible as possible, is especially important for historical structures which are a significant part of cultural heritage. The purpose of this paper is to show the necessity of the FE model updating procedure for a historical building. In accordance with this purpose, experimental and numerical dynamic characteristics of the historical Santa Maria Church in Trabzon, Turkey was evaluated and FE model updating procedure was carried out. The following conclusions are drawn from the study:

- The first three experimental and initial numerical frequencies were obtained between 4.46-7.68Hz and 5.90-10.34Hz for the church building, respectively. Also, experimental damping ratios were obtained between 1.36-3.17%.
- Experimental and numerical mode shapes of the church building were obtained as transverse, longitudinal and torsional modes.

The maximum difference between the experimental and initial numerical frequencies was 34.81%. To reduce the differences between the numerical and experimental frequencies, the model updating procedure was employed. With the model updating procedure, the maximum difference was minimized from 34.81% to 2.22%.

Declaration of Conflict of Interests

The authors declare that there is no conflict of interest. They have no known competing financial interests or personal relationships that could have appeared to influence the work reported in this paper.

References

[1.] Moravej, H., Chan, T.H.T., Nguyen, K.-D. and Jesus, A. (2019). Vibration-based bayesian model updating of civil engineering structures applying Gaussian procedure metamodel. Advances in Structural Engineering 22 (16): 3487-3502. doi: 10.1177/1369433219858723.

[2.] Venanzi, I., Kita, A., Cavalagli, N., Ierimonti, L. and Ubertini, F. (2020). Earthquake-induced damage localization in an historic masonry tower through long-term dynamic monitoring and FE model calibration. Bulletin of Earthquake Engineering 18: 2247-2274. doi: 10.1007/s10518-019-00780-4.

[3.] Günaydın, M., Adanur, S. and Altunışık, A.C. (2019). Experimental investigation on acceptable difference value in modal parameters for model updating using RC building models. Structural Engineering International, 29 (1): 150-159. doi: 10.1080/10168664.2018.1517019.

[4.] Zivanovic, S., Pavic, A. and Reynolds, P. (2007). Finite element modelling and updating of a lively footbridge: the complete procedure. Journal of Sound Vibration 301 (1): 126–145 5. doi: 10.1016/j.jsv.2006.09.024.

[5.] [5] Sevim, B., Bayraktar, A., Altunışık, A.C., Atamtürktür, S. and Birinci, F. (2011). Finite element model calibration effects on the earthquake response of masonry arch bridges. Finite Elements in Analysis and Design 47 (7): 621-634. doi: 10.1016/j.finel.2010.12.011.

[6.] Saisi, A., Gentile, C. and Guidobaldi, M. (2015). Post-earthquake continuous dynamic monitoring of the Gabbia tower in mantua, Italy. Construction and Building Materials 81: 101-112. doi: 10.1016/j.conbuildmat.2015.02.010.

[7.] Bergamo, O., Campione, G., Donadello, S. and Russo, G. (2015). In-situ NDT testing procedure as an integral part of failure analysis of historical masonry arch bridges. Engineering Failure Analysis 57: 31-55. doi: 10.1016/j.engfailanal.2015.07.019.

[8.] Ceroni, F., Sica, S., Pecce, M.R. and Garofano, A. (2014). Evaluation of the natural vibration frequencies of a historical masonry building accounting for SSI. Soil Dynamics and Earthquake Engineering 64: 95–101. doi: 10.1016/j.soildyn.2014.05.003.

[9.] Torres, W., Almazán, J.L., Sandoval, C. and Boroschek, R. (2017). Operational modal analysis and FE model updating of the Metropolitan Cathedral of Santiago, Chile. Engineering Structures 143: 169-188. doi: 10.1016/j.engstruct.2017.04.008.

[10.] Lacanna, G., Ripepe, M., Marchetti, E., Coli, M. and Garzonio, C.A. (2016). Dynamic response of the Baptistery of San Giovanni in Florence, Italy, based on ambient vibration test. Journal of Cultural Heritage 20: 632-640. doi: 10.1016/j.culher.2016.02.007.

[11.] Standoli, G., Giordano, E., Milani, G. and Clementi, F. (2021). Model updating of historical belfries based on oma identification techniques. International Journal of Architectural Heritage, 15 (1): 132-156. doi: 10.1080/15583058.2020.1723735.

[12.] Van Overschee, P. and De Moor, B.L. (1996). Subspace identification for linear systems: Theory, Implementation and Applications. 1st ed. Dordrecht, The Netherlands. Kluwer Academic Publishers.

[13.] Jacobsen, N. J., Andersen, P. and Brincker, R. (2006). Using enhanced frequency domain decomposition as a robust technique to harmonic excitation in operational modal analysis. Proceedings of ISMA2006: International Conference on Noise & Vibration Engineering, September 18-20. Leuven, Belgium.

[14.] ABAQUS/Standard. V. 6.14. 2014. Dassault systémes simulia corp. Providence: Rhode Island, USA.

[15.] Saloustros, S., Pelà, L., Roca, P. and Portal, J. (2015). Numerical analysis of structural damage in the church of the Poblet monastery. Engineering Failure Analysis 48: 41–61. doi: 10.1016/j.engfailanal.2014.10.015.

[16.] Carpinteri, A., Invernizzi, S. and Lacidogna, G. (2005). In situ damage assessment and nonlinear modelling of a historical masonry tower. Engineering Structures 27: 387–395. doi: 10.1016/j.engstruct.2004.11.001.

[17.] Betti, M. and Vignoli, A. (2011). Numerical assessment of the static and seismic behavior of the basilica of Santa Maria all'Impruneta (Italy). Construction and Building Materials 25: 4308–4324. doi: 10.1016/j.conbuildmat.2010.12.028.

[18.] [Sorour, M.M., Parsekian, G.A., Duchesne, D., Paquette, J., Mufti, A., Jaeger, L. and Shrive, N.G. (2009). Evaluation of young's Modulus for Stone Masonry Walls under Compression. 11th Canadian Masonry Symposium, Toronto, Ontario.

PACE-2023

International Congress on Phenomenological Aspects in Civil Engineering

Research Article

20-23 June 2023

Investigation of Dynamic Characteristics of Blast Effects on Reinforced Concrete Structure Models with Different Geometrical Properties

Fatma Önalan[1], Fezayil Sunca[2], Ahmet Can Altunışık*[,3]

[1] *Ankara Water and Sewerage Administration, 06050 Ankara, Turkey*

[2] *Department of Civil Engineering, Faculty of Engineering, Sivas Cumhuriyet University, 58140 Sivas, Turkey*

[3] *Department of Civil Engineering, Faculty of Engineering, Karadeniz Technical University, 61080 Trabzon, Turkey*

Corresponding Author E-mail:ahmetcan8284@hotmail.com

Keywords

Explicit Analysis, Buildings., Blast Load, Explosives., Concrete strength..

Abstract

Engineering structures such as buildings, highways, hospitals and bridges are all necessary structures for people to maintain their basic lives. In recent years, with the development of technology and the increase in wars, we have been witnessing the effects of the explosion phenomenon that occurred as a result of accidents or terrorist attacks in daily life. Within the scope of this study, the effect of explosions occurring in different scenarios around a building was examined. Within the scope of the study, a parametric study was carried out on a total of 72 scenarios using two different building models, 6 different explosive weights and 6 different concrete strength classes, and the dynamic responses of the elements constituting the building were examined. When the data obtained as a result of the studies are examined, it has been determined that the strength class of the concrete material, which constitutes the majority of the building, the explosive weight and distance, as well as the presence of the hollow geometry in the structure are of great importance and play an active role. Explosion resistant structures can be constructed using the parameters explained in the light of the results obtained.

1. Introduction

With the Second World War, it is seen that the analytical and experimental studies on the effects of explosive types and those who tried them, on the behaviors caused by explosions in the scientific field, also took place in the literature. The explosion effect from the 1950s to the present continues to increase with the processes going through them and the analytically advancing and future technology. It shows that it pays more and more attention to the consequences of terrorist bomb attacks, especially in the last twenty years.

Empirical, experimental and numerical studies have been carried out by many scientists to determine the dynamic responses of structures as a result of the explosion event. First of all, in the 1950s, Newmark (1953) [1] presented suggestions for the design of structures resistant to explosion effects, determined the calculation steps, and defined the numerical relation that determines the explosion load pressure function. In later studies [2,3,4,5,6] various empirical formulas were developed to measure the pressure values caused by the explosion on the structural element, and numerical studies related to the subject were continued. Although the obtained numerical relations are useful in reading the pressure effect on the building element, they are not sufficient for today.

On the other hand, when the experimental studies on reinforced concrete structures are examined, almost all of the studies were carried out on only a single load-bearing element [7,8,9]. The data obtained from experimental studies, on the other hand, are limited in the literature due to the complexity of the explosion phenomenon and limited measurability [10,11].

In the literature, in the measurement of dynamic responses of reinforced concrete structures; Finite Element (FE) method in building type structures [12,13,14,15,16], in studies for retaining walls [17,18], in bridges and dams [19,20,21] handled using. When the aforementioned studies are examined, using the vibrations caused by the explosive material types and the ground movements caused by the explosion, the dynamic responses of the structural bearing elements, reliability analyzes, load residual capacity, collapse mechanisms, etc., under variable parameters such as explosive weight and distance, responses have been evaluated.

Scope of this study, the effects of explosive weight and distance on different concrete strength classes on a reinforced concrete single-storey building type building model with two different geometrical properties are discussed. In the first stage of the study, a numerical modeling of a

structure built according to the conditions of the Turkish Earthquake Code (2018) [22] was carried out on the ANSYS Workbench [23] program in order to measure the reactions to occur in the explosion event in a partially confined environment. Subsequently, the created model was transferred to ANSYS Autodyn [24] for explicit analysis within the ANSYS program. Obtained results are given comparatively on the graph.

2. Blast Theory

The detonation of high-intensity explosives leads to blast waves. The blast waves produce a shock wave effect that spreads from the explosion center to the atmosphere with hemispherical form. After the shock wave releases from the center of the explosion, it reaches the maximum pressure (P_{so}) and speed value in a short time like a millisecond. As the shock wave moves away from the explosion center, the surface area expands and the pressure value gradually decreases. This process continues until a balance is achieved with the air surrounding the shock wave. This process is defined as the positive phase duration (to). During the propagation of the shock wave, the pressure value in the region behind of the shock wave falls below the ambient pressure and creates negative pressure (P^-_{so}). This process, which creates a vacuum effect, is defined as the negative phase duration (t-o). The time-history graph of blast wave pressure is given in Fig.1. Examined in the literature, generally duration of the blast approximately 2,5-3 milliseconds and value of P_{so} can reach to big overpressures.

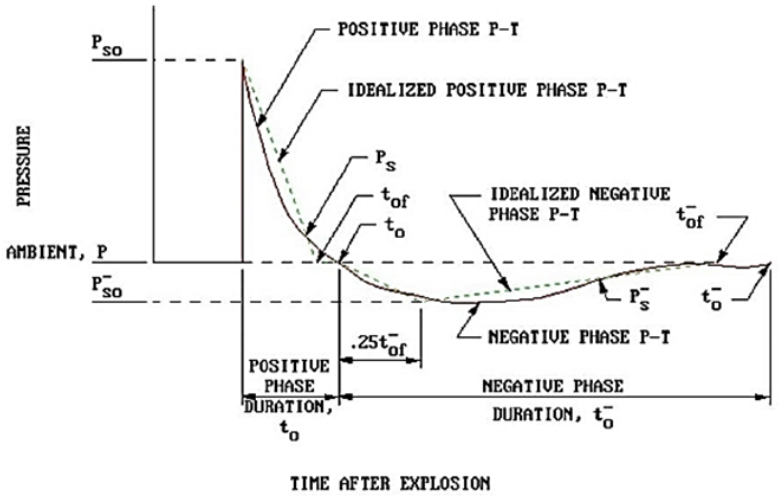

Figure 1. Pressure wave-distance interaction related to blasting

3. Finite Element Model

In this research, two building models were selected in this study. In Model I, gas escape is easily provided from the door and window openings on all facades, and in Model II, the rear facade walls of the building are assumed to be void-free to prevent explosion pressures leaving the building. The length of the building is 9000 mm (X axis), width is 6200 mm (Z axis), height is 3000 mm (Y axis), foundation depth and cantilever are determined as 500 mm. The columns cross-section was selected as 600 × 300 mm, beams cross section was 500 × 300 mm, and the slabs thickness was 120 mm. brick wall properties was selected, thick 100 mm and high 2500 mm. The slab thickness is selected as 12 cm. The buildings contain six columns and the cross-section dimensions of the columns is 30 × 60 cm. For all columns, the confinement bars are φ8/100 mm (confinement zone), φ8/195 mm (other regions) and longitudinal bars are 6φ20. The dimensions of the beams are 30 × 50 cm. The reinforcing bars of beams are 6φ16. For all beams, confinement bars are determined as φ8/100 mm (confinement zone) and φ8/200 mm (other regions). B420C (f_{yk} =420 MPa) steel class is selected for all load-bearing elements. The walls are constituted using brick elements that are 45% hollow ratio according to the Turkısh Earthquake Code. The concrete material properties used in the finite element model of buildings are summarized of Table 1 and other materials properties given Table 2 respectively.

Table 1. Concrete material properties finite element of buildings

Concrete strength						
	C25/30	C30/37	C35/45	C40/50	C45/55	C50/60
fc(MPa)	25.00	30.00	35.00	40.00	45.00	50.00
Poisson Ratio				0.20		

Table 2. Material properties finite element of buildings

Material Component	Material Type	Density (g/cm^3)	Compressive trength (MPa)
Reinforcing Bar	B420C	2.40	420.00
Infill Wall	Brick	0.69	5.00

The FE models of the buildings are constituted in ANSYS Workbench software. To perform explicit analyses of the buildings, the FE models are transferred into ANSYS Autodyn software. The Lagrange theory is used for solid elements. Air volume and TNT explosives are modeled according to Euler's theory.

The FE models of the buildings are given in Fig. 2. The detonation is a phenomenon that occurs in a very short time period. To observe the differences in pressure change, the analysis time should be chosen appropriately. The analyses times are considered as 3ms and the increment interval of 0.01ms. In the blasting analyses, 29 gauge points are selected to monitor the blasting responses of the buildings. These gauge points are specified various important regions such as joints of load-bearing elements, brick walls, and structural elements-infill wall interaction regions to determine the blasting responses of the different facades of buildings. These selected gauge points are given in Fig. 3.

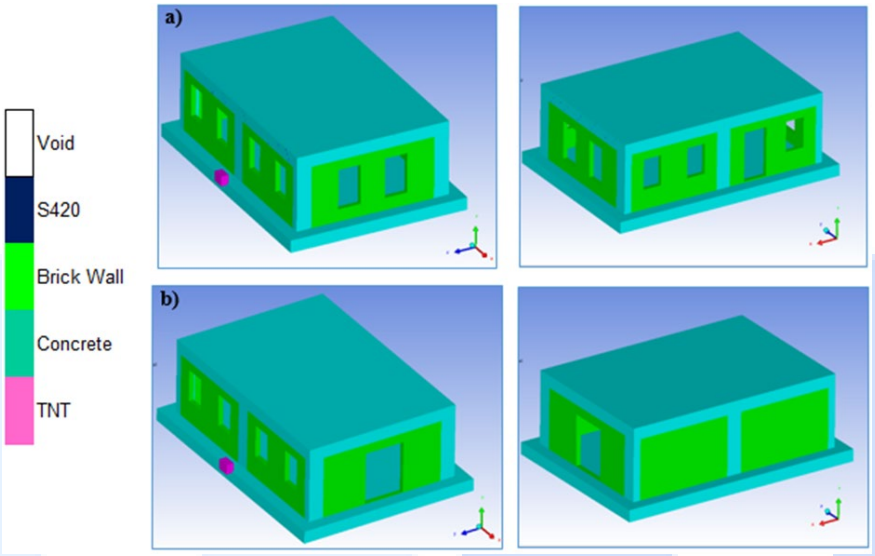

Figure 2. Finite element models of the building models (a. Model I, b. Model II)

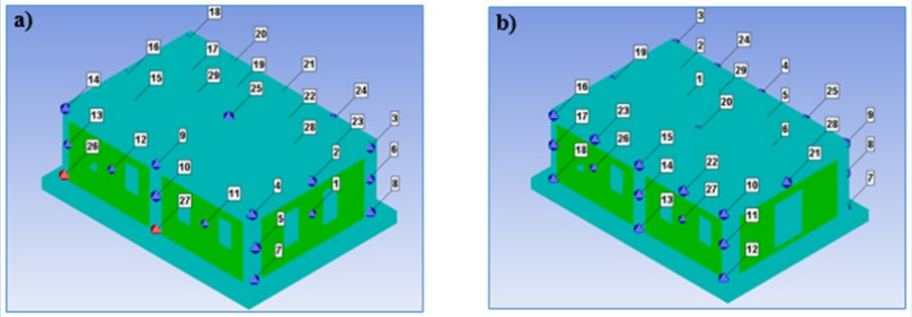

Figure 3. Gauge points (a. Model I, b. Model II)

4. Explicit Analysis

In the analysis of structures, the maximum responses obtained from numerical studies are generally guiding in our understanding of structural behavior. Therefore, the critical measurement points at which maximum responses are obtained in structural elements and infill walls were determined to compare the results of 72 explicit analyzes. The maximum responses of the structural elements were obtained from gauge 27 for Model 1 and from gauge 13 for Model 2. Also, gauge 12 and gauge 26 are critical points for the infill walls of Model 1 and Model 2, respectively. The common feature of these gauge points is that they are located on the building facades and are closest to the explosion center. The four critical gauge points chosen for both structural members and infill walls are given in Figure 4.

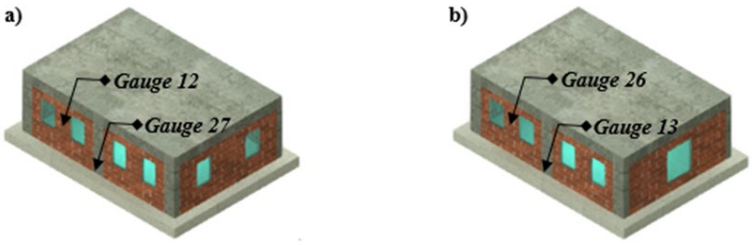

Figure 4. Critical gauge points at the front façade of models (a. Model I, b. Model II)

To determine the effects of concrete strength, TNT charge weight, and the opening ratio in infill walls on the blasting responses, the peak pressures are comparatively investigated. Figs. 5-8 present the time-history of peak pressures obtained from the critical gauge points on the load-bearing elements and infill walls of Model 1 and Model 2.

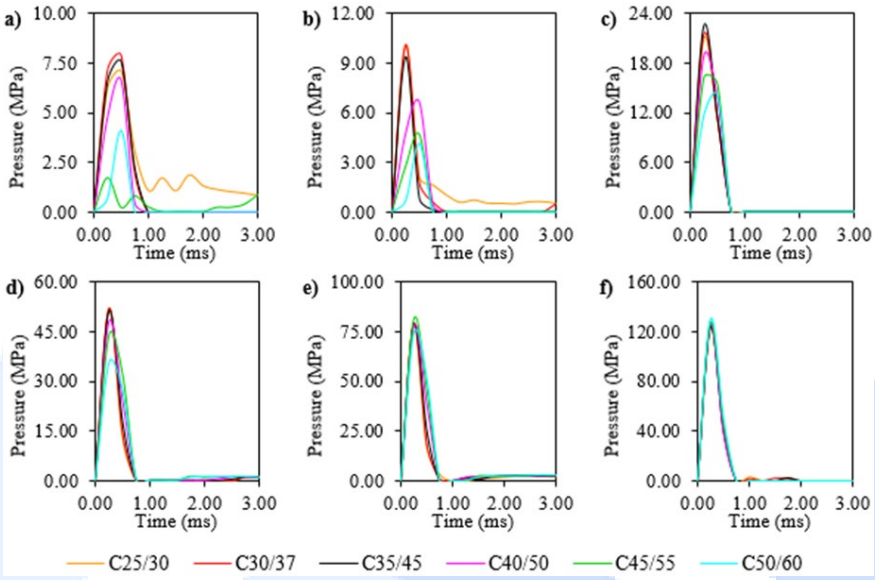

Figure 5. The time-histories of peak pressures obtained from the load-bearing elements of Model 1 (charge weight; a. 5kg, b. 10kg, c. 25kg, d. 50kg, e. 100kg, f. 200kg)

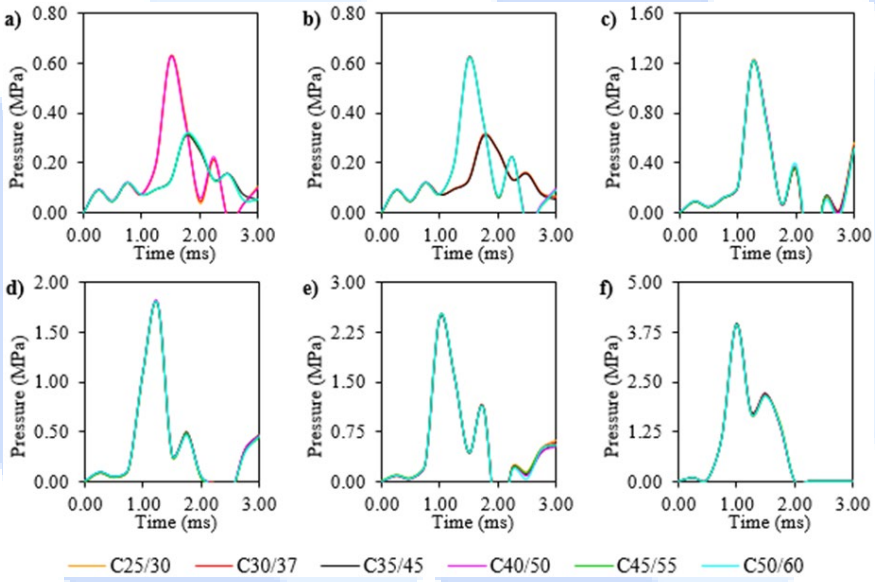

Figure 6. The time-histories of peak pressures obtained from the infill walls of Model 1 (charge weight; a. 5kg, b. 10kg, c. 25kg, d. 50kg, e. 100kg, f. 200kg)

The maximum differences between the peak pressures of Model 1 and Model 2 due to the openings in infill walls are determined as 64.45% for 5kg TNT, 68.95% for 10kg TNT, 34.54% for 25kg TNT, 18.86% for 50kg TNT, 11.66% for 100kg TNT, and 13.26% for 200kg TNT.

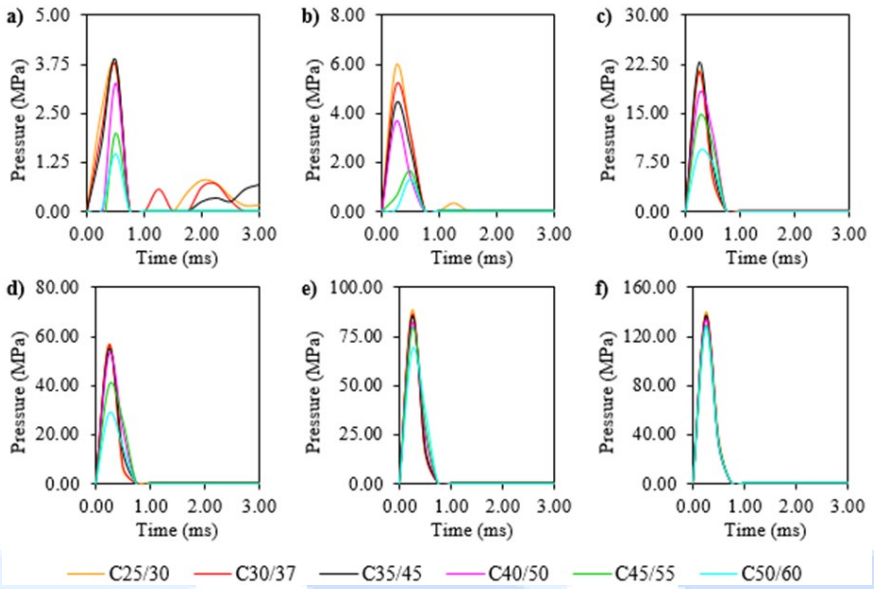

Figure 7. The time-histories of peak pressures obtained from the load-bearing elements of Model 2 (charge weight; a. 5kg, b. 10kg, c. 25kg, d. 50kg, e. 100kg, f. 200kg)

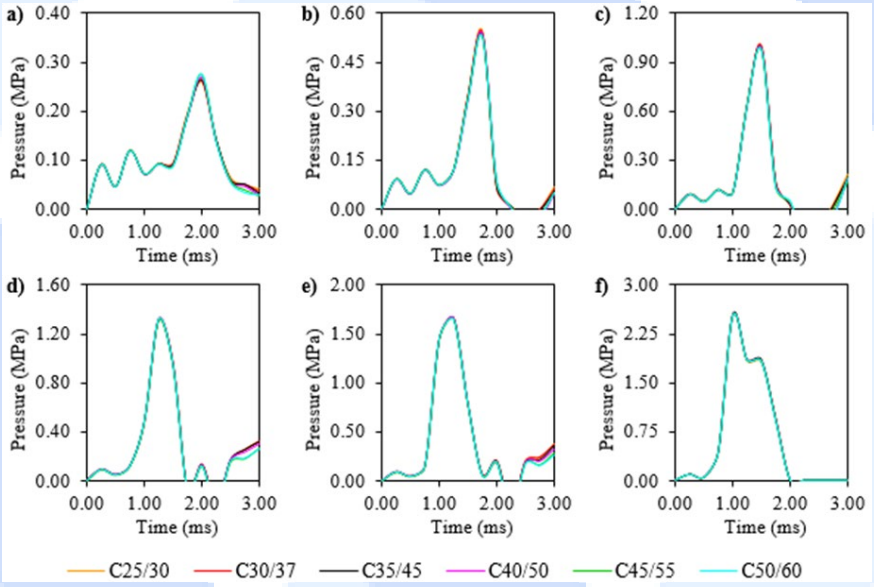

Figure 8. The time-histories of peak pressures obtained from the infill walls of Model 2 (charge weight; a. 5kg, b. 10kg, c. 25kg, d. 50kg, e. 100kg, f. 200kg)

Figs. 9-10 comparatively present the time-history of displacements obtained from the critical gauge points on the load-bearing elements for each model. In Model 1, the displacements of the structural elements increase from 1.88mm to 85.48mm for C25/30, 1.89mm to 84.65mm for C30/37, 1.95mm to 80.43mm for C35/45, 2.00mm to 75.11mm for C40/50, 1.82mm to 69.41mm for C45/55, and 1.48mm to 63.43mm for C50/60 with the increasing of explosive material weights from 5kg to 200kg. Similar upward trends are observed in Model 2 depending on the increase in the TNT weights. The increases in maximum displacements obtained from the structural elements of Model 2 are determined from 0.63mm to 99.54mm for C25/30, 0.79mm to 95.91mm for C30/37, 0.67mm to 92.73mm for C35/45, 0.74mm to 86.89mm for C40/50, 0.70mm to 80.55mm for C45/55, and 0.68mm to 75.60mm for C50/60. It is also observed from the Figs. 18, 20, and 22 that the maximum displacements of the infill walls increase by nearly 20.63 times for Model 1 and 22.21 times for Model 2 with the increase of weights of TNT from 5kg to 200kg.

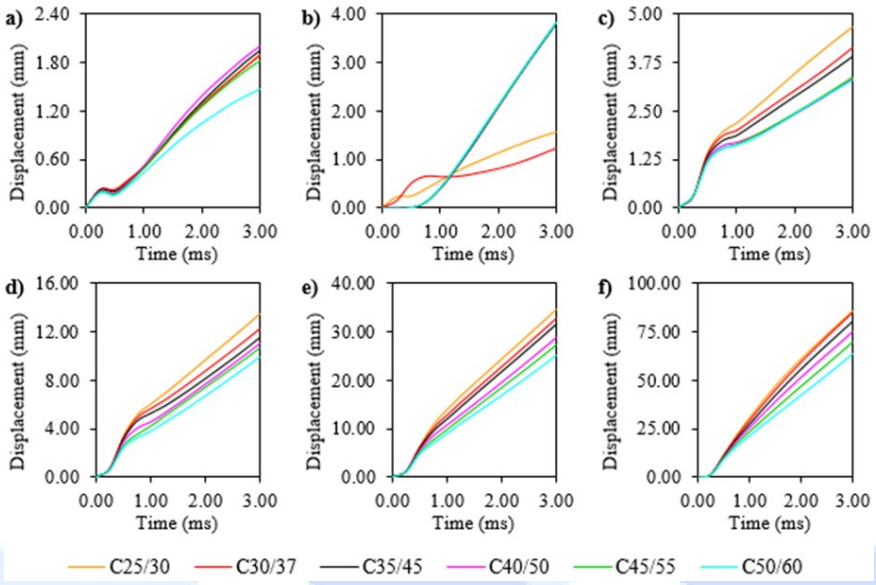

Figure 9. The time-histories of maximum displacements obtained from load-bearing elements of Model I (charge weight; a. 5kg, b. 10kg, c. 25kg, d. 50kg, e. 100kg, f. 200kg)

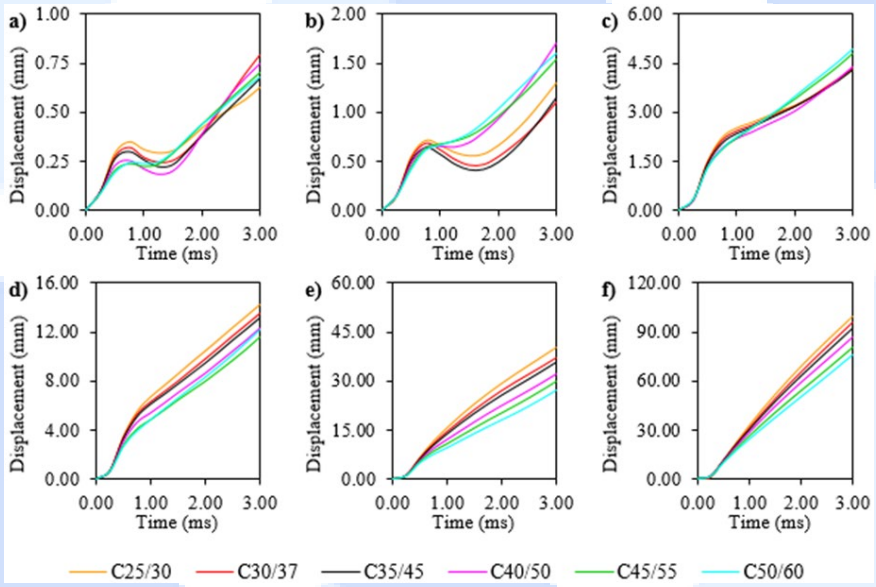

Figure 10. The time-histories of maximum displacements obtained from load-bearing elements of Model II (charge weight; a. 5kg, b. 10kg, c. 25kg, d. 50kg, e. 100kg, f. 200kg)

The released-total energies obtained from selected explosion material weights and absorbed-total energies by the air volume are plotted in Fig. 11. It can be seen from Fig. 11 that the released energies are determined as 0.18×1014μJ for 5kg TNT, 0.36×1014μJ for 10kg TNT, 0.90×1014μJ for 25kg TNT, 1.8×1014μJ for 50kg TNT, 3.6×1014μJ for 100kg TNT, and 7.2×1014μJ for 200kg TNT.

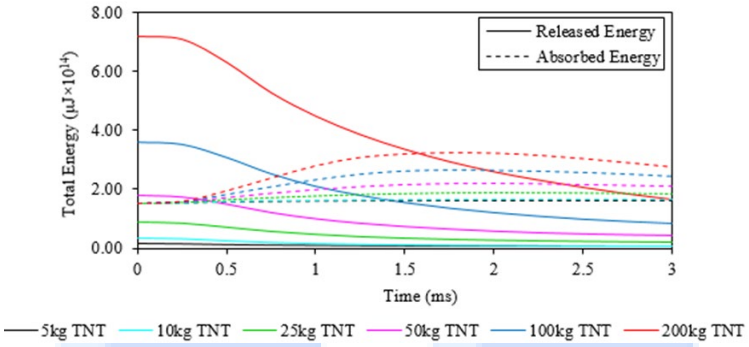

Figure 11. The time-histories of released energies by explosives and absorbed by air volume

5. Result and Discussions

As a result of the blasting analyses, the damage contour diagrams of Model 1 and Model 2 are plotted and are presented in Figs. 12 and 13. Similar damage distributions are observed in all blasting scenarios and concrete strengths, as the absorbed energies by the concrete and brick materials are negligible. Therefore, damage distributions of buildings exposed to different TNT explosives for the C25/30 and C50/60 concrete strengths are given in Figs. 14 and 15. With the increase in explosive weight, the damages increased significantly for both models. During the analyses, the damages on the load-bearing elements and infill walls are concentrated in gauge 27 and gauge 12 for Model 1 and gauge 13 and gauge 26 for Model 2, respectively. These gauge points are located on the façades of buildings and are closest to the explosion center.

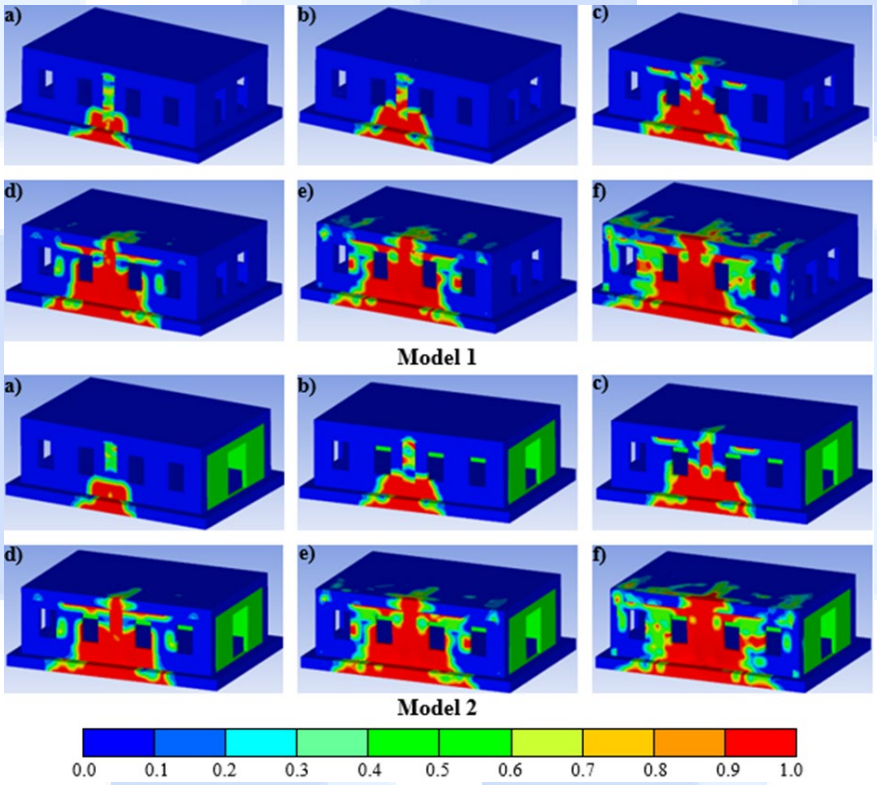

Figure 12. The damage contour diagrams obtained from C25/30 concrete strength for Model 1 and Model 2 (charge weight; a. 5kg, b. 10kg, c. 25kg, d. 50kg, e. 100kg, f. 200kg)

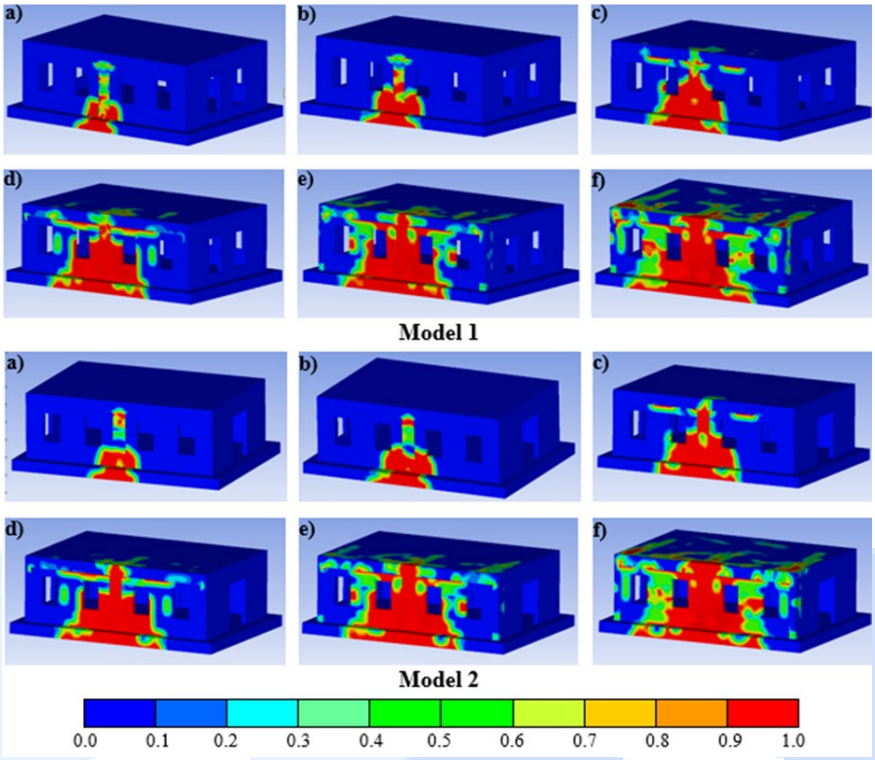

Figure 13. The damage contour diagrams obtained from C25/30 concrete strength for Model 1 and Model 2 (charge weight; a. 5kg, b. 10kg, c. 25kg, d. 50kg, e. 100kg, f. 200kg)

6. Conclusion

This study aims to assess the blasting responses and damages of RC buildings subjected to explosions. For this purpose, the explicit analyses are carried out by taking into account the effects of different TNT explosive weight, concrete strength, and different geometrical type of building. The blasting analyzes revealed that the wall openings caused crucial changes in the dynamic response of RC buildings. The differences of up to 68.95% were observed between the peak pressures obtained from the load-bearing elements of models due to window and door openings. The displacements of the load-bearing elements and infill walls were significantly affected by explosive weights. As the explosive weight increases, the displacements from both buildings also incrementally increase. As a result of the study carried out using 72 different scenarios, it was determinated that higher resistance against explosion and lower displacements were obtained in structures with hollow geometric structure and high strength concrete class.

Declaration of Conflict of Interests

The authors declares that there is no conflict of interest. They have no known competing financial interests or personal relationships that could have appeared to influence the work reported in this paper.

References

[1.] N.W.Newmark, An Engineering Approach to Blast Desingn. American Society of Civil Engineers (1953).

[2.] Brode, H.L.: Numerical solutions of spherical blast waves. J. Appl.Phys. 26(6), 766–775 (1955)

[3.] Henrych, J.; Major, R.: The dynamics of explosion and its use. Elsevier, Amsterdam (1979)

[4.] Kingery, C.N.; Bulmash, G.: Air blast parameters from TNT spherical air burst and hemispherical burst, technical report ARBRL-TR02555: AD-B082 713. US Army Ballistic Research Laboratory Aberdeen Proving Ground, Maryland (1984)

[5.] Kinney, G.F.; Graham, K.J.: Explosive shocks in air. Springer Publishing Company, Berlin (1985)

[6.] Mills, C.A.; The design of concrete structure to resist explosions and weapon effects. In: Proceedings of the 1st international conference on concrete for hazard protections. Edinburgh, 27–30 Sept 1987, pp. 61–73.

[7.] Codina, R.; Ambrosini, D.; de Borbón, F.: Experimental and numerical study of a RC member under a close-in blast loading. Eng.Struct. 127, 145–158 (2016). https://doi.org/10.1016/j.engstruct.2016.08.035

[8.] Dua, A.; Braimah, A.; Kumar, M.: Experimental and numerical investigation of rectangular reinforced concrete columns under contact explosion effects. Eng. Struct. 205, 109891 (2020). https://doi.org/10.1016/j.engstruct.2019.109891

[9.] Liu, L.; Zong, Z.; Ma, Z.J.; Qian, H.; Gan, L.: Experimental study on behavior and failure mode of psrc bridge pier under close-in blast loading. J. Bridg. Eng. 26(2), 04020124 (2021). https://doi.org/10.1061/(asce)be.1943-5592.0001662

[10.] Heggelund, S.; Brekken, K.; Ingier, P.; Christensen, S.O.: Global response of a three-story building exposed to blast loading. Multidiscip. Digit. Publ. Inst. Proc. 2(8), 386 (2018). https://doi.org/10. 3390/ICEM18-05211

[11.] Norén-Cosgriff, K.M.; Ramstad, N.; Neby, A.; Madshus, C.: Building damage due to vibration from rock blasting. Soil Dyn. Earthq. Eng. 138, 106331 (2020). https://doi.org/10.1016/j.soildyn.2020. 106331

[12.] Jayasooriya, R.; Thambiratnam, D.P.; Perera, N.J.; Kosse, V.: Blast and residual capacity analysis of reinforced concrete framed buildings. Eng. Struct. 33(12), 3483–3495 (2011). https://doi.org/10.1016/j.engstruct.2011.07.011

[13.] Kelliher, D.; Sutton-Swaby, K.: Stochastic representation of blast load damage in a reinforced concrete building. Struct. Saf. 34(1),407–417 (2012). https://doi.org/10.1016/j.strusafe.2011.08.001

[14.] Abdollahzadeh, G.; Faghihmaleki, H.: Seismic-explosion riskbased robustness index of structures. Int. J. Damage Mech. 26(4), 523–540 (2017). https://doi.org/10.1177/1056789516651919

[15.] Syed, Z.I.; Mohamed, O.A.; Murad, K.; Kewalramani, M.: Performance of earthquake-resistant rcc frame structures under blast explosions. Procedia Engineering 180, 82–90 (2017)

[16.] Sevim, B.; Toy, A.T.: Blasting response of a two-storey rc building under different charge weight of tnt explosives. Iran. J. Sci. Technol. Trans. Civ. Eng. 44(2), 565–577 (2019)

[17.] Yusof, M.A.; Rosdi, R.N.; Nor, N.M.; Ismail, A.; Yahya, M.A.; Peng, N.C.: Simulation of reinforced concrete blast wall subjected to air blast loading. J. Asian Sci. Res. 4(9), 522–533 (2014)

[18.] Toy, A.T.; Sevim, B.: Numerically and empirically determination of blasting response of a RC retaining wall under TNT explosive. Adv. Concr. Constr. 5(5), 493–512 (2017). https://doi.org/10.12989/acc.2017.5.5.493

[19.] Andreou, M.; Kotsoglou, A.; Pantazopoulou, S.: Modelling blast effects on a reinforced concrete bridge. Adv. Civ. Eng. 2016, 1–11 (2016). https://doi.org/10.1155/2016/4167329

[20.] Hu, Z.-J.; Wu, L.; Zhang, Y.-F.; Sun, L.: Dynamic responses of concrete piers under close-in blast loading. Int. J. Damage Mech. 25(8),1235–1254 (2016). https://doi.org/10.1177/1056789516653245

[21.] Chen, J.; Liu, X.; Xu, Q.: Numerical simulation analysis of damage mode of concrete gravity dam under close-in explosion. KSCE J. Civ. Eng. 21(1), 397–407 (2017). https://doi.org/10.1007/s12205-016-1082-4

[22.] TEC (2018). Turkish Earthquake Code, Disaster and Emergency Management Presidency, Ankara, Turkey.

[23.] ANSYS Workbench (2016), Swanson Analyses System, Ansys Inc, USA

[24.] ANSYS Autodyn (2016), Swanson Analyses System, Ansys Inc, USA

PACE-2023
International Congress on the Phenomenological Aspects of Civil Engineering

PACE-2023
International Congress on Phenomenological Aspects in Civil Engineering

Research Article
20-23 June 2023

A Numerical Investigation on Determining the ideal Size and Geometry of Hollow Block-Shaped Concrete Specimens for Indirect Tensile Strength Testing

Ayşegül Durmuş Demir*,[1] Hatice Süleymanoğlu[1]
[1]*Karadeniz Technical University, Department of Civil Engineering, 61080, Trabzon, Turkey*
Corresponding Author E-mail: aysegul@ktu.edu.tr

Keywords

Indirect test,
Direct test,
Tensile strength,
Concrete,
Finite element method.

Abstract

Although the compressive strength is often regarded as the primary mechanical property of concrete, it is crucial to acknowledge the significance of tensile strength in concrete design, experimental analysis, and numerical modeling. Until now, indirect methods have been employed to measure the tensile strength of concrete. Despite their widespread acceptance, they do not provide an accurate representation of the actual tensile strength of concrete. In this study, a new approach to determine concrete tensile strength is introduced. A hollow block-shaped specimen and a pull by push loading apparatus that allows to use uniaxial compression machine were designed. A parametric study was performed with the ANSYS commercial program, which is based on the finite element method, to determine the ideal geometry and size of the proposed specimen. In order to serve as a reference, a numerical model of the direct tensile strength test was also performed. This study, demonstrated an ideal specimen that exhibits a stress distribution along the specimen length that is closer to the tensile strength of concrete compared to direct tensile testing, while also providing a more uniform stress distribution. However, the recommended test method should also be experimentally validated.

1. Introduction

Concrete holds the distinction of being the most extensively utilized construction material globally, with an annual consumption of approximately 33 billion metric tons [1]. The compressive strength of concrete is widely considered the primary measure of its overall quality and serves as a direct indicator of the material's capacity to withstand loads in structural applications [2-4]. Conducting compressive strength tests is a relatively simple process, and the obtained results often exhibit correlations with other properties of concrete that typically necessitate more complex testing methods [2, 5]. However, tensile strength of concrete is also a crucial design parameter to consider. In particular, the initiation and prediction of cracking in the tension zone of reinforced concrete elements, which poses a direct challenge for the design of water-retaining structures or structures with special durability requirements, depend on the tensile behavior. Additionally, the failure of reinforced concrete structures in shear occurs through the formation of diagonal tension cracks, hence shear strength is directly related to tensile strength [6].

Despite the significant importance placed on investigating the tensile strength of concrete, many challenges in this field remain unresolved. Uniaxial testing is required to determine the basic tensile properties, but so far, due to the challenges involved in applying a pure tensile force to plain concrete specimens, there are no standardized tests specifically designed for direct tension measurement [2, 6]. Over the years, various indirect tensile testing methods have been developed to overcome the difficulties associated with conducting direct tensile strength tests, such as holding, gluing and secondary stresses introduced in the loading process. The tensile strength of concrete can be evaluated through various tests employing different specimen geometries. These tests include direct tension tests conducted on briquettes or dumbbell-shaped specimens [7-10], flexural tests performed on beams, splitting tests carried out on cylinders or cubes, ring-tensile tests [11], fluid-pressured test [12], the double-punch test [13] and compression to tension test [14, 15]

Concrete strength is not an inherently absolute property like certain other material properties. It is influenced by factors such as the shape and size of the specimen, the preparation of the sample, and the method of loading, which can lead to varying results. Therefore, as a result of applying different test methods to specimens produced from concrete of the same quality, different tensile strength values are obtained. Among the commonly accepted methods, the tensile strength values obtained follow a specific sequence: flexural tensile strength > splitting tensile strength > direct tensile strength [16]. In order to obtain results closer to the direct pull test, which gives more realistic results for concrete

tensile strength, this study aims to determine the ideal specimen size and geometry for the proposed indirect tension test approach by comparing with the direct tension method.

2. The Proposed Indirect Test Method

The apparatus described below was designed to apply tensile load to the proposed hollow block specimen by using uniaxial compression machine. The apparatus is schematically represented in Fig. 1. The pull by push apparatus consists of four parts (Fig. 1(a)): two rigid steel frame bottom (part 1) and top sections (part 2) to be placed below and above the specimen and two rigid semi-circular steel loading elements to be placed bottom and top of the hollow in the specimen to transmit the pressure load to the specimen as tension (part 3 and part 4).

The set up procedure of pull by push apparatus is consisted of four stages, as shown in Fig. 1. Firstly, the bottom rigid frame is placed on compression machine. Then, the hollow block concrete specimen is vertically positioned inside the bottom frame and the top rigid frame placed on the specimen. Finally, semi-circular steel loading elements are inserted into the top and bottom of the hollow, respectively. The top and bottom loading elements are moved upward and downward, respectively, as the hydraulic press pushes the rigid frames in the opposite directions (Fig. 1 (c)). As the press continues to compress, the tensile stress in the specimen increases until failure occurs.

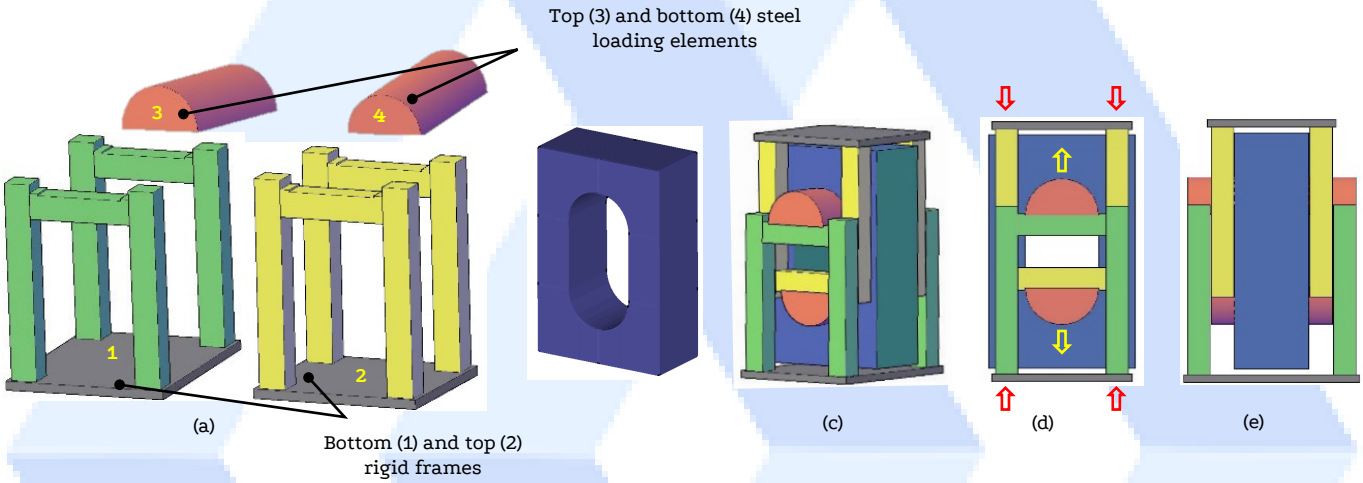

Figure 1. (a) The components of the pull by push apparatus , (b) proposed specimen , (c) perspective, (d) front and (e) side view of the experimental set-up

3. Numerical Modeling

To examine the stress distribution in a hollow block indirect tensile strength test (HBT) specimen, a series of numerical analyses were carried out using ANSYS software [17] which contain special elements and material models for brittle materials like concrete. Additionally, a cylindrical direct tensile strength test (DTT) specimen with an aspect ratio of two was also modeled and analyzed (Fig. 2). The concrete specimens and the semi-circular steel loading elements on which the load is applied were modeled with solid elements. The considered solid elements are isoperimetric eight node-brick element with three degrees of freedom per node. Solid65 that allows cracking in tension and crushing in compression was used to model concrete and Solid185 was used to model semi-circular steel loading elements. The accurate characterization of the interaction between concrete specimen and steel loading elements is a crucial aspect in the analysis. Various methods have been described in technical literature to simulate the contact mechanism between two distinct surfaces, depending on the nature of the problem. To simulate the interaction between concrete and steel loading elements in three-dimensional problem, a surface-to-surface contact algorithm was chosen. In the analysis, the reciprocal surfaces of the concrete and steel bars are designated as the target and contact surfaces, respectively. Since the steel loading element is more rigid than the concrete, it is assigned as the target surface (Targe170), while the surface of the concrete is considered the contact surface (Conta174) (Fig. 2). The contact status between these two surfaces is regularly evaluated at Gauss integration points. To model the interaction between these two different materials, the Coulomb friction model was employed.

The Willam-Warnke failure criterion was utilized to enable the prediction of failure occurrence in concrete specimen. Initially, the material was assumed to be linear elastic until a crack formed. Once a crack initiated, the program recalculated the changes in normal and shear stresses. The re-calculated shear stresses were transferred by the plasticity due to the generated open and closed cracks. A shear transfer coefficient of 0.7 was used for closed cracks, while a coefficient of 0.2 was used for open cracks.

In order to achieve adequate solution convergence, multiple finite element models with different meshes were examined. The aim was to determine the appropriate mesh density that would yield satisfactory results. The mesh length in the concrete specimen model was deliberately set to 1 mm in the straight sections of the hollow and vicinity of the semi-circular parts of the hollow, as this region is considered the most critical area for the initiation of failure. The mesh length progressively increased as the distance from the semi-circular parts of the hollow increased. Fig. 2 illustrates the specific meshing configuration used in the analysis.

Nonlinear static analyses were performed using the full Newton-Raphson method. In the case of displacement-controlled loading, the total displacement was achieved by dividing it into several sub-steps.

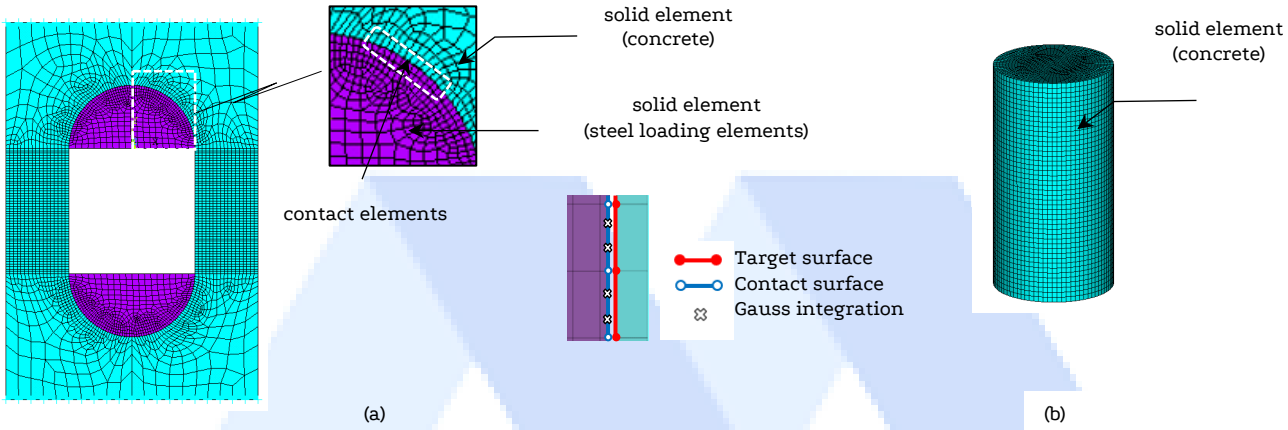

Figure 2. Finite element model for (a) proposed HBT specimen and (b) DTT specimen

4. Description of the considered concrete specimens

The failure mechanism of the specimens with different hollow sizes were investigated by numerical analyses to evaluate whether it occurs under uniaxial tensile stress. Given that concrete consists of elements with varying strengths, it is a reasonable assumption that the greater the volume of concrete under stress, the higher the likelihood of containing an element with an extreme (low) strength [17]. Based on that, the block was designed with dimensions of 200 mm in length, 100 mm in width, and 300 mm in height, considering the need to provide sufficient area for tension while modeling the hollow (Fig. 3). This hollow enables the application of tensile force to the specimen, and its shape allows for the consideration of defects in concrete.

In the analysis, three different hollow diameters (D) were considered: 60 mm, 80 mm, and 100 mm. And, three different lengths (L) were taken into account to represent the straight section of the hollow: 80 mm, 100 mm, and 120 mm. Each diameter value was analyzed for three different length values. A cylindrical specimen with a diameter of 75 mm and a height of 150 mm was also considered as a direct tensile strength test specimen. All specimen shapes and dimensions considered are illustrated in Fig. 3. By comparing the obtained principal tensile stress distribution in the event of failure with those obtained from direct tensile strength tests, the final hollow dimensions were determined.

The elasticity modulus (E_c) and Poisson ratio (ν_c) of concrete specimen, were interpreted as 30000 MPa and 0.2, respectively. The tensile strength of concrete was considered as 3 MPa. The semi-circular steel loading elements were characterized by an interpreted elasticity modulus (E_c) of 200000 MPa and a Poisson's ratio (ν_c) of 0.3. Due to the lubrication of the interface during the experiments, the friction of coefficient was considered as 0.2 between the concrete specimen and steel loading elements for all analyses.

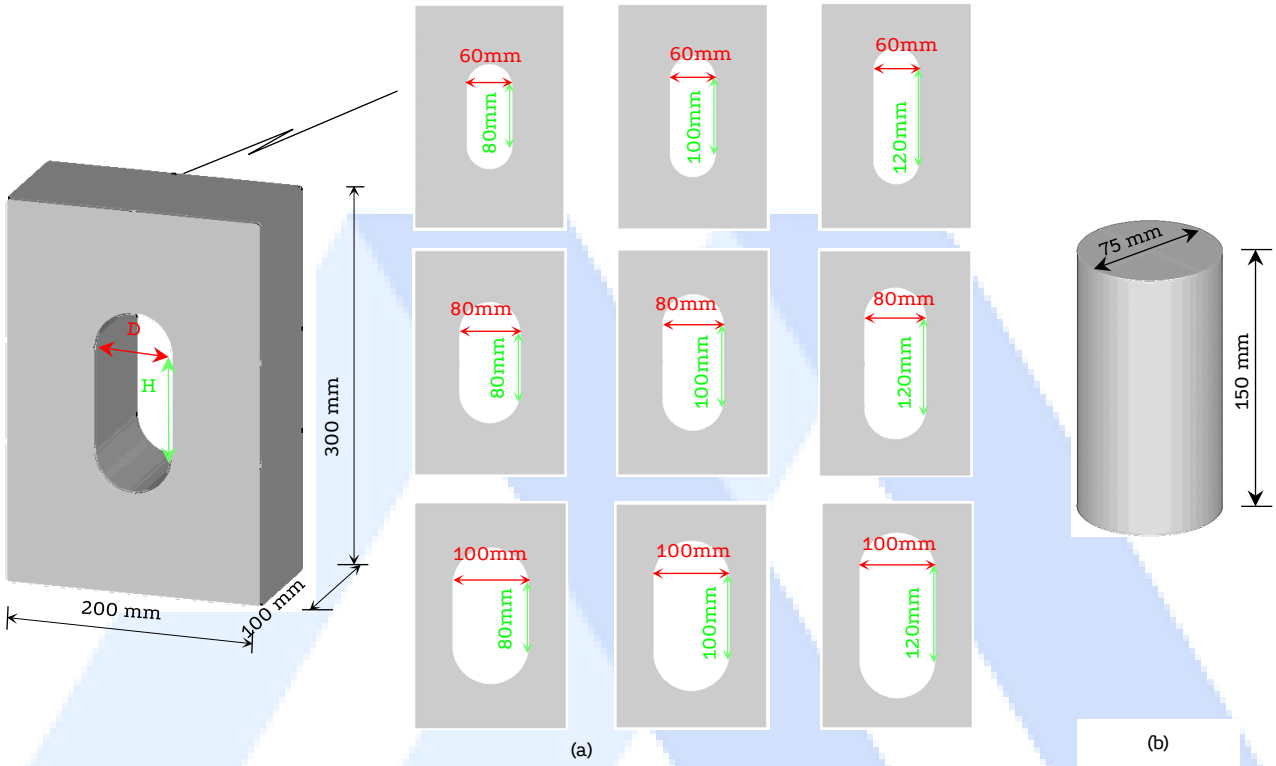

Figure 3. Considered dimensions of the (a) proposed HBT specimen and DTT specimen

5. Results and Discussion

Nine different analyses were conducted, considering various combinations of parameters such as the diameter of the hollow and the length of the straight section within the hollow. This study examined three different diameters and, for each diameter, three different lengths of the straight section were investigated. Furthermore, a direct tensile test analysis was performed to compare the obtained results. The results were analyzed parametrically, focusing on the distribution of the first principal stress along the length of the straight section of the hollow and the types of crack propagation observed in the considered specimens. The models analyzed through Direct Tensile Strength Test and the ones analyzed through the Hollow Block Tensile Strength Test are denoted by the abbreviations DTT and HBT, respectively. In this context, HBT_D60-L80 represents a hollow block specimen with a diameter of 60 mm and a length of 80 mm.

The comparisons of the obtained first principal stresses along the measurement length of the considered HBT specimens and DTT specimen were given in Fig. 4. When these three graphs are examined, the stress values occurring throughout the measurement length of the specimen are smaller for all considered hollow lengths for the specimens with 60 mm hollow diameter compared to the DTT. As the intended hollow diameter in the specimen increases, the stress values occurring in the middle section of the specimen tend to be closer to the tensile strength of the concrete material compared to DTT. Therefore, this situation increases the probability of fractures occurring in the middle section of the specimen under tension, due to potential defects in the concrete.

The hollow diameter (D) was determined as 100 mm. As can be seen from Figure 2.c, a specimen with this diameter allows for obtaining a stress value closer to the tensile strength of concrete compared to the DTT, as well as achieving a more uniform stress distribution. When considering the values of L for the 100 mm hollow diameter, it can be observed that the results are similar for three different L values. In order to allow for obtaining more realistic tensile strength results by considering potential defects in the concrete, it was determined that the specimen under tension should be kept as long as possible. Therefore, L was set to 100 mm.

The crack propagations of the considered HBT specimens are shown in Fig. 5. In numerical modeling, due to the heterogeneous nature of concrete, possible defects in the material cannot be taken into account. Therefore, as expected, cracks occurred at the ends of the hollow where the stress was greatest. However, based on the obtained stress distribution, the proposed sample also allows possible defects in the material to be taken into account. For this reason, it is expected that fractures will occur in the middle sections of the hollow in experimental studies.

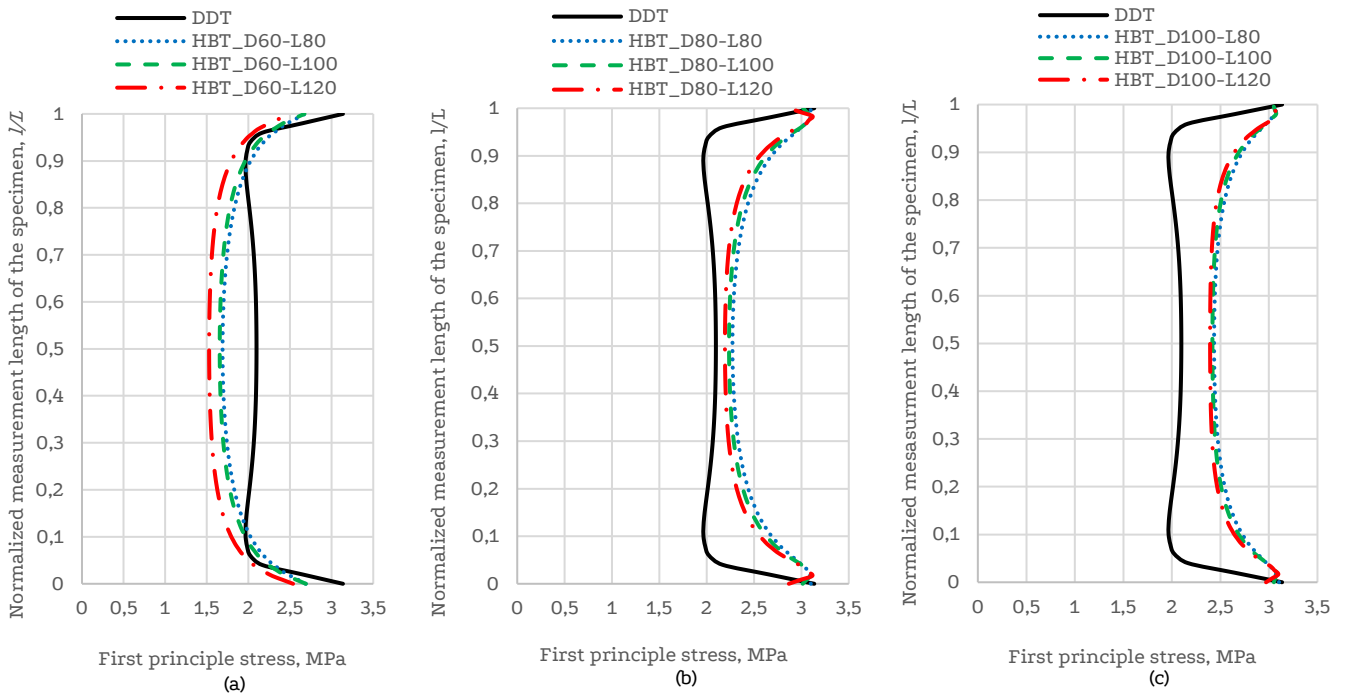

Figure. 4. Comparisons of first principle stress distribution along the normalized length of the considered HBT and DTT specimens for hollow diameter of (a) 60mm (b) 80mm and (c)100mm

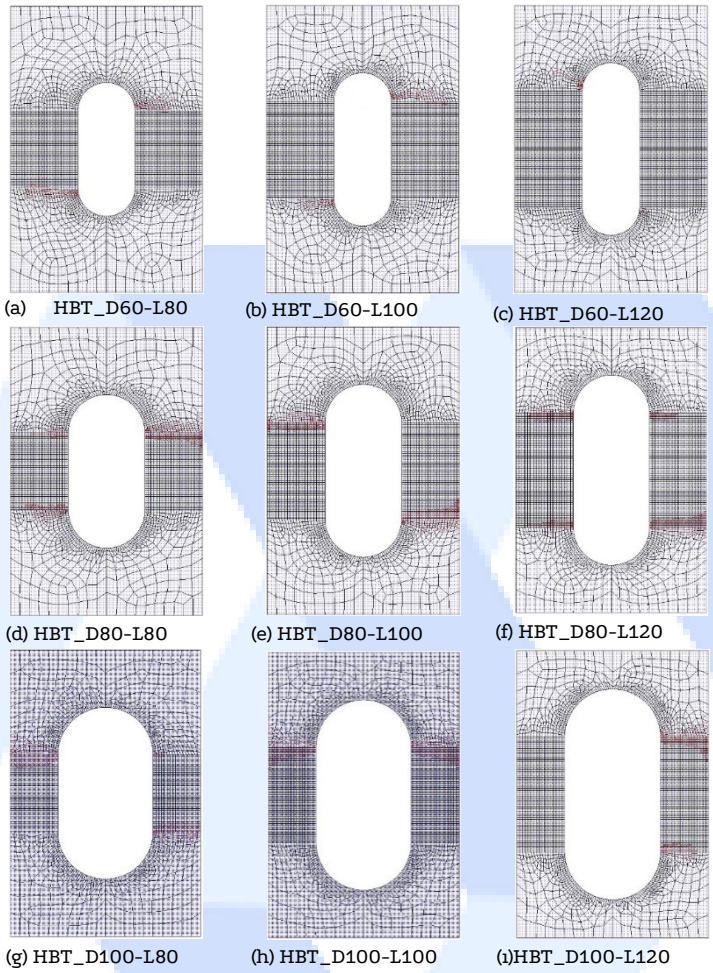

Figure. 5. Crack propagations of the considered HBT specimens

6. Conclusions

The HBT method is a novel technique for determining tensile strength of concrete. This method has several advantages, such as

- removing the time-consuming sample preparation problem of direct tensile strength test (DTT) due to gluing and holding steps,
- eliminating invalid failure modes caused by adhesives used in DTT,
- allowing the use of uniaxial compression machine,
- controlling the failure mode of concrete under uniaxial tensile stress conditions,
- providing a more uniform stress distribution along the length of the specimen compared to the DTT,
- enabling for obtaining a stress distribution that is closer to the tensile strength of the concrete material over a broader area along the specimen compared to DTT and
- allowing to take into account the probable defects in concrete specimens that determines the strength of the entire specimen.

Based on the findings of this numerical study, it is recommended to conduct further research on the HBT test to enhance its effectiveness and establish it as a widely adopted method for determining the tensile strength of concrete.

Declaration of Conflict of Interests

The authors declare that there is no conflict of interest. They have no known competing financial interests or personal relationships that could have appeared to influence the work reported in this paper.

References

[1.] Nogueira, Carnot L., A new method to test concrete tensile and shear strength with cylindrical specimens. ACI Materials Journal 115:6 (2018) 909-923.

[2.] LU, A., Preliminary assessment of the base variables for standardizing the pressure tension test, Master's thesis, McGill University, Canada (2015).

[3.] Chen, X., Huang, W., & Zhou, J., Effect of moisture content on compressive and split tensile strength of concrete. Indian Journal of Engineering & Materials Sciences, 19 (2012) 427-435.

[4.] Bungey, J. H., Smillard, S. G., & Grantham, M. G., Testing of Concrete in Structures (4th Ed. ed.). Oxon: Taylor & Francis (2006).

[5.] Ozyildirim, C., & Carino, N. J., Concrete Strength Testing. In J. F. Lamond & J. H. Pielert (Eds.), Significance of tests and properties of concrete and concrete-making materials. Philadelphia, PA: ASTM (2006).

[6.] Kassas, A. A., Studies on the tensile strength of concrete, Master's thesis, Middle East Technical University, Turkey (1978).

[7.] ASTM D2936-08, Standard Test Method for Direct Tensile Strength of Intact Rock Core Specimens. Annual Book of ASTM Standards, vol. 4, ASTM, West Conshohocken, PA.

[8.] N.X. Xie, W.Y. Liu, Determining tensile properties of mass concrete by direct tensile test, ACI Mater. J. 86:3 (1989) 214–219.

[9.] W. Zheng, A.K.H. Kwan, P.K.K. Lee, Direct tension test of concrete, ACI Mater. J. 98:1 (2001) 63–71.

[10.] A. Ghaffar, M.A. Chaudhry, M. Kamran Ali, A new approach for measurement of tensile strength of concrete, J. Res. Sci. Bahauddin Zakariya Univ., Multan, Pakistan 16:1 (2005) 1–9.

[11.] D.J. Hannant, The tensile strength of concrete: a review paper, Struct. Eng. 50:7 (1972) 253–257.

[12.] Cantillo, V., & Guzmán, A., Fluid-pressured test to measure tensile strength of concrete. Journal of materials in civil engineering, 26:4 (2014) 776-780.

[13.] W.F. Chen, B.E. Trumbauer, Double-punch test and tensile strength of concrete, J. Mater. ASTM 7:2 (1972) 148–154.

[14.] Sarfarazi, V., Haeri, H., Ebneabbasi, P., Shemirani, A. B., & Hedayat, A., Determination of tensile strength of concrete using a novel apparatus. Construction and Building Materials, 166 (2018) 817-832.

[15.] Haeri, H., Sarfarazi, V., & Hedayat, A., Suggesting a new testing device for determination of tensile strength of concrete. Struct. Eng. Mech, 60:6 (2016) 939-952.

[16.] Erdoğan, T. Y., Concrete. METU Press Publishing Company (2003) (In Turkish).

[17.] ANSYS Software ANSYS Inc., Canonsburg, PA, USA.

[18.] Neville, A. M., Properties of concrete. London: Longman (1995)

Keyword Index